

Persistent Radicals in Natural Product Synthesis: A Biomimetic
Approach to Resveratrol Oligomers

by

Kevin Joseph Romero

A dissertation submitted in partial fulfillment
of the requirements for the degree of
Doctor of Philosophy
(Chemistry)
in The University of Michigan
2020

Doctoral Committee:

Professor Corey R. J. Stephenson, Chair
Professor Pavel Nagorny
Professor Alison R. H. Narayan
Professor David H. Sherman

Kevin J. Romero

kevjrom@umich.edu

ORCID iD: 0000-0001-7604-3996

© Kevin J. Romero 2020

to J.R., Renee, Alexis, and Kaitlin – for your unwavering love and support

ACKNOWLEDGEMENTS

“For the things we have to learn before we can do them, we learn by doing them.”
— Aristotle, The Nicomachean Ethics

The work described in this dissertation represents the summit of my academic career, and it was during this climb that I learned about so much more than chemistry. I have been blessed with numerous opportunities that have helped me to arrive at where I am today, so now I must take a moment to give my utmost thanks to those that have assisted in my academic journey. To Professor Corey Stephenson, thank you for taking me on as a graduate student in your group at the end of my first year at Michigan four years ago. Undoubtedly, I was the greenest recruit of my cohort entering the group, so, in hindsight, I do not take such a decision lightly. I appreciate the faith you expressed in me and the support you have given throughout the years since to help me to achieve my goals. I would not be the chemist and person I am today without your unwavering commitment to excellence and pushing the perceived boundary of the status quo. To Professor Derek Pratt, thank you for the guiding influence you have also had on our interdisciplinary and collaborative project and the mentorship you provided through the years. To Professor Alison Narayan, thank you for the opportunity to rotate in your group during my first year at Michigan. That was certainly a formative experience for me, and I will always appreciate the one-on-one conversations we had as I was trying to find my way as a young chemist. To Professor Pavel Nagorny and Professor David Sherman, as well as Prof. Narayan, thank

you for agreeing to serve on my thesis committee and for all of your helpful suggestions and guidance over the course of my time at Michigan. To Professor Elizabeth Atkinson, who first inspired my interest in organic chemistry, thank you for always fostering my curiosity about the subject and inspiring me to pursue a graduate education. To Professor Brian Gilbert, thank you for helping me to find my path at Linfield and beyond, and for teaching me to appreciate the power of a cold beer after a long day. To Professor Jim Diamond, thank you for extending the first opportunity to conduct chemistry research as an undergraduate, setting in motion a process that brought me to where I am today. I very much appreciate the support these three faculty from Linfield provided by encouraging me to seek out additional research opportunities through summer REU programs, and I thank Professor Michael Jewett at Northwestern University and Professor Yuriy Román at the Massachusetts Institute of Technology for the opportunities to work with their groups and learn from their talented graduate students and postdocs as I broadened my research horizons. Finally, I must thank my high school chemistry teacher, Mr. Bruce Campbell, for always pushing me to never simply be content with the correct answer and instead demanding that “why” and “how” be the focus – an approach that has continually guided me throughout my academic career.

I would also like to briefly take a moment to thank the excellent administrative support here at Michigan, specifically Liz Oxford and Katie Foster, as they have always provided clear guidance for graduate students. In addition, this department offers outstanding technical support from Eugenio Alvarado and Chris Kojiro (NMR), Jim Windak and Paul Lennon (HRMS, IR, SFC), and Roy Wentz (Glassblowing). I must particularly thank Roy

for the custom electrochemistry glassware he constructed for our lab in addition to fixing the many pieces of glassware I broke over the last five years.

I have had the pleasure of working with an excellent group of colleagues during my graduate studies, and their talent and drive have inspired me to constantly improve in my own work. First, I would like to thank the senior students and postdocs of the Stephenson group when I joined – Daryl Staveness, Mitch Keylor, Verner Lofstrand, Joel Beatty, Markus Kaerkaes, Xu Zhu, Tim Monos, Irene Bosque, Gabe Magallanes, Theresa Williams, and Martin Sevrin – for their mentorship and guidance during my early years in the group. Mitch requires special recognition, as he was my rotation mentor during my first year and was critical in helping me to learn the fundamentals of synthetic organic chemistry from an operational standpoint; furthermore, his guidance and influence in research directions have persisted throughout my PhD studies, as much of the work described herein derives from or is inspired by work previously investigated by Mitch or Bryan Matsuura (a Stephenson group alumnus I also very much thank). Daryl is another who deserves special thanks for being a sounding board for many of my ideas as well as for being an impressive wealth of knowledge from which I continue to learn. I will always be grateful to Irene for conducting the initial proof of concept experiments for our electrochemistry project (see Chapter 2) and to Irene and Gabe for teaching me the fundamentals of synthetic organic electrochemistry. Xu was also an excellent colleague during the summer we shared in the group as he initially evaluated to homolytic bond migration (see Chapter 3), providing important groundwork for that key step from which I was able to achieve the vitisin total synthesis described within.

Excellent colleagues have continued to join the Stephenson group in the years that followed my arrival, and it has been a pleasure working each of them, including Ted McClain, Matt Galliher, Logan Combee, James Collins, Maddie Sowden, Dirk Alpers, Cheng Yang, Anthony Allen, Efrey Noten, Beca Roldan, Alex Harmata, Nick Watson, Alex Levashkevich, Racquel Edjoc and Ethan Strobel. In particular, I must thank Matt, with whom a significant portion of this journey has been shared. We have worked together on the resveratrol project for three years, publishing a tutorial *Chem. Soc. Rev.* (Chapter 1) and an *Angew. Chem.* paper (Chapter 2), and I am very excited to see where he and Beca Roldan, who recently joined the project, will take things in the years to come. Ted also was an idea sounding board for me while in the lab, and I appreciated his input and knowledge of organometallics as I investigated the key C–H arylation step for the vitisin synthesis. Logan has proven indispensable since joining the group, and his intimate knowledge of the inner workings of HPLC and UPLC instruments was critical in helping me to complete the final stages of my graduate work. Finally, I would be remiss if I did not thank Ethan, a very bright and talented undergraduate who worked with me for the better part of two years. His contributions to the resveratrol project are many, but most importantly I would like to thank him for his help in completing the vitisin synthesis (Chapter 3).

Most importantly, my time in the Stephenson group would not nearly have been the same without those in my cohort – Rory McAtee, Alex Sun, and Taylor Sodano. Together we traversed the ups and downs of a graduate education, and I could not have asked for better lab mates during the last five years. I think the thing I appreciate the most about working alongside each of them has been the diversity of thought and personality exhibited across

the four of us. We have learned so much together and from each other, and I am very excited to see where our careers in the pharmaceutical industry will lead.

“Education is the kindling of a flame, not the filling of a vessel.”
— Socrates

Outside of the lab, I have received tremendous support from family and friends, and some of the lab mates I have already mentioned assumed dual roles of colleague and friend in this journey. Ted and Gabe, in particular, have always been in my corner and I have come to rely upon their friendship. I must also thank Sam Krier and Ian Coker, two friends from Linfield who have been understanding of my time commitments these past five years but nonetheless have helped me to find ways to continue to grow our friendship and support each other from across the country. My uncle, Jeff Roelofs, has been an extremely generous source of support for me here in Michigan by regularly opening his home to my friends and I for days on the boat. My extended family, near and far, including aunts and uncles and cousins and grandparents have all expressed their love and support for me in many ways over this journey, and I appreciate all of it. However, above all else, I am indebted to the support of my parents and my sister. My mother, Renee Roelofs, was undoubtedly one of the first to help kindle the flame of my educational curiosity. She was my first role model in science, and she has always challenged me to seek out a life in which I might use my talents to improve the lives of those around me. My father, J.R. Romero, has always kept me grounded in the knowledge that regardless of the highs and lows that life may bring, it goes on; this mentality has served me well in graduate school. Furthermore, as my first coach, he taught me the importance of teamwork to achieve a common goal – a lesson that will remain for rest of my life. Some might say it is rare for an older sibling to look up to their younger sibling, but I have become used to it. My sister, Alexis Romero, taught me

that with the right amount of determination, grit, and heart any challenge can be overcome. These three have always been simply a phone call away, and our conversations were an important and consistent relief from the stress and trials of graduate school.

I have two women left to thank for their influence on me professionally and personally to this point. The first is Dr. Brittany Baguley, whose guidance resulted in my attendance at Linfield College, my pursuit of summer research projects and REUs, and, ultimately, my choice to go to graduate school. She was instrumental in setting me on the path to discovering my passion for synthetic organic chemistry. On July 10th, 2016, the summer after my first year at Michigan, Brittany died from cardiac arrest resulting from scleroderma. She was 38 years old. While her infectious excitement for chemistry tragically left the world that day, her memory was a source of inspiration for me over the course of my graduate work and remains so to this day.

Finally, I must thank my partner – Kaitlin Kentala. She has been an unwavering pillar of support when it comes to my graduate work as well as my personal growth. Graduate school can be a significant strain on any relationship and adding the 242 miles between us as we have each pursued our PhDs has not made it any easier. Regardless, I have found a refuge in Kaitlin that I did not know could exist, and I am certain that I would not be in the position I am today without her by my side. Keith, Diane, Hope, Jake, and the extended Kentala family have also become an amazing support system to me, and I would be remiss if I did not thank them as well. The completion of this dissertation represents the closing of one chapter in my relationship with Kaitlin, and I have no doubt the chapters to follow will be bountiful with her steadfast love and support.

TABLE OF CONTENTS

DEDICATIONS	ii
ACKNOWLEDGEMENTS	iii
LIST OF FIGURES	xii
LIST OF TABLES	xix
LIST OF ABBREVIATIONS	xxi
ABSTRACT	xxv
CHAPTER 1: RADICALS AS KEY INTERMEDIATES IN NATURAL PRODUCT SYNTHESIS	1
1.1 Introduction	1
1.2 Radical stability and persistence	2
1.3 Stabilized radicals in natural product synthesis	4
1.3.1 α -Acyl radicals in natural product synthesis	6
1.3.2 Benzyl radicals in natural product synthesis	11
1.3.3 Tertiary radicals in natural product synthesis	17
1.4 The persistent radical effect	21
1.5 Persistent radicals in natural product synthesis	23

1.5.1	Natural product syntheses harnessing TEMPO for key steps	24
1.5.2	Persistent phenoxy radicals for the synthesis of resveratrol oligomers.....	28
1.6	Conclusions	31
CHAPTER 2: DEVELOPMENT OF AN ELECTROCHEMICAL DIMERIZATION OF PHENYLPROPANOID SCAFFOLDS AND THE EVALUATION OF THEIR ANTIOXIDANT ACTIVITIES.....		
		32
2.1	Introduction	32
2.2	Anodic electrochemistry in natural product synthesis	35
2.3	Electrochemical Dimerization of Phenylpropenoid Scaffolds	44
2.4	Synthesis and Biological Evaluation of Natural Product Analogs.....	53
2.5	Quinone Methide Dimers are Potent Radical Trapping Antioxidants	57
2.6	Conclusions	61
2.7	Experimental Procedures and Spectral Data	63
CHAPTER 3: TOTAL SYNTHESIS OF RESVERATROL TETRAMERS VITISIN A & VITISIN D: HARNESSING A PERSISTENT RADICAL EQUILIBRIUM FOR A HOMOLYTIC BOND MIGRATION		
		176
3.1	Introduction	176
3.2	Prior biomimetic efforts in resveratrol oligomer synthesis	182
3.3	Prior <i>de novo</i> efforts in resveratrol oligomer synthesis.....	189
3.3.1	Quinone methide cyclizations to access resveratrol dimers	190
3.3.2	Construction of 5-membered rings for resveratrol oligomer synthesis	197

3.3.3	Synthesis of higher-order resveratrol oligomers	206
3.4	Discovery of a C8–C8' to C3–C8' homolytic bond migration	212
3.5	Synthesis of vitisin A & D	218
3.6	Biological activity of resveratrol tetramers	240
3.7	Future directions – efforts toward resveratrol trimers.....	248
3.8	Conclusions	252
3.9	Experimental Procedures and Spectral Data	253
	References.....	335

LIST OF FIGURES

Figure 1.1. Gomberg's discovery of the triphenylmethyl radical (1.4).....	1
Figure 1.2. Selected kinetic and thermodynamic parameters of some C-centered radicals. ^a Lifetimes are based upon a radical concentration of 10 ⁻⁵ M. ^b Calculated using CBS-QB3. ⁹	3
Figure 1.3. Curran's synthesis of hirsutene (1.15) via a double radical cyclization.	4
Figure 1.4. Approaches by Procter and Reisman to pleuromutilin (1.34) via ketyl radical cyclizations to deliver intermediate α -acyl radicals.....	7
Figure 1.5. Chen's asymmetric synthesis of ageliferin (1.39) leveraging 5-exo-trig/6-endo- trig sequential cyclizations.	9
Figure 1.6. Inoue's synthesis of resiniferatoxin (1.48) featuring a 3-component radical coupling strategy.....	10
Figure 1.7. Boger's synthesis of vinblastine (1.52) leveraging the fragmentation of catharanthine (1.50).	12
Figure 1.8. The Stephenson group's approach to multiple alkaloids derived from catharanthine (1.50).	13
Figure 1.9. Approaches to pyrroloindolinyl radicals starting from bromopyrroloindoline precursors.....	15
Figure 1.10. Wang's synthesis of (\pm)-flustramide B (1.76)	17

Figure 1.11. Overman's tertiary radical coupling to set vicinal stereocenters for the synthesis of marine sponge terpenoids.	18
Figure 1.12. Reisman's synthesis of maecocrystal Z (1.99) featuring a ketyl radical cyclization.....	20
Figure 1.13. Synthesis of matrine analogs by Miranda and co-workers.....	21
Figure 1.14. The persistent radical effect imparts selectivity in radical-radical coupling reactions.....	23
Figure 1.15. Jahn's use of TEMPO to leverage the persistent radical effect for the synthesis of natural products.	25
Figure 1.16. Theodorakis' use of TEMPO for the synthesis of (-)-fusarisetin A (1.131)..	26
Figure 1.17. Knowles' use of TEMPO for the synthesis of pyrroloindoline natural products.	27
Figure 1.18. Stephenson's synthesis of quadrangularin A (1.152) and pallidol (1.153). ...	28
Figure 1.19. Discovery of dynamic equilibrium between quinone methide dimers and radical monomers.....	29
Figure 1.20. Synthesis of resveratrol tetramers from a persistent radical equilibrium.	30
Figure 2.1. Early examples of organic electrochemical reactions.	33
Figure 2.2. General schematic of electrochemical cells for organic reactions.	34
Figure 2.3. Corey's synthesis of (+)-pentacyclosqualene (2.15) enabled by a Kolbe electrolysis reaction.	36
Figure 2.4. Yamamura's synthesis of (±)-8,14-cedranoxide (2.24) featuring an electrochemical formal (5+2) cycloaddition.....	37

Figure 2.5. Tan and co-workers semisynthesis of aspidofractinine alkaloids using anodic oxidation under potentiostatic conditions.	38
Figure 2.6. Moeller's synthesis of (+)-linalool oxide (2.35) utilizing a polarity reversal approach enabled by anodic oxidation.	39
Figure 2.7. Moeller's synthesis of (-)-alliacol A (2.43) utilizing an electrochemical enol-furan coupling.	40
Figure 2.8. Trauner's synthesis of (-)-heptemerone B (2.56) and (-)-guanacastepene E (2.57) using an anodic furan-enol coupling.	42
Figure 2.9. Baran's synthesis of dixiamycin B (2.61) featuring an oxidative electrochemical N-N dimerization as the final step.	43
Figure 2.10. Anodic oxidation of 2.62 affords complex mixtures of products (2.63a-j)...	46
Figure 2.11. Watanabe's approach to furofuran lignans based on electrochemical dimerization of cinnamic acid derivatives.	47
Figure 2.12. Measurement of the oxidation potential of 1.151 by cyclic voltammetry.	48
Figure 2.13. Substrate scope for the C8–C8' electrochemical dimerization of 4-hydroxystilbenes.	51
Figure 2.14. Electrochemical C3–C8' dimerization occurs for multiple phenylpropenoid monomers.	52
Figure 2.15. Compounds evaluated for initial study of radical-trapping activity.	54
Figure 2.16. Preparation of ^t Bu ₄ -quadrangularin A analogs to evaluate RTA activity.	55
Figure 2.17. Representative data for the RTA activity of the A) resveratrol and B) quadrangularin A analogs.	56

Figure 2.18. A) Mechanism of Peroxyl Inhibition for hindered phenols. B) Mechanistic Hypothesis of Peroxyl Inhibition with QMDs.	58
Figure 2.19. Representative data for the RTA activity of quinone methide dimers.	58
Figure 2.20. Mechanistic possibilities for RTA activity of QMDs.	60
Figure 3.1. Stilbenoid compounds isolated by Langcake and Pryce while investigating pathogen defense response in <i>Vitis vinifera</i>	177
Figure 3.2. Resveratrol (2.78) arises from the phenylpropanoid pathway and undergoes oligomerization via phenoxy radical intermediates.	179
Figure 3.3. Dimerization of the monolignols proceeds through stereoselective coupling of phenoxy radical intermediates.	180
Figure 3.4. Dirigent protein hypothesis for resveratrol dimerization.	181
Figure 3.5. Hou's synthesis of quadrangularin A (1.152) featuring an arene protecting group strategy.	186
Figure 3.6. Li's approach to protected tetraaryl furan dimers and pallidol (1.153).	188
Figure 3.7. Snyder's synthesis of ampelopsin D (3.31) and ampelopsin F (3.15).	191
Figure 3.8. Snyder's synthesis of quadrangularin A (1.152) and pallidol (1.153).	192
Figure 3.9. Nicolaou's synthesis of hopeahainol A (3.50) and hopeanol (3.52).	193
Figure 3.10. Snyder's synthesis of hopeahainol A (3.50) and hopeanol (3.52).	195
Figure 3.11. Snyder's synthesis of hopeahainol D (3.65) and heimiol A (3.66).	196
Figure 3.12. Chen's synthesis of malibatol A (3.69) and shoreaphenol (3.70).	197
Figure 3.13. Various approaches to diarylindanones utilizing palladium catalysis.	198
Figure 3.14. Kim and Choi's approach to 2,3-diarylbenzofurans using C–H activation.	200
Figure 3.15. Elofsson's approach to ampelopsin B (3.85) and ϵ -viniferin (3.1).	202

Figure 3.16. Yao's synthesis of ampelopsin F (3.15).....	203
Figure 3.17. Shaw's asymmetric synthesis of (+)- δ -viniferin (3.5) using a C–H insertion strategy.....	204
Figure 3.18. Snyder's approach to DHB rings relying upon homologation and cyclization from aryl bromides.	205
Figure 3.19. Snyder's modular approach to resveratrol trimers and tetramers.	207
Figure 3.20. Snyder's synthesis of vaticanol A (3.119) harnessing three quinone methide cyclizations.	209
Figure 3.21. Snyder and Wright's synthesis of caraphenol A (3.131).	211
Figure 3.22. van't Hoff analysis of the 1.151/1.156 equilibrium reveals the C8–C8' bond dissociation enthalpy & suggests 1.156 is persistent at elevated temperatures.	212
Figure 3.23. Development of a radical DHB synthesis protocol.	213
Figure 3.24. Proposed mechanism for radical DHB synthesis.	214
Figure 3.25. van't Hoff analysis of the 2.69c/3.140 equilibrium shows irreversibility at elevated temperatures.	215
Figure 3.26. Homolysis of the C8–C8' bond of 2.69c at elevated temperature results in homolytic bond migration to the C3–C8' bond.	216
Figure 3.27. Computational investigations of the C8–C8' to C3–C8' homolytic bond migration reveal a clear C3-substituent effect on the free energy of the reaction.	217
Figure 3.28. Proposed biosynthesis of the C3–C8' resveratrol tetramers.....	219
Figure 3.29. Synthetic hypothesis to access vitisin tetramers via a homolytic bond migration strategy.....	220
Figure 3.30. Initial studies of the homolytic bond migration targeting the vitisins.....	221

Figure 3.31. Snyder's homologation-DHB synthesis approach to access 3.161.....	223
Figure 3.32. Retrosynthetic analysis for the synthesis of key DHB fragment 3.162.....	224
Figure 3.33. Synthesis of the key benzofuran following Kim and Choi's approach.	225
Figure 3.34. First generation synthesis of TBS-protected <i>trans</i> -DHB 3.175.	226
Figure 3.35. Second generation synthesis of key DHB fragment 3.175.....	227
Figure 3.36. Preparation of silyl protected ϵ -viniferin analog 3.189.....	229
Figure 3.37. Electrochemical dimerization of 3.189 affords key <i>bis</i> -quinone methide tetramer 3.190.....	230
Figure 3.38. Crossover experiment between 2.69c and 3.192 demonstrates that the persistent radicals escape the solvent cage during the homolytic bond migration.	231
Figure 3.39. Homolytic bond migration proceeds via relative configuration of 3.191. ..	231
Figure 3.40. Proposed mechanism for the conversion of 3.191 to 3.199 & 3.200.	232
Figure 3.41. Synthesis of vitisin A (3.146) from 3.191 via homolytic bond migration and acid-mediated cyclization.	233
Figure 3.42. Preparation of 3.206/3.207 from 3.191 via homolytic bond migration and desilylation sequence.	236
Figure 3.43. Synthesis of vitisin D (3.148) via Friedel-Crafts cyclizations from the vitisin B scaffold.....	239
Figure 3.44. Synthetic hypothesis for resveratrol trimers from radical DHB formation.	248
Figure 3.45. Diastereoconvergent cyclization affords synthesis of quinone methide intermediate 3.210.	249
Figure 3.46. Radical DHB synthesis with 3.210 leads to two resveratrol trimer cores. ..	250

Figure 3.47. Radical DHB synthesis offers an approach for the unified synthesis of higher-order resveratrol oligomers..... 251

LIST OF TABLES

Table 2.1. Products from anodic oxidation of 2.62 under varying conditions.	46
Table 2.2. Optimization of Electrochemical Dimerization Procedure.....	49
Table 2.3. Comparison of radical trapping antioxidant activity of resveratrol, pallidol, quadrangularin A and their synthetic precursors with α -tocopherol and BHT. ⁴⁴	54
Table 2.4. Comparison of inhibition rate constants (k_{inh}) and stoichiometry (n) for substituted QMDs, stilbenoid phenols, and quadrangularin A analogs during inhibited co-oxidations of 1-hexadecene (2.9 M) and PBD-BODIPY (10 μ M) initiated by AIBN (6 mM) at 37 °C, t BuOO t Bu (87 mM) at 70 °C, and dicumyl peroxide (1 mM) at 100 °C.	167
Table 2.5. Summary of enthalpies (ΔH , ΔH^\ddagger), free energies (ΔG , ΔG^\ddagger), and corresponding computed second order rate constants (k) for the addition of methyl peroxy radical to or hydrogen atom transfer (HAT) from a truncated analog of 2.69e in the gas phase at 37 °C.	168
Table 3.1. Biomimetic dimerizations accessing C3–C8' resveratrol oligomers.	183
Table 3.2. Biomimetic dimerization of resveratrol (2.78) to ϵ -viniferin (3.1).....	185
Table 3.3. Li's synthesis of pallidol (1.153) and ampelopsin F (3.15).	187
Table 3.4. Li's use of halides as C3-blocking groups for resveratrol dimerization.	189
Table 3.5. Unsuccessful attempts at debenylation of 3.150.....	222
Table 3.6. Optimization of the C–H arylation of 3.180 to access 3.181.....	228
Table 3.7. Investigation of C3/5 desilylation conditions to access vitisin B (3.10).	235

Table 3.8. Unsuccessful attempts at C5c-desilylation.	237
Table 3.9. Comparison of literature and observed ^1H NMR data for vitisin A (3.146)...	301
Table 3.10. Comparison of literature and observed ^{13}C NMR data for vitisin A (3.146).	302
Table 3.11. Comparison of literature and observed ^1H NMR data for vitisin D (3.148).	308
Table 3.12. Comparison of literature and observed ^{13}C NMR data for vitisin D (3.148).	309
Table 3.13. Enthalpies and free energies (in kcal/mol) for the dimerization of resveratrol radicals to dimers.	320
Table 3.14. Relative enthalpies and free energies (in kcal/mol) for R = tBu and TMS. .	320

LIST OF ABBREVIATIONS

9-BBN	9-borabicyclo(3.3.1)nonane
°C	degrees Celsius
δ	chemical shift in parts per million
μL	microliters
μM	micromolar
A	amps
A β	amyloid- β
Abs	absorbance
Ac	acetyl
AChE	acetylcholinesterase
AIBN	azobisisobutyronitrile
aq.	aqueous
Ar	aryl
BASF	Badische Anilin und Soda Fabrik
BDE	bond dissociation enthalpy
BHT	2,6-di- <i>tert</i> -butyl-4-hydroxytoluene
Bn	benzyl
Boc	<i>tert</i> -butyloxycarbonyl
BOM	benzyloxymethyl
Bu	<i>n</i> -butyl
bpy	2,2'-bipyridine
BRSM	yield based on recovered starting material
Cbz	carboxybenzyl
CE	counter electrode
cm	centimeters
Cp	cyclopentadienyl
d	doublet
DBU	1,8-diazabicyclo[5.4.0]undec-7-ene
DCC	dicyclohexylcarbodiimide
DCE	dichloroethane
DCM	dichloromethane
dd	doublet of doublets
DDQ	2,3-dichloro-5,6-dicyano-1,4-benzoquinone
dF(CF ₃)ppy	2-(2,4-difluorophenyl)-5-(trifluoromethyl)pyridine
dCF ₃ ,Me-ppy	2-(2,4-di(trifluoromethyl)phenyl)-5-methylpyridine
DHB	dihydrobenzofuran
(DHQ)-PHAL	Hydroquinine 1,4-phthalazinediyl diether
DIBAL-H	diisobutylaluminum hydride

(+)-DIP-Cl	(+)- <i>B</i> -chlorodiisopinocampheylborane
DIPEA	diisopropyl ethyl amine
DMAP	4-dimethylaminopyridine
DMDO	dimethyldioxirane
DMF	dimethylformamide
DMP	Dess-Martin periodinane
DMS	dimethyl sulfide
DMSO	dimethyl sulfoxide
DPPH	1,1-diphenyl-2-picrylhydrazyl radical
dr	diastereomeric ratio
dtbbpy	4,4'-di- <i>tert</i> -butyl-2,2'-bipyridine
EC ₅₀	half maximal effective concentration
EDG	electron-donating group
ee	enantiomeric excess
<i>E_p</i>	peak half-cell electrochemical potential
EPR	electron paramagnetic resonance
equiv	molar equivalents
ESI	electrospray ionization
Et	ethyl
EtOH	ethanol
EWG	electron-withdrawing group
EY	Eosin Y
F	faraday
FMO	frontier molecular orbital
FTIR	Fourier transform infrared spectroscopy
g	grams
h	hours
H8-TRIP BINOL phosphate	<i>n</i> -tetrabutylammonium (2 <i>r</i> ,6 <i>s</i>)-2,6-bis(2,4,6-triisopropylphenyl)-8,9,10,11,12,13,14,15-octahydrodiantho[2,1- <i>d</i> :1',2'- <i>f</i>][1,3,2]dioxaphosphepin-4-olate 4-oxide
H ₂ B-PMHC	BODIPY-2,2,5,7,8-pentamethyl-6-hydroxy-chromane
HAT	hydrogen atom transfer
HCV	hepatitis C virus
HMDS	hexamethyldisilazide
HMPA	hexamethylphosphoramide
HPLC	high performance liquid chromatography
HRMS	high resolution mass spectrometry
HRP	horseradish peroxidase
HWE	Horner-Wadsworth-Emmons
Hz	Hertz
IBX	2-iodoxybenzoic acid
IC ₅₀	half maximal inhibitory concentration
^{<i>i</i>} Pr	isopropyl
IR	infrared
<i>J</i>	coupling constant in units of Hertz
<i>k_r</i>	radical recombination rate constant

L	liters
<i>L</i> -Men	<i>L</i> -menthol
LED	light emitting diode
LFP	laser flash photolysis
m	multiplet
M	molar concentration
mA	milliamps
<i>m</i> CPBA	<i>meta</i> -chloroperoxybenzoic acid
Me	methyl
MeCN	acetonitrile
MeOH	methanol
mg	milligrams
MHz	megahertz
min	minutes
mm	millimeters
mmol	millimoles
MOM	methyloxymethyl
mol	moles
MsCl	methanesulfonyl chloride
MsOH	methanesulfonic acid
NBS	<i>N</i> -bromosuccinimide
NF- κ B	nuclear factor kappa-light-chain-enhancer of activated B cells
nM	nanomolar
nm	nanometers
NMR	nuclear magnetic resonance
NPhth	phthalimide
[O]	oxidant
OTf	triflate
<i>p</i> -TsOH	<i>para</i> -toluenesulfonic acid
PCET	proton coupled electron transfer
PG	protecting group
Piv	pivalate
PMB	<i>para</i> -methoxybenzyl protecting group
ppm	parts per million
ppy	2-phenylpyridine
PRE	persistent radical effect
q	quartet
QMD	quinone methide dimer
RE	reference electrode
ROS	reactive oxygen species
RSE	radical stabilization energy
rt	room temperature
RTA	radical trapping antioxidant
RVC	reticulated vitreous carbon
s	singlet

S-(+)-Monophos	(S)-(+)-(3,5-Dioxa-4-phosphacyclohepta[2,1-a;3,4-a']dinaphthalen-4-yl)dimethylamine
SAR	structure activity relationship
SOMO	singly occupied molecular orbital
t	triplet
TBAF	tetra- <i>n</i> -butyl ammonium fluoride
TBS	<i>tert</i> -butyl-dimethylsilyl
TBDPS	<i>tert</i> -butyl-diphenylsilyl
^t Bu	<i>tert</i> -butyl
^t BuOH	<i>tert</i> -butanol
TEMPO	2,2,6,6-tetramethylpiperidin-1-oxyl
TFA	trifluoroacetic acid
THF	tetrahydrofuran
TIPS	triisopropylsilyl
TIPS-EBX	1-((triisopropylsilyl)ethynyl)-1λ ³ -benzo[d][1,2]iodaoxol-3(1H)-one
TLC	thin layer chromatography
TMP	2,2,6,6-tetramethylpiperidinyl
TMS	trimethylsilyl
TsCl	toluenesulfonyl chloride
TTMSS	tris(trimethylsilyl)silane
UPLC	ultra performance liquid chromatography
UV	ultraviolet
V	volts
WE	working electrode

ABSTRACT

Since their discovery 120 years ago, carbon-centered free radicals have captivated the attention of organic chemists worldwide. As the thermodynamic and kinetic properties of radical reactions have been studied, it has been recognized that open-shell intermediates offer complementary and orthogonal modes of reactivity when compared to traditional polar mechanisms. Persistent radicals, which by definition have higher kinetic barriers for reactivity, serve to increase the selectivity with which radical reactions occur through the persistent radical effect – a phenomenon that has recently begun to be leveraged for synthesis. The work described herein seeks to advance the field of radical chemistry in the context of employing persistent radicals for synthesis through synergistic combination of physical organic chemistry and chemical synthesis. In particular, these efforts target chemical synthesis of oligomers from the resveratrol class of natural products – an extensive and structurally diverse set of polyphenols to which a broad range of biological activities has been ascribed – with the goal of better understanding the mechanism(s) by which these compounds are biologically active. Chapter 1 summarizes the state of the field of radical chemistry in the context of natural product synthesis, concluding with a discussion of how persistent radicals have begun to be employed. The inspiration for the synthetic approach described in the subsequent chapters derives from the final example in which, during the course of a natural product total synthesis campaign, a key equilibrium between persistent phenoxy radicals and their dimeric adducts was discovered and

leveraged to access C8–C8' resveratrol dimers and tetramers. Chapter 2 details how a mild, sustainable, and scalable approach for the generation of these persistent radicals was developed by relying upon electrochemical oxidation. This new method enabled the synthesis of a set of natural product analogs for initial structure-activity relationship (SAR) analysis of the compounds as radical trapping antioxidants (RTAs). Surprisingly, it was determined during the course of this study that the persistent radicals are more potent RTAs than any of the polyphenols evaluated, calling into question the exact cellular role these compounds fulfill in nature. Finally, Chapter 3 describes how thermodynamic study of the equilibrium between the persistent phenoxy radicals and the corresponding C8–C8' dimers resulted in the discovery of a C8–C8' to C3–C8' homolytic bond migration. This reaction was subsequently leveraged as the key step for the synthesis of the resveratrol tetramers vitisin A and vitisin D – two members of a subset of resveratrol oligomers to which perhaps the most interesting biological activity has been attributed. This chapter concludes with a discussion of where this project is headed in terms of the use of these persistent radicals for intermolecular C8–C10' bond-forming reactions to access resveratrol trimers. In total, the strategy developed herein for resveratrol oligomer synthesis mimics the proposed manner in which Nature constructs these complex molecules, offering a direct route for the evaluation of their pharmacological potential.

CHAPTER 1: Radicals as Key Intermediates in Natural Product Synthesis

*Portions of this chapter have been published in:
Romero, K. J.; Galliher, M. S.; Pratt, D. A.; Stephenson, C. R. J. *Chem. Soc. Rev.*
2018, *47*, 7851–7866.

1.1 Introduction

In 1900, here at the University of Michigan, Professor Moses Gomberg published the remarkable finding that trivalent carbon can exist. While attempting to prepare the sterically encumbered compound hexaphenylethane (**1.2**) from triphenylmethyl chloride (**1.1**) using a Wurtz coupling, Prof. Gomberg instead formed peroxide **1.3** (Figure 1.1). Proposing that **1.3** arose due to incorporation of atmospheric O₂ into the hydrocarbon during its formation, he carried out the reaction under an atmosphere of CO₂, where he obtained not **1.2**, but an unidentifiable reactive unsaturated compound he suggested to be the triphenylmethyl radical **1.4**.¹ This seminal report was met with heavy skepticism, as it was the first example of trivalent carbon; however, after significant debate in the literature,² numerous experiments pointed to the same conclusion – carbon-centered radicals exist. Later, the dynamic equilibrium between **1.4** and the dimer **1.5** – which comprised 99.99% of the material isolated by Gomberg – was demonstrated.³ Though Gomberg concluded his ground-breaking publication by stating that he wished to “reserve the field” for himself, the

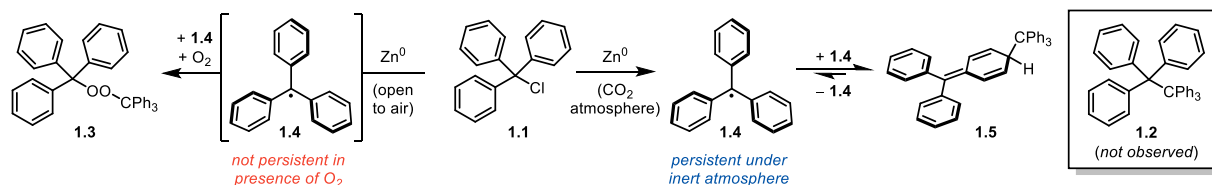


Figure 1.1. Gomberg's discovery of the triphenylmethyl radical (**1.4**).

intrigue surrounding trivalent carbon spawned the field of radical chemistry. Starting as a fundamental curiosity, radicals have become valuable intermediates in the synthesis of small and large molecules in both academic and industrial settings around the world.

1.2 Radical stability and persistence

The triphenylmethyl radical (**1.4**) provides a good starting point to introduce the concepts of radical stability and radical persistence, which were first defined by Griller and Ingold.⁴ The triphenylmethyl radical is relatively stable; the C-H bond strength in triphenylmethane (81 kcal/mol) is significantly lower than that in methane (105 kcal/mol), reflecting the stabilizing interactions between the unpaired electron on the central carbon atom and the π orbitals of the three attached phenyl rings which serve to delocalize it.^{5,6} The triphenylmethyl radical can also be persistent; in the absence of O₂, it makes up roughly 0.01% of a sample of **1.5**. However, in the presence of O₂, the triphenylmethyl radical is not persistent. Since persistence is a kinetic characteristic, it depends on reaction conditions. Stability, which is a thermodynamic property, is inherent to the electronic structure of the radical.

Griller and Ingold proposed that the adjective persistent be used “to describe a radical that has a lifetime significantly greater than methyl under the same conditions.”⁴ In contrast, methyl and other short-lived radicals are described as transient. These definitions are based upon the kinetics with which radicals decay when generated in dilute solutions, which are characterized by the recombination rate constant k_r (this despite the fact that radical recombination is often competitive with disproportionation; moreover, it should be acknowledged that the radicals are rarely generated from their corresponding dimers, so recombination is not actually the ideal term to describe this process given such poor

radical	k_r ($M^{-1}s^{-1}$)	$t_{1/2}$ (s) ^a	RSE (kcal/mol)
1.6	1.1×10^{10}	9.1×10^{-6}	0.0
1.7	8.5×10^9	1.2×10^{-5}	17
1.8	2.3×10^9	4.3×10^{-5}	15
1.9	8.1×10^9	1.2×10^{-5}	9
1.10	2.5×10^8	4.0×10^{-4}	17 ^b
1.11	2.0×10^2	5.0×10^2	9 ^b
1.12	n/a	days	11 ^b

The figure shows chemical structures for radicals 1.6 through 1.12. 1.6 is a methyl radical, 1.7 is an allyl radical, 1.8 is a phenyl radical, 1.9 is a 2-methylpropan-2-yl radical, 1.10 is a 2,4,6-tri-tert-butylphenyl radical, 1.11 is a 2,2,6,6-tetramethylpiperidin-1-yl radical, and 1.12 is a 2,2,6,6-tetramethylpiperidin-1-yl radical with a phenyl group. To the right, a reaction scheme shows two molecules of a radical R• reacting with a rate constant k_r to form either a dimer R-CR(R)-CR(R)-R or a molecule R-CR(R)-R and an alkene R-CH=CH-R.

Figure 1.2. Selected kinetic and thermodynamic parameters of some C-centered radicals. ^aLifetimes are based upon a radical concentration of 10^{-5} M. ^bCalculated using CBS-QB3.⁷

applicability to most radicals). Illustrative kinetic parameters of selected carbon-centered radicals are given in Figure 1.2.

Griller and Ingold also suggested “that ‘stabilized’ should be used to describe a carbon-centered radical, R^\bullet , when the R–H bond strength is less than the appropriate C–H bond strength in an alkane”.⁴ The difference of the C–H BDE of a given hydrocarbon from methane is often used as a measure of the so-called ‘radical stabilization energy (RSE)’ afforded by the substituent(s) attached to the central carbon atom, so these are also included in Figure 1.2.⁷ Although radical stability and persistence are often used interchangeably, it is evident from the data collected in Figure 1.2 that they should not. For example, while introduction of a vinyl or phenyl substituent on methyl significantly increases stability, the solution lifetime is essentially unchanged.^{8,9} However, introduction of substituents that hinder dimerization and/or disproportionation of the radicals increase persistence – even if they do not increase the stability of the radical.⁴ In fact, substitutions that increase persistence often decrease the stability of the radical by localizing the electron spin (e.g. **1.12**).^{7,10} Another consideration in evaluating the persistence of a radical (which is not included in Ingold and Griller’s definition) is the reversibility of the radical (re)combination reaction. A radical with a relatively short lifetime in solution can be highly persistent if the

material (**1.14**), generating key primary radical **1.20** to initiate the tandem cyclization events. Sequential *5-exo-trig/5-exo-dig* cyclization reactions thus proceeded to afford the desired tricyclic scaffold, and the sequence is terminated by hydrogen atom transfer from tributyl tin hydride to yield the natural product (**1.15**). In the years since this report, such an approach to radical generation and reactivity has become widespread due to the predictability with which these radical reactions occur.

With the foregoing in mind, the following sections will highlight examples from natural product synthesis in which both stabilized and persistent radicals feature as intermediates in a key step. In terms of stabilized carbon-centered radicals, the sections are organized by the three most often encountered species – α -acyl, benzyl, and tertiary radicals. Representative examples will be presented in each section in which the given radical is featured, and the stereoelectronic factors contributing to the stability of these transient species are described at the beginning of each section. Curran's synthesis of hirsutene (**1.15**, *vide supra*) demonstrates how the selected examples are presented, with emphasis placed upon the proposed mechanism of the key radical reaction. As the knowledge regarding radical reactivity and selectivity has increased, intermolecular reactions have become feasible and are now a mainstay in the field of complex molecule synthesis, and as such, many of the examples will underscore this advancement in the field. Furthermore, as understanding surrounding persistent radicals has been adopted in the synthetic organic community, their intentional use for natural product synthesis has flourished. Examples wherein the persistent radical TEMPO ((2,2,6,6-tetramethylpiperidin-1-yl)oxidanyl) has been utilized to establish persistent radical equilibria with transient radicals for several natural product syntheses will be presented. Finally, this chapter will conclude with a

discussion of the work by my colleagues Dr. Bryan Matsuura and Dr. Mitch Keylor that directly inspired and laid the foundation for the research described in Chapters 2 and 3 – the use of persistent phenoxyl radicals for the synthesis and biological evaluation of oligomeric natural products derived from resveratrol. For additional reading regarding the use of radicals for organic small molecule synthesis, excellent contributions from Fischer, Curran, and Studer should be consulted.^{12–15}

1.3.1 α -Acyl radicals in natural product synthesis

Conjugated radicals are versatile intermediates in natural product total syntheses, as additions to activated alkenes are a common and particularly convenient means to access polycyclic systems, as exemplified in Curran's hirsutene synthesis. The stability of conjugated radicals is derived directly from delocalization of the unpaired electron across three atoms. In terms of frontier molecular orbitals (FMOs), the singly occupied molecular orbital (SOMO) of the radical mixes with the adjacent π -orbitals to form a new set of molecular orbitals across the three atoms. For example, the α -C–H bond for acetaldehyde has a BDE of 94 kcal/mol, whereas the C–H BDE for ethane is reported to be 101 kcal/mol – giving a RSE of 7 kcal/mol.⁶ This section describes the utility of these stabilized radicals for natural product synthesis.

In 2009, Procter and co-workers reported a strategy for the synthesis of the natural product pleuromutilin (**1.34**) with the goal of providing a versatile platform for analog synthesis (Figure 1.4).^{16,17} Derivatives of this natural product have been shown to inhibit bacterial protein synthesis through interactions with the 50S ribosomal subunit; therefore, it was anticipated that this scaffold could be utilized for the development of new antibacterial agents. The authors envisioned that a SmI₂-mediated cyclization cascade from

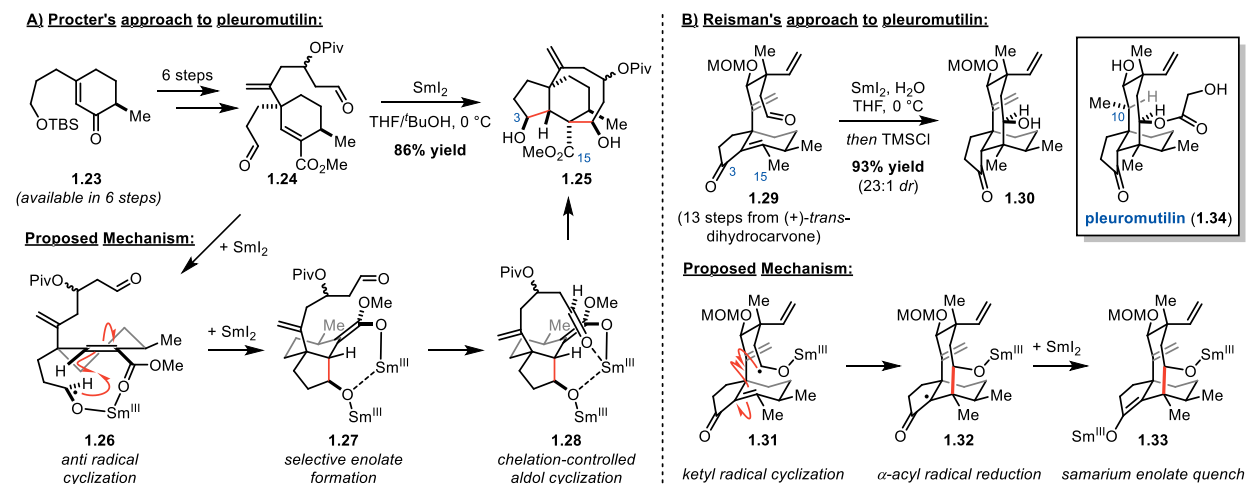
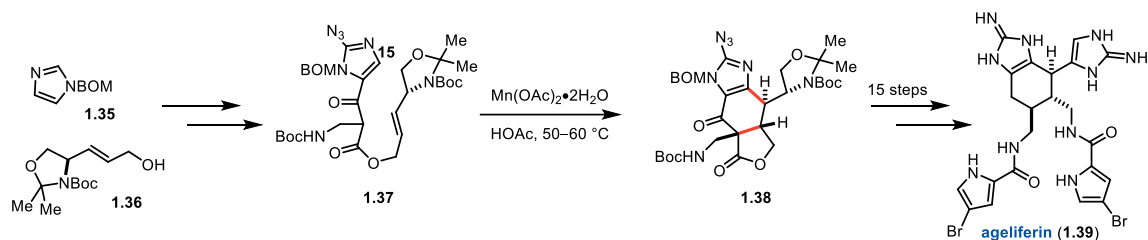


Figure 1.4. Approaches by Procter and Reisman to pleuromutilin (1.34) via ketyl radical cyclizations to deliver intermediate α -acyl radicals.

dialdehyde **1.24** would provide rapid access to the 5/6/8 fused tricyclic core of the target compound. Dialdehyde **1.24** was prepared in six steps from unsaturated ketone **1.23** to set up the key transformation. Treatment of dialdehyde **1.24** with SmI_2 in a 5:1 mixture of THF/ BuOH at $0\text{ }^\circ\text{C}$ afforded tricycle **1.25** in 86% yield, selectively forming four contiguous stereocenters in a single step. The authors suggest that the aldehyde proximal to the ester is first to react, generating ketyl radical **1.26** upon reaction with SmI_2 . The Sm-coordinated ketyl radical **1.26** is thus poised to undergo a 5-*exo-trig* cyclization onto the unsaturated ester, resulting in a stabilized α -keto radical. While the stabilization of such an intermediate radical presumably imparts some degree of thermodynamic driving force, the chelation between the ester and ketyl radical (**1.26**) is proposed to be the critical component for achieving the selective cyclization. Procter and co-workers suggest that this stabilized radical is further reduced by a second equivalent of SmI_2 to access enolate **1.27**, and subsequent coordination by samarium to the distal aldehyde affords a selective aldol cyclization to finish the cascade. This dialdehyde cyclization cascade provides rapid access to tricycle **1.25**, realizing the desired scaffold to enable the preparation of pleuromutilin

(**1.34**) and natural product analogs. Reisman and co-workers also employed a SmI₂-mediated cyclization in their 2018 synthesis of **1.34**. Starting from (+)-*trans*-dihydrocarvone, they prepared aldehyde **1.29** in 13 steps, featuring an elegant oxidative transposition to furnish the ketone at C3. Subsequent treatment of **1.29** with SmI₂ and H₂O at 0 °C delivers ketyl radical **1.31**, which cyclizes into the α,β -unsaturated ketone in an 8-*exo-trig* reaction to deliver α -acyl radical **1.32**. An additional equivalent of SmI₂ reduces **1.32** to form the samarium enolate **1.33**. Remarkably, the authors report that this entire process converting **1.29** to **1.33** occurs in just 5 minutes, at which point chlorotrimethylsilane (TMSCl) is added to quench **1.33**. The reaction proceeds in 93% yield and 23:1 *dr* to deliver the carbocyclic core of the natural product. A key consideration when comparing the approaches by Procter and Reisman is the oxidation states at C3 and C15 at the end of each respective cyclization. In Procter's synthesis, C3 is at the alcohol oxidation state, while C15 is an ester. Both are in the incorrect oxidation state relative to **1.34**, and Procter and co-workers required numerous redox manipulations to complete their synthesis. Reisman and co-workers clearly learned from Procter's approach and developed a strikingly similar cyclization; however, their cyclization product (**1.30**) exhibits the correct oxidation state at both C3 and C15, thus significantly fewer manipulations were subsequently required to achieve the natural product. In fact, only four additional steps were required to access **1.34**, including a clever transannular [1,5]-hydrogen atom transfer to reduce the olefin at C10 to the corresponding methyl group in pleuromutilin.

In 2011, Chen and co-workers reported the asymmetric synthesis of the dimeric natural product ageliferin (**1.39**, Figure 1.5).¹⁸ This pyrrole–imidazole alkaloid is thought to arise in nature from a [4+2] dimerization of hymenidin. Multiple *de novo* syntheses have been



Proposed Mechanism:

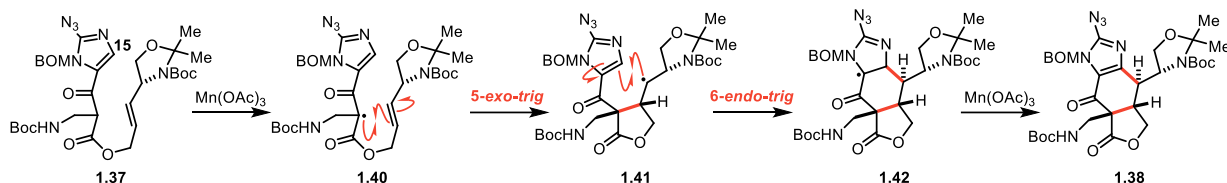


Figure 1.5. Chen's asymmetric synthesis of ageliferin (1.39) leveraging 5-*exo*-trig/6-*endo*-trig sequential cyclizations.

reported; however, Chen and co-workers sought to mimic the proposed biosynthetic pathway via a radical addition sequence to form the key 6-membered ring. Their critical β -keto ester intermediate (**1.37**) was treated with $\text{Mn}(\text{OAc})_3$, which is well known to selectively oxidize β -keto esters to form α -keto radicals.¹⁹ A 5-*exo*-trig cyclization of the resultant radical onto the pendant alkene yields a 5-membered lactone and a transient secondary radical (**1.41**). A subsequent 6-*endo*-trig cyclization of intermediate **1.41** produces α -keto radical **1.42**, which is further oxidized to the desired product (**1.38**). Interestingly, in a prior study, Chen and Tan investigated this transformation and found that the identity of the C15 substituent had a major influence on the regiochemical outcome of the second cyclization.²⁰ When an electron withdrawing group is present at C15, the double 5-*exo*-trig cyclization yields spirocyclic products; however, when the C15 substituent is hydrogen, then the 5-*exo*/6-*endo* product is formed.

In 2017, Inoue and co-workers completed the total synthesis of resiniferatoxin (**1.48**), a daphnane diterpenoid that is a potent ion channel protein agonist (Figure 1.6).²¹ This natural product presents a unique synthetic challenge, as it features a *trans*-fused 5/7/6-tricyclic

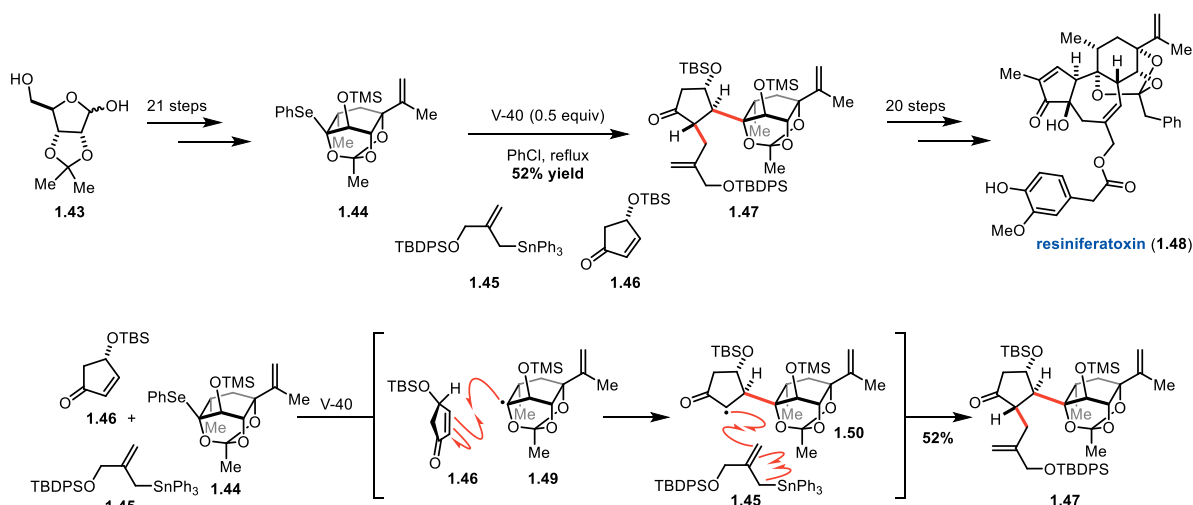


Figure 1.6. Inoue's synthesis of resiniferatoxin (1.48) featuring a 3-component radical coupling strategy.

core as well as a cage-like orthoester component. The authors sought to develop a radical coupling strategy for the synthesis of this densely oxygenated natural product, recognizing that radical reactivity can be highly tolerant of polar functional groups. In particular, they proposed that a three-component radical coupling could bring together the A- and C-rings in a diastereoselective manner while also forming the necessary side chain for a subsequent cyclization to access the 7-membered B-ring. Following successful model studies, they arrived at the three components needed for this critical transformation in 20 steps. Subjecting these materials to the optimized reaction conditions afforded the desired product in 52% yield. The radical coupling reaction is initiated by V-40 – a variant of AIBN (**1.16**) wherein the geminal dimethyl-bearing carbons have been replaced with cyclohexyl groups. The authors propose that radical substitution on the phenylselenide yields tertiary radical **1.49** which adds to unsaturated ketone (**1.46**) with the TBS ether controlling the facial selectivity of the addition. This first reaction forms the stabilized α -keto radical **1.50**, which subsequently adds to the allyl stannane **1.45**, liberating the persistent triphenyl tin radical ($\text{Ph}_3\text{Sn}^\bullet$) which can carry the chain. This three-component coupling occurs with excellent

control to furnish the *trans*-configuration for the cyclic ketone that is ultimately reflected in the natural product. The authors suggest that the success of this reaction relies upon the electronic match of each coupling component. Radical **1.49** is nucleophilic due to donation from the adjacent oxygen atom; therefore, it reacts selectively with the electrophilic unsaturated ketone (**1.46**). Electron-deficient radical **1.50** then adds to the electron rich allyl stannane (**1.45**) to afford the desired product. Upon successful execution of the three-component coupling strategy, Inoue and co-workers close the B-ring and append the appropriate ester side chain to arrive at the natural product following an additional 20 steps.

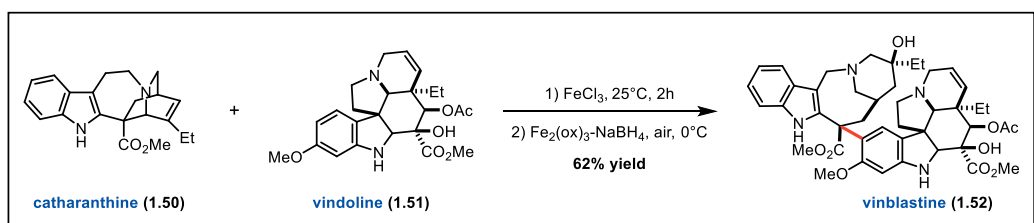
1.3.2 Benzyl radicals in natural product synthesis

Benzyl radical intermediates are widely utilized in natural product synthesis due to their relative stability. Benzyl radical stability is attributed to the delocalization of electron density through the neighboring arenyl π -orbitals. Namely, the overlap between the aryl π -orbitals and the singly occupied molecular orbital (SOMO) nominally localized to the benzylic carbon atom enables radical delocalization; this is similar to the α -keto radical stability discussed in the previous section. The lower bond dissociation enthalpy of the C–H bond in toluene (90 kcal/mol versus 105 kcal/mol of the C–H bond in methane) arises from the stability of the benzyl radical.²² The following section will describe how radicals adjacent to aromatic rings have been utilized in recent natural product syntheses.

Catharanthine (**1.50**) is a polycyclic natural product that has been utilized as a starting point for several semisynthetic efforts to access a variety of structurally related alkaloid natural products. It contains an indole and an isoquinuclidine ring, and these fragments are connected by the seven-membered C-ring. Catharanthine is easily accessed from cell cultures in synthetically useful quantities; thus, its abundance and resulting commercial

availability has fuelled multiple semisynthetic efforts. The utility of **1.50** as a synthetic precursor for related alkaloids is enabled by the ease with which the C16-C21 bond undergoes oxidative fragmentation to the benzylic radical intermediate **1.54** (Figure 1.7).

The Boger group published a remarkable total synthesis of vinblastine (**1.52**) in 2008 in which the key step involved the coupling of catharanthine (**1.50**) and vindoline (**1.51**) via the radical-induced fragmentation of **1.50** (Figure 1.7).²³ Vinblastine (**1.52**) is a potent inhibitor of microtubule formation and mitosis and is a key anticancer drug target. In Boger's synthesis of vinblastine, catharanthine (**1.50**) is treated with FeCl₃ to form the amine radical cation **1.53**. This intermediate presumably undergoes rapid C16–C21 fragmentation, affording benzyl radical **1.54**. Subsequent oxidation of **1.54** gives intermediate **1.55**, which acts as the electrophile in a Friedel-Crafts coupling reaction with vindoline (**1.51**) to give **1.56**. This fragmentation and coupling sequence was originally developed by Kutney and co-workers in 1988 to access 3'-4'-anhydrovinblastine (**1.57**),



Proposed Mechanism:

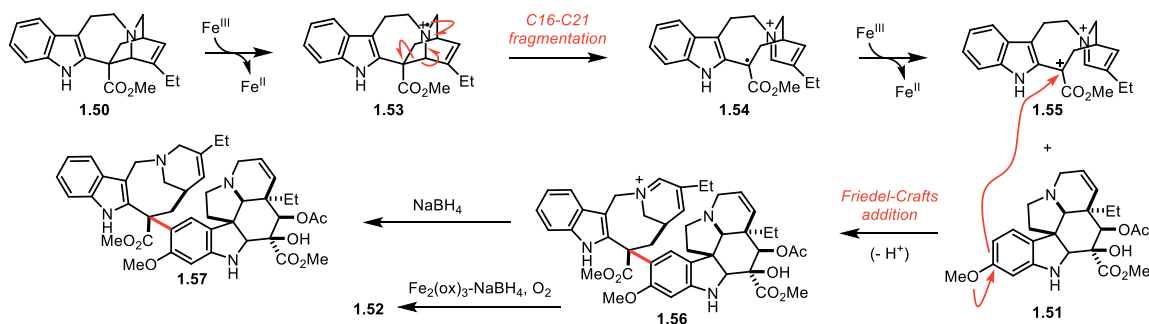


Figure 1.7. Boger's synthesis of vinblastine (1.52) leveraging the fragmentation of catharanthine (1.50).

which was obtained by reduction of **1.56** with NaBH₄.²⁴ Boger and co-workers instead leveraged conditions (Fe₂(ox)₃-NaBH₄/O₂) that enabled reduction of the iminium and stereoselective oxidation of the C15'–C20' double bond in a single pot. This decisive step affords the C20' tertiary alcohol of vinblastine (**1.52**) in 43% yield under optimized conditions.

While Boger demonstrated that alkaloid natural products can be accessed through the FeCl₃-mediated single electron oxidation and fragmentation of catharanthine, my colleague, Dr. Joel Beatty, was able to show this can also be accomplished with photoredox catalysis. In 2014, he achieved the syntheses of (-)-pseudotabersonine (**1.60**), (+)-coronaridine (**1.61**), and (-)-pseudovincadifformine (**1.62**) (Figure 1.8).²⁵ The key step to the syntheses of **1.60-1.62** involved the formation of a common intermediate (**1.59**) by the photoredox-mediated fragmentation of catharanthine (**1.50**). Excitation of the photocatalyst and reductive quench with **1.50** yields amine radical cation **1.53**.

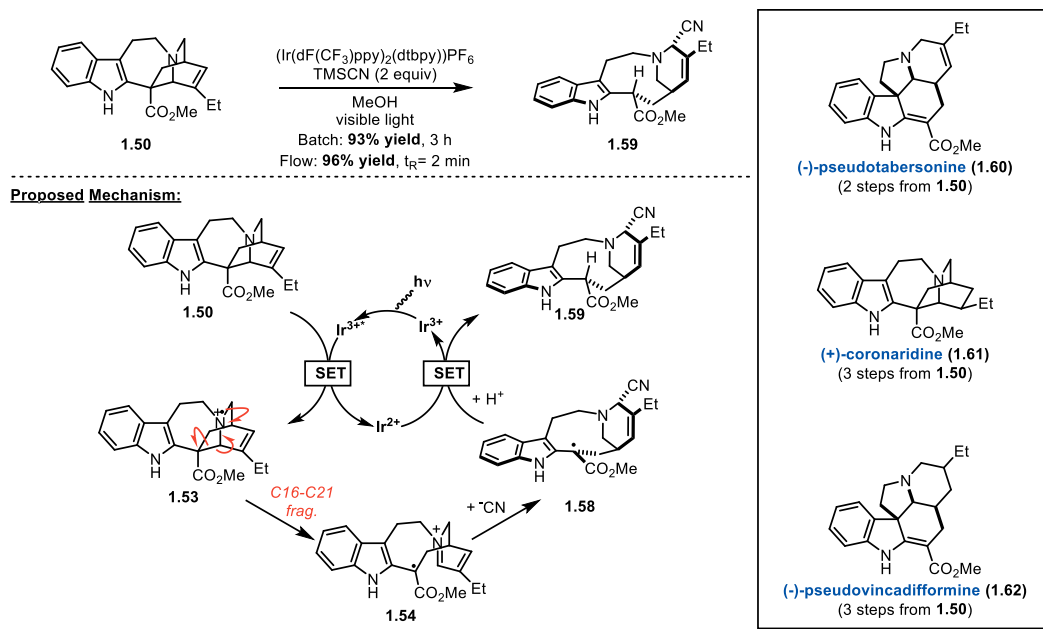


Figure 1.8. The Stephenson group's approach to multiple alkaloids derived from catharanthine (**1.50**).

Fragmentation of the C16–C21 bond occurs in the same way as discussed in Boger's synthesis of vinblastine, generating the stabilized benzyl radical **1.54**. This stabilized radical survives the addition of cyanide to the iminium group, forming **1.58**, before reduction by the photocatalyst and subsequent protonation gives **1.59**. This transformation was achieved via batch reaction (93% yield) as well as by utilizing continuous flow processing (96% yield), demonstrating the versatility of photoredox catalysis for natural product synthesis. From **1.59**, the desired natural products (**1.60-1.62**) were synthesized in 1 or 2 additional steps.

Pyrroloindoline-containing alkaloids comprise an important family of natural products which are endowed with a wide array of biological activities. Due to their pharmaceutical potential, numerous synthetic efforts have been made to access and evaluate these molecules. A common approach for their synthesis is the utilization of benzyl-like pyrroloindolinyl radicals (*e.g.* **1.64** and **1.70**, Figure 1.9) to incorporate this heterocyclic motif. Two of the most common ways to access pyrroloindolinyl radical intermediates involve the use of the corresponding bromopyrroloindoline precursor as well as tryptamine/tryptamide precursors.

A bromopyrroloindoline was first used as a precursor to a pyrroloindolinyl radical by the Crich group in 1994 (Figure 1.9A).²⁶ Their total synthesis of (+)-*ent*-debromoflustramine B (**1.66**) involved a radical allylation of bromopyrroloindoline **1.63** using allyl tributyltin. Radical initiation relied on thermolysis of AIBN and subsequent reaction with an allyl stannane to liberate the tributyl tin radical. As seen in prior examples, dehalogenation of **1.63** can then occur to give pyrroloindoline radical **1.64**. Allylation of the radical (**1.64**) by a second equivalent of the allyl stannane produced the allyl adduct

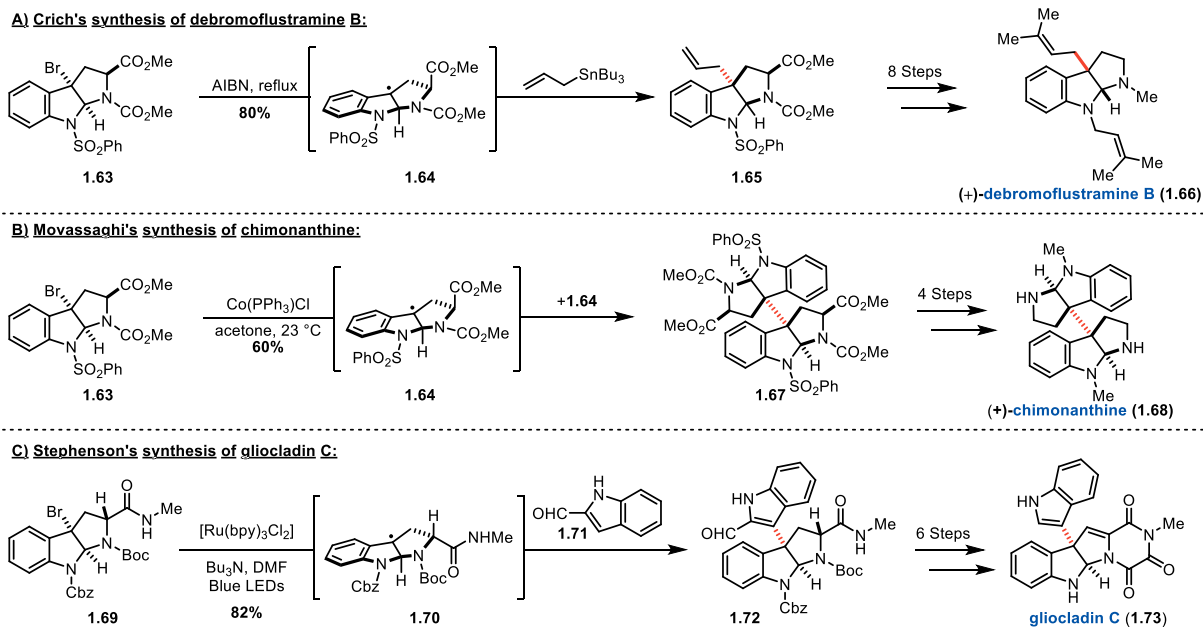


Figure 1.9. Approaches to pyrroloindolinyl radicals starting from bromopyrroloindoline precursors.

1.65 in 80% yield and provided a key intermediate from which **1.66** could be produced in 8 additional steps.

The Movassaghi group leveraged this approach in the synthesis of (+)-chimonanthine (**86**), (+)-folicanthine, and (-)-calycanthine in 2007 (Figure 1.9B).²⁷ Generation of the radical **1.64** from **1.63** proved ineffective under most photolytic, thermolytic, and reductive conditions. The authors believed that a rapid radical activation was needed to achieve the subsequent second-order dimerization to obtain **1.67**; therefore, they turned to a cobalt-mediated halide activation strategy. It was found that $\text{CoCl}(\text{PPh}_3)_3$ met these requirements and produced **1.67** in good yield (60% yield) and excellent selectivity. The authors propose two possible mechanisms for this transformation. The first involves bromide abstraction by the cobalt complex, followed by homodimerization of **1.64**. They also suggest that formal oxidative insertion of Co^{I} into the C–Br bond could be operative, and in this case homodimerization would precede a fragmentation-recombination mechanism that replaces

the C–Co bonds with C–C bonds to furnish the desired product. Regardless of the mechanism, this reaction occurs by homodimerization of the enantiopure pyrroloindoline monomers in a diastereoselective fashion, providing the desired dimer in 99% *ee* on multigram scale. Photoredox chemistry has also been utilized to promote radical formation from bromopyrroloindolines (Figure 1.9C). In 2011, my predecessors in the Stephenson group demonstrated the capacity of photoredox catalysis to realize the formation of radical **1.70** and applied it to the synthesis of gliocladin C (**1.73**).²⁸ A Ru^{II}-based photocatalyst was used to successfully generate this pyrroloindoline radical in a halide reduction mechanism. Pyrroloindoline radical **1.70** was then coupled to C3 of indole-2-carboxaldehyde **1.71** to give the corresponding captodatively-stabilized radical. Subsequent oxidation and rearomatization afforded the desired indole-adduct product (**1.72**) in 82% yield. From this intermediate, the synthesis of gliocladin C (**1.73**) was finished in 6 additional steps.

Intermediate pyrroloindolinyl radicals have also been generated *in situ* by the cyclization of nitrogen-centered radicals onto the indole functionality of tryptamines and tryptamides. The 2017 total synthesis of flustramide B (**1.76**, Figure 1.10) by the Wang group demonstrates that activated tryptamides can be used to generate these radicals *in situ* (Scheme 12).²⁹ Tryptamides that contain N-aryloxy groups can be photolyzed to the amidyl radical (e.g. **1.79**). Eosin Y was used as a photocatalyst to perform a single electron reduction of bromotryptamide containing di-nitrophenoxyl group **1.73** in the presence of green light. It is proposed that reduction occurs at the dinitrophenoxyl arene which subsequently fragments to the dinitro phenolate (**1.78**) and amidyl radical **1.79**, which undergoes a *5-endo-trig* cyclization to generate the key pyrroloindolinyl radical **1.80**. Conjugate addition of the bisphenylsulfone **1.74** furnishes intermediate **1.75** which can then

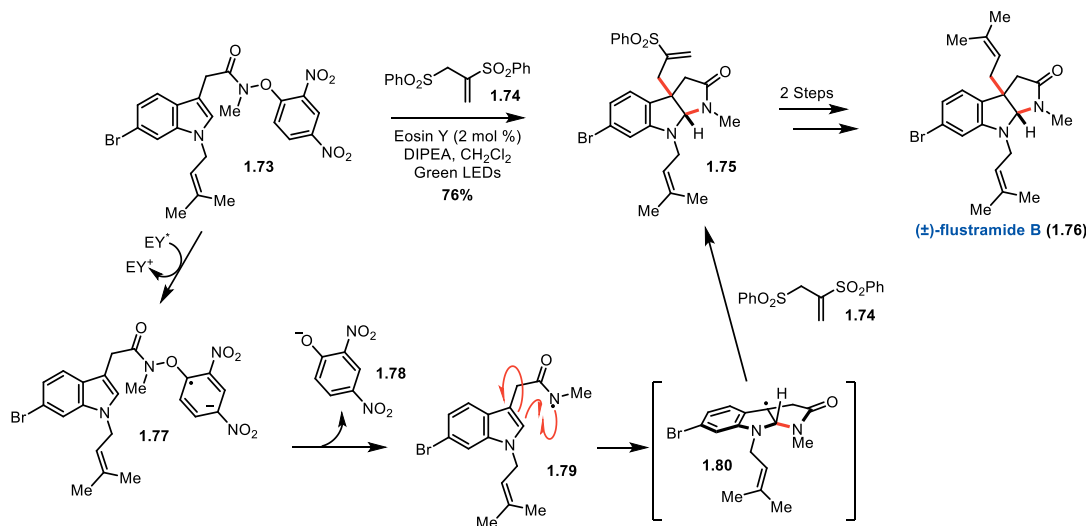


Figure 1.10. Wang's synthesis of (±)-flustramide B (1.76)

be converted to (±)-flustramide B (1.76) in 2 steps. The formation of the stabilized pyrroloindoline radical was supported by the isolation of the TEMPO adduct when carried out in the presence of TEMPO. Knowles and co-workers recently reported an approach to pyrroloindolines in which they also employ amidyl radicals from tryptamine precursors.³⁰ These intermediates undergo 5-*exo-trig* cyclizations to give the key pyrroloindoline radicals that are trapped by TEMPO, and the TEMPO-adduct can be utilized in subsequent steps. As this approach relies upon the use of a persistent radical for synthesis, it will be discussed in full detail in Section 1.5.1.

1.3.3 Tertiary radicals in natural product synthesis

Tertiary carbon-centered radicals are some of the most utilized free radical-based building blocks in complex molecule synthesis, and they are stabilized by hyperconjugation whereas steric hindrance contributes to their persistence. Stability via hyperconjugation arises from σ -bond donation to the SOMO from bonds alpha to the radical center. This stability is reflected in the diminished BDE of the C2–H in 2-methylpropane (97 kcal/mol), which corresponds with the formation of *tert*-butyl radical.⁶ Increased steric bulk around

the radical center decreases the likelihood of self-quenching through dimerization events, thereby conferring persistence to these species. As a result, tertiary radicals can be used for predictable and controlled reactions in both intra- and intermolecular contexts. The following section describes the use of tertiary radicals in natural product synthesis.

The syntheses of (-)-aplyviolene (**1.93**), (+)-cheloviolene A (**1.94**) & B (**1.95**), and (+)-dendrillolide C (**1.92**) were produced by the Overman group.^{31,32} These natural products are marine sponge-derived diterpenes with biological activities that remain unexplored. The conserved 7/5-fused bicyclic core in addition to the vicinal stereocenters between the 5-membered rings provide a challenging target for the development of synthetic methods. The successful synthesis of these natural products relied on the utilization of tertiary radical

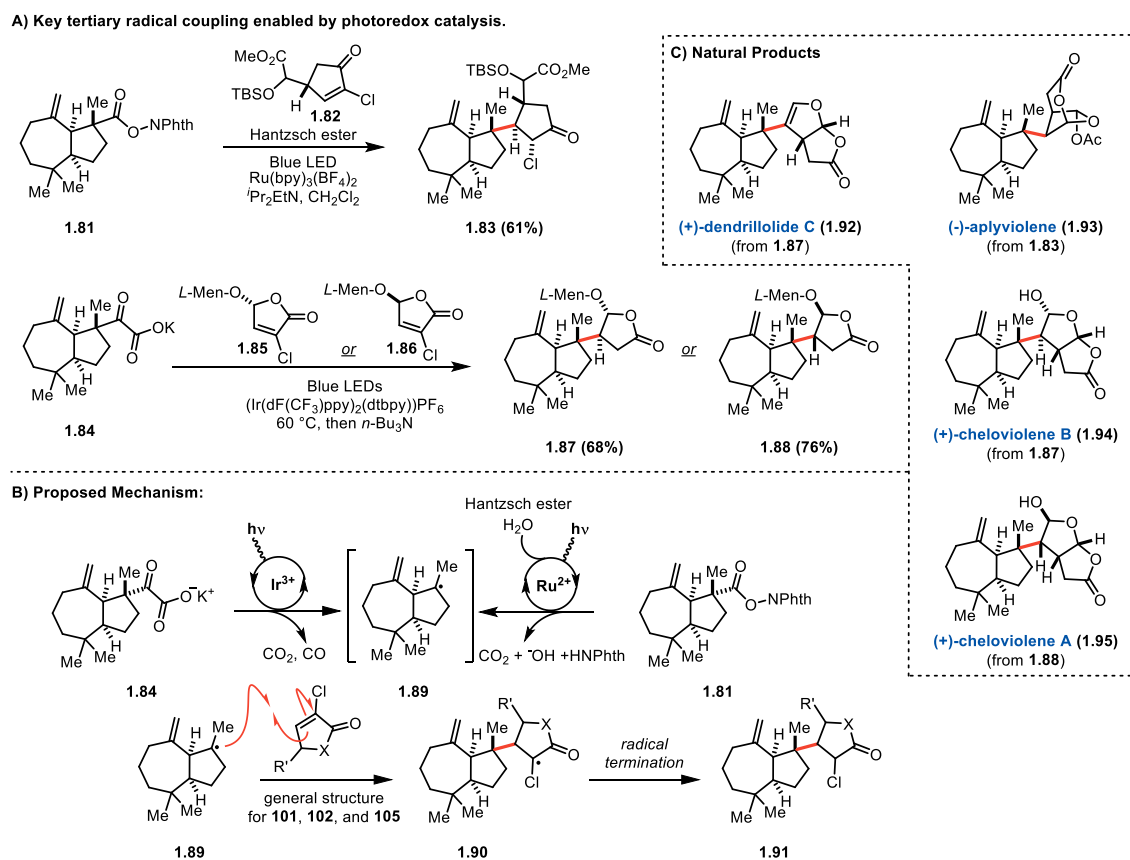


Figure 1.11. Overman's tertiary radical coupling to set vicinal stereocenters for the synthesis of marine sponge terpenoids.

intermediates generated via photoredox catalysis (Figure 1.11). The key step developed for the synthesis of **1.93** was the radical-conjugate addition to obtain intermediate **1.83** from the N-oxy phthalimide ester (**1.81**) (Figure 1.11A). The authors propose that irradiation of the Ru(bpy)₃(BF₄)₂ photoredox catalyst enables single electron transfer to **1.81** to form the corresponding radical anion, and subsequent fragmentation produces the tertiary radical intermediate (**1.89**) (Figure 1.11B). This tertiary radical then undergoes conjugate addition to form the cyclopentanone adduct (**1.83**) in 61% yield. This intermolecular radical coupling reaction provides excellent control (>20:1 *dr*) over the formation of the key vicinal stereocenters. From the cyclopentanone adduct (**1.83**), the desired natural product (**1.93**) was synthesized in an additional 9 steps. This success inspired the use of this transformation for the subsequent syntheses of **1.92**, **1.94**, and **1.95** (Figure 1.11C). The radical precursor used for this route was the α -keto carboxylate (**1.84**) which yields the tertiary radical **1.89** upon single electron oxidation and successive decarboxylation and decarbonylation. Radical conjugate addition onto either enantiomer of the L-menthol enone adduct (**1.85** & **1.86**) provided a means to access both (+)-cheloviolene A (**1.95**) and B (**1.94**) as well as (+)-dendrillolide C (**1.92**).

The synthesis of (-)-maoecrystal Z (**1.99**) by Reisman and co-workers embraces the conversion of tertiary radical intermediates for selective radical cyclization cascades (Figure 1.12).³³ Maoecrystal Z is closely related to the 6,7-*seco-ent*-kauranoid natural products which includes maoecrystal V and to which anticancer biological properties has been ascribed.³⁴ For the formation of the complex polycyclic core, the Reisman group employed a cyclization cascade which features tertiary radical **1.101** as a key intermediate. The authors propose that the aldehyde distal to the spirocycle is reduced first, perhaps due

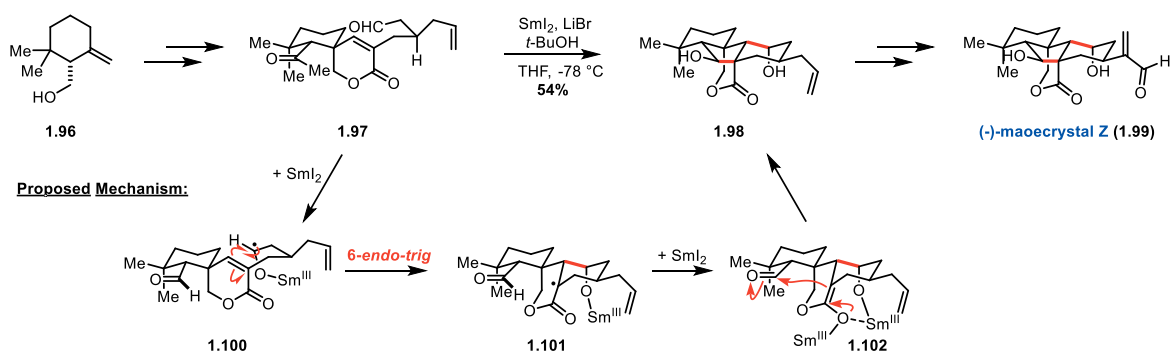
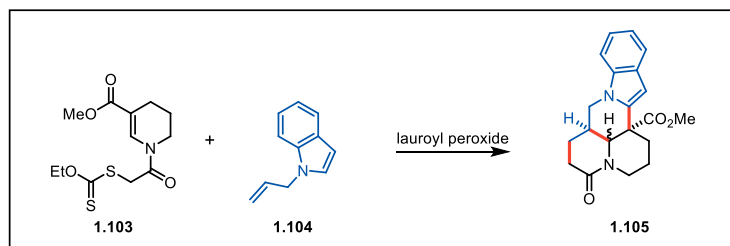


Figure 1.12. Reisman's synthesis of maoecrystal Z (1.99) featuring a ketyl radical cyclization.

to its greater steric accessibility relative to the aldehyde adjacent to the geminal dimethyl group. Single electron reduction forms ketyl radical **1.100**, which selectively undergoes a 6-endo-trig cyclization to afford tertiary radical **1.101**. Presumably there is an equilibrium between the 6-endo-trig and 5-exo-trig cyclization pathways, however, the authors propose that subsequent reduction of stabilized radical **1.101** drives the reaction in favor of forming enolate **1.102**. An aldol cyclization then yields the desired product (**1.98**). The proposed order of reactivity is supported by the isolation of monocyclized byproduct, which is suggested to arise from premature protonation of enolate **1.102**. From intermediate **1.98**, Reisman and co-workers access maoecrystal Z in 3 additional steps.

Synthetic efforts by the Miranda group towards matrine analogs showcases the thermodynamic stability of tertiary radicals (Figure 1.13).³⁵ Matrine alkaloid natural products possess a wide array of biological activities including antipyretic, analgesic, and anti-inflammatory properties. This family of molecules share a conserved fused-heterocyclic core as seen in analog **1.105**. The Miranda group aimed to form this polycyclic core by a radical cyclization cascade, and they envisioned the following mechanism would rapidly access the desired analogs. Initially, the alpha-keto radical (**1.107**) is formed from the reaction of xanthate ester (**1.103**) with lauroyl peroxide. This intermediate then



Proposed Mechanism:

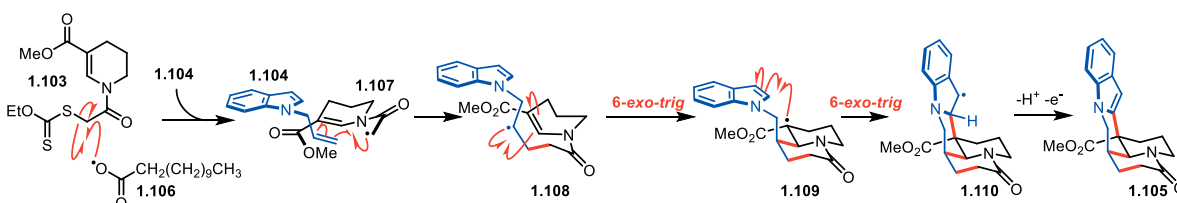


Figure 1.13. Synthesis of matrine analogs by Miranda and co-workers.

undergoes radical addition to N-allyl indole (**1.104**), resulting in a secondary radical intermediate (**1.107**). Cyclization onto the neighboring cyclic enamine moiety gives tertiary radical intermediate (**1.108**). Subsequent cyclization onto the indole produces a benzylic radical (**1.109**). Further cyclization leads to a radical (**1.110**), and the matrine analog (**1.105**) is formed upon rearomatization. This intermolecular coupling forms two 6-membered rings in a single step to provide rapid access to the desired natural product analogs. This example includes each type of radical intermediate discussed thus far – α -acyl, benzylic, and tertiary. These radicals, though stabilized, are presumed to be transient and short-lived in solution. The following sections will discuss how persistent radicals impart selectivity to reactions by influencing the apparent lifetime of all radicals in solution.

1.4 The persistent radical effect

Of the persistent radicals utilized in organic chemistry, 2,2,6,6-tetramethylpiperidin-1-oxyl, or TEMPO (**1.118**, Figure 1.15), is most prevalent. TEMPO is a stable radical that exists as a red-orange solid at room temperature. It was first prepared by Lebedev and Kazarnowskii in 1960 by oxidizing 2,2,6,6-tetramethylpiperidine with hydrogen

peroxide.³⁶ The stability of TEMPO can be attributed largely to resonance, while its persistence, largely to sterics. The stability is evident upon consideration of the O-H BDE of the corresponding hydroxylamine (**1.145**, Figure 1.17), which has been reported to be 69 kcal/mol – approx. 35 kcal/mol lower than a typical O–H bond.^{6,37} The four methyl groups flanking the aminoxyl radical prevent dimerization, and the lack of adjacent C-H bonds prevents disproportionation to nitron and hydroxylamine.

The selectivity observed in many of the reactions which utilize TEMPO is governed by the persistent radical effect (PRE). Fischer and Ingold were among the first to observe and characterize this intriguing phenomenon in which systems containing both persistent and transient radicals afforded remarkably selective product distributions.³⁸ There are two main criteria necessary for the persistent radical effect to be operative: a) of the radical intermediates formed in a given reaction, one is more persistent than the other(s), meaning it has a significantly slower termination rate, and b) the radical intermediates are generated in effectively equivalent rates. When such criteria are met, the initial rapid termination of transient radicals in solution results in a system in which the persistent radical has a significantly larger concentration than any transient radical. Such an excess of the persistent radical serves to drive the reaction forward in a selective fashion.¹² Figure 1.14 provides a generic example of this scenario. A radical initiation event creates a system in which both the transient radical R• (red) and the persistent radical P• (blue) are present in solution. R• rapidly undergoes termination events, therefore its concentration in solution remains relatively low. On the contrary, P• maintains a relatively high concentration in solution due to its persistence, thereby resulting in a system in which $[P•] \gg [R•]$. This “buildup” in $[P•]$ increases the favorability of coupling to R•, and the irreversible formation of the R–P

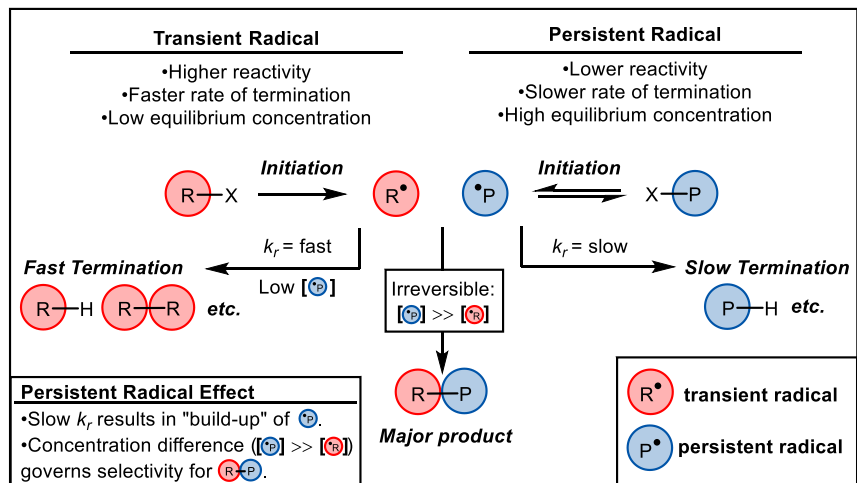


Figure 1.14. The persistent radical effect imparts selectivity in radical-radical coupling reactions.

heterocoupled product ultimately drives the reaction. In other words, the persistent radical effect favors the formation of $R-P$ due to the persistence of P^\bullet in solution. The following section will highlight how TEMPO has been utilized to leverage the PRE for the synthesis of natural products.

1.5 Persistent radicals in natural product synthesis

While Curran's synthesis of hirsutene (**1.15**) inspired numerous efforts to employ transient radicals for natural product synthesis, the analogous use of persistent radicals has lagged behind in comparison despite the inherent selectivity with which these unique intermediates react. Leifert and Studer recently published a review describing how various groups have leveraged the persistent radical effect,³⁹ though given the number of studies that are conducted in model systems – not applied to a specific target of interest – it is reasonable to argue that the use of persistent radicals for natural product synthesis is still in its infancy. The following sections describe efforts in which natural product syntheses have relied upon the employment of persistent radicals directly in key steps in the route.

1.5.1 Natural product syntheses harnessing TEMPO for key steps

The Jahn group has pioneered the use of TEMPO to leverage the persistent radical effect to achieve geometrically challenging radical cyclization for natural product synthesis. In particular, they sought to develop a method to access the diazabicyclo[2.2.2]octane core of the asperparaline and stephacidin alkaloid families.⁴⁰ They envisioned that single electron oxidation of enolate **1.111** would afford a radical capable of undergoing a 6-*exo-trig* cyclization. Unfortunately, oxidation of **1.111** with ferrocenium hexafluorophosphate (Cp₂FePF₆) at 0 °C only afforded the dimerization product; furthermore, running the reaction at room temperature afforded only trace amounts of the desired product (Figure 1.15A). The addition of TEMPO to the reaction conditions was critical to achieving the desired cyclization, and indeed **1.115** was isolated in 34% yield after oxidation of **1.111** with Cp₂FePF₆ in the presence of TEMPO (**1.118**). Interestingly, Jahn and co-workers reported that TEMPO-adduct **1.112** was not observed in the reaction, suggesting that a rapid equilibrium occurs between TEMPO and **1.113** which effectively reduces the concentration of **1.113** to slow its dimerization and enable the cyclization to compete.

In a similar vein, the Jahn group has utilized TEMPO-derived alkoxyamines as radical-precursors for key transformations in natural product synthesis. For example, in their formal synthesis of bicyclomycin (**1.121**), they prepared TEMPO-adduct **1.116** in three steps from the readily available materials (Figure 1.15B).⁴¹ Thermolysis of the alkoxyamine C–O bond in **1.116** at 130 °C enabled 8-*exo-trig* cyclization onto the appended allene to access the desired bicyclic core (**1.120**) of the natural product. Once again, the presence of TEMPO (**1.118**) enabled the researchers to minimize the concentration of the transient radicals derived from both starting material (**1.117**) and product (**1.119**), precluding dimerization

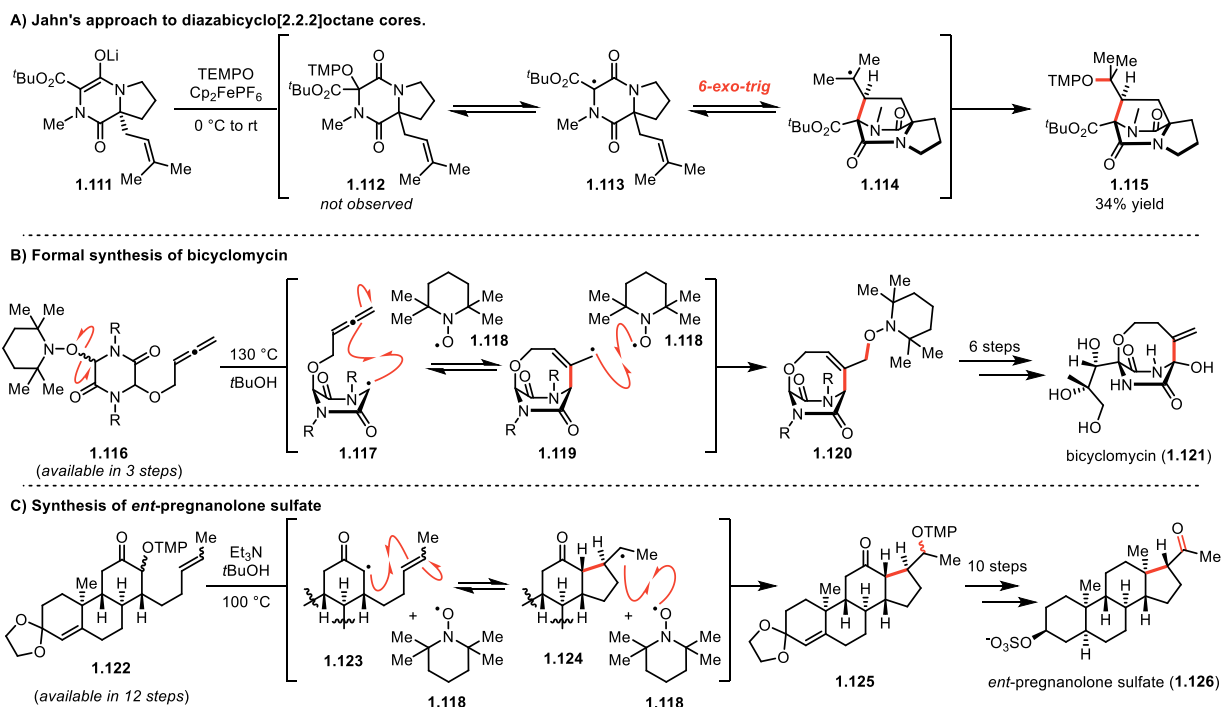


Figure 1.15. Jahn's use of TEMPO to leverage the persistent radical effect for the synthesis of natural products.

and/or disproportionation reactions. The desired natural product can subsequently be completed from intermediate **1.120** in only 6 steps.

The Jahn group also used this approach in their synthesis and biological evaluation of *ent*-pregnanolone sulfate (**1.126**, Figure 1.15C).⁴² They prepared TEMPO-adduct **1.122** in 12 steps prior to targeting the final cyclization of the steroid core employing the PRE. Thermolysis of **1.122** established the desired equilibrium, and the desired *5-exo-trig* reaction occurred to afford **1.125**. The steroid core was then converted to the desired product in 10 steps. This approach to radical cyclization reactions based on the persistent radical effect has multiple benefits. The preparation of TEMPO-adducts **1.116** and **1.122** occurs via enolate oxygenation in one step, directly accessing a compound activated for radical cyclization. These reactions are not dependent upon a chemical additive to initiate the radical reaction – instead thermolysis of the C–O bond initiates the persistent radical

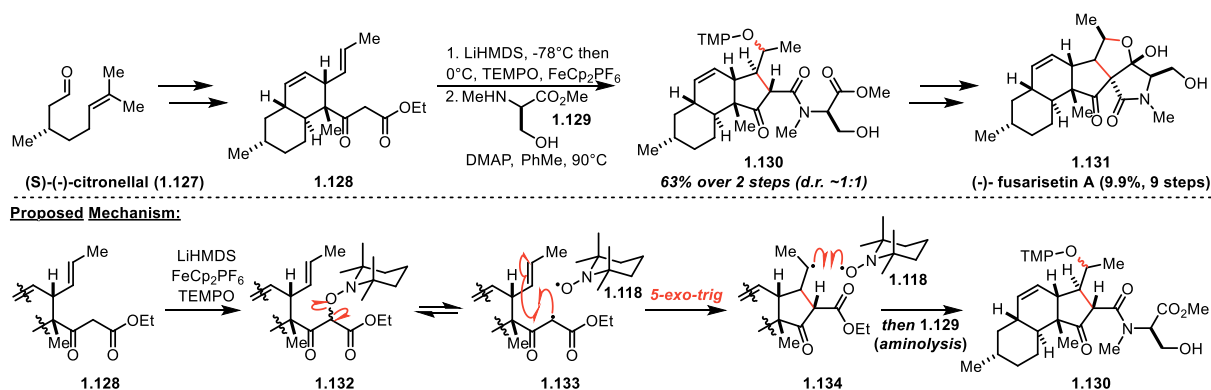
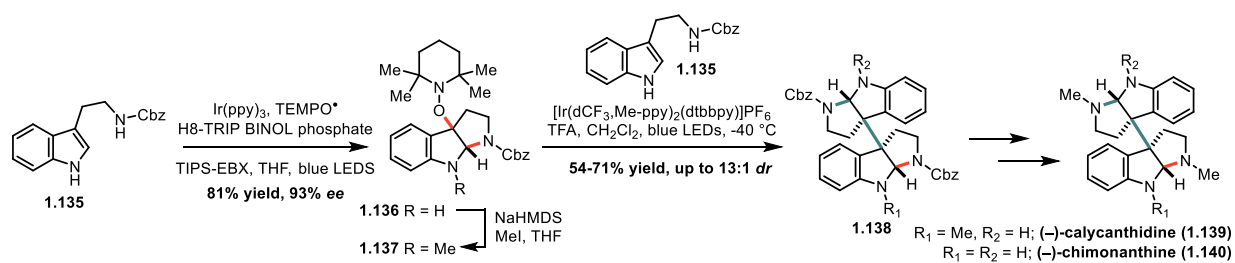


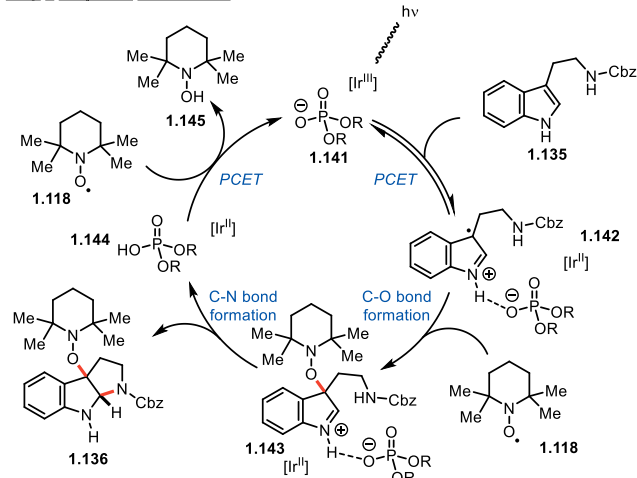
Figure 1.16. Theodorakis' use of TEMPO for the synthesis of (-)-fusarisetin A (1.131). equilibrium, which funnels the transient radicals along the desired reaction path. These examples from the Jahn group demonstrate the elegance with which the persistent radical effect can be harnessed for the synthesis of natural products.

Following Jahn's pioneering efforts, the Theodorakis group successfully demonstrated that TEMPO can be used to leverage the persistent radical effect in their synthesis of (-)-fusarisetin A (1.131, Figure 1.16) in 2012.⁴³ Compound 1.131 has demonstrated some inhibitory activity against acinar morphogenesis (77 μM), cell migration (7.7 μM) and cell invasion (26 μM) in the invasive breast cancer cell line MB-231. The key radical cyclization is facilitated by TEMPO (1.118) which forms an adduct (1.132) with the initially generated malonyl radical (1.133) – the same mechanism as Jahn's seminal examples. Tandem aminolysis of the ester motif was achieved in this one-pot transformation to afford the aminated TEMPO adduct (1.130) as a 1:1 mixture of diastereomers in 63% yield over the 2 steps. The total synthesis of (-)-fusarisetin A (1.131) was completed in just 9 steps with 9.9% overall yield.

A recent report from the Knowles group provides another demonstration of how TEMPO can be used to tame transient radical intermediates (Figure 1.17).³⁰ They proposed the use of TEMPO to trap the radical cation arising from single electron oxidation of a



Step 1 Proposed Mechanism:



Step 2 Proposed Mechanism:

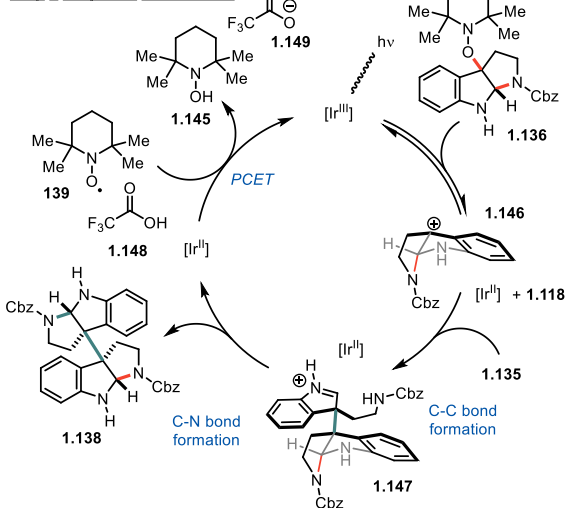


Figure 1.17. Knowles' use of TEMPO for the synthesis of pyrroloindoline natural products.

protected tryptamine starting material. The formation of the hydrogen bond between a chiral phosphate base to the indole N–H of the tryptamine decreases the tryptamine oxidation potential allowing the excited iridium polypyridyl photocatalyst to perform a single electron oxidation from the tryptamine-phosphate complex, thereby oxidizing the tryptamine **1.135** to radical cation **1.142**. The radical is trapped by TEMPO (**1.118**), and the iminium ion is trapped by addition of the pendant amine, affording TEMPO adduct **1.143**. Furthermore, this process is rendered enantioselective by the chirality induced from the phosphate base (**1.141**). A subsequent oxidation of **1.136** with a second photocatalyst accesses a system in which benzyl cation **1.146** is presumed to be stabilized by TEMPO (**1.118**) through a mesolytic cleavage and recombination equilibrium. Nucleophilic attack by a second tryptamine equivalent (**1.135**) quenches this stabilized benzyl cation, and

cyclization onto the resulting iminium (**1.147**) completes the two-step dimerization process. Oxidation of the reduced photocatalyst by the liberated TEMPO turns over the catalytic cycle. TEMPO is regenerated via the oxidation of TEMPOH by TIPS-EBX, an exogenous oxidant. This unique approach from the Knowles group demonstrates the versatility of TEMPO to both induce selectivity for the coupling of reactive intermediates and serve as a redox mediator in conjunction with a photocatalyst in natural product synthesis.

1.5.2 Persistent phenoxy radicals for the synthesis of resveratrol oligomers

Numerous natural products are proposed to have biosyntheses based upon stabilized or persistent radical intermediates. One such example is the resveratrol class of natural products (this natural product class is discussed in detail in Chapter 3).⁴⁴ Oligomers derived from resveratrol have shown widespread biological activities; these results coupled with their structural complexity has inspired synthetic efforts from a number of research groups. My colleagues in the Stephenson group, Dr. Bryan Matsuura and Dr. Mitch Keylor, initiated synthetic efforts that sought to develop a biomimetic approach to these natural products based on the hypothesis that Nature constructs these molecules by stereoselectively coupling phenoxy radical intermediates. They first accomplished the syntheses of pallidol (**1.153**) and quadrangularin A (**1.152**) from common quinone methide dimer (QMD) intermediate **1.151** (Figure 1.18).⁴⁵ In their bio-inspired dimerization step, protected resveratrol analog **1.150** was deprotonated and subjected to single electron

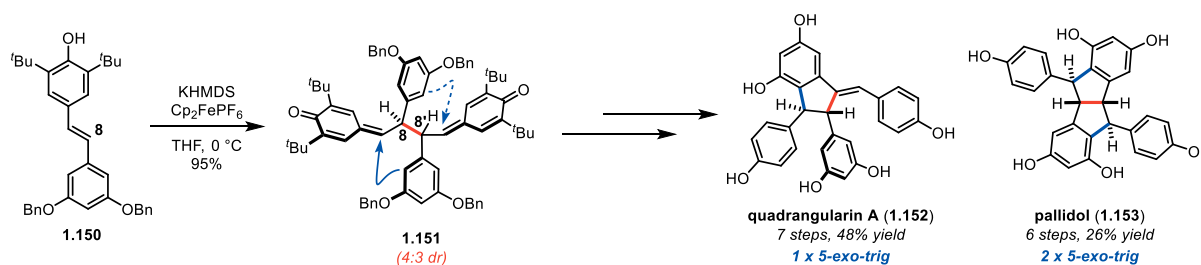


Figure 1.18. Stephenson's synthesis of quadrangularin A (1.152) and pallidol (1.153).

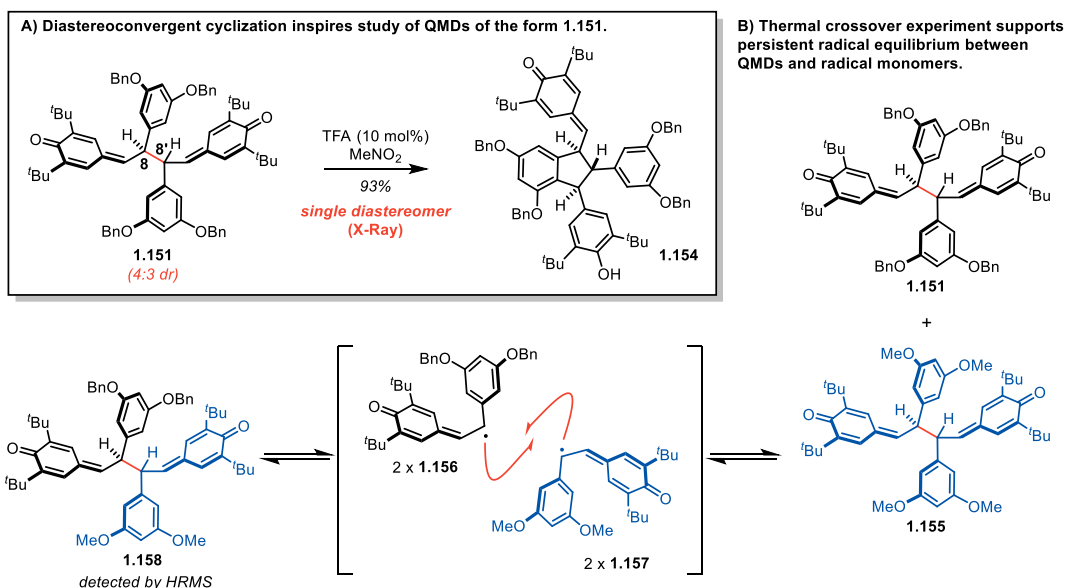


Figure 1.19. Discovery of dynamic equilibrium between quinone methide dimers and radical monomers.

oxidation to yield the key intermediate (**1.151**). Subsequent Lewis-acid mediated cyclizations and deprotections of **1.151** afforded pallidol (**1.153**) and quadrangularin A (**1.152**) with good synthetic efficiency.

Upon further investigation of the cyclization conditions for **1.151**, they found that treatment of QMD **1.151** with 10 mol% of trifluoroacetic acid afforded the cyclized quinone methide **1.154** as a single diastereomer in 93% yield (Figure 1.19A). The conversion of **1.151** (as a 4:3 mixture of diastereomers) to the *trans,trans*-indane product **1.154** was confirmed by X-ray crystallography. Control experiments suggested that this diastereoconvergent cyclization did not arise from a prototropic mechanism; instead, based on a 1969 report from Becker and the work of Moses Gomberg (*vide supra*), a radical mechanism was hypothesized to be responsible for the observed reactivity.⁴⁶ To test this hypothesis, a thermal crossover experiment was performed between **1.151** and **1.155**, and a statistical mixture of products was observed which was consistent with the proposed radical mechanism (Figure 1.19B). Subsequent experimentation with **1.151** revealed that

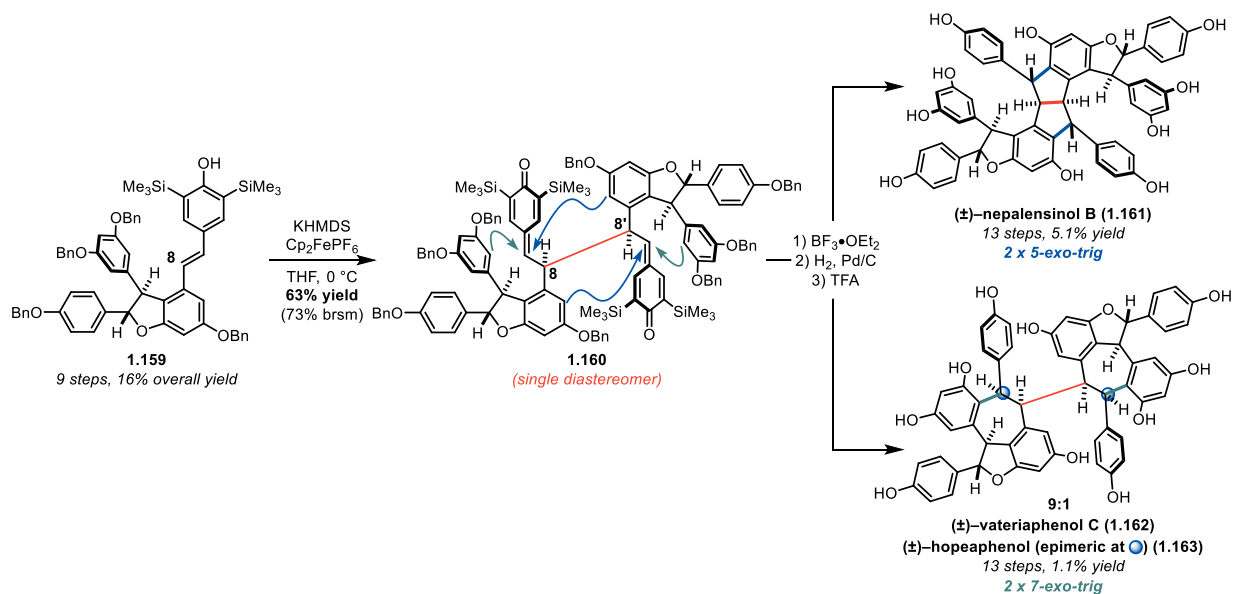


Figure 1.20. Synthesis of resveratrol tetramers from a persistent radical equilibrium. the C8–C8' bond dissociation enthalpy (BDE) was a mere 17.0 ± 0.7 kcal/mol, which is only slightly higher than the Gomberg dimer.⁴⁷

An analogous approach was applied to the synthesis of higher-order resveratrol oligomers (Figure 1.20).⁴⁸ Upon preparing racemic ϵ -viniferin analog **1.159** (9 steps, 16% yield), subsection of this material to the same dimerization conditions afforded **1.160** as a single diastereomer. This bis-quinone methide tetramer was found to have a slightly weaker C8–C8' BDE of just 16.4 ± 0.5 kcal/mol, and it is believed that the highly reversible homolysis and recombination of the radicals contributes to the observed diastereoselectivity. The assignment of the relative configuration of **1.160** was based largely upon the outcome of the subsequent cyclization. It is possible that the isolated isomer of **1.160** is of a different configuration than the one that reacts due to the dynamic homolysis-recombination equilibrium. Lewis-acid mediated cyclization afforded two reaction modes – the double 5-*exo-trig* and double 7-*exo-trig* reactions. Subsequent hydrogenolysis of the benzyl ethers followed by protodesilylation to remove the C3-silyl substituents afforded resveratrol tetramers nepalensinol B (**1.161**) and vateriaphenol C

(**1.162**) in just 13 steps and 5.1% and 1.1% overall yield, respectively. The persistent radical effect was critical to the selective outcome of these syntheses, as they were able to successfully dimerize racemic, prochiral material to a single diastereomer in good yield, enabling the first syntheses of these two resveratrol tetramers.

1.6 Conclusions

The utility of radicals within the context of natural product synthesis has been demonstrated through the examples presented herein. Radicals can be stabilized by stereoelectronic factors and rendered persistent by their steric environments. When used with the appropriate conditions, radical intermediates can react with regio- and stereoselective control to achieve elaborate molecular architectures. Stabilized radicals can react in predictable manifolds and persistent radicals provide a means to improve selectivity for reactions involving transient radicals that are otherwise difficult to achieve. Once thought to be limited to intramolecular cyclizations (e.g. Curran's hirsutene synthesis), the field has advanced to include many examples of intermolecular radical reactivity, resulting in the expanded use of radical intermediates in complex molecule synthesis. It seems likely that not only will radical transformations be a mainstay in the synthetic chemistry toolbox for the synthesis of natural products, but that their use will continue to grow.

CHAPTER 2: Development of an Electrochemical Dimerization of Phenylpropenoid Scaffolds and the Evaluation of Their Antioxidant Activities

*Portions of this chapter have been published in:

Romero, K. J.; Galliher, M. S.; Raycroft, M. A. R.; Chauvin, J.-P. R.; Bosque, I.; Pratt, D. A.; Stephenson, C. R. J. *Angew. Chem. Int. Ed.* **2018**, *57* (52), 17125–17129.

2.1 Introduction

While the field of radical chemistry originated at the turn of the 20th century with Gomberg's seminal discovery of the persistent triphenylmethyl radical, the field of electrochemistry commenced a century earlier with Volta's invention of the "Volta pile", or more commonly known as the battery.⁴⁹ Volta communicated his findings to the president of the Royal Society, Sir Joseph Banks, who subsequently shared the exciting news with Anthony Carlisle and William Nicholson.⁵⁰ These two set out immediately to validate Volta's work, and, in doing so, they observed that wetting the Volta pile resulted in the evolution of a gas. In fact, Carlisle and Nicholson had split water into its elemental constituents – hydrogen and oxygen – in the first known electrochemical reaction.

In the context of electroorganic synthesis, it is Professor Michael Faraday of the Royal Institution of Great Britain who is credited with the seminal work based on his 1834 report of the synthesis of ethane from the electrolysis of an acetate solution (Figure 2.1).^{51,52} Faraday's work inspired the Kolbe electrolysis, whereby anodic oxidation converts fatty acid carboxylates to the corresponding hydrocarbon dimers with concomitant

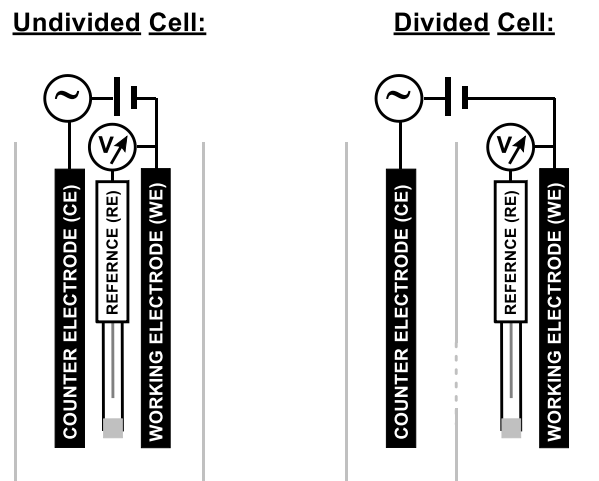


Figure 2.2. General schematic of electrochemical cells for organic reactions.

reaction. Under this reaction paradigm, the cell potential will increase over time, a phenomenon that was first observed by Haber in 1898.⁵² In 1942, Hickling invented the *potentiostat* – a device by which the electrochemical cell potential could be held constant with variable current. This discovery afforded a new mode of electrochemical reactivity, which is referred to as *potentiostatic* conditions. Under this reaction paradigm, the electrochemical cell potential is held constant, creating an upper limit of the reactivity that can occur. The current subsequently decreases over time until all reactions that can occur at the given cell potential have completed. This mode of reactivity requires a third electrode, which is referred to as a *reference* electrode (Figure 2.2). The reference electrode contains a standard electrochemical half-cell, typically Ag/Ag⁺ or saturated calomel, which is used to measure the potential at the *working* electrode by comparison. The working electrode is the electrode (either anode or cathode) at which the reaction of interest occurs (Figure 2.2). For example, in an oxidation reaction the working electrode is the anode, and the *counter electrode* is the cathode. Potentiostatic conditions afford direct control of the potential at the working electrode, thereby resulting in precise control of the chemistry that can occur. A reference electrode may also be included under galvanostatic conditions, serving to

measure the potential over the course of the reaction. However, as the reference electrode has no bearing on the current passing through the cell, it is not required for galvanostatic reactivity. A final consideration for the construction of electrochemical cells is whether there exists a physical barrier between the anodic and cathodic reactions (Figure 2.2). In an *undivided cell*, the electrodes are the same solution, and every reagent in solution can access each electrode. In a *divided cell*, the electrodes are separated by a semi-permeable membrane designed to only allow for the passage of electrolytes, thereby separating the anodic and cathodic reactions. While these reaction setups can be more complex, the segregation of electrodes in a divided cell helps to avoid the premature oxidation of cathodic products and *vice versa*.^{57,58} For additional reading regarding the fundamentals of organic electrochemistry, excellent contributions from Moeller, Sperry and Wright, Frontana-Urbe and co-workers, as well as Waldvogel and co-workers should be consulted.^{59–63} The following section presents a selection of examples where anodic electrochemistry has been utilized for a key step in natural product synthesis.

2.2 Anodic electrochemistry in natural product synthesis

Electrochemically mediated organic synthesis renders electrons as reagents, avoiding the need for stoichiometric additives, thereby enabling direct redox manipulations in the theoretically simplest manner.⁶⁴ As a result, electrochemistry offers a unique alternative to traditional methods for the synthesis of complex molecules and natural products.⁵⁷ The first example of an organic electrochemical reaction for natural product synthesis is exhibited in Prof. E. J. Corey's synthesis of (+)-pentacyclosqualene (**2.15**) and α - and β -onoceradienes (**2.17** and **2.16**, respectively) in 1958 (Figure 2.3).⁶⁵ Following a report from Ruzicka and Janot,⁶⁶ the authors converted the bicyclic terpene alcohol sclareol (**2.7**) to

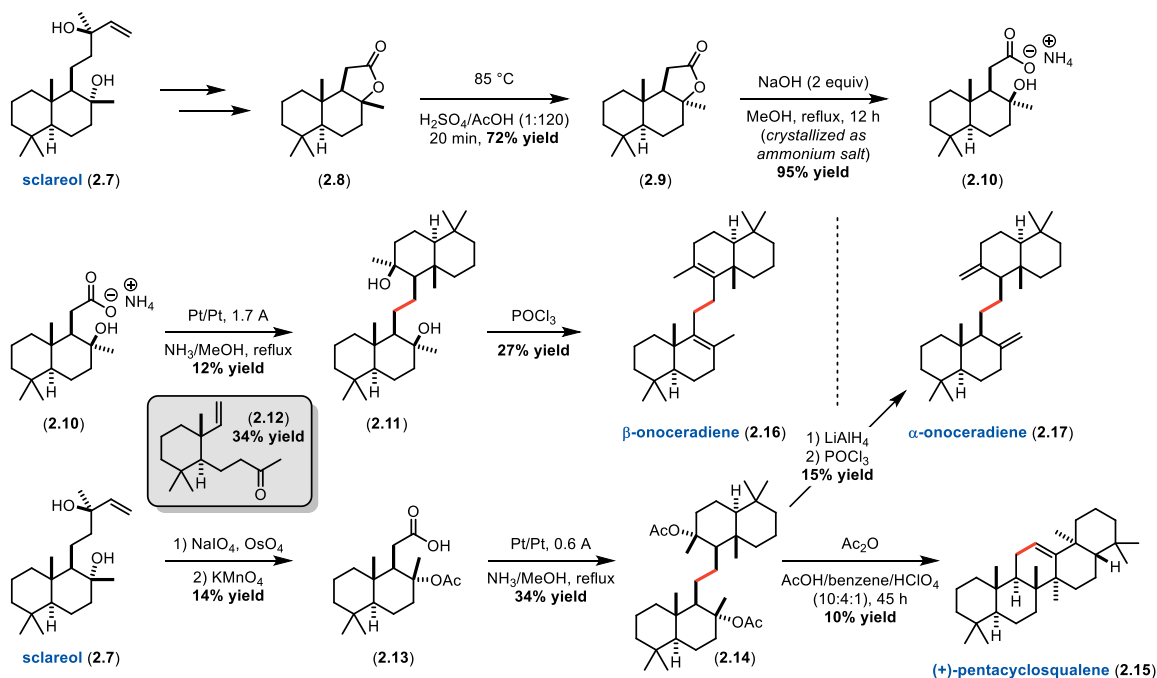


Figure 2.3 Corey's synthesis of (+)-pentacyclosqualene (2.15) enabled by a Kolbe electrolysis reaction.

lactone **2.8**. Subsequent acid-mediated epimerization followed by hydrolysis of the lactone delivered the requisite ammonium salt starting material (**2.10**) for a late-stage dimerization enabled by the Kolbe electrolysis. Treatment of **2.10** to anodic oxidation under galvanostatic conditions delivered dimer **2.11** in 12% yield along with the β-scission product (**2.12**) in 34% yield. These results were realized after a brief optimization in which the authors observed that increasing reaction concentration favored the formation of the desired dimer (**2.11**). Alternatively, sclareol (**2.7**) was converted to acetate **2.13**, which delivered nearly a three-fold increase in yield (34%) in the electrochemical conversion to **2.14**. Acid-mediated dehydration of **2.14** delivered (+)-pentacyclosqualene (**2.15**). Furthermore, dehydration of **2.11** delivered β-onoceradiene (**2.16**), whereas reduction of **2.14** followed by dehydration afforded α-onoceradiene (**2.17**). These early efforts from Corey demonstrated that electrochemistry is a useful tool for natural product synthesis.

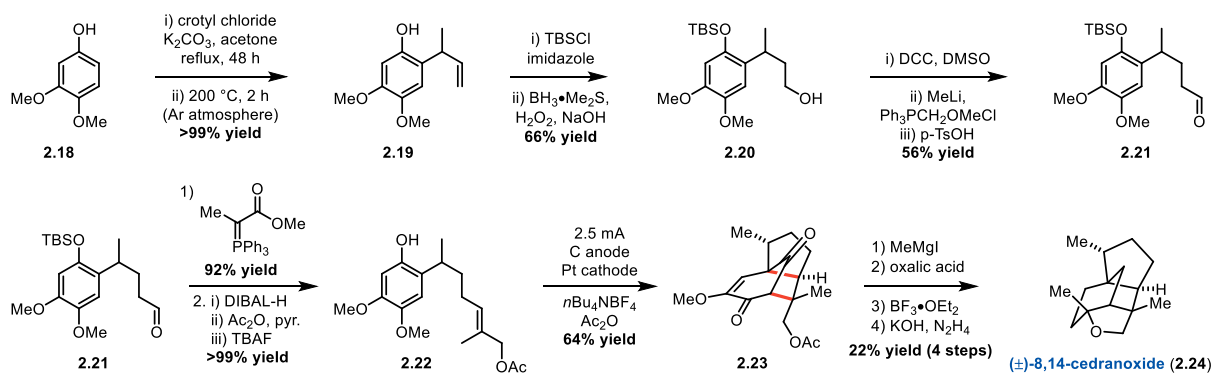


Figure 2.4. Yamamura's synthesis of (±)-8,14-cedranoxide (2.24) featuring an electrochemical formal (5+2) cycloaddition.

In 1987, Yamamura and co-workers reported the synthesis of (±)-8,14-cedranoxide (2.24) utilizing an electrochemical formal (5+2) cycloaddition (Figure 2.4).⁶⁷ Starting from 3,4-dimethoxyphenol (2.18), alkylation followed by a Claisen rearrangement is reported to deliver 2.19 in quantitative yield. Subsequent silyl protection of the phenol is followed by hydroboration-oxidation to access primary alcohol 2.20, and a Pfitzner-Moffatt oxidation,⁶⁸ Wittig homologation, and deprotection sequence affords 2.21. A second Wittig reaction, this time with a stabilized ylide to ensure *E*-selectivity⁶⁹ was followed by reduction of the newly incorporated ester down to the alcohol, acetylation of the alcohol, and phenol deprotection to give compound 2.22. With the desired starting material in hand, the authors set out to implement the proposed electrochemical formal (5+2) cycloaddition. They found that by utilizing a glassy carbon anode and a platinum cathode they could effect the desired transformation in 64% yield by passing 2.5 mA of current (at a cell potential between +900–1200 mV vs. SCE, ~2 F/mol) through a reaction mixture containing the starting material (2.22) and tetrabutylammonium tetrafluoroborate electrolyte dissolved in acetic anhydride. The tricyclic product 2.23 was then treated with MeMgI to deliver a 1,2-addition to the α,β -unsaturated ketone followed by oxalic acid to reveal the ketone from the methyl enol ether. A Lewis-acid mediated cyclization closed the tetrahydrofuran moiety, and, finally, a Wolff-

Kishner reduction yielded the desired natural product (\pm)-8,14-cedranoxide (**2.24**). The rapid increase in complexity afforded by the conversion of **2.22** to **2.23** demonstrates that electrochemical transformations can be integral in natural product synthesis; in fact, these sorts of phenol-alkene intramolecular cycloaddition reactions have been featured in numerous synthetic efforts.⁷⁰

Tan and co-workers further demonstrated the selectivity with which anodic oxidation can be employed for late-stage functionalization in natural product synthesis.⁷¹ In 2001 these researchers studied the electrochemical oxidation of aspidofractinine-type alkaloids, resulting in the semi-syntheses of kopsidine A–C (**2.27–2.29**) (Figure 2.5). They began their investigation by measuring the oxidation potentials of their starting materials using cyclic voltammetry.⁷² Kopsingine (**2.25**), which had been previously isolated from *Kopsia teoi*,⁷³ exhibited two irreversible oxidation waves at 0.78 V and 1.38 V versus a Ag/AgCl reference electrode. Presumably the first oxidation corresponds to the tertiary amine, while the second oxidation can be attributed to the methoxyarene moiety.⁷⁴ The authors utilize platinum electrodes with Et₄NClO₄ (1 M) as the electrolyte in a CH₂Cl₂/MeCN solvent mixture with two equivalents of 2,6-lutidine to conduct their bulk electrolysis experiment under potentiostatic conditions. The authors allow for the consumption of 2.1 faradays/mol, which corresponds to the removal of 2 equivalents of electrons from the starting material, at a constant potential of 0.87 V vs. Ag/AgCl to afford the conjugated iminium salt **2.26**. A

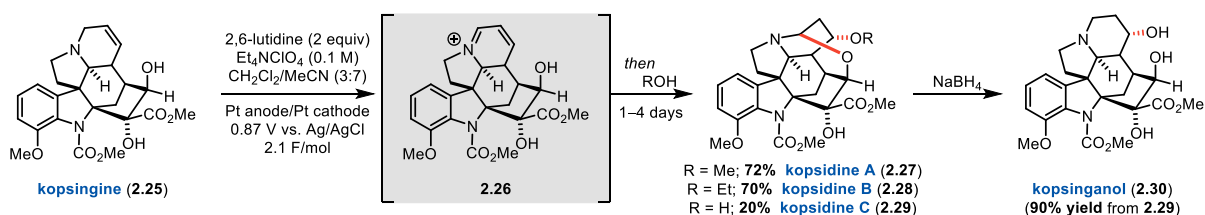


Figure 2.5. Tan and co-workers semisynthesis of aspidofractinine alkaloids using anodic oxidation under potentiostatic conditions.

solvent exchange with MeOH and subsequent stirring for a day served to precipitate out the electrolyte and convert **2.26** to kopsidine A (**2.27**). Similar treatment with EtOH afforded kopsidine B (**2.28**), and treatment with water gave kopsidine C (**2.29**), albeit in diminished yield relative to the other two while requiring extended reaction time (4 days). Kopsidine C was also further converted to kopsinganol (**2.30**) via reductive cleavage of the amination with sodium borohydride. The general approach of leveraging anodic amine oxidation for α -amino functionalization (typically forming amination) is referred to as the Shono oxidation,⁷⁵ and it has been employed for numerous natural product and complex molecule syntheses.^{76–78} This example from Tan and co-workers elegantly demonstrates the selectivity with which organic electrochemistry can be leveraged for late-stage functionalization in complex molecule synthesis.

In the same year, Moeller and Duan leveraged the reactivity of enol ether radical cations in their synthesis of (+)-linalool oxide (**2.35**) (Figure 2.6).⁷⁹ Their approach was based upon the idea that oxidation of enol ethers to the radical cation results in a polarity reversal, inviting nucleophilic attack by pendant alcohols and providing a novel approach to access tetrahydrofuran and tetrahydropyran rings.^{59,80} Their synthesis commenced with an asymmetric dihydroxylation of commercially available ketone **2.31** to afford diol **2.32**, and a Wittig olefination gave enol ether **2.33**. The authors then subjected **2.33** to anodic oxidation under galvanostatic conditions (2F/mol, 8 mA) using a reticulated vitreous carbon

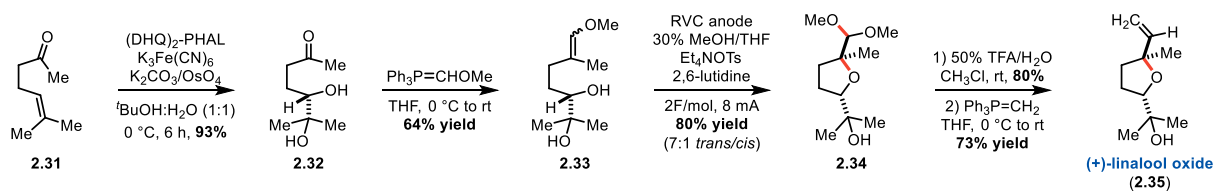


Figure 2.6. Moeller's synthesis of (+)-linalool oxide (2.35) utilizing a polarity reversal approach enabled by anodic oxidation.

(RVC) anode with 2,6-lutidine as the base and Et₄NOTs as the electrolyte in 30% MeOH/THF to deliver the desired tetrahydrofuran product **2.34** in 80% yield as a 7:1 mixture of *trans* and *cis* isomers. Hydrolysis of the acetal followed by a second Wittig olefination delivered (+)-linalool oxide (**2.35**). This rapid synthesis of **2.35** demonstrates the power of polarity reversal that is enabled by electrochemical reactions.

Moeller followed these efforts with the 2004 synthesis of (-)-alliacol A (**2.43**) relying upon a tandem anodic coupling–Friedel-Crafts alkylation approach (Figure 2.7).⁸¹ The authors started by preparing α,β -unsaturated ketone **2.36** in 4 steps from readily available materials. This material was subjected to asymmetric conjugate addition using *S*-(+)-Monophos and a methyl cuprate to set the key stereocenter in **2.37** that would provide asymmetric induction for the following steps. Formation of the silyl enol ether under standard conditions afforded **2.38**, providing the desired platform for the anodic coupling step. Moeller again utilized galvanostatic conditions (15.3 mA, 2.1 F/mol) to enact the desired oxidation at an RVC anode, and subsequent acidic treatment delivered the aromatized product **2.39**. A Garegg-Samuelsson reaction⁸² converted the primary alcohol to an intermediate iodide, and subsequent treatment with silver nitrate initiated a Friedel-Crafts cyclization to afford tricyclic ketone **2.40**. A series of redox manipulations converted

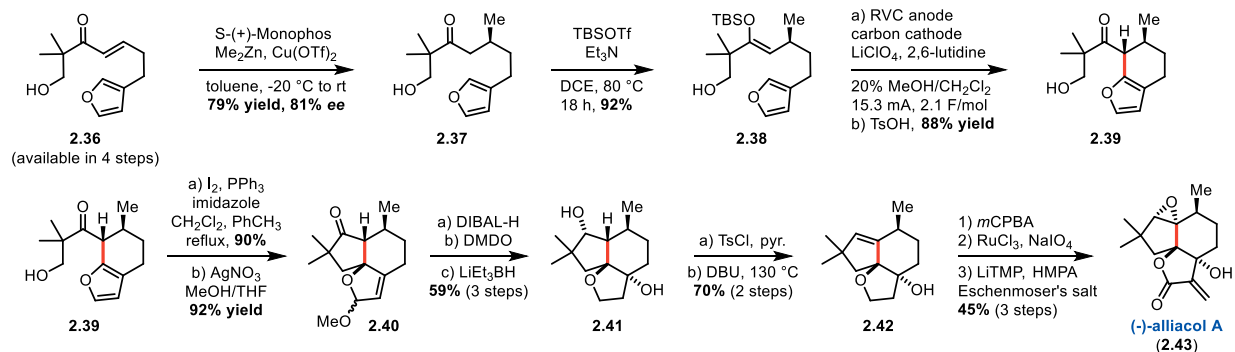


Figure 2.7. Moeller's synthesis of (-)-alliacol A (2.43) utilizing an electrochemical enol-furan coupling.

2.40 to **2.41**, and selective activation and elimination of the secondary alcohol delivered **2.42**. Finally, the desired product **2.43** was realized after a series of oxidations and alkylation with Eschenmoser's salt to afford the α,β -unsaturated lactone. Unfortunately, the authors determined by optical rotation that their product, (-)-alliacol A (**2.43**), was the opposite enantiomer relative to the natural product; therefore, the *R*-(+)-Monophos ligand is required to access the natural material. Regardless, Moeller yet again demonstrated the utility of electrochemical polarity reversal to couple two nucleophiles and forge a key C–C bond in complex molecule synthesis.

Another example of enol-furan anodic coupling was leveraged by the Trauner group in their synthesis of (-)-heptemerone B (**2.56**) and (-)-guanacastepene E (**2.57**) (Figure 2.8).⁸³ Trauner and co-workers recognized that formation of the 7-membered ring central to these natural products would be the critical element for a successful synthesis, and they chose to split this ring into two fragments from a retrosynthetic standpoint. Synthesis of the left-hand fragment commenced with an asymmetric reduction of ketone **2.44** using (+)-*B*-chlorodiisopinocampheylborane [(+)-DIP-Cl]⁸⁴ to access (+)-**2.45** with good yield and enantioselectivity. The newly formed stereocenter provided modest diastereomeric control (ca. 5:1) in the subsequent Heck reaction to furnish the key six-membered ring (**2.46**). The alcohol was then silyl protected, and the pendant alkene was converted to a primary iodide following hydroboration-oxidation and a Garegg-Samuels reaction, delivering **2.47** in good yield. A chiral auxiliary-mediated carbonyl-ene reaction previously reported by Whitesell and co-workers⁸⁵ was employed for the preparation of **2.49**, setting both stereocenters for the right-hand fragment. Benzyl protection followed by reductive cleavage of the auxiliary afforded aldehyde **2.50**, which was next treated with vinyl

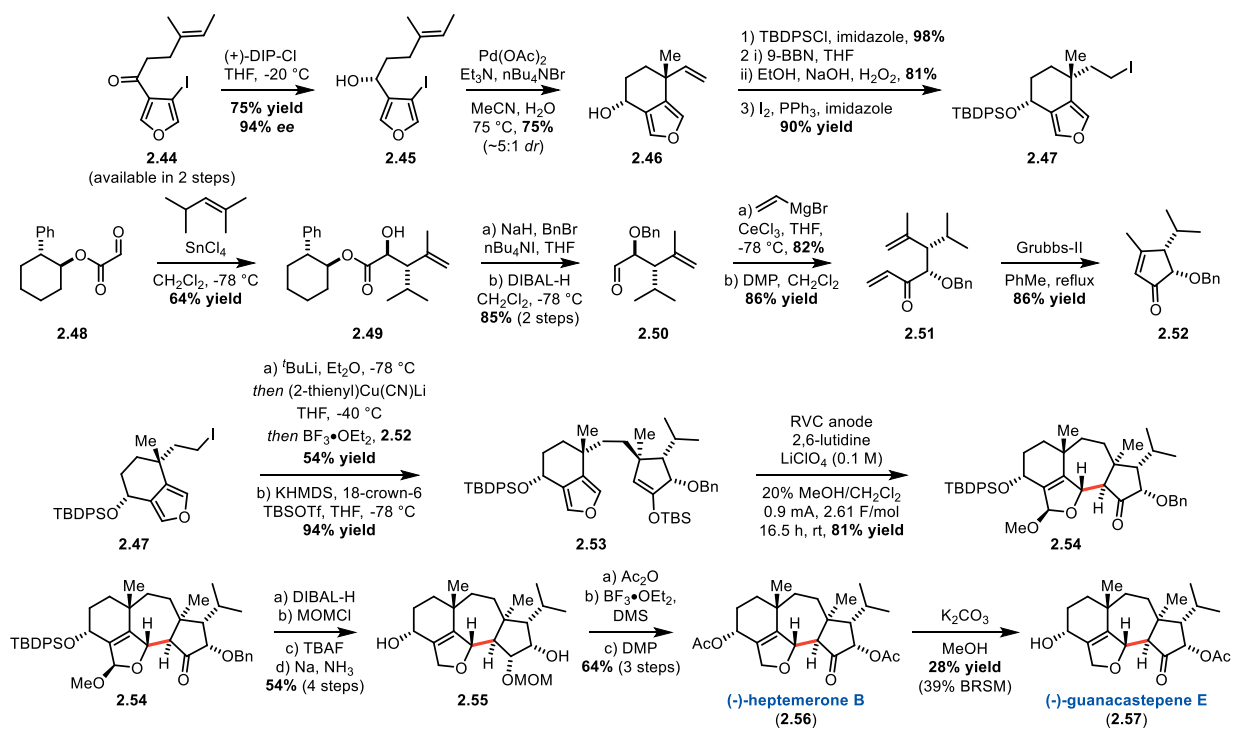


Figure 2.8. Trauner's synthesis of (-)-heptemerone B (2.56) and (-)-guanacastepene E (2.57) using an anodic furan-enol coupling.

magnesium bromide followed by Dess-Martin-periodinane (DMP) to give diene **2.51**.⁸⁶ Finally, a ring-closing metathesis utilizing the second-generation Grubbs catalyst⁸⁷ afforded the α,β -unsaturated ketone **2.52**. At this point the two fragments were coupled by converting **2.47** to a cuprate and activating **2.52** with a Lewis-acid to promote the desired conjugate addition. Subsequent formation of the silyl enol ether set the stage for the key anodic coupling step. Drawing inspiration from the precedent established by Moeller and others (*vide supra*), **2.53** was subjected to galvanostatic oxidation (0.9 mA, 2.61 F/mol) at an RVC anode using 2,6-lutidine as the base with LiClO₄ (0.1 M) as the electrolyte in 20% MeOH/CH₂Cl₂. This protocol furnished the desired seven-membered ring in **2.54** in 81% yield as a single isomer. Trauner and co-workers were now set to access the desired natural products and accomplished this by reducing both the acetal and ketone in **2.54** followed by a series of protecting group manipulations to realize **2.55**. Acetylation of the two free

alcohols in **2.55** was followed by MOM deprotection and oxidation of the revealed alcohol to the ketone to deliver (-)-heptemerone B (**2.56**). Finally, (-)-guanacastepene E (**2.57**) was prepared by hydrolysis of the more sterically accessible acetate group. This excellent contribution from Trauner and co-workers, featuring a clever fragment coupling approach, further demonstrates how electrochemical reactivity can serve to access key C–C bonds in natural product synthesis.

Recently, the Baran group has become a leader in the field of electrochemical organic synthesis, providing multiple examples of late-stage natural product functionalization enabled by electrochemistry. Their initial contributions came during their efforts to complete the total synthesis of the bis-carbazole natural product dixiamycin B (**2.61**) in 2014 (Figure 2.9).⁸⁸ Having prepared xiamycin A (**2.60**) in 14 steps, the final challenge facing Baran and co-workers was the N–N dimerization required to deliver **2.61**. These researchers were unable to effect the dimerization of simple carbazole (**2.58**) as a model system after evaluating a range of traditional chemical oxidants; therefore, they turned to electrochemistry in an attempt to solve this problem. Analysis by cyclic voltammetry revealed the onset potential for oxidation to be near +1.2 V, and bulk electrolysis experiments revealed conditions at which the model dimerization would occur. Treatment of carbazole (**2.58**) to oxidation at a carbon anode under potentiostatic conditions (+1.2 V

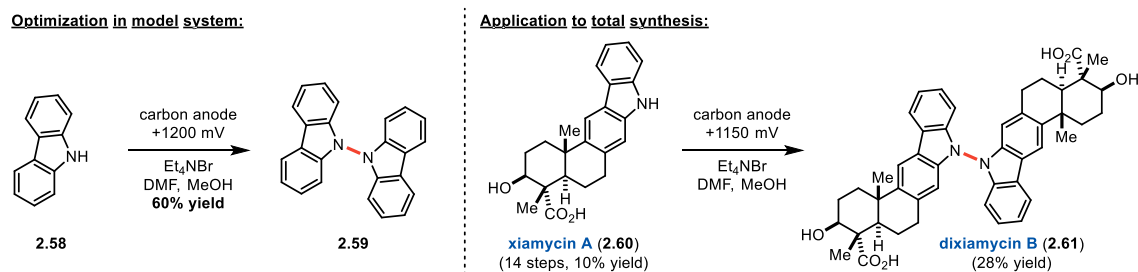


Figure 2.9. Baran's synthesis of dixiamycin B (2.61) featuring an oxidative electrochemical N–N dimerization as the final step.

vs. Ag/AgCl, 18 h) with Et₄NBr (0.1 M) as the electrolyte in 5% MeOH/DMF afforded 60% yield of the desired product (**2.59**). These conditions were applied to the dimerization of xiamycin A (**2.60**) with only slight variation (+1.15 V vs. Ag/AgCl) and the desired product dixiamycin B (**2.61**) was accessed in 28% yield. The Baran group has contributed numerous electrochemical methods following this initial report, including a robust allylic oxidation protocol,⁸⁹ in addition to review⁵⁷ and tutorial⁶⁴ articles describing contemporary uses of electrochemistry for synthesis.

The examples presented highlighted how anodic electrochemistry has been employed for natural product synthesis; however, it is important to note that cathodic chemistry has also been utilized for complex molecule and natural product synthesis.^{57,58} The following section describes our own foray into this exciting and continually growing field.

2.3 Electrochemical Dimerization of Phenylpropenoid Scaffolds

Polyphenolic natural products arising from stilbene- or styrene-derived monomers have drawn substantial interest due to a wide range of observed biological activities, including their widely-touted antioxidant properties.^{90,91} Within this broad class of secondary metabolite natural products, resveratrol and its oligomers have recently received significant attention,⁴⁴ inspiring our efforts in the Stephenson group to synthesize these natural products for biological evaluation (see Section 1.5.2 for a discussion of the synthetic efforts that occurred in the Stephenson group prior to projects described herein).^{45,48} The synthetic approach we have adopted in the Stephenson group has been to target these molecules with biomimetic synthesis based on the hypothesis that resveratrol oligomerization proceeds through phenoxy radical intermediates (see Section 3.1 for a full discussion of the biosynthetic hypothesis for resveratrol and its oligomers). Other research groups following

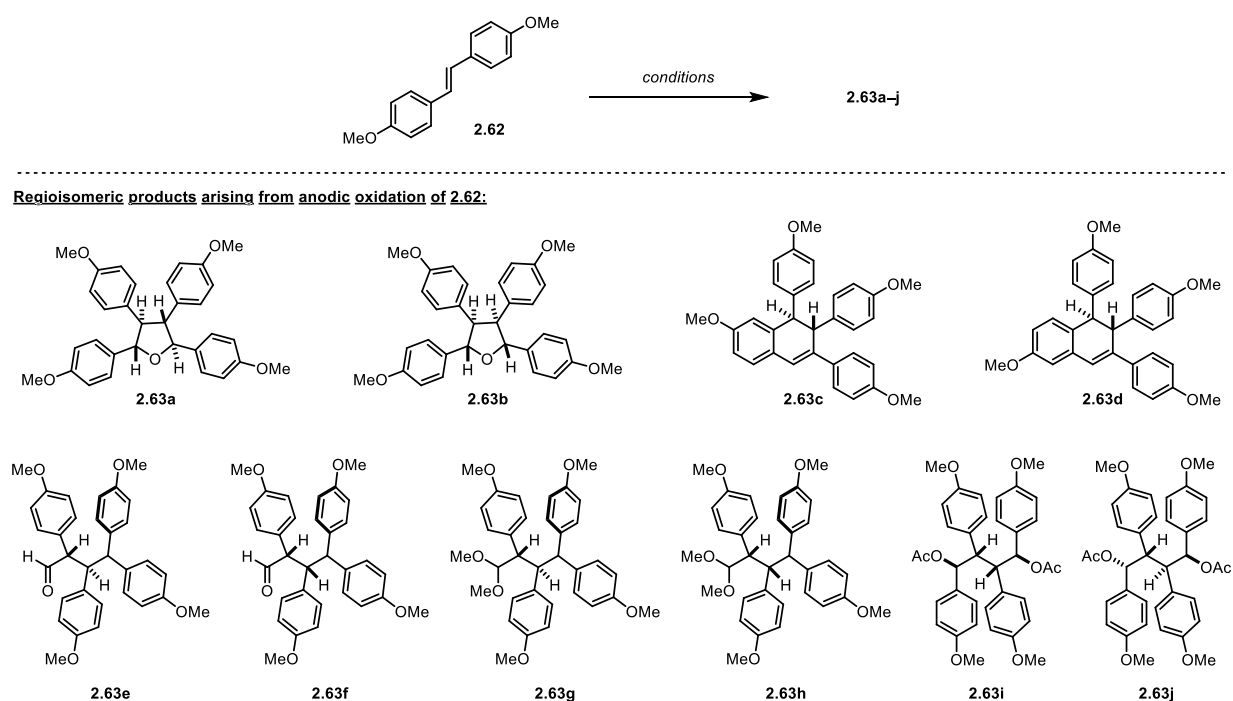
this synthetic strategy have used enzymatic catalysis or single-electron oxidants for the dimerization of resveratrol-derived scaffolds.^{44,92-94} My colleagues in the Stephenson group, Dr. Bryan Matsuura and Dr. Mitch Keylor, developed a reaction protocol that employed ferrocenium hexafluorophosphate as a mild stoichiometric oxidant to promote dimerization of protected resveratrol derivatives, which ultimately enabled the total synthesis of several dimeric and tetrameric resveratrol natural products.^{45,48} While these conditions were high-yielding and afforded excellent regioselectivity, we sought to develop a catalytic method that would translate more readily to other systems, especially those that may be prone to overoxidation. We previously investigated the use of photocatalysis to achieve this goal.⁴⁵ Unfortunately, competing energy transfer pathways resulted in stilbene isomerization, while stoichiometric terminal oxidants led to decomposition of the products and/or starting materials. Therefore, an alternative method for catalytic phenol oxidation was desired.

Anodic electrochemistry offered an attractive option to achieve a mild and catalytic dimerization protocol as it has been broadly employed in natural product and complex molecule synthesis (*vide supra*). However, efforts to apply this approach in the context of phenylpropenoid natural product total synthesis have been limited by low yields and lack of regiocontrol. For example, Kam and co-workers investigated the dimerization of stilbene radical cations arising from anodic oxidation, finding that, while electrochemical conditions and arene substitution had some influence on the regiochemical outcome, in all cases regioisomeric mixtures were generated (Table 2.1 & Figure 2.10).⁹⁵ Unsurprisingly, the incorporation of weak nucleophiles such as methanol and acetate resulted in the corresponding adducts resulting from nucleophilic trapping of the radical cation

Table 2.1. Products from anodic oxidation of 2.62 under varying conditions.

Entry	Conditions ^a	Isolated yield of 2.63 isomers										
		a	b	c	d	e	f	g	h	i	j	total
1	MeCN/0.2 M LiClO ₄ , +0.84 V	56	22	1	5	5						89
2	MeCN/0.2 M LiClO ₄ ^b , +0.84 V	17	8	4	22							51
3	1% H ₂ O/MeCN/0.2 M LiClO ₄ ^b , +0.88 V	38	20	2	7	3						70
4	25% MeOH/DCM/0.2 M LiClO ₄ , +0.80 V					11	3	28	14			56
5	25% MeOH/DCM/0.2 M LiClO ₄ ^b , +0.80 V							40	10			50
6	0.25 M NaOAc, 25% AcOH/MeCN/0.1 M LiClO ₄ , +0.80V									40	22	62

^aPt anode, Pt cathode, vs Ag/AgNO₃, ^bNonaqueous workup

**Figure 2.10. Anodic oxidation of 2.62 affords complex mixtures of products (2.63a-j).**

intermediates. The researchers followed up this study with a second report investigating the influence of ortho-substituted nucleophilic groups during anodic stilbene oxidation.⁹⁶

Again, complex product distributions were realized, with arene substitution and reaction conditions having only modest influence on the outcome. Watanabe and co-workers also took an anodic oxidation approach for the synthesis of furofuran lignans yangambin (**2.68a**), sesamin (**2.68b**), and eudesmin (**2.68c**) (Figure 2.11). They utilized L-proline as a chiral auxiliary to influence the stereochemical outcome of the dimerization step with

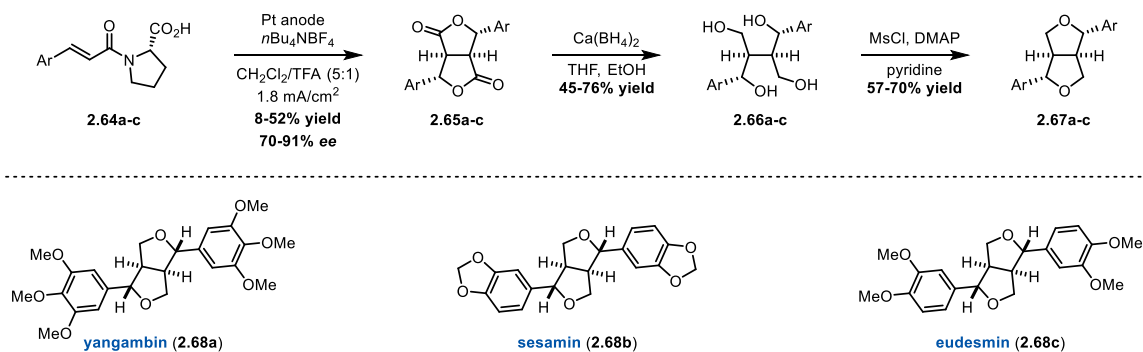


Figure 2.11. Watanabe's approach to furofuran lignans based on electrochemical dimerization of cinnamic acid derivatives.

modest to good enantioselectivity, but the yields of this key step were modest at best. Conversion of the dilactone scaffold **2.65** to the desired natural products occurred by reduction and activation/elimination, and after recrystallization the authors were able to access the enantiomerically pure natural products.

Given the state of the art in the field, we posited that an electrochemical approach to resveratrol dimerization would be a nice contribution; furthermore, we hypothesized that we might be able to expand the scope of dimerization substrates beyond our prior ferrocenium-mediated conditions. Though sometimes viewed as intimidating, the setup of electrochemical reactions is quite straightforward, and, for anodic chemistry, many reactions can be conducted on the benchtop open to the atmosphere. As a result, we also hypothesized that the development of an electrochemical dimerization protocol would prove to be enabling for the synthesis of additional resveratrol-derived oligomeric natural products.

To determine whether the desired dimerization reaction would be feasible under anodic oxidation conditions, we began by interrogating the oxidation potential of the target substrate (**1.150**) using cyclic voltammetry (Figure 2.12). Alongside Dr. Irene Bosque, it was discovered that direct oxidation of **1.150** begins to occur above +0.6 V (vs. Ag/AgCl)

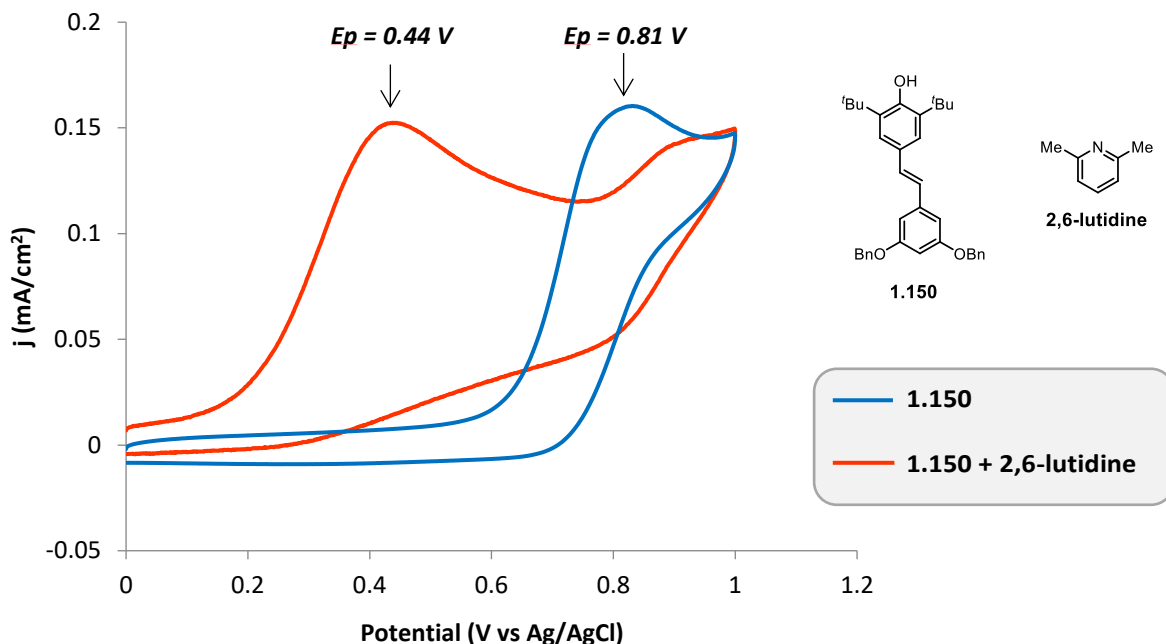
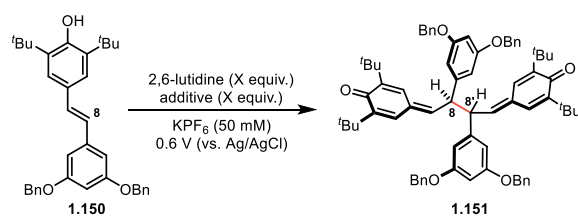


Figure 2.12. Measurement of the oxidation potential of 1.151 by cyclic voltammetry. with a peak oxidation potential of +0.81 V. The inclusion of a weak base, 2,6-lutidine, served to decrease the oxidation potential of the system, as oxidation began to occur substantially above +0.2 V, with a peak oxidation potential of +0.44 V. This result is consistent with observations by Corduneanu and co-workers in their investigation of the effect of pH on the oxidation potential of resveratrol in which they also noticed a lowering of the oxidation potential through the addition of base.⁹⁷ This presumed proton-coupled oxidation presented exactly the mild reaction conditions desired for the development of an anodic dimerization protocol for **1.150**.⁹⁸ The initial attempt at electrochemical dimerization of **1.150** sought to recapitulate the ferrocenium-mediated conditions,⁴⁵ positing that the well-known, low and reversible oxidation potential of ferrocene ($E_{1/2}$ (Fc⁺/Fc) = 0.40 V vs SCE) would allow for the use of sub-stoichiometric equivalents of the oxidant.⁹⁹ Gratifyingly, an excellent yield was achieved using only 10 mol% of ferrocene and 2 equivalents of 2,6-lutidine (Table 2.2, Entry 1). It was speculated that the oxidative dimerization of **1.150** could occur without the need for a metal catalyst; indeed

Table 2.2. Optimization of Electrochemical Dimerization Procedure.

Entry	Scale (mmol)	Additive (equiv.)	2,6-lut. (equiv.)	Solvent (ratio)	Time (h)	Isolated Yield (%)
1	0.1	Fc (0.1)	2.0	MeCN	0.5	94
2	0.1	-	2.0	MeCN	0.5	99
3	0.1	-	0.2	MeCN	0.5	99
4	0.1	-	0	MeCN	0.5	0
5	0.3	-	0.2	MeCN	1	90
6	0.3	-	0.2	MeCN:CH ₂ Cl ₂ (2:1)	1	95
7	0.9	-	0.2	MeCN:CH ₂ Cl ₂ (2:1)	5	99
8	3.6	-	0.2	MeCN:CH ₂ Cl ₂ (2:1)	12	95
9	193	-	2.0	MeCN:CH ₂ Cl ₂ (3:2)	18	99

the bulk electrochemical processing of monomer **1.150** proved highly effective in the absence of ferrocene as an electrochemical mediator (Table 2.2, Entry 2), generating the desired product in near quantitative yield after just 30 min at +0.6 V. Furthermore, it was observed that only a sub-stoichiometric amount of base was needed (Table 2.2, Entry 3), and the reaction did not occur at the same set potential when base was excluded (Table 2.2, Entry 4). Upon increasing the scale of the reaction (from 0.1 mmol to 0.3 mmol), deposition of insoluble dimeric products on the surface of the electrodes was found to inhibit the reaction (Table 2.2, Entry 5), an issue that was ameliorated through the addition of dichloromethane as a co-solvent. Importantly, these optimized conditions proved readily scalable (Table 2.2, Entries 6-9), including operation on multi-gram scale while still maintaining high yields ($\geq 95\%$). In addition to the efficiency, the operational simplicity of this method is viewed as a definitive benefit, as it is carried out on the benchtop, open to atmosphere, and only requires the addition of an electrolyte and a single, readily available

reagent. Furthermore, column chromatography is generally not required, increasing the attractiveness of this method for multi-step synthetic routes. This is best reflected in Entry 9 of Table 2.2, which represents a 100 gram scale reaction that was conducted by my colleague Matt Galliher, resulting in a conversion rate of ~11 mmol/hr (or ~5.5 g/h) to access this key synthetic intermediate (**1.151**). Remarkably, this reaction was conducted on the benchtop in a 4-L beaker, requiring only ~3.2 L of solvent and reaching completion after just 18 hours. Unfortunately, Entry 9 was conducted after the paper describing this method was published, but nonetheless it represents a remarkable example of the potential that electrochemistry holds for enabling natural product synthesis.

With these optimized and scalable conditions in hand, the scope of this reaction was next evaluated. Given the knowledge that **1.156** (the radical arising from C8–C8' homolysis of **1.151**) was persistent, we envisioned that the synthesis of a range of these compounds would enable a physical organic evaluation of the variables contributing to their persistence. The corresponding stilbene substrates were prepared from the benzyl halides or benzaldehydes using the ever reliable Wittig olefination.¹⁰⁰ Variation of the resorcinol protecting group (**2.69a-b**), including the oxidatively labile PMB ether,¹⁰¹ did not have a significant effect on the outcome of the dimerization reaction (Figure 2.13). When the *tert*-butyl substituents at C3 were exchanged with trialkylsilyl groups (**2.69c-d**), the yield diminished presumably due to the decreased persistence of the corresponding radical precursor which was previously measured by laser flash photolysis (LFP) by our collaborators in the Pratt group at the University of Ottawa.⁴⁸ It was apparent that both electron-withdrawing and electron-donating groups were tolerated at each position of the parent resorcinol ring, as reactions proceeded with a wide-variety of electronically distinct

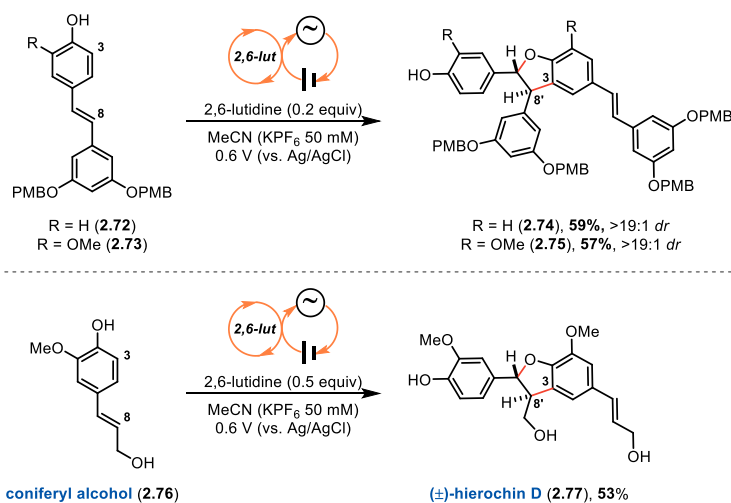


Figure 2.14. Electrochemical C3–C8' dimerization occurs for multiple phenylpropenoid monomers.

purification, which is highly advantageous for multi-step synthesis and provides an attractive alternative to stoichiometric dimerization methods.

The removal of one of the C3 blocking groups resulted in C3–C8' dimerization, enabling direct access to the cores of the natural products δ -viniferin (**2.74**) and shegansu B (**2.75**) exclusively as the *trans*-diastereomers (Figure 2.14), consistent with prior biomimetic dimerization studies of these types of hydroxystilbenes.⁹¹ As a result, the regioselectivity for this transformation is controlled exclusively by the presence or absence of a C3-blocking group. Furthermore, based upon the shared biosynthetic hypothesis between resveratrol and lignan dimers,⁴⁴ the electrochemical dimerization strategy was extended to the lignol monomer coniferyl alcohol (**2.76**). While minimal conversion was observed under the optimized conditions, simply increasing the amount of 2,6-lutidine afforded modest conversion to the neolignan dimer hierochin D (**2.77**) (Figure 2.14). As a result, we developed a unified electrochemical dimerization method for phenylpropenoid scaffolds to enable facile synthesis of these complex molecules.

2.4 Synthesis and Biological Evaluation of Natural Product Analogs

Having developed a mild, operationally simple, and scalable electrochemical dimerization protocol, the next goal was to utilize this method to facilitate the synthesis of resveratrol oligomer analogs for biological study. The Stephenson group had previously teamed up with the Pratt group at the University of Ottawa to investigate the antioxidant activity of quadrangularin A (**1.152**) and pallidol (**1.153**), and this project was a direct follow-up to that earlier study.⁴⁵ Resveratrol (**2.78**) and the oligomers derived from it have garnered wide-spread attention due to their purported therapeutic potential,^{102,103} and it has been proposed that the biological mechanism of action for these polyphenolic compounds is to act as radical-trapping antioxidants (RTAs). While this hypothesis is reasonable from a thermodynamic perspective, RTA activity is a function of kinetics, and, most importantly, evaluation of these kinetics must occur in biologically relevant systems.¹⁰⁴ With that in mind, my colleagues set out to evaluate the RTA hypothesis for resveratrol activity. They compared peroxy radical trapping activities in homogeneous organic solution, lipid bilayers, and cell culture (Table 2.3). It is well established that peroxy radicals are involved in lipid peroxidation, and this process has been associated with numerous degenerative diseases against which resveratrol has been implicated to be active.^{105,106} The solution studies were conducted in chlorobenzene utilizing the peroxy radical clock approach,^{107,108} which is a kinetic competition experiment by which the rate constant for peroxy radical inhibition (k_{inh}) for a given antioxidant is derived from antioxidant concentration dependence of lipid autoxidation products. As seen in Table 2.3, none of the compounds evaluated performed better than α -tocopherol (**2.82**), which is a component of vitamin E and nature's ubiquitous radical-trapping antioxidant.¹⁰⁹ These results alone suggest that this

Table 2.3. Comparison of radical trapping antioxidant activity of resveratrol, pallidol, quadrangularin A and their synthetic precursors with α -tocopherol and BHT.⁴⁵

Compound	Solution		Lipid Bilayers		Cells	Cytotoxicity
	k_{inh}^a (PhCl) / $M^{-1}s^{-1}$	$k_{rel, b} n^c$ (ROO• _{lipid}) ^d	$k_{rel, b} n^c$ (ROO• _{aq}) ^d	EC_{50} / μM	EC_{50} / μM	
2.78	2.0×10^5	<0.01	<0.01	12.6 ± 0.9	118 ± 14	
1.153	8.5×10^4	<0.01	<0.01	8.1 ± 0.9	205 ± 11	
1.152	2.3×10^5	<0.01	<0.1	3.4 ± 0.4	63.5 ± 3.0	
2.82	3.2×10^6	$1.8 \pm 0.2, 2.0$	$1.3 \pm 0.1, 2.0$	0.15 ± 0.01	>100	
2.79	$(5.9 \pm 0.8) \times 10^4$	$17.9 \pm 3.3, 1.8 \pm 0.1$	$21.0 \pm 6.8, 1.8 \pm 0.1$	0.051 ± 0.004	10.2 ± 0.3	
2.81	$(2.1 \pm 0.3) \times 10^4$	<0.01	<0.01	0.39 ± 0.07	10.2 ± 0.4	
2.80	$(6.2 \pm 0.9) \times 10^4$	$7.5 \pm 0.6, 1.9 \pm 0.1$	<0.1	0.21 ± 0.03	8.7 ± 0.5	
2.83	$(2.2 \pm 0.1) \times 10^4$	<0.01	<0.01	12.7 ± 1.5	49.5 ± 2.0	

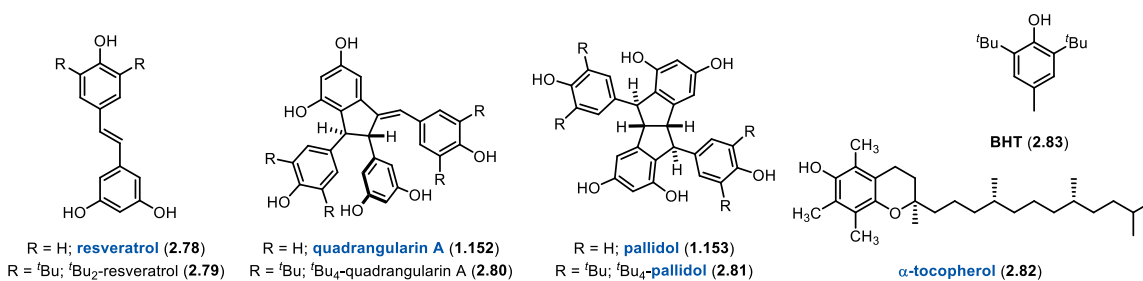


Figure 2.15. Compounds evaluated for initial study of radical-trapping activity.

set of resveratrol-derived compounds do not owe their biological activities to a radical-trapping mechanism. Analysis of RTA activity in lipid bilayers was again conducted using a kinetic competition, in this case using a fluorogenic α -tocopherol derivative to determine relative rates of activity (k_{rel}),^{110,111} the results of which can be found in Table 2.3. The only compounds that demonstrated activity relative to the fluorophore were *tert*-butyl-resveratrol (**2.79**) and *tert*-butyl-quadrangularin A (**2.80**). These two compounds also demonstrated activity with greater potency than α -tocopherol (**2.82**) in cellular assays; as a result, we sought to utilize the newly developed electrochemical dimerization protocol to follow up on these data.

The preparation of analogs of **2.79** had already been completed, as these compounds were the precursors to **2.69e-o** (see Figure 2.13); therefore, conversion of **2.69e-o** to the corresponding ^tBu₄-quadrangularin A (**2.80**) analogs was required for the desired follow up

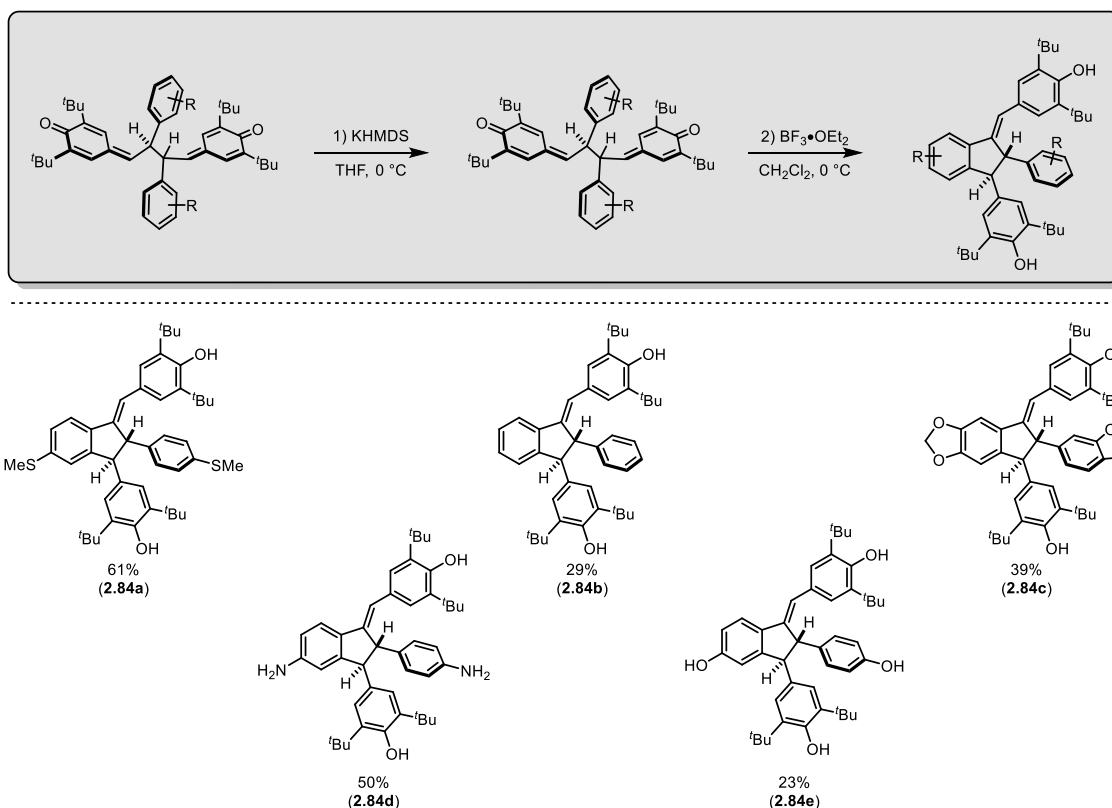


Figure 2.16. Preparation of *t*Bu₄-quadrangularin A analogs to evaluate RTA activity.

study. This was accomplished following the route developed previously for the synthesis of **1.152** (Figure 2.16). First, isomerization of one of the quinone methides in the **2.69** scaffold to the *trans*-stilbene was accomplished by treatment with base. Next, a Friedel-Crafts cyclization onto the remaining quinone methide was achieved upon Lewis-acid activation to deliver the desired analogs. Unfortunately, the compounds with electron-withdrawing groups (derived from **2.69k-o**) did not cyclize, even upon exposure to elevated temperatures, limiting the scope of analogs that were prepared by this approach.

The biological analysis discussed for the remainder of this section (as well as the work described in Section 2.5) was conducted by collaborators in Prof. Derek Pratt's research group at the University of Ottawa – Dr. Mark Raycroft and Dr. Jean-Philippe Chauvin – whose contributions and insight were instrumental in understanding the activity of these

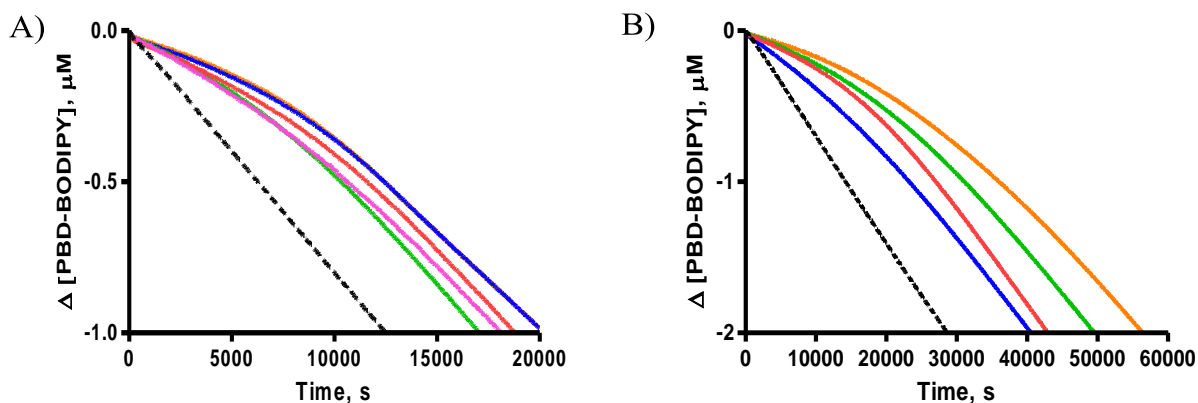
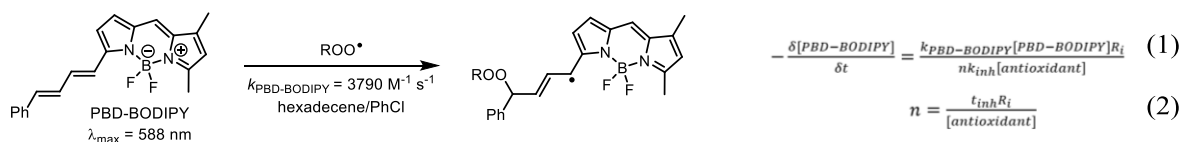


Figure 2.17. Representative data for the RTA activity of the A) resveratrol and B) quadrangularin A analogs.

compounds. The resveratrol and quadrangularin A analogs were evaluated for their ability to inhibit co-oxidations of PBD-BODIPY and 1-hexadecene in chlorobenzene at 37 °C (Figure 2.17).¹¹² PBD-BODIPY enables quantitative determination of the reaction progress of the autoxidation by UV-vis spectrophotometry; its consumption by reaction with chain-carrying peroxy radicals is associated with a loss of absorbance at 588 nm (Figure 2.17). The uninhibited decay of PBD-BODIPY is represented by the black line in each plot. Both the resveratrol (Figure 2.17A) and quadrangularin A (Figure 2.17B) analogs slow down the rate of decay of PBD-BODIPY, however neither completely inhibits autoxidation, which would be observed as a horizontal line indicating complete preservation of absorbance at 588 nm. Kinetic analysis of the reaction progress data according to Eqs. 1 and 2 enables determination of the rate constant for the reaction of the RTA with peroxy radicals (k_{inh}) as well as the reaction stoichiometry (n). The full set of data for these experiments is tabulated in Section 2.7, and the general trends in the data are described here. The quadrangularin A analogs are all good RTAs, as their inhibition rate constants are roughly

one order of magnitude greater than BHT (**2.83**, $k_{\text{inh}} = 2 \times 10^4 \text{ M}^{-1}\text{s}^{-1}$), the quintessential hindered phenolic RTA.⁴⁵ Substitution around the resorcinol ring has little impact on the reactivity of the quadrangularin A analogs, and most k_{inh} values are within experimental error of each other. These results are consistent with the hypothesis that quadrangularin A and its *tert*-butylated derivatives inhibit autoxidation via H-atom transfer from the (hindered) phenolic moiety. The same can be said for the resveratrol analogs as well; the k_{inh} for all compounds evaluated is on the order of $10^5 \text{ M}^{-1}\text{s}^{-1}$; substitution of the resorcinol ring in the parent compound has minimal effect on the radical-trapping activity. While these compounds outstrip BHT (**2.83**), they still leave something to be desired when compared to α -tocopherol (**2.82**, $k_{\text{inh}} \sim 10^6 \text{ M}^{-1}\text{s}^{-1}$). These results only serve to further support the hypothesis that the biological activity of resveratrol (and resveratrol-derived oligomers) does not involve peroxy radical trapping.

2.5 Quinone Methide Dimers are Potent Radical Trapping Antioxidants

The resveratrol and quadrangularin A analogs demonstrated good, but not excellent, RTA activity. During the course of this investigation, we began to question how the quinone methide dimers (QMDs) might perform as RTAs. Initially, it was hypothesized that the two equivalents of persistent radical derived from each QMD would serve as a radical trap in the same way that TEMPO can be used to interrogate radical mechanisms through the persistent radical effect (see Section 1.4 for a discussion of the persistent radical effect).⁷ One well established problem with hindered phenols (i.e. BHT, **2.83**) as RTAs is the inverse temperature dependence for their activity. Hindered phenols function by first succumbing to hydrogen atom transfer (HAT) to “trap” one equivalent of a radical species, followed by radical-radical combination, forming a peroxide in the case of peroxy radical inhibition,

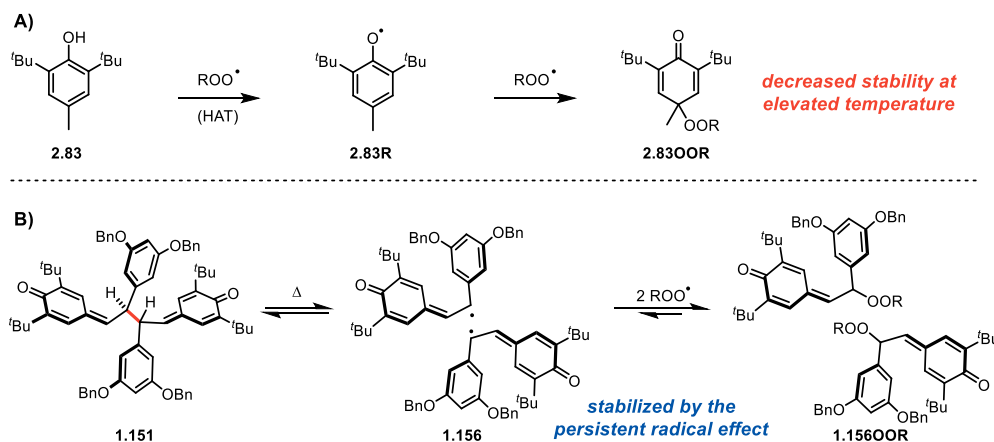


Figure 2.18. A) Mechanism of Peroxyl Inhibition for hindered phenols. B) Mechanistic Hypothesis of Peroxyl Inhibition with QMDs.

to “trap” the second equivalent (Figure 2.18A). Peroxides such as **2.83OOR** have decreased stability at elevated temperature, and decomposition regenerates an equivalent of peroxy radical, thereby mitigating the radical trapping activity. Given the previously established equilibrium between QMD **1.151** and persistent radical **1.156**, and in particular the knowledge that the equilibrium favors formation of **1.156** at elevated temperatures,⁴⁸ it was hypothesized that QMDs such as **1.151** could actually be more potent RTAs at elevated temperature (Figure 2.18B). Therefore, the same RTA analysis was conducted on the set of QMDs that were generated from electrochemical dimerization, and, gratifyingly, these compounds were excellent RTAs. As seen in Figure 2.19, in all cases the QMDs studied

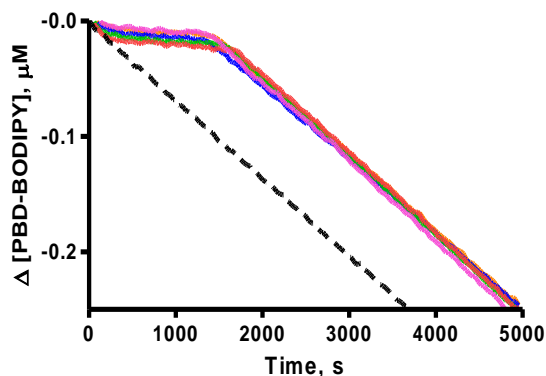


Figure 2.19. Representative data for the RTA activity of quinone methide dimers.

fully inhibit autoxidation of PBD-BODIPY, which is indicated by the horizontal line for the first 2000 seconds of the experiment. Once the antioxidant is fully consumed, the absorbance at 588 nm falls off at the same rate as the uninhibited line (black), resulting in the discontinuity observed in Figure 2.19. The tabulated data (k_{inh}) for each QMD evaluated can be found in Section 2.7. In general, despite being devoid of phenolic moieties, the QMDs are >10-fold more reactive ($k_{\text{inh}} \sim 10^6 \text{ M}^{-1}\text{s}^{-1}$) than the quadrangularin A derivatives. Interestingly, monomeric quinone methides have been reported to be modest RTAs,¹¹³ suggesting that the QMD scaffold is unique.

Mechanistic possibilities for the surprising reactivity of the QMDs are presented in Figure 2.20. At first glance, Mechanism 1 can be excluded solely on the basis of the magnitude of k_{inh} determined from the inhibited autoxidations ($k_{\text{inh}} = 2\text{-}3 \times 10^6 \text{ M}^{-1}\text{s}^{-1}$). Hydrogen atom transfer from a C–H bond is established to be a relatively slow reaction, even when highly thermodynamically favorable.¹¹⁴ Indeed, the CBS-QB3-predicted¹¹⁵ rate constants for HAT (k_{HAT}) from a truncated form of the unsubstituted dimer to a model (methyl)peroxyl radical is a mere $6 \text{ M}^{-1}\text{s}^{-1}$ (see Section 2.7 for the optimized structures, their energies, and the rate constants estimated therefrom). Mechanism 2 requires tautomerization of the QMD; however, upon exposing NMR samples of QMD to deuterated methanol (CD_3OD), no deuterium incorporation was observed. Tautomerization of the QMD is not spontaneous and instead requires base. Furthermore, if tautomerization were to occur, the phenolic tautomer would be expected to exhibit similar reactivity to the monomeric resveratrol derivative from which the QMD is derived ($k_{\text{inh}} \sim 10^5 \text{ M}^{-1}\text{s}^{-1}$).

Although the addition of peroxyl radicals to carbon-carbon double bonds is well-known, it generally features in the propagation of autoxidation of unsaturated substrates (e.g.

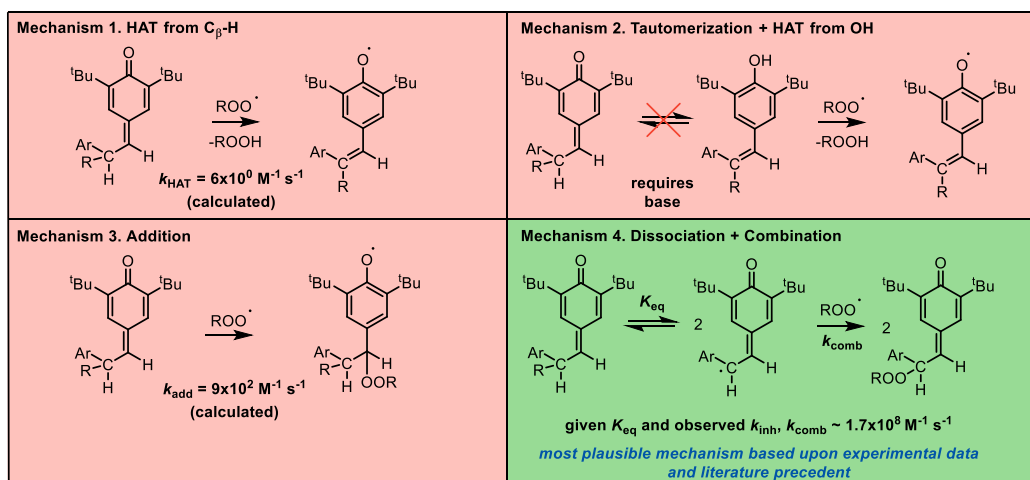


Figure 2.20. Mechanistic possibilities for RTA activity of QMDs.

styrene), not in its inhibition; as a result, Mechanism 3 has little precedent. The primary difference in the current context is that the resultant radical (a hindered phenoxyl) is unreactive to O_2 and does not propagate the autoxidation. Moreover, not only does peroxyl radical addition produce a more stabilized phenoxyl radical, the thermodynamics are also greatly enhanced by aromatization of the quinone methide. However, RTA activity is purely a function of kinetics, and CBS-QB3 predicts a rate constant (k_{add}) of $9 \times 10^2 \text{ M}^{-1} \text{ s}^{-1}$.¹ This value is in excellent agreement with results from Volodkin and co-workers in which they determined that simple quinone methides react as modest antioxidants ($k_{\text{inh}} \sim 10^3 \text{ M}^{-1} \text{ s}^{-1}$),¹¹³ however it is three orders of magnitude lower than experimental observations for the QMDs, suggesting that radical addition to the quinone methide is not the operative mechanism for the observed RTA activity.

The final possible mechanism – Mechanism 4 – corresponds to the initial hypothesis for the activity of QMDs; that is, the persistent phenoxyl radicals arising from C8–C8' homolysis capture peroxyl radicals in a manner analogous to the persistent radical effect.⁷ Upon initial consideration, this did not seem likely given the small amount of phenoxyl radical present at equilibrium in the autoxidation experiments ($K_{\text{eq}} = 5.5 \times 10^{-10} \text{ M}$ at 37°C

for **1.151/1.156**). For example, at the beginning of an autoxidation inhibited by 1 μM of **1.151**, the concentration of **1.156** is ~ 23 nM. Given the assumption that this equilibrium is established faster than propagation of the autoxidation, then $k_{\text{inh}}[\mathbf{1.151}] = k_{\text{comb}}[\mathbf{1.156}]$, such that $k_{\text{comb}} \sim 43(4.0 \times 10^6 \text{ M}^{-1} \text{ s}^{-1}) \sim 1.7 \times 10^8 \text{ M}^{-1} \text{ s}^{-1}$. This derived value for the rate constant of RTA activity for the persistent phenoxy radical **1.156** is in excellent agreement with a report from Jonsson and co-workers whereby they determined that stabilized phenoxy radicals react with peroxy radicals on the order of $10^8 \text{ M}^{-1} \text{ s}^{-1}$.¹¹⁶ These results, in addition to ongoing work from collaborators in the Pratt lab, suggest that the initial hypothesis was correct – quinone methide dimers are excellent RTAs due to the persistent radical effect. While the preceding presents a summary overview of the data supporting Mechanism 4, a complete investigation of the RTA activity of QMDs, including assays conducted in biologically relevant media (i.e. lipid bilayers) and how/why they differ from simple quinone methides is currently being finalized by collaborators in the Pratt group, and the full mechanistic analysis of these compounds will be reported in due course.

2.6 Conclusions

Electrochemistry has become an enabling tool for the generation of reactive intermediates under mild and selective reaction conditions for complex molecule synthesis. Anodic oxidation is readily coupled with the reduction of protons, perhaps the simplest electrochemical transformation, and has seen numerous applications in total synthesis. Electrochemistry will only become more widespread in organic synthesis as the technological barrier to its implementation is lowered. We have leveraged anodic oxidation for the generation of persistent phenoxy radicals from which natural products and natural product analogs are readily synthesized. The electrochemical reactions are quite robust,

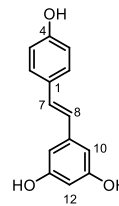
providing key synthetic intermediates (or, in one example, a natural product) in excellent yields with impressive scalability. The development of this method enabled further study of the quadrangularin A natural product scaffold, lending further support to the conclusion that resveratrol-derived natural products do not act as radical trapping antioxidants in nature. Finally, it was discovered that the quinone methide dimers arising from anodic oxidation are themselves potent radical trapping antioxidants due to a dynamic equilibrium with persistent phenoxy radicals and the persistent radical effect, and further investigation is ongoing to understand the function and potential utility of these compounds.

2.7 Experimental Procedures and Spectral Data

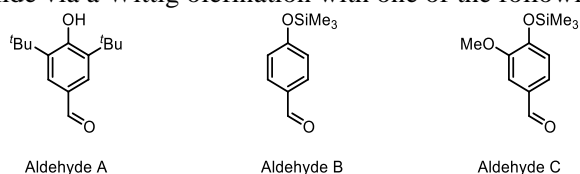
General Procedures: Unless specifically noted otherwise, all glassware was flame-dried under vacuum (~0.5 Torr) and cooled under inert atmosphere (N₂ or Ar) prior to use. Each reaction container was charged with a Teflon/PTFE-coated magnetic stir bar and sealed with a rubber septum to maintain a positive pressure of inert atmosphere (N₂ or Ar). Reagents sensitive to the atmosphere were transferred via syringe or cannula as necessary. Reaction conversion was evaluated using analytical thin-layer chromatography (TLC) using Merck silica gel 60 F254 TLC plates. TLC plates were visualized under a dual short wave/long wave UV lamp and/or stained using solutions of *p*-anisaldehyde or potassium permanganate or ceric ammonium molybdate. Stained plates were developed over a heat gun as needed. Reactions were purified via flash column chromatography either with RediSep®*R_F* Gold silica columns using a Teledyne Isco CombiFlash *R_F* automated purification system or manually using 230-400 mesh silica gel. Either sodium sulfate or magnesium sulfate were utilized to exclude water from worked up reactions, and the solvent was removed on Büchi rotary evaporators and/or a Welch vacuum pump. All electrochemical experiments were acquired using either a CH1620E electrochemical analyzer (from CH Instruments) or a uSTAT4000 4-Channel Potentiostat/Galvanostat (from Metrohm USA). Cyclic voltammetry measurements were performed in five-neck cells (3 mL) using a three-electrode set-up in which the working electrode was glassy carbon (3 mm diameter), the counter/auxiliary electrode was a platinum wire, and the reference electrode was Ag/AgCl (3 M KCl, from CHInstruments). Bulk electrolysis experiments were performed on discovery scale in open 10-mL vials and in a beaker of the appropriate size (15 – 40 mL) for the subsequent scale-up experiments. These reactions used RVC panels (reticulated vitreous carbon, 100 ppi, 0.25-inch thickness, 3% relative density, from McMaster Carr) as the working or counter/auxiliary electrodes and a Ag/AgCl (3 M KCl) reference electrode.

Reaction Materials: Commercially available reagents were used without further purification unless specified. Organic solvents (acetonitrile, dichloromethane, diethyl ether, dimethylformamide, dimethyl sulfoxide, methanol, tetrahydrofuran, and toluene) and amine bases (triethylamine, pyridine, N,N-diisopropylethylamine, and diisopropylamine) were purified prior to use with a Phoenix Solvent Drying System from JC-Meyer Solvent Systems and PureSolv Micro amine drying columns from Innovative Technology, respectively, and kept under a pressure of argon. Solutions of organolithium reagents and Grignard reagents were purchased from Acros Organics and titrated prior to use.

Product Analysis: Product names were obtained using ChemDraw Professional 16.0 from Perkin Elmer. For racemic compounds, the name corresponds to the depicted structure. Nuclear magnetic resonance (NMR) spectra were obtained using an internal deuterium lock on Varian Inova 500 or Varian VNMR 500 and 700 spectrometers. For ¹H spectra, chemical shifts were referenced to the center line of the residual solvent signal (CDCl₃: δ 7.26; acetone-*d*₆: δ 2.05) and are reported in parts per million (ppm). Signal multiplicity is reported as follows: (br = broad, s = singlet, d = doublet, t = triplet, dd = doublet of doublets, ddd = doublet of doublet of doublets, m = multiplet), and the associated coupling constants are given in Hertz. For ¹³C spectra, experiments were completely heterodecoupled (broadband) and chemical shifts are reported as ppm using the center line of the solvent signal as reference (CDCl₃: δ 77.16; acetone-*d*₆: δ 29.92). The following resveratrol numbering scheme was used for the assignment of ¹H and ¹³C NMR signals. High-resolution mass spectra (HRMS) were acquired using a Micromass AutoSpec Ultima Magnetic Sector mass spectrometer using electrospray ionization (ESI), positive ion mode. We thank James Windak and Paul Lennon at the University of Michigan, Department of Chemistry Instrumentation Facility for conducting the HRMS experiments. Infrared spectra were acquired using a Perkin-Elmer Spectrum BX FT-IR spectrophotometer using an ATR mount with a ZnSe crystal.



General Stilbene preparation: Unless otherwise specified, stilbene substrates were prepared from the benzyl alcohol or benzyl bromide via a Wittig olefination with one of the following aldehydes:



3,5-di-*tert*-butyl-4-hydroxybenzaldehyde (aldehyde A), commercially available;
 4-((trimethylsilyl)oxy)benzaldehyde (aldehyde B), from silyl protection of 4-hydroxybenzaldehyde;
 3-methoxy-4-((trimethylsilyl)oxy)benzaldehyde (aldehyde C), from silyl protection of vanillin.

Starting from the benzyl alcohol:

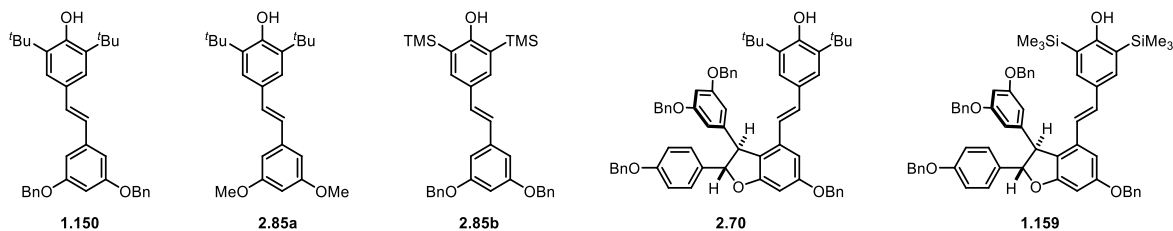
A solution of triphenylphosphine (0.97 g, 3.71 mmol) in dry THF (2.5 mL) was sparged with N₂ (18G needle, 5 min) and was added dropwise to a solution of (benzyl) alcohol (2.97 mmol) and carbon tetrabromide (1.31 3.71 mmol) in dry THF (4.5 mL) that had been previously sparged (18G needle, 5 min.) in a 50 mL flame-dried round bottom flask and chilled to 0 °C. The mixture was stirred at room temperature for 16 h followed by dropwise addition of methanol (1 mL). The mixture was diluted with EtOAc (100 mL) and added to a separatory funnel and the organic phase was washed with a 1:1:1 mixture of 10% bicarbonate solution, saturated Na₂S₂O₃, and DI water solution (100mL). The organic phase was washed with brine and dried over Na₂SO₄. The organic phase was then concentrated under reduced pressure and purified by silica gel (pre-neutralized) column chromatography and eluted with 10:1 (hexane/ ethyl acetate) to afford the brominated product.

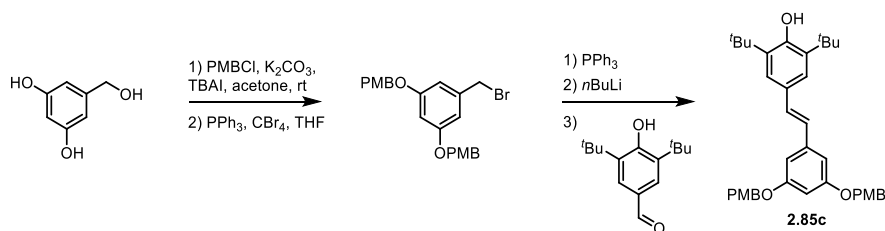
Starting from the benzyl bromide:

The benzyl bromide was added to a flame-dried round bottom flask charged with a stir bar and fitted with a reflux condenser and dissolved in toluene (0.15 – 0.20 M). To the stirring solution was added triphenylphosphine (1.5 equiv.), and the reaction was heated to 100 °C for 12 hours. After cooling the reaction mixture to room temperature, the white phosphonium salt was collected via vacuum filtration, and any excess triphenylphosphine was rinsed away with hexanes. The phosphonium salt was dried under vacuum for >24 hours prior to use in the Wittig olefination to ensure full removal of residual solvent and water.

The phosphonium salt was added to a flame-dried, 3-neck, round bottom flask charged with stir bar and fitted with a reflux condenser. The salt was suspended in solvent (toluene or THF, 0.1 M), and to the stirring mixture was added *n*BuLi (1.6 or 2.5 M, 1.00 equiv.). After 30 minutes, the reaction mixture had become a brilliant red, clear solution, at which point the aldehyde was added under a stream of nitrogen, and the reaction was heated at reflux for 12 hours. After cooling the reaction mixture to room temperature, the reaction was quenched with saturated aqueous ammonium chloride, diluted with ethyl acetate, and added to a separatory funnel containing additional aqueous ammonium chloride. The layers were separated, and the aqueous layer was extracted with additional ethyl acetate. The combined organic layers were washed with brine, dried over magnesium sulfate, and concentrated under reduced pressure. The crude stilbene products were purified via flash column chromatography (see characterization data for specific chromatography conditions).

The following substrates were prepared following previously reported conditions.^{45,48}





(2.85c) (*E*)-4-(3,5-bis((4-methoxybenzyl)oxy)styryl)-2,6-di-*tert*-butylphenol

Commercially available 3,5-dihydroxybenzyl alcohol (2.0 g, 14.3 mmol) was added to flask charged with potassium carbonate (2.25 equiv., 4.44 g) and tetrabutylammonium iodide (0.2 equiv., 1.05 g), and the solids were dissolved/suspended in acetone (42 mL). To the stirring reaction mixture was added 4-methoxybenzyl chloride (2.20 equiv., 4.26 mL), and the reaction was allowed to stir at room temperature for 16 hours. Upon completion, the reaction was diluted with ethyl acetate and poured into a separatory funnel containing deionized water. The layers were separated, and the aqueous layer was extracted with additional portions of ethyl acetate. The combined organic layer was washed with brine, dried over magnesium sulfate, and concentrated under reduced pressure to afford the crude product, which was carried forward without further purification. The PMB-protected material (2.18g, 5.72 mmol) was subjected to the general procedure using toluene as the solvent for the olefination with aldehyde A. The product was purified by column chromatography (4% to 28% ethyl acetate in hexanes) to afford (*E*)-4-(3,5-bis((4-methoxybenzyl)oxy)styryl)-2,6-di-*tert*-butylphenol (2.06g, 62% yield).

$R_f = 0.22$ (ethyl acetate/hexanes 1:9; UV)

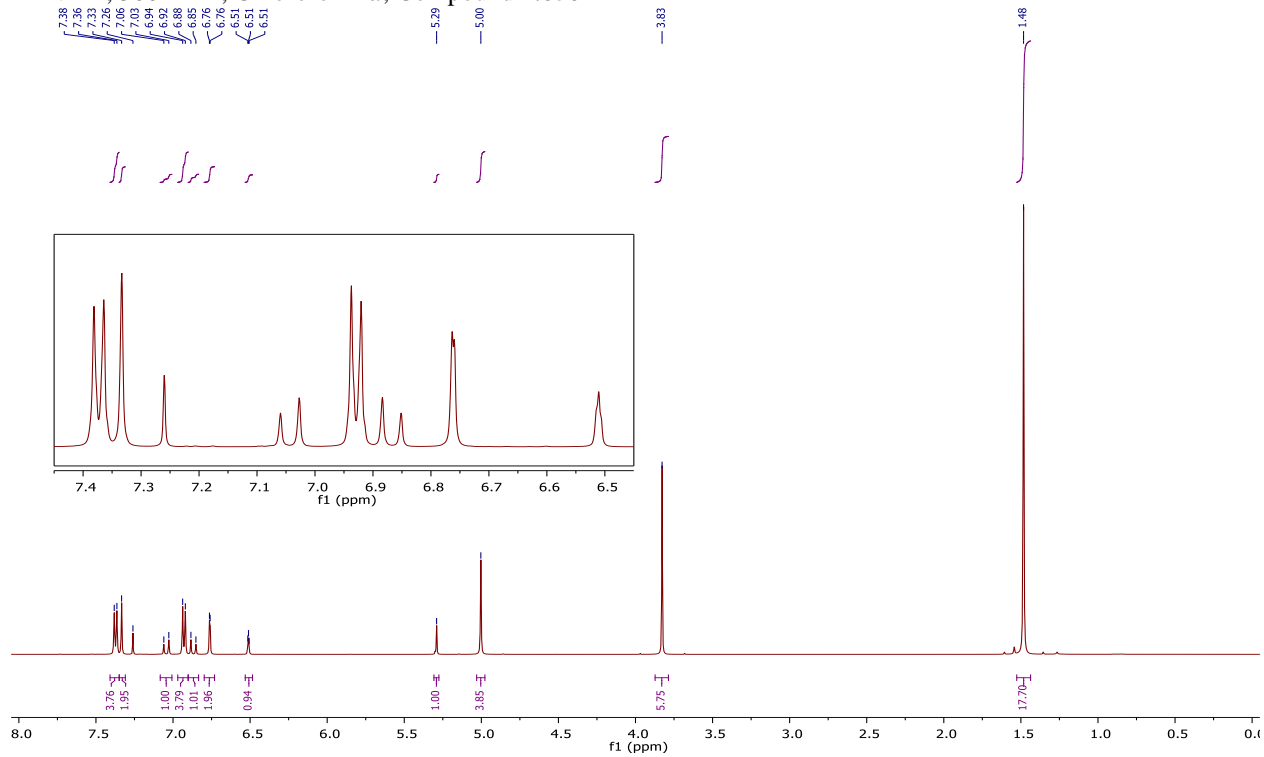
$^1\text{H NMR}$ (500 MHz, Chloroform-*d*) δ 7.37 (d, $J = 8.6$ Hz, 4H), 7.33 (s, 2H), 7.04 (d, $J = 16.1$ Hz, 1H), 6.93 (d, $J = 8.6$ Hz, 4H), 6.87 (d, $J = 16.1$ Hz, 1H), 6.76 (d, $J = 2.2$ Hz, 2H), 6.51 (t, $J = 2.2$ Hz, 1H), 5.29 (s, 1H), 5.00 (s, 4H), 3.83 (s, 6H), 1.48 (s, 18H).

$^{13}\text{C NMR}$ (126 MHz, Chloroform-*d*) δ 160.32, 159.61, 154.08, 140.13, 136.29, 130.26, 129.44, 129.17, 128.56, 125.92, 123.66, 114.15, 105.56, 101.24, 70.04, 55.47, 34.53, 30.43.

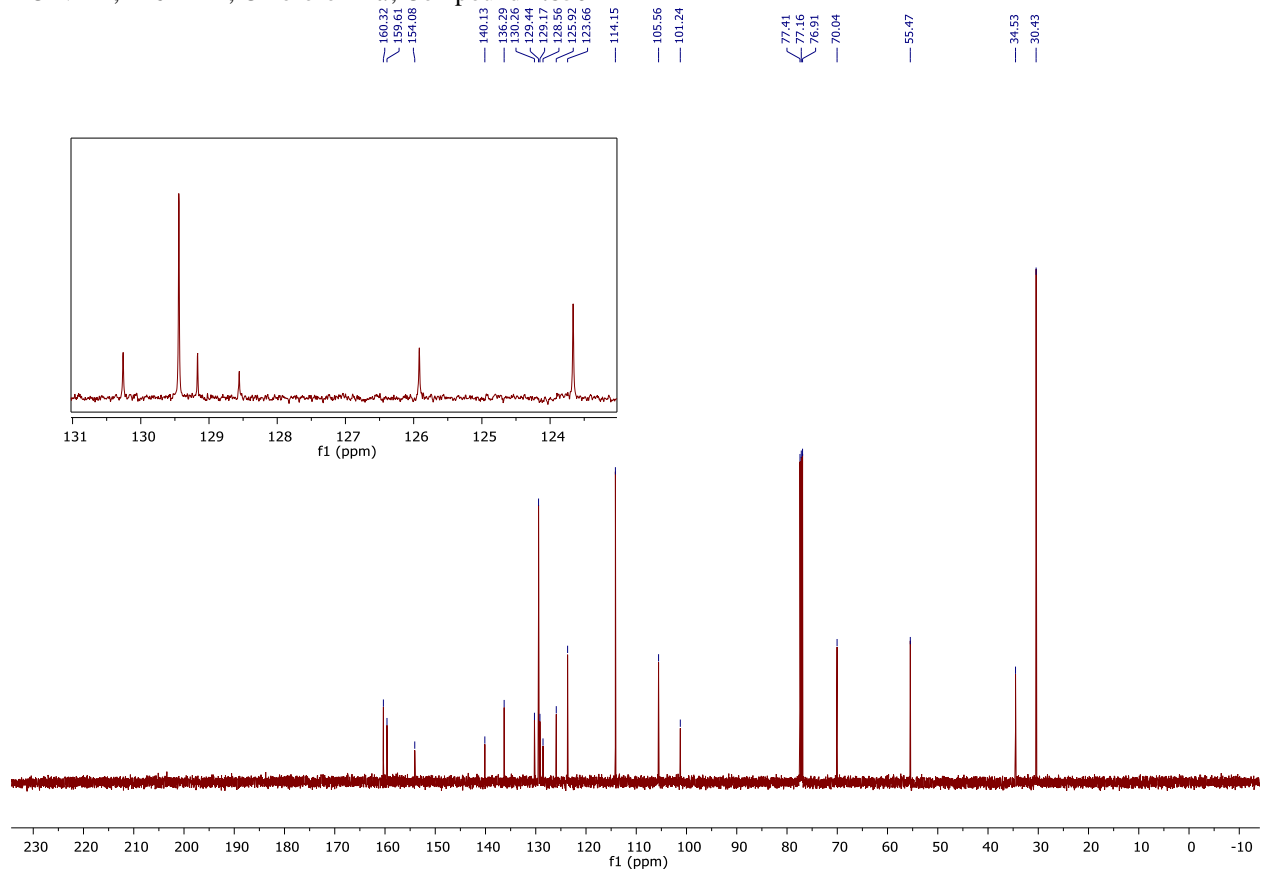
IR (Neat): 3606, 2965, 1577, 1515, 1439, 1245, 1147, 1046, 1026, 967, 858 cm^{-1} ;

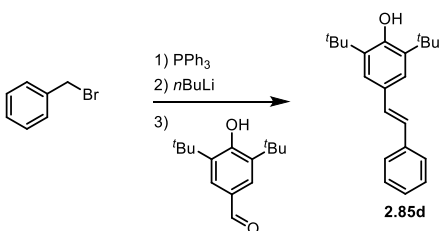
HRMS (ESI) m/z calculated for $\text{C}_{38}\text{H}_{45}\text{O}_5^+$ ($[\text{M}+\text{H}]^+$) 581.3262, found 581.3267.

¹H NMR, 500 MHz, Chloroform-*d*, Compound **2.85c**



¹³C NMR, 126 MHz, Chloroform-*d*, Compound **2.85c**





(2.85d) (*E*)-2,6-di-*tert*-butyl-4-styrylphenol

Commercially available benzyl bromide ((bromomethyl)benzene, 1.1 g, 6.4 mmol) was subjected to the general procedure using toluene as the solvent for the olefination with aldehyde A. The product was purified by column chromatography (2% to 12% ethyl acetate in hexanes) to afford (*E*)-2,6-di-*tert*-butyl-4-styrylphenol (1.64 g, 83% yield). The acquired ¹H and ¹³C NMR spectra were consistent with those reported in the literature.

R_f = 0.31 (ethyl acetate/hexanes 1:9; UV)

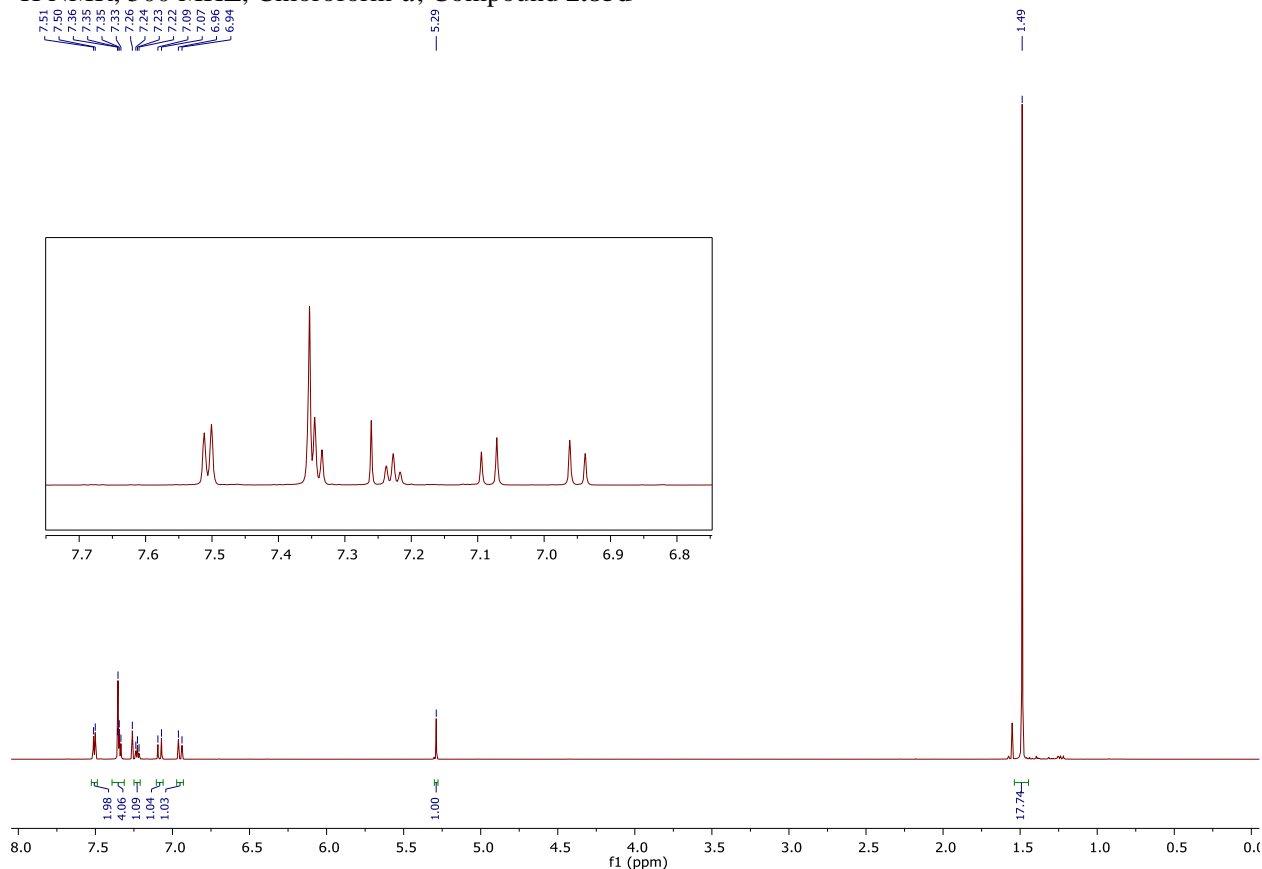
¹H NMR (500 MHz, Chloroform-*d*) δ 7.50 (d, *J* = 7.6 Hz, 2H), 7.35 (s, 2H), 7.34 (t, *J* = 7.5 Hz, 1H), 7.23 (t, *J* = 7.3 Hz, 1H), 7.08 (d, *J* = 16.3 Hz, 1H), 6.95 (d, *J* = 16.2 Hz, 1H), 5.28 (s, 1H), 1.49 (s, 18H).

¹³C NMR (126 MHz, Chloroform-*d*) δ 153.99, 138.09, 136.28, 129.70, 128.73, 127.11, 126.33, 126.00, 123.57, 34.53, 30.44.

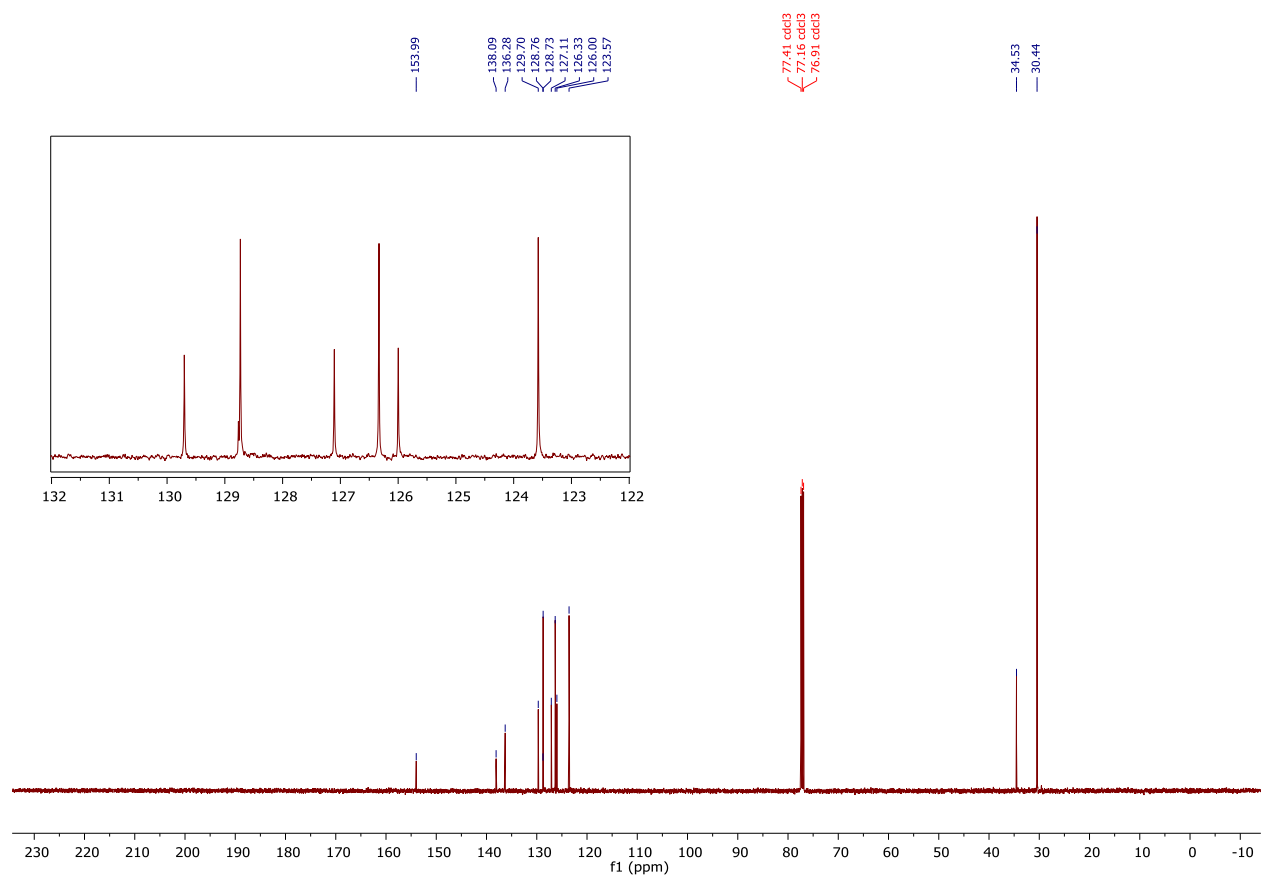
IR (Neat): 3616, 2953, 1470, 1235, 1137, 1118, 957 cm⁻¹;

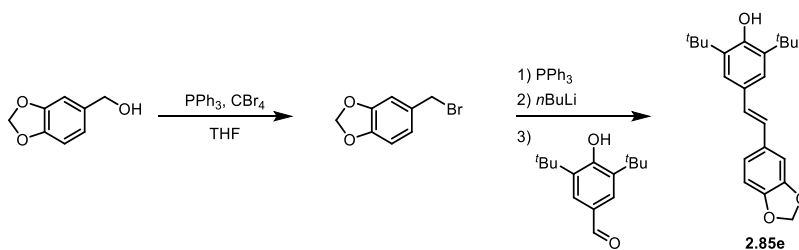
HRMS (ESI) *m/z* calculated for C₂₂H₂₉O⁺ ([M+H]⁺) 309.2213, found 309.2206.

¹H NMR, 500 MHz, Chloroform-*d*, Compound **2.85d**



^{13}C NMR, 126 MHz, Chloroform-*d*, Compound **2.85d**





(2.85e) (*E*)-4-(2-(benzo[*d*][1,3]dioxol-5-yl)vinyl)-2,6-di-*tert*-butylphenol

Commercially available benzyl alcohol (benzo[*d*][1,3]dioxol-5-ylmethanol, 1.00g, 6.6 mmol) was subjected to the general procedure using toluene as the solvent for the olefination with aldehyde A. The product was purified by column chromatography (2% to 12% ethyl acetate in hexanes) to afford (*E*)-4-(2-(benzo[*d*][1,3]dioxol-5-yl)vinyl)-2,6-di-*tert*-butylphenol (1.72 g, 74% yield).

$R_f = 0.26$ (ethyl acetate/hexanes 1:9; UV)

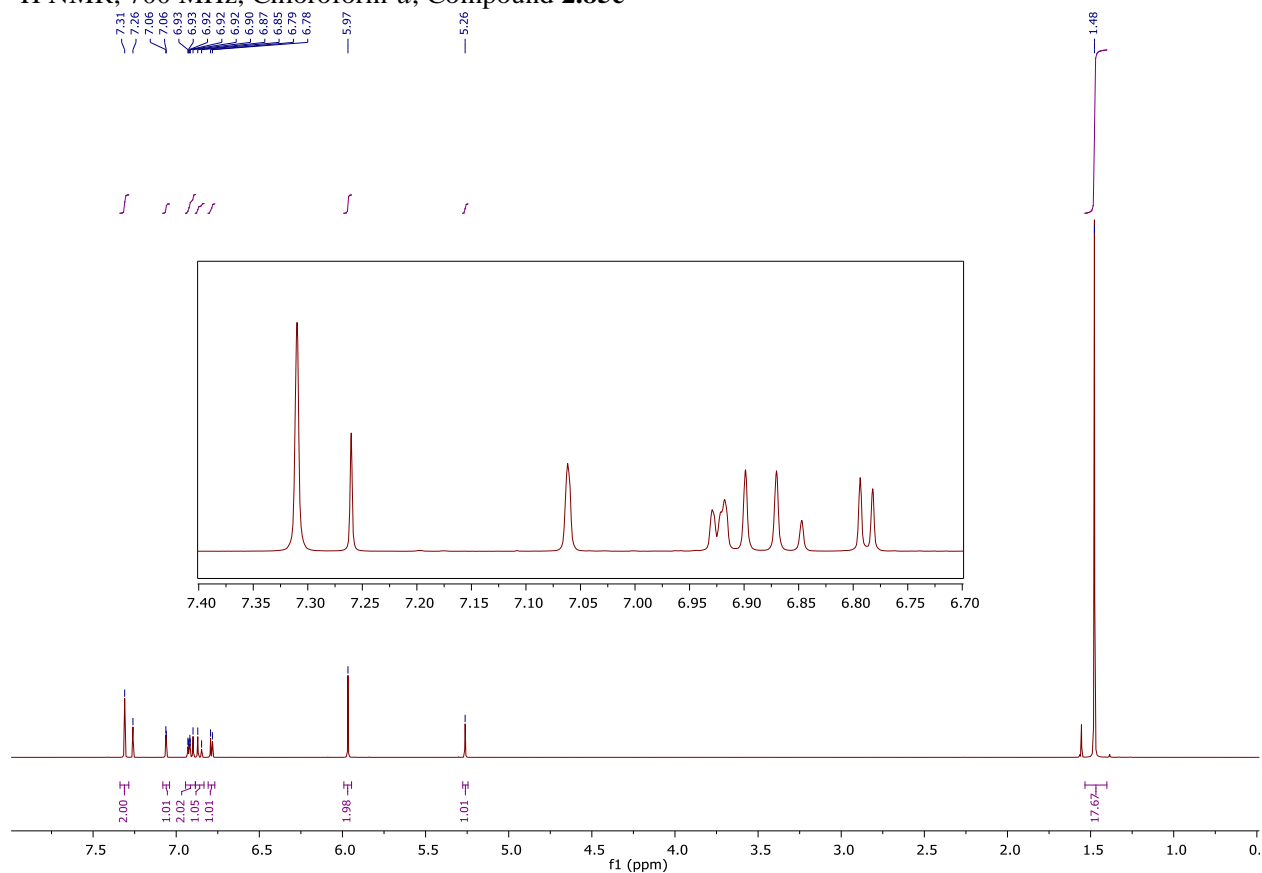
$^1\text{H NMR}$ (700 MHz, Chloroform-*d*) δ 7.31 (s, 2H), 7.06 (s, 1H), 6.92 (d, $J = 8.0$ Hz, 1H), 6.91 (d, $J = 16.2$ Hz, 1H), 6.86 (d, $J = 16.2$ Hz, 1H), 6.79 (d, $J = 8.0$ Hz, 1H), 5.97 (s, 2H), 5.26 (s, 1H), 1.48 (s, 18H).

$^{13}\text{C NMR}$ (126 MHz, Chloroform-*d*) δ 153.79, 148.22, 146.94, 136.28, 132.69, 128.82, 128.10, 125.71, 123.36, 121.03, 108.50, 105.52, 101.16, 34.53, 30.44.

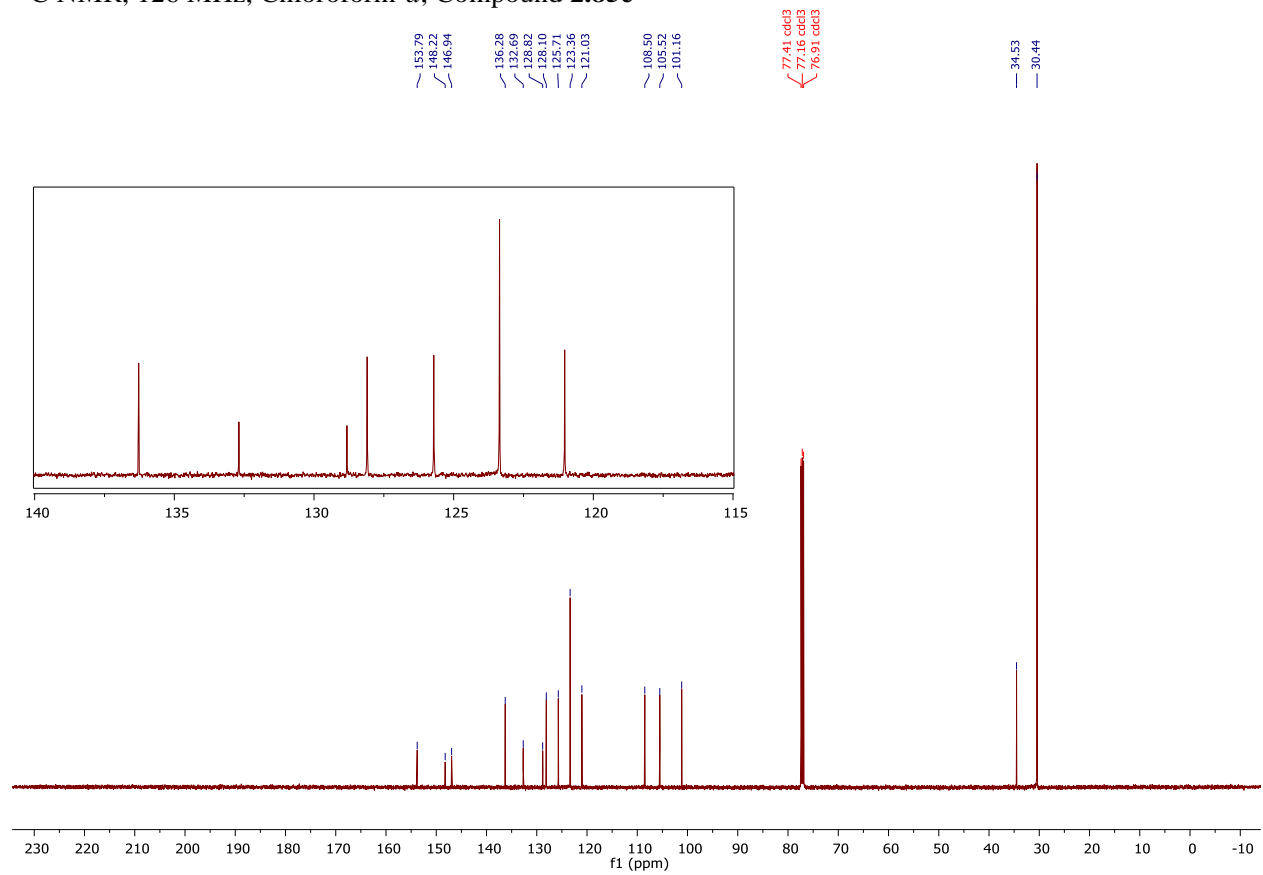
IR (Neat): 3625, 2955, 1486, 1435, 1249, 1135, 1036, 950 cm^{-1} ;

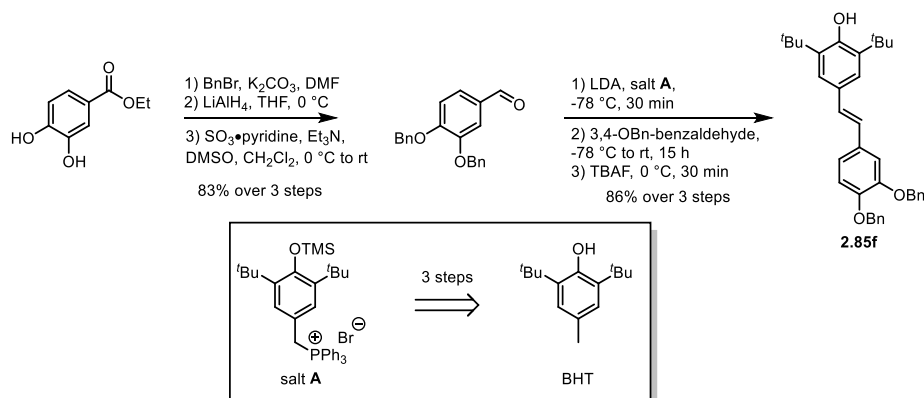
HRMS (ESI) m/z calculated for $\text{C}_{23}\text{H}_{29}\text{O}_3^+$ ($[\text{M}+\text{H}]^+$) 353.2111, found 353.2107.

$^1\text{H NMR}$, 700 MHz, Chloroform-*d*, Compound **2.85e**



^{13}C NMR, 126 MHz, Chloroform-*d*, Compound **2.85e**





(2.85f) (E)-4-(3,4-bis(benzyloxy)styryl)-2,6-di-tert-butylphenol

Freshly distilled diisopropylamine (1.04 mmol, 146 μ L) was added to a flame-dried heart-shaped flask, dissolved in freshly distilled THF (2 mL), and cooled to -78 °C. To the stirring solution was added *n*BuLi (1.00 mmol, 400 μ L, 2.5 M), and the solution was allowed to stir at the same temperature for 30 min. Meanwhile, in a 3-neck round bottom flask, the phosphonium salt **A** (1.00 mmol, 634 mg, available in 3 steps⁴⁸) was suspended in freshly distilled THF (10 mL) and cooled to -78 °C. The freshly prepared LDA solution was added to the phosphonium salt suspension via cannula, and the ylid was allowed to form at the same temperature for 30 min, turning the solution deep red. To a flame-dried heart-shaped flask was added 3,4-benzyloxybenzaldehyde (0.80 mmol, 255 mg, available in 3 steps via alkylation, reduction, and oxidation), and the solid was dissolved in THF (5 mL). The aldehyde solution was added to the ylid via cannula, and the reaction was allowed to warm to room temperature overnight (~15 hours). The reaction was subsequently cooled to 0 °C, and a solution of TBAF (1.00 mmol, 1.00 mL, 1.0 M) was added. The desilylation was allowed to occur for 30 min, at which point the reaction was quenched via the addition of saturated ammonium chloride, diluted with EtOAc, and added to a separatory funnel containing deionized water. The layers were separated, and the aqueous layer was extracted with additional portions of EtOAc. The combined organic layers were washed with brine, dried over magnesium sulfate, and concentrated under reduced pressure. The crude product was purified by flash column chromatography (10% to 60% CH₂Cl₂ in Hexanes) to afford the stilbene product (360 mg, 86% yield).

R_f = 0.30 (CH₂Cl₂/hexanes 1:1; UV)

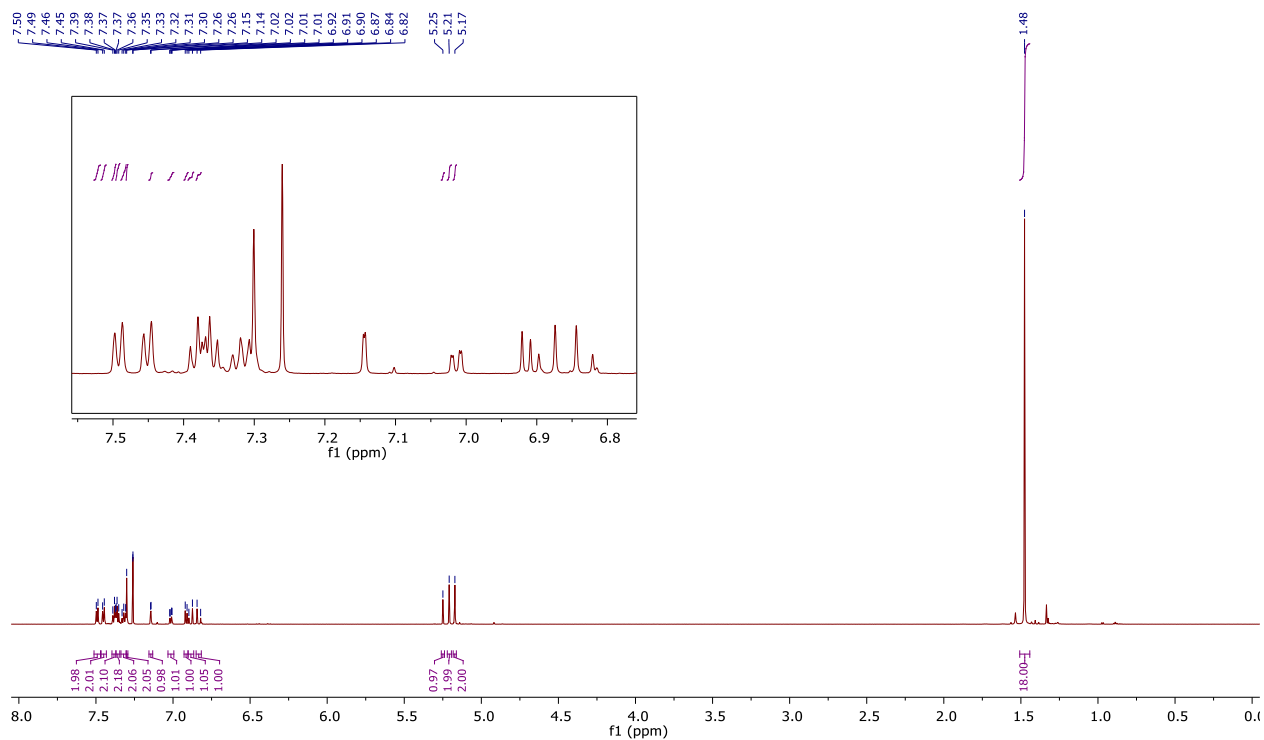
¹H NMR (700 MHz, Chloroform-*d*) δ 7.49 (d, *J* = 7.5 Hz, 2H), 7.45 (d, *J* = 7.5 Hz, 2H), 7.40 – 7.37 (m, 2H), 7.37 – 7.35 (m, 2H), 7.34 – 7.30 (m, 2H), 7.30 (s, 2H), 7.14 (d, *J* = 2.0 Hz, 1H), 7.01 (dd, *J* = 8.3, 2.0 Hz, 1H), 6.91 (d, *J* = 8.3 Hz, 1H), 6.89 (d, *J* = 16.2 Hz, 1H), 6.83 (d, *J* = 16.2 Hz, 1H), 5.25 (s, 1H), 5.21 (s, 2H), 5.17 (s, 2H), 1.48 (s, 18H).

¹³C NMR (176 MHz, Chloroform-*d*) δ 153.77, 149.34, 148.56, 137.52, 137.49, 136.26, 132.10, 128.90, 128.63, 128.61, 128.28, 127.95, 127.91, 127.58, 127.45, 125.64, 123.36, 120.14, 115.39, 112.86, 71.62, 71.55, 34.53, 30.45.

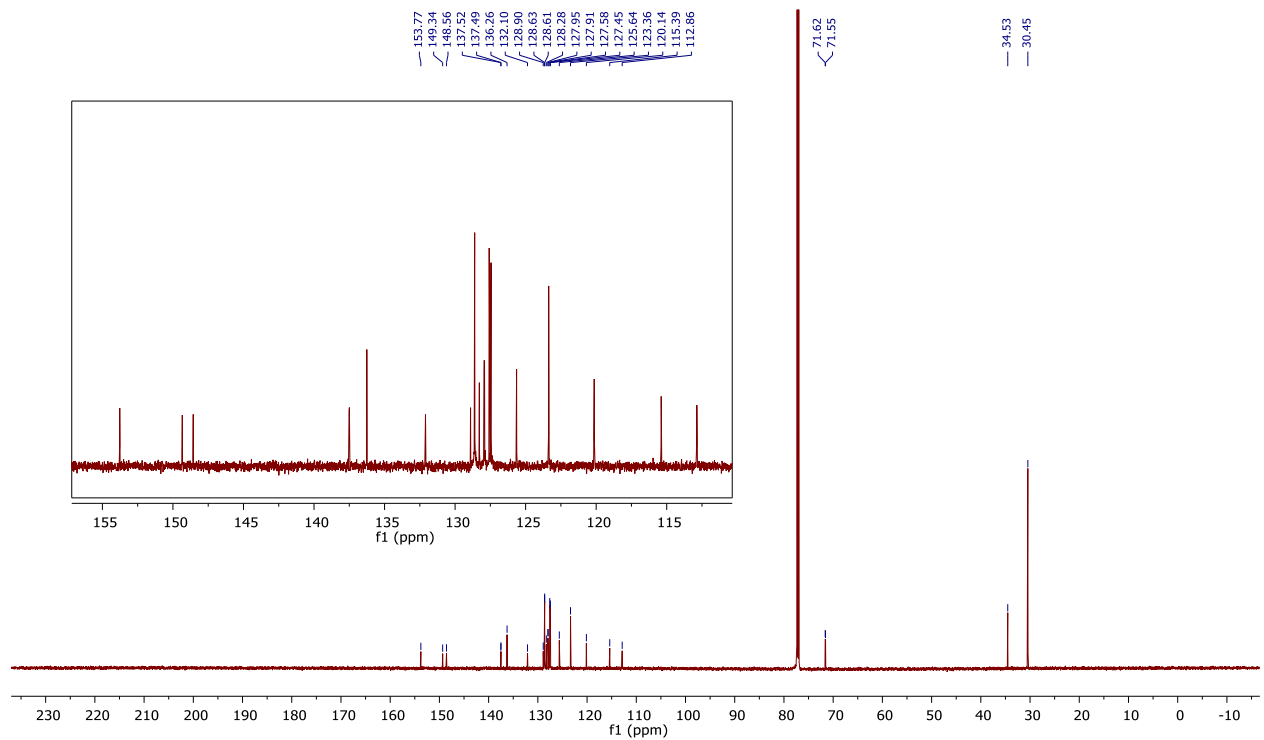
IR (Neat): 3617, 2951, 1680, 1595, 1504, 1255, 1133, 1016, 729, 695 cm⁻¹;

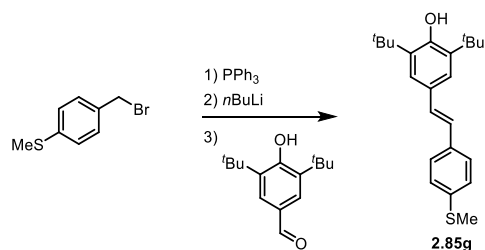
HRMS (ESI) *m/z* calculated for NaC₃₆H₄₀O₃⁺ ([M+Na]⁺) 543.2870, found 543.2873.

¹H NMR, 700 MHz, Chloroform-*d*, Compound **2.85f**



¹³C NMR, 176 MHz, Chloroform-*d*, Compound **2.85f**





(2.85g) (*E*)-2,6-di-tert-butyl-4-(4-(methylthio)styryl)phenol

Commercially available benzyl bromide ((4-(bromomethyl)phenyl)(methyl)sulfane, 1.0 g, 4.6 mmol) was subjected to the general procedure using toluene as the solvent for the olefination with aldehyde A. The product was purified by column chromatography (2% to 12% ethyl acetate in hexanes) to afford (*E*)-2,6-di-tert-butyl-4-(4-(methylthio)styryl)phenol (1.35 g, 82% yield).

R_f = 0.34 (ethyl acetate/hexanes 1:9; UV)

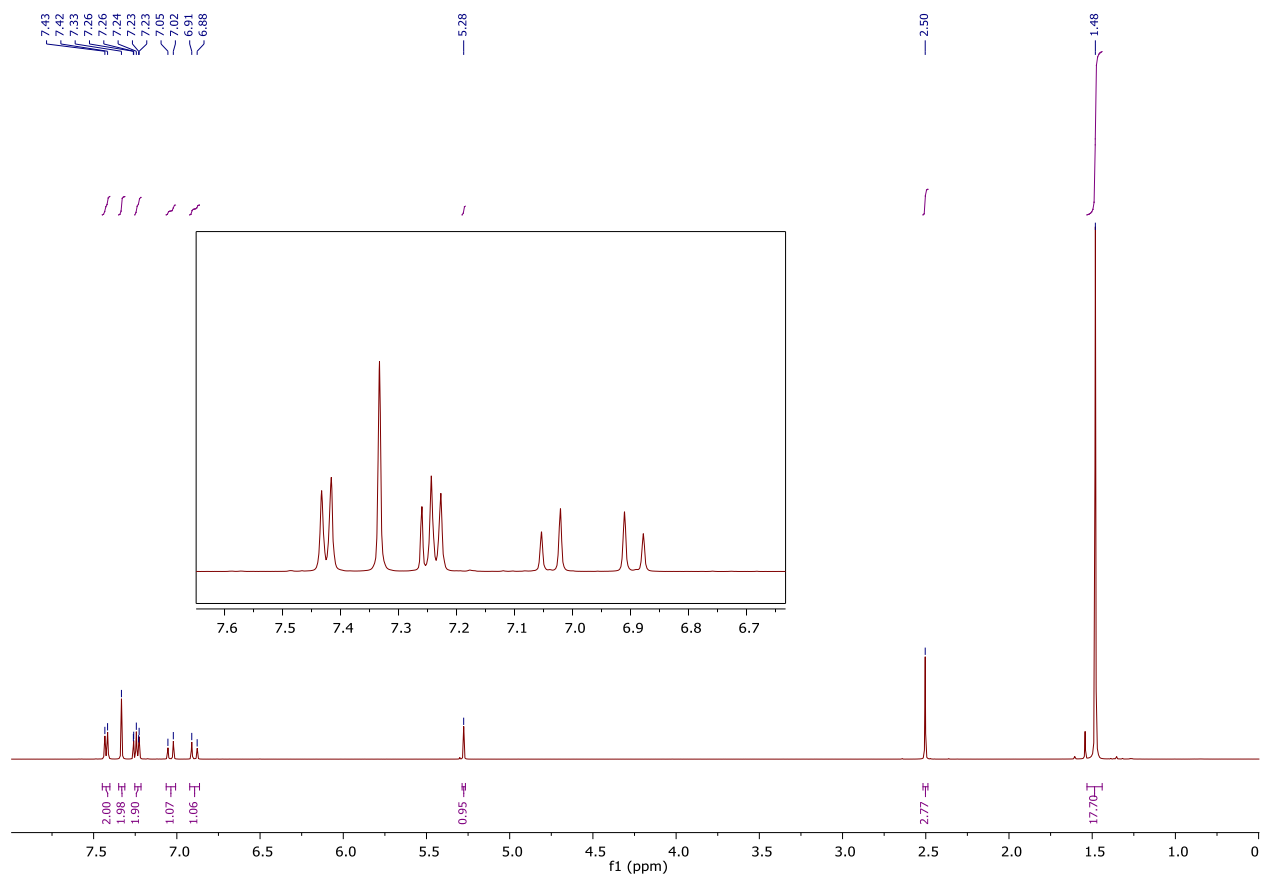
¹H NMR (500 MHz, Chloroform-*d*) δ 7.42 (d, *J* = 8.1 Hz, 2H), 7.33 (s, 2H), 7.24 (d, *J* = 8.4 Hz, 2H), 7.04 (d, *J* = 16.2 Hz, 1H), 6.89 (d, *J* = 16.2 Hz, 1H), 5.28 (s, 1H), 2.50 (s, 3H), 1.48 (s, 18H).

¹³C NMR (126 MHz, Chloroform-*d*) δ 153.96, 137.00, 136.30, 135.20, 129.18, 128.73, 127.04, 126.72, 125.31, 123.50, 34.53, 30.44, 16.18.

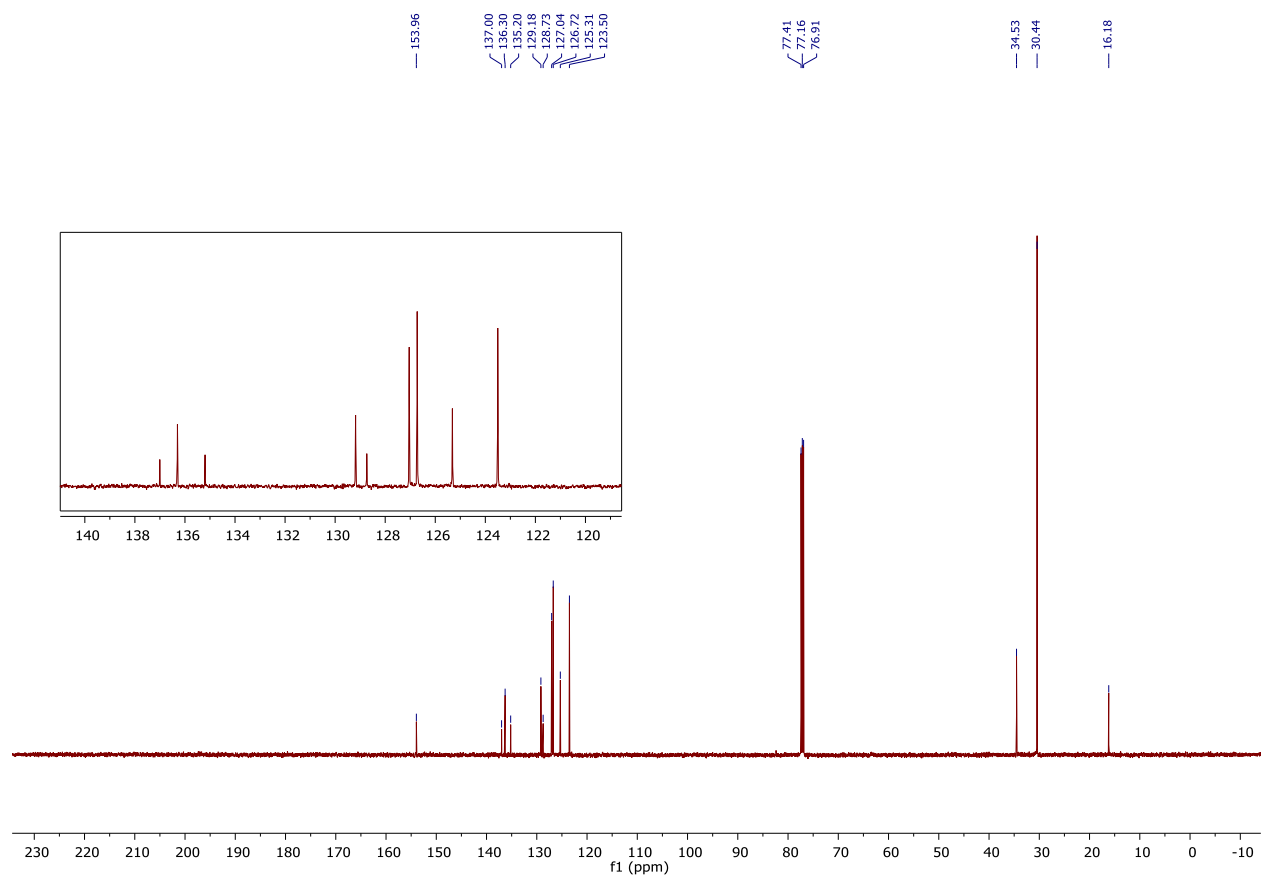
IR (Neat): 3616, 2955, 1435, 1249, 1184, 962, 800 cm⁻¹;

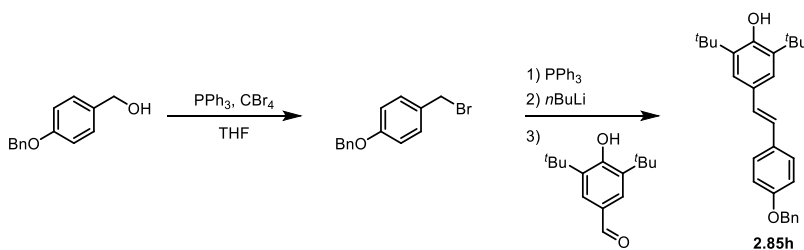
HRMS (ESI) *m/z* calculated for C₂₃H₃₁OS⁺ ([M+H]⁺) 355.2090, found 355.2087.

¹H NMR, 500 MHz, Chloroform-*d*, Compound **2.85g**



^{13}C NMR, 126 MHz, Chloroform-*d*, Compound **2.85g**





(2.85h) (*E*)-4-(4-(benzyloxy)styryl)-2,6-di-*tert*-butylphenol

Commercially available benzyl alcohol ((4-(benzyloxy)phenyl)methanol, 1.00g, 4.7 mmol) was subjected to the general procedure using toluene as the solvent for the olefination with aldehyde A. The product was purified by column chromatography (2% to 12% ethyl acetate in hexanes) to afford (*E*)-4-(4-(benzyloxy)styryl)-2,6-di-*tert*-butylphenol (1.52g, 78% yield).

$R_f = 0.28$ (ethyl acetate/hexanes 1:9; UV)

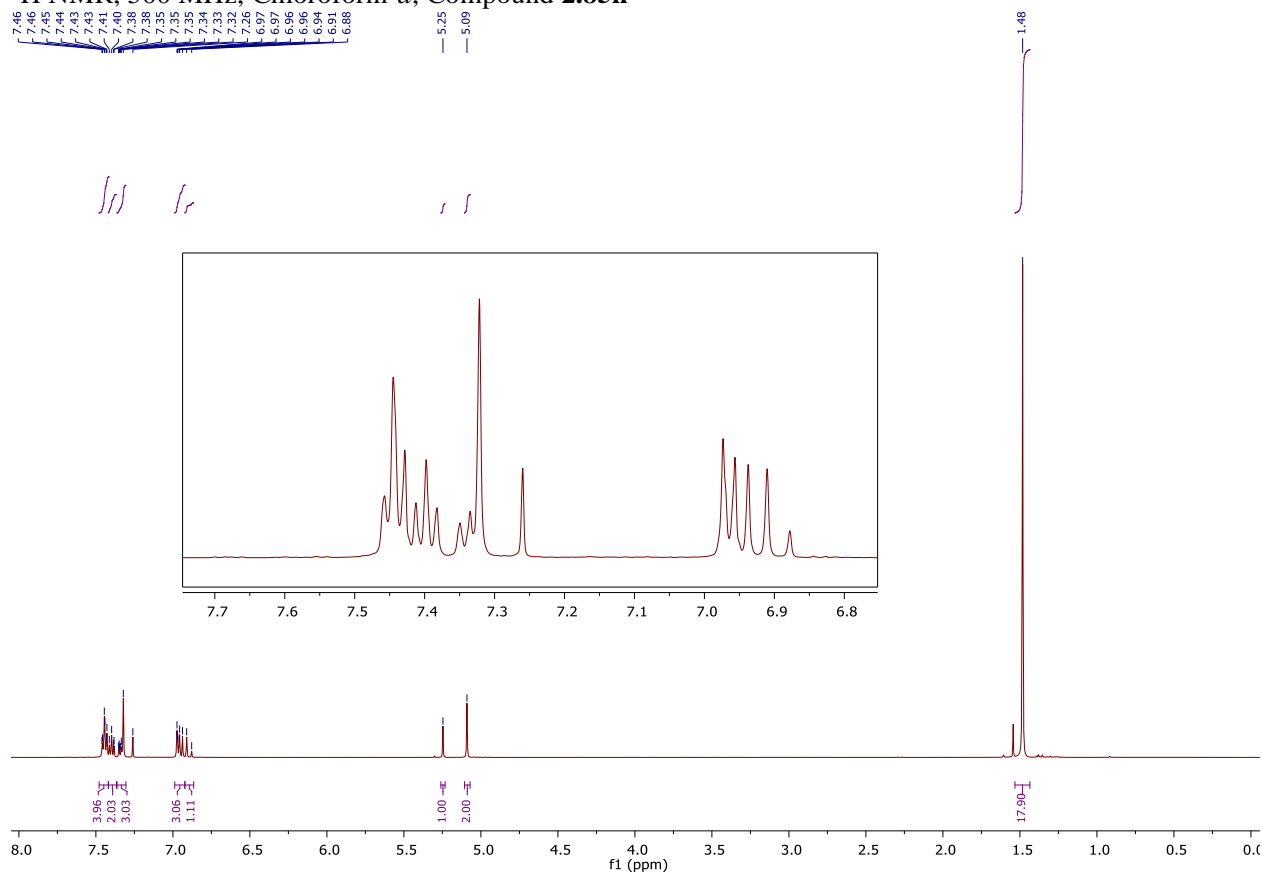
$^1\text{H NMR}$ (500 MHz, Chloroform-*d*) δ 7.44 (d, $J = 7.1$ Hz, 2H), 7.44 (d, $J = 8.6$ Hz, 2H), 7.40 (t, $J = 7.6$ Hz, 2H), 7.33 (t, $J = 7.3$ Hz, 1H), 7.32 (s, 2H), 6.96 (d, $J = 8.6$ Hz, 2H), 6.95 (d, $J = 16.2$ Hz, 1H), 6.89 (d, $J = 16.3$ Hz, 1H), 5.25 (s, 1H), 5.09 (s, 2H), 1.48 (s, 18H).

$^{13}\text{C NMR}$ (126 MHz, Chloroform-*d*) δ 158.20, 153.69, 137.16, 136.24, 131.21, 129.05, 128.73, 128.11, 127.83, 127.63, 127.48, 125.53, 123.30, 115.17, 70.22, 34.53, 30.45.

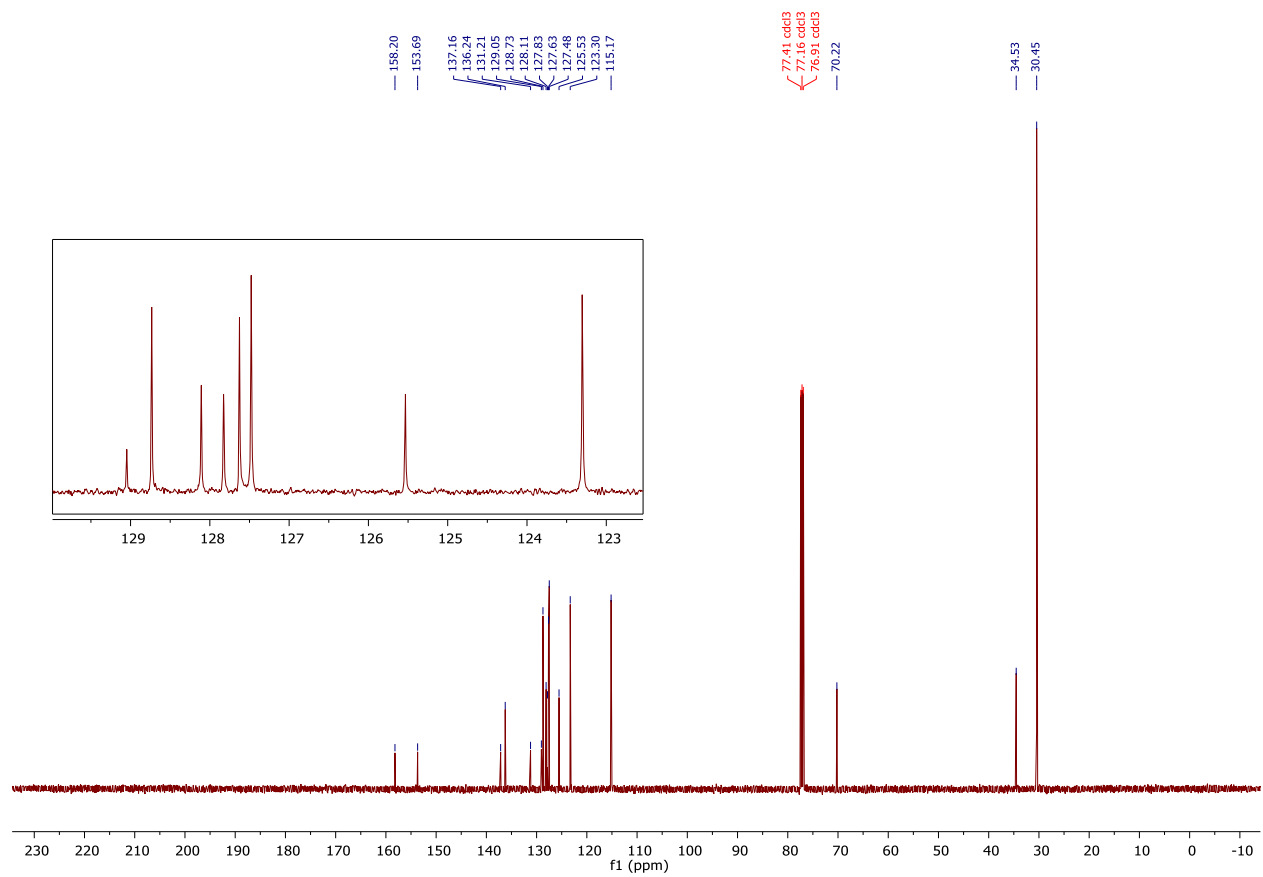
IR (Neat): 3628, 2953, 1606, 1510, 1465, 1233, 1175, 1010, 954, 745 cm^{-1} ;

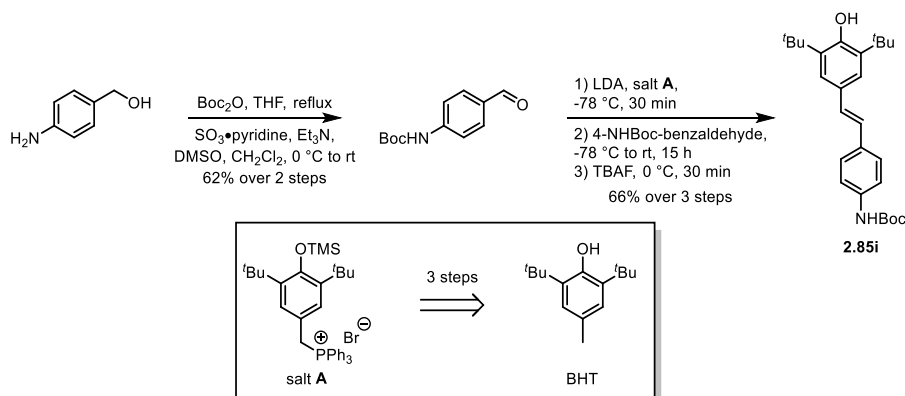
HRMS (ESI) m/z calculated for $\text{C}_{29}\text{H}_{35}\text{O}_2^+$ ($[\text{M}+\text{H}]^+$) 415.2632, found 415.2632.

$^1\text{H NMR}$, 500 MHz, Chloroform-*d*, Compound **2.85h**



^{13}C NMR, 126 MHz, Chloroform-*d*, Compound **2.85h**





(2.85i) *tert*-butyl (*E*)-(4-(3,5-di-*tert*-butyl-4-hydroxystyryl)phenyl)carbamate

Freshly distilled diisopropylamine (3.41 mmol, 478 μ L) was added to a flame-dried heart-shaped flask, dissolved in freshly distilled THF (10 mL), and cooled to -78 $^{\circ}$ C. To the stirring solution was added *n*BuLi (3.28 mmol, 1.31 mL, 2.5 M), and the solution was allowed to stir at the same temperature for 30 min. Meanwhile, in a 3-neck round bottom flask, the phosphonium salt **A** (3.28 mmol, 2.08 g) was suspended in freshly distilled THF (25 mL) and cooled to -78 $^{\circ}$ C. The freshly prepared LDA solution was added to the phosphonium salt suspension via cannula, and the ylid was allowed to form at the same temperature for 30 min, turning the solution deep red. To a flame-dried heart-shaped flask was added 4-NHBoc-benzaldehyde (2.62 mmol, 580 mg, available in 2 steps via Boc protection and oxidation), and the solid was dissolved in THF (10 mL). The aldehyde solution was added to the ylid via cannula, and the reaction was allowed to warm to room temperature overnight (\sim 15 hours). The reaction was subsequently cooled to 0 $^{\circ}$ C, and a solution of TBAF (3.28 mmol, 3.28 mL, 1.0 M) was added. The desilylation was allowed to occur for 30 min, at which point the reaction was quenched via the addition of saturated ammonium chloride, diluted with EtOAc, and added to a separatory funnel containing deionized water. The layers were separated, and the aqueous layer was extracted with additional portions of EtOAc. The combined organic layers were washed with brine, dried over magnesium sulfate, and concentrated under reduced pressure. The crude product was purified by flash column chromatography (20% to 100% CH_2Cl_2 in Hexanes) to afford the stilbene product (1.00 g, 90% yield).

$R_f = 0.30$ (CH_2Cl_2 /hexanes 3:1; UV)

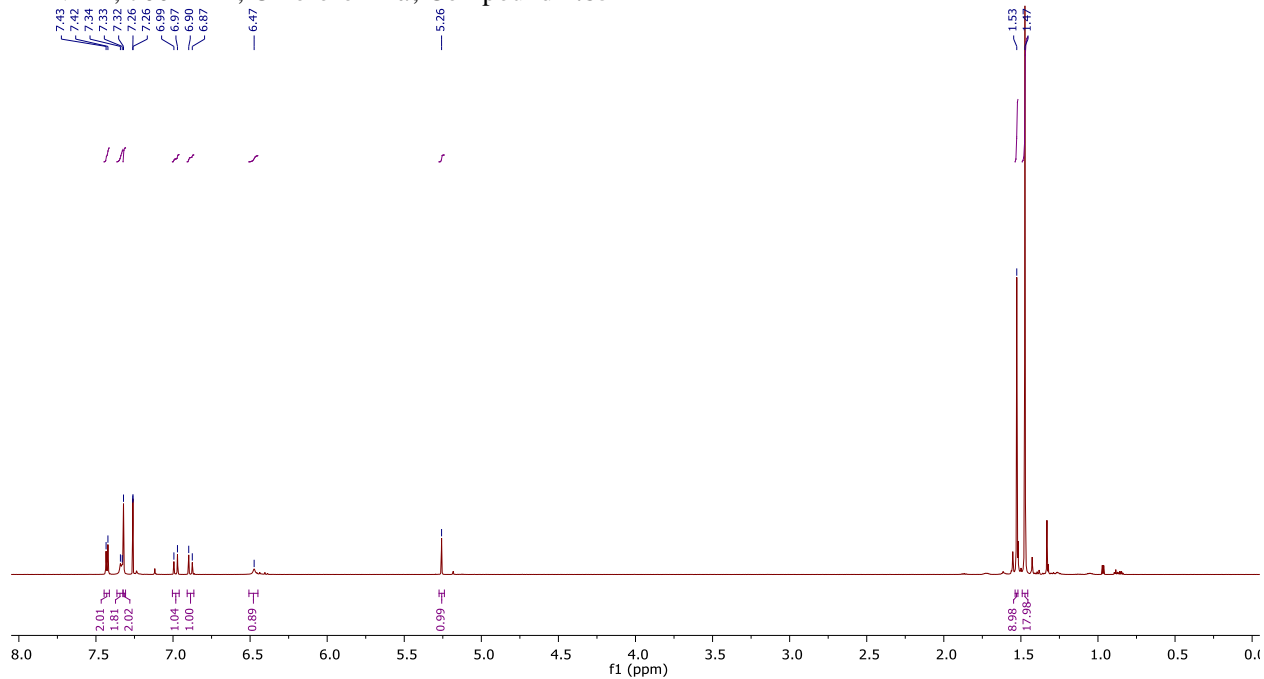
^1H NMR (700 MHz, Chloroform-*d*) δ 7.43 (d, $J = 8.4$ Hz, 2H), 7.34 (d, $J = 8.3$ Hz, 2H), 7.32 (s, 2H), 6.98 (d, $J = 16.2$ Hz, 1H), 6.89 (d, $J = 16.2$ Hz, 1H), 6.47 (s, 1H), 5.26 (s, 1H), 1.53 (s, 9H), 1.47 (s, 18H).

^{13}C NMR (176 MHz, Chloroform-*d*) δ 153.79, 152.77, 137.31, 136.22, 133.06, 128.87, 128.36, 126.93, 125.42, 123.39, 118.69, 80.71, 34.52, 30.43, 28.50.

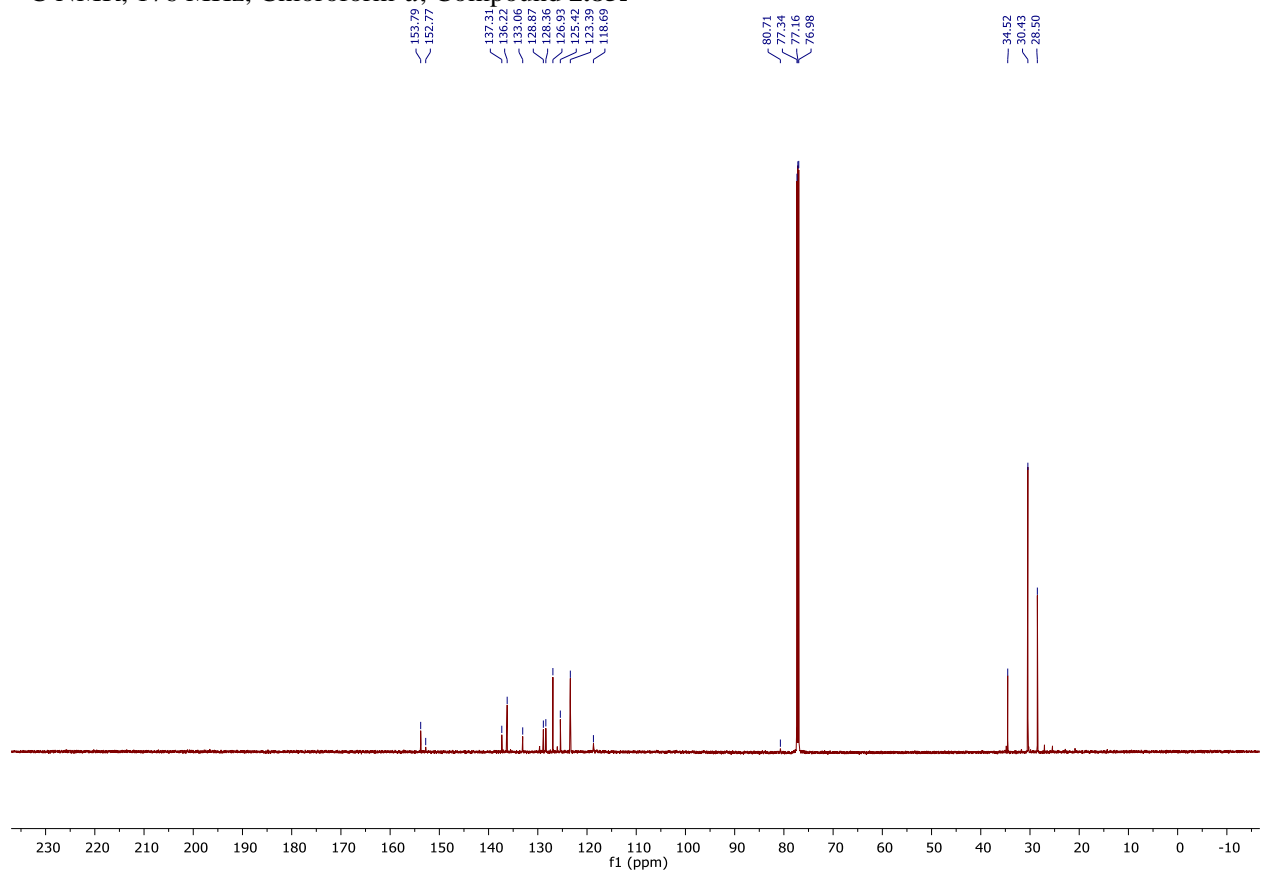
IR (Neat): 3623, 3325, 2957, 1709, 1600, 1521, 1234, 1153, 1051, 740 cm^{-1} ;

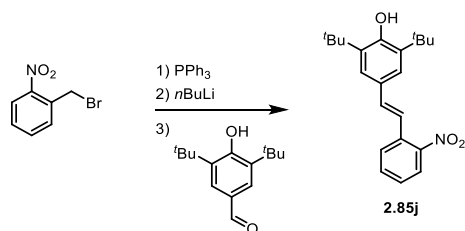
HRMS (ESI) m/z calculated for $\text{NaC}_{27}\text{H}_{37}\text{NO}_3^+$ ($[\text{M}+\text{Na}]^+$) 446.2666, found 446.2660.

¹H NMR, 700 MHz, Chloroform-*d*, Compound **2.85i**



¹³C NMR, 176 MHz, Chloroform-*d*, Compound **2.85i**





(2.85j) (*E*)-2,6-di-*tert*-butyl-4-(2-nitrostyryl)phenol

Commercially available benzyl bromide (1-(bromomethyl)-2-nitrobenzene, 1.0 g, 4.6 mmol) was subjected to the general procedure using toluene as the solvent for the olefination. The product was purified by column chromatography (2% to 12% ethyl acetate in hexanes) to afford (*E*)-2,6-di-*tert*-butyl-4-(2-nitrostyryl)phenol (927 mg, 57% yield).

R_f = 0.38 (ethyl acetate/hexanes 1:9; UV)

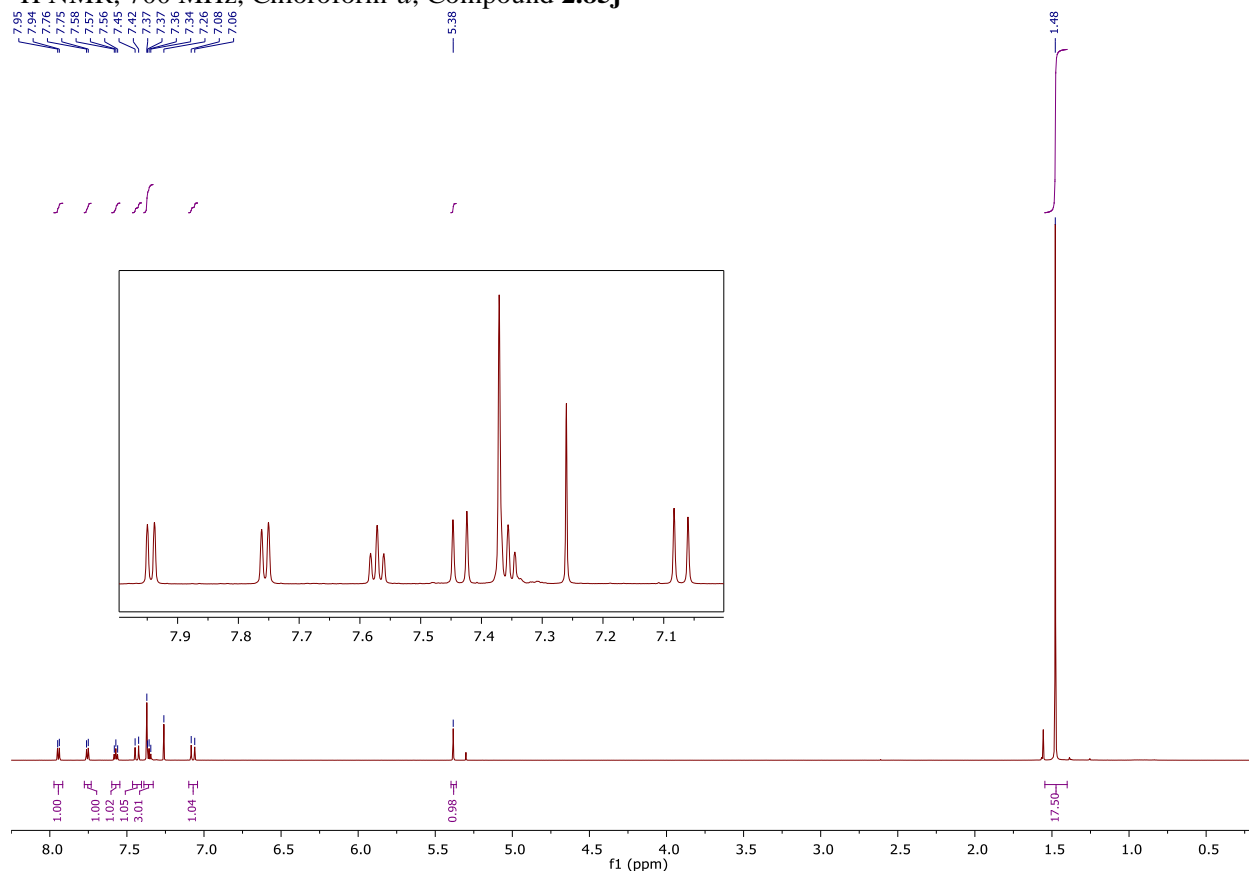
^1H NMR (700 MHz, Chloroform-*d*) δ 7.94 (d, J = 8.1 Hz, 1H), 7.76 (d, J = 7.9 Hz, 1H), 7.57 (t, J = 7.6 Hz, 1H), 7.44 (d, J = 16.0 Hz, 1H), 7.37 (s, 3H), 7.36 (t, J = 7.7 Hz, 3H), 7.07 (d, J = 16.0 Hz, 1H), 5.38 (s, 1H), 1.48 (s, 18H).

^{13}C NMR (176 MHz, Chloroform-*d*) δ 154.83, 147.95, 136.44, 135.03, 133.80, 133.07, 128.09, 128.05, 127.40, 124.91, 124.29, 120.65, 34.52, 30.38.

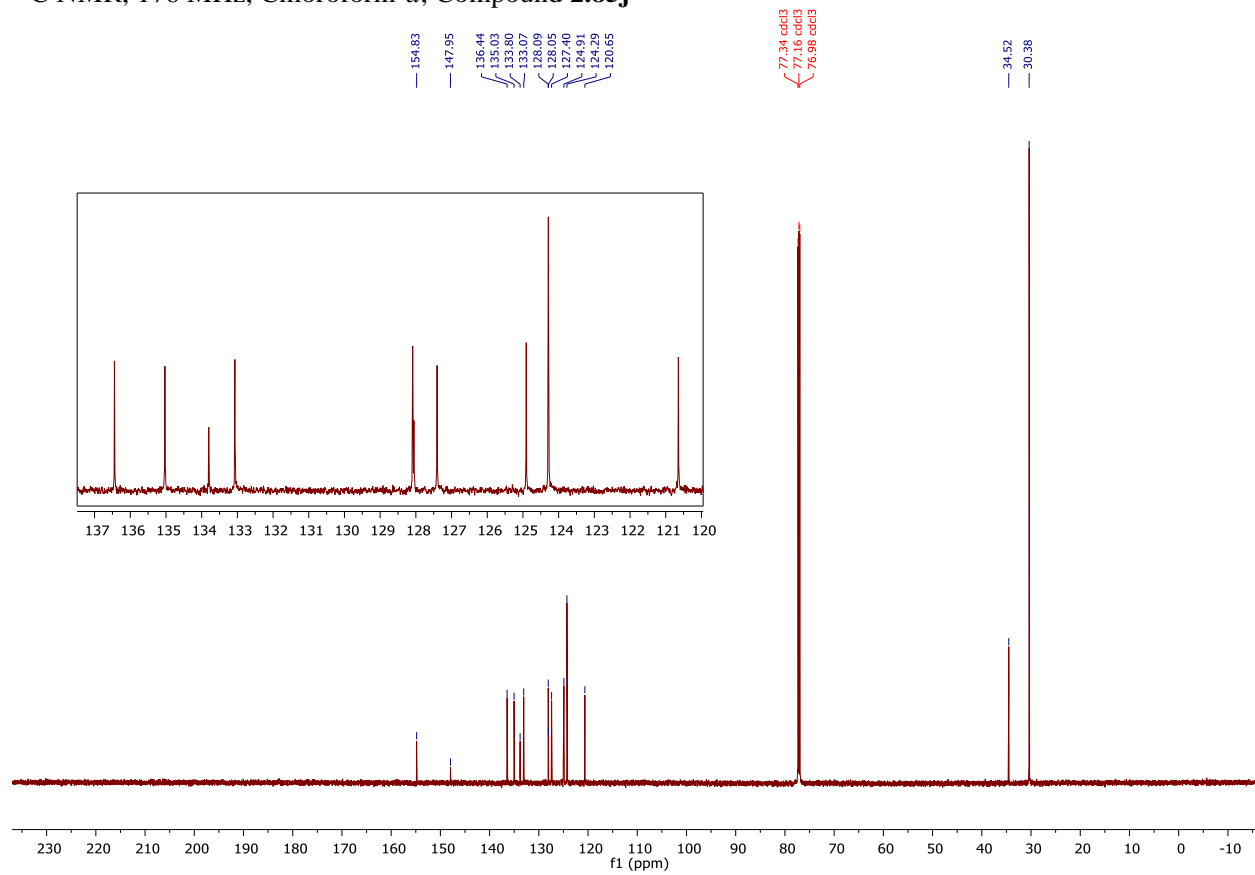
IR (Neat): 3626, 2961, 1626, 1603, 1515, 1348, 1233, 1150, 965, 742 cm^{-1} ;

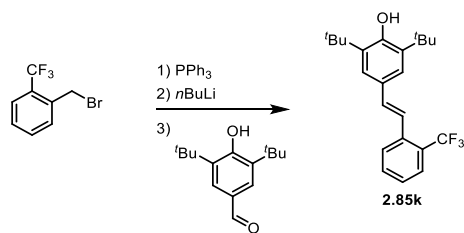
HRMS (ESI) m/z calculated for $\text{C}_{22}\text{H}_{28}\text{NO}_3^+$ ($[\text{M}+\text{H}]^+$) 354.2064, found 354.2064.

^1H NMR, 700 MHz, Chloroform-*d*, Compound **2.85j**



^{13}C NMR, 176 MHz, Chloroform-*d*, Compound **2.85j**





(2.85k) (*E*)-2,6-di-*tert*-butyl-4-(2-(trifluoromethyl)styryl)phenol

Commercially available benzyl bromide (1-(bromomethyl)-2-(trifluoromethyl)benzene, 0.79 g, 3.29 mmol) was subjected to the general procedure using THF as the solvent for the olefination. The product was purified by column chromatography (2% to 12% ethyl acetate in hexanes) to afford (*E*)-2,6-di-*tert*-butyl-4-(2-(trifluoromethyl)styryl)phenol (989 mg, 73% yield).

$R_f = 0.40$ (ethyl acetate/hexanes 1:9; UV)

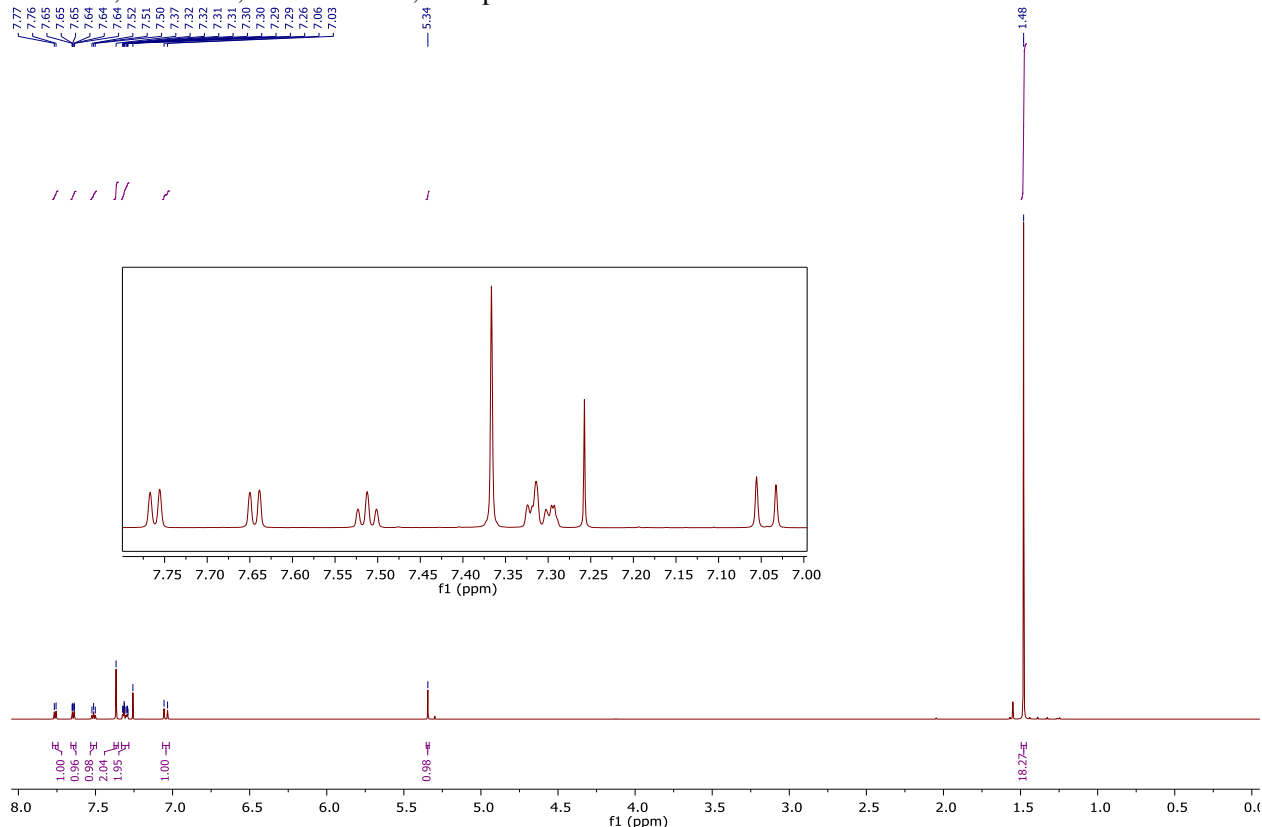
$^1\text{H NMR}$ (700 MHz, Chloroform-*d*) δ 7.76 (d, $J = 7.9$ Hz, 1H), 7.66 – 7.63 (m, 1H), 7.51 (t, $J = 7.6$ Hz, 1H), 7.37 (s, 2H), 7.33 – 7.28 (m, 2H), 7.04 (d, $J = 16.0$ Hz, 1H), 5.34 (s, 1H), 1.48 (s, 18H).

$^{13}\text{C NMR}$ (176 MHz, Chloroform-*d*) δ 154.48, 137.16, 136.34, 133.57, 131.92, 128.37, 127.32 (q, $J_{\text{C-F}} = 29$ Hz), 126.90, 126.71, 125.99 (q, $J_{\text{C-F}} = 6.2$ Hz), 124.66 (q, $J_{\text{C-F}} = 275$ Hz), 124.03, 121.71, 34.50, 30.36.

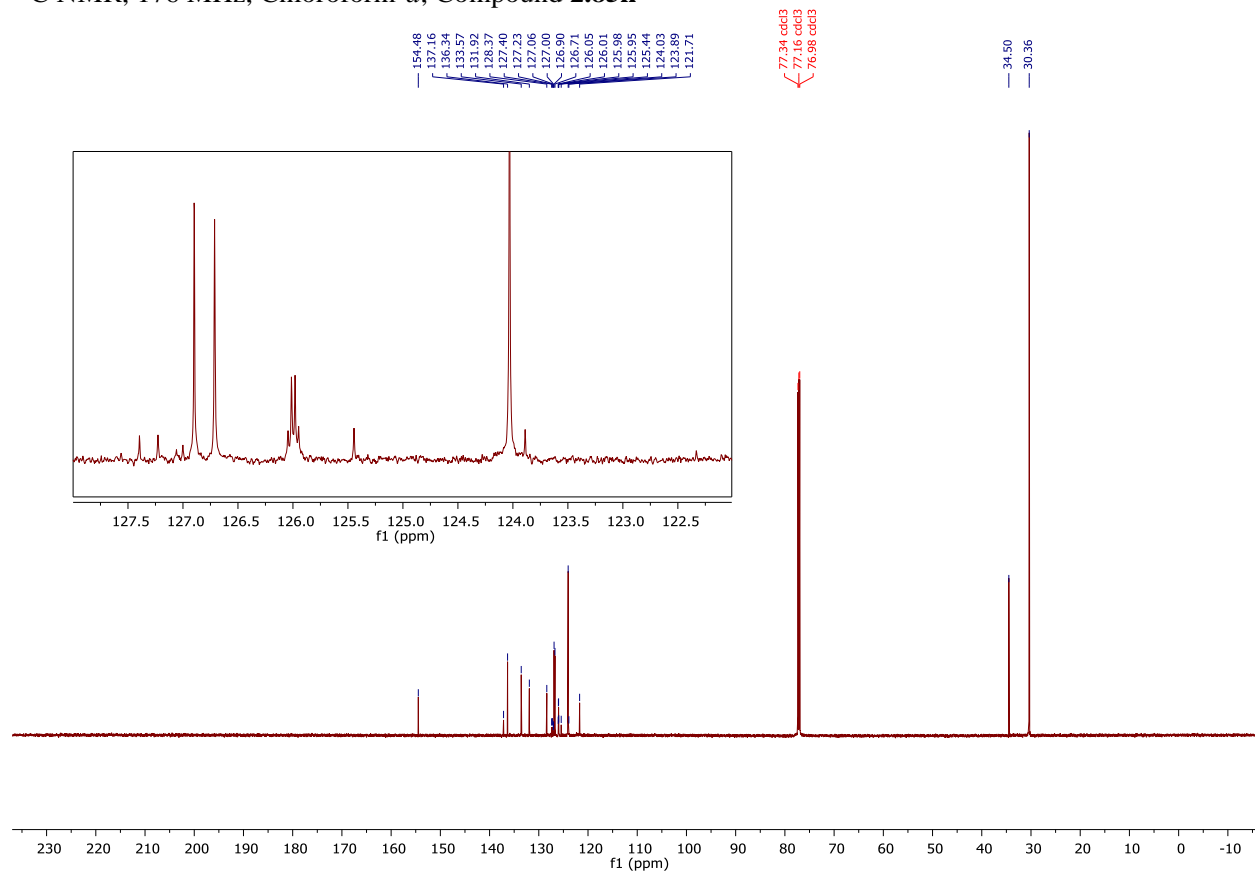
IR (Neat): 3636, 2956, 1435, 1422, 1308, 1122, 1035, 960, 753 cm^{-1} ;

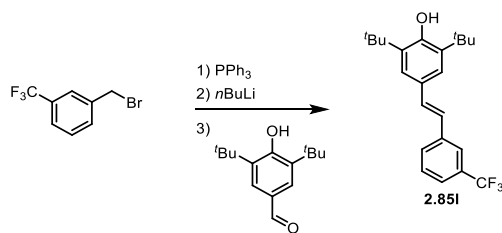
HRMS (ESI) m/z calculated for $\text{C}_{23}\text{H}_{28}\text{F}_3\text{O}^+$ ($[\text{M}+\text{H}]^+$) 377.2087, found 377.2084.

$^1\text{H NMR}$, 700 MHz, Chloroform-*d*, Compound **2.85k**



^{13}C NMR, 176 MHz, Chloroform-*d*, Compound **2.85k**





(2.85I) (*E*)-2,6-di-*tert*-butyl-4-(3-(trifluoromethyl)styryl)phenol

Commercially available benzyl bromide (1-(bromomethyl)-3-(trifluoromethyl)benzene, 0.78 g, 3.25 mmol) was subjected to the general procedure using THF as the solvent for the olefination. The product was purified by column chromatography (2% to 12% ethyl acetate in hexanes) to afford (*E*)-2,6-di-*tert*-butyl-4-(3-(trifluoromethyl)styryl)phenol (1.06 g, 87% yield).

$R_f = 0.40$ (ethyl acetate/hexanes 1:9; UV)

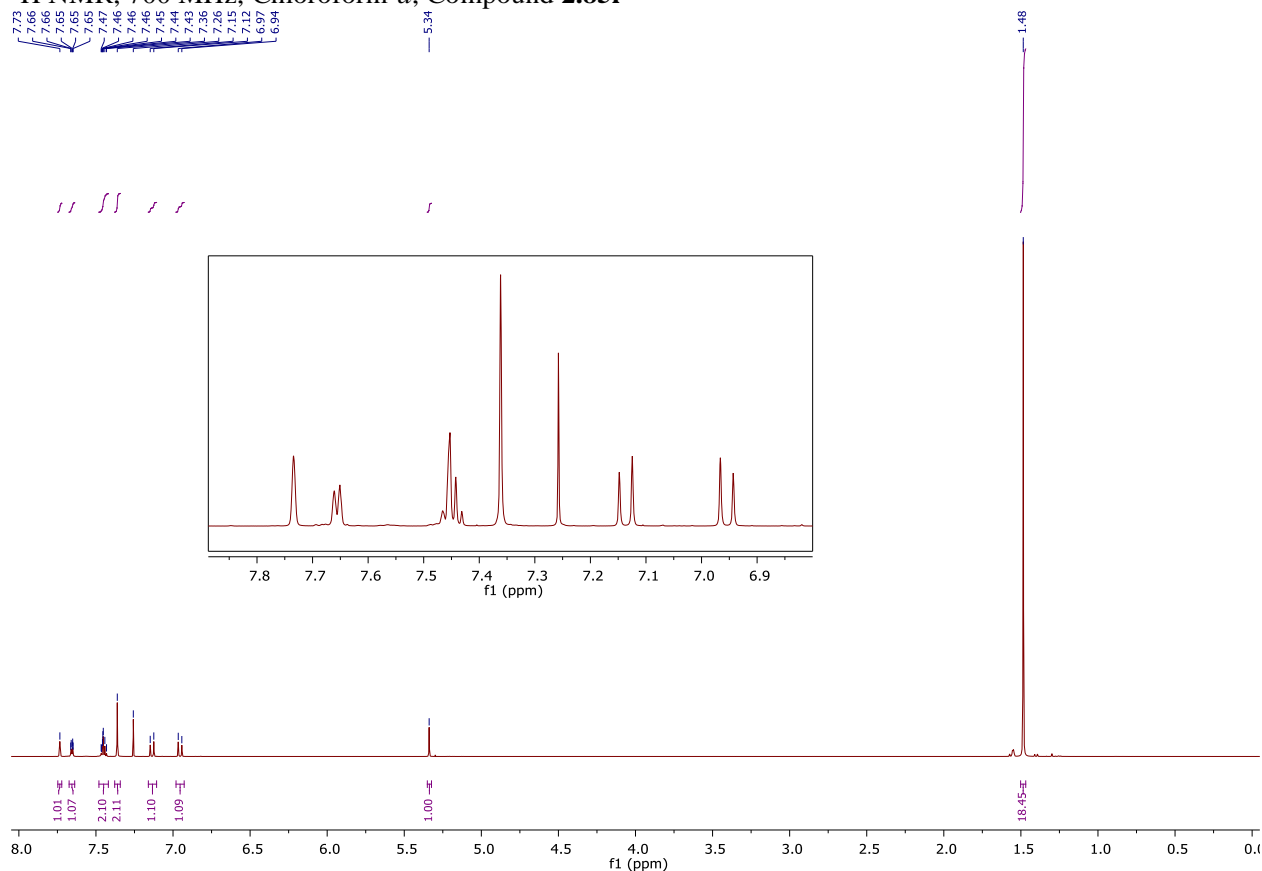
$^1\text{H NMR}$ (700 MHz, Chloroform-*d*) δ 7.73 (s, 1H), 7.66 (dd, $J = 7.0, 1.9$ Hz, 1H), 7.48 – 7.42 (m, 2H), 7.36 (s, 2H), 7.14 (d, $J = 16.2$ Hz, 1H), 6.95 (d, $J = 16.2$ Hz, 1H), 5.34 (s, 1H), 1.48 (s, 18H).

$^{13}\text{C NMR}$ (176 MHz, Chloroform-*d*) δ 154.42, 138.85, 136.38, 131.48, 131.13 (q, $J_{\text{C-F}} = 32$ Hz), 129.33, 129.14, 128.11, 124.37 (q, $J_{\text{C-F}} = 273$ Hz), 124.33, 123.82, 123.51 (q, $J_{\text{C-F}} = 3.5$ Hz), 122.88 (q, $J_{\text{C-F}} = 3.5$ Hz), 34.54, 30.41.

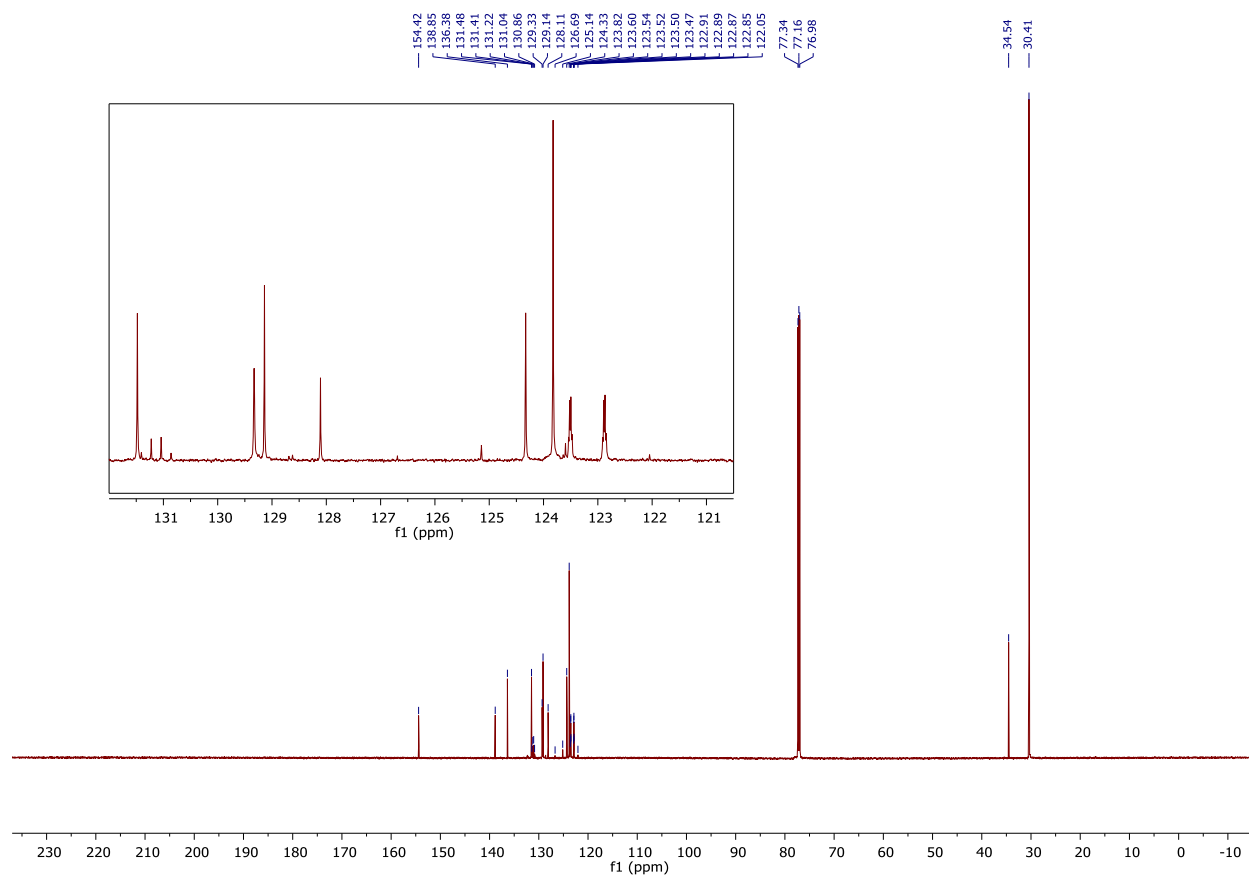
IR (Neat): 3639, 2957, 1655, 1437, 1328, 1163, 1121, 1073 cm^{-1} ;

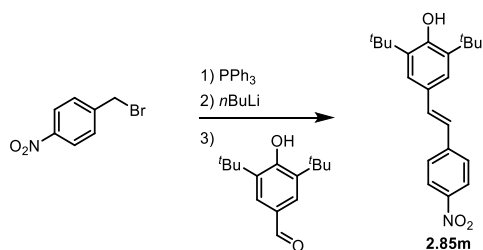
HRMS (ESI) m/z calculated for $\text{C}_{23}\text{H}_{28}\text{F}_3\text{O}^+$ ($[\text{M}+\text{H}]^+$) 377.2087, found 377.2093.

$^1\text{H NMR}$, 700 MHz, Chloroform-*d*, Compound **2.85I**



^{13}C NMR, 176 MHz, Chloroform-*d*, Compound **2.851**





(2.85m) (E)-2,6-di-*tert*-butyl-4-(4-nitrostyryl)phenol

Commercially available benzyl bromide (1-(bromomethyl)-4-nitrobenzene, 1.0 g, 4.6 mmol) was subjected to the general procedure using toluene as the solvent for the olefination with aldehyde A. The product was purified by column chromatography (2% to 12% ethyl acetate in hexanes) to afford (E)-2,6-di-*tert*-butyl-4-(4-nitrostyryl)phenol (990 mg, 61% yield).

R_f = 0.38 (ethyl acetate/hexanes 1:9; UV)

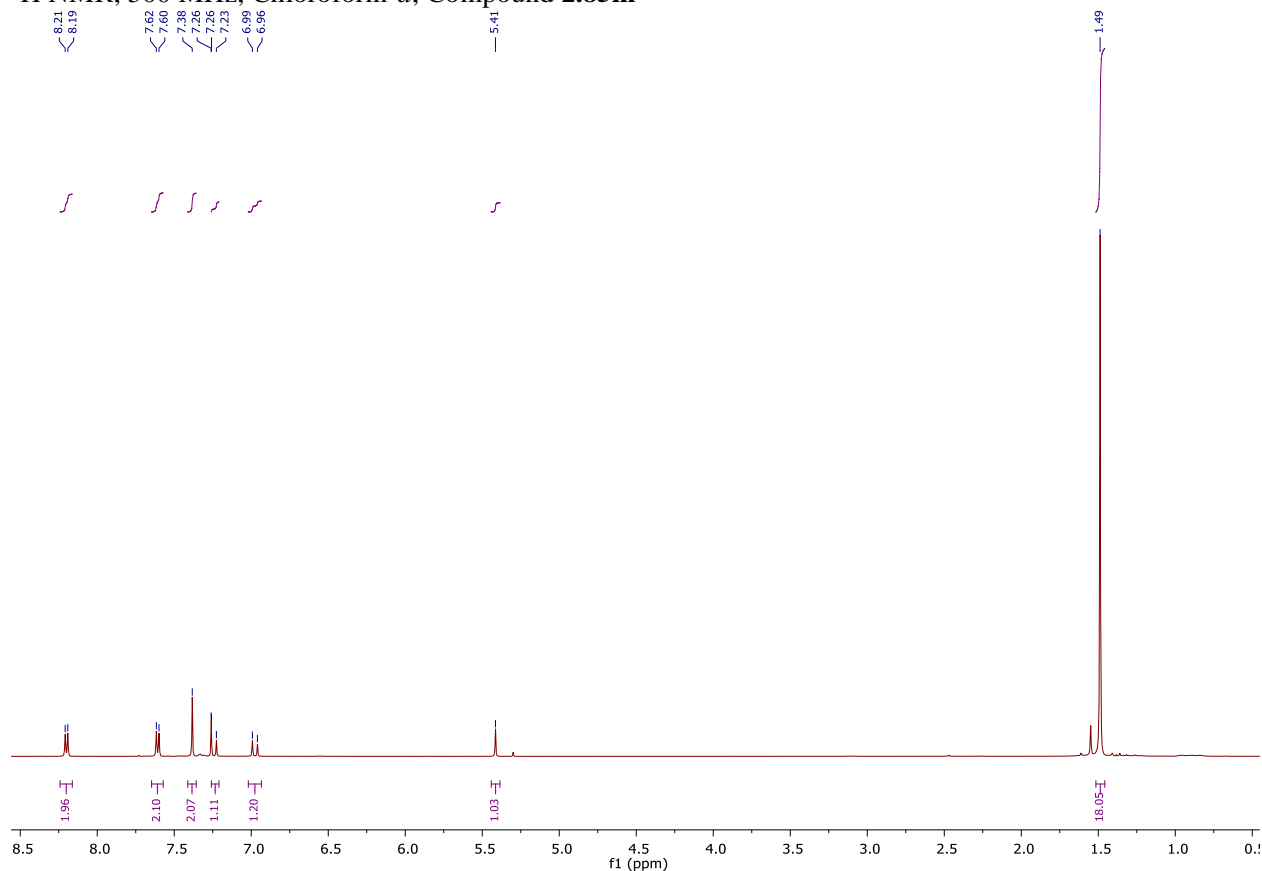
¹H NMR (500 MHz, Chloroform-*d*) δ 8.20 (d, *J* = 8.5 Hz, 2H), 7.60 (d, *J* = 8.6 Hz, 2H), 7.38 (s, 2H), 7.24 (d, *J* = 16.1 Hz, 2H), 6.97 (d, *J* = 16.2 Hz, 1H), 5.41 (s, 1H), 1.48 (s, 18H).

¹³C NMR (126 MHz, Chloroform-*d*) δ 155.07, 146.40, 144.77, 136.56, 134.49, 127.69, 126.53, 124.29, 123.44, 34.56, 30.39.

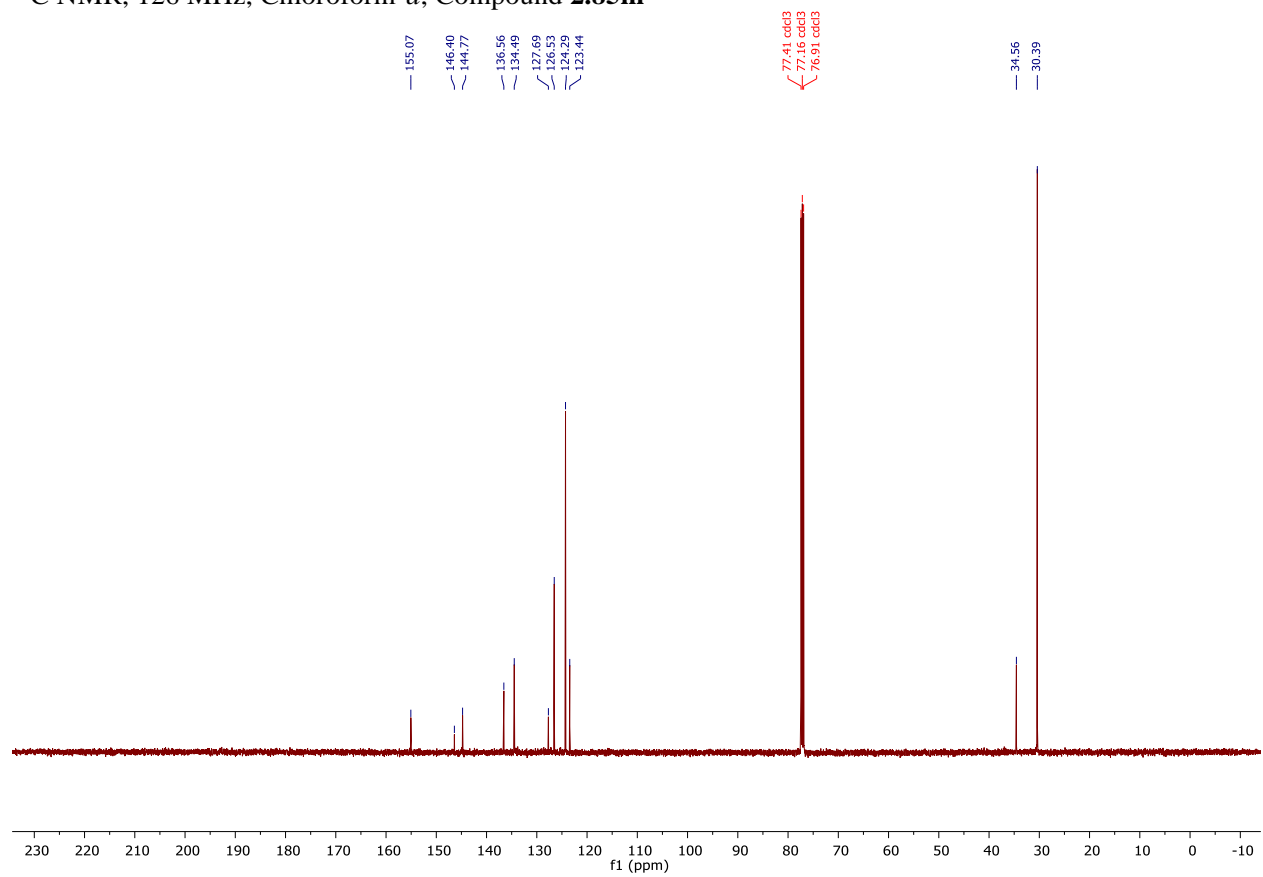
IR (Neat) 3618, 2955, 1629, 1595, 1505, 1428, 1332, 1117, 973, 861, 748 cm⁻¹;

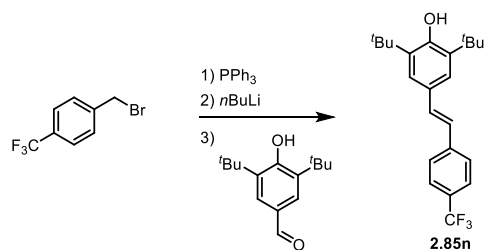
HRMS (ESI) *m/z* calculated for C₂₂H₂₈NO₃⁺ ([M+H]⁺) 354.2064, found 354.2068.

¹H NMR, 500 MHz, Chloroform-*d*, Compound **2.85m**



^{13}C NMR, 126 MHz, Chloroform-*d*, Compound **2.85m**





(2.85n) (*E*)-2,6-di-*tert*-butyl-4-(4-(trifluoromethyl)styryl)phenol

Commercially available benzyl bromide (1-(bromomethyl)-4-(trifluoromethyl)benzene, 1.0 g, 4.18 mmol) was subjected to the general procedure using THF as the solvent for the olefination. The product was purified by column chromatography (2% to 12% ethyl acetate in hexanes) to afford (*E*)-2,6-di-*tert*-butyl-4-(4-(trifluoromethyl)styryl)phenol (1.15 g, 77% yield).

R_f = 0.40 (ethyl acetate/hexanes 1:9; UV)

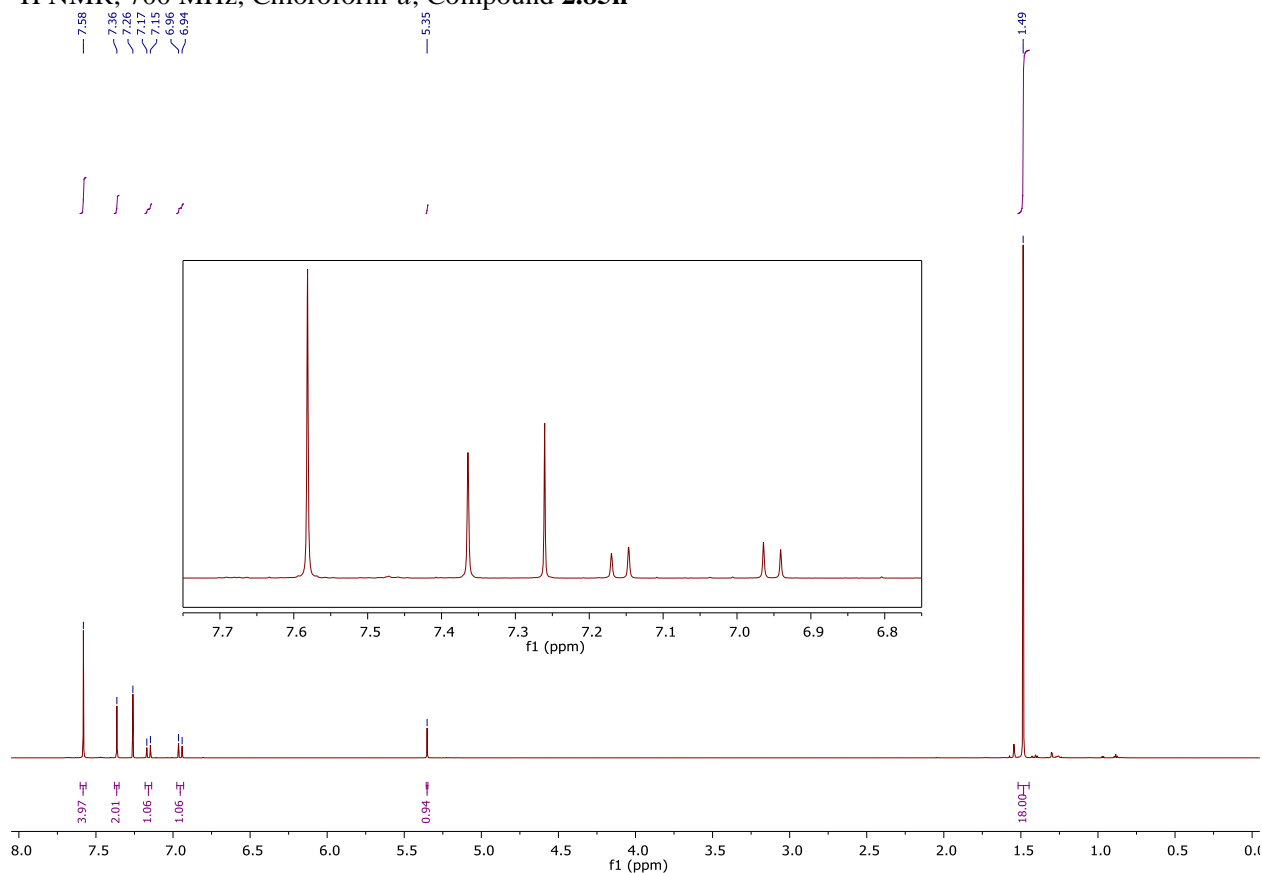
¹H NMR (700 MHz, Chloroform-*d*) δ 7.58 (s, 4H), 7.36 (s, 2H), 7.16 (d, *J* = 16.3 Hz, 1H), 6.95 (d, *J* = 16.2 Hz, 1H), 5.35 (s, 1H), 1.49 (s, 18H).

¹³C NMR (176 MHz, Chloroform-*d*) δ 154.56, 141.63, 136.43, 132.26, 128.71 (q, *J* = 32 Hz), 128.11, 126.33, 125.68 (q, *J* = 3.5 Hz), 124.52 (q, *J* = 271 Hz), 124.32, 123.93, 34.54, 30.41.

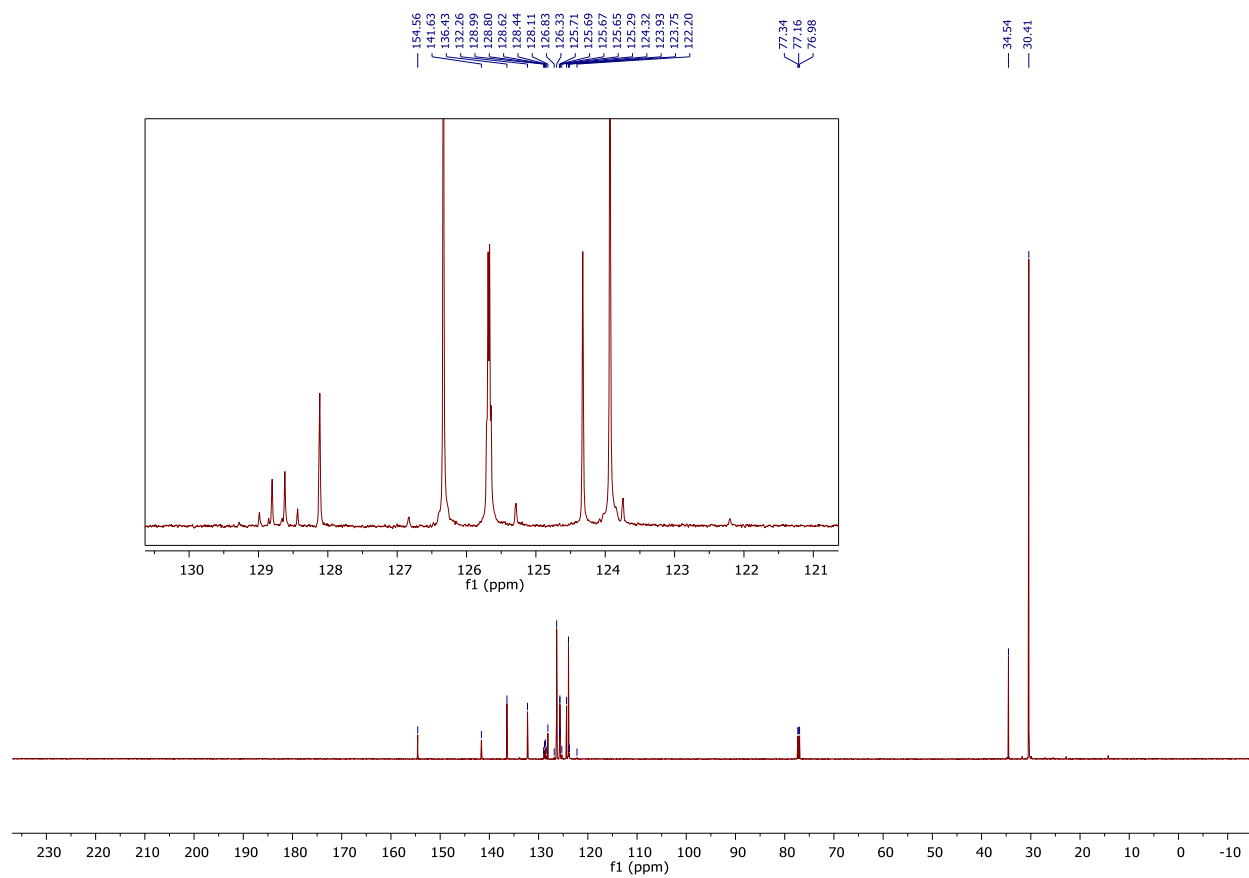
IR (Neat): 3636, 2955, 1435, 1422, 1308, 1122, 1035, 960, 753 cm⁻¹;

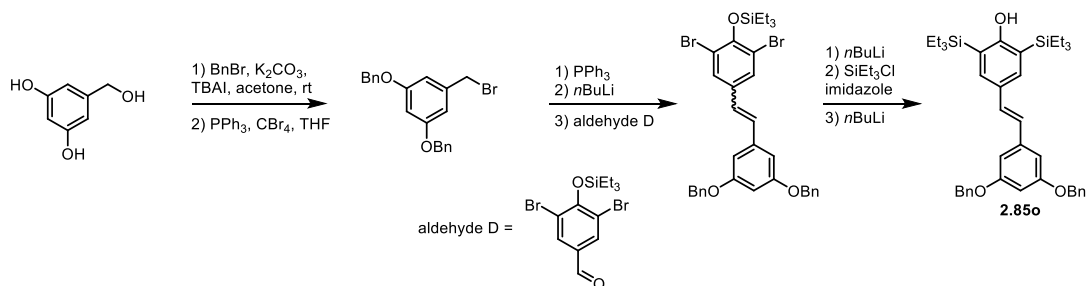
HRMS (ESI) *m/z* calculated for C₂₃H₂₈F₃O⁺ ([M+H]⁺) 377.2087, found 377.2084.

¹H NMR, 700 MHz, Chloroform-*d*, Compound **2.85n**



^{13}C NMR, 176 MHz, Chloroform-*d*, Compound **2.85n**





(2.85o) (*E*)-4-(3,5-bis(benzyloxy)styryl)-2,6-bis(triethylsilyl)phenol

Commercially available 3,5-dihydroxybenzyl alcohol (2.0 g, 14.3 mmol) was added to flask charged with potassium carbonate (2.25 equiv., 4.44 g) and tetrabutylammonium iodide (0.2 equiv., 1.05 g), and the solids were dissolved/suspended in acetone (42 mL). To the stirring reaction mixture was added 4-methoxybenzyl chloride (2.20 equiv., 3.74 mL), and the reaction was allowed to stir at room temperature for 16 hours. Upon completion, the reaction was diluted with ethyl acetate and poured into a separatory funnel containing deionized water. The layers were separated, and the aqueous layer was extracted with additional portions of ethyl acetate. The combined organic layer was washed with brine, dried over magnesium sulfate, and concentrated under reduced pressure to afford the crude product, which was carried forward without further purification. The benzyl-protected material (2.22 g, 5.79 mmol) was subjected to the general procedure using THF as the solvent for the olefination with aldehyde D, which is available from silyl protection of commercially available 3,5-dibromo-4-hydroxybenzaldehyde. The product was purified by column chromatography (2% to 12% ethyl acetate in hexanes, 2% increments, 2 column volumes each, then 2 column volumes at both 16% and 20%) to afford both olefin isomers in a ~1:1 ratio (2.26 g, 69% yield combined). The *E*-isomer (900 mg, 1.59 mmol) was carried forward and dissolved in THF, and the reaction mixture was cooled to -78 °C. *n*BuLi (1.0 equiv, 1.6 M in hexanes, 993 μL) was added dropwise to the stirring solution, and the reaction was held at temperature for 15 min prior to being allowed to warm to room temperature. The retro-Brook rearrangement was quenched and worked up following the general procedure. The resulting product was silyl protected following standard conditions, then subjected to the same retro-Brook reaction to afford the product (*E*)-4-(3,5-bis(benzyloxy)styryl)-2,6-bis(triethylsilyl)phenol (861 mg, 85% yield).

R_f = 0.37 (ethyl acetate/hexanes 1:9; UV)

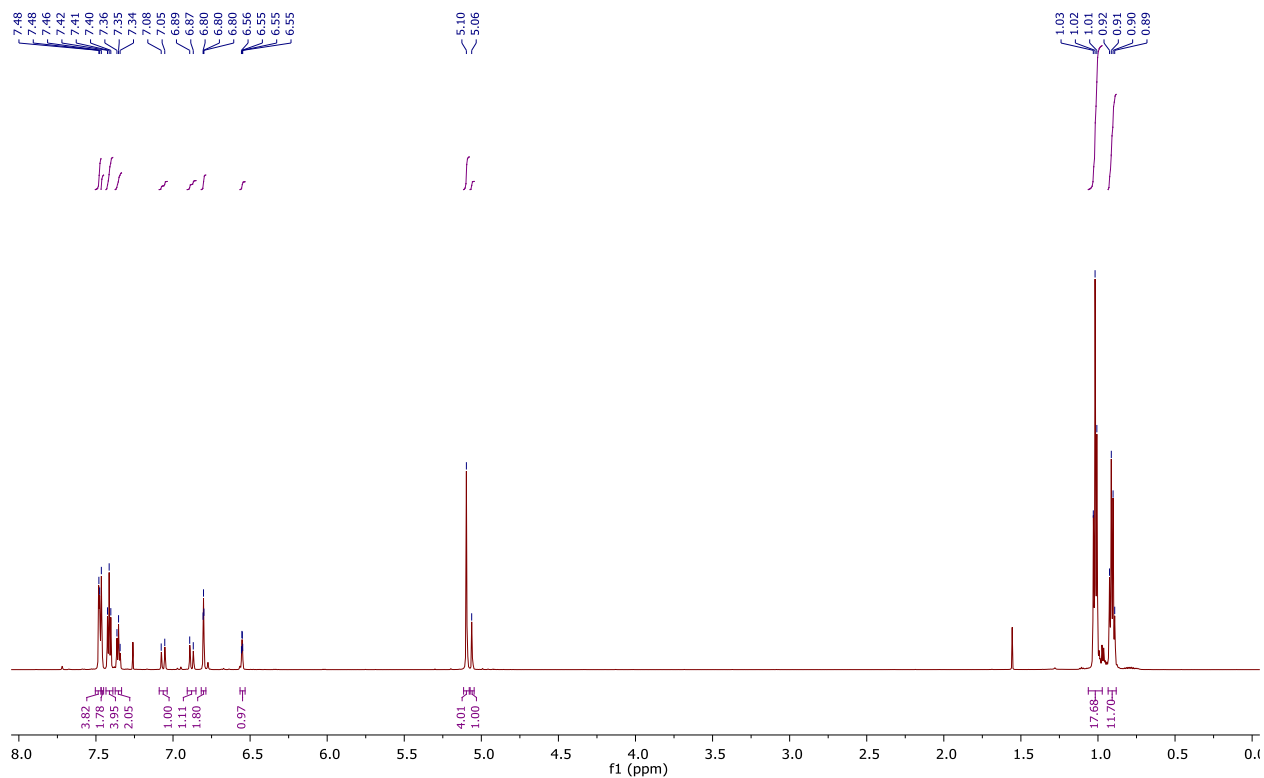
¹H NMR (700 MHz, Chloroform-*d*) δ 7.48 (d, *J* = 3.5 Hz, 4H), 7.46 (s, 2H), 7.41 (t, *J* = 7.5 Hz, 4H), 7.35 (t, *J* = 7.2 Hz, 2H), 7.07 (d, *J* = 16.1 Hz, 1H), 6.88 (d, *J* = 16.2 Hz, 1H), 6.80 (t, *J* = 1.8 Hz, 2H), 6.55 (q, *J* = 2.0 Hz, 1H), 5.10 (s, 4H), 5.06 (s, 1H), 1.02 (t, *J* = 8.0 Hz, 18H), 0.91 (q, *J* = 7.7 Hz, 12H).

¹³C NMR (176 MHz, Chloroform-*d*) δ 166.04, 160.27, 140.16, 137.07, 136.01, 129.77, 129.09, 128.72, 128.12, 127.72, 125.88, 121.44, 105.62, 101.18, 70.25, 7.70, 3.98.

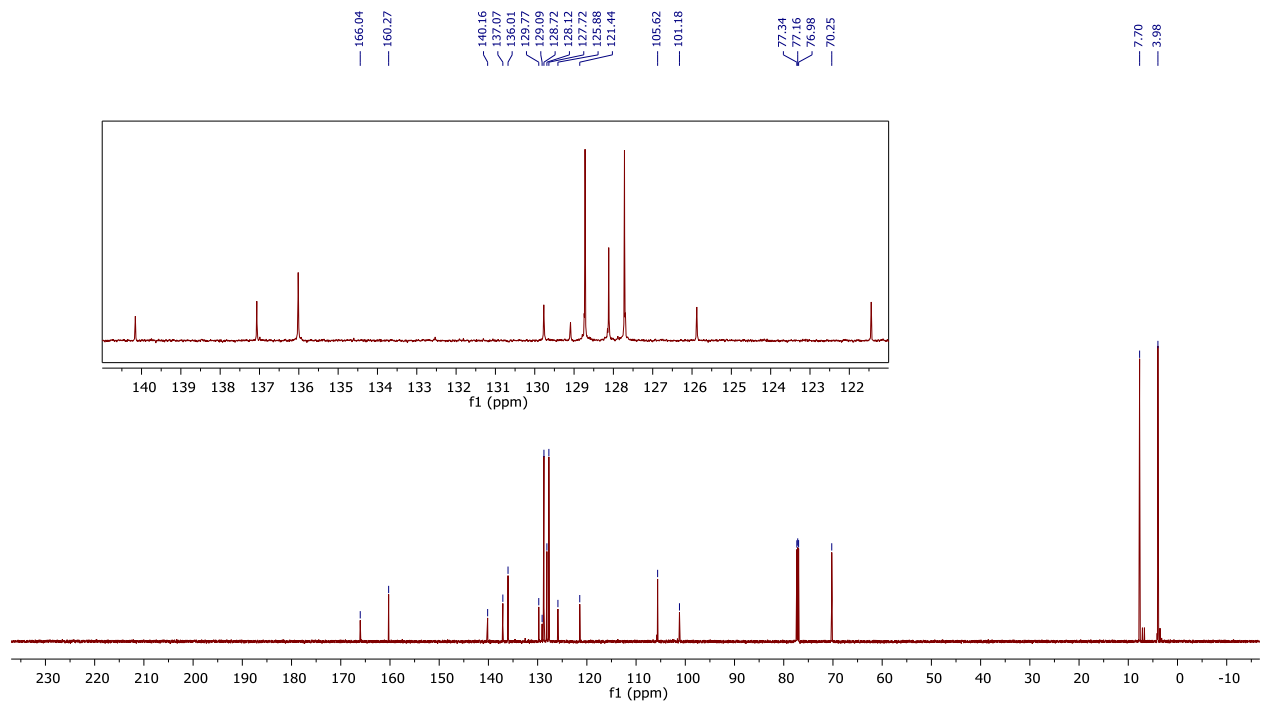
IR (Neat): 3592, 2951, 2870, 1591, 1453, 1397, 1161, 1144, 1060, 1004, 953, 723, 692 cm⁻¹;

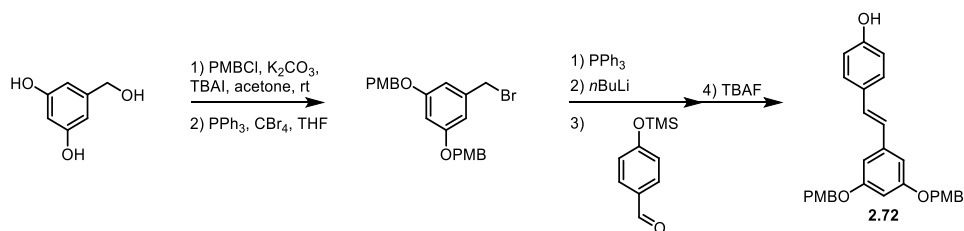
HRMS (ESI) *m/z* calculated for C₄₀H₅₃O₃Si₂⁺ ([M+H]⁺) 637.3528, found 637.3535.

¹H NMR, 700 MHz, Chloroform-*d*, Stilbene **2.85o**



¹³C NMR, 176 MHz, Chloroform-*d*, Stilbene **2.85o**





(2.72) (*E*)-4-(3,5-bis((4-methoxybenzyl)oxy)styryl)phenol

Commercially available 3,5-dihydroxybenzyl alcohol (2.0 g, 14.3 mmol) was added to flask charged with potassium carbonate (2.25 equiv., 4.44 g) and tetrabutylammonium iodide (0.2 equiv., 1.05 g), and the solids were dissolved/suspended in acetone (42 mL). To the stirring reaction mixture was added 4-methoxybenzyl chloride (2.20 equiv., 4.26 mL), and the reaction was allowed to stir at room temperature for 16 hours. Upon completion, the reaction was diluted with ethyl acetate and poured into a separatory funnel containing deionized water. The layers were separated, and the aqueous layer was extracted with additional portions of ethyl acetate. The combined organic layer was washed with brine, dried over magnesium sulfate, and concentrated under reduced pressure to afford the crude product, which was carried forward without further purification. A portion of the PMB-protected benzyl alcohol (783 mg, 2.06 mmol) was subjected to the general procedure using toluene as the solvent for the olefination with aldehyde B. Upon completion of the olefination, the reaction was cooled to 0 °C, and TBAF (1.0 equiv., 1.0 M in THF, 2.06 mL) was added dropwise. The reaction was allowed to stir for 30 min, at which point it was quenched and worked up following the general procedure. The product was purified by column chromatography (8% to 40% ethyl acetate in hexanes) to afford the desired product (478 mg, 49% yield).

$R_f = 0.30$ (ethyl acetate/hexanes 3:7; UV)

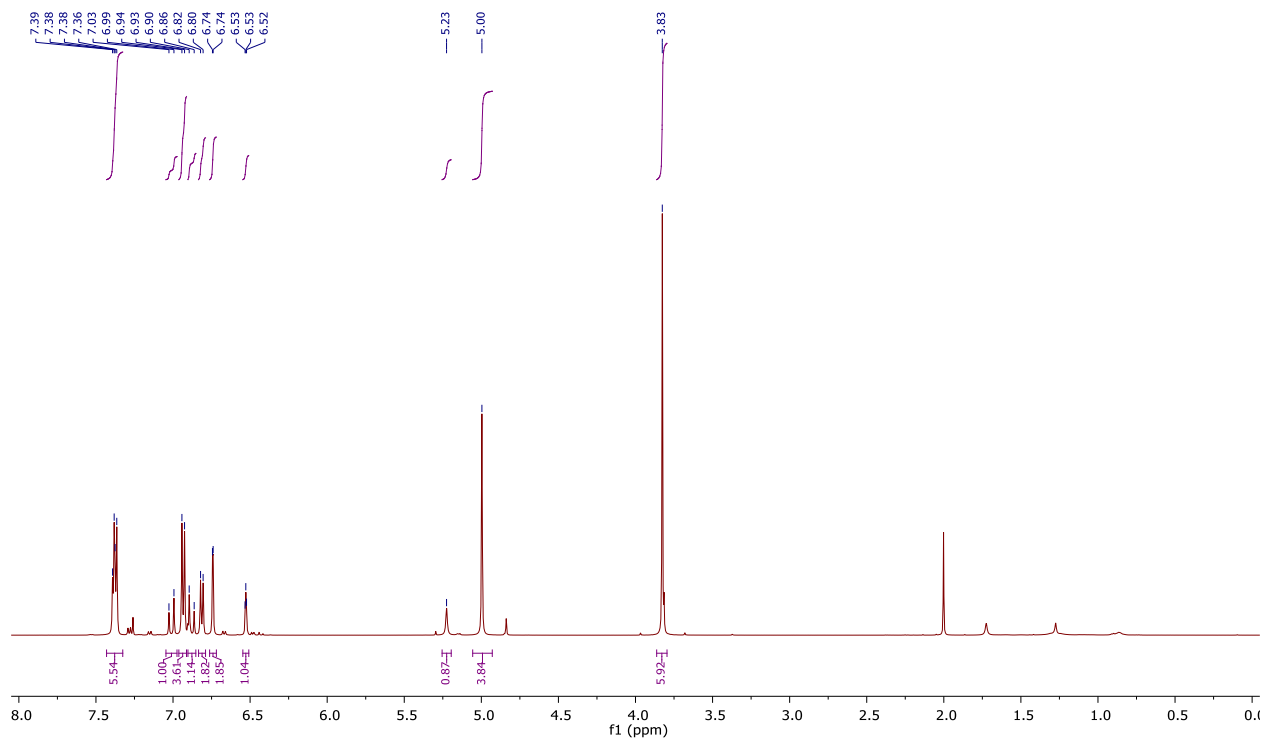
$^1\text{H NMR}$ (500 MHz, Chloroform-*d*) δ 7.38 (d, $J = 8.3$ Hz, 2H), 7.37 (d, $J = 8.5$ Hz, 4H), 7.01 (d, $J = 16.2$ Hz, 1H), 6.93 (d, $J = 8.6$ Hz, 4H), 6.88 (d, $J = 16.2$ Hz, 1H), 6.81 (d, $J = 8.3$ Hz, 2H), 6.74 (d, $J = 2.2$ Hz, 2H), 6.53 (d, $J = 2.3$ Hz, 1H), 5.23 (s, 1H), 5.00 (s, 4H), 3.83 (s, 6H).

$^{13}\text{C NMR}$ (126 MHz, Chloroform-*d*) δ 160.14, 159.45, 155.45, 139.65, 130.02, 129.33, 128.95, 128.73, 127.99, 126.52, 115.63, 114.03, 105.57, 101.24, 69.92, 55.32.

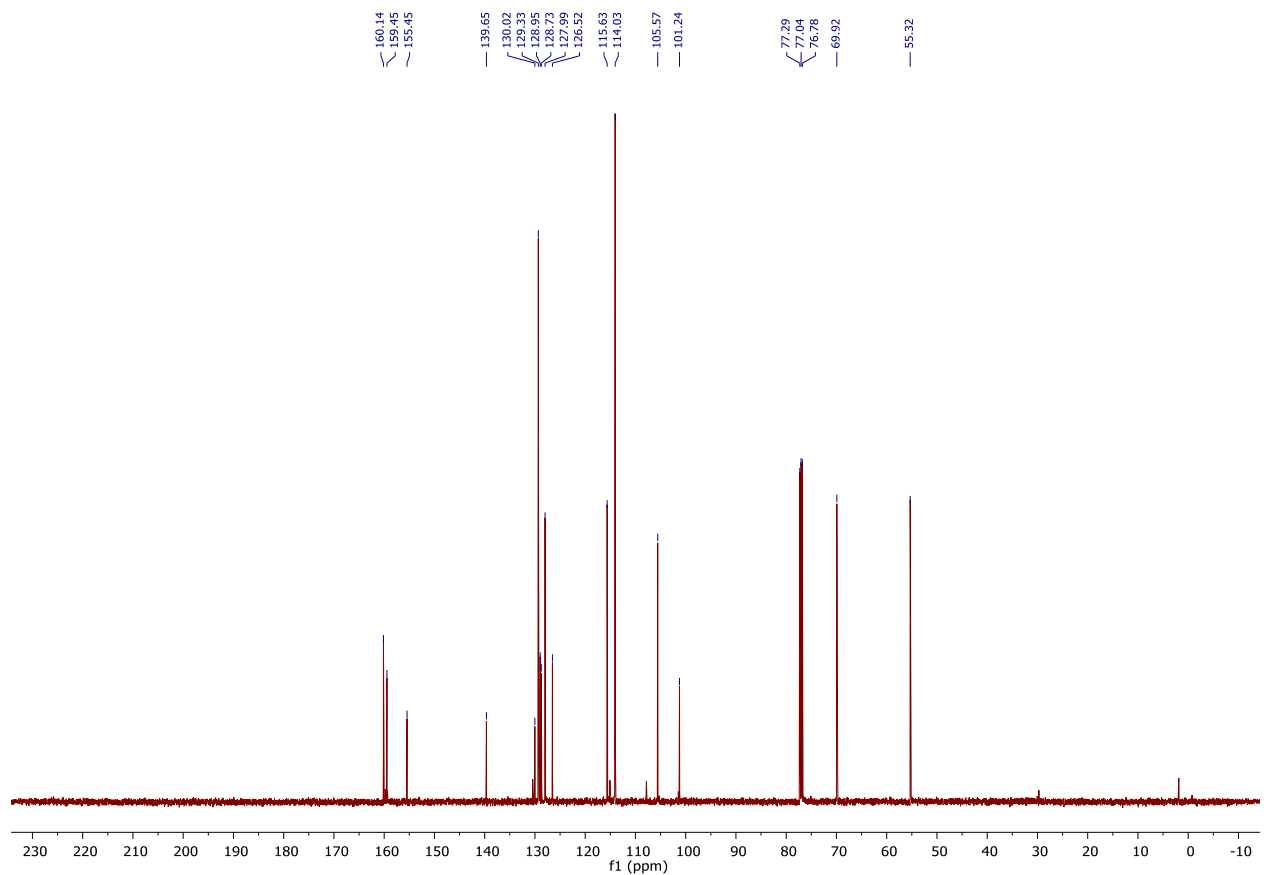
IR (Neat): 3608, 2953, 1611, 1580, 1514, 1436, 1245, 1144, 1030 cm^{-1} ;

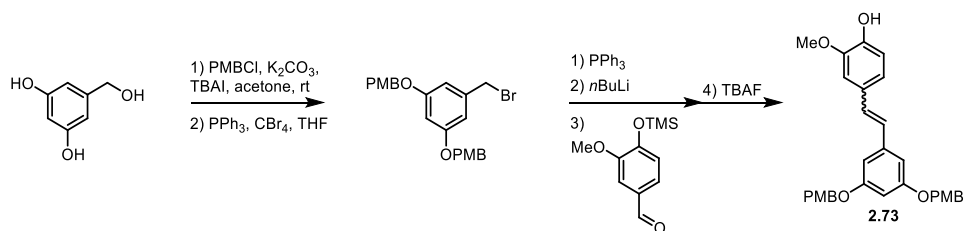
HRMS (ESI) m/z calculated for $\text{C}_{30}\text{H}_{29}\text{O}_5^+$ ($[\text{M}+\text{H}]^+$) 469.2010, found 469.2007.

¹H NMR, 500 MHz, Chloroform-*d*, Compound **2.72**



¹³C NMR, 126 MHz, Chloroform-*d*, Compound **2.72**





(2.73) (*E*)-4-(3,5-bis((4-methoxybenzyl)oxy)styryl)-2-methoxyphenol

Commercially available 3,5-dihydroxybenzyl alcohol (2.0 g, 14.3 mmol) was added to flask charged with potassium carbonate (2.25 equiv., 4.44 g) and tetrabutylammonium iodide (0.2 equiv., 1.05 g), and the solids were dissolved/suspended in acetone (42 mL). To the stirring reaction mixture was added 4-methoxybenzyl chloride (2.20 equiv., 4.26 mL), and the reaction was allowed to stir at room temperature for 16 hours. Upon completion, the reaction was diluted with ethyl acetate and poured into a separatory funnel containing deionized water. The layers were separated, and the aqueous layer was extracted with additional portions of ethyl acetate. The combined organic layer was washed with brine, dried over magnesium sulfate, and concentrated under reduced pressure to afford the crude product, which was carried forward without further purification. A portion of the PMB-protected material (734 mg, 1.93 mmol) was subjected to the general procedure using toluene as the solvent for the olefination with aldehyde C. Upon completion of the olefination, the reaction was cooled to 0 °C, and TBAF (1.0 equiv., 1.0 M in THF, 1.93 mL) was added dropwise. The reaction was allowed to stir for 30 min, at which point it was quenched and worked up following the general procedure. The product was purified by column chromatography (8% to 40% ethyl acetate in hexanes) to afford the desired product as a ~3.6:1 E:Z mixture (762 mg, 79% yield).

$R_f = 0.32$ (ethyl acetate/hexanes 3:7; UV)

E-isomer:

$^1\text{H NMR}$ (700 MHz, Chloroform-*d*) δ 7.37 (d, $J = 8.4$ Hz, 4H), 7.03 (d, $J = 1.8$ Hz, 1H), 7.01 (dd, $J = 8.2, 1.8$ Hz, 1H), 7.00 (d, $J = 15.9$ Hz, 1H), 6.93 (d, $J = 8.4$ Hz, 4H), 6.91 (d, $J = 8.1$ Hz, 1H), 6.87 (d, $J = 15.9$ Hz, 1H), 6.52 (t, $J = 2.5$ Hz, 1H), 5.67 (s, 1H), 5.00 (s, 4H), 3.95 (s, 3H), 3.83 (s, 6H).

$^{13}\text{C NMR}$ (126 MHz, Acetone-*d*₆) δ 160.30, 159.58, 146.83, 145.82, 139.70, 129.90, 129.40, 129.28, 129.06, 126.55, 120.71, 114.69, 114.13, 108.42, 105.63, 101.38, 70.01, 56.03, 55.42.

Z-isomer:

$^1\text{H NMR}$ (700 MHz, Chloroform-*d*) δ 7.28 (d, $J = 8.6$ Hz, 4H), 6.88 (d, $J = 8.6$ Hz, 4H), 6.80 (dd, $J = 7.6, 1.8$ Hz, 1H), 6.79 (d, $J = 7.6$ Hz, 1H), 6.77 (d, $J = 1.5$ Hz, 1H), 6.54 (d, $J = 2.2$ Hz, 2H), 6.48 (d, $J = 12.1$ Hz, 1H), 6.46 (t, $J = 2.3$ Hz, 1H), 6.44 (d, $J = 12.1$ Hz, 1H), 5.57 (s, 1H), 4.84 (s, 4H), 3.81 (s, 6H), 3.62 (s, 3H).

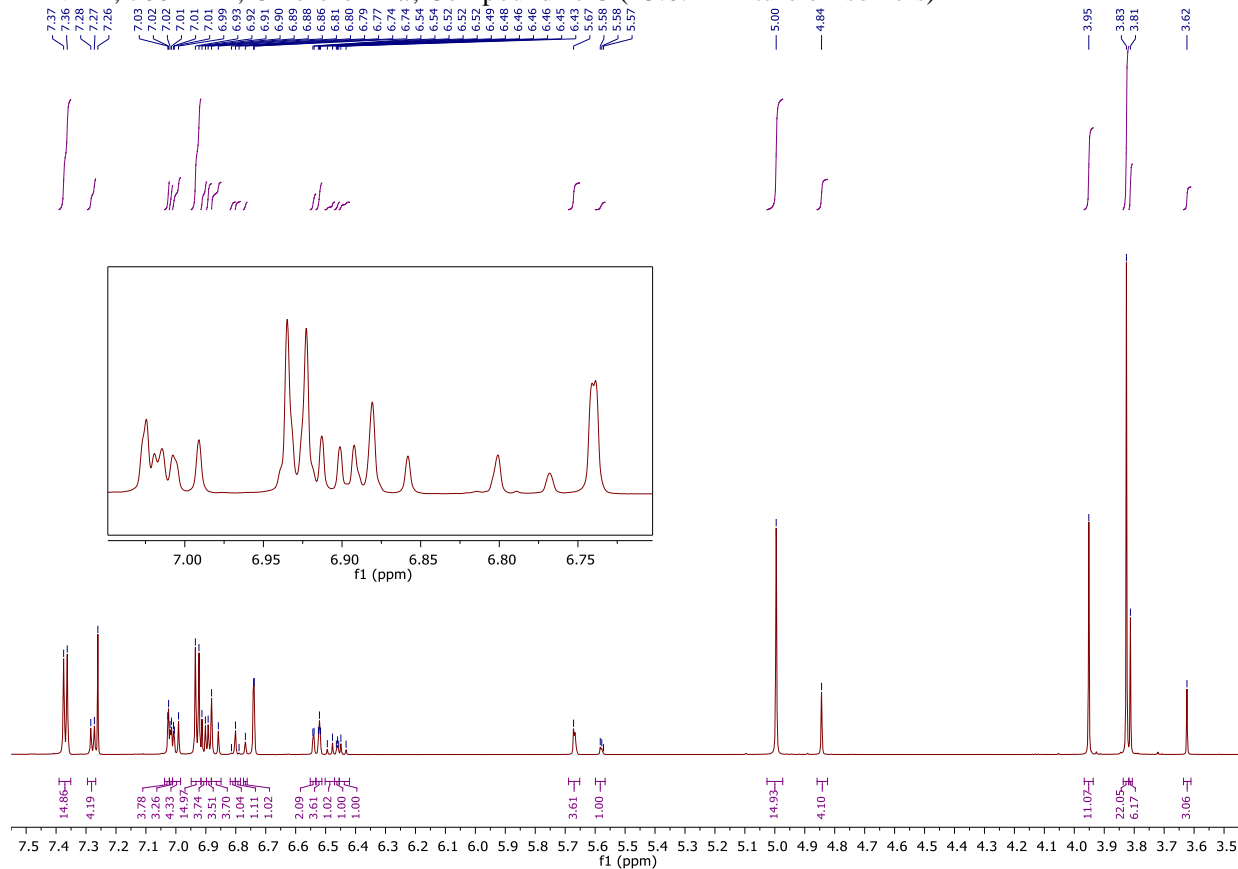
$^{13}\text{C NMR}$ (126 MHz, Acetone-*d*₆) δ 159.95, 159.51, 146.08, 145.08, 139.74, 130.53, 129.90, 128.61, 124.41, 122.87, 121.77, 114.07, 112.30, 111.42, 107.93, 101.44, 69.88, 55.75, 55.42.

Mixture of isomers:

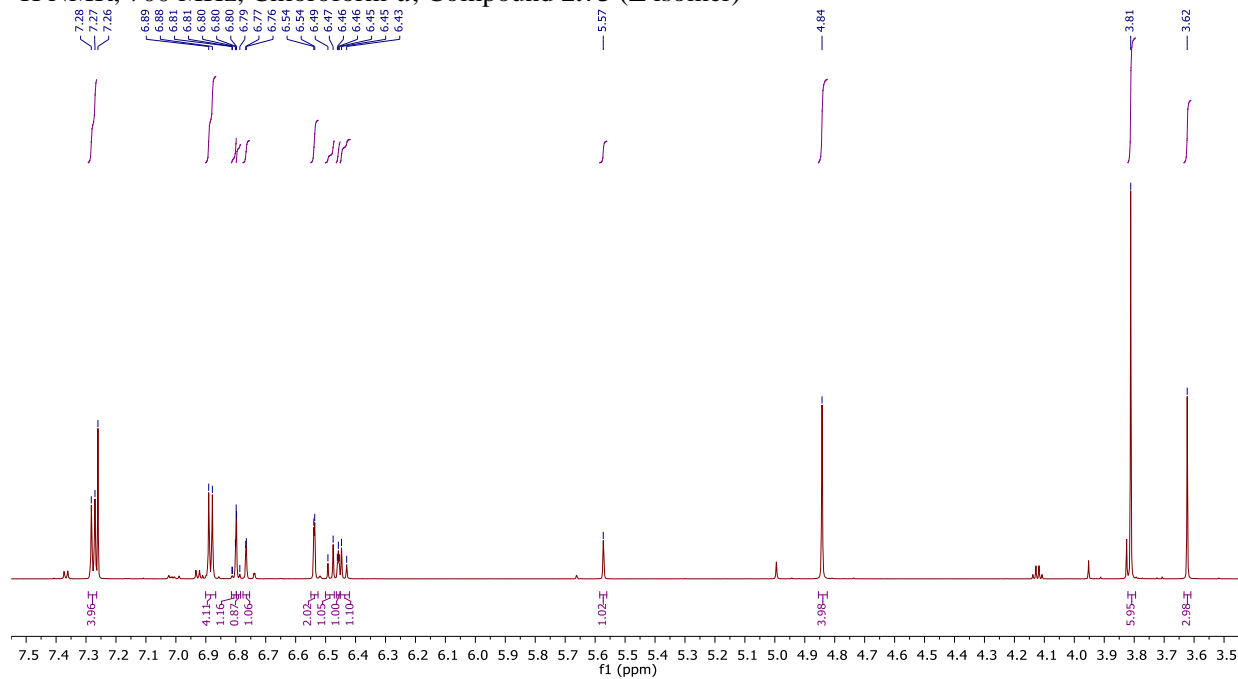
IR (Neat): 3522, 2954, 2869, 1592, 1454, 1353, 1287, 1212, 1194, 1157, 1149, 1056, 1037, 963, 828, 732, 695, 634 cm^{-1} ;

HRMS (ESI) m/z calculated for $\text{C}_{31}\text{H}_{31}\text{O}_6^+$ ($[\text{M}+\text{H}]^+$) 499.2115, found 499.2111.

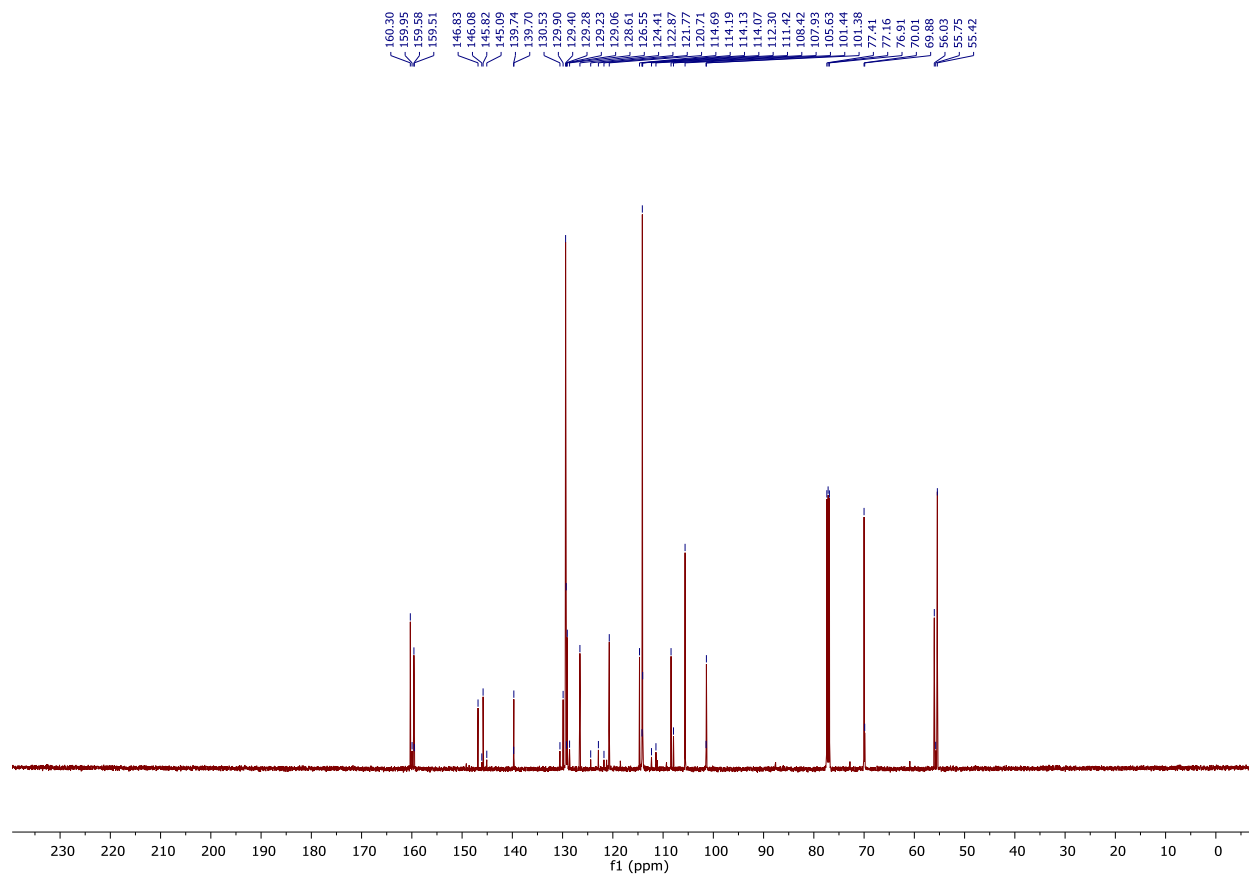
¹H NMR, 700 MHz, Chloroform-*d*, Compound **2.73** (~3.6:1 mixture of isomers)



¹H NMR, 700 MHz, Chloroform-*d*, Compound **2.73** (Z isomer)

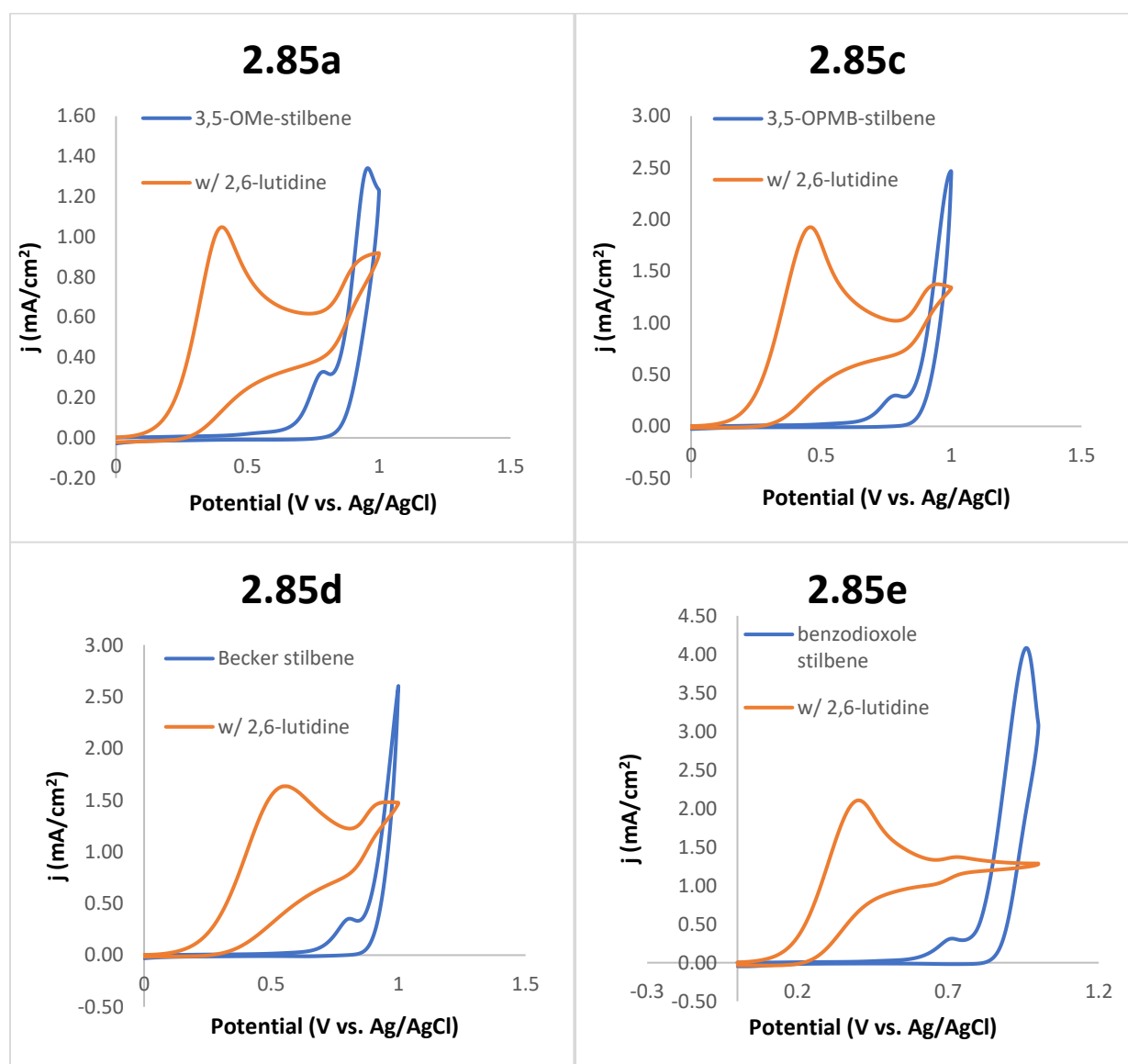


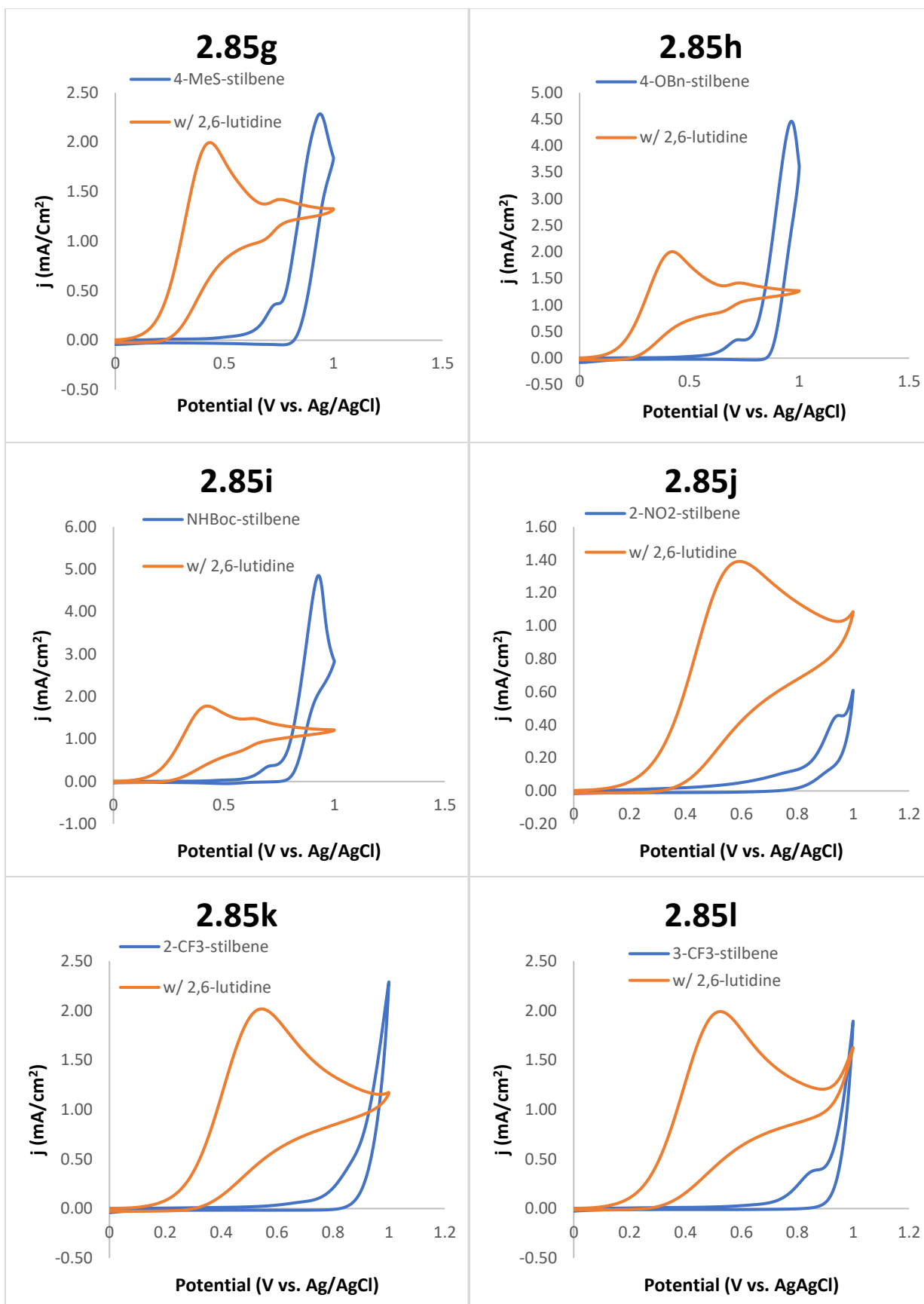
^{13}C NMR, 126 MHz, Chloroform-*d*, Compound **2.73** (~3.6:1 mixture of isomers)

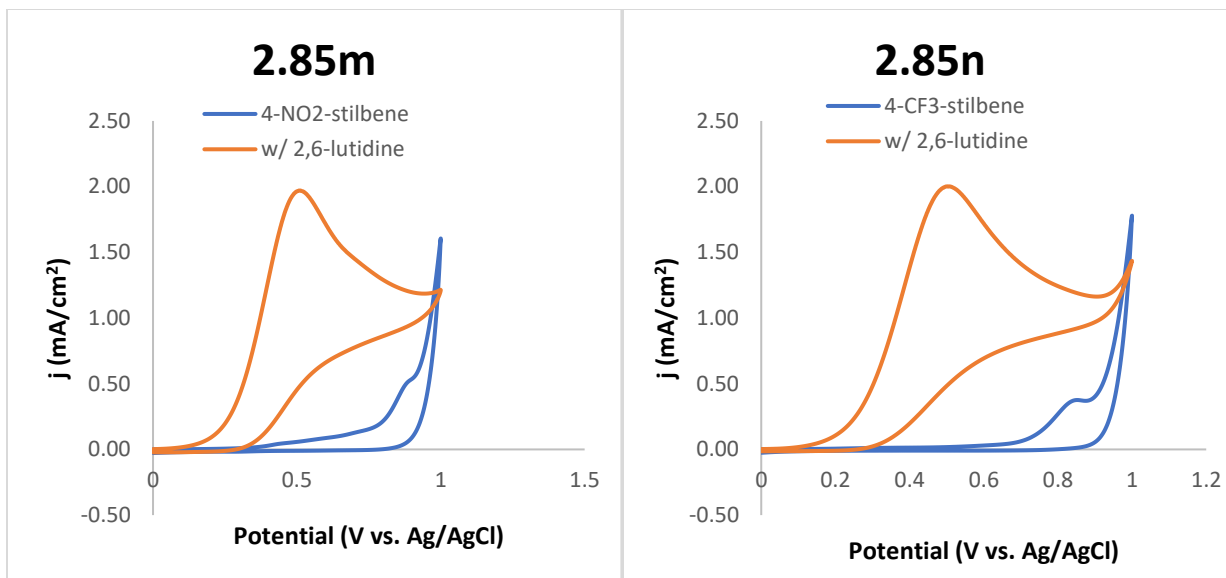


Cyclic Voltammetry Experimental Procedure: For each stilbene substrate, two cyclic voltammetry experiments were conducted. The first was to measure oxidation of the substrate (green or blue curve), while the second was to measure oxidation in the presence of 2,6-lutidine (orange curve). The stilbene substrate (0.03 mmol) and the electrolyte (Bu_4NPF_6 , 0.3 mmol, 116 mg) were dissolved in acetonitrile (3 mL). For the experiments with base, 2,6-lutidine (0.03 mmol, 3.5 μL) was added. The solution was transferred to a 5-neck electrochemical cell, which was outfitted with a working electrode (glassy carbon, 3 mm diameter, surface area = 0.0707 cm^2), reference electrode (Ag/AgCl, 3 M aq. KCl), and counter/auxiliary electrode (platinum wire). The electrochemical cell was connected to the CHI620E electrochemical analyzer, and the potential was swept from 0.0 V to +1.0 V in two sweep segments at a scan rate of 100 mV/s to afford the observed cyclic voltammograms. It can be seen in the data below that direct oxidation of the electron rich substrates occurs between +0.8 to +1.0 V, however direct oxidation of electron deficient substrates occurs beyond +1.0 V. In the presence of 2,6-lutidine, oxidation occurs below +0.6 V in all cases, suggesting that +0.6 V is a sufficient potential to attain the desired reactivity.

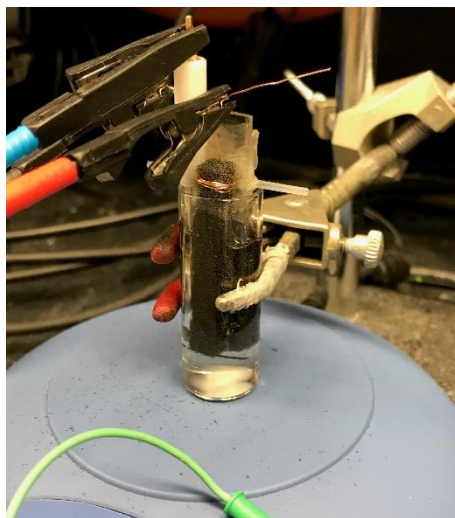
Cyclic Voltammetry Data:



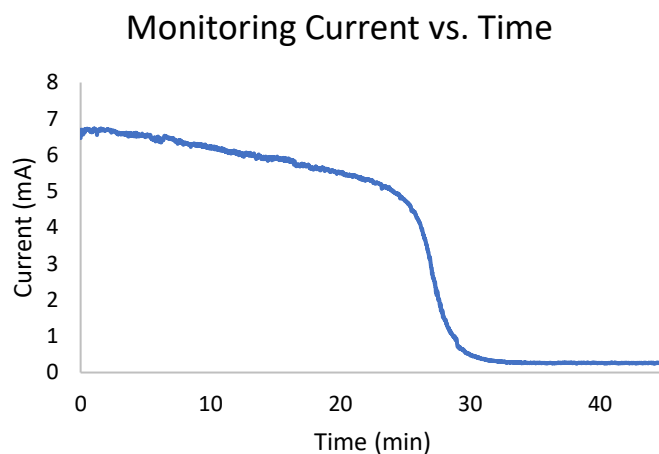




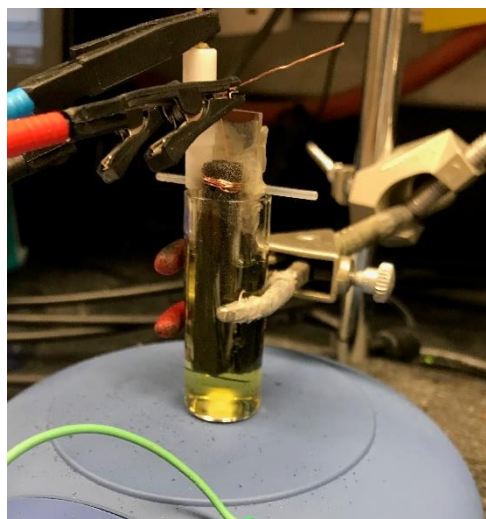
General Dimerization Procedure¹¹⁷: The starting phenol (0.1 mmol) was added to a reaction vial with KPF_6 (74 mg, 0.4 mmol) and 2,6-lutidine (2.3 μL , 0.02 mmol) and dissolved in acetonitrile (8 mL). Two pieces of 0.25 x 2-inch RVC panel (0.25 inch thickness) were cut. To each, a hole was made near one end, and copper wire was placed through the hole and wrapped around the top of each electrode. One end of the wire was left free in to connect to the alligator clips. These electrodes were carefully placed into the reaction vial along with the reference electrode (Ag/AgCl in 3 M KCl) and a divider (**see image**). The alligator clips were connected such that the reference and working electrodes were adjacent to each other, while the counter electrode was opposite the divider. Care was taken to ensure the copper wire was not submerged in solvent, nor the active components of the alligator clips touching each other. The reaction was stirred at 750 rpm for 1-2 h at a constant voltage of 0.6 V. A chronoamperogram was recorded to follow the course of the reaction. Upon completion of the reaction, the electrodes were removed and rinsed into a collection flask with DCM (~40 mL). The contents of the reaction vial were also rinsed into the collection flask. The solvent was removed on the rotovap, the crude material was resuspended in DCM, and the electrolyte was filtered away with a plug of Celite. The filtrate was then concentrated to afford the product, which did not require further purification. The diastereomeric ratios were determined by integration of the aryl protons on the quinone methide. When these were overlapping with other aryl signals, the δ -protons of the quinone methide were integrated to determine dr.



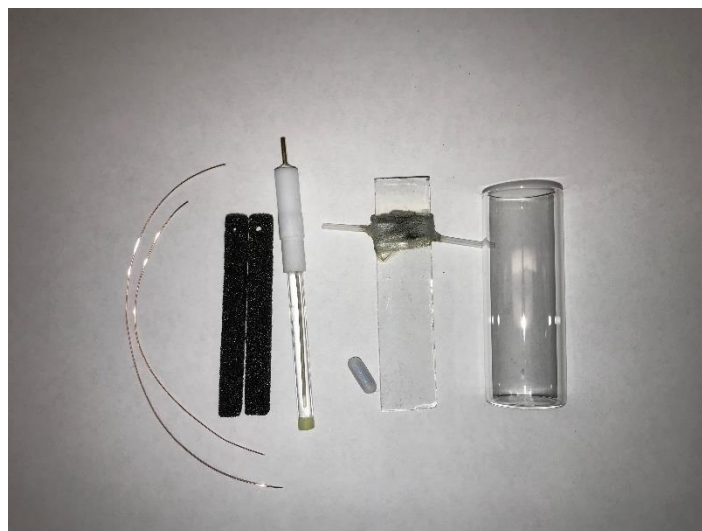
Prior to electrolysis



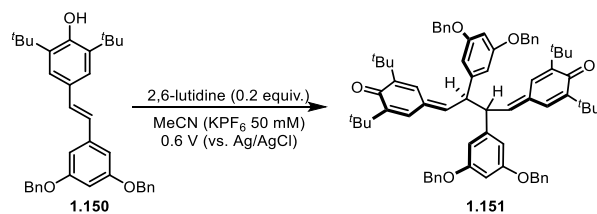
Sample chronoamperogram



After electrolysis



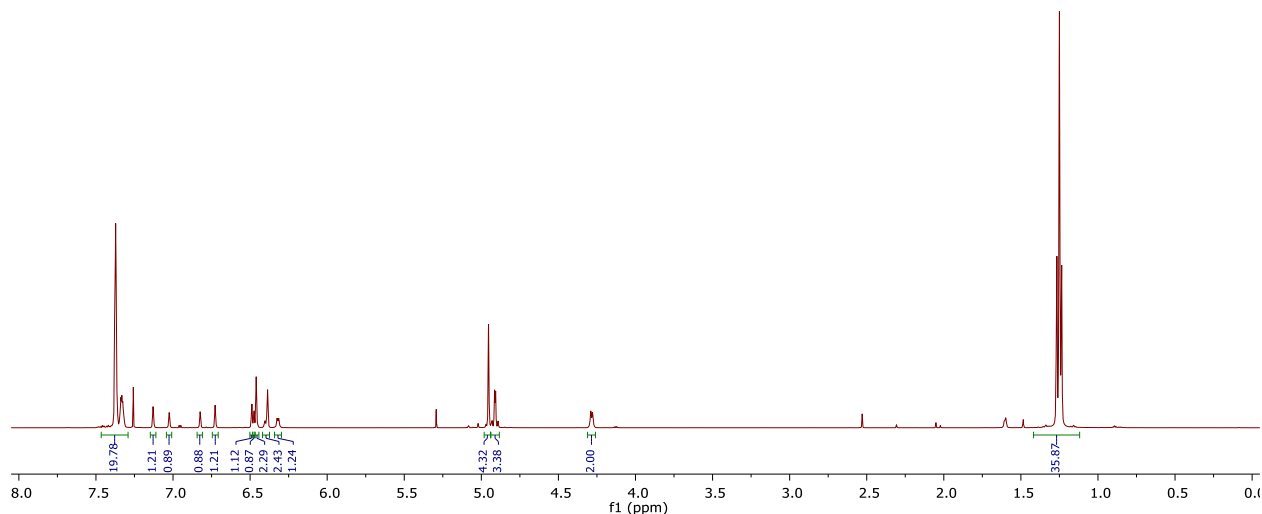
Reaction components

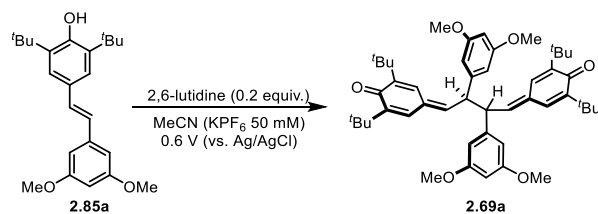


(1.151) 4,4'-((2R,3R)-2,3-bis(3,5-bis(benzyloxy)phenyl)butane-1,4-diylidene)bis(2,6-di-tert-butylcyclohexa-2,5-dien-1-one)

Stilbene **1.150** (0.1 mmol, 52.1 mg) was subjected to the general dimerization procedure, affording bis-quinone methide **1.151** (51.7 mg, 99% yield, 4:3 dr). The ^1H NMR spectrum was identical to the previous report for this compound.⁴⁵

^1H NMR (CDCl_3 , 500 MHz): δ 7.40 – 7.30 (m, 20H), β -H's of quinone methides: 7.12 (major diastereomer, d, $J = 2.2$ Hz, 2H), 7.02 (minor diastereomer, d, $J = 2.0$ Hz, 2H), 6.82 (minor diastereomer, d, $J = 2.2$ Hz, 2H), 6.72 (major diastereomer, d, $J = 2.0$ Hz, 2H); δ -H's of quinone methides: 6.41 – 6.37 (minor diastereomer, m, 2H), 6.33 – 6.29 (major diastereomer, m, 2H); 6.48 (major diastereomer, t, $J = 2.1$ Hz, 2H), 6.47 (minor diastereomer, t, $J = 2.2$ Hz, 2H), 6.45 (major diastereomer, d, $J = 2.1$ Hz, 4H), 6.38 (minor diastereomer, d, $J = 2.2$ Hz, 4H), 4.96 (major diastereomer, d, $J = 11.5$ Hz, 4H), 4.94 (major diastereomer, d, $J = 11.5$ Hz, 4H), 4.91 (minor diastereomer, d, $J = 11.5$ Hz, 4H), 4.89 (minor diastereomer, d, $J = 11.5$ Hz, 4H), 4.28 (m, overlap, sp^3 methines of both diastereomers, 4H), 1.26 (minor diastereomer *t*Bu's, s, 18H), 1.24 (major diastereomer *t*Bu's, s, 36H), 1.23 (minor diastereomer *t*Bu's, s, 18H).

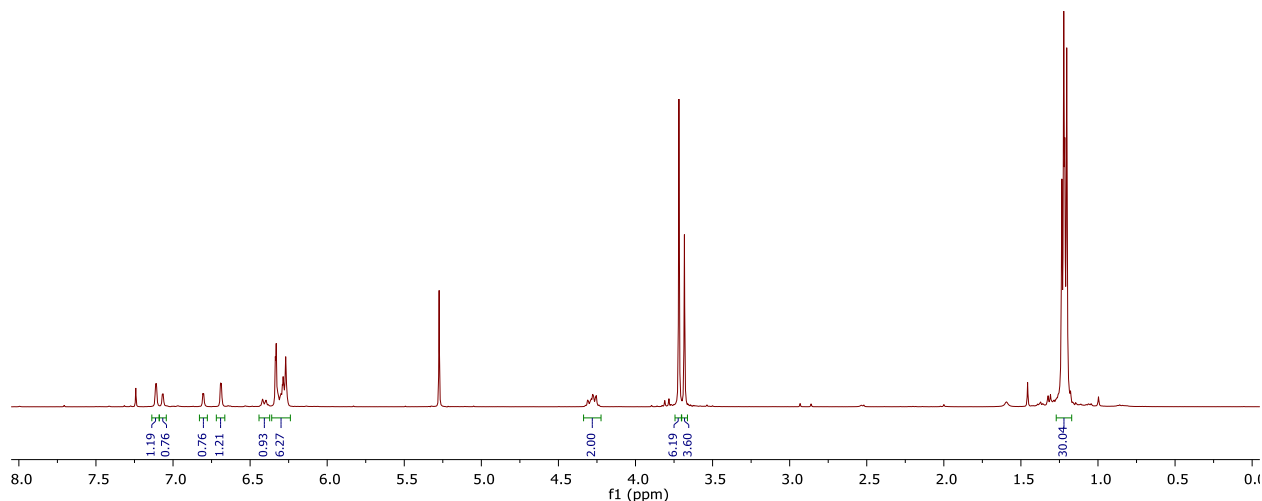


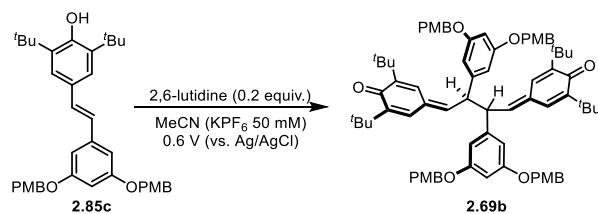


(2.69a) 4,4'-((2*R*,3*R*)-2,3-bis(3,5-dimethoxyphenyl)butane-1,4-diylidene)bis(2,6-di-*tert*-butylcyclohexa-2,5-dien-1-one)

Stilbene **2.85a** (0.1 mmol, 36.9 mg) was subjected to the general dimerization procedure, affording bis-quinone methide **2.69a** (36.5mg, 99% yield, 3:2 dr). The ^1H NMR spectrum was identical to the previous report for this compound.⁴⁵

^1H NMR (CDCl₃, 700 MHz): δ β -H's of quinone methides: 7.13 (major diastereomer, d, $J = 1.9$ Hz, 2H), 7.09 (minor diastereomer, d, $J = 2.0$ Hz, 2H), 6.82 (minor diastereomer, d, $J = 2.2$ Hz, 2H), 6.71 (major diastereomer, d, $J = 2.2$ Hz, 2H); δ -H's of quinone methides: 6.43 (minor diastereomer, m, 2H), 6.33 (major diastereomer, m, 2H); 6.35 (Ar-H major diastereomer, d, $J = 2.1$ Hz, 4H), 6.31 (Ar-H major diastereomer, t, $J = 2.1$ Hz, 2H), 6.29-6.27 (Ar-H's minor diastereomer, overlap, 6H), 4.34 – 4.30 (minor diastereomer sp³ methines, m, 2H), 4.30 – 4.26 (major diastereomer sp³ methines, m, 2H), 3.74 (major diastereomer –OMe's, s, 12H), 3.70 (minor diastereomer –OMe's, s, 12H), 1.25 (minor diastereomer *t*Bu's, s, 18H), 1.24 (major diastereomer *t*Bu's, s, 18H), 1.23 (minor diastereomer *t*Bu's, s, 18H), 1.22 (major diastereomer *t*Bu's, s, 18H).





(2.69b) 4,4'-((2*R*,3*R*)-2,3-bis(3,5-bis((4-methoxybenzyl)oxy)phenyl)butane-1,4-diylidene)bis(2,6-di-*tert*-butylcyclohexa-2,5-dien-1-one)

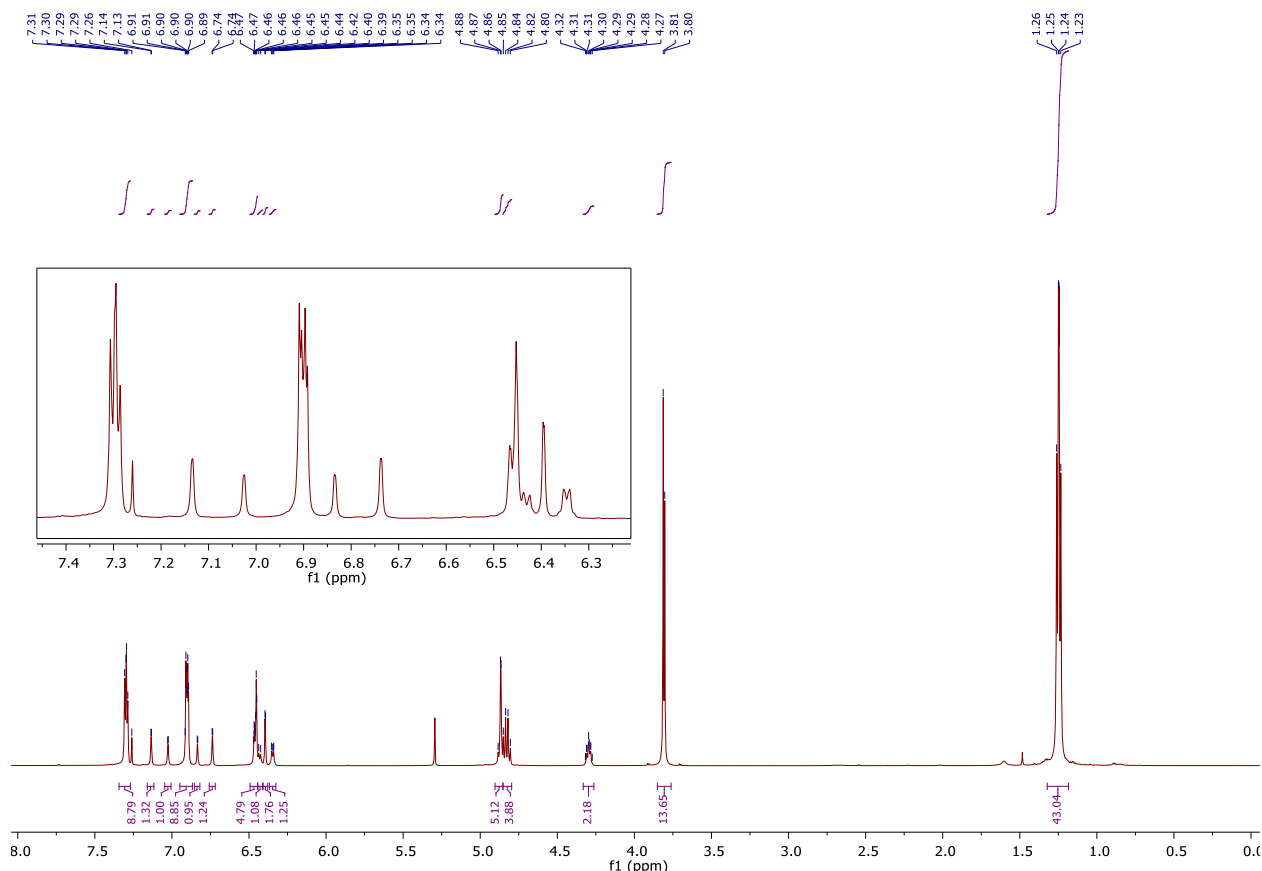
Stilbene **2.85c** (0.1 mmol, 58.1 mg) was subjected to the general dimerization procedure, affording bisquinone methide **2.69b** (57.8 mg, 99% yield, 5:4 dr).

¹H NMR (700 MHz, Chloroform-*d*) δ 7.30 (m, 16H), 7.13 (β -H, major diastereomer, d, $J = 2.4$ Hz, 2H), 7.03 (β -H, minor diastereomer, d, $J = 2.4$ Hz, 2H), 6.90 (m, 16H), 6.83 (β -H, minor diastereomer, d, $J = 2.4$ Hz, 2H), 6.74 (β -H, major diastereomer, d, $J = 2.4$ Hz, 2H), 6.46 (m, 8H), 6.43 (δ -H, minor diastereomer, d, $J = 8.8$ Hz, 2H), 6.39 (minor diastereomer, d, $J = 2.2$ Hz, 4H), 6.35 (δ -H, major diastereomer, dd, $J = 7.2, 2.5$ Hz, 2H), 4.87 (d, $J = 2.6$ Hz, 8H), 4.83 (q, $J = 10.6$ Hz, 8H), 4.30 (m, sp³ methines of both diastereomers, 4H), 3.81 (s, 12H), 3.80 (s, 12H), ^tBu signals: 1.26 (s, 18 H), 1.25 (s, 18H), 1.24 (s, 18 H), 1.23 (s, 18 H).

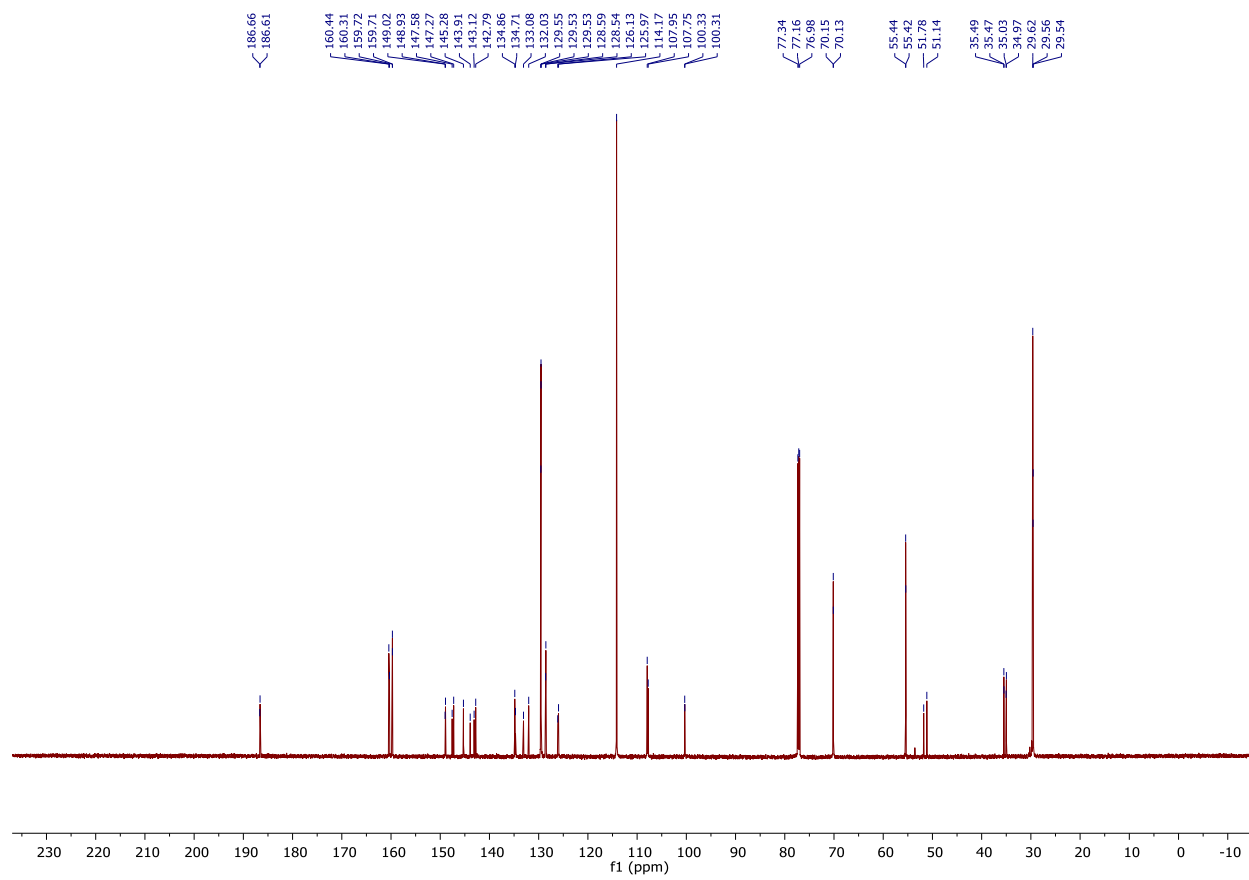
¹³C NMR (176 MHz, Chloroform-*d*) δ 186.66, 186.61, 160.44, 160.31, 159.72, 159.71, 149.02, 148.93, 147.58, 147.27, 145.28, 143.91, 143.12, 142.79, 134.86, 134.71, 133.08, 132.03, 129.55, 129.53, 128.59, 128.54, 126.13, 125.97, 114.17, 107.95, 107.75, 100.33, 100.31, 70.15, 70.13, 55.44, 55.42, 51.78, 51.14, 35.49, 35.47, 35.03, 34.97, 29.62, 29.56, 29.54.

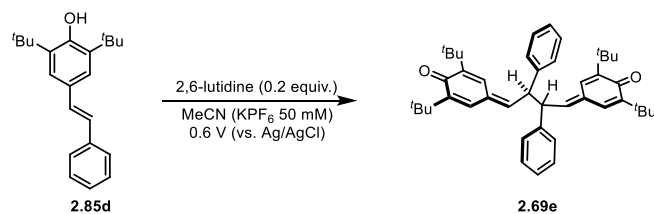
IR (Neat): 2955, 2929, 1611, 1577, 1515, 1439, 1245, 1147, 1046, 1026, 967, 858 cm⁻¹;

HRMS (ESI) m/z calculated for C₇₆H₈₇O₁₀⁺ ([M+H]⁺) 1159.6294, found 1159.6278.



^{13}C NMR, 176 MHz, Chloroform-*d*, Dimer **2.69b**





(2.69e) 4,4'-((2R,3R)-2,3-diphenylbutane-1,4-diylidene)bis(2,6-di-*tert*-butylcyclohexa-2,5-dien-1-one)
 Stilbene **2.85d** (0.1 mmol, 33 mg) was subjected to the general dimerization procedure, affording bis-quinone methide **2.69e** (32.6 mg, 99% yield, 4:3 dr).

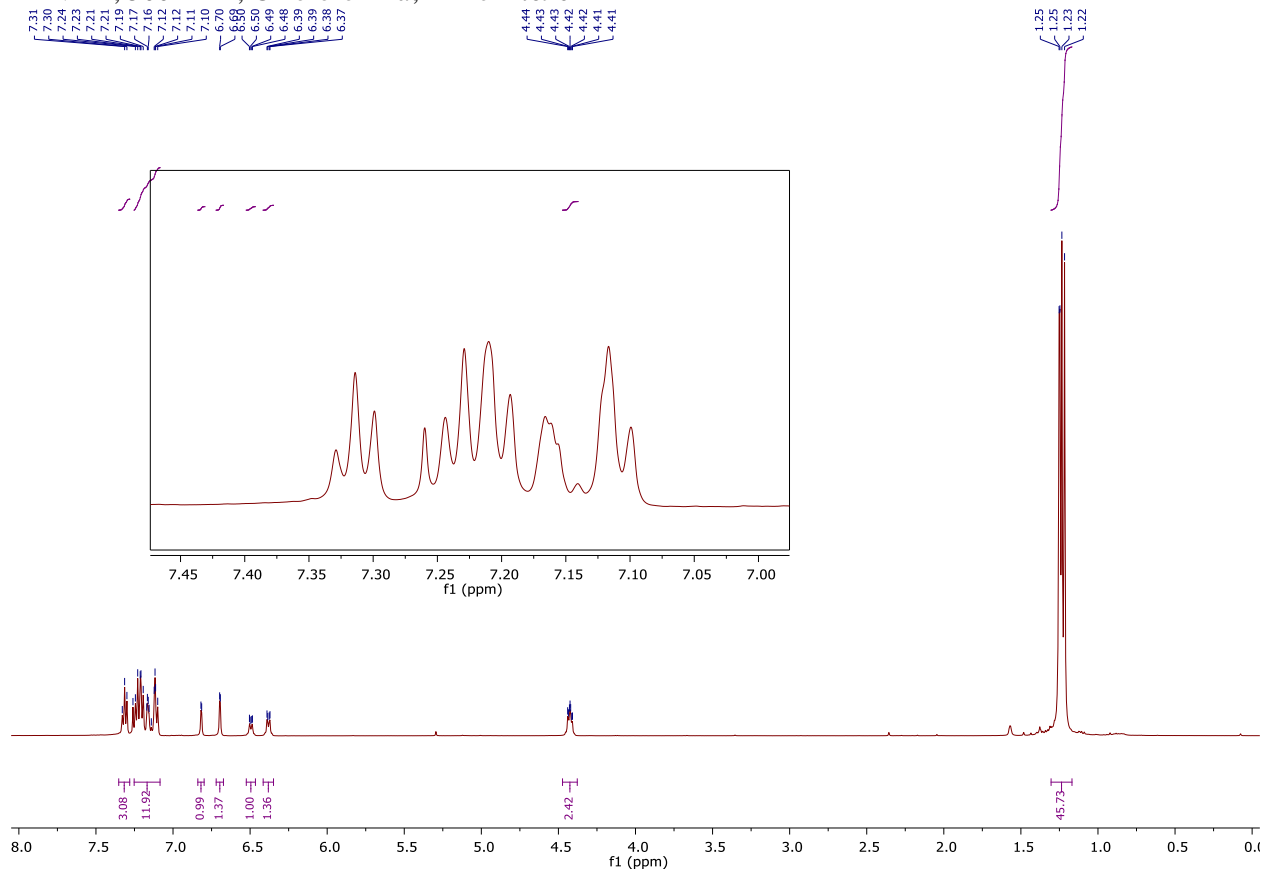
¹H NMR (500 MHz, Chloroform-*d*) δ 7.31 (t, *J* = 7.5 Hz, 4H), 7.25 – 7.08 (m, 20H), β-H's of quinone methides: 6.82 (minor diastereomer, d, *J* = 2.4 Hz, 2H), 6.70 (major diastereomer, d, *J* = 2.4 Hz, 2H), δ-H's of quinone methides: 6.52 – 6.47 (minor diastereomer, m, 2H), 6.42 – 6.35 (major diastereomers, m, 2H), 4.42 (m, sp³ methines of both diastereomers, 4H), ^tBu signals: 1.25 (s, 18 H), 1.25 (s, 18H), 1.23 (s, 18 H), 1.22 (s, 18 H).

¹³C NMR (126 MHz, Chloroform-*d*) δ 186.59, 186.55, 149.11, 148.91, 147.61, 147.32, 145.47, 144.98, 141.14, 140.63, 134.67, 132.76, 132.02, 129.17, 128.97, 128.47, 128.27, 127.55, 127.23, 126.07, 125.94, 51.68, 51.31, 35.52, 35.49, 35.03, 34.95, 29.60, 29.56, 29.52.

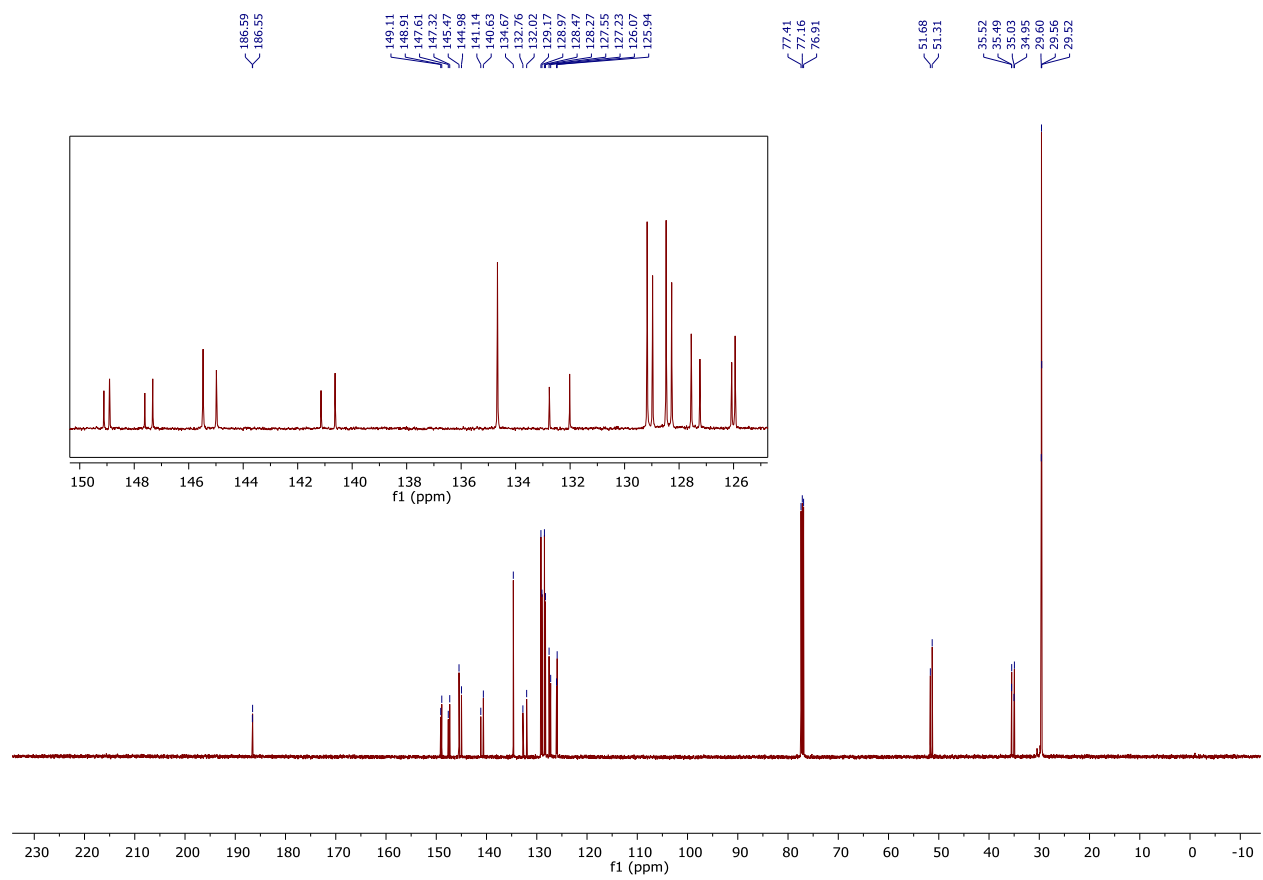
IR (Neat): 2951, 2915, 1614, 1577, 1453, 1358, 1257, 917, 883, 759, 697 cm⁻¹;

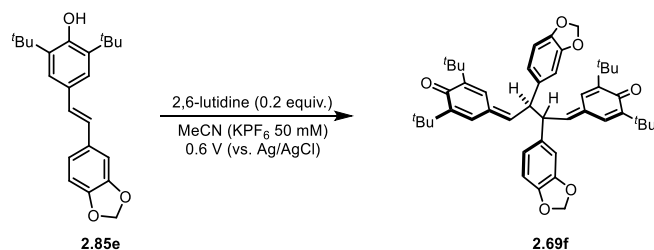
HRMS (ESI) *m/z* calculated for NaC₄₄H₅₄O₂⁺ ([M+Na]⁺) 637.4016, found 637.4012.

¹H NMR, 500 MHz, Chloroform-*d*, Dimer **2.69e**



^{13}C NMR, 126 MHz, Chloroform-*d*, Dimer **2.69e**





(2.69f) 4,4'-((2R,3R)-2,3-bis(benzo[d][1,3]dioxol-5-yl)butane-1,4-diylidene)bis(2,6-di-tert-butylcyclohexa-2,5-dien-1-one)

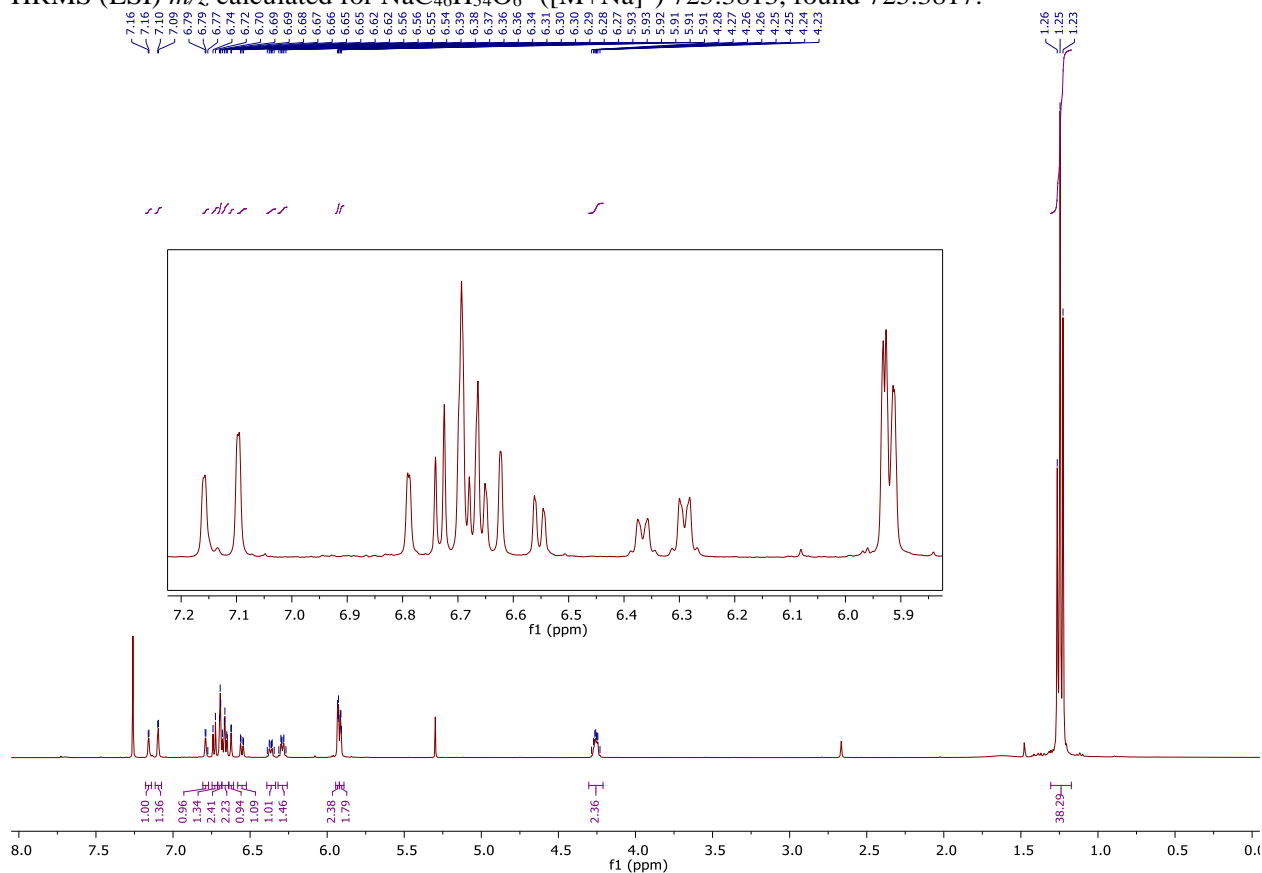
Stilbene **2.85e** (0.1 mmol, 35.2 mg) was subjected to the general dimerization procedure, affording bis-quinone methide **2.69f** (34.7 mg, 99% yield, 3:2 dr).

$^1\text{H NMR}$ (500 MHz, Chloroform-*d*) δ 7.16 (minor diastereomer, d, $J = 2.4$ Hz, 2H), 7.10 (major diastereomer, d, $J = 2.4$ Hz, 2H), 6.79 (minor diastereomer, d, $J = 2.3$ Hz, 2H), 6.73 (minor diastereomer, d, $J = 7.9$ Hz, 2H), 6.69 (d, $J = 1.6$ Hz, 4H), 6.68 – 6.64 (m, 4H), 6.62 (d, $J = 1.7$ Hz, 2H), 6.55 (dd, $J = 8.0, 1.7$ Hz, 2H), 6.36 (δ -H, minor diastereomer, dt, $J = 8.7, 4.4$ Hz, 2H), 6.32 – 6.26 (δ -H, minor diastereomer, m, 2H), 5.93 (d, $J = 2.3$ Hz, 4H), 5.91 (d, $J = 2.1$ Hz, 4H), 4.30 – 4.21 (sp^3 methines of both diastereomers, m, 4H), ^tBu signals: 1.26 (s, 18 H), 1.25 (s, 36 H), 1.23 (s, 18 H).

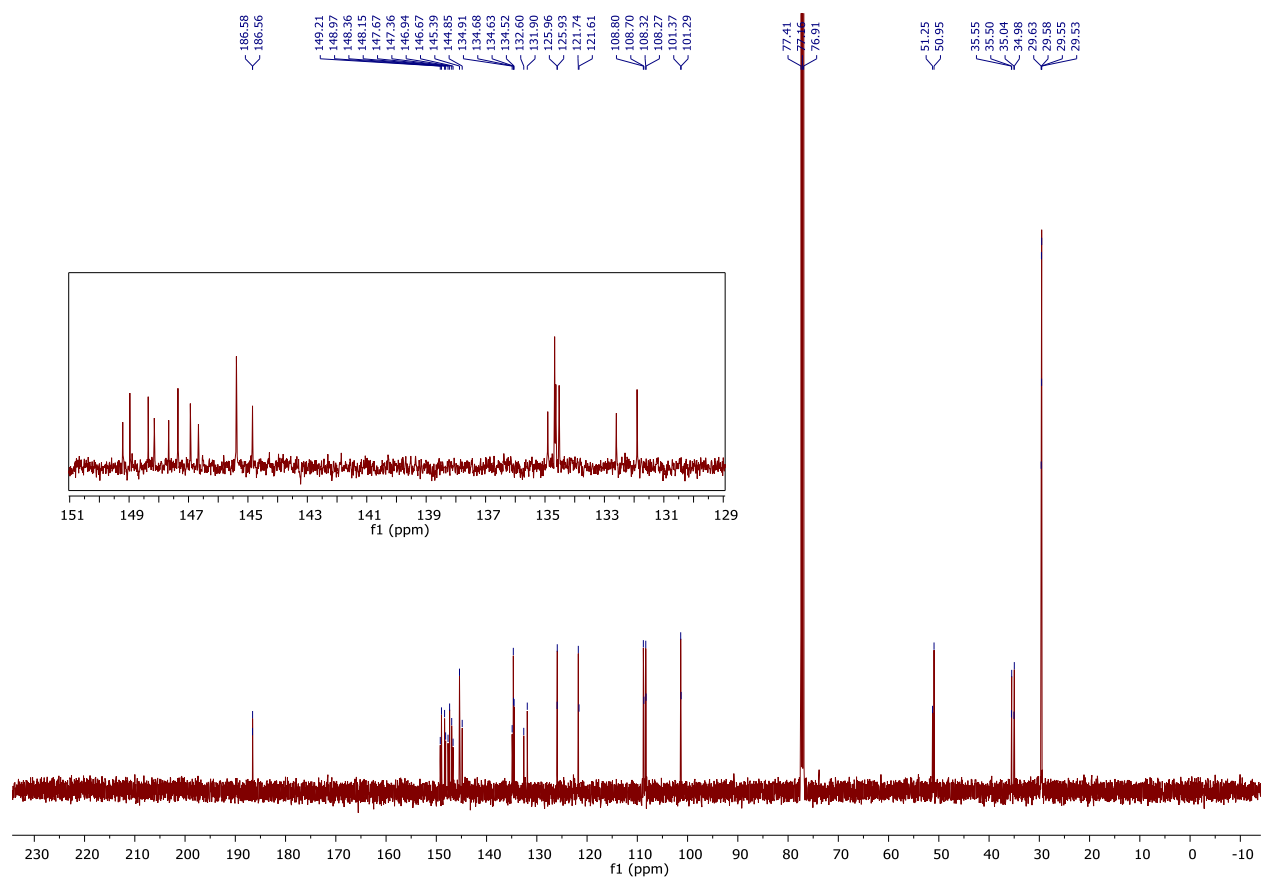
$^{13}\text{C NMR}$ (126 MHz, Chloroform-*d*) δ 186.58, 186.56, 149.21, 148.97, 148.36, 148.15, 147.67, 147.36, 146.94, 146.67, 145.39, 144.85, 134.91, 134.68, 134.63, 134.52, 132.60, 131.90, 125.96, 125.93, 121.74, 121.61, 108.80, 108.70, 108.32, 108.27, 101.37, 101.29, 51.25, 50.95, 35.55, 35.50, 35.04, 34.98, 29.63, 29.58, 29.55, 29.53.

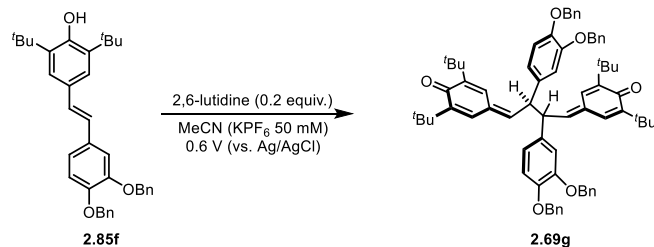
IR (Neat): 2954, 2914, 2361, 2336, 1616, 1539, 1362, 1243, 1034, 924, 808 cm^{-1} ;

HRMS (ESI) m/z calculated for $\text{NaC}_{46}\text{H}_{54}\text{O}_6^+$ ($[\text{M}+\text{Na}]^+$) 725.3813, found 725.3817.



^{13}C NMR, 126 MHz, Chloroform-*d*, Dimer **2.69f**





(2.69g) 4,4'-((2*R*,3*R*)-2,3-bis(3,4-bis(benzyloxy)phenyl)butane-1,4-diyldiene)bis(2,6-di-tert-butylcyclohexa-2,5-dien-1-one)

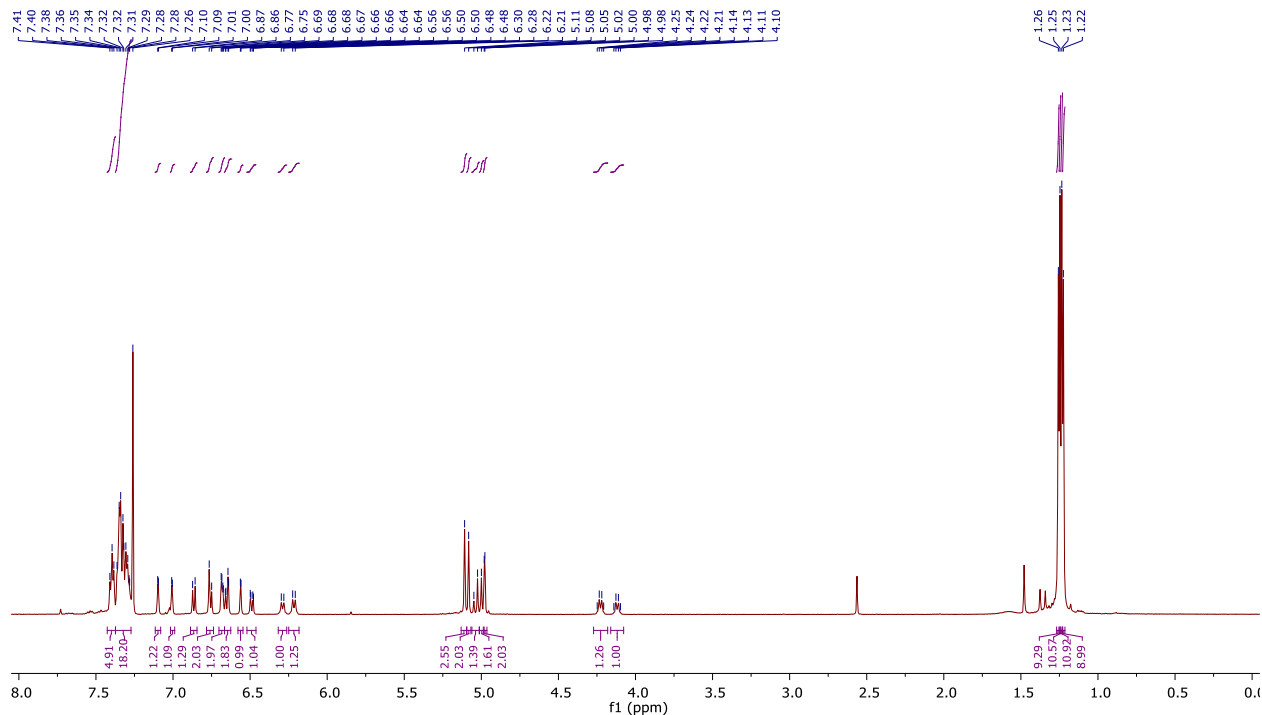
Stilbene **2.85f** (0.1 mmol, 52.1 mg) was subjected to the general dimerization procedure, affording bis-quinone methide **2.69g** (48.9 mg, 94% yield, 5:4 dr).

¹H NMR (500 MHz, Chloroform-*d*) δ 7.40 (t, *J* = 6.5 Hz, 4H), 7.37 – 7.27 (m, 16H), 7.10 (major diastereomer, d, *J* = 2.3 Hz, 1H), 7.01 (minor diastereomer, d, *J* = 2.1 Hz, 1H), 6.86 (major diastereomer, d, *J* = 8.2 Hz, 1H), 6.77 (s, 1H), 6.76 (d, *J* = 8.0 Hz, 1H), 6.68 (m, 2H), 6.67 – 6.63 (m, 2H), 6.56 (minor diastereomer, d, *J* = 2.0 Hz, 1H), 6.49 (minor diastereomer, dd, *J* = 8.3, 2.0 Hz, 1H), 6.29 (minor diastereomer, d, *J* = 8.2 Hz, 1H), 6.22 (major diastereomer, d, *J* = 8.4 Hz, 1H), 5.11 (major diastereomer, s, 2H), 5.08 (minor diastereomer, s, 2H), 5.04 (major diastereomer, d, *J* = 11.9 Hz, 1H), 5.00 (major diastereomer, d, *J* = 11.9 Hz, 1H), 4.98 (minor diastereomer, s, 2H), 4.23 (major diastereomer, d, *J* = 8.2 Hz, 1H), 4.12 (minor diastereomer, d, *J* = 8.0 Hz, 1H), 1.26 (s, 9H), 1.25 (s, 9H), 1.23 (s, 9H), 1.22 (s, 9H).

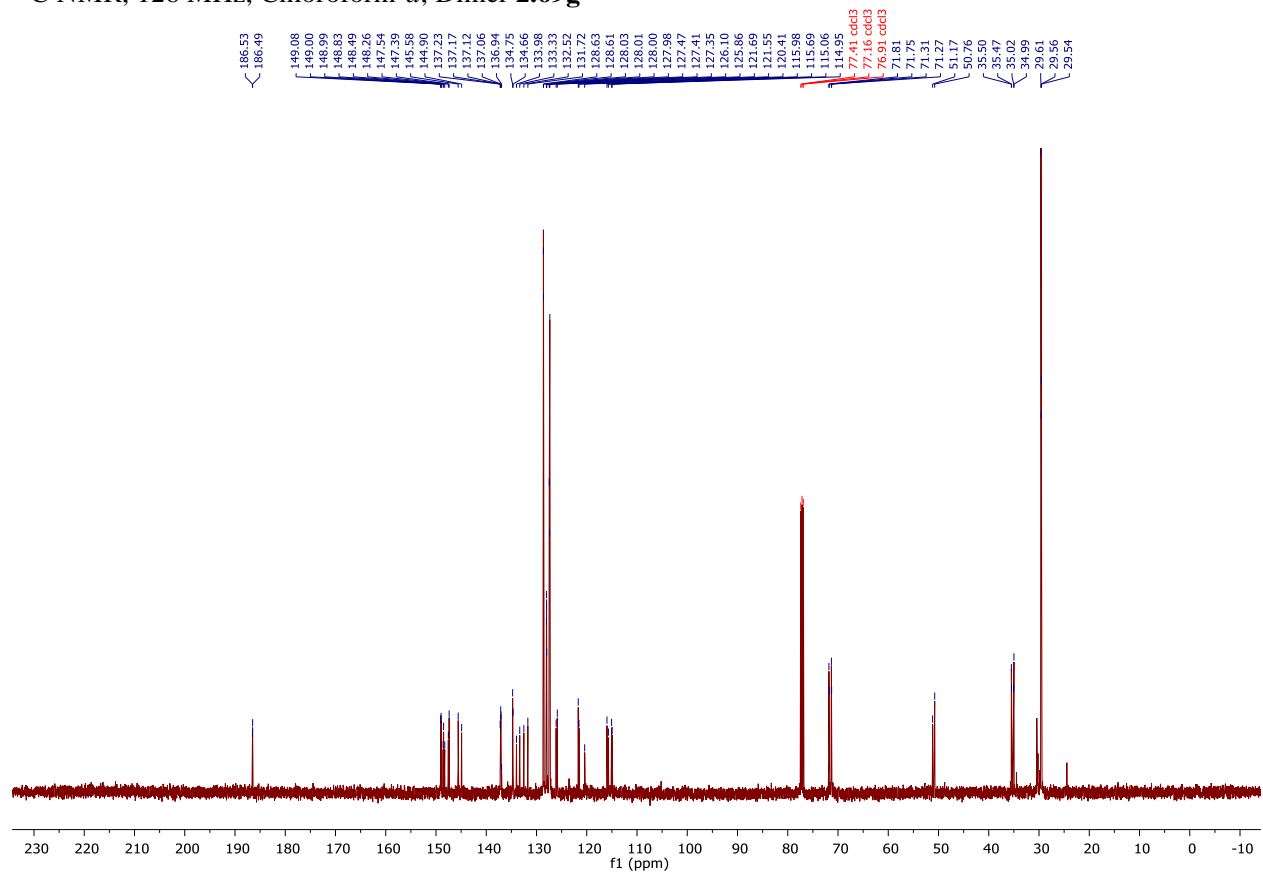
¹³C NMR (126 MHz, Chloroform-*d*) δ 186.53, 186.49, 149.08, 149.00, 148.99, 148.83, 148.49, 148.26, 147.54, 147.39, 145.58, 144.90, 137.23, 137.17, 137.12, 137.06, 136.94, 134.75, 134.66, 133.98, 133.33, 132.52, 131.72, 128.63, 128.61, 128.03, 128.01, 128.00, 127.98, 127.47, 127.41, 127.35 (2C), 126.10, 125.86, 121.69, 121.55, 120.41, 115.98, 115.69, 115.06, 114.95, 71.81, 71.75, 71.31, 71.27, 51.17, 50.76, 35.50, 35.47, 35.02, 34.99, 29.61 (2C), 29.56, 29.54.

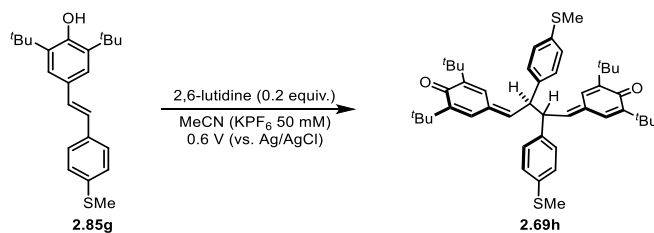
IR (Neat): 2960, 2867, 1616, 1510, 1453, 1358, 1262, 1136, 1021, 734, 697 cm⁻¹;

HRMS (ESI) *m/z* calculated for NaC₇₂H₇₈O₆⁺ ([M+Na]⁺) 1061.5691, found 1061.5672.



¹³C NMR, 126 MHz, Chloroform-*d*, Dimer **2.69g**





(2.69h) 4,4'-((2*R*,3*R*)-2,3-bis(4-(methylthio)phenyl)butane-1,4-diylidene)bis(2,6-di-*tert*-butylcyclohexa-2,5-dien-1-one)

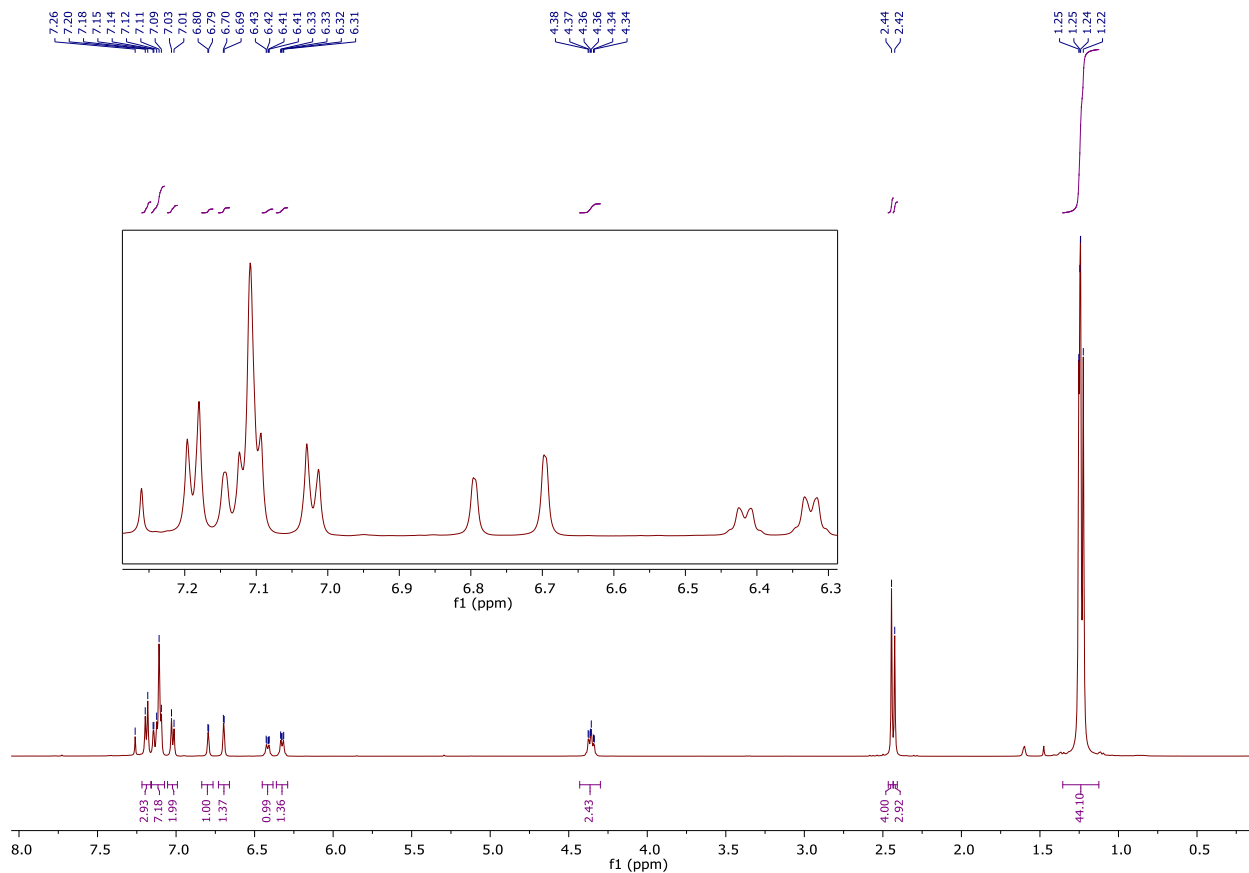
Stilbene **2.85g** (0.1 mmol, 35.5 mg) was subjected to the general dimerization procedure, affording bisquinone methide **2.69h** (32.9 mg, 93% yield, 4:3 dr).

¹H NMR (500 MHz, Chloroform-*d*) δ 7.19 (major diastereomer, d, *J* = 8.0 Hz, 4H), 7.12 (m, 12H), 7.02 (minor diastereomer, d, *J* = 8.0 Hz, 4H), β-H's of quinone methides: 6.80 (minor diastereomer, d, *J* = 2.4 Hz, 2H), 6.70 (major diastereomer, d, *J* = 2.4 Hz, 2H), δ-H's of quinone methides: 6.42 (minor diastereomer, dd, *J* = 7.2, 2.4 Hz, 2H), 6.36 – 6.29 (major diastereomer, m, 2H), 4.43 – 4.30 (sp³ methines of both diastereomers, m, 4H), 2.44 (s, 3H), 2.42 (s, 3H), ^tBu signals: 1.25 (s, 18 H), 1.25 (s, 18H), 1.24 (s, 18 H), 1.22 (s, 18 H).

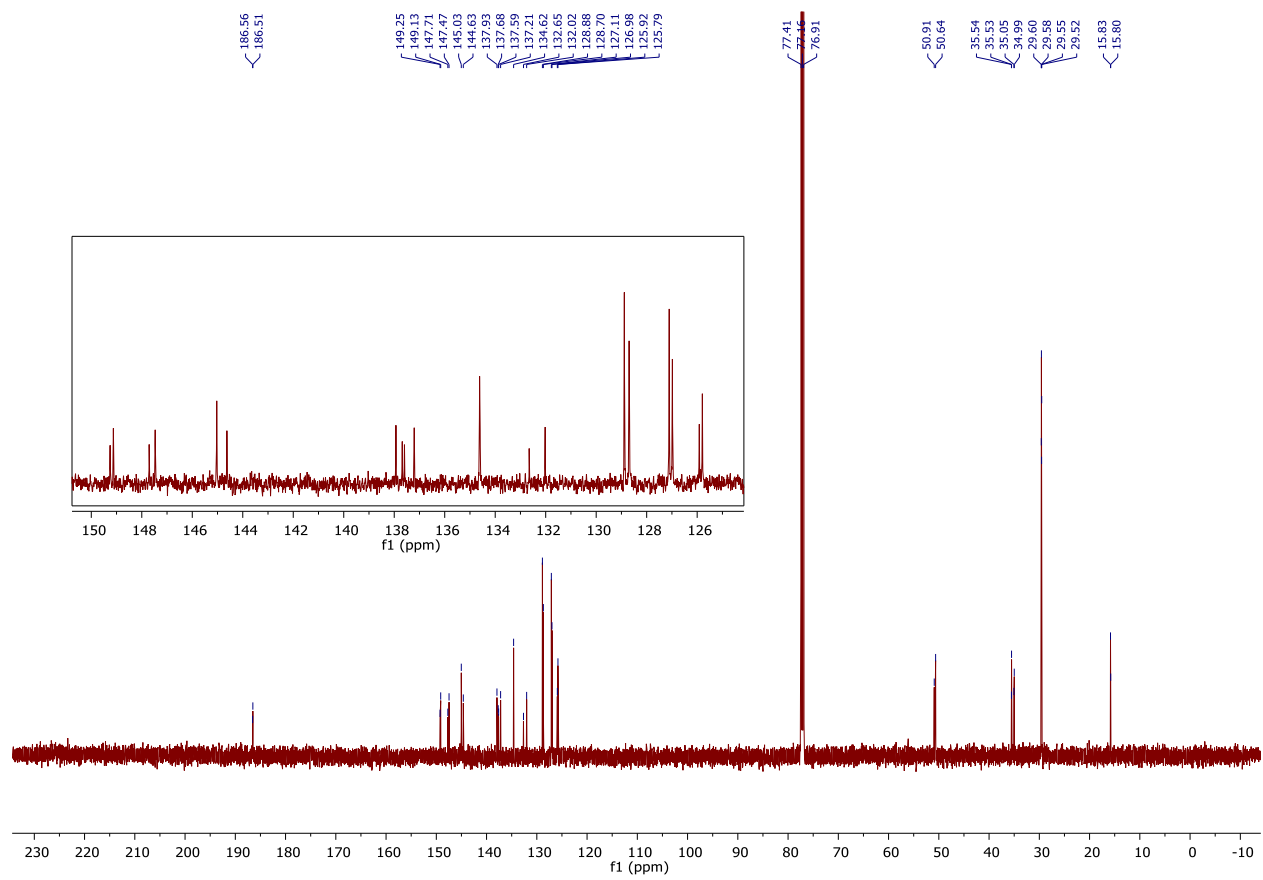
¹³C NMR (126 MHz, Chloroform-*d*) δ 186.56, 186.51, 149.25, 149.13, 147.71, 147.47, 145.03, 144.63, 137.93, 137.68, 137.59, 137.21, 134.62, 132.65, 132.02, 128.88, 128.70, 127.11, 126.98, 125.92, 125.79, 50.91, 50.64, 35.54, 35.53, 35.05, 34.99, 29.60, 29.58, 29.55, 29.52, 15.83, 15.80.

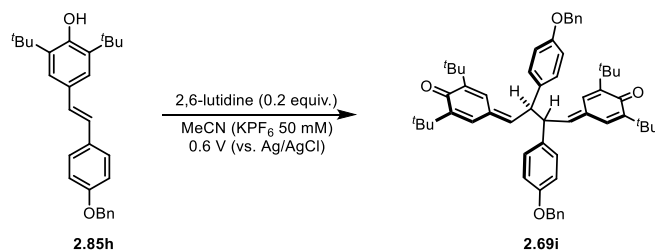
IR (Neat): 2960, 2906, 1698, 1591, 1437, 1358, 1262, 1096, 1023, 846, 815, 740 cm⁻¹;

HRMS (ESI) *m/z* calculated for NaC₄₆H₅₈O₂S₂⁺ ([M+Na]⁺) 729.3770, found 729.3773.



^{13}C NMR, 126 MHz, Chloroform-*d*, Dimer **2.69h**





(2.69i) 4,4'-((2*R*,3*R*)-2,3-bis(4-(benzyloxy)phenyl)butane-1,4-diylidene)bis(2,6-di-*tert*-butylcyclohexa-2,5-dien-1-one)

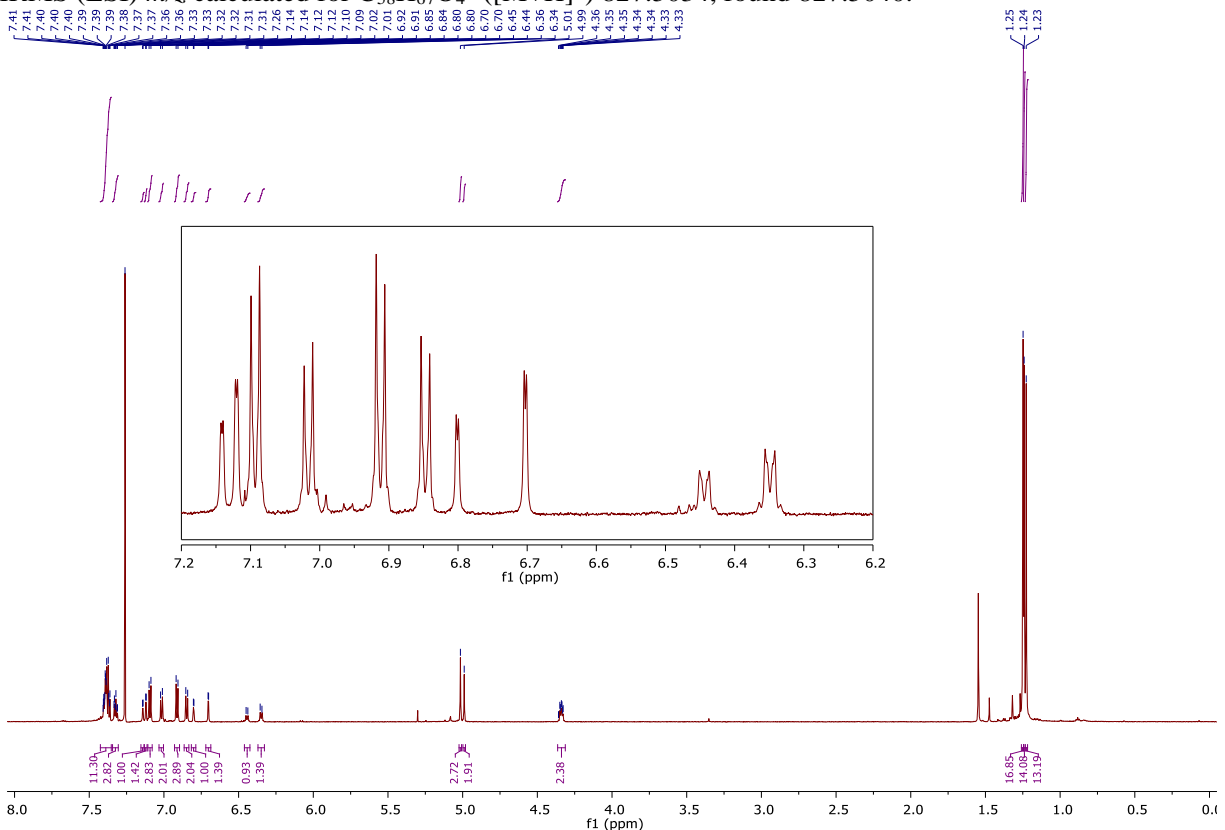
Stilbene **2.69i** (0.1 mmol, 41.5 mg) was subjected to the general dimerization procedure, affording bisquinone methide **2.85h** (39.3 mg, 95% yield, 3:2 dr).

$^1\text{H NMR}$ (700 MHz, Chloroform-*d*) δ 7.43 – 7.35 (m, 16H), 7.34 – 7.31 (m, 4H), 7.14 (β -H, minor diastereomer, d, $J = 2.4$ Hz, 2H), 7.12 (β -H, major diastereomer, d, $J = 2.4$ Hz, 2H), 7.09 (major diastereomer, d, $J = 8.7$ Hz, 4H), 7.02 (minor diastereomer, d, $J = 8.7$ Hz, 4H), 6.91 (major diastereomer, d, $J = 8.7$ Hz, 4H), 6.85 (minor diastereomer, d, $J = 8.7$ Hz, 4H), 6.80 (β -H, minor diastereomer, d, $J = 2.4$ Hz, 2H), 6.70 (β -H, major diastereomer, d, $J = 2.4$ Hz, 2H), 6.44 (δ -H, minor diastereomer, d, $J = 8.2$ Hz, 2H), 6.35 (δ -H, major diastereomer, d, $J = 8.4$ Hz, 2H), 5.01 (major diastereomer, s, 4H), 4.99 (minor diastereomer, s, 4H), 4.31 (sp³ methines of both diastereomers, m, 4H), ^tBu signals: 1.25 (s, 36H), 1.24 (s, 18H), 1.23 (s, 18H).

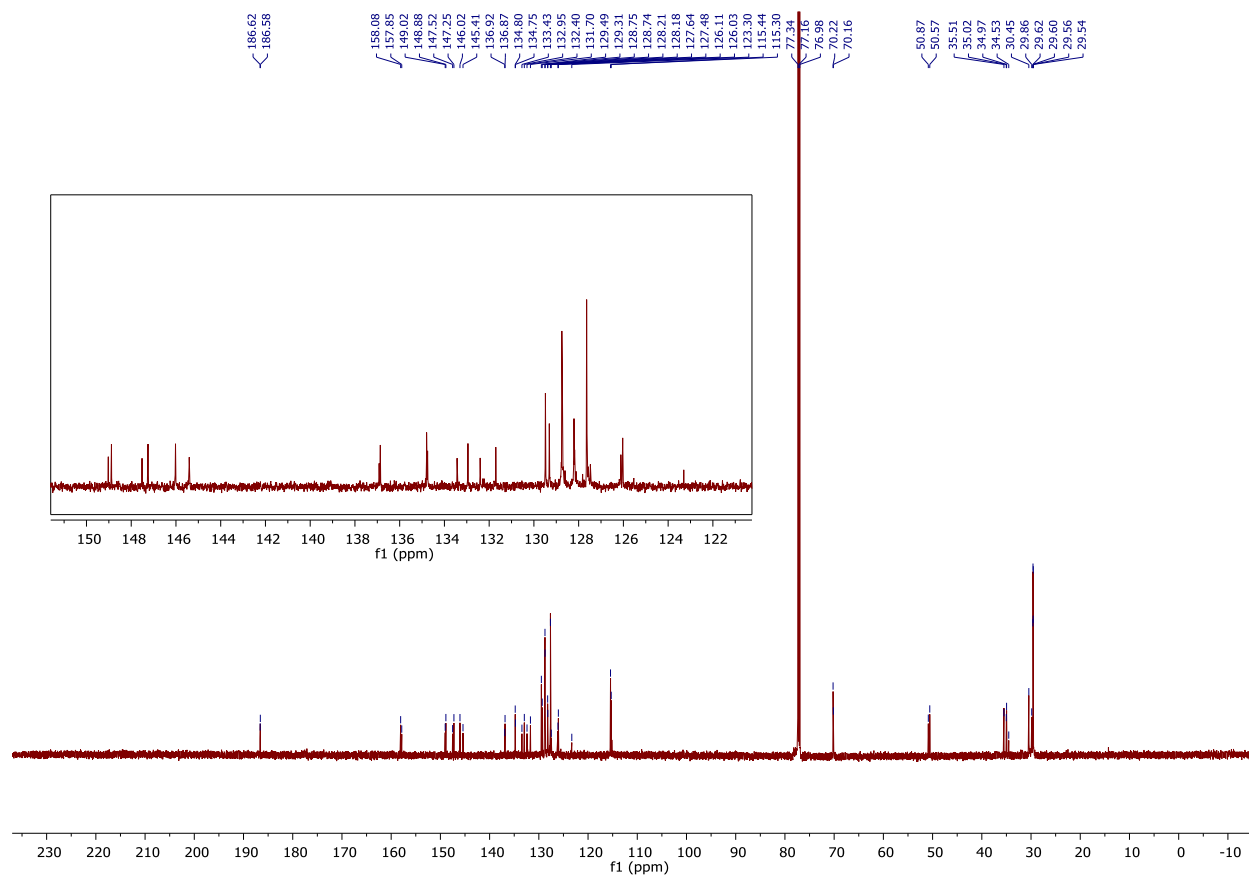
$^{13}\text{C NMR}$ (176 MHz, Chloroform-*d*) δ 186.62, 186.58, 158.08, 157.85, 149.02, 148.88, 147.52, 147.25, 146.02, 145.41, 136.92, 136.87, 134.80, 134.75, 133.43, 132.95, 132.40, 131.70, 129.49, 129.31, 128.75, 128.74, 128.21, 128.18, 127.64, 127.48, 126.11, 126.03, 123.30, 115.44, 115.30, 70.22, 70.16, 50.87, 50.57, 35.51, 35.02, 34.97, 34.53, 30.45, 29.86, 29.62, 29.60, 29.56, 29.54.

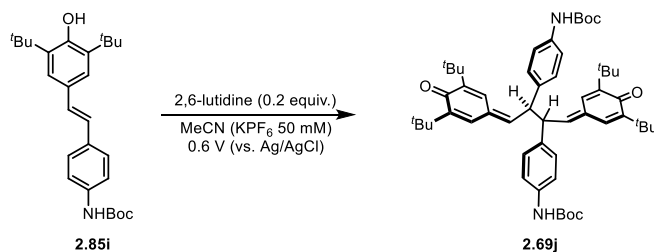
IR (Neat): 2954, 2918, 1608, 1569, 1510, 1358, 1245, 1018, 824, 740, 695 cm⁻¹;

HRMS (ESI) m/z calculated for C₅₈H₆₇O₄⁺ ([M+H]⁺) 827.5034, found 827.5040.



^{13}C NMR, 176 MHz, Chloroform-*d*, Dimer **2.69i**





(2.69j) Di-tert-butyl (((2*R*,3*R*)-1,4-bis(3,5-di-tert-butyl-4-oxocyclohexa-2,5-dien-1-ylidene)butane-2,3-diyl)bis(4,1-phenylene))dicarbamate

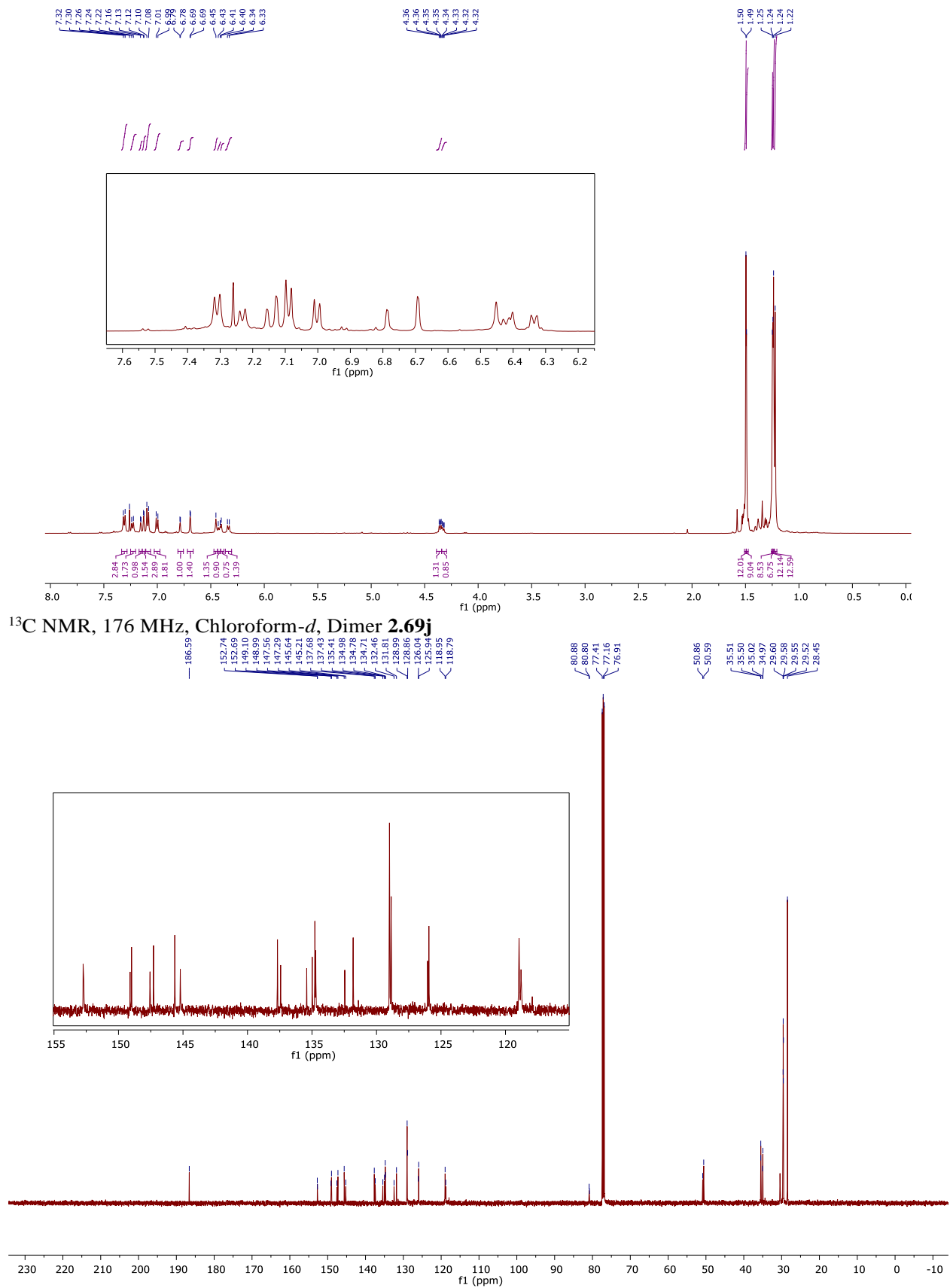
Stilbene **2.85i** (0.1 mmol, 42.4 mg) was subjected to the general dimerization procedure, affording bisquinone methide **2.69j** (40.7 mg, 95% yield, 3:2 dr).

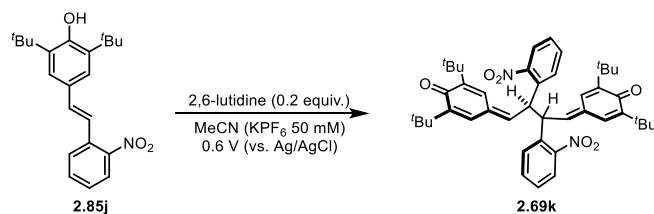
$^1\text{H NMR}$ (500 MHz, Chloroform-*d*) δ 7.31 (major diastereomer, d, $J = 8.2$ Hz, 2H), 7.23 (minor diastereomer, d, $J = 8.1$ Hz, 2H), 7.16 (minor diastereomer, d, $J = 2.3$ Hz, 1H), 7.13 (major diastereomer, d, $J = 2.3$ Hz, 2H), 7.09 (major diastereomer, d, $J = 8.2$ Hz, 2H), 7.00 (minor diastereomer, d, $J = 8.1$ Hz, 2H), 6.79 (minor diastereomer, d, $J = 2.3$ Hz, 1H), 6.69 (major diastereomer, d, $J = 2.3$ Hz, 1H), 6.45 (major diastereomer, s, 1H), 6.42 (minor diastereomer, d, $J = 9.2$ Hz, 1H), 6.40 (minor diastereomer, s, 1H), 6.34 (major diastereomer, d, $J = 8.9$ Hz, 1H), 4.35 (major diastereomer, dd, $J = 7.3, 2.4$ Hz, 1H), 4.33 (minor diastereomer, dd, $J = 7.4, 2.3$ Hz, 1H), 1.50 (major diastereomer, s, 9H), 1.49 (minor diastereomer, s, 9H), 1.25 (minor diastereomer, s, 9H), 1.24 (minor diastereomer, s, 9H), 1.24 (major diastereomer, s, 9H), 1.22 (major diastereomer, s, 9H).

$^{13}\text{C NMR}$ (126 MHz, Chloroform-*d*) δ 186.60, 186.59, 152.74, 152.69, 149.10, 148.99, 147.56, 147.29, 145.64, 145.21, 137.68, 137.43, 135.41, 134.98, 134.78, 134.71, 132.46, 131.81, 128.99, 128.86, 126.04, 125.94, 118.95, 118.79, 80.88, 80.80, 50.86, 50.59, 35.51, 35.50, 35.02, 34.97, 29.60, 29.58, 29.55, 29.52, 28.45 (2C).

IR (Neat): 3333, 2954, 2864, 1715, 1611, 1521, 1361, 1231, 1153, 1049, 818 cm^{-1} ;

HRMS (ESI) m/z calculated for $\text{NaC}_{54}\text{H}_{72}\text{N}_2\text{O}_6^+$ ($[\text{M}+\text{Na}]^+$) 867.5283, found 867.5276.





(2.69k) 4,4'-((2*R*,3*R*)-2,3-bis(2-nitrophenyl)butane-1,4-diylidene)bis(2,6-di-*tert*-butylcyclohexa-2,5-dien-1-one)

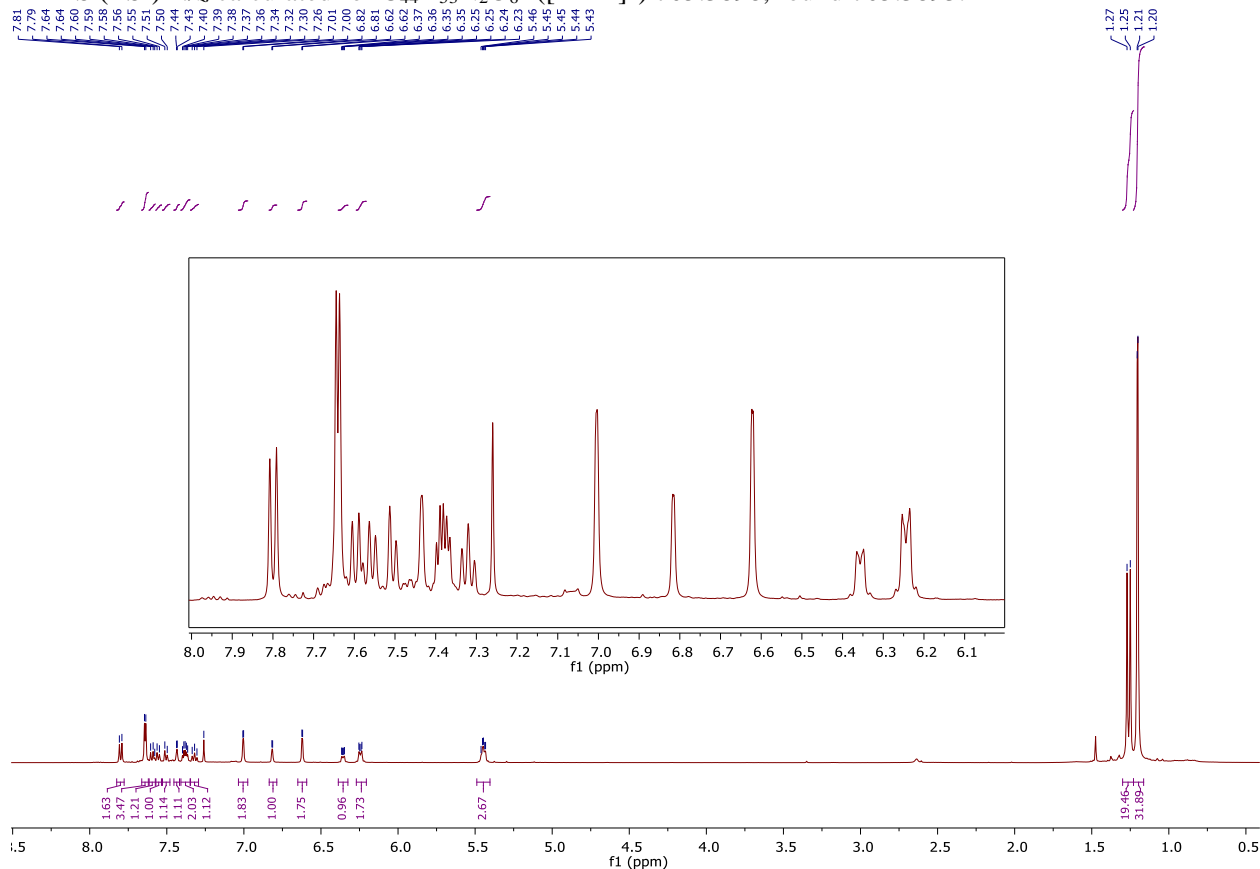
Stilbene **2.85j** (0.1 mmol, 35.3 mg) was subjected to the general dimerization procedure, affording bis-quinone methide **2.69k** (32.8 mg, 93% yield, 2:1 dr).

$^1\text{H NMR}$ (500 MHz, Chloroform-*d*) δ 7.80 (d, $J = 8.1$ Hz, 2H), 7.64 (d, $J = 4.3$ Hz, 4H), 7.61 – 7.57 (m, 2H), 7.56 (dd, $J = 7.5, 1.4$ Hz, 2H), 7.50 (dd, $J = 8.0, 1.4$ Hz, 2H), 7.44 (d, $J = 2.2$ Hz, 2H), 7.38 (dt, $J = 8.4, 4.3$ Hz, 2H), 7.35 – 7.30 (m, 2H), 7.00 (β -H, major diastereomer, d, $J = 2.4$ Hz, 2H), 6.82 (β -H, major diastereomer, d, $J = 2.3$ Hz, 2H), 6.62 (δ -H, minor diastereomer, dd, $J = 6.5, 2.6$ Hz, 2H), 6.25 (δ -H, major diastereomer, dd, $J = 7.1, 2.8$ Hz, 2H), 5.49 – 5.41 (m, 4H), ^tBu signals: 1.27 (s, 18 H), 1.25 (s, 18H), 1.20 (s, 18 H), 1.20 (s, 18 H).

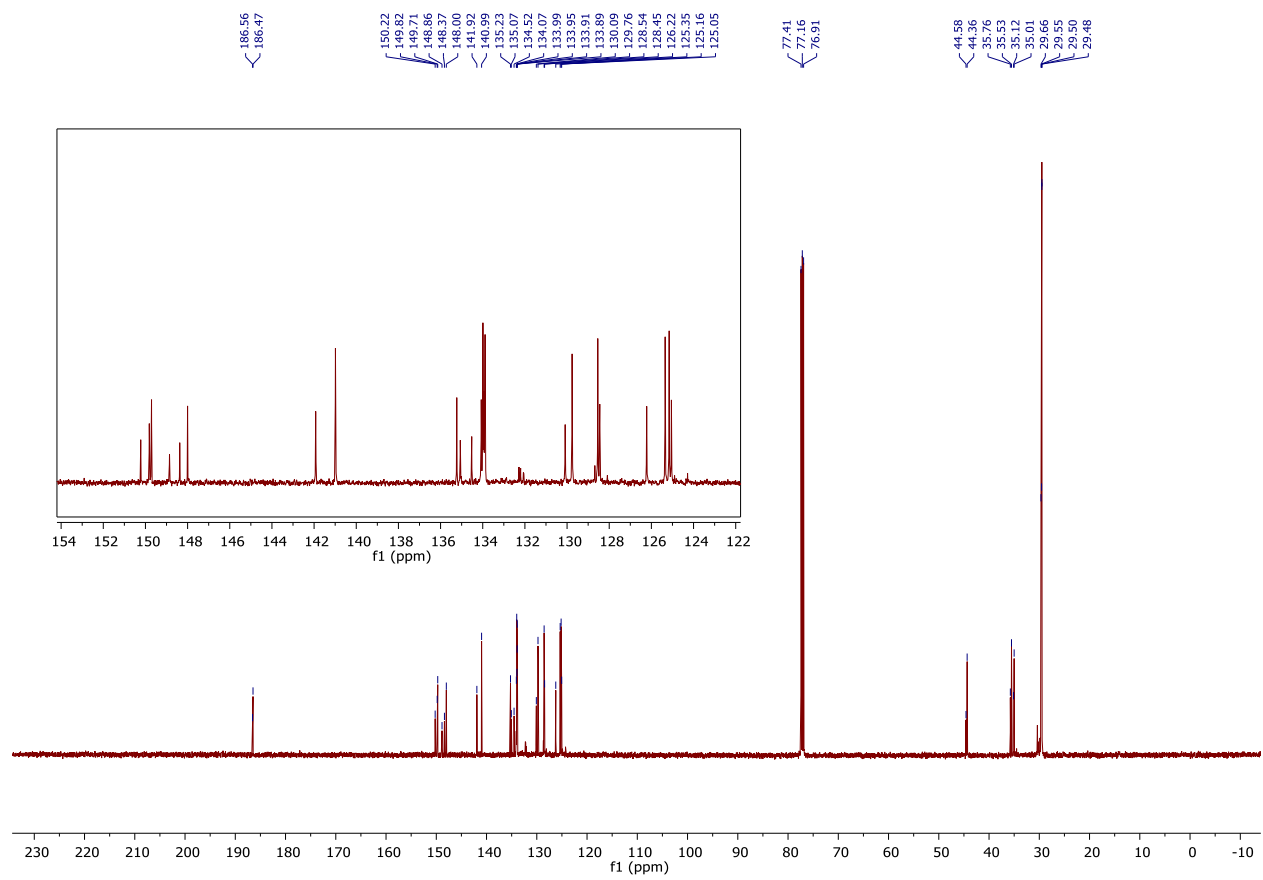
$^{13}\text{C NMR}$ (126 MHz, Chloroform-*d*) δ 186.56, 186.47, 150.22, 149.82, 149.71, 148.86, 148.37, 148.00, 141.92, 140.99, 135.23, 135.07, 134.52, 134.07, 133.99, 133.95, 133.91, 133.89, 130.09, 129.76, 128.54, 128.45, 126.22, 125.35, 125.16, 125.05, 44.58, 44.36, 35.76, 35.53, 35.12, 35.01, 29.66, 29.55, 29.50, 29.48.

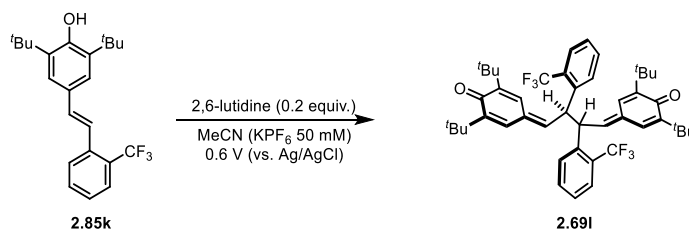
IR (Neat): 2956, 2917, 1616, 1520, 1345, 1255, 918, 886, 822, 782, 729 cm^{-1} ;

HRMS (ESI) m/z calculated for $\text{C}_{44}\text{H}_{53}\text{N}_2\text{O}_6^+$ ($[\text{M}+\text{H}]^+$) 705.3898, found 705.3893.



^{13}C NMR, 126 MHz, Chloroform-*d*, Dimer **2.69k**





(2.691) 4,4'-((2*R*,3*R*)-2,3-bis(2-(trifluoromethyl)phenyl)butane-1,4-diylidene)bis(2,6-di-*tert*-butylcyclohexa-2,5-dien-1-one)

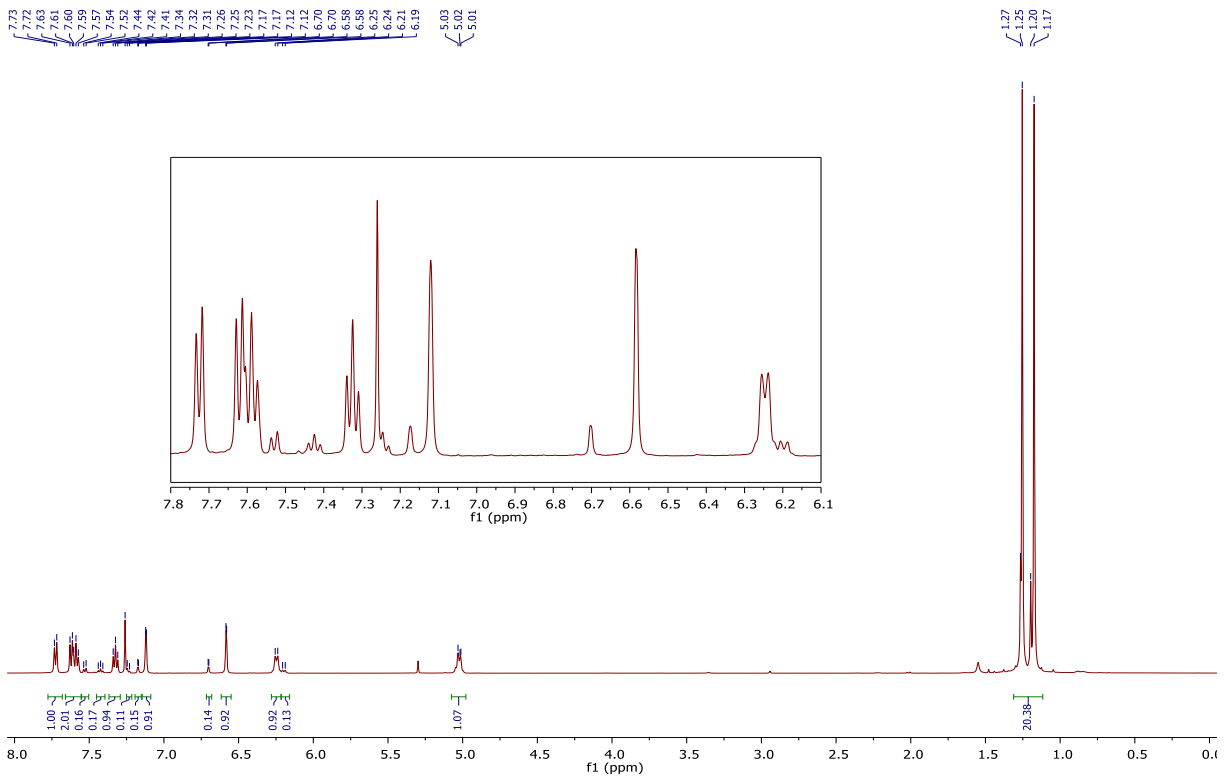
Stilbene **2.85k** (0.1 mmol, 37.6 mg) was subjected to the general dimerization procedure, affording bisquinone methide **2.691** (36.8 mg, 98% yield, 5:1 dr).

¹H NMR (500 MHz, Chloroform-*d*) δ 7.73 (major diastereomer, d, $J = 7.9$ Hz, 2H), 7.62 (major diastereomer, d, $J = 8.0$ Hz, 2H), 7.59 (major diastereomer, t, $J = 7.7$ Hz, 2H), 7.53 (minor diastereomer, d, $J = 8.0$ Hz, 2H), 7.42 (minor diastereomer, t, $J = 7.7$ Hz, 2H), 7.32 (major diastereomer, t, $J = 7.7$ Hz, 2H), 7.24 (minor diastereomer, t, $J = 7.7$ Hz, 2H), β -H's of quinone methides: 7.17 (minor diastereomer, d, $J = 2.3$ Hz, 2H), 7.12 (major diastereomer, d, $J = 2.5$ Hz, 2H), 6.70 (minor diastereomer, d, $J = 2.4$ Hz, 2H), 6.58 (major diastereomer, d, $J = 2.3$ Hz, 2H), δ -H's of quinone methides: 6.25 (major diastereomer, d, $J = 8.6$ Hz, 2H), 6.20 (minor diastereomer, d, $J = 8.8$ Hz, 2H), 5.03 (sp³ methines of both diastereomers, m, 4H), ^tBu signals: 1.27 (minor diastereomer, s, 18H), 1.25 (major diastereomer, s, 18H), 1.20 (minor diastereomer, s, 18H), 1.17 (major diastereomer, s, 18H),

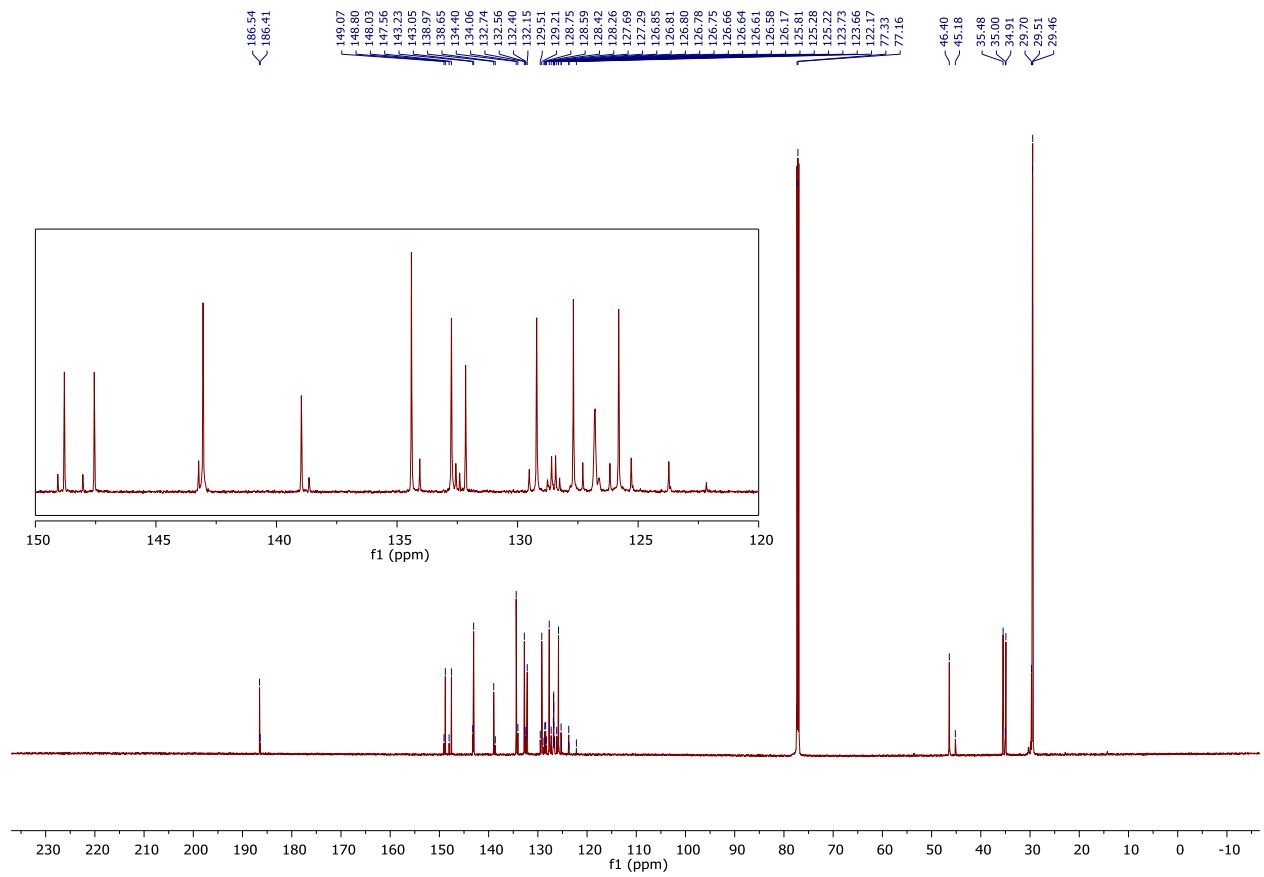
¹³C NMR (176 MHz, Chloroform-*d*) δ 186.54, 186.41, 149.07, 148.80, 148.03, 147.56, 143.23, 143.05, 138.97, 138.65, 134.40, 134.06, 132.74, 132.56, 132.40, 132.15, 129.51, 129.21, 128.50 (major diastereomer, q, $J = 28$ Hz), 128.44 (minor diastereomer, q, $J = 28$ Hz), 127.69, 127.29, 126.80 (major diastereomer, q, $J = 5.3$ Hz), 126.62 (minor diastereomer, q, $J = 5.3$ Hz), 126.17, 125.81, 124.50 (major diastereomer, q, $J = 273$ Hz), 124.43 (minor diastereomer, q, $J = 273$ Hz), 46.40, 45.18, 35.48, 35.00, 34.91, 29.70, 29.51, 29.46.

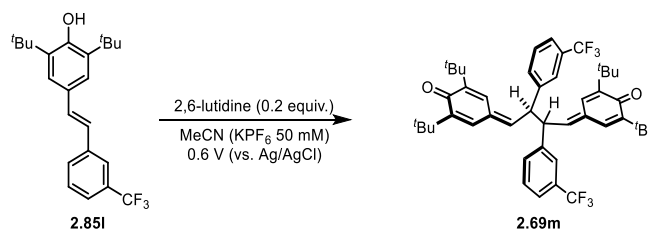
IR (Neat): 3005, 2957, 2918, 1614, 1569, 1453, 1363, 1310, 1155, 1111, 1032, 931, 765 cm⁻¹;

HRMS (ESI) m/z calculated for NaC₄₆H₅₂F₆O₂⁺ ([M+Na]⁺) 773.3764, found 773.3772.



¹³C NMR, 176 MHz, Chloroform-*d*, Dimer **2.691**





(2.69m) 4,4'-((2*R*,3*R*)-2,3-bis(3-(trifluoromethyl)phenyl)butane-1,4-diylidene)bis(2,6-di-*tert*-butylcyclohexa-2,5-dien-1-one)

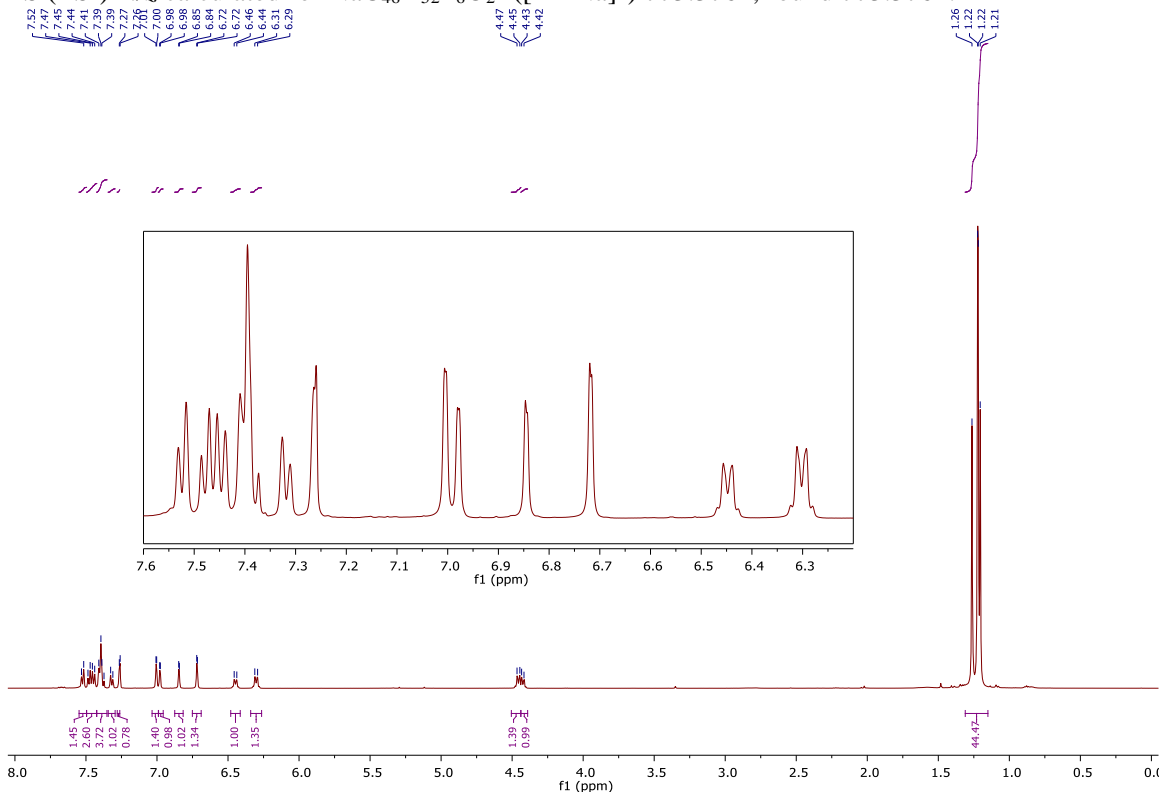
Stilbene **2.85I** (0.1 mmol, 37.6 mg) was subjected to the general dimerization procedure, affording bisquinone methide **2.69m** (36.4 mg, 97% yield, 4:3 dr).

¹H NMR (500 MHz, Chloroform-*d*) δ 7.52 (major diastereomer, d, *J* = 7.8 Hz, 2H), 7.46 (m, 4H), 7.43 – 7.35 (m, 6H), 7.32 (minor diastereomer, d, *J* = 7.8 Hz, 2H), 7.26 (minor diastereomer, s, 2H), β-H's of quinone methides: 7.01 (major diastereomer, d, *J* = 2.4 Hz, 2H), 6.98 (minor diastereomer, d, *J* = 2.4 Hz, 2H), 6.85 (minor diastereomer, d, *J* = 2.4 Hz, 2H), 6.72 (major diastereomer, d, *J* = 2.4 Hz, 2H), δ-H's of quinone methides: 6.45 (minor diastereomer, d, *J* = 9.5 Hz, 1H), 6.30 (major diastereomer, d, *J* = 9.9 Hz, 1H), 4.46 (sp³ methine of major diastereomer, d, *J* = 10.0 Hz, 1H), 4.42 (sp³ methine of minor diastereomer, d, *J* = 9.6 Hz, 1H), ^tBu signals: 1.26 (minor diastereomer, s, 18H), 1.22 (major diastereomer, s, 18H), 1.22 (major diastereomer, s, 18H), 1.21 (minor diastereomer, s, 18H),

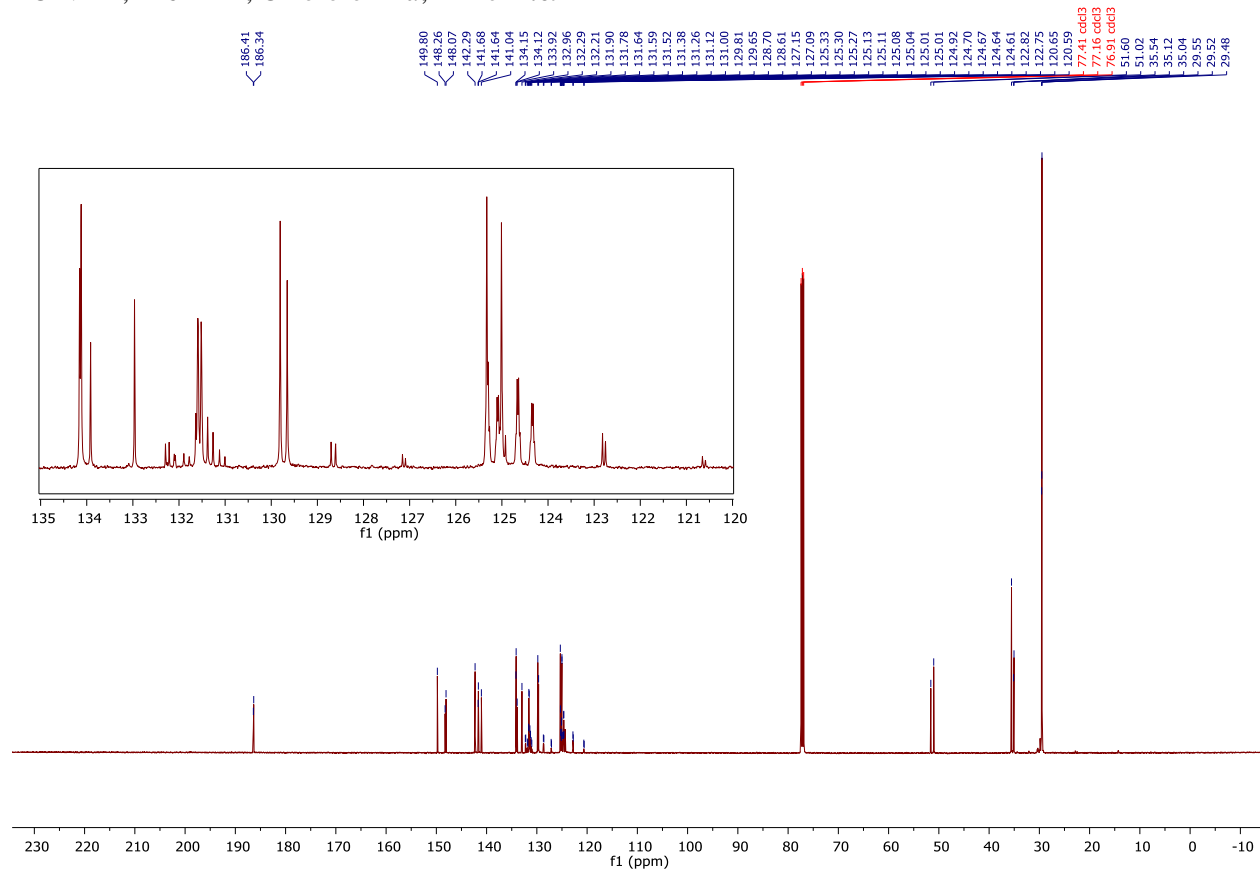
¹³C NMR (126 MHz, Chloroform-*d*) δ 186.41, 186.34, 149.80, 148.26, 148.07, 142.29, 141.68, 141.64, 141.04, 134.15, 134.12, 133.92, 132.96, 132.29, 132.21, 131.59, 131.52, 131.51 (q, *J* = 32 Hz), 131.39 (q, *J* = 32 Hz), 129.81, 129.65, 128.70, 128.61, 125.33, 125.31 (q, *J* = 3.8 Hz), 125.09 (q, *J* = 3.8 Hz), 125.01, 124.65 (q, *J* = 3.8 Hz), 124.34 (q, *J* = 3.8 Hz), 123.90 (q, *J* = 271 Hz), 123.83 (q, *J* = 271 Hz), 51.60, 51.02, 35.54, 35.12, 35.04, 29.55, 29.52, 29.48.

IR (Neat): 2959, 1617, 1571, 1448, 1390, 1324, 1252, 1162, 1124, 1069, 883, 813 cm⁻¹;

HRMS (ESI) *m/z* calculated for NaC₄₆H₅₂F₆O₂⁺ ([M+Na]⁺) 773.3764, found 773.3762.



¹³C NMR, 126 MHz, Chloroform-*d*, Dimer **2.69m**





(2.69n) 4,4'-((2*R*,3*R*)-2,3-bis(4-nitrophenyl)butane-1,4-diyldiene)bis(2,6-di-*tert*-butylcyclohexa-2,5-dien-1-one)

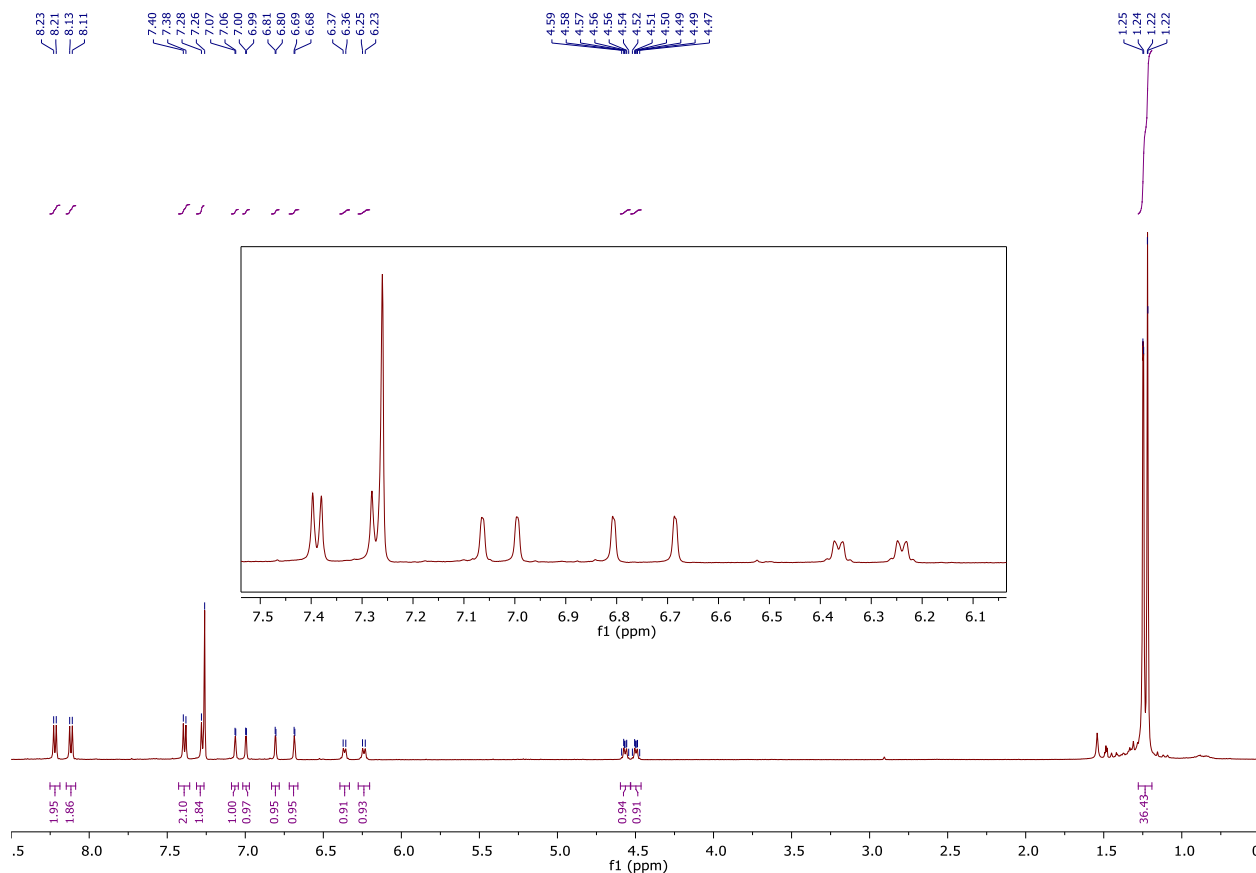
Stilbene **2.85m** (0.1 mmol, 35.3 mg) was subjected to the general dimerization procedure, affording bisquinone methide **2.69n** (32.5 mg, 92% yield, 1:1 dr).

$^1\text{H NMR}$ (500 MHz, Chloroform-*d*) δ 8.22 (d, $J = 8.4$ Hz, 4H), 8.12 (d, $J = 8.4$ Hz, 4H), 7.39 (d, $J = 8.3$ Hz, 4H), 7.27 (d, $J = 8.4$ Hz, 4H), β -H's of quinone methides: 7.06 (d, $J = 2.4$ Hz, 2H), 7.00 (d, $J = 2.4$ Hz, 2H), 6.81 (d, $J = 2.4$ Hz, 2H), 6.68 (d, $J = 2.4$ Hz, 2H), δ -H's of quinone methides: 6.36 (d, $J = 8.5$ Hz, 2H), 6.24 (d, $J = 8.8$ Hz, 2H), sp^3 methines: 4.60 – 4.53 (m, 2H), 4.53 – 4.46 (m, 2H), 1.25 (s, 18H), 1.24 (s, 18H), 1.22 (s, 18H).

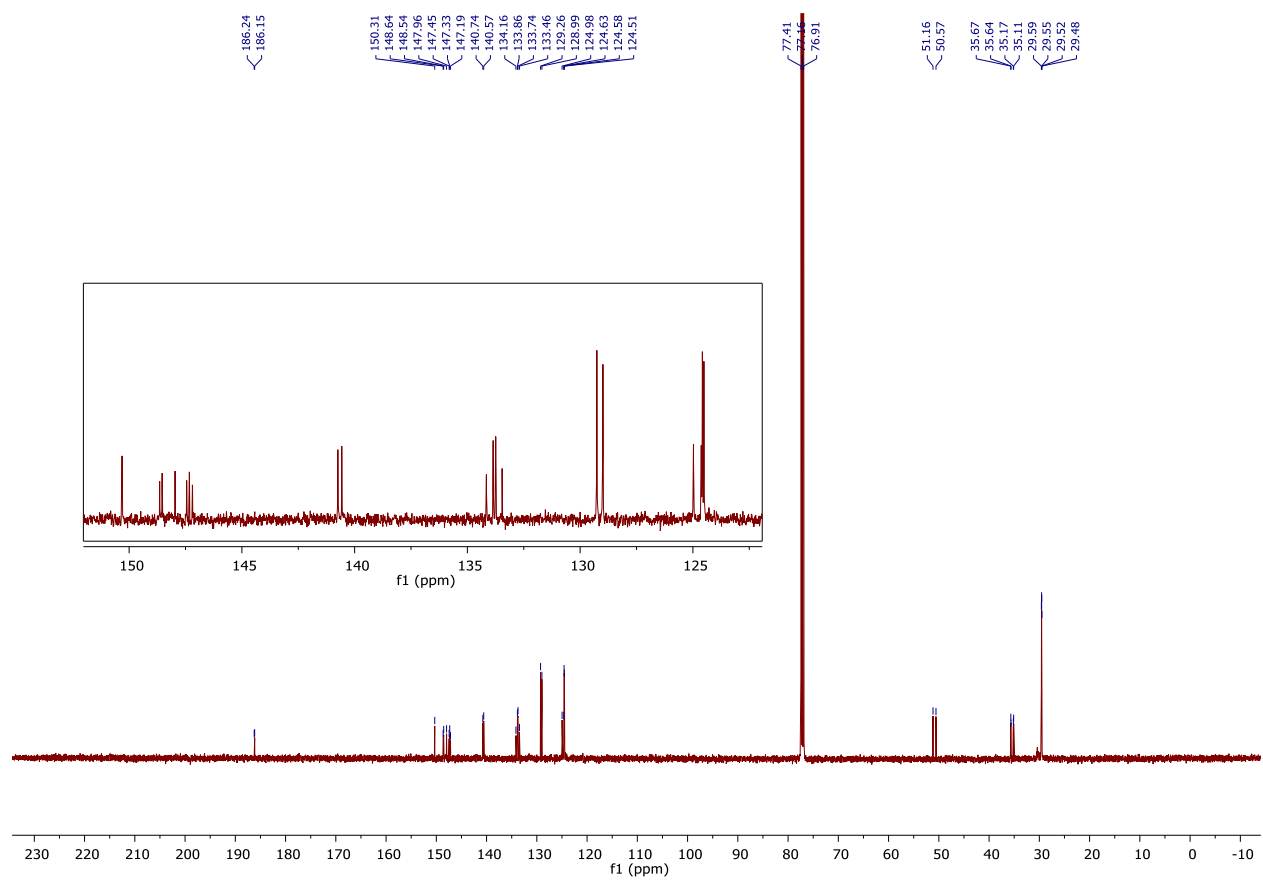
$^{13}\text{C NMR}$ (126 MHz, Chloroform-*d*) δ 186.24, 186.15, 150.31, 148.64, 148.54, 147.96, 147.45, 147.33, 147.19, 140.74, 140.57, 134.16, 133.86, 133.74, 133.46, 129.26, 128.99, 124.98, 124.63, 124.58, 124.51, 51.16, 50.57, 35.67, 35.64, 35.17, 35.11, 29.59, 29.55, 29.52, 29.48.

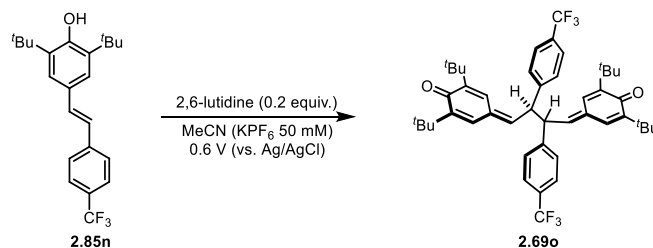
IR (Neat): 2953, 1613, 1518, 1344, 1254, 913, 857, 706 cm^{-1} ;

HRMS (ESI) m/z calculated for $\text{C}_{44}\text{H}_{52}\text{N}_2\text{O}_6^+$ ($[\text{M}+\text{Na}]^+$) 727.3718, found 727.3723.



^{13}C NMR, 126 MHz, Chloroform-*d*, Dimer **2.69n**





(2.69o) 4,4'-((2*R*,3*R*)-2,3-bis(4-(trifluoromethyl)phenyl)butane-1,4-diyldiene)bis(2,6-di-*tert*-butylcyclohexa-2,5-dien-1-one)

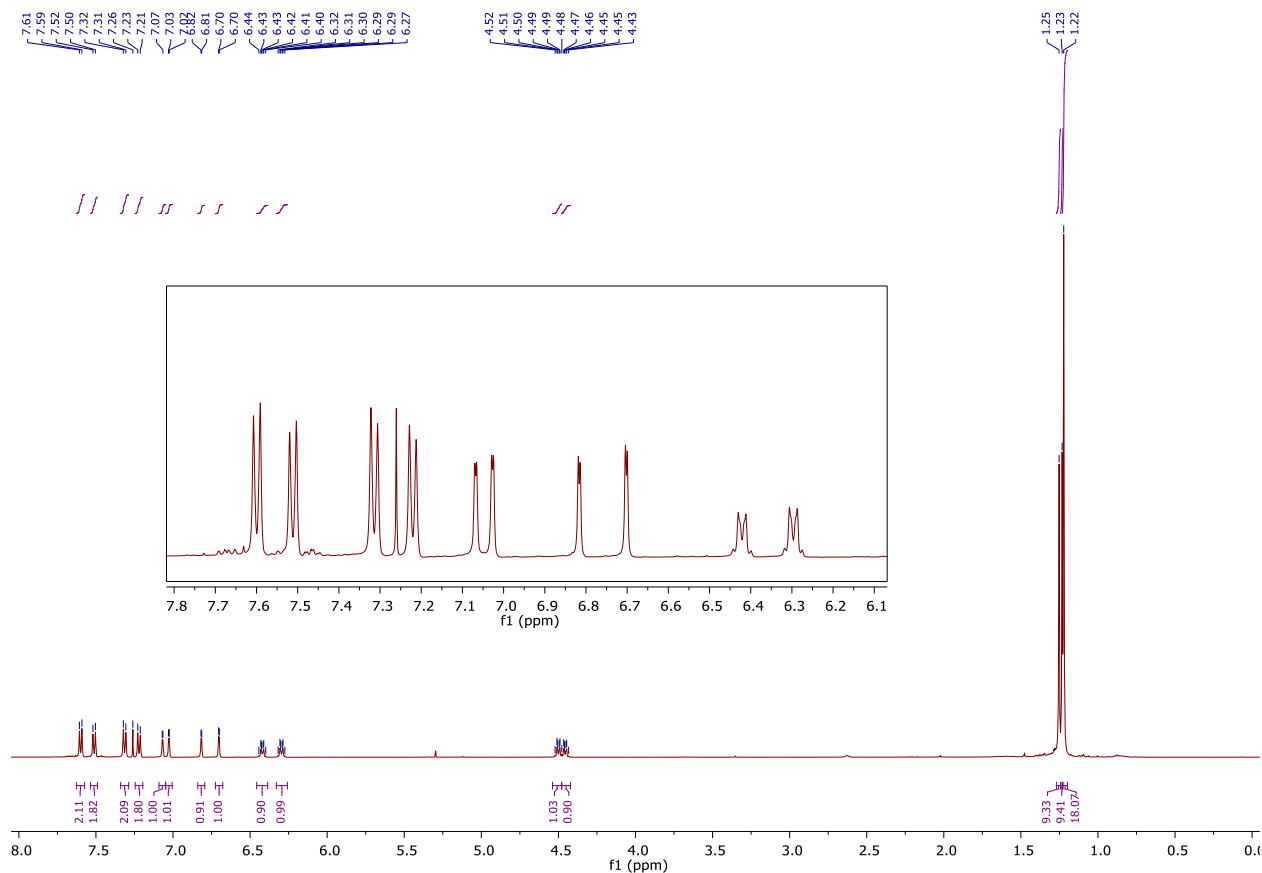
Stilbene **2.85n** (0.1 mmol, 37.6 mg) was subjected to the general dimerization procedure, affording bisquinone methide **2.69o** (33.8 mg, 90% yield, 1:1 dr).

$^1\text{H NMR}$ (500 MHz, Chloroform-*d*) δ 7.60 (d, $J = 8.1$ Hz, 4H), 7.51 (d, $J = 8.1$ Hz, 4H), 7.31 (d, $J = 8.0$ Hz, 4H), 7.22 (d, $J = 8.1$ Hz, 4H), 7.07 (d, $J = 2.4$ Hz, 2H), 7.03 (d, $J = 2.4$ Hz, 2H), 6.82 (d, $J = 2.4$ Hz, 2H), 6.70 (d, $J = 2.4$ Hz, 2H), 6.46 – 6.39 (m, 2H), 6.33 – 6.26 (m, 2H), 4.50 (dd, $J = 7.4, 2.4$ Hz, 2H), 4.46 (dt, $J = 8.7, 6.3$ Hz, 2H), 1.25 (s, 18H), 1.23 (s, 18H), 1.22 (s, 36H).

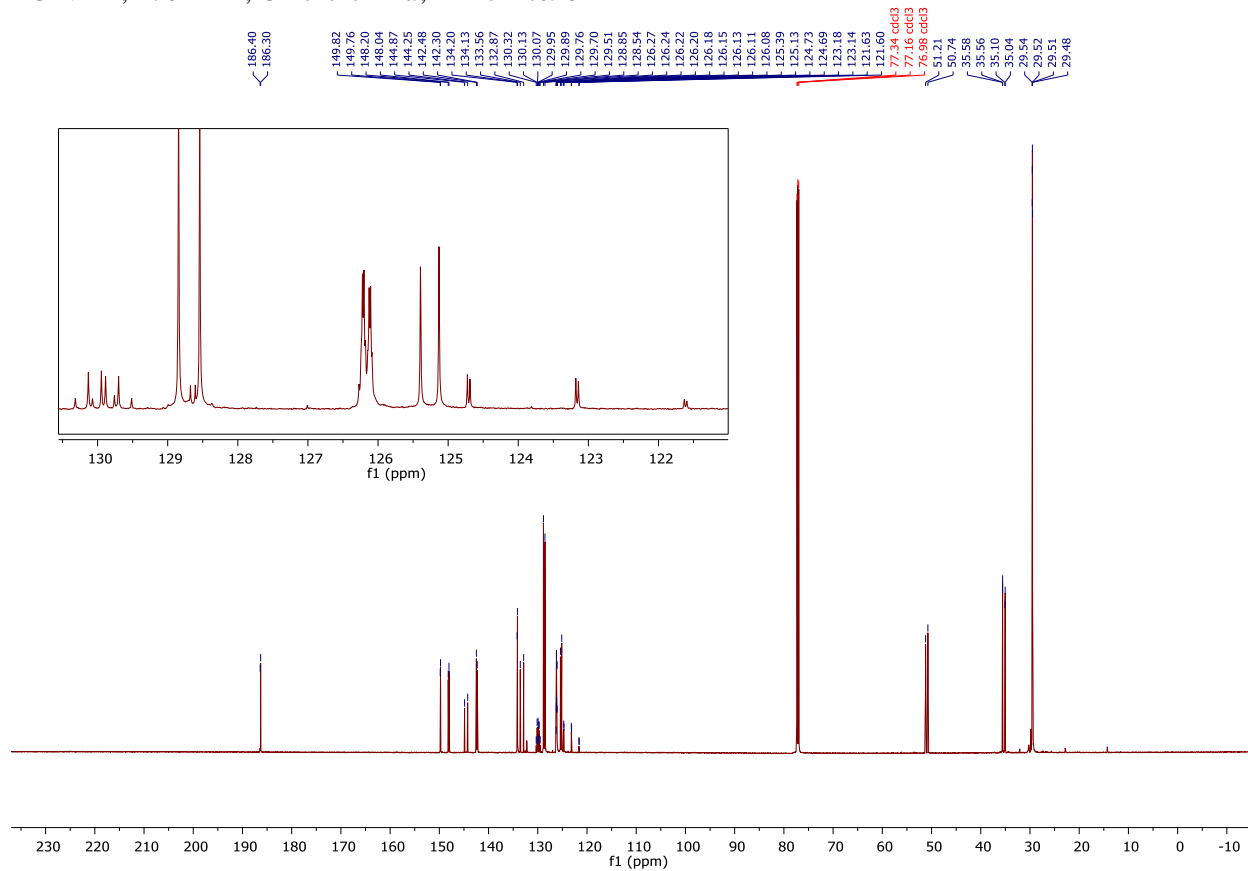
$^{13}\text{C NMR}$ (176 MHz, Chloroform-*d*) δ 186.40, 186.30, 149.82, 149.76, 148.20, 148.04, 144.87, 144.25, 142.48, 142.30, 134.20, 134.13, 133.56, 132.87, 130.04 (q, $J = 33$ Hz), 129.80 (q, $J = 32$ Hz), 128.85, 128.54, 126.21 (q, $J = 3.5$ Hz), 126.12 (q, $J = 3.5$ Hz), 125.39, 125.13, 123.96 (q, $J = 273$ Hz), 123.92 (q, $J = 273$ Hz), 51.21, 50.74, 35.58, 35.56, 35.10, 35.04, 29.54, 29.52, 29.51, 29.48.

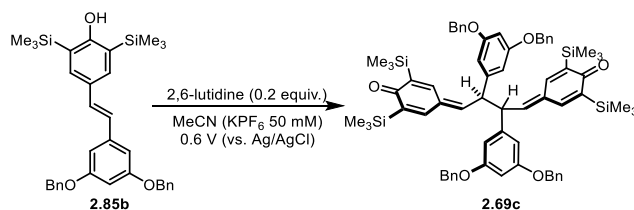
IR (Neat): 2955, 1612, 1571, 1361, 1322, 1165, 1105, 1067, 883, 834 cm^{-1} ;

HRMS (ESI) m/z calculated for $\text{NaC}_{46}\text{H}_{52}\text{F}_6\text{O}_2^+$ ($[\text{M}+\text{H}]^+$) 773.3764, found 773.3769.



^{13}C NMR, 176 MHz, Chloroform-*d*, Dimer **2.69o**



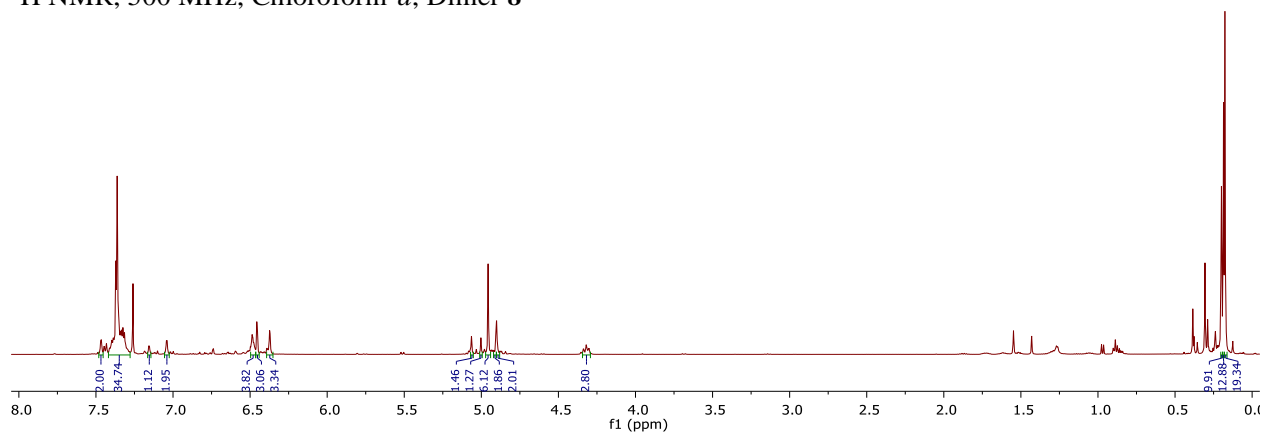


(2.69c) 4,4'-((2*R*,3*R*)-2,3-bis(3,5-bis(benzyloxy)phenyl)butane-1,4-diylidene)bis(2,6-bis(trimethylsilyl)cyclohexa-2,5-dien-1-one)

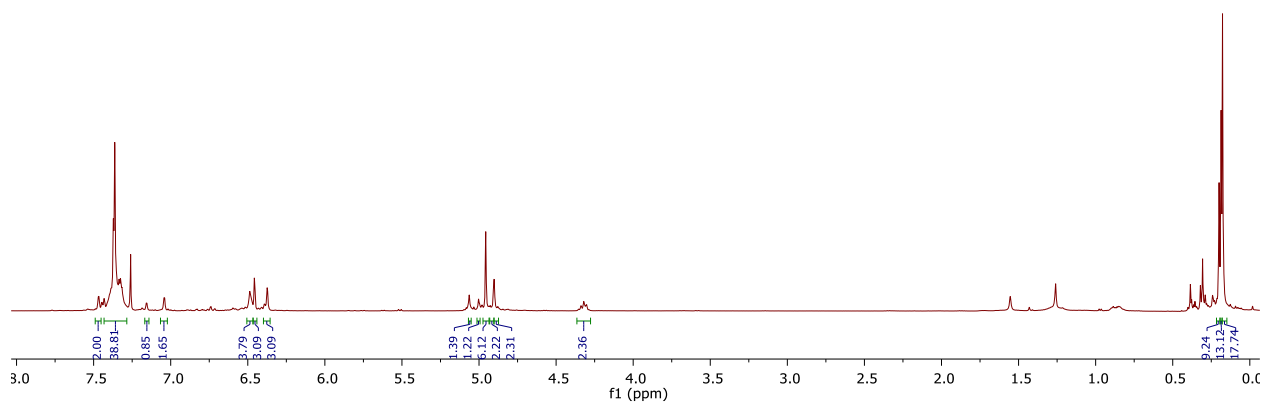
Stilbene **2.85b** (0.1 mmol, 55 mg) was subjected to the general dimerization procedure, and the crude reaction mixture was purified by flash column chromatography (0 to 15% EtOAc in Hexanes) to afford bis-quinone methide **8** (35.8 mg, 65% yield, 2:1 dr). The ^1H NMR spectrum was identical to the previous report for this compound.⁴⁸

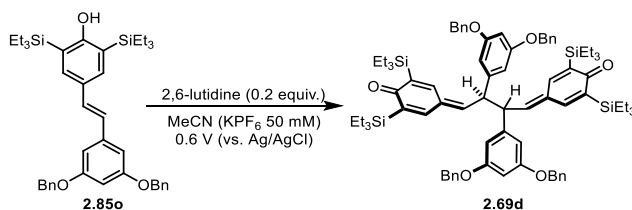
^1H NMR (500 MHz, CDCl_3 , 25 °C) δ : 7.47 (d, $J = 2.5$ Hz, 2H, major), 7.45 – 7.28 (m, 32H), 7.15 (d, $J = 2.5$ Hz, 2H, minor), 7.04 (d, $J = 2.5$ Hz, 2H, major), 6.50 – 6.47 (m, overlap, 4H), 6.45 (d, $J = 2.2$ Hz, 4H, major), 6.38 (m, 4H), 6.37 (d, $J = 2.2$ Hz, 4H, minor), 5.07 (d, $J = 9.3$ Hz, 2H, minor), 4.99 (d, $J = 9.3$ Hz, 2H, minor), 4.96 (s, 8H, major/minor overlap), 4.91 (d, $J = 11.2$ Hz, 2H, major), 4.89 (d, $J = 11.2$ Hz, 2H, major), 4.36 – 4.28 (m, overlap, 4H, major/minor), 0.20 (s, 18H, minor), 0.19 (s, 18H, minor), 0.18 (s, 36H, major)

^1H NMR, 500 MHz, Chloroform-*d*, Dimer **8**



^1H NMR, 500 MHz, Chloroform-*d*, Compound **4b**⁴⁸





(2.69d) 4,4'-((2*R*,3*R*)-2,3-bis(3,5-bis(benzyloxy)phenyl)butane-1,4-diylidene)bis(2,6-bis(triethylsilyl)cyclohexa-2,5-dien-1-one)

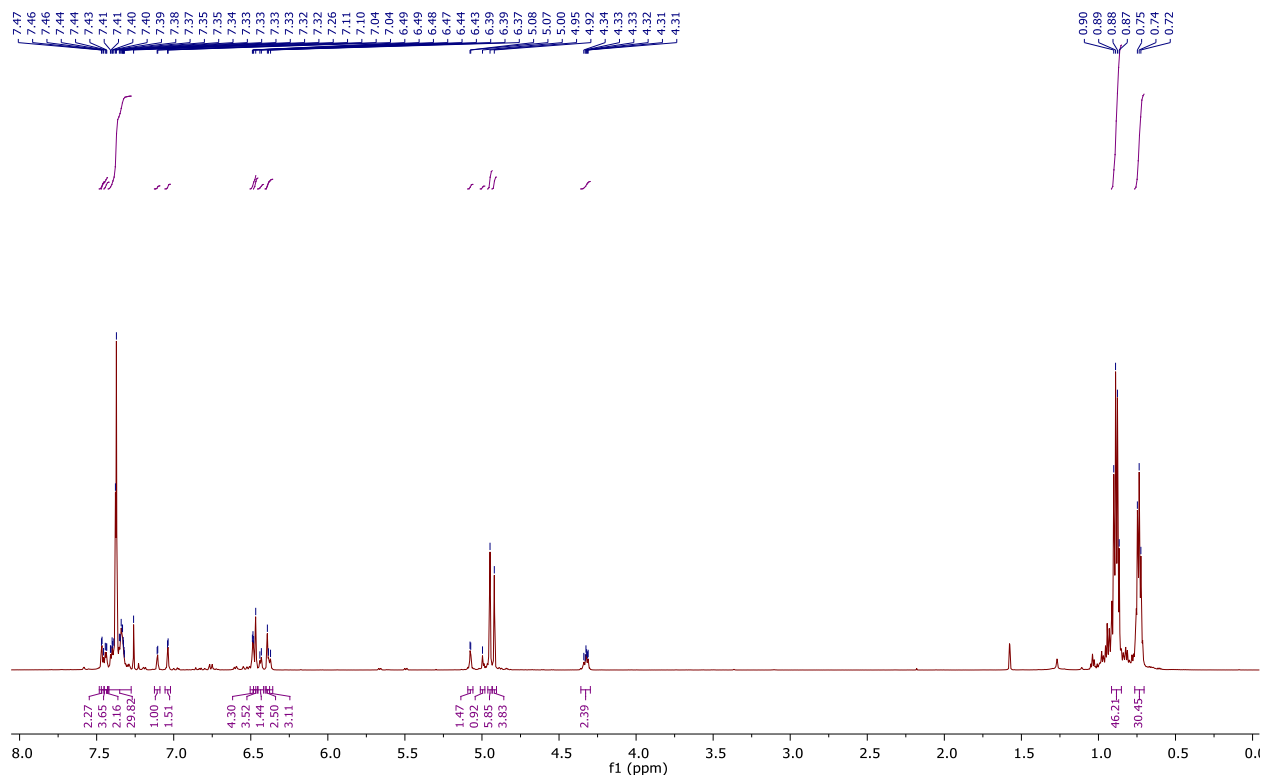
Stilbene **2.85o** (0.1 mmol, 63.7 mg) was subjected to the general dimerization procedure, and the crude reaction mixture was purified by flash column chromatography (0 to 15% EtOAc in Hexanes) to afford bisquinone methide **2.69d** (43.4 mg, 68% yield, 2:1 dr).

^1H NMR (700 MHz, Chloroform-*d*) δ 7.47 (d, $J = 2.6$ Hz, 2H), 7.45 (d, $J = 7.8$ Hz, 4H), 7.44 (d, $J = 2.6$ Hz, 2H), 7.42 – 7.28 (m, 30H), 7.11 (d, $J = 2.6$ Hz, 1H), 7.04 (d, $J = 2.6$ Hz, 2H), 6.50 – 6.47 (m, 4H), 6.47 (s, 4H), 6.44 (d, $J = 6.8$ Hz, 1H), 6.39 (s, 3H), 6.38 (d, $J = 9.6$ Hz, 3H), 5.08 (d, $J = 3.1$ Hz, 1H), 5.00 (s, 1H), 4.95 (s, 6H), 4.92 (s, 4H), 4.32 (td, $J = 8.5, 7.1, 4.5$ Hz, 2H), 0.88 (q, $J = 8.1$ Hz, 46H), 0.76 – 0.70 (m, 30H).

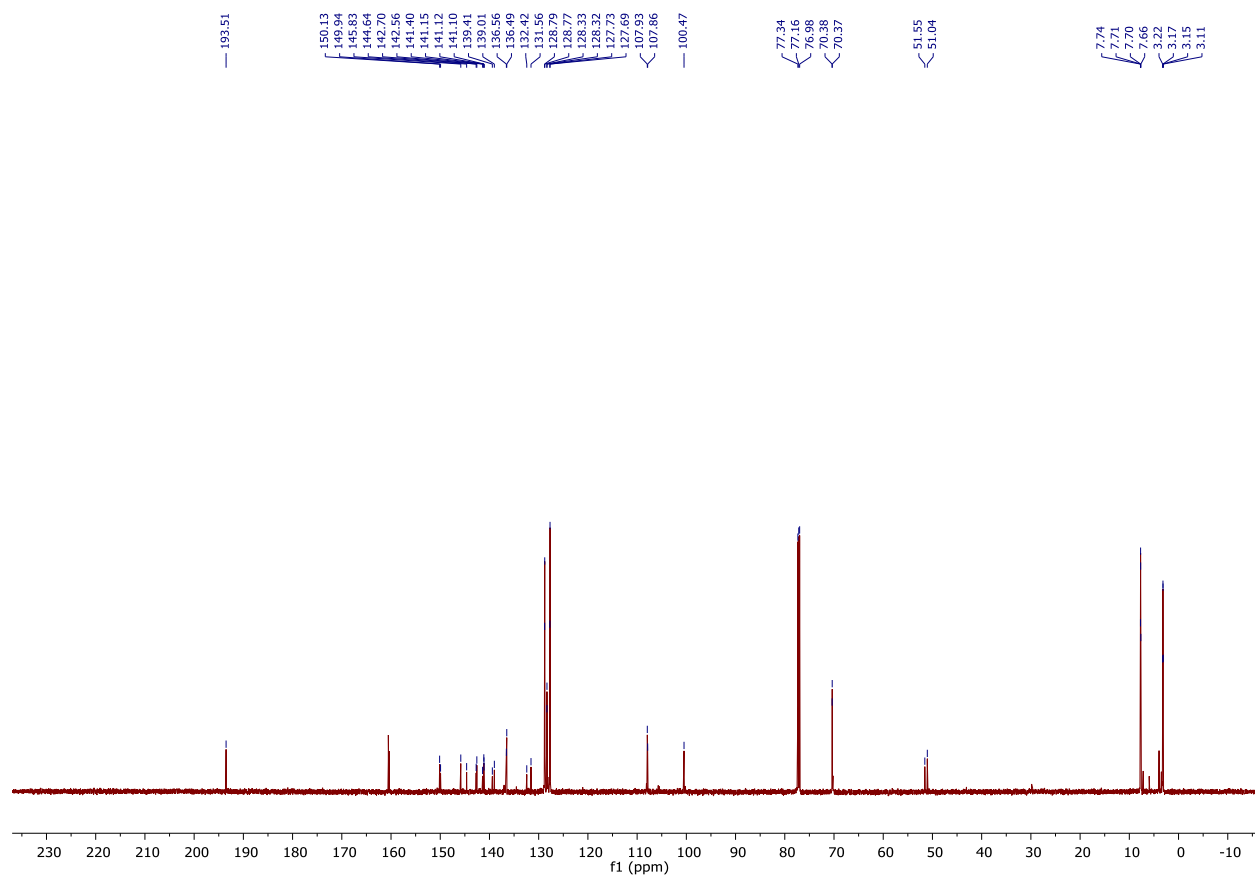
^{13}C NMR (176 MHz, Chloroform-*d*) δ 193.51, 150.13, 149.94, 145.83, 144.64, 142.70, 142.56, 141.40, 141.15, 141.12, 141.10, 139.41, 139.01, 136.56, 136.49, 132.42, 131.56, 128.79, 128.77, 128.33, 128.32, 127.73, 127.69, 107.93, 107.86, 100.47, 70.38, 70.37, 51.55, 51.04, 7.74, 7.71, 7.70, 7.66, 3.22, 3.17, 3.15, 3.11.

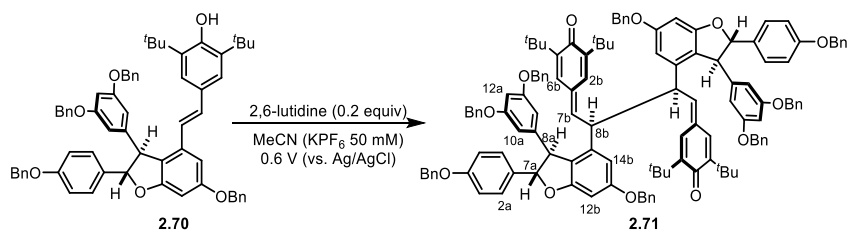
IR (Neat): 2957, 2898, 1588, 1456, 1248, 1158, 1051, 841, 734, 695, 619 cm^{-1} ;

HRMS (ESI) m/z calculated for $\text{C}_{80}\text{H}_{103}\text{O}_6\text{Si}_4^+$ ($[\text{M}+\text{H}]^+$) 1271.6826, found 1271.6816.



^{13}C NMR, 176 MHz, Chloroform-*d*, Dimer **2.69d**



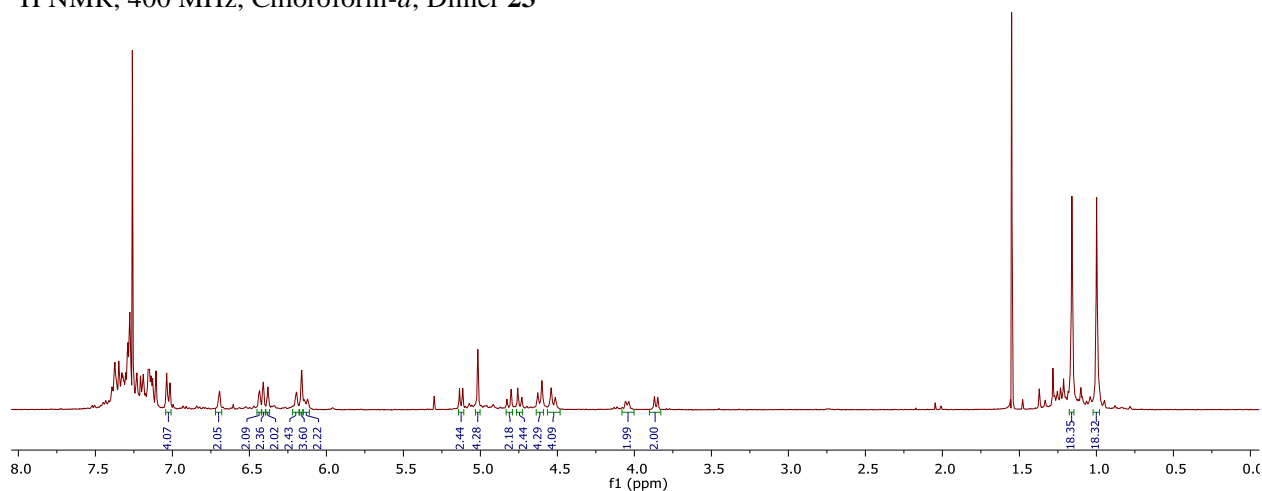


(2.71) 4,4'-((2*S*,3*S*)-2,3-bis((2*S*,3*S*)-6-(benzyloxy)-2-(4-(benzyloxy)phenyl)-3-(3,5-bis(benzyloxy)phenyl)-2,3-dihydrobenzofuran-4-yl)butane-1,4-diylidene)bis(2,6-di-*tert*-butylcyclohexa-2,5-dien-1-one)

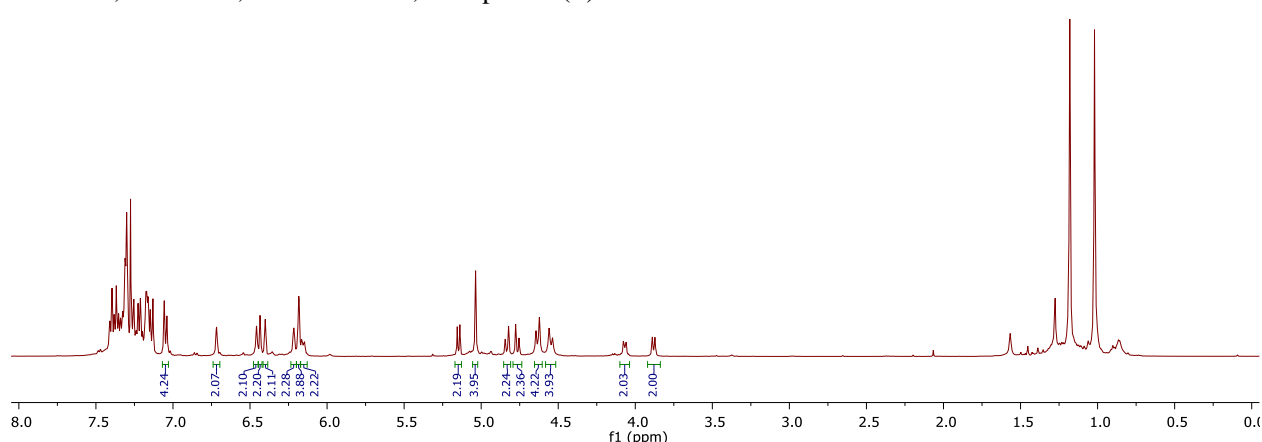
Stilbene **2.70** (0.05 mmol, 45 mg) was subjected to the general dimerization procedure, affording bis-quinone methide **2.71** (40 mg, 89% yield, >19:1 dr). The ^1H NMR spectrum was identical to the previous report for this compound.⁴⁸

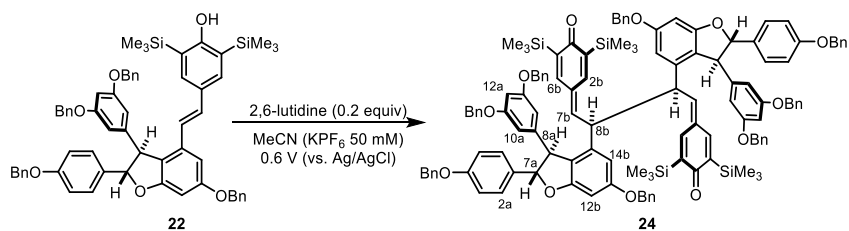
^1H NMR (700 MHz, CDCl_3 , 50 $^\circ\text{C}$) δ : 7.52 – 7.12 (m, 40H, $-\text{OCH}_2\text{C}_6\text{H}_5$), 7.10 (d, $J = 8.5$ Hz, 4H, C2a–H), 7.01 (d, $J = 8.5$ Hz, 4H, C3a–H), 6.70 (s, 2H, C14b–H), 6.42 (s, 2H, C2/6b–H), 6.39 (s, 2H, C12b–H), 6.37 (s, 2H, C12a–H), 6.23 (s, 2H, C2/6b–H), 6.16 (s, 4H, C10a–H), 6.11 (dd, br, $J = 7.3, 9.2$ Hz, 2H, C7b–H), 5.11 (d, $J = 8.1$ Hz, 2H, C7a–H), 5.04 (d, $J = 12.5$ Hz, 2H, C4a– $\text{OCH}_2\text{C}_6\text{H}_5$), 5.02 (d, $J = 12.5$ Hz, 2H, C4a– $\text{OCH}_2\text{C}_6\text{H}_5$), 4.83 (d, $J = 10.8$ Hz, 2H, C13b– $\text{OCH}_2\text{C}_6\text{H}_5$), 4.77 (d, $J = 10.8$ Hz, 2H, C13b– $\text{OCH}_2\text{C}_6\text{H}_5$), 4.62 (d, $J = 11.1$ Hz, 4H, C11a– $\text{OCH}_2\text{C}_6\text{H}_5$), 4.56 (d, $J = 11.1$ Hz, 4H, C11a– $\text{OCH}_2\text{C}_6\text{H}_5$), 4.06 (dd, br, $J = 7.9, 9.2$ Hz, 2H, C8b–H), 3.87 (d, $J = 8.1$ Hz, 2H, C8a–H), 1.17 (s, 18H, C3/5b– $\text{C}(\text{CH}_3)_3$), 1.00 (s, 18H, C3/5b– $\text{C}(\text{CH}_3)_3$).

^1H NMR, 400 MHz, Chloroform-*d*, Dimer **23**



^1H NMR, 500 MHz, Chloroform-*d*, Compound (\pm)-**5a**⁴⁸



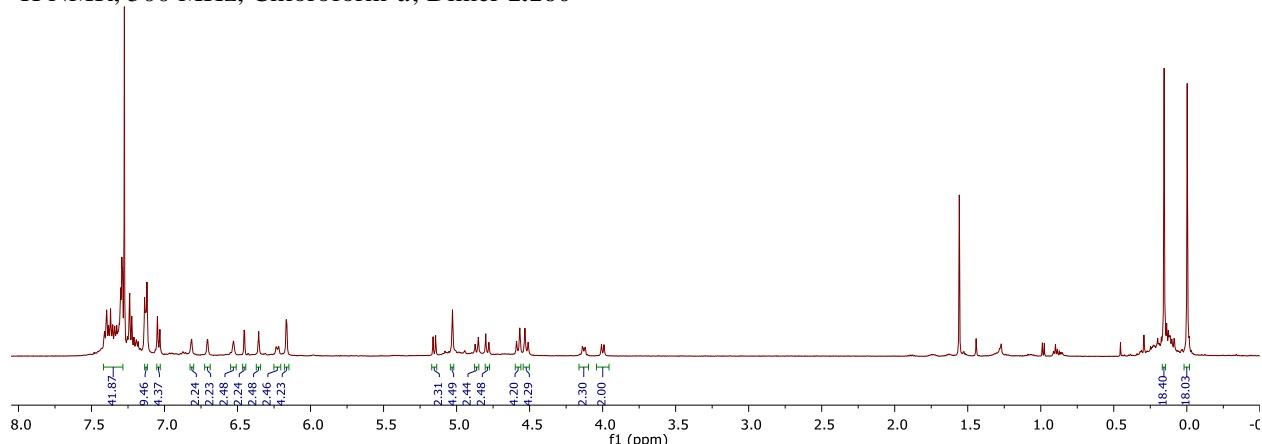


(1.160) 4,4'-((2*S*,3*S*)-2,3-bis((2*S*,3*S*)-6-(benzyloxy)-2-(4-(benzyloxy)phenyl)-3-(3,5-bis(benzyloxy)phenyl)-2,3-dihydrobenzofuran-4-yl)butane-1,4-diylidene)bis(2,6-bis(trimethylsilyl)cyclohexa-2,5-dien-1-one)

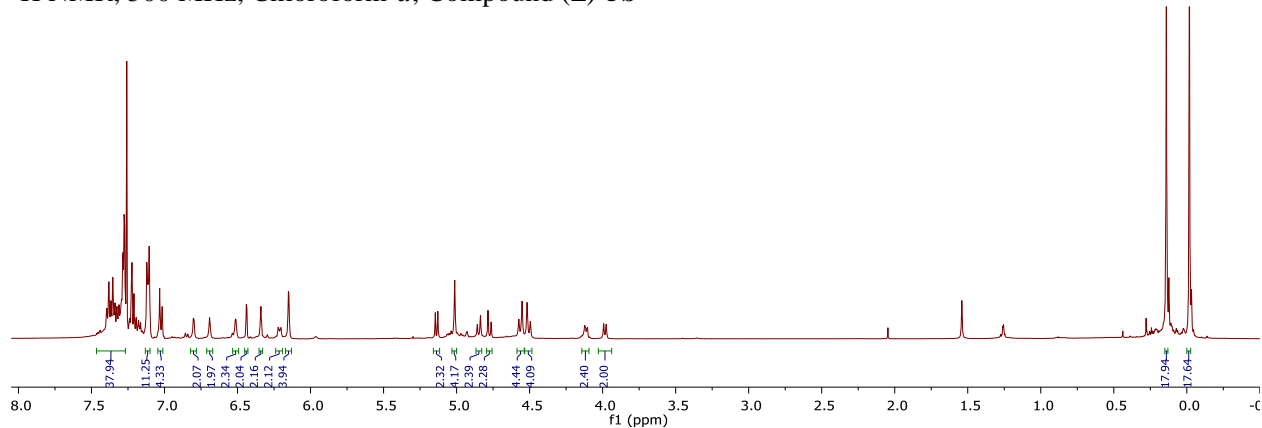
Stilbene **1.159** (0.039 mmol, 37 mg) was subjected to the general dimerization procedure, affording bisquinone methide **1.160** (21 mg, 57% yield, >19:1). The ^1H NMR spectrum was identical to the previous report for this compound.⁴⁸

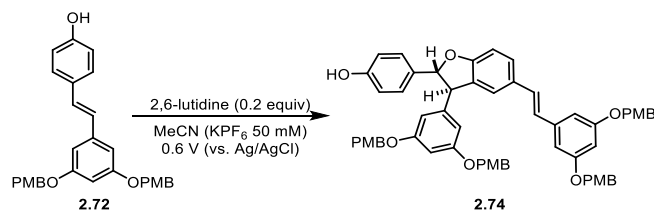
^1H NMR (500 MHz, CDCl_3 , 25 °C) δ : 7.44 – 7.10 (m, 40H, $-\text{OCH}_2\text{C}_6\text{H}_5$), 7.11 (d, $J = 8.6$ Hz, 4H, C2a–H), 7.03 (d, $J = 8.6$ Hz, 4H, C3a–H), 6.80 (d, $J = 2.2$ Hz, 2H, C2/6b–H), 6.69 (s, br, 2H, C14b–H), 6.51 (d, br, $J = 2.2$ Hz, 2H, C2/6b–H), 6.44 (d, $J = 2.2$ Hz, 2H, C12b–H), 6.34 (t, $J = 2.0$ Hz, 2H, C12a–H), 6.21 (dd, $J = 7.7, 9.9$ Hz, 2H, C7b–H), 6.15 (d, $J = 2.0$ Hz, 4H, C10a–H), 5.14 (d, $J = 8.6$ Hz, 2H, C7a–H), 5.01 (s, 4H, C4a– $\text{OCH}_2\text{C}_6\text{H}_5$), 4.85 (d, $J = 11.0$ Hz, 2H, C13b– $\text{OCH}_2\text{C}_6\text{H}_5$), 4.77 (d, $J = 11.0$ Hz, 2H, C13b– $\text{OCH}_2\text{C}_6\text{H}_5$), 4.56 (d, $J = 11.0$ Hz, 4H, C11a– $\text{OCH}_2\text{C}_6\text{H}_5$), 4.51 (d, $J = 11.0$ Hz, 4H, C11a– $\text{OCH}_2\text{C}_6\text{H}_5$), 4.11 (dd, $J = 7.7, 9.9$ Hz, 2H, C8b–H), 3.99 (d, $J = 8.6$ Hz, 2H, C8a–H), 0.14 (s, 18H, C3/5b– $\text{Si}(\text{CH}_3)_3$), -0.02 (s, 18H, C3/5b– $\text{Si}(\text{CH}_3)_3$).

^1H NMR, 500 MHz, Chloroform-*d*, Dimer **1.160**



^1H NMR, 500 MHz, Chloroform-*d*, Compound (\pm)-**5b**⁴⁸





(2.74) 4-((2R,3R)-3-(3,5-bis((4-methoxybenzyl)oxy)phenyl)-5-((E)-3,5-bis((4-methoxybenzyl)oxy)styryl)-2,3-dihydrobenzofuran-2-yl)phenol

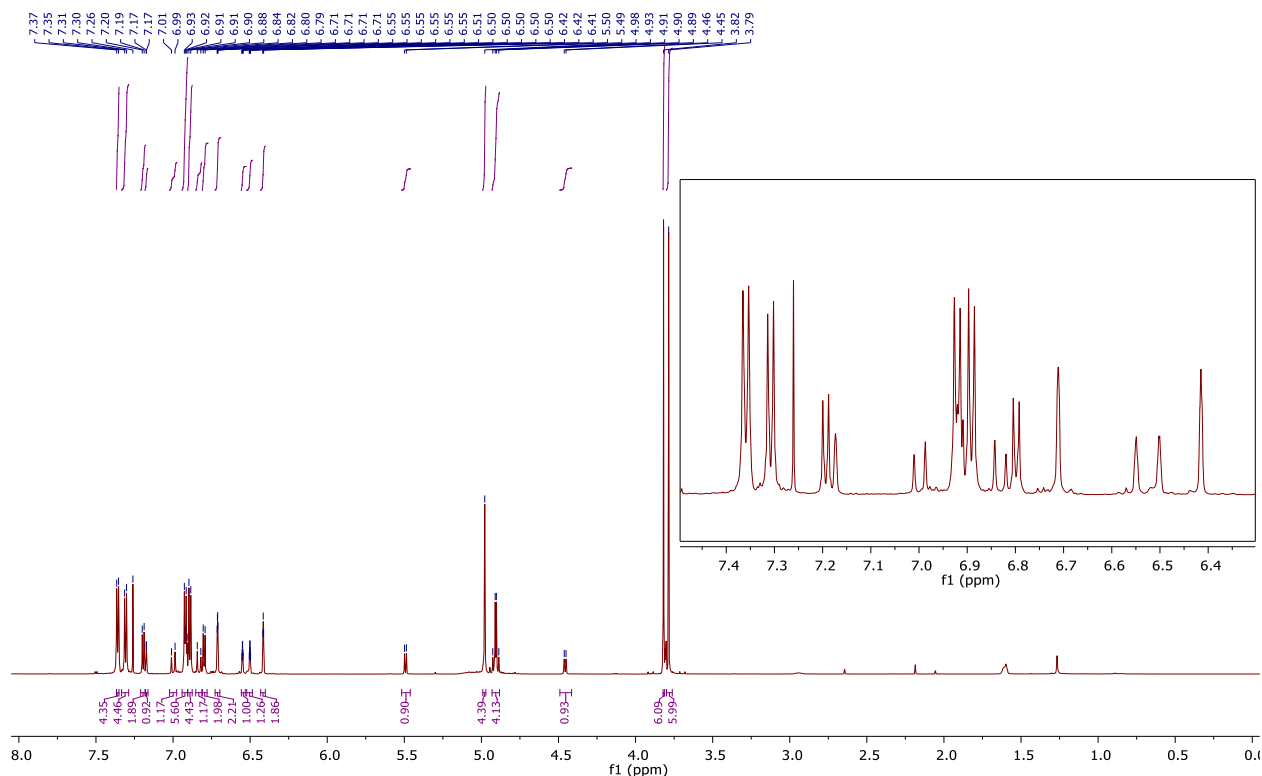
Stilbene **2.72** (0.1 mmol, 46.9 mg) was subjected to the general dimerization procedure. The crude product was purified via flash column chromatography (1% to 5% Acetone in CH₂Cl₂) to afford the dihydrobenzofuran **2.74** (27.5 mg, 59% yield, >19:1 dr).

¹H NMR (700 MHz, Chloroform-*d*) δ 7.36 (d, *J* = 8.4 Hz, 4H), 7.31 (d, *J* = 8.6 Hz, 4H), 7.19 (d, *J* = 8.5 Hz, 2H), 7.17 (d, *J* = 1.7 Hz, 1H), 7.00 (d, *J* = 16.2 Hz, 1H), 6.92 (d, *J* = 8.3, 4H), 6.91 (d, *J* = 8.5, 2H), 6.89 (d, *J* = 8.5 Hz, 4H), 6.83 (d, *J* = 16.2 Hz, 1H), 6.80 (d, *J* = 8.6 Hz, 2H), 6.71 (dd, *J* = 2.3, 1.2 Hz, 2H), 6.55 (td, *J* = 2.3, 1.0 Hz, 1H), 6.50 (td, *J* = 2.2, 1.2 Hz, 1H), 6.42 (t, *J* = 1.9 Hz, 2H), 5.49 (d, *J* = 8.2 Hz, 1H), 4.98 (s, 4H), 4.93 – 4.88 (m, 4H), 4.46 (d, *J* = 8.2 Hz, 1H), 3.82 (s, 6H), 3.79 (s, 6H).

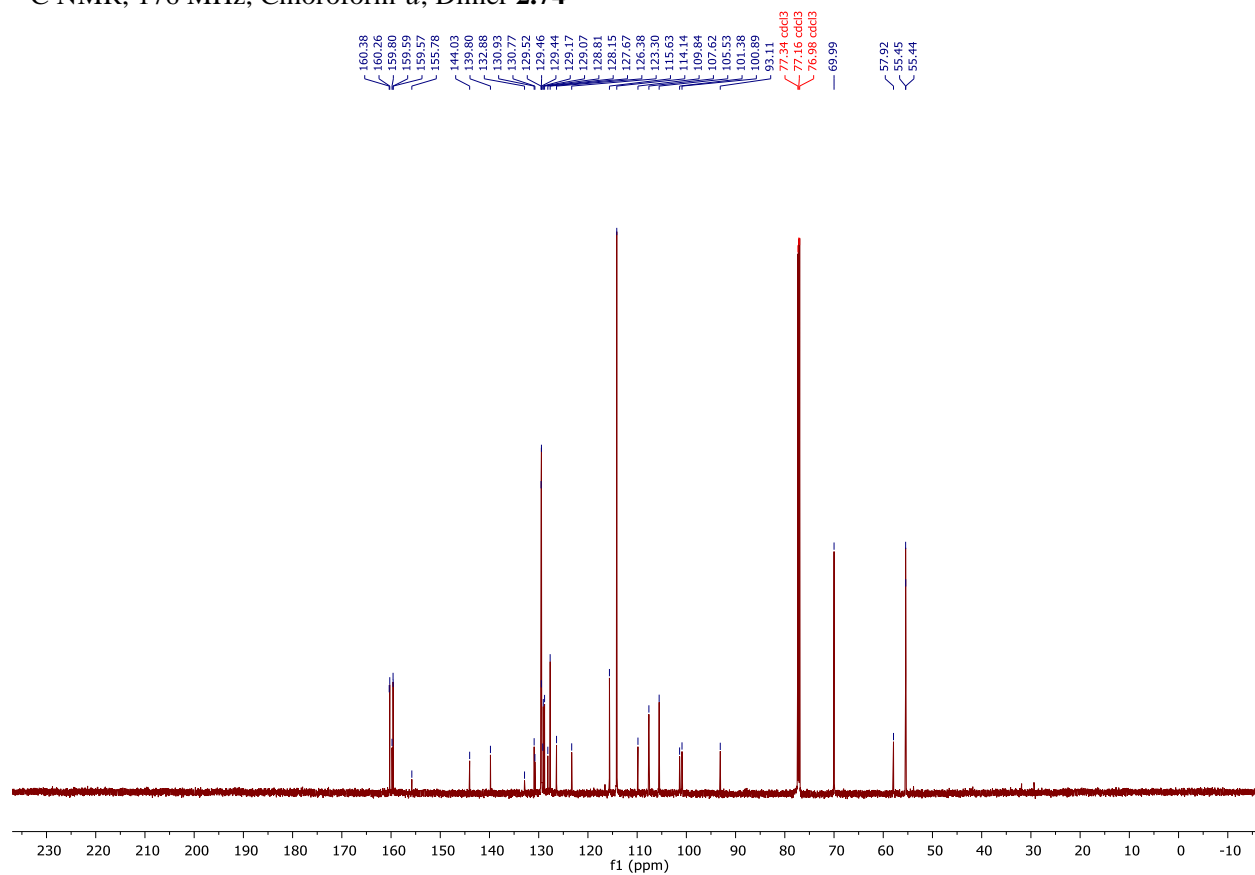
¹³C NMR (176 MHz, Chloroform-*d*) δ 160.38, 160.26, 159.80, 159.59, 159.57, 155.78, 144.03, 139.80, 132.88, 130.93, 130.77, 129.52, 129.46, 129.44, 129.17, 129.07, 128.81, 128.15, 127.67, 126.38, 123.30, 115.63, 114.14, 109.84, 107.62, 105.53, 101.38, 100.89, 93.11, 69.99, 57.92, 55.45, 55.44.

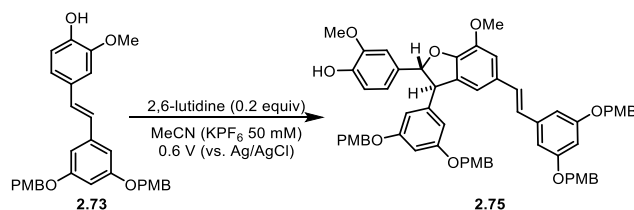
IR (Neat): 3391, 2932, 2835, 1585, 1512, 1440, 1301, 1244, 1146, 1030, 818 cm⁻¹;

HRMS (ESI) *m/z* calculated for C₆₀H₅₅O₁₀⁺ ([M+H]⁺) 935.3790, found 935.3800.



^{13}C NMR, 176 MHz, Chloroform-*d*, Dimer **2.74**





(2.75) 4-((2*R*,3*R*)-3-(3,5-bis((4-methoxybenzyl)oxy)phenyl)-5-((*E*)-3,5-bis((4-methoxybenzyl)oxy)styryl)-7-methoxy-2,3-dihydrobenzofuran-2-yl)-2-methoxyphenol

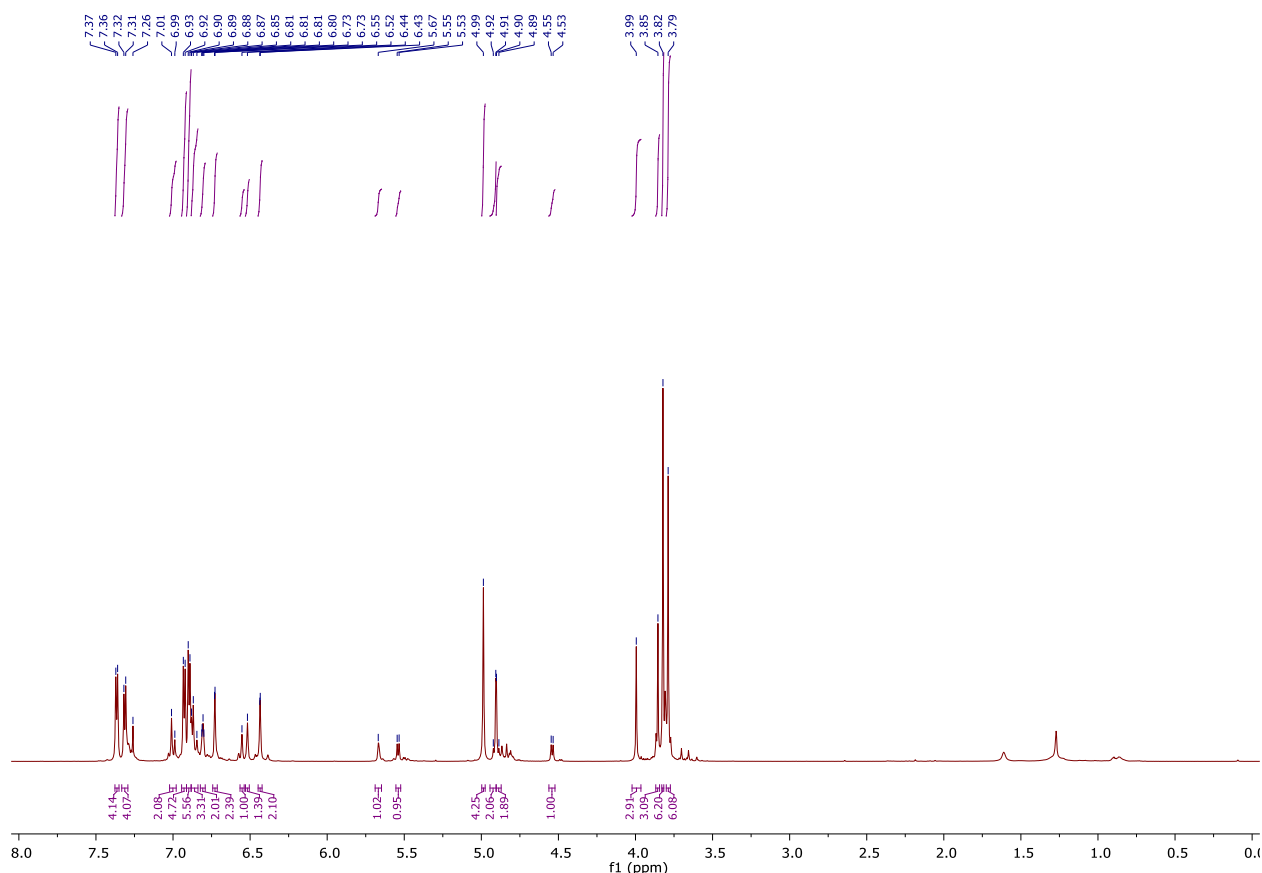
Stilbene **2.73** (0.1 mmol, 49.9 mg) was subjected to the general dimerization procedure. The crude product was purified via flash column chromatography (1% to 5% Acetone in CH₂Cl₂) to afford the dihydrobenzofuran **2.75** (28.4 mg, 57% yield, >19:1 dr).

¹H NMR (700 MHz, Chloroform-*d*) δ 7.37 (d, *J* = 8.1 Hz, 4H), 7.31 (d, *J* = 8.3 Hz, 4H), 7.00 (d, *J* = 15.0 Hz, 2H), 6.93 (d, *J* = 8.2 Hz, 5H), 6.90 (d, *J* = 7.8 Hz, 6H), 6.88 – 6.84 (m, 3H), 6.81 (d, *J* = 4.1 Hz, 2H), 6.74 – 6.71 (m, 2H), 6.55 (s, 1H), 6.52 (s, 1H), 6.45 – 6.42 (m, 2H), 5.67 (s, 1H), 5.54 (d, *J* = 8.8 Hz, 1H), 4.99 (s, 4H), 4.91 (d, *J* = 11.2 Hz, 2H), 4.89 (d, *J* = 11.0 Hz, 2H), 4.54 (d, *J* = 8.8 Hz, 1H), 3.99 (s, 3H), 3.85 (s, 3H), 3.82 (s, 6H), 3.79 (s, 6H).

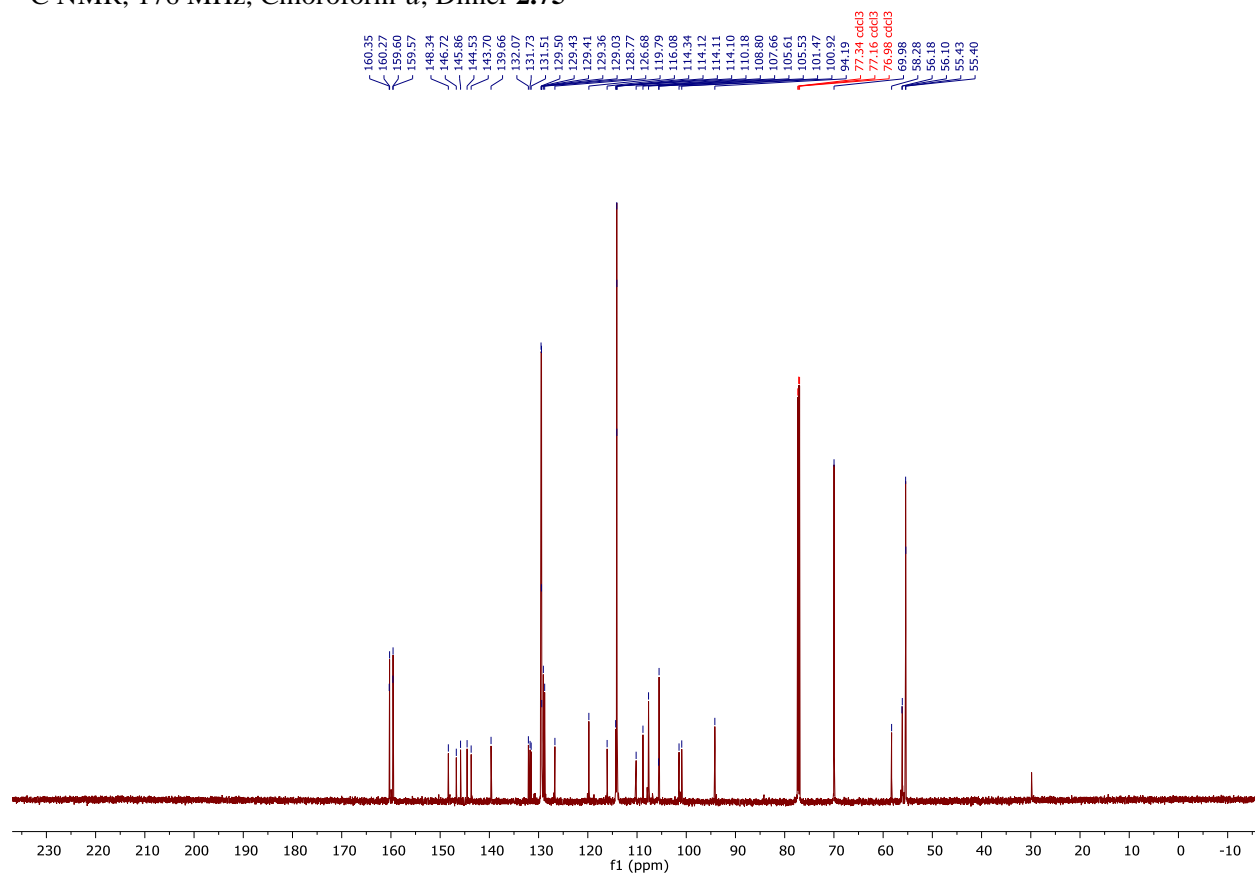
¹³C NMR (176 MHz, Chloroform-*d*) δ 160.35, 160.27, 159.60, 159.57, 148.34, 146.72, 145.86, 144.53, 143.70, 139.66, 132.07, 131.73, 131.51, 129.50, 129.43, 129.41, 129.36, 129.03, 128.77, 126.68, 119.79, 116.08, 114.34, 114.12, 114.11, 114.10, 110.18, 108.80, 107.66, 105.61, 105.53, 101.47, 100.92, 94.19, 69.98, 58.28, 56.18, 56.10, 55.43, 55.40.

IR (Neat): 3395, 2999, 2934, 2833, 1585, 1512, 1439, 1302, 1245, 1150, 1032, 824, 734 cm⁻¹;

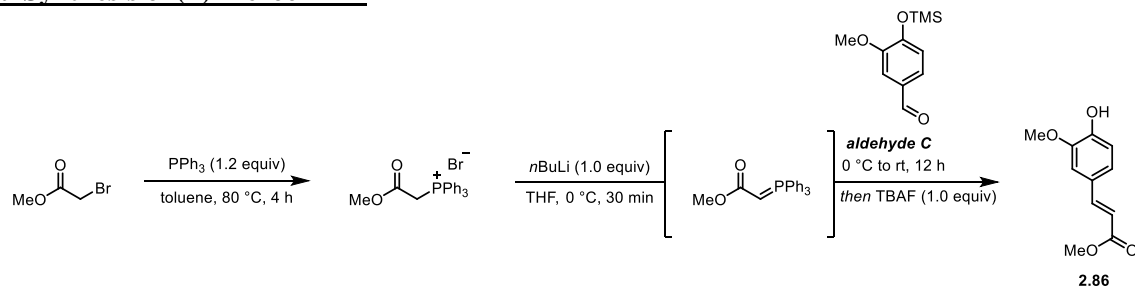
HRMS (ESI) *m/z* calculated for C₆₂H₅₉O₁₂⁺ ([M+H]⁺) 995.4001, found 995.3979.



^{13}C NMR, 176 MHz, Chloroform-*d*, Dimer **2.75**



Total Synthesis of (\pm)-hierochin D



(**2.86**) methyl (*E*)-3-(4-hydroxy-3-methoxyphenyl)acrylate

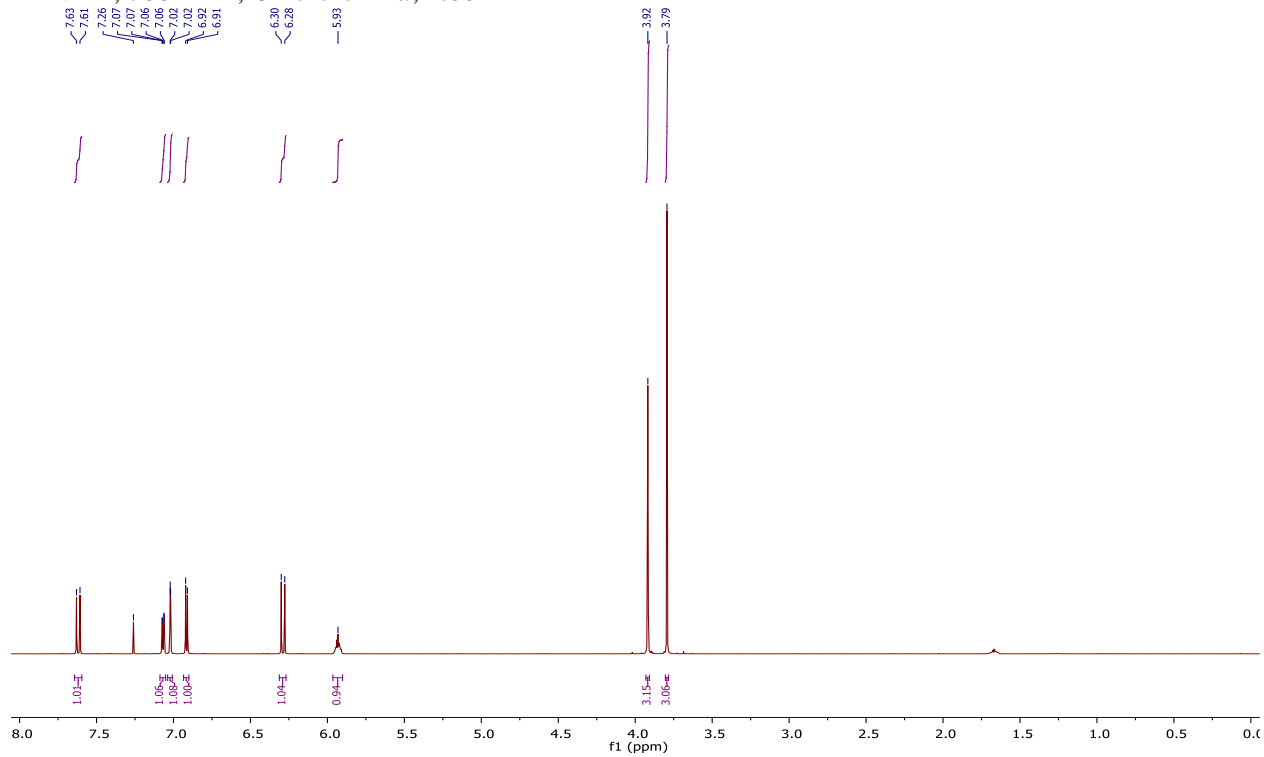
Commercially available methyl bromoacetate (1.42 mL, 15 mmol) was dissolved in toluene (60 mL) in a flame-dried round bottom flask. To the stirring solution was added triphenylphosphine (18 mmol, 4.72g), and the reaction was heated to 80 °C for 4 hours. Upon cooling the reaction mixture to room temperature, the white solid product was collected via vacuum filtration, and any excess triphenylphosphine was rinsed away with hexanes. The product was dried under vacuum for >24 hours to ensure full removal of solvent and water prior to use in the subsequent olefination.

To a flame-dried, three-neck, round bottom flask was added methyl acetophosphonium bromide (5.35 mmol, 2.22 g), which was subsequently suspended in THF (15 mL) and cooled on ice to 0 °C. To the stirring suspension was added *n*BuLi (5.35 mmol, 2.14 mL, 2.5 M in hexanes), and the reaction mixture was allowed to stir at temperature for 30 minutes to form the ylide. In a separate flame-dried, heart-shaped flask, TMS-vanillin (aldehyde C, 5.35 mmol, 1.20 g) was dissolved in THF (20 mL). The aldehyde was added to the ylide solution via cannula, and the reaction was allowed to warm to room temperature over 12 hours. The reaction was subsequently cooled on ice to 0 °C, and TBAF (5.35 mmol, 5.35 mL, 1.0 M in THF) was added. The reaction was allowed to warm to room temperature over 1 hour, at which point it was quenched by the addition of saturated ammonium chloride, diluted with EtOAc, then transferred to a separatory funnel containing additional saturated ammonium chloride. The layers were separated, and the aqueous layer was extracted with additional EtOAc. The combined organic layers were washed with brine, dried over magnesium sulfate, and concentrated under reduced pressure. The crude product was purified via flash column chromatography (6-42% EtOAc in Hexanes, 7-step gradient, 2 column volumes per step) to afford the product **2.86** as a clear, colorless, oil (857 mg, 77% yield). The ¹H and ¹³C NMR spectra of the product was consistent with the data previously reported in the literature.¹¹⁸

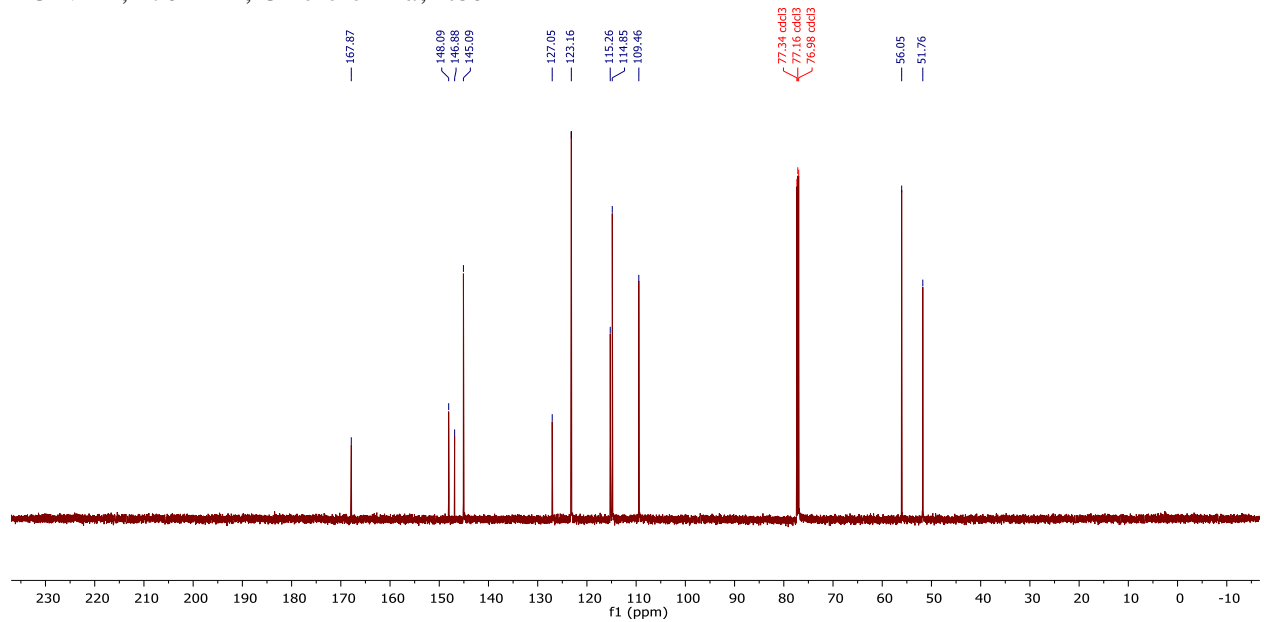
¹H NMR (700 MHz, Chloroform-*d*) δ 7.62 (d, *J* = 15.9 Hz, 1H), 7.07 (dd, *J* = 8.3, 1.9 Hz, 1H), 7.02 (d, *J* = 1.9 Hz, 1H), 6.92 (d, *J* = 8.2 Hz, 1H), 6.29 (d, *J* = 15.9 Hz, 1H), 5.93 (s, 1H), 3.92 (s, 3H), 3.79 (s, 3H).

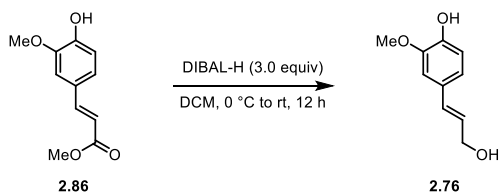
¹³C NMR (176 MHz, Chloroform-*d*) δ 167.87, 148.09, 146.88, 145.09, 127.05, 123.16, 115.26, 114.85, 109.46, 56.05, 51.76.

¹H NMR, 700 MHz, Chloroform-*d*, 2.86



¹³C NMR, 176 MHz, Chloroform-*d*, 2.86



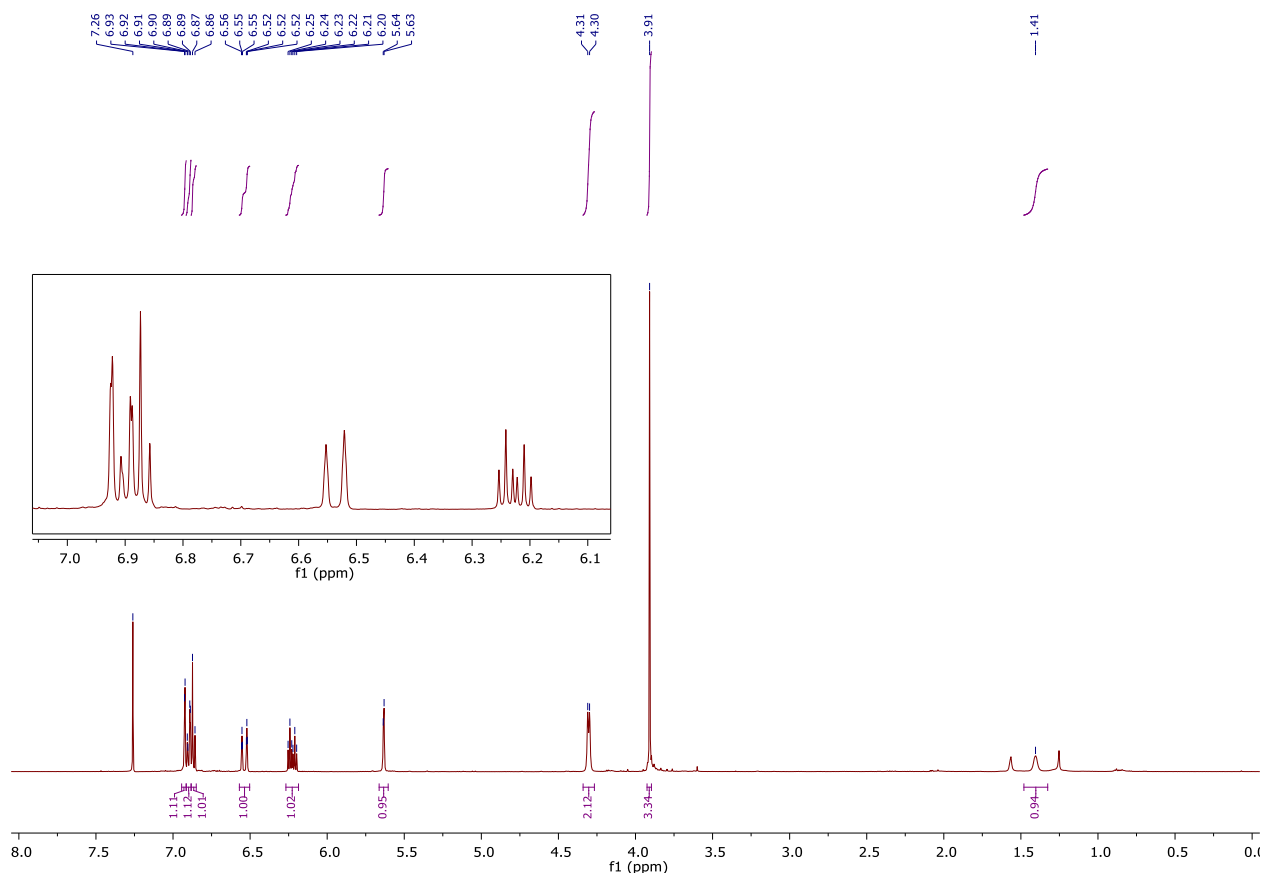


coniferyl alcohol (2.76) ((E)-4-(3-hydroxyprop-1-en-1-yl)-2-methoxyphenol)

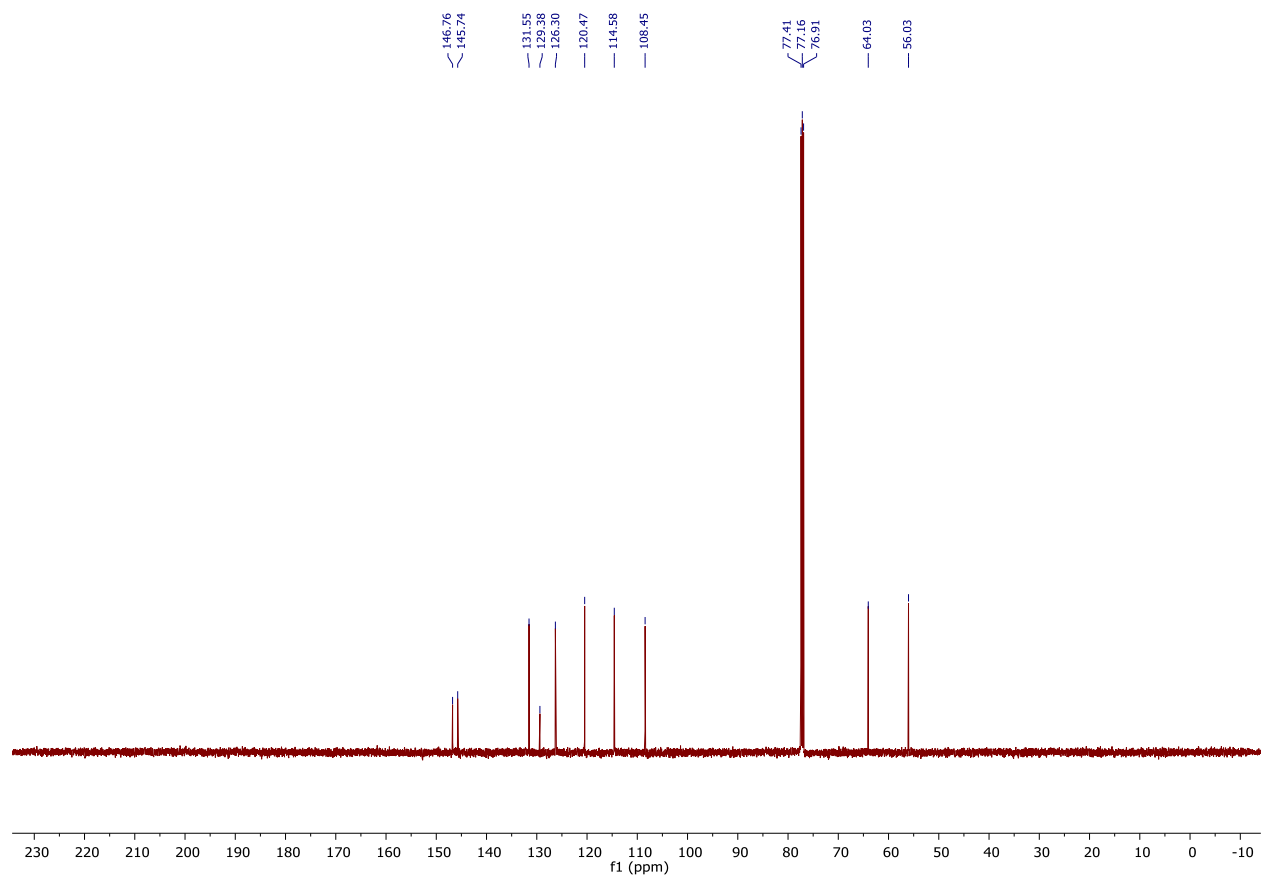
Compound **2.86** (1.12 mmol, 233 mg) was dissolved in DCM under inert atmosphere, and the stirring solution was cooled to 0 °C on ice. A solution of diisobutylaluminum hydride (3.36 mmol, 3.36 mL, 1.0 M in DCM) was added dropwise to the stirring solution, causing the reaction to change from colorless to slightly yellow. The reaction mixture was held at 0 °C for 10 minutes, at which point it was allowed to warm to room temperature over 12 hours. The reaction was quenched slowly with 4mL of Rochelle's salt, turning the mixture cloudy. The mixture was let to stir at room temperature for >6 hours, at which point it was diluted with DI water and transferred to a separatory funnel. The layers were separated, and the aqueous layer was washed with multiple portions of DCM. The combined organic layers were washed with brine, dried over magnesium sulfate, and concentrated under reduced pressure. The crude product was purified via flash column chromatography (28-98% EtOAc in Hexanes, 5 step gradient, 2 column volumes per step) to afford the product **2.76** as a white solid (167 mg, 83% yield). The ¹H and ¹³C NMR spectra of the product was consistent with the data previously reported in the literature.¹¹⁹

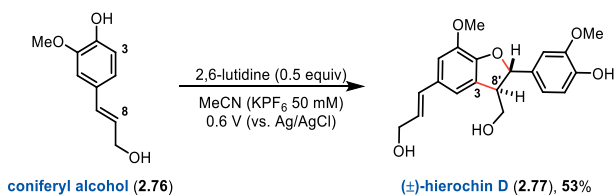
¹H NMR (500 MHz, Chloroform-*d*) δ 6.92 (d, *J* = 1.8 Hz, 1H), 6.90 (dd, *J* = 8.1, 1.8 Hz, 1H), 6.87 (d, *J* = 8.1 Hz, 1H), 6.54 (dt, *J* = 15.8, 1.6 Hz, 1H), 6.23 (dt, *J* = 15.8, 6.0 Hz, 1H), 5.63 (d, *J* = 2.8 Hz, 1H), 4.30 (d, *J* = 5.9 Hz, 2H), 3.91 (s, 3H), 1.41 (s, 1H).

¹³C NMR (126 MHz, Chloroform-*d*) δ 146.76, 145.74, 131.55, 129.38, 126.30, 120.47, 114.58, 108.44, 64.04, 56.03.



^{13}C NMR, 126 MHz, Chloroform-*d*, **2.76**



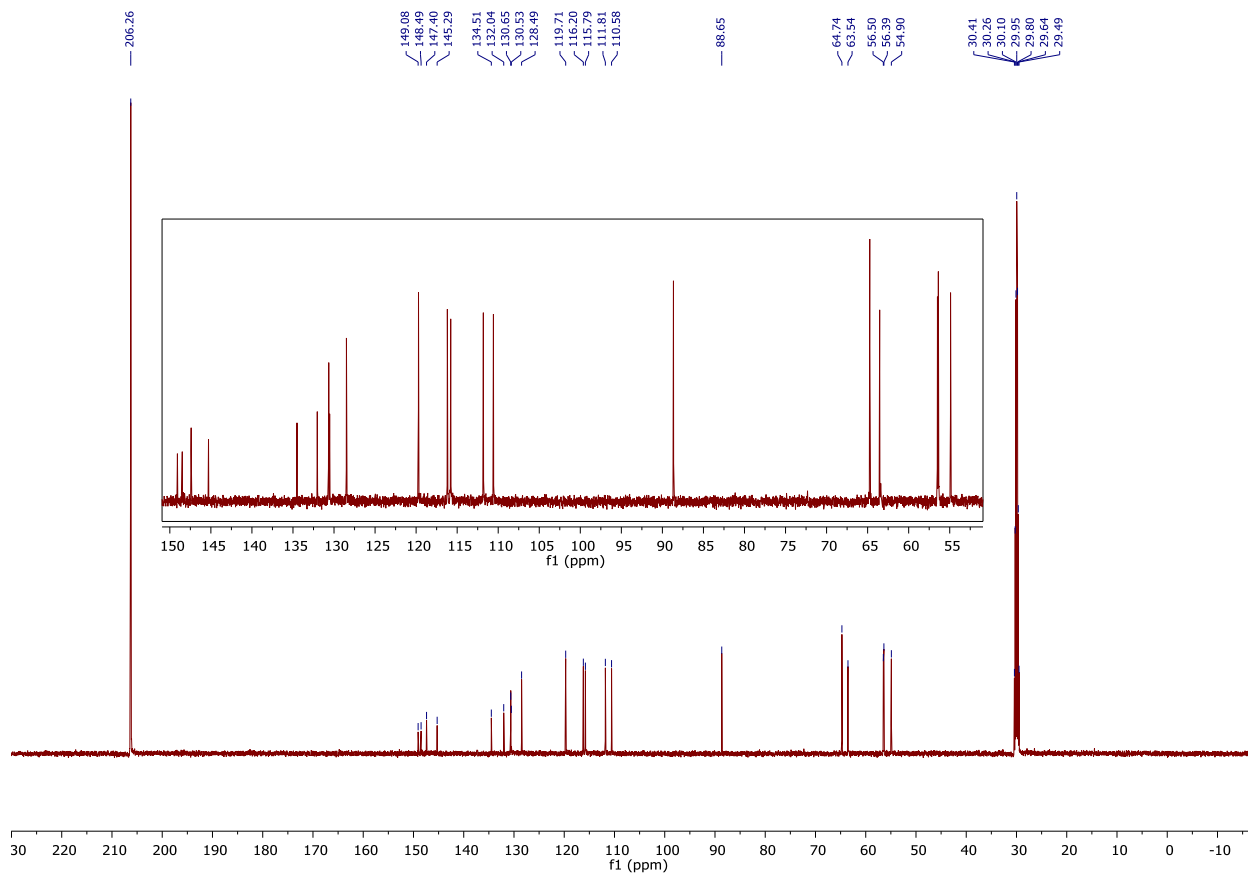


(±)-hierochin D (2.77) 4-((2*S*,3*R*)-3-(hydroxymethyl)-5-((*E*)-3-hydroxyprop-1-en-1-yl)-7-methoxy-2,3-dihydrobenzofuran-2-yl)-2-methoxyphenol

Coniferyl alcohol (**2.76**, 0.1 mmol, 18 mg) was subjected to the general dimerization conditions (see page S42), with the only variation being the amount of 2,6-lutidine (5.8 μ L, 0.05 mmol). The crude reaction material was purified via flash column chromatography to afford (±)-hierochin D (**2.77**) as a colorless oil (9.4 mg, 53% yield). The ^{13}C NMR was consistent with the previous report for this compound.¹²⁰

^{13}C NMR (126 MHz, Acetone- d_6) δ 148.97, 148.38, 147.29, 145.18, 134.40, 131.93, 130.54, 130.42, 128.38, 119.60, 116.09, 115.68, 111.70, 110.47, 88.54, 64.63, 63.43, 56.39, 56.28, 54.79.

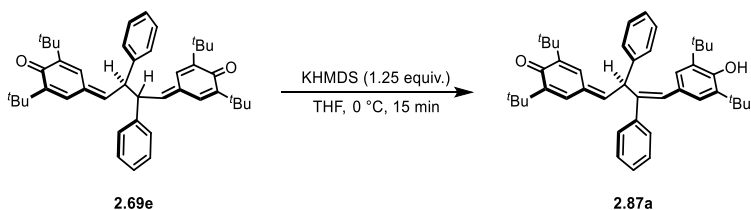
^{13}C NMR, 126 MHz, Chloroform- d , **2.77**



Natural Product Analog Synthesis:

Tautomerization of BQM dimer to MQM dimer – General Procedure:

The starting BQM dimer was added to a reaction vial charged with a stir bar. The atmosphere was evacuated and replaced with nitrogen, and the starting material was dissolved in THF. The reaction solution was cooled in an ice bath to 0 °C, and potassium bis(trimethylsilyl)amide (KHMDS) was added as a solution (1.25 equiv., 0.7 M in toluene). The reaction was allowed to stir until the starting material consumed based on TLC analysis. The reaction was quenched by the addition of aqueous saturated ammonium chloride, diluted with EtOAc, and transferred to a separatory funnel containing additional aq. sat. NH₄Cl. The layers were separated, and the aqueous layer was extracted with additional portions of ethyl acetate. The combined organic layers were washed with brine, dried over magnesium sulfate, and concentrated under reduced pressure. The crude product was further purified by flash column chromatography.



(2.87a) (*S,Z*)-2,6-di-*tert*-butyl-4-(4-(3,5-di-*tert*-butyl-4-hydroxyphenyl)-2,3-diphenylbut-3-en-1-ylidene)cyclohexa-2,5-dien-1-one

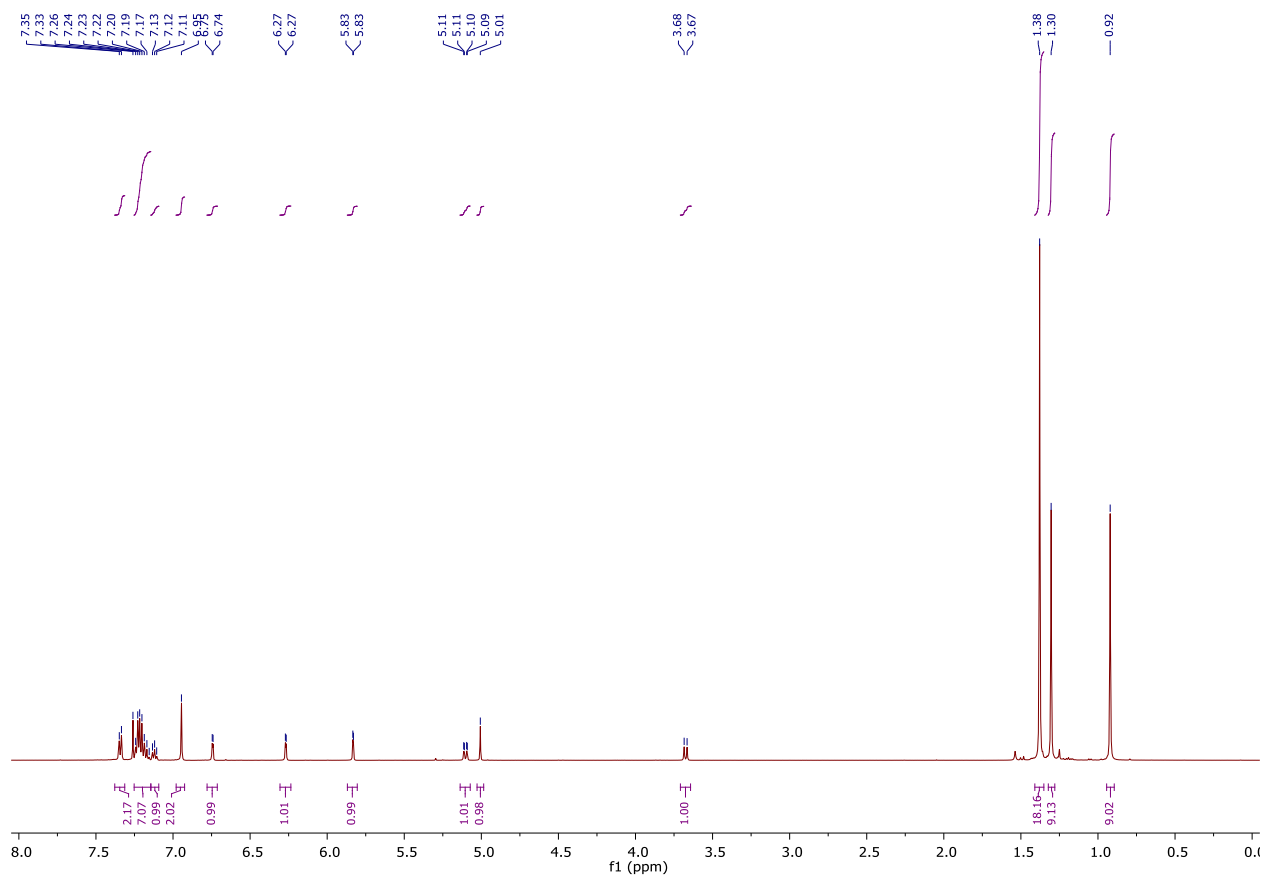
Dimer **2.69e** (0.026 mmol, 16 mg) was subjected to the tautomerization conditions, and the crude product was purified by flash column chromatography (10–50% DCM/Hexanes) to afford MQM **2.87a** (10 mg, 62% yield).

^1H NMR (500 MHz, Chloroform-*d*) δ 7.34 (d, $J = 7.0$ Hz, 2H), 7.25 – 7.14 (m, 7H), 7.12 (t, $J = 6.8$ Hz, 1H), 6.95 (s, 2H), 6.74 (d, $J = 2.7$ Hz, 1H), 6.27 (d, $J = 2.7$ Hz, 1H), 5.83 (d, $J = 1.9$ Hz, 1H), 5.10 (dd, $J = 9.5, 2.0$ Hz, 1H), 5.01 (s, 1H), 3.67 (d, $J = 9.5$ Hz, 1H), 1.38 (s, 18H), 1.30 (s, 9H), 0.92 (s, 9H).

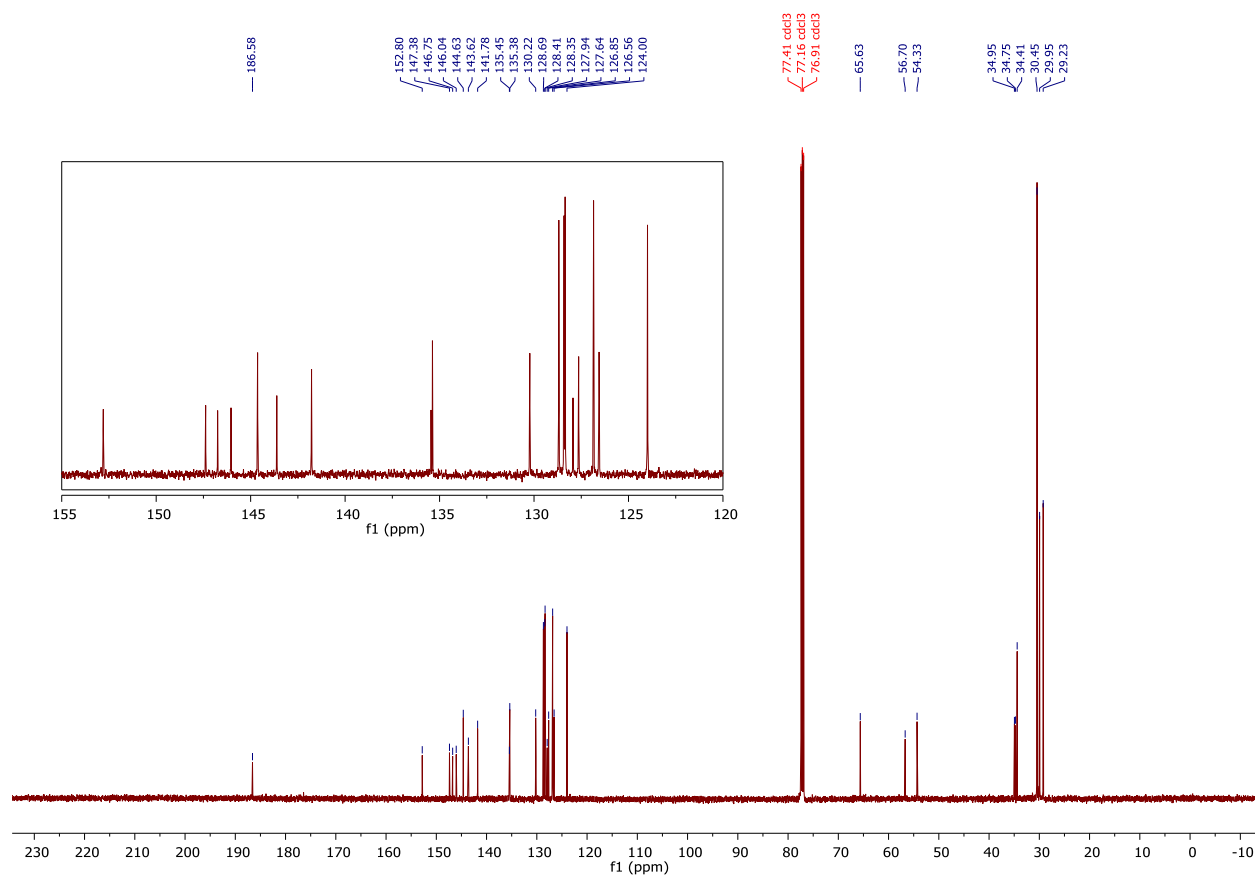
^{13}C NMR (126 MHz, Chloroform-*d*) δ 186.41, 152.63, 147.21, 146.57, 145.86, 144.46, 143.44, 141.60, 135.28, 135.20, 130.05, 128.51, 128.24, 128.18, 127.76, 127.47, 126.68, 126.39, 123.82, 65.46, 56.53, 54.16, 34.78, 34.58, 34.23, 30.28, 29.77, 29.06.

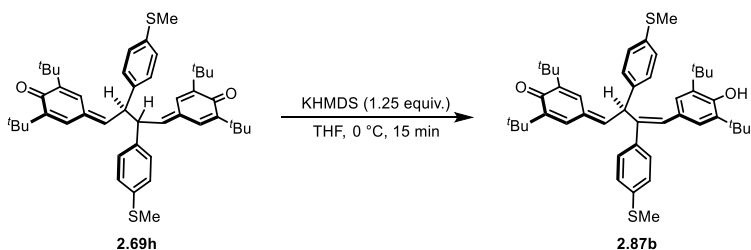
IR (Neat): 3623, 2954, 2912, 1653, 1437, 1366, 1192, 1116, 886, 734, 700 cm^{-1} ;

HRMS (ESI) m/z calculated for $\text{C}_{44}\text{H}_{55}\text{O}_2^+$ ($[\text{M}+\text{H}]^+$) 615.4197, found 615.4194.



^{13}C NMR, 126 MHz, Chloroform-*d*, Tautomer **2.87a**





(2.87b) (*S,Z*)-2,6-di-*tert*-butyl-4-(4-(3,5-di-*tert*-butyl-4-hydroxyphenyl)-2,3-bis(4-(methylthio)phenyl)but-3-en-1-ylidene)cyclohexa-2,5-dien-1-one

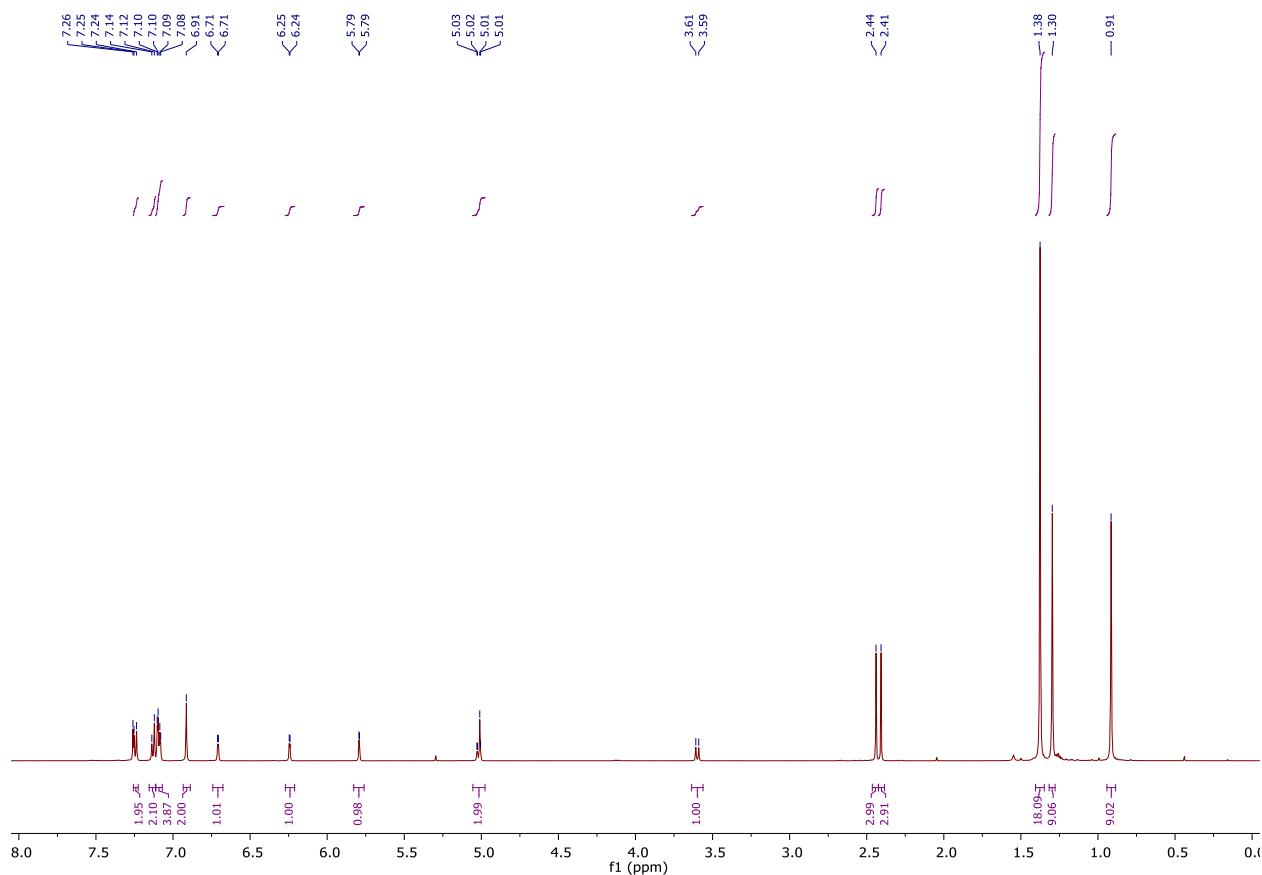
Dimer **2.69h** (0.021 mmol, 15 mg) was subjected to the tautomerization conditions, and the crude product was purified by flash column chromatography (10-50% DCM/Hexanes) to afford MQM **2.87b** (14.8 mg, 99% yield).

^1H NMR (500 MHz, Chloroform-*d*) δ 7.24 (d, $J = 8.2$ Hz, 2H), 7.13 (d, $J = 8.2$ Hz, 2H), 7.10 (d, $J = 8.2$ Hz, 2H), 7.09 (d, $J = 8.2$ Hz, 2H), 6.91 (s, 2H), 6.71 (d, $J = 2.7$ Hz, 1H), 6.24 (d, $J = 2.7$ Hz, 1H), 5.79 (d, $J = 1.9$ Hz, 1H), 5.02 (dd, $J = 9.2, 2.0$ Hz, 1H), 5.01 (s, 1H), 3.60 (d, $J = 9.6$ Hz, 1H), 2.44 (s, 3H), 2.41 (s, 3H), 1.38 (s, 18H), 1.30 (s, 9H), 0.91 (s, 9H).

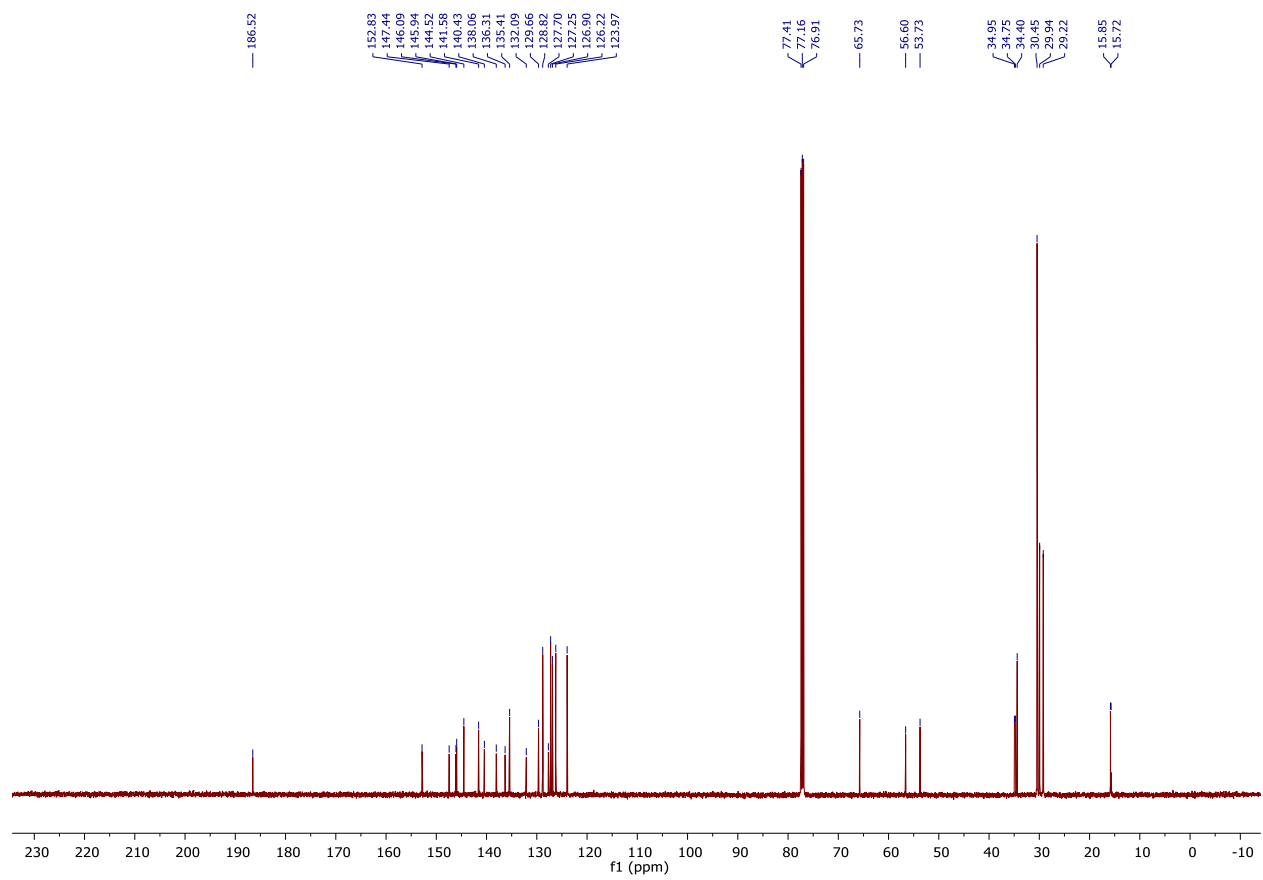
^{13}C NMR (126 MHz, Chloroform-*d*) δ 186.52, 152.83, 147.44, 146.09, 145.94, 144.52, 141.58, 140.43, 138.06, 136.31, 135.41, 132.09, 129.66, 128.82, 127.70, 127.25, 126.90, 126.22, 123.97, 65.73, 56.60, 53.73, 34.95, 34.75, 34.40, 30.45, 29.94, 29.22, 15.85, 15.72.

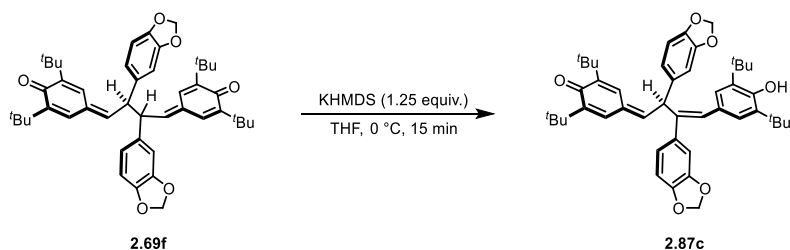
IR (Neat): 3645, 2960, 1659, 1496, 1439, 1363, 1316, 1237, 1150, 1094, 891, 814, 728 cm^{-1} ;

HRMS (ESI) m/z calculated for $\text{C}_{46}\text{H}_{59}\text{O}_2\text{S}_2^+$ ($[\text{M}+\text{H}]^+$) 707.3951, found 707.3940.



^{13}C NMR, 126 MHz, Chloroform-*d*, Tautomer **2.87b**





(2.87c) (*S,Z*)-4-(2,3-bis(benzo[*d*][1,3]dioxol-5-yl)-4-(3,5-di-*tert*-butyl-4-hydroxyphenyl)but-3-en-1-ylidene)-2,6-di-*tert*-butylcyclohexa-2,5-dien-1-one

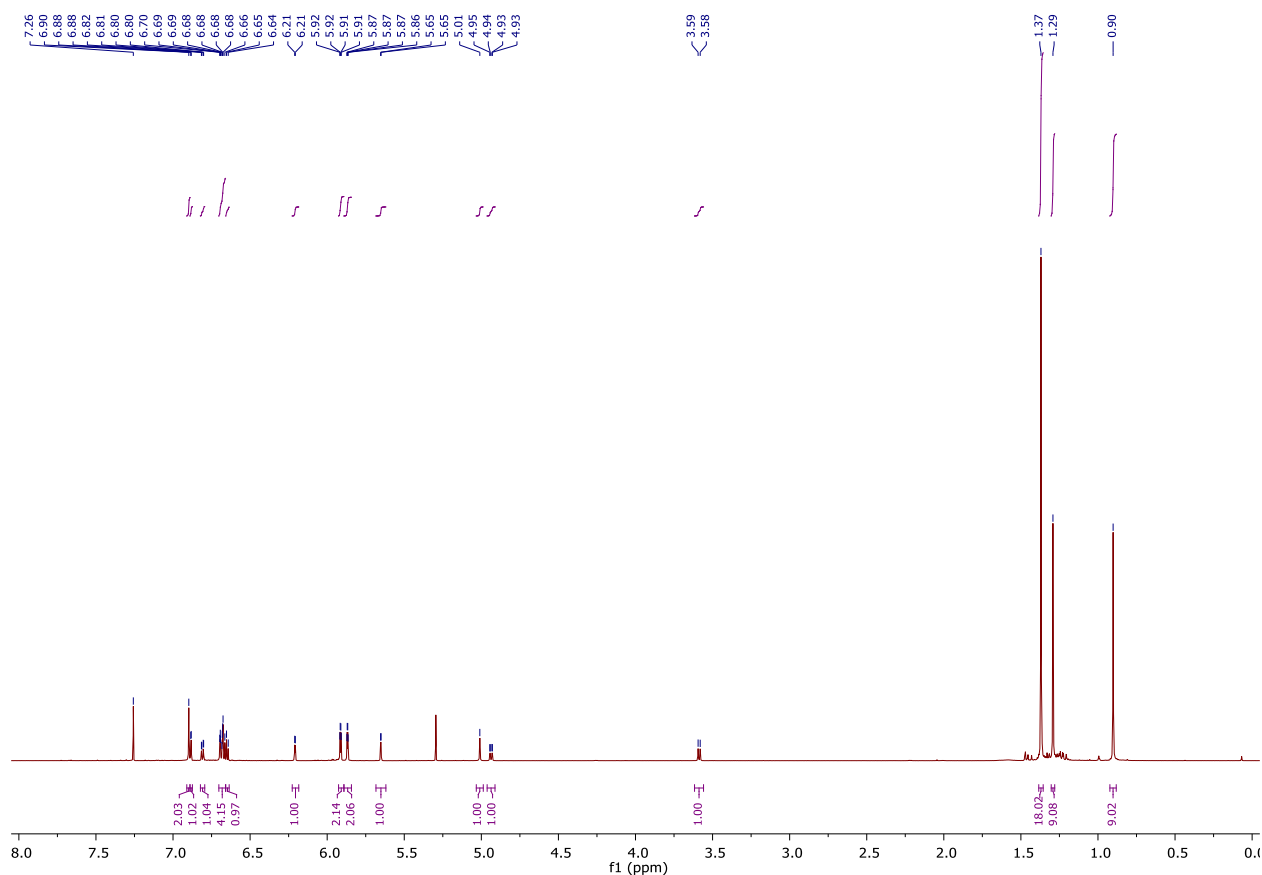
Dimer **2.69f** (0.021 mmol, 14.7 mg) was subjected to the tautomerization conditions, and the crude product was purified by flash column chromatography (10–50% DCM/Hexanes) to afford MQM **2.87c** (9 mg, 61% yield).

$^1\text{H NMR}$ (700 MHz, Chloroform-*d*) δ 6.90 (s, 2H), 6.88 (d, $J = 1.8$ Hz, 1H), 6.81 (dd, $J = 8.1, 1.8$ Hz, 1H), 6.70 – 6.66 (m, 4H), 6.65 (d, $J = 7.8$ Hz, 1H), 6.21 (d, $J = 2.7$ Hz, 1H), 5.93 – 5.89 (m, 2H), 5.89 – 5.84 (m, 2H), 5.65 (d, $J = 1.9$ Hz, 1H), 5.01 (s, 1H), 4.94 (dd, $J = 9.5, 2.0$ Hz, 1H), 3.59 (d, $J = 9.5$ Hz, 1H), 1.37 (s, 18H), 1.29 (s, 9H), 0.90 (s, 9H).

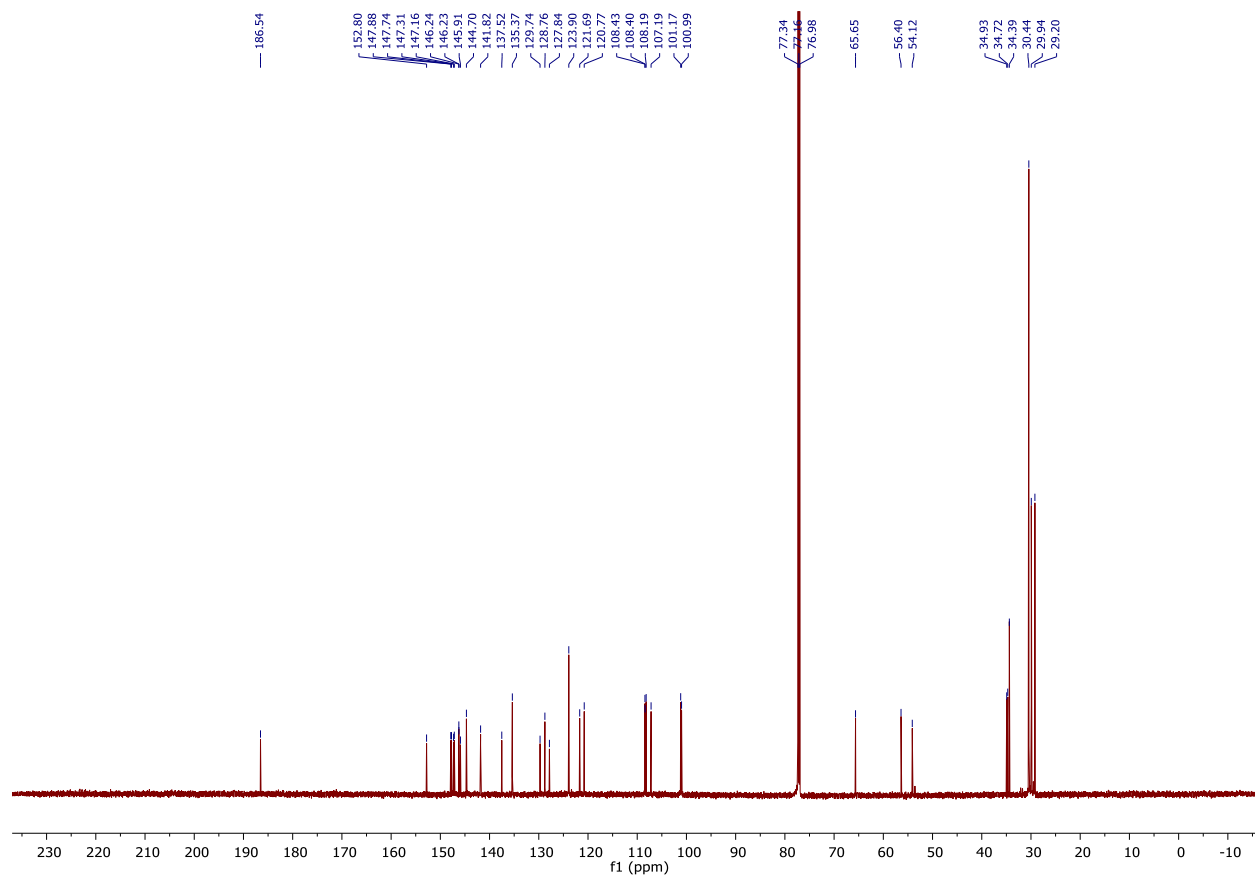
$^{13}\text{C NMR}$ (176 MHz, Chloroform-*d*) δ 186.54, 152.80, 147.88, 147.74, 147.31, 147.16, 146.24, 146.23, 145.91, 144.70, 141.82, 137.52, 135.37, 129.74, 128.76, 127.84, 123.90, 121.69, 120.77, 108.43, 108.40, 108.19, 107.19, 101.17, 100.99, 65.65, 56.40, 54.12, 34.93, 34.72, 34.39, 30.44, 29.94, 29.20.

IR (Neat): 3628, 2955, 2905, 1653, 1635, 1503, 1436, 1363, 1235, 1038, 933, 809, 729 cm^{-1} ;

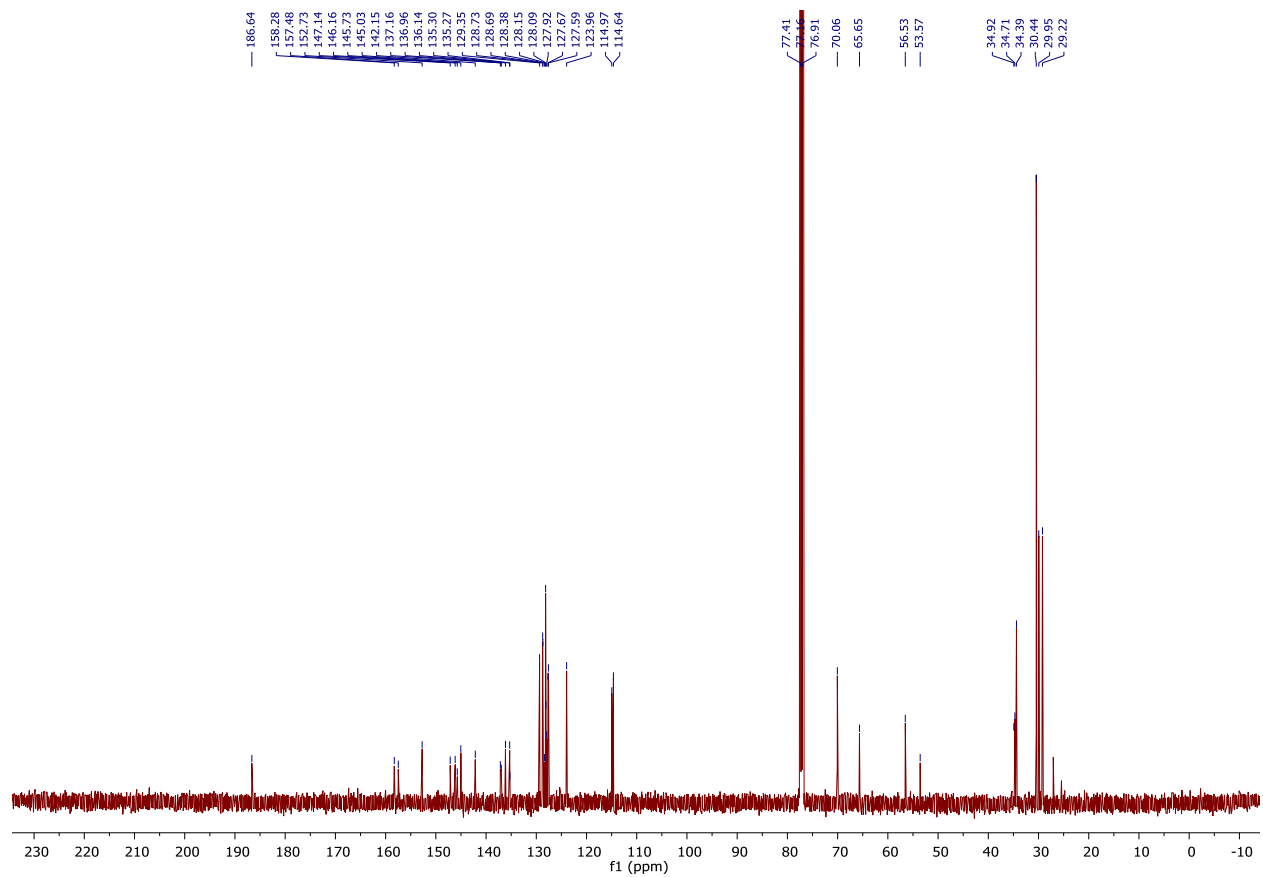
HRMS (ESI) m/z calculated for $\text{C}_{46}\text{H}_{55}\text{O}_6^+$ ($[\text{M}+\text{H}]^+$) 703.3993, found 703.3985.

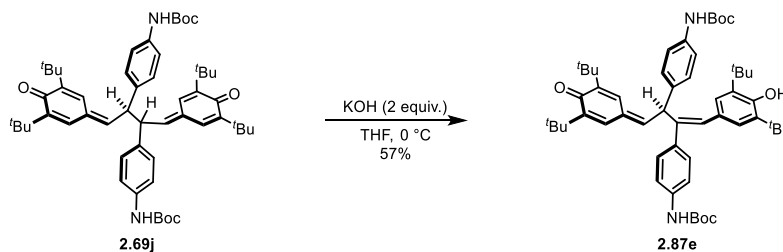


^{13}C NMR, 176 MHz, Chloroform-*d*, Tautomer **2.87c**



^{13}C NMR, 176 MHz, Chloroform-*d*, Tautomer **2.87d**



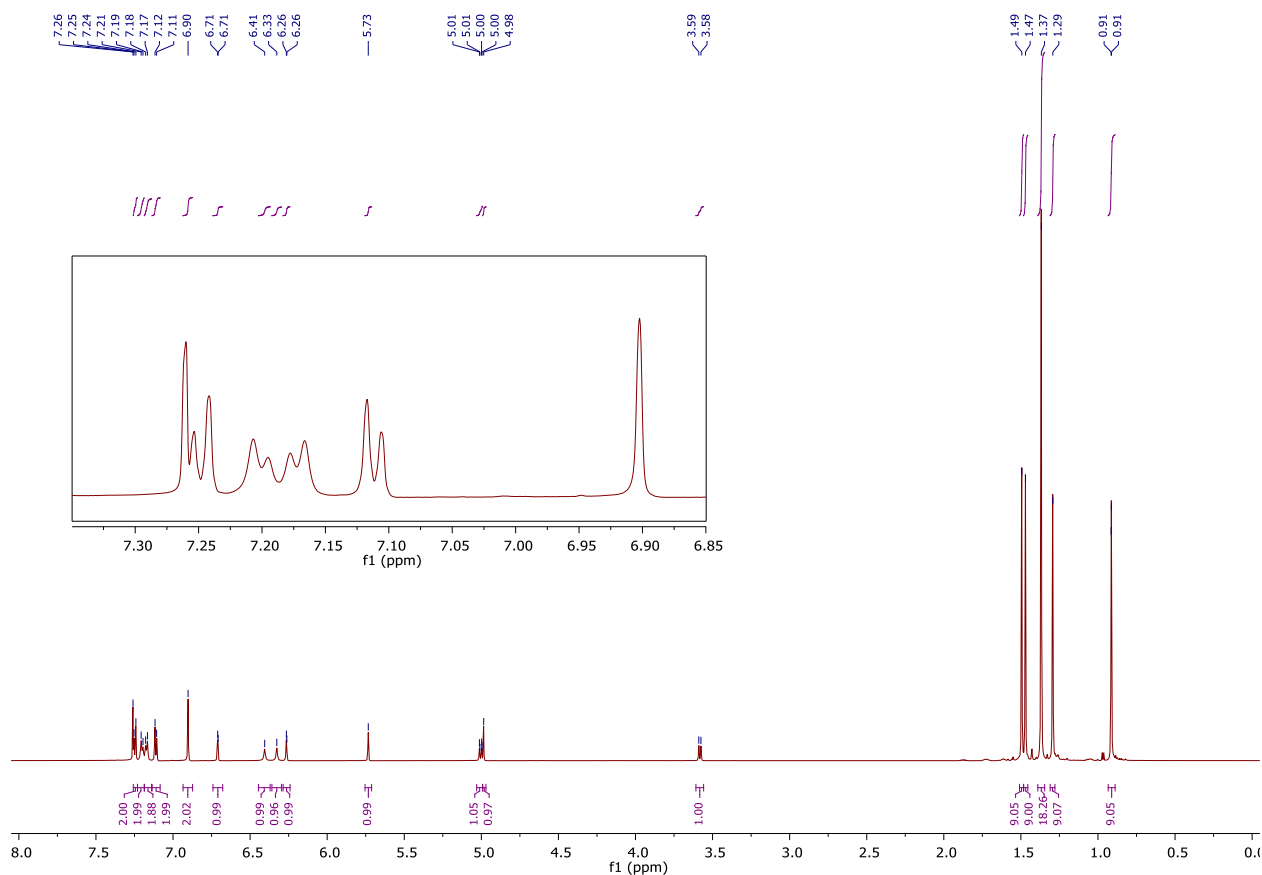


(2.87e) tert-butyl (S,Z)-4-(3-(4-((tert-butoxycarbonyl)amino)phenyl)-4-(3,5-di-tert-butyl-4-hydroxyphenyl)-1-(3,5-di-tert-butyl-4-oxocyclohexa-2,5-dien-1-ylidene)but-3-en-2-yl)phenylcarbamate

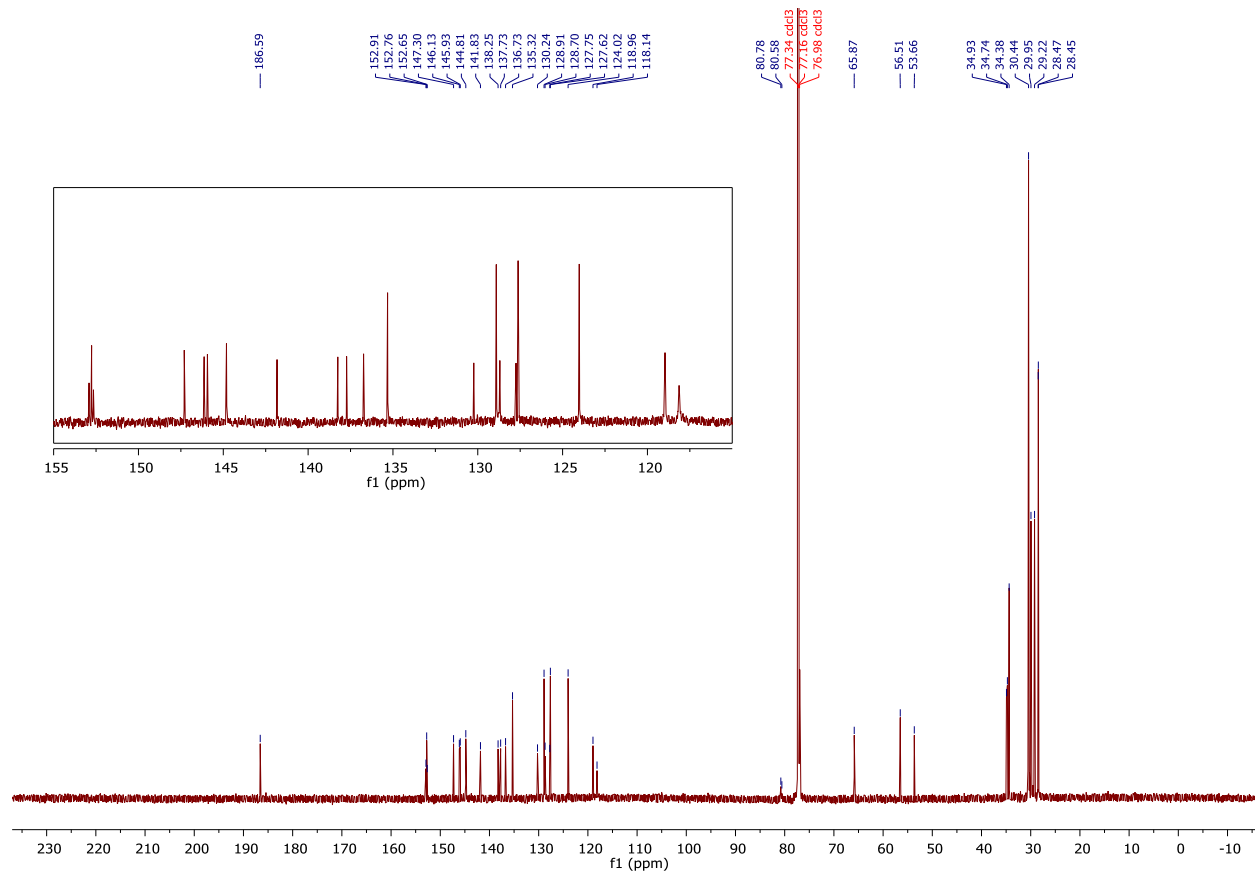
Dimer **2.69j** (1.18 mmol, 1.00 g) was subjected to the tautomerization conditions using KOH (133 mg, 2 equiv.) as the base. The crude product was purified by column chromatography (20–100% DCM/Hexanes) to afford **2.87e** (570 mg, 57% yield).

^1H NMR (700 MHz, Chloroform-*d*) δ 7.25 (d, $J = 8.4$ Hz, 2H), 7.20 (d, $J = 8.4$ Hz, 2H), 7.17 (d, $J = 8.2$ Hz, 2H), 7.11 (d, $J = 8.4$ Hz, 2H), 6.90 (s, 2H), 6.71 (d, $J = 2.7$ Hz, 1H), 6.41 (s, 1H), 6.33 (s, 1H), 6.26 (d, $J = 2.7$ Hz, 1H), 5.73 (d, $J = 1.9$ Hz, 1H), 5.00 (dd, $J = 9.6, 2.0$ Hz, 1H), 4.98 (s, 1H), 3.58 (d, $J = 9.7$ Hz, 1H), 1.49 (s, 9H), 1.47 (s, 9H), 1.37 (s, 18H), 1.29 (s, 9H), 0.91 (s, 9H).

^{13}C NMR (176 MHz, Chloroform-*d*) δ 186.59, 152.91, 152.76, 152.65, 147.30, 146.13, 145.93, 144.81, 141.83, 138.25, 137.73, 136.73, 135.32, 130.24, 128.91, 128.70, 127.75, 127.62, 124.02, 118.96, 118.14, 80.78, 80.58, 65.87, 56.51, 53.66, 34.93, 34.74, 34.38, 30.44, 29.95, 29.22, 28.47, 28.45.

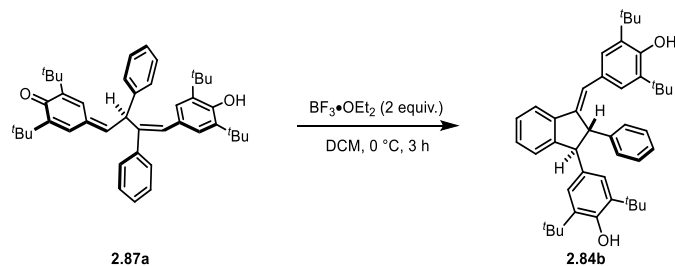


^{13}C NMR, 176 MHz, Chloroform-*d*, Tautomer **2.87e**



Cyclization of MQM dimer to quadrangularin A core:

The starting material was dried down into a flame-dried round bottom flask charged with stir bar. The atmosphere was evacuated and replaced with N₂, and the starting material was dissolved in CH₂Cl₂ (0.01 M reaction concentration). The solution was cooled to the reaction temperature, and BF₃•OEt₂ (2 equiv.) was added dropwise. The reaction was allowed to stir for 3 hours, at which point it was raised from the ice bath and quenched via the addition of saturated NaHCO₃. Once the reaction had thawed, it was poured into a separatory funnel, and the layers were separated. The aqueous layer was extracted with additional portions of CH₂Cl₂, and the combined organic layers were washed with brine, dried over magnesium sulfate, and concentrated under reduced pressure. The crude product was purified by column chromatography.



(2.84b) 2,6-di-tert-butyl-4-((1*S*,2*S*)-3-((*E*)-3,5-di-tert-butyl-4-hydroxybenzylidene)-2-phenyl-2,3-dihydro-1*H*-inden-1-yl)phenol

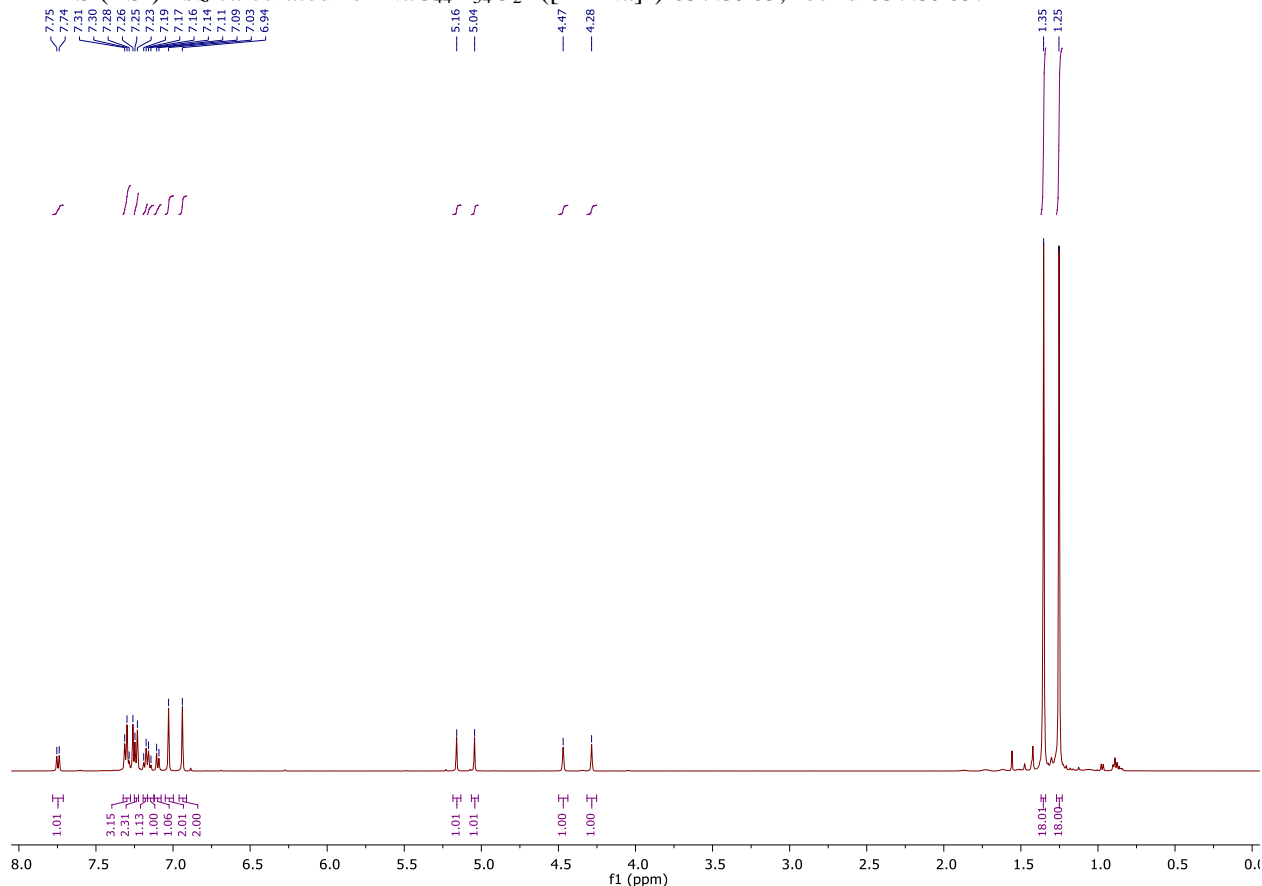
Compound **2.87a** (330 mg, 0.537 mmol) was subjected to the standard cyclization conditions at 0 °C with $\text{BF}_3 \cdot \text{OEt}_2$ (0.132 mL, 1.07 mmol), and the crude product was purified by column chromatography (3%, 6%, 9%, 12%, 17%, 26%, 37%, 51%, DCM/Hexanes, 2 CV per step) to afford compound **2.84b** (154 mg, 47% yield).

^1H NMR (500 MHz, Chloroform-*d*) δ 7.75 (d, $J = 7.7$ Hz, 1H), 7.31 (m, 3H), 7.24 (d, $J = 7.9$ Hz, 2H), 7.18 (d, $J = 7.9$ Hz, 1H), 7.15 (d, $J = 7.9$ Hz, 1H), 7.10 (d, $J = 7.5$ Hz, 1H), 7.03 (s, 2H), 6.94 (s, 2H), 5.16 (s, 1H), 5.04 (s, 1H), 4.47 (s, 1H), 4.28 (s, 1H), 1.35 (s, 18H), 1.25 (s, 18H).

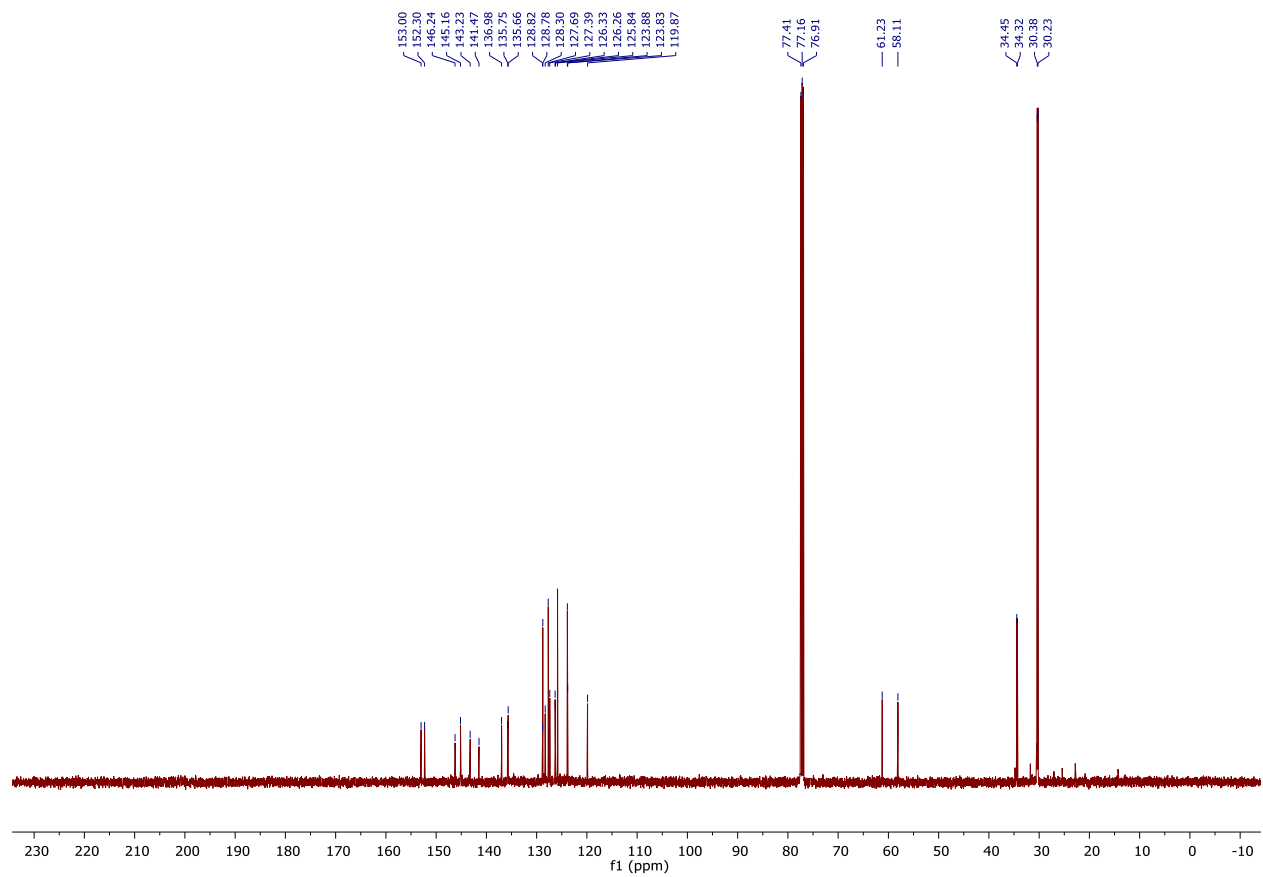
^{13}C NMR (126 MHz, Chloroform-*d*) δ 153.00, 152.30, 146.24, 145.16, 143.23, 141.47, 136.98, 135.75, 135.66, 128.82, 128.78, 128.30, 127.69, 127.39, 126.33, 126.26, 125.84, 123.88, 123.83, 119.87, 61.23, 58.11, 34.45, 34.32, 30.38, 30.23.

IR (Neat): 3616, 2953, 1470, 1311, 1235, 1137, 957, 767, 694 cm^{-1} ;

HRMS (ESI) m/z calculated for $\text{NaC}_{44}\text{H}_{54}\text{O}_2^+$ ($[\text{M}+\text{Na}]^+$) 637.3965, found 637.3965.



¹³C NMR, 176 MHz, Chloroform-*d*, Analog Core **2.84b**





(2.84a) 2,6-di-*tert*-butyl-4-((1*S*,2*S*)-3-((*E*)-3,5-di-*tert*-butyl-4-hydroxybenzylidene)-6-(methylthio)-2-(4-(methylthio)phenyl)-2,3-dihydro-1*H*-inden-1-yl)phenol

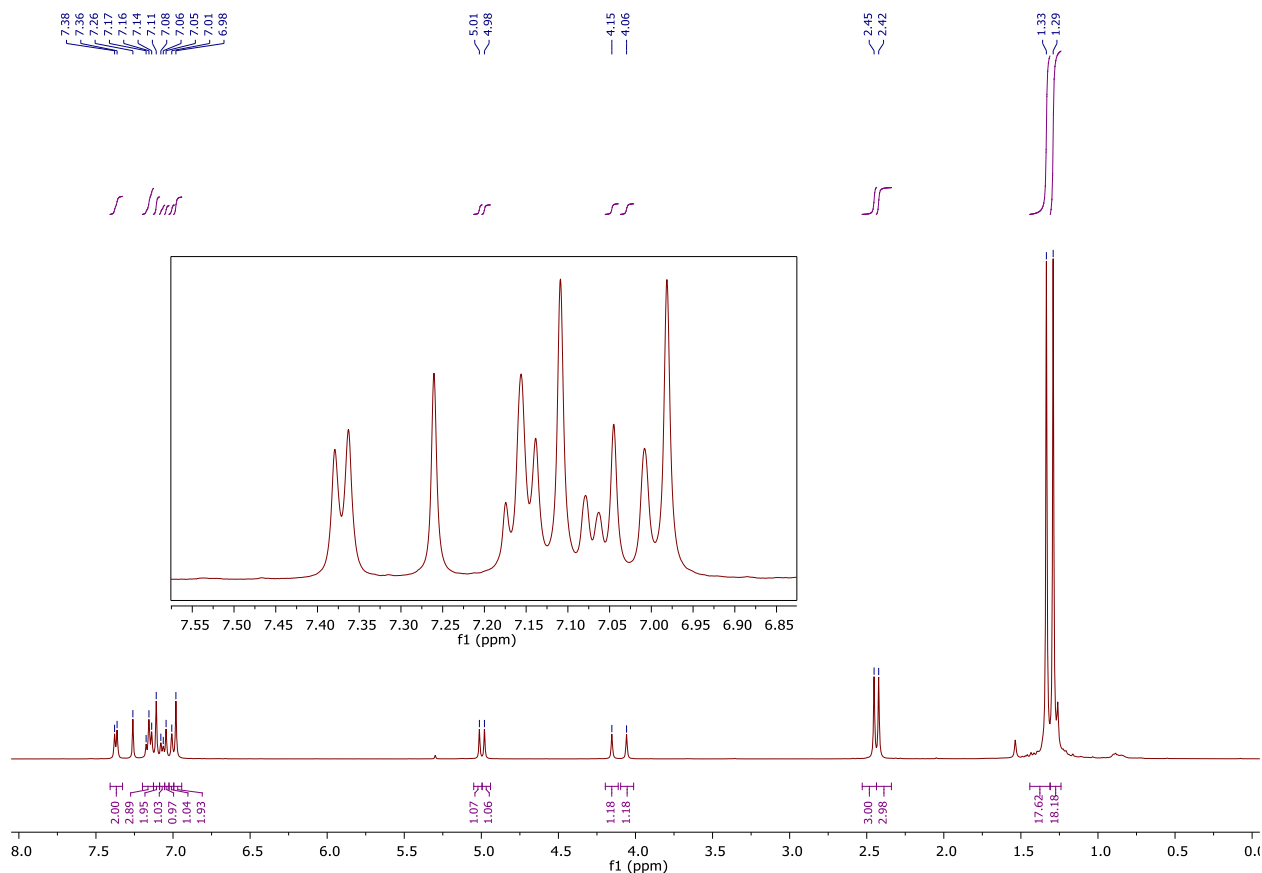
Compound **2.87b** (96 mg, 0.136 mmol) was subjected to the standard cyclization conditions at 0 °C with $\text{BF}_3 \cdot \text{OEt}_2$ (0.034 mL, 0.27 mmol), and the crude product was purified by column chromatography (10% to 50% DCM/Hexanes) to afford compound **2.84a** (59 mg, 62% yield).

^1H NMR (500 MHz, Chloroform-*d*) δ 7.37 (d, $J = 8.1$ Hz, 2H), 7.16 (m, 3H), 7.11 (s, 2H), 7.07 (d, $J = 7.9$ Hz, 1H), 7.05 (s, 1H), 7.01 (s, 1H), 6.98 (s, 2H), 5.01 (s, 1H), 4.98 (s, 1H), 4.15 (s, 1H), 4.06 (s, 1H), 2.45 (s, 3H), 2.42 (s, 3H), 1.33 (s, 18H), 1.29 (s, 18H).

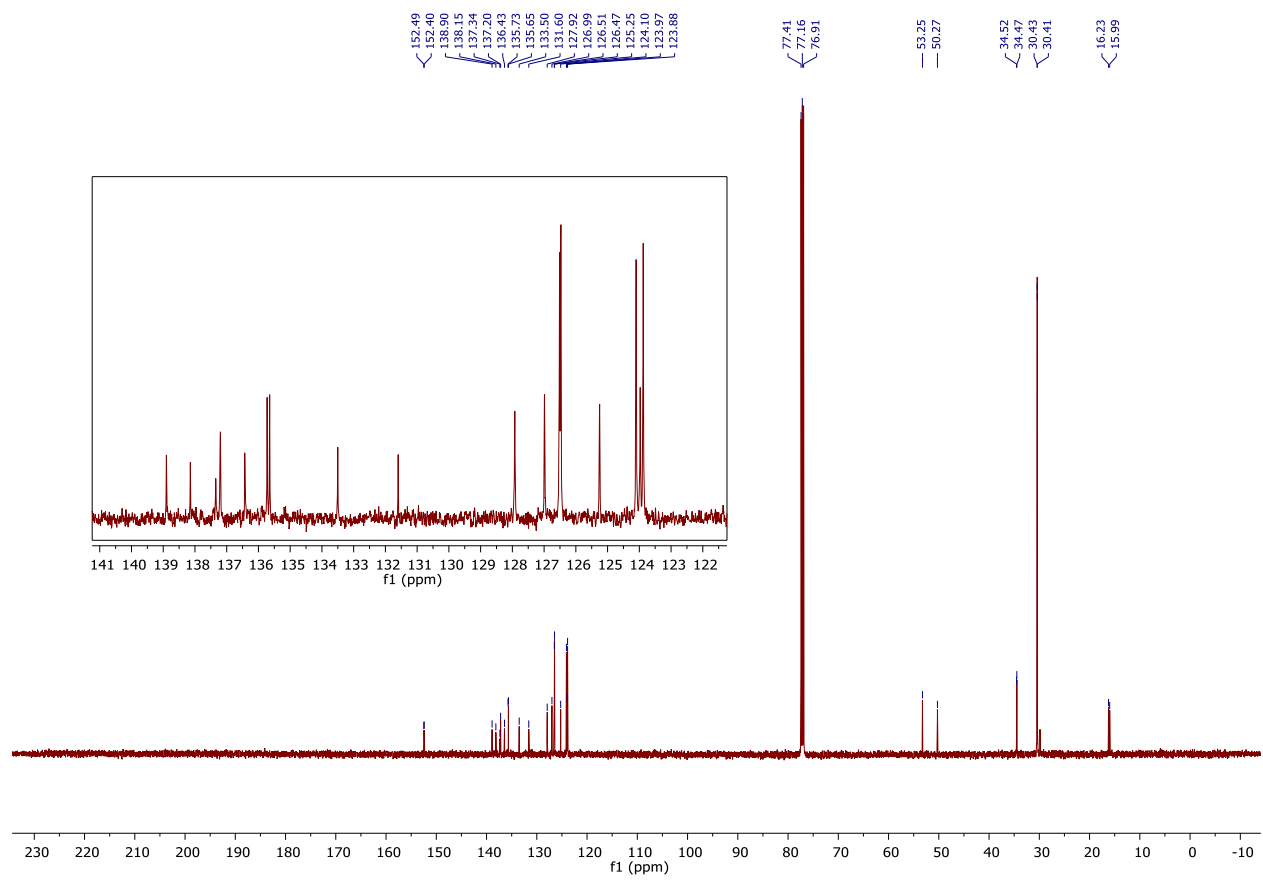
^{13}C NMR (126 MHz, Chloroform-*d*) δ 152.49, 152.40, 138.90, 138.15, 137.34, 137.20, 136.43, 135.73, 135.65, 133.50, 131.60, 127.92, 126.99, 126.51, 126.47, 125.25, 124.10, 123.97, 123.88, 53.25, 50.27, 34.52, 34.47, 30.43, 30.41, 16.23, 15.99.

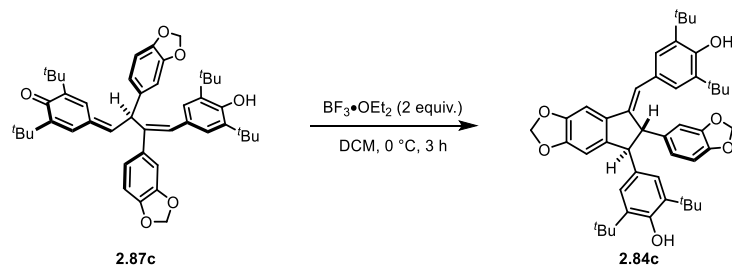
IR (Neat): 3614, 2957, 2920, 1597, 1434, 1240, 1150, 1119, 883, 821, 790, 765 cm^{-1} ;

HRMS (ESI) m/z calculated for $\text{C}_{46}\text{H}_{58}\text{O}_2\text{S}_2^+$ ($[\text{M}]^+$) 706.3873, found 706.3872.



^{13}C NMR, 126 MHz, Chloroform-*d*, Analog Core **2.84a**





(2.84c) 4-((1*S*,2*S*)-6-(benzyloxy)-2-(4-(benzyloxy)phenyl)-3-((*E*)-3,5-di-*tert*-butyl-4-hydroxybenzylidene)-2,3-dihydro-1*H*-inden-1-yl)-2,6-di-*tert*-butylphenol

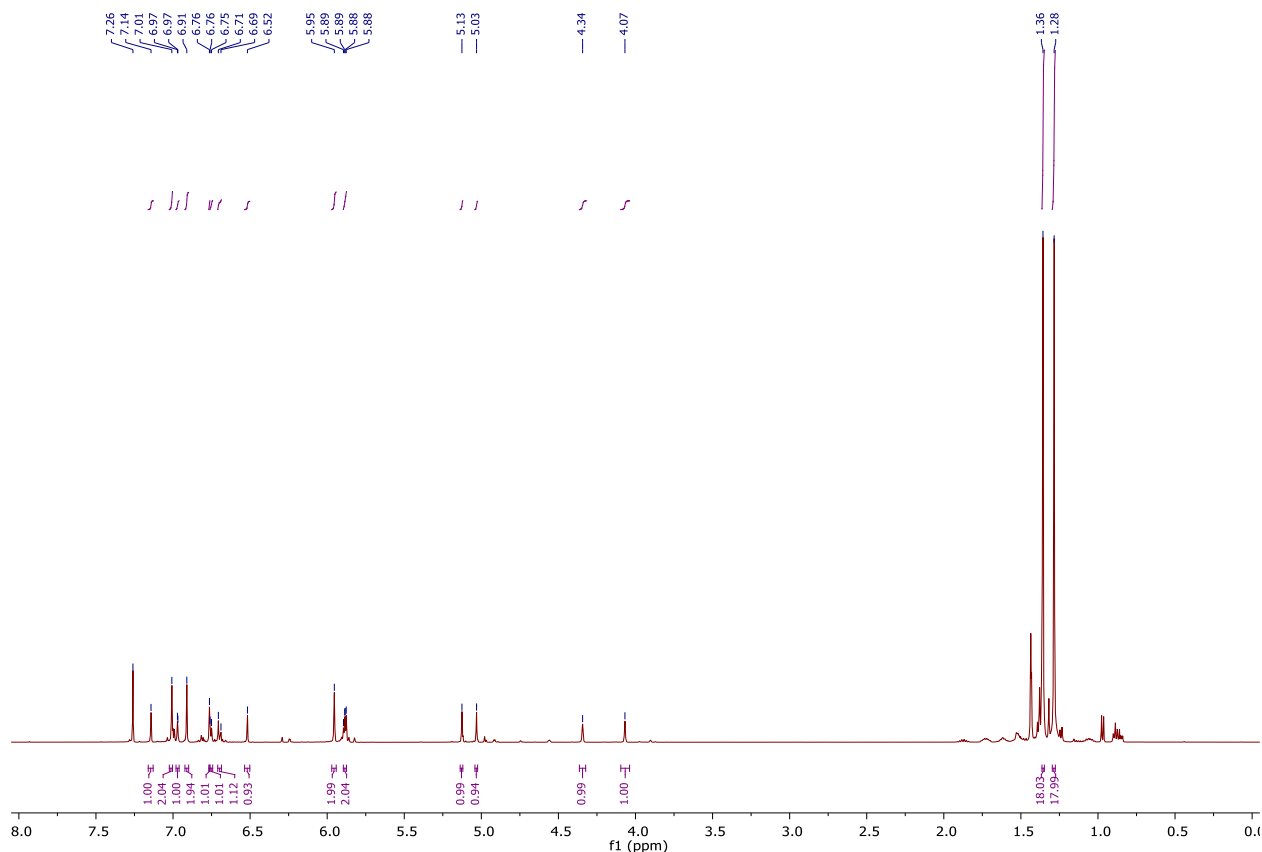
Compound **2.87c** (102 mg, 0.145 mmol) was subjected to the standard cyclization conditions at 0 °C with $\text{BF}_3 \bullet \text{OEt}_2$ (0.036 mL, 0.29 mmol), and the crude product was purified by column chromatography (10% to 50% DCM/Hexanes) to afford compound **2.84c** (65 mg, 64% yield).

^1H NMR (500 MHz, Chloroform-*d*) δ 7.14 (s, 1H), 7.01 (s, 2H), 6.97 (d, $J = 1.4$ Hz, 1H), 6.91 (s, 2H), 6.76 (s, 1H), 6.75 (d, $J = 4.6$ Hz, 1H), 6.70 (d, $J = 8.4$ Hz, 1H), 6.52 (s, 1H), 5.95 (s, 2H), 5.88 (dd, $J = 5.2, 3.7$ Hz, 2H), 5.13 (s, 1H), 5.03 (s, 1H), 4.34 (s, 1H), 4.07 (s, 1H), 1.36 (s, 18H), 1.28 (s, 18H).

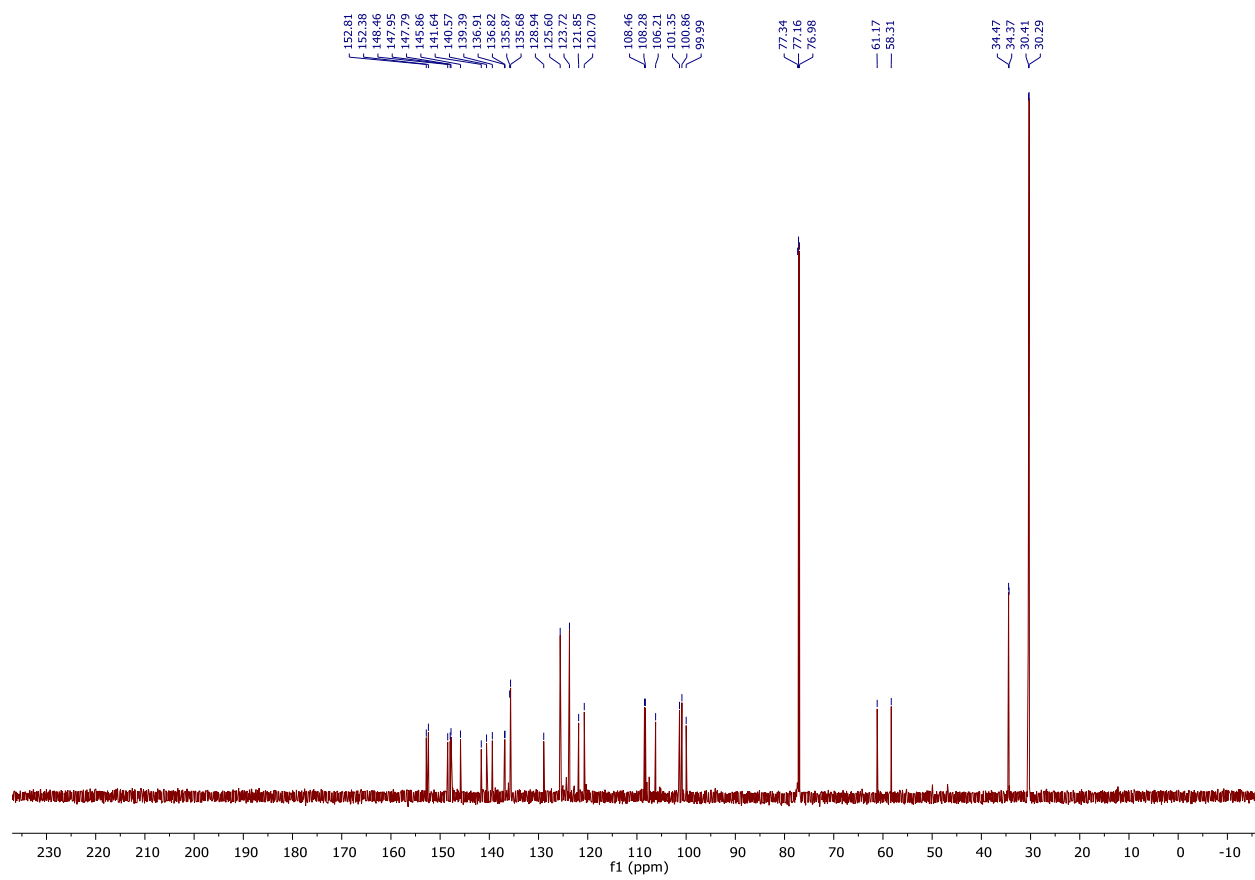
^{13}C NMR (176 MHz, Chloroform-*d*) δ 152.81, 152.38, 148.46, 147.95, 147.79, 145.86, 141.64, 140.57, 139.39, 136.91, 136.82, 135.87, 135.68, 128.94, 125.60, 123.72, 121.85, 120.70, 108.46, 108.28, 106.21, 101.35, 100.86, 99.99, 61.17, 58.31, 34.47, 34.37, 30.41, 30.29.

IR (Neat): 3634, 2957, 2912, 1476, 1431, 1231, 1150, 1035, 936, 737 cm^{-1} ;

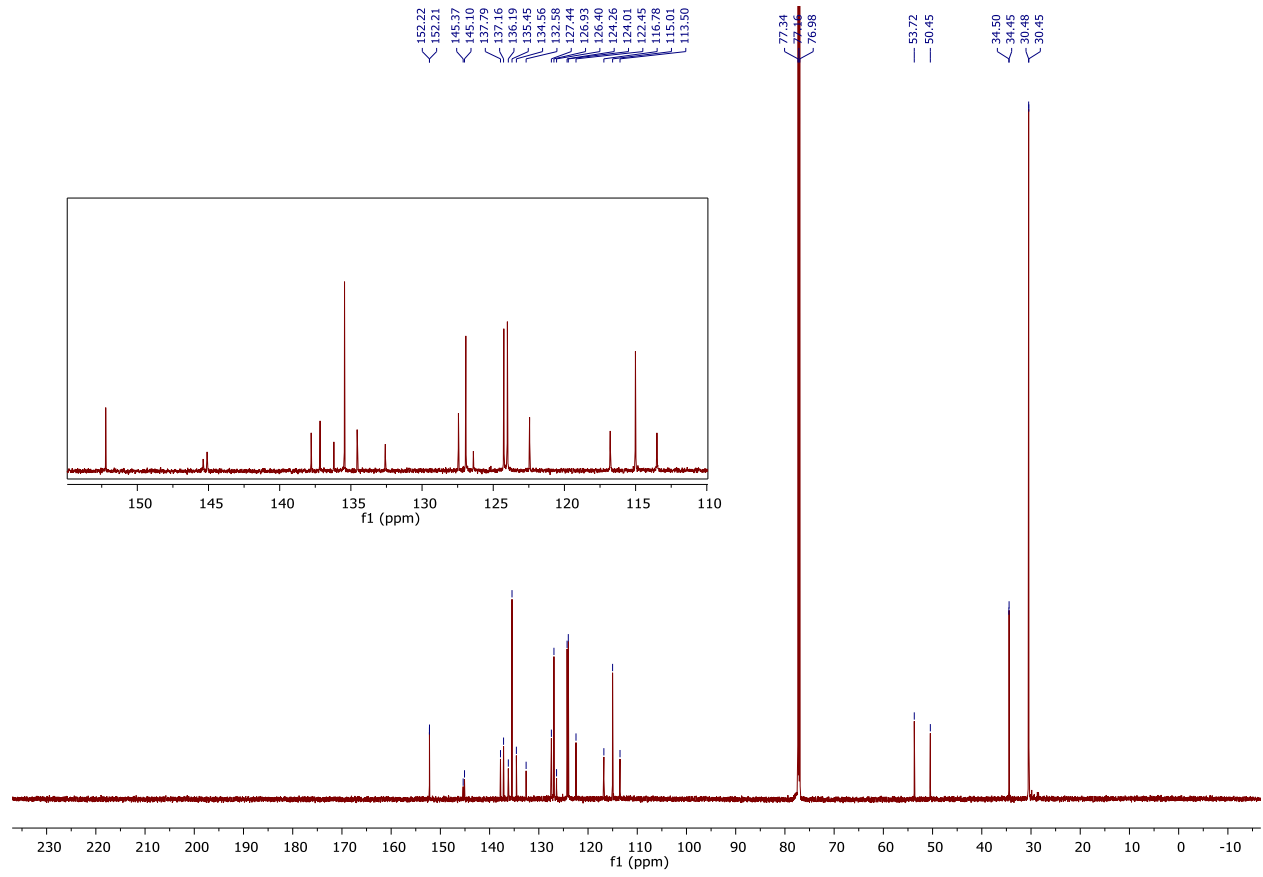
HRMS (ESI) m/z calculated for $\text{C}_{46}\text{H}_{54}\text{O}_6^+$ ($[\text{M}]^+$) 702.3915, found 702.3900.



¹³C NMR, 176 MHz, Chloroform-*d*, Analog Core **2.84c**



¹³C NMR, 176 MHz, Chloroform-*d*, Analog Core **2.84d**





(2.88) 4-((1*S*,2*S*)-6-(benzyloxy)-2-(4-(benzyloxy)phenyl)-3-((*E*)-3,5-di-*tert*-butyl-4-hydroxybenzylidene)-2,3-dihydro-1*H*-inden-1-yl)-2,6-di-*tert*-butylphenol

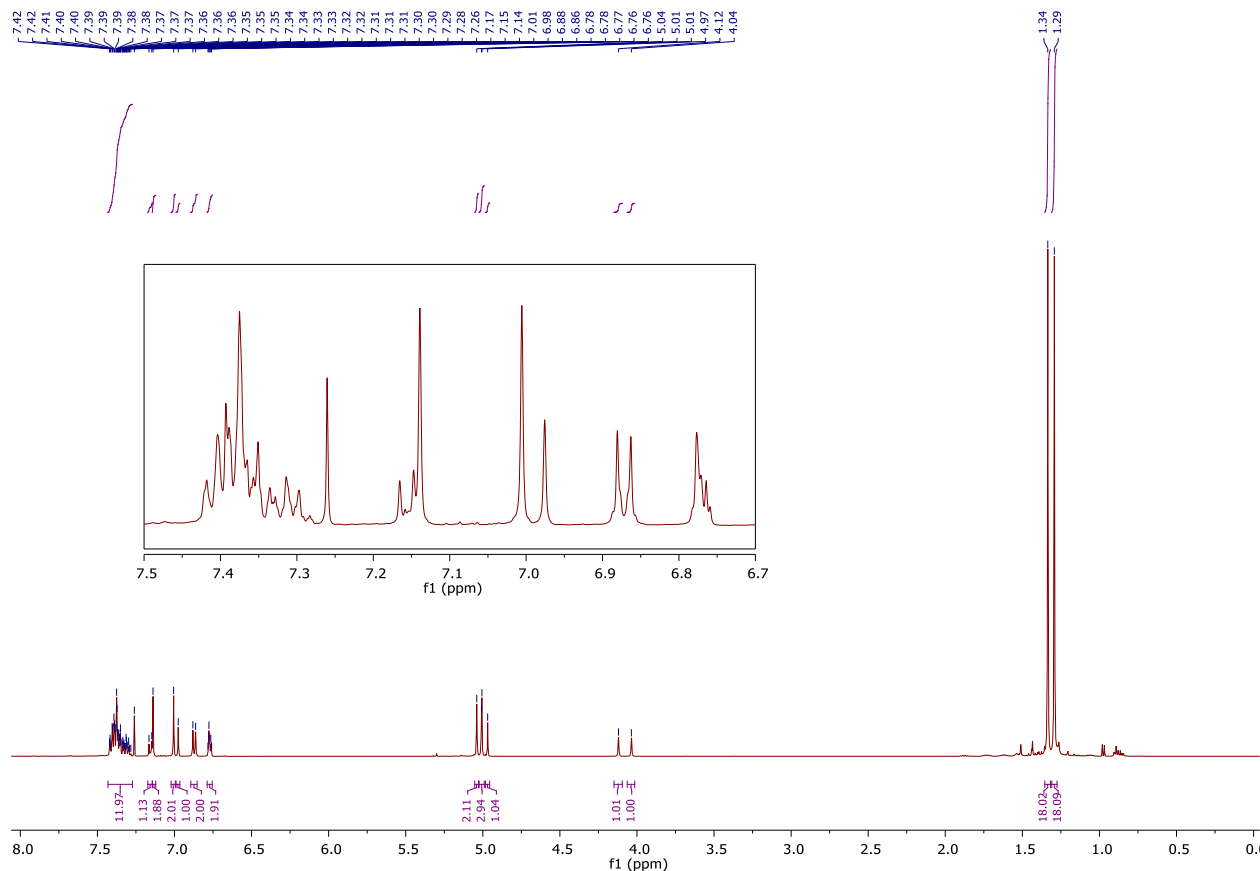
Compound **2.87d** (120 mg, 0.145 mmol) was subjected to the standard cyclization conditions at 0 °C with $\text{BF}_3 \cdot \text{OEt}_2$ (0.036 mL, 0.29 mmol), and the crude product was purified by column chromatography (10% to 50% DCM/Hexanes) to afford compound **2.88** (100 mg, 83% yield).

^1H NMR (500 MHz, Chloroform-*d*) δ 7.43 – 7.27 (m, 12H), 7.16 (d, $J = 9.1$ Hz, 1H), 7.14 (s, 2H), 7.01 (s, 2H), 6.98 (s, 1H), 6.87 (d, $J = 8.9$ Hz, 2H), 6.77 (m, 2H), 5.04 (s, 2H), 5.01 (s, 2H), 5.01 (s, 1H), 4.97 (s, 1H), 4.12 (s, 1H), 4.04 (s, 1H), 1.34 (s, 18H), 1.29 (s, 18H).

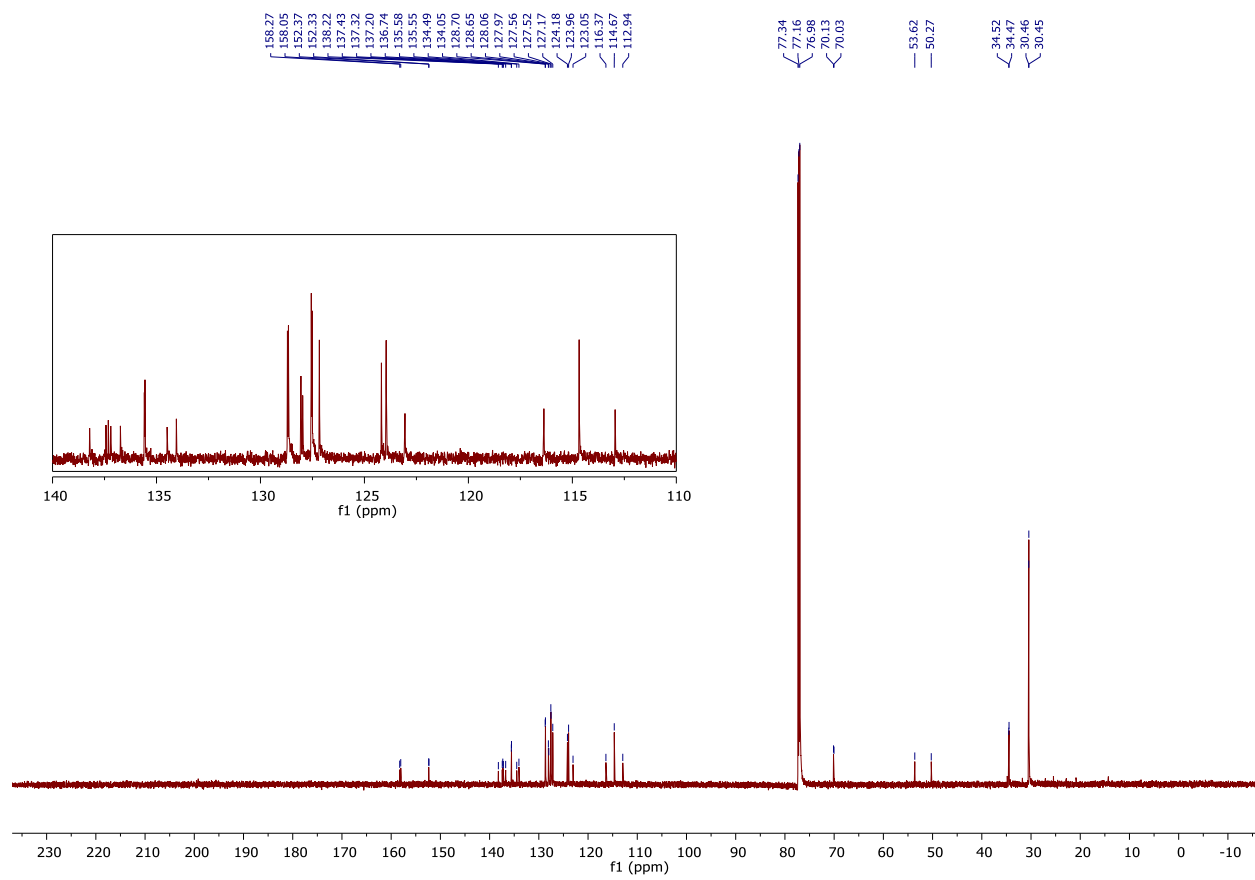
^{13}C NMR (176 MHz, Chloroform-*d*) δ 158.27, 158.05, 152.37, 152.33, 138.22, 137.43, 137.32, 137.20, 136.74, 135.58, 135.55, 134.49, 134.05, 128.70, 128.65, 128.06, 127.97, 127.56, 127.52, 127.17, 124.18, 123.96, 123.05, 116.37, 114.67, 112.94, 70.13, 70.03, 53.62, 50.27, 34.52, 34.47, 30.46, 30.45.

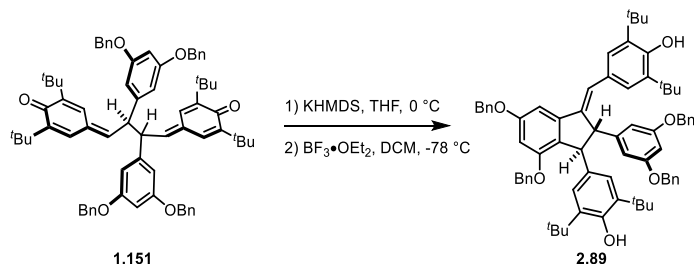
IR (Neat): 3634, 3589, 2957, 2870, 1647, 1594, 1507, 1434, 1237, 1158, 1136, 1029, 734, 697 cm^{-1} ;

HRMS (ESI) m/z calculated for $\text{C}_{58}\text{H}_{66}\text{O}_4^+$ ($[\text{M}]^+$) 826.4956, found 826.4952.



^{13}C NMR, 176 MHz, Chloroform-*d*, Analog Core **2.88**

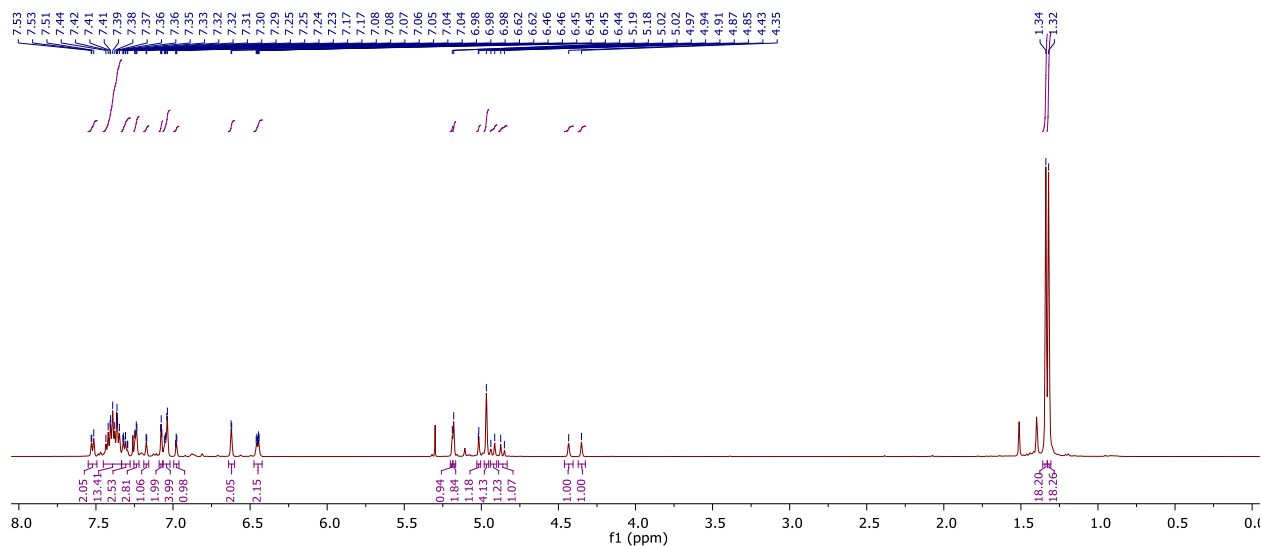




(2.89) 4-((1S,2S)-5,7-bis(benzyloxy)-2-(3,5-bis(benzyloxy)phenyl)-3-((E)-3,5-di-tert-butyl-4-hydroxybenzylidene)-2,3-dihydro-1H-inden-1-yl)-2,6-di-tert-butylphenol

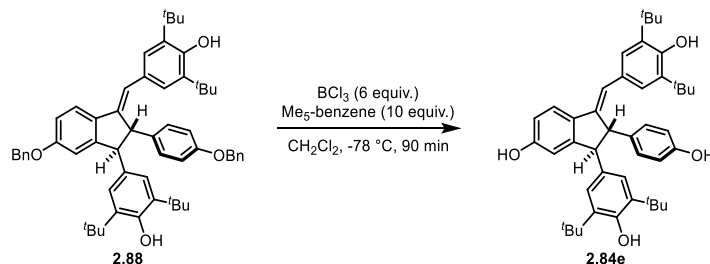
QMD **1.151** (500 mg, 0.481 mmol) was subjected to the standard tautomerization conditions, and the crude product was subjected to the cyclization conditions at $-78\text{ }^{\circ}\text{C}$ with $\text{BF}_3 \cdot \text{OEt}_2$ (128 μL , 0.962 mmol, 2.0 equiv.). The product was purified by column chromatography (0% to 20% EtOAc in Hexanes) to afford compound **2.89** (452 mg, 90% yield). The ^1H NMR spectrum was consistent with the prior report for this compound.⁴⁵

^1H NMR (500 MHz, Chloroform-*d*) δ 7.55 – 7.49 (m, 2H), 7.45 – 7.33 (m, 13H), 7.33 – 7.28 (m, 3H), 7.24 (t, $J = 2.8$ Hz, 3H), 7.19 – 7.16 (m, 1H), 7.08 (d, $J = 1.8$ Hz, 2H), 7.05 (dd, $J = 7.2, 2.7$ Hz, 4H), 6.98 (t, $J = 1.9$ Hz, 1H), 6.62 (d, $J = 2.1$ Hz, 2H), 6.45 (dt, $J = 5.4, 2.0$ Hz, 2H), 5.19 (s, 1H), 5.18 (s, 2H), 5.02 (d, $J = 1.6$ Hz, 1H), 4.97 (s, 4H), 4.93 (d, $J = 12.4$ Hz, 1H), 4.86 (d, $J = 12.0$ Hz, 1H), 4.43 (s, 1H), 4.35 (s, 1H), 1.34 (s, 18H), 1.32 (s, 18H).



Lewis-acid mediated benzyl deprotection of compound S21:

The starting material (1 equiv.) was dried down in a flame-dried round bottom flask charged with a stir bar. Pentamethylbenzene (10-20 equiv.) was added in a single portion, and the solids were dissolved in dichloromethane (0.01 M reaction concentration) under inert atmosphere. The reaction mixture was cooled to -78 °C, at which point BCl₃ (6-12 equiv., 1.0 M in CH₂Cl₂) was added via syringe, turning reaction mixture deep purple. The reaction was stirred at this temperature for 1.5 h, at which point it was lifted from dry ice bath and quenched with saturated NaHCO₃. The reaction was stirred vigorously while the ice thawed and until the reaction mixture stopped changing colors. Once the quench was complete (at this point the reaction was a pale-yellow color), the reaction was poured into a separatory funnel containing DI H₂O. The layers were separated, and the aqueous layer was extracted with additional CH₂Cl₂. The combined organic layers were washed with brine, dried over MgSO₄ and concentrated under reduced pressure. The crude material was purified by flash chromatography using 0 to 15% Acetone in DCM gradient.



(2.84e) (2S,3S)-1-((E)-3,5-di-tert-butyl-4-hydroxybenzylidene)-3-(3,5-di-tert-butyl-4-hydroxyphenyl)-2-(4-hydroxyphenyl)-2,3-dihydro-1H-inden-5-ol

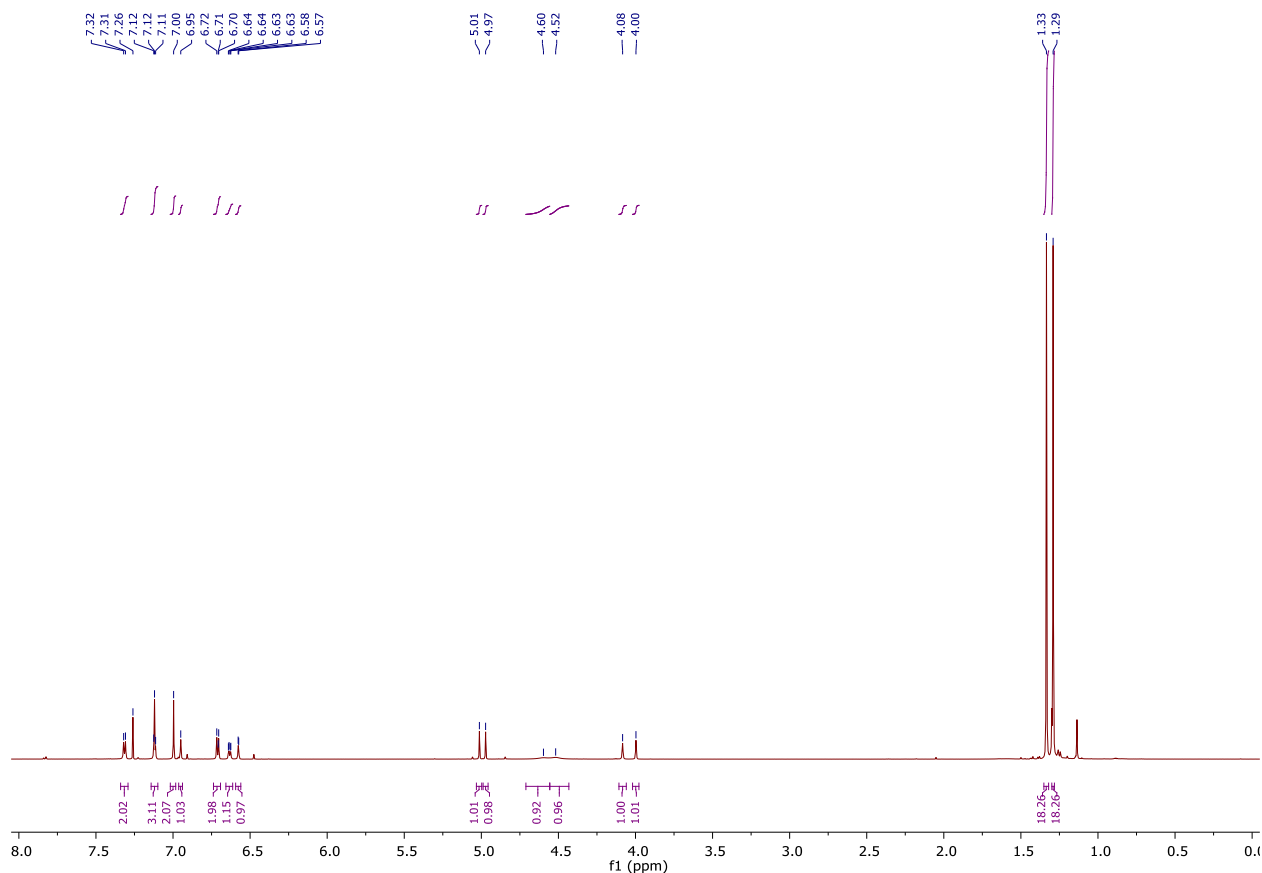
Compound **2.88** (73 mg, 0.088 mmol) was subjected to the standard deprotection conditions with pentamethylbenzene (134 mg, 0.88 mmol) and BCl_3 (0.53 mL, 0.53 mmol) to afford compound **2.84e** (49 mg, 86% yield).

^1H NMR (700 MHz, Chloroform-*d*) δ 7.31 (d, $J = 8.3$ Hz, 2H), 7.12 (s, 2H), 7.12 (d, $J = 8.1$ Hz, 1H), 7.00 (s, 2H), 6.95 (s, 1H), 6.71 (d, $J = 8.7$ Hz, 2H), 6.63 (dd, $J = 8.1, 2.8$ Hz, 1H), 6.58 (d, $J = 2.5$ Hz, 1H), 5.01 (s, 1H), 4.97 (s, 1H), 4.60 (s, 1H), 4.52 (s, 1H), 4.08 (s, 1H), 4.00 (s, 1H), 1.33 (s, 18H), 1.29 (s, 18H).

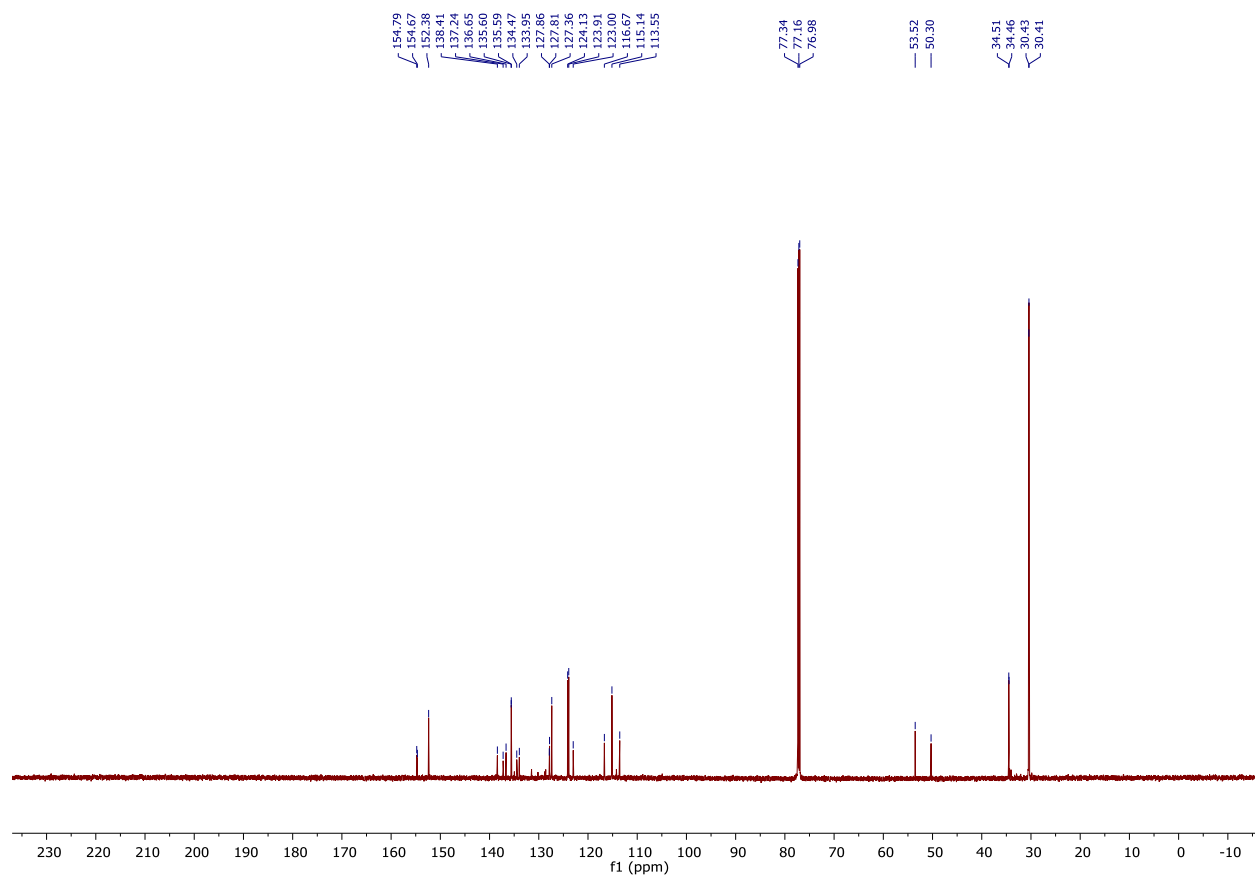
^{13}C NMR (176 MHz, Chloroform-*d*) δ 154.79, 154.67, 152.38, 138.41, 137.24, 136.65, 135.60, 135.59, 134.47, 133.95, 127.86, 127.81, 127.36, 124.13, 123.91, 123.00, 116.67, 115.14, 113.55, 53.52, 50.30, 34.51, 34.46, 30.43, 30.41.

IR (Neat): 3628, 2959, 1656, 1595, 1558, 1507, 1459, 1361, 1244, 1197, 1024, 878, 836, 668 cm^{-1} ;

HRMS (ESI) m/z calculated for $\text{C}_{44}\text{H}_{55}\text{O}_4^+$ ($[\text{M}+\text{H}]^+$) 647.4021, found 647.4029.



¹³C NMR, 176 MHz, Chloroform-*d*, Analog Core **2.84e**



Analysis of Radical-Trapping Antioxidant Activity:

Kinetic Data

General Procedure for Inhibited Autoxidations

The inhibited autoxidations were carried out following our reported method.¹¹² All autoxidations of 1-hexadecene (2.9 M) and PBD-BODIPY (10 μ M) were initiated by AIBN (6 mM) in chlorobenzene at 37 °C. A 3.5-mL quartz cuvette was charged with PhCl (0.44 mL), 1-hexadecene (2.00 mL). The cuvette was preheated to 37 °C in a thermostatted sample holder of a UV-vis spectrophotometer and allowed to equilibrate for approximately 15 min. To the cuvette was added PBD-BODIPY (12.5 μ L of a 2.00 mM stock solution in 1,2,4-trichlorobenzene) and AIBN (50 μ L of a 300 mM stock solution in chlorobenzene). The solution was thoroughly mixed prior to monitoring the uninhibited co-autoxidation via the disappearance of the PBD-BODIPY probe at 588 nm for 10 min to ensure the reaction was proceeding at a constant rate. Finally, the antioxidant under investigation was added (5.0 μ L of a 2.5 mM solution in chlorobenzene), the solution was mixed thoroughly, and the absorbance readings were resumed. The resulting Abs vs time data were processed as previously reported.¹¹² The rate of initiation ($R_i = 1.3 \times 10^{-9} \text{ Ms}^{-1}$) and second order rate constant for propagation for the dye ($k_{\text{PBD-BODIPY}} = 3792 \text{ M}^{-1}\text{s}^{-1}$) necessary to compute stoichiometric data (n) and inhibition rate constants (k_{inh}) were determined using PMC as a standard, which has an established stoichiometry of 2.^{121,122} An analogous procedure was conducted at the elevated temperatures (70 °C and 100 °C) using the corresponding initiators.

Table 2.4. Comparison of inhibition rate constants (k_{inh}) and stoichiometry (n) for substituted QMDs, stilbenoid phenols, and quadrangularin A analogs during inhibited co-oxidations of 1-hexadecene (2.9 M) and PBD-BODIPY (10 μ M) initiated by AIBN (6 mM) at 37 °C, *t*BuOO*t*Bu (87 mM) at 70 °C, and dicumyl peroxide (1 mM) at 100 °C.

QMDs	37 °C		70 °C		100 °C	
	k_{inh} ($10^5 \text{ M}^{-1}\text{s}^{-1}$)	n	k_{inh} ($10^5 \text{ M}^{-1}\text{s}^{-1}$)	n	k_{inh} ($10^5 \text{ M}^{-1}\text{s}^{-1}$)	n
2.69f	48 ± 9	1.8 ± 0.1	59 ± 10	1.6 ± 0.1	4.3 ± 0.3	0.44 ± 0.01
2.69i	48 ± 8	1.7 ± 0.1	44 ± 2	1.6 ± 0.1	ND	ND
2.69h	46 ± 6	1.8 ± 0.1	59 ± 4	1.4 ± 0.1	5.1 ± 0.1	0.49 ± 0.01
2.69e	45 ± 3	1.8 ± 0.1	86 ± 6	1.7 ± 0.1	9.0 ± 0.9	0.52 ± 0.01
1.151	40 ± 8	2.0 ± 0.1	120 ± 10	1.9 ± 0.1	13 ± 0.9	0.61 ± 0.05
2.69m	41 ± 4	1.8 ± 0.1	110 ± 10	1.6 ± 0.1	ND	ND
2.69o	43 ± 9	1.8 ± 0.1	98 ± 10	1.6 ± 0.1	7.2 ± 0.9	0.50 ± 0.02
2.69l	45 ± 3	1.9 ± 0.1	62 ± 8	1.4 ± 0.1	ND	ND
2.69n	45 ± 6	1.3 ± 0.1	40 ± 10	1.2 ± 0.1	ND	ND
2.69k	42 ± 9	1.5 ± 0.1	47 ± 10	1.0 ± 0.1	ND	ND
Stilbenes	k_{inh} ($10^5 \text{ M}^{-1}\text{s}^{-1}$)	n	k_{inh} ($10^5 \text{ M}^{-1}\text{s}^{-1}$)	n	k_{inh} ($10^5 \text{ M}^{-1}\text{s}^{-1}$)	n
2.85e	2.1 ± 0.2	2.2 ± 0.1	6.2 ± 0.3	1.6 ± 0.1	2.9 ± 0.1	1.1 ± 0.1
2.85h	3.1 ± 0.2	2.1 ± 0.1	11 ± 1	1.9 ± 0.1	ND	ND
2.85g	1.7 ± 0.1	2.2 ± 0.1	5.9 ± 0.7	1.5 ± 0.1	2.8 ± 0.3	1.1 ± 0.1
2.85d	1.6 ± 0.1	2.0 ± 0.3	4.6 ± 0.4	1.5 ± 0.1	2.6 ± 0.2	1.0 ± 0.1
1.150	1.4 ± 0.1	2.3 ± 0.1	19 ± 5	1.7 ± 0.1	2.5 ± 0.1	1.3 ± 0.1
2.85l	1.1 ± 0.2	2.3 ± 0.3	3.7 ± 0.1	1.5 ± 0.1	ND	ND
2.85n	1.3 ± 0.1	2.3 ± 0.1	3.5 ± 0.4	1.6 ± 0.2	2.3 ± 0.2	1.2 ± 0.1
2.85k	1.0 ± 0.1	2.3 ± 0.3	3.6 ± 0.4	1.3 ± 0.1	ND	ND
2.85m	1.0 ± 0.1	2.3 ± 0.1	2.8 ± 0.3	1.6 ± 0.1	ND	ND
2.85j	1.0 ± 0.1	2.3 ± 0.1	2.7 ± 0.2	1.4 ± 0.1	ND	ND
Quad A analogs	k_{inh} ($10^5 \text{ M}^{-1}\text{s}^{-1}$)	n	k_{inh} ($10^5 \text{ M}^{-1}\text{s}^{-1}$)	n	k_{inh} ($10^5 \text{ M}^{-1}\text{s}^{-1}$)	n
2.84c	1.3 ± 0.1	4.1 ± 0.1	2.8 ± 0.3	4.2 ± 0.4	1.9 ± 0.2	3.6 ± 0.1
2.84e	2.6 ± 0.4	5.5 ± 0.5	16 ± 1	6.3 ± 0.4	ND	ND
2.84a	0.8 ± 0.1	3.8 ± 0.1	1.2 ± 0.1	3.5 ± 0.3	1.6 ± 0.1	2.0 ± 0.1
2.84b	1.0 ± 0.1	4.1 ± 0.3	2.2 ± 0.2	4.0 ± 0.3	1.7 ± 0.1	2.9 ± 0.1
2.89	1.1 ± 0.1	3.8 ± 0.3	2.7 ± 0.4	3.5 ± 0.4	1.9 ± 0.1	2.8 ± 0.1

Computational Data⁴⁴

Table 2.5. Summary of enthalpies (ΔH , ΔH^\ddagger), free energies (ΔG , ΔG^\ddagger), and corresponding computed second order rate constants (k) for the addition of methyl peroxy radical to or hydrogen atom transfer (HAT) from a truncated analog of **2.69e** in the gas phase at 37 °C.

<i>Mechanism</i>	<i>Position</i>	ΔH , (<i>kcal mol⁻¹</i>)	ΔG , (<i>kcal mol⁻¹</i>)	ΔH^\ddagger , (<i>kcal mol⁻¹</i>)	ΔG^\ddagger , (<i>kcal mol⁻¹</i>)	k^a (<i>M⁻¹s⁻¹</i>)
HAT	C _β -H	-15.7	-15.3	7.5	19.0	6
Addition	C _α	-31.5	-19.4	-1.7	10.8	4 × 10 ⁶

$$k = \frac{RT}{P} \cdot \frac{k_B T}{h} e^{\frac{-\Delta G^\ddagger}{RT}}$$

^a Computed using where T = 310.15 K.

Optimized Gaussian Structures and CBS-QB3¹¹⁵ or DFT Energies (Hartree)

Methyl peroxy radical

H₃COO•

CBS-QB3 Enthalpy = -189.954731 CBS-QB3 Free Energy = -189.985243

0 2

C	1.09605900	-0.18318300	0.00000000
H	1.87467700	0.57860700	-0.00001500
H	1.14885000	-0.80070400	0.89699800
H	1.14883700	-0.80072700	-0.89698300
O	-0.15733600	0.54388600	0.00000000
O	-1.18625300	-0.27864500	0.00000000

Methyl hydroperoxide

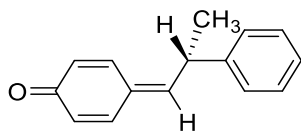
H₃COOH

CBS-QB3 Enthalpy = -190.589542 CBS-QB3 Free Energy = -190.620447

0 1

C	1.12961700	-0.22363900	0.02672600
H	1.97292100	0.47126800	0.02466400
H	1.14400500	-0.82582200	0.94203100
H	1.18954700	-0.87767200	-0.84877800
O	-0.01619300	0.60684200	-0.03138300
O	-1.16412600	-0.28550800	-0.09072600
H	-1.64161900	0.00339000	0.69859800

Truncated dimer

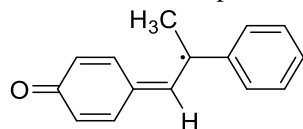


CBS-QB3 Enthalpy = -654.002976 CBS-QB3 Free Energy = -654.060994

0 1

C	-2.28497800	0.40886900	-1.38146900
C	-3.55270400	-0.03922500	-1.32815500
C	-4.13529300	-0.56092000	-0.07890600
C	-3.23865900	-0.55847700	1.09408900
C	-1.97179800	-0.10764000	1.02679200
H	-1.87418700	0.78842400	-2.31241000
H	-4.20081500	-0.03800300	-2.19697400
H	-3.66131800	-0.94226000	2.01572400
H	-1.34982200	-0.12439600	1.91411400
C	-1.40780200	0.40947300	-0.21456200
C	-0.14133100	0.88393400	-0.33638800
H	0.15649000	1.24391200	-1.31988600
O	-5.28793700	-0.97120500	-0.01361300
C	0.93072100	0.98559600	0.71399400
C	2.15417900	0.17948500	0.27509100
C	2.43091400	-1.05007100	0.87987500
C	3.00520900	0.62664700	-0.74224100
C	3.53098300	-1.81010100	0.48913600
H	1.77888600	-1.41666800	1.66618900
C	4.10408800	-0.13185400	-1.13742500
H	2.81702700	1.57620900	-1.23132600
C	4.37188000	-1.35298100	-0.52222200
H	3.72971200	-2.75869500	0.97523300
H	4.75316900	0.23292500	-1.92573000
H	5.22845900	-1.94234200	-0.82872500
C	1.25966000	2.46665200	1.00604200
H	1.57784500	2.99577200	0.10458500
H	0.38007500	2.98079300	1.40032500
H	2.06455800	2.53733300	1.74154700
H	0.57301500	0.54030300	1.64432900

C-H HAT radical product (truncated dimer)

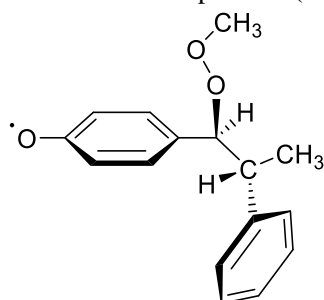


CBS-QB3 Enthalpy = -653.393246 CBS-QB3 Free Energy = -653.450284

0 2

C	1.52663700	-0.17878300	-0.06031300
C	2.26612700	1.04646900	-0.05163000
C	3.63125800	1.05609200	-0.05797800
C	4.41372500	-0.17389500	-0.07235200
C	3.64436100	-1.41088100	-0.11084300
C	2.28208000	-1.39605400	-0.11637600
H	1.74048500	1.98910300	-0.07297000
H	4.18983800	1.98508300	-0.06360700
H	4.20631700	-2.33724000	-0.13798000
H	1.73406700	-2.33262400	-0.14873300
C	0.09559100	-0.30235800	-0.05597100
H	-0.23773000	-1.30730800	-0.29735500
C	-0.90681300	0.59889900	0.18954500
C	-2.31412300	0.15072700	0.07608700
C	-3.30656300	1.03105100	-0.39201800
C	-2.71066100	-1.15268400	0.42751200
C	-4.62699500	0.61798900	-0.53178300
H	-3.03832200	2.04156900	-0.67632200
C	-4.03301100	-1.56037100	0.29989500
H	-1.98216700	-1.84097800	0.83868200
C	-4.99806500	-0.67954400	-0.18603900
H	-5.36792600	1.31206600	-0.91227100
H	-4.31363000	-2.56608300	0.59198900
H	-6.02906600	-0.99866600	-0.28584100
O	5.65560200	-0.16513300	-0.06495700
C	-0.67848700	2.04011600	0.58017800
H	0.15428900	2.12915000	1.27928800
H	-0.44885500	2.67090900	-0.28670000
H	-1.56247000	2.45544600	1.06398500

Addition radical product (truncated dimer)

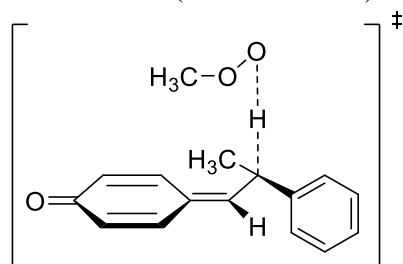


CBS-QB3 Enthalpy = -844.008115 CBS-QB3 Free Energy = -844.077218

0 2

C	1.68586100	-0.73545200	-0.94678200
C	2.03864400	-2.05690200	-1.04386900
C	1.65692100	-3.01393600	-0.01965400
C	0.89517400	-2.49267000	1.10074700
C	0.55651100	-1.16384100	1.17166500
H	1.98969400	-0.02773600	-1.70968300
H	2.61367700	-2.43783300	-1.87997300
H	0.61296200	-3.19839200	1.87314800
H	-0.01169700	-0.79243000	2.01765600
C	0.93550600	-0.26276200	0.15473600
O	1.97130500	-4.22160000	-0.09771200
O	1.58857600	2.04790200	-0.20443700
O	2.61138400	1.96629700	0.84596800
C	3.78537300	2.50236300	0.26894200
H	4.52260200	2.46789200	1.07383500
H	4.12979300	1.89716600	-0.57569200
H	3.63454500	3.53954000	-0.04808300
C	0.53023100	1.19587100	0.22243000
C	-0.67504300	1.54242800	-0.70021500
H	0.27533000	1.45818500	1.25591200
C	-1.89282900	0.70535500	-0.33377400
C	-2.36613100	-0.27753900	-1.20731200
C	-2.57489100	0.90298300	0.87332900
C	-3.48544600	-1.04383900	-0.88862100
H	-1.85000100	-0.44796500	-2.14632700
C	-3.69261200	0.13833500	1.19677100
H	-2.23685900	1.66374000	1.56895000
C	-4.15235100	-0.83895000	0.31597800
H	-3.83382500	-1.80139600	-1.58165800
H	-4.20687700	0.30800700	2.13631100
H	-5.02313000	-1.43390300	0.56681800
C	-0.98133300	3.05080000	-0.68657800
H	-1.22038800	3.40135600	0.32101200
H	-0.12719900	3.62451100	-1.04555200
H	-1.84128200	3.26025700	-1.32687200
H	-0.37898200	1.26472500	-1.71711200

C-H HAT TS (truncated dimer)



TS frequency: -1557.85 cm^{-1}

CBS-QB3 Enthalpy = -843.945793

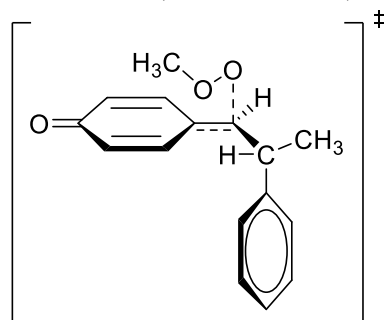
CBS-QB3 Free Energy =

-844.015840

0 2

C	2.25564500	-0.81459400	-1.31202000
C	3.59164400	-1.00867700	-1.27621500
C	4.34095000	-0.94392700	-0.01493100
C	3.53661400	-0.67398800	1.18686700
C	2.19873300	-0.47972300	1.13376700
H	1.72389600	-0.86184400	-2.25735800
H	1.65699900	-0.30200500	2.05014700
C	1.47427800	-0.52309700	-0.12151100
C	0.11527300	-0.32322000	-0.28906400
H	-0.22338500	-0.43776100	-1.31608500
O	5.55794900	-1.10835800	0.03910700
C	-0.95338200	0.11339200	0.59345900
H	-0.98829400	1.32936100	0.26126100
O	-0.99624200	2.63019100	-0.02807000
O	-0.04681900	2.76958300	-1.00881500
C	1.15191800	3.32650200	-0.45026100
H	1.58793500	2.64444600	0.28311000
H	1.82813900	3.45106200	-1.29669400
H	0.93127600	4.29146200	0.01023200
C	-0.78138600	0.19480600	2.11318300
H	-0.60022900	-0.79575900	2.54330900
H	0.03185600	0.86149900	2.40191900
H	-1.69744200	0.58282100	2.56083200
C	-2.32405400	-0.39026600	0.18827000
C	-3.44985900	0.43555600	0.30836200
C	-2.50351700	-1.70092100	-0.27188600
C	-4.71588900	-0.03568000	-0.02300300
H	-3.32776700	1.46076400	0.63874700
C	-3.77214400	-2.17439200	-0.60011000
H	-1.64639200	-2.36002900	-0.35910000
C	-4.88216500	-1.34322800	-0.47742900
H	-5.57354200	0.62163600	0.06581100
H	-3.89129700	-3.19433200	-0.94836100
H	-5.86931600	-1.70967500	-0.73514600
H	4.16560400	-1.21728600	-2.17165600
H	4.07690800	-0.64693800	2.12640000

Addition TS (truncated dimer)



TS frequency: -343.37 cm^{-1}

CBS-QB3 Enthalpy = -843.960367

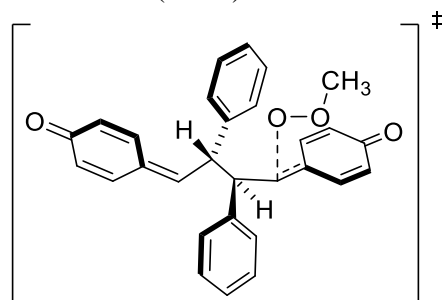
CBS-QB3 Free Energy =

-844.028986

0 2

C	0.96314500	-0.76857400	-0.75517100
C	1.83634300	-1.75262400	-1.08048400
C	2.84270300	-2.24399300	-0.12820700
C	2.84016200	-1.60372700	1.19251200
C	1.96163900	-0.62042300	1.49770000
H	0.22717400	-0.43962100	-1.47830900
H	1.82743000	-2.22622800	-2.05555400
H	3.57672000	-1.95858700	1.90398000
H	1.98057100	-0.15155200	2.47654100
C	0.97599200	-0.15653500	0.55037100
O	3.63885800	-3.13567600	-0.42560300
O	1.35833300	2.52336000	0.56707000
O	1.45649800	2.81734500	-0.75543500
C	2.78161800	2.51858200	-1.22898300
H	2.79283600	2.84364900	-2.26985300
H	3.51406800	3.07645700	-0.64293800
H	2.97189500	1.44691100	-1.15775400
C	0.11111800	0.87785900	0.91263100
C	-1.10441000	1.33029600	0.13304000
H	-0.76303100	1.59726800	-0.87257200
H	0.14440000	1.17923200	1.95527200
C	-1.73255800	2.58771200	0.76472600
H	-2.57633300	2.93237100	0.16356300
H	-2.10800700	2.36997500	1.76906300
H	-0.99437700	3.38714100	0.83252300
C	-2.14961600	0.22465600	-0.01552300
C	-2.75441500	-0.00316100	-1.25515700
C	-2.56682600	-0.54188100	1.07849300
C	-3.74636600	-0.97085000	-1.40242800
H	-2.44737600	0.58550300	-2.11425100
C	-3.55574100	-1.51108400	0.93481700
H	-2.11460600	-0.38633700	2.05227600
C	-4.14944200	-1.72962700	-0.30691000
H	-4.20104800	-1.13240100	-2.37351500
H	-3.86193900	-2.09794800	1.79366400
H	-4.91795600	-2.48583000	-0.41895600

Addition TS (dimer)



TS frequency: -398.43 cm^{-1}

DFT Enthalpy = -1420.677955

DFT Free Energy = -1420.774397

0 2

C	0.60031500	2.05824600	-0.77530600
C	0.75794700	2.68832800	-2.01173100
C	1.55020200	3.82910900	-2.13686000
C	2.19360300	4.35635900	-1.02139000
C	2.03749900	3.73949600	0.21969400
C	1.24612200	2.60228100	0.34237400
H	0.25358100	2.28765000	-2.88553500
H	1.65988900	4.30507700	-3.10482300
H	2.81086000	5.24239300	-1.11549500
H	2.53569300	4.14404000	1.09344200
H	1.12928000	2.13182200	1.31290800
C	-0.26601800	0.80745700	-0.65062800
H	-0.65354100	0.58365300	-1.64854100
C	0.58847600	-0.45477700	-0.21551700
H	0.70380600	-0.41268100	0.86323600
C	-0.09534900	-1.77858300	-0.56242100
C	-0.57209500	-2.61394400	0.45107800
C	-0.23990800	-2.19606200	-1.89276900
C	-1.18412900	-3.82841500	0.14669800
H	-0.48070200	-2.29802400	1.48299800
C	-0.85186000	-3.40854500	-2.19920000
H	0.12826900	-1.57519900	-2.70275000
C	-1.32742200	-4.23009800	-1.17855700
H	-1.55098700	-4.46020200	0.94790300
H	-0.95236300	-3.71394000	-3.23473300
H	-1.80262400	-5.17505700	-1.41541800
C	1.94713100	-0.42463400	-0.86423100
H	1.95496400	-0.26059900	-1.93908900
C	3.15304500	-0.61833900	-0.27149600
C	3.33403600	-0.85067100	1.15626800
C	4.36065200	-0.59801200	-1.09043500
C	4.55484800	-1.04107200	1.69126700
H	2.45971200	-0.87193200	1.79590100
C	5.58667100	-0.78537200	-0.56832200
H	4.23704300	-0.42258000	-2.15498300
C	5.78329600	-1.02375900	0.87262700
H	4.69372400	-1.21472500	2.75235800
H	6.48169800	-0.76914800	-1.17951300
C	-2.79696000	0.78924200	-0.00077400
C	-3.20596700	-0.26628500	-0.89096000
C	-3.83191900	1.52426900	0.68723200

C	-4.51622300	-0.55791500	-1.08332400
H	-2.44820900	-0.84131600	-1.40644800
C	-5.14645400	1.24916000	0.50544900
H	-3.52542700	2.32092700	1.35695700
C	-5.58433400	0.17857900	-0.39767200
H	-4.83088200	-1.34823500	-1.75490300
H	-5.92639000	1.80772700	1.00998700
O	6.89284500	-1.19451600	1.36391300
O	-6.77616500	-0.08491000	-0.57011800
C	-1.46158100	1.14673700	0.23837500
H	-1.33283400	2.05465700	0.81129200
O	-1.02977200	0.19349100	2.02623500
O	-1.67266300	0.82133800	3.05310100
C	-2.64791700	-0.06212400	3.63054900
H	-2.15070500	-0.94196400	4.04459000
H	-3.11966800	0.51642200	4.42559700
H	-3.38238700	-0.35591500	2.87988800

CHAPTER 3: Total Synthesis of Resveratrol Tetramers Vitisin A & Vitisin D: Harnessing a Persistent Radical Equilibrium for a Homolytic Bond Migration

Portions of this chapter have been published in:

Romero, K. J.; Keylor, M. H.; Griesser, M.; Zhu, X.; Strobel, E. J.; Pratt, D. A.; Stephenson, C. R. J. *J. Am. Chem. Soc.* **2020**, *142*, 6499-6504

3.1 Introduction

Resveratrol (**2.78**) and its oligomers are stilbenoid natural products produced as secondary metabolites across multiple plant families;⁴⁴ however, it was a 1992 report that brought resveratrol to the attention of the general public when Siemann and Creasy disclosed that **2.78** was present in significant quantities in red wine while also noting that it was found in many traditional East Asian folk medicines.^{123,124} At the time, resveratrol (**2.78**) was suggested to be the solution to the “French Paradox” – the observation that the French population specifically had a low incidence of mortality due to coronary heart disease relative to other populations despite a diet that resulted in elevated risk factors, such as high fat and cholesterol consumption.¹²⁵ It has since been suggested that red wine has cardioprotective properties, though the relationship between red wine consumption and the French Paradox is still debated in the literature.^{126,127} Beyond the French Paradox, resveratrol has been suggested to have broad biological activity, including antioxidant,¹²⁸ antidiabetic,^{129,130} and anticancer properties,¹³¹ and numerous investigations into resveratrol biological activity have been conducted despite poor bioavailability.^{102,132–137}

Resveratrol oligomers arise in nature as part of a biological defense mechanism for many plant compounds, and these secondary metabolite natural products have been isolated as dimer, trimers, tetramers, and higher-order oligomers – all derived from **2.78**.⁴⁴ Langcake and Pryce first reported this biological role for these compounds in 1976 when they observed fluorescent lesions on the leaves of *Vitis vinifera* after infection with two plant pathogens, gray mold (*Botrytis cinerea*) and downy mildew (*Plasmopara viticola*).¹³⁸ They determined that **2.78** was responsible for the observed fluorescence, and they observed that both fungal infection and damage from ultraviolet light irradiation resulted in an increased expression of **2.78** concentrated near the lesion.¹³⁹ Subsequent investigations determined that **2.78** exhibited poor antifungal activity; however, the oligomeric natural products ϵ -viniferin (**3.1**) and α -viniferin (**3.2**) both displayed potent antifungal activity and were observed in higher concentrations relative to **2.78** at the site of inoculation (Figure 3.1).¹⁴⁰ Langcake and Pryce, in addition to Coggon and co-workers (who isolated the first resveratrol tetramer, hopeaphenol¹⁴¹), proposed that resveratrol oligomers arose through an oxidative oligomerization process, suggesting that **2.78** was the precursor to the active phytoalexins – plant secondary metabolites produced to counter infection – in a similar manner to that reported for lignan phytoalexins, such as licarin A.¹⁴² Langcake and Pryce subsequently validated this hypothesis by oxidation of resveratrol with horseradish

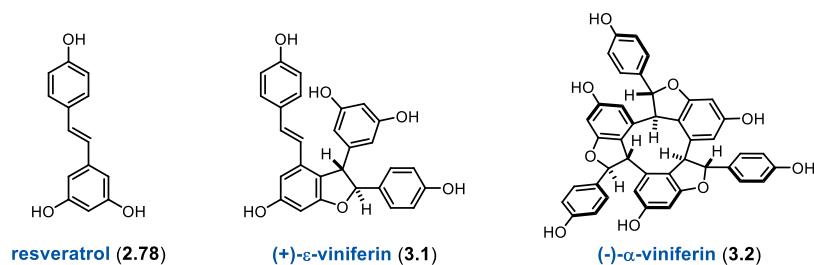


Figure 3.1. Stilbenoid compounds isolated by Langcake and Pryce while investigating pathogen defense response in *Vitis vinifera*.

peroxidase and hydrogen peroxide,^{143,144} thus demonstrating that the resveratrol and lignan oligomers share a common biosynthetic oligomerization mechanism.⁴⁴

Resveratrol is produced in plants through the phenylpropanoid pathway, which is responsible for the biosynthesis of all aromatic secondary metabolites (Figure 3.2).⁹⁰ L-phenylalanine is converted through a series of enzymatic transformations to coumaroyl-CoA, at which point a series of Claisen condensations and decarboxylations with malonyl-CoA affords a linear tetraketide intermediate (**3.3**) that is common to all phenylpropanoids, including stilbenes, flavonoids, and chalcones. Under homeostatic control, plants constitutively express chalcone synthase, which converts **3.3** via an intramolecular Claisen condensation to compounds such as naringenin (**3.4**); however, stilbene synthase is upregulated in response to numerous environmental stimuli, such as fungal inoculation or UV irradiation as demonstrated by Langcake and Pryce (*vide supra*), and instead this enzyme mediates an intramolecular aldol condensation with concomitant decarboxylation to deliver resveratrol (**2.78**). While the enzymatic processes that synthesize phenylpropanoid monomers, such as **2.78**, have been thoroughly characterized,⁹⁰ the same cannot be said for the oxidative oligomerization that gives rise to dimeric and higher-order resveratrol oligomers. In the absence of enzymatic characterization, the biosynthetic oligomerization of resveratrol has been proposed by analogy to the lignans (*vide infra*).⁴⁴

It is proposed that oxidative oligomerization of **2.78** occurs through single electron oxidation and deprotonation to access phenoxyl radical intermediates, of which the major resonance structures (**A–D**) are depicted in Figure 3.2. Coupling between radicals **A** and **B** forges the C3–C8' connection, and subsequent rearomatization of the phenol and cyclization onto the intermediate quinone methide gives δ -viniferin (**3.5**). Coupling

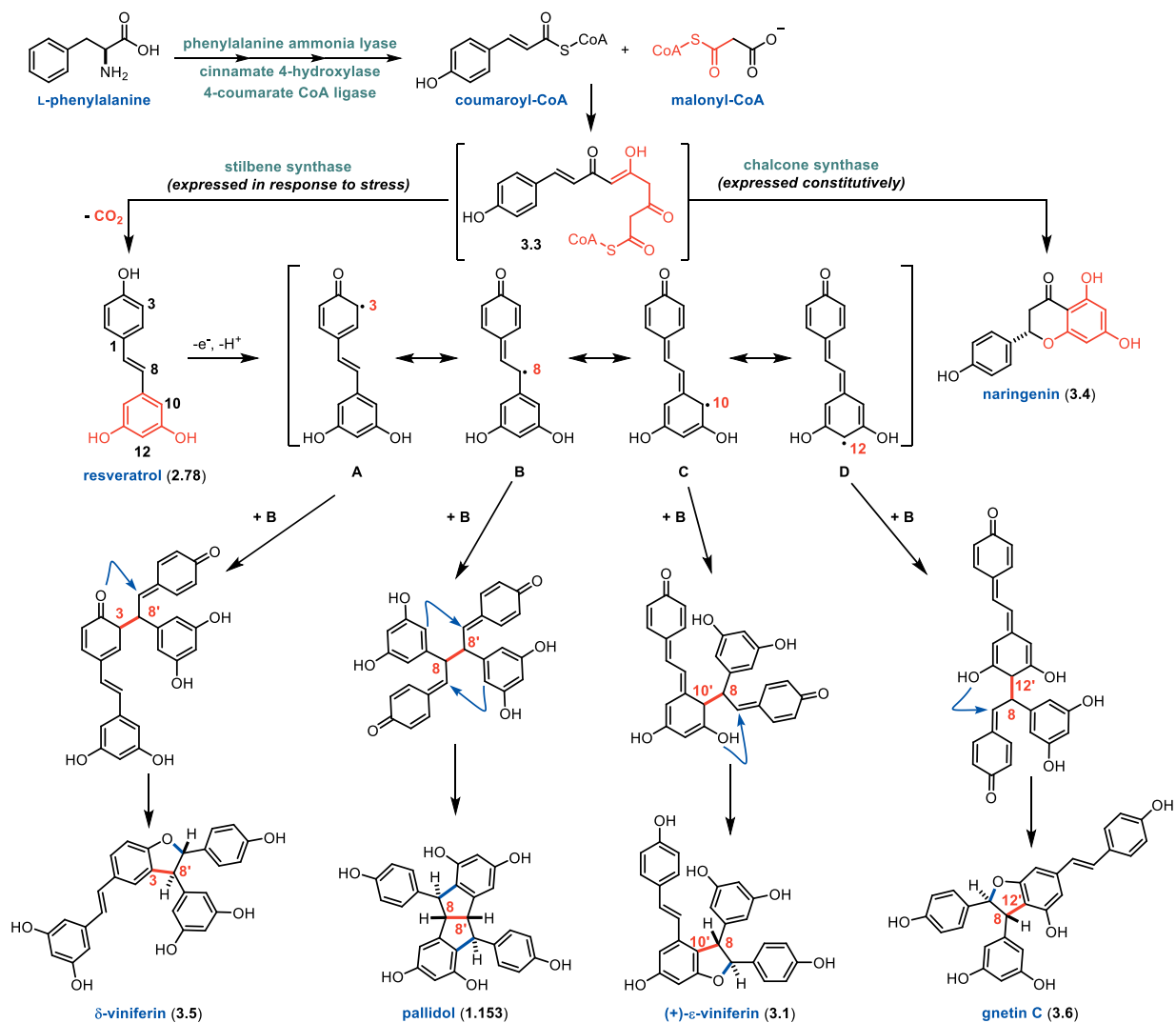


Figure 3.2. Resveratrol (2.78) arises from the phenylpropanoid pathway and undergoes oligomerization via phenoxyl radical intermediates.

between two **B** radicals accesses the C8–C8' connection, and subsequent Friedel-Crafts cyclization of the resorcinols onto the quinone methides gives pallidol (**1.153**). Coupling between radicals **B** and **C** delivers the C8–C10' connection, and, after cyclization of the phenol on the quinone methide, ϵ -viniferin (**3.1**) is formed. Finally, coupling between radicals **B** and **D** delivers the C8–C12' connection, and gnetin C (**3.6**) is formed upon cyclization of the phenol onto the quinone methide. Remarkably, these molecules are

isolated as single enantiomers in nature, suggesting that the radical coupling and cyclization events are stereoselective and likely enzymatically mediated.⁴⁴

The lignans arise from dimerization of the monolignols – coniferyl alcohol (**2.76**), coumaryl alcohol (**3.7**), and sinapyl alcohol (**3.8**) – which are compounds that are also produced by the phenylpropanoid pathway.⁹⁰ The process by which dimerization of these compounds occurs is depicted in Figure 3.3 using coniferyl alcohol (**2.76**) as a representative example. Phenol oxidation and deprotonation gives a phenoxy radical intermediate, of which the major contributing resonance structures are **E–G**. Combination between radicals **F** and **G** affords the C5–C8' connection; subsequent tautomerization and cyclization onto the quinone methide gives hierochin D (**2.77**). Alternatively, coupling between two **G** radicals affords the C8–C8' connection, and cyclization of the pendant alcohols onto the quinone methides affords (+)-pinoresinol (**3.9**). The biosynthesis of **3.9**,

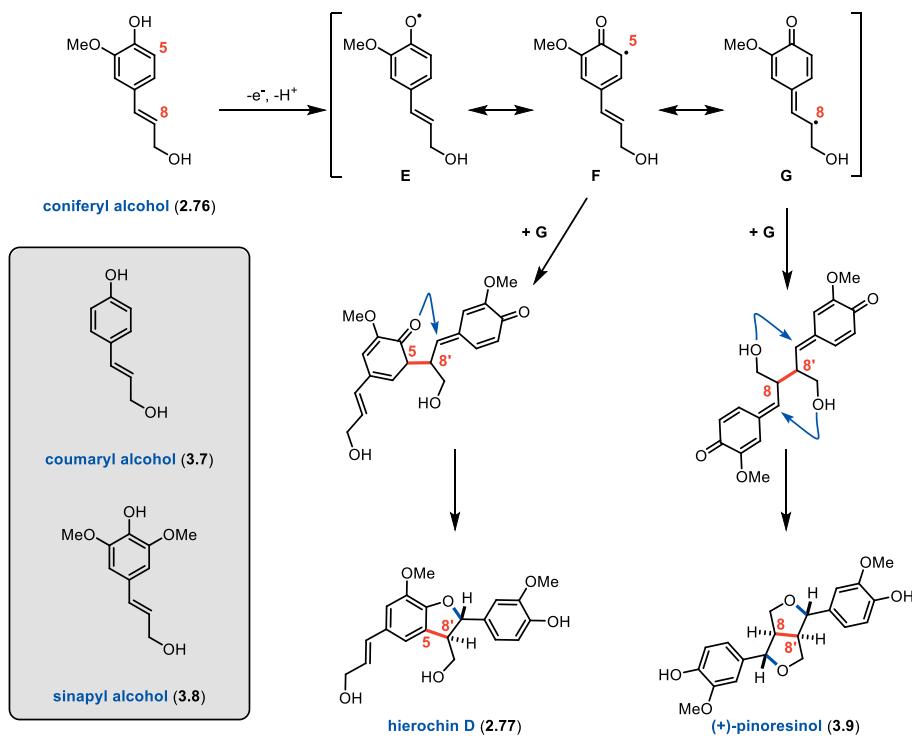


Figure 3.3. Dimerization of the monolignols proceeds through stereoselective coupling of phenoxy radical intermediates.

in particular, was demonstrated by Davin and Lewis to be enzyme-mediated to account for the synthesis of chiral material.^{145,146} These researchers isolated a remarkable protein, *FiDIR1*, which they observed to mediate the conversion of **2.76** to **3.9** in a regio- and enantiospecific fashion. Interestingly, this “dirigent” protein (from the Latin word *dirigere*, meaning to align or guide) does not demonstrate oxidase activity.¹⁴⁷ Instead, it operates by capturing and dimerizing radical **G** upon oxidation of **2.76** faster than the background, non-mediated dimerization process. Davin and Lewis demonstrated this activity with both enzymatic and inorganic oxidants to fully support the notion that radical formation is completely decoupled from C–C bond formation and cyclization for lignan biosynthesis. Schaller and co-workers followed up this seminal discovery by isolating *AtDIR6*, which provides the opposite enantiomer of **3.9**, providing further evidence that there exists biosynthetic machinery for the enantioselective synthesis of phenylpropanoid oligomers.¹⁴⁸ Importantly, in the absence of dirigent protein, complex mixtures of racemic regioisomers are observed upon oxidation of **2.76**, and, as the following section will describe, the same is true for resveratrol (**2.78**).⁴⁴ The leading hypothesis is that enantiospecific resveratrol biosynthesis is also mediated by dirigent proteins (Figure 3.4); however, there have yet to

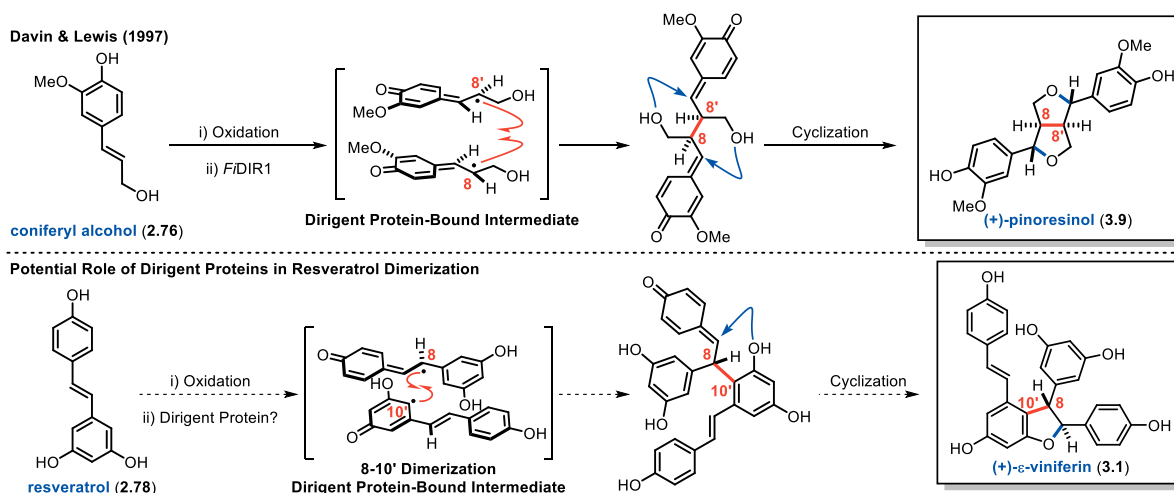


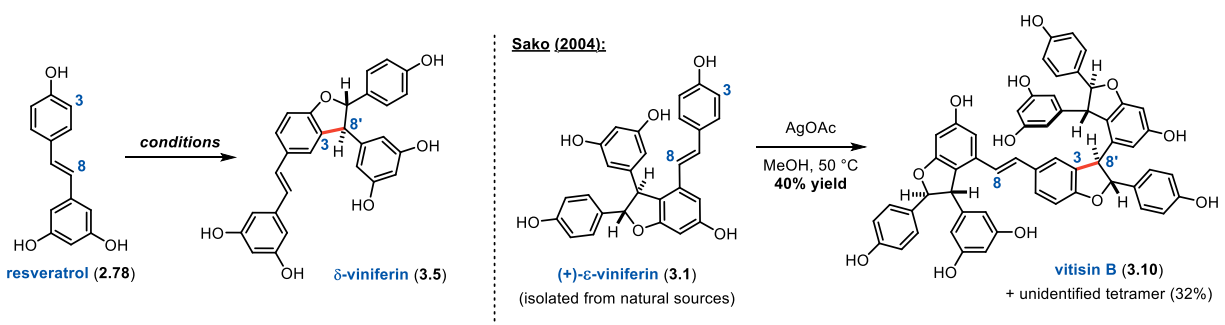
Figure 3.4. Dirigent protein hypothesis for resveratrol dimerization.

be any reports identifying these critical cellular components. As such, this hypothesis has not been corroborated, and clearly more work is required to fully explain the biosynthesis of the resveratrol natural product class.

3.2 Prior biomimetic efforts in resveratrol oligomer synthesis

The concept of biomimetic synthesis can be traced back to Robinson's one-step synthesis of tropinone via a double Mannich reaction – a remarkably elegant approach that was well ahead of its time.^{149,150} Simply mixing succinaldehyde, methylamine, and acetonedicarboxylic acid under acidic conditions at elevated temperatures afforded a series of condensation reactions followed by two decarboxylation events to deliver the natural product in the same manner that is proposed to occur in nature.¹⁵¹ In the years that have followed, biomimetic synthesis has been generally accepted as the most direct route to accessing complex natural products; however, in the absence of enzymatic influence, selectivity issues abound. The resveratrol natural products are a perfect example of this problem. The proposed biogenesis of resveratrol oligomers represents a rapid increase in complexity in a highly convergent fashion, offering an attractive approach to the preparation of these molecules. However, as this section will describe, the intermediacy of the delocalized phenoxy radical results in regioselectivity issues based on the myriad of C–C bond forming events that can occur. Furthermore, chemoselectivity also becomes problematic, as the oxidation potential of resveratrol is similar to the dimeric products, which can lead to undesired overoxidation. Finally, the possible modes of Friedel-Crafts cyclization that occurs after the initial radical coupling only increase as higher order oligomers are formed, further adding to the selectivity issues. Nonetheless, many research groups have undertaken a biomimetic approach to resveratrol oligomers in order to evaluate

Table 3.1. Biomimetic dimerizations accessing C3–C8' resveratrol oligomers.



Entry*	Reaction Conditions	Yield of 3.5	Ref.
1	Cu ^{II} SO ₄ , MeCN, rt	16%	152
2	DPPH, MeOH	18%	153
3	Various Peroxidases, Acetone/EtOH	13-21%	154
4	Laccase, <i>n</i> -BuOH	31%	155
5	HRP/H ₂ O ₂	40%	143
6	Galvinoxyl radical, ethanol, rt	41%	156
7	Graphitic carbon nitride (<i>h</i> ν , 410 nm), lutidine, air, MeCN, rt	85%	157
8	AgOAc, MeOH, 50 °C	86%	158
9	MnO ₂ , CH ₂ Cl ₂ , rt	91%	154
10	HRP/H ₂ O ₂ , H ₂ O/Acetone, pH 8	93%	159
11	FeCl ₃ , Acetone, rt	97%	154

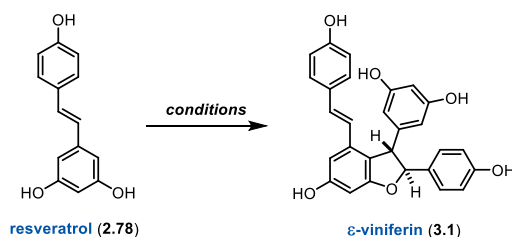
*Entries are organized by reaction yield.

their proposed biosynthesis, elucidate structure during isolation studies, and begin to investigate the biological activity of this natural product class.

As mentioned in the previous section, Langcake and Pryce were the first to evaluate oxidation conditions for the dimerization of resveratrol.¹⁴³ They subjected resveratrol (2.78) to enzymatic oxidation conditions developed by Sarkanen and Wallis,¹⁶⁰ and they observed the formation of the C3–C8' coupling product δ -viniferin (3.5) in 40% isolated yield (Table 3.1, Entry 5). In the years that have followed, numerous research groups have reported the dimerization of 2.78 to 3.5 under enzymatic,^{155,159,161,162} organic,^{153,156} inorganic,^{152,154,158} and photochemical¹⁵⁷ oxidation conditions (Table 3.1). The contributions from Sako and co-workers (Table 3.1, Entry 8) are particularly noteworthy as they were able to extend this strategy to the C3–C8' dimerization of (+)- ϵ -viniferin (3.1) to access vitisin B (3.10) in 40% yield in addition to 32% yield of an unidentified tetrameric

compound.¹⁵⁸ Niwa and co-workers followed up this report by demonstrating that both MnO₂ and FeCl₃ afforded higher yields of δ -viniferin (Table 3.1, Entries 9 and 11), however these conditions were not extended beyond the dimer system.¹⁵⁴

While the C3–C8' dimerization of resveratrol can be achieved in excellent yield and regioselectivity (albeit in a racemic fashion), this connection motif is not broadly observed across the natural product class; in fact, the C3–C8' bond is essentially limited to δ -viniferin and the vitisin tetramers, vitisin A–D.⁴⁴ On the other hand, the C8–C10' bond exhibited in ϵ -viniferin (**3.1**) is found in the majority of higher order resveratrol oligomers. Therefore, the selective dimerization of resveratrol to ϵ -viniferin is critical for accessing biomimetic syntheses of resveratrol trimers, tetramers, and beyond. The 4-hydroxystilbene motif is preserved upon dimerization of resveratrol to ϵ -viniferin, and, as a result, the oxidation potentials for each of these compounds have been reported to be within error of each other.¹⁵⁸ The comparable reactivity between starting material and desired product results in a chemoselectivity challenge that has yet to be solved (Table 3.2, Entries 1–3).^{154,163} However, a 1998 report from Pezet provides an enzymatic solution to this selectivity problem.¹⁶⁴ The author reported the isolation of a 32-kDa laccase-like stilbene oxidase from *Botrytis cinerea* – a plant pathogen – and found that this enzyme converted resveratrol to ϵ -viniferin in 97% yield (Table 3.2, Entry 4). While these results are undoubtedly exciting in regards to accessing this critical material for entry into higher order oligomers, two important caveats significantly dampen the excitement regarding this report: 1) the author did not measure the optical rotation of the ϵ -viniferin produced in this fashion, and 2) these reactions were conducted on microgram scale. As the scale-up of enzymatic reactions has become prominent in the biocatalysis field,¹⁶⁵ revisiting Pezet's results with the goal of

Table 3.2. Biomimetic dimerization of resveratrol (2.78) to ϵ -viniferin (3.1).

Entry	Reaction Conditions	Yield	Ref.
1	FeCl ₃ , MeOH/H ₂ O, rt	30%	163
2	K ₃ Fe(CN) ₆ , K ₂ CO ₃ , MeOH/H ₂ O, rt	22%	154
3	Tl(NO ₃) ₃ , MeOH, -50 °C	30%	154
4	<i>B. cinerea</i> laccase-like stilbene oxidase	97%	164

developing a preparative approach to ϵ -viniferin, especially if such an approach was enantioselective, might be a worthwhile endeavor to facilitate higher-order resveratrol oligomer synthesis.

The final major bond connection for resveratrol oligomer synthesis, the C8–C8' bond, has also been accessed from a biomimetic approach. Indeed, many of the conditions described above that afforded either δ -viniferin or ϵ -viniferin gave products arising from C8–C8' oligomerization as well.⁴⁴ Niwa and co-workers reported a thorough evaluation of oxidation conditions and provided an initial proof of concept for reagent controlled regioselectivity, but the yields and selectivities were modest at best.¹⁵⁴ A significant step forward in guiding the selectivity with which resveratrol dimerization occurs took place in 2006 when Hou and co-workers unveiled an arene protecting group strategy for the synthesis of quadrangularin A (Figure 3.5).⁹² These researchers “protected” the C3-position of the resveratrol scaffold with *tert*-butyl groups to eliminate the possibility of C3–C8' coupling, drawing inspiration from studies of lignan biosynthesis from Müller and Wallis.^{166,167} The requisite *t*Bu-resveratrol (**2.79**) to investigate oxidative oligomerization was prepared in 7 steps. Starting from benzoic acid **3.11**, a 4-step sequence involving Fisher esterification, benzyl protection, ester reduction, and alcohol activation afforded benzyl

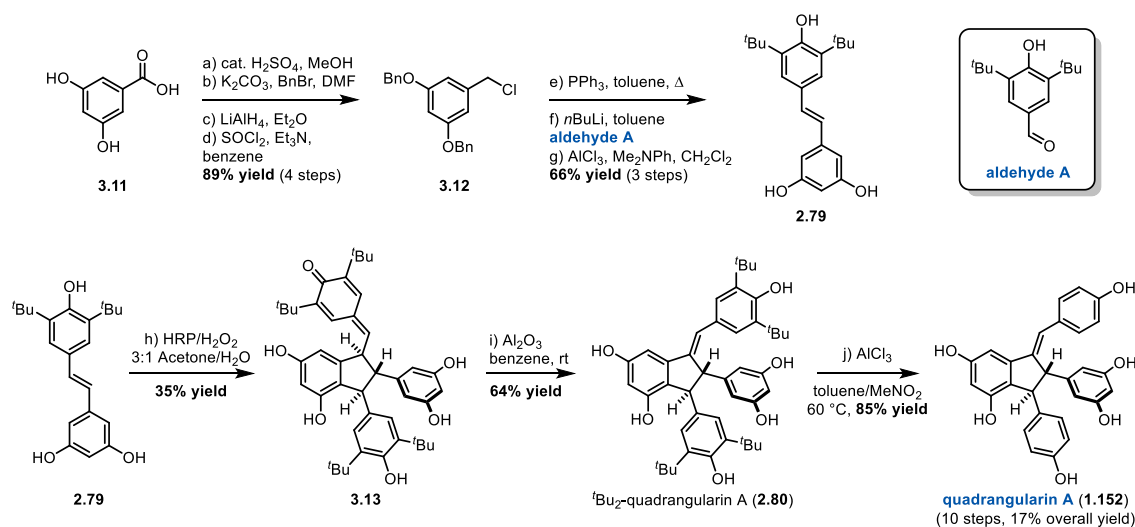
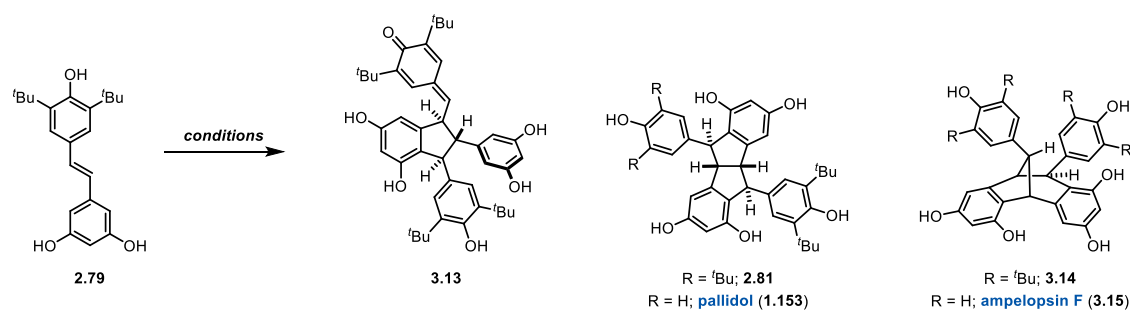


Figure 3.5. Hou's synthesis of quadrangularin A (1.152) featuring an arene protecting group strategy.

chloride **3.12**. This material was converted to the corresponding phosphonium salt upon treatment with triphenylphosphine in toluene at reflux and subsequently utilized for a Wittig olefination with BHT-derived aldehyde A.^a Finally, debenzoylation under Lewis acid conditions afforded **2.79**. Subjection of *t*Bu-resveratrol (**2.79**) to HRP/ H_2O_2 delivered the indane product **3.13** in 35% yield, and treatment with Al_2O_3 afforded isomerization to *t*Bu-quadrangularin A (**2.80**). Finally, a retro-Friedel Crafts reaction mediated by AlCl_3 delivered quadrangularin A (**1.152**) in 10 steps and 17% overall yield.

Following these efforts, Li and co-workers evaluated additional inorganic oxidation conditions for the dimerization of *t*Bu-resveratrol (**2.79**).⁹³ One important note in discussing this work is that the authors reported reaction results in conversion, not isolated yield, and the mass balance was not always completely accounted for (Table 3.3). Regardless, they found that the cyclized quinone methide product **3.13** was produced upon oxidation with either silver carbonate or manganese oxide (Entries 1-2), whereas oxidation with iron (III)

^a Hou and co-workers prepared this aldehyde from BHT. It is now commercially available from multiple vendors.

Table 3.3. Li's synthesis of pallidol (1.153) and ampelopsin F (3.15).

Entry	Reaction Conditions	Dimerization Conversion		
		3.13	2.81	3.14
1	Ag ₂ CO ₃ , CH ₂ Cl ₂	59%	-	-
2	MnO ₂ , CH ₂ Cl ₂	54%	-	-
3	FeCl ₃ •6H ₂ O, benzene/acetone (2:1)	-	55%	-
4	FeCl ₃ •6H ₂ O, CH ₂ Cl ₂	-	-	45%

chloride hexahydrate resulted in two cyclization events after the initial C8–C8' coupling. In a 2:1 mixture of benzene and acetone, the pallidol scaffold (**2.81**) was favored (Entry 3), whereas in dichloromethane the ampelopsin F scaffold (**3.14**) was produced (Entry 4). These results are consistent with the reports from Niwa and Velu demonstrating that choice of both solvent and oxidant can have a significant influence on the regiochemical outcome of dimerization.^{154,168} Finally, the authors were able to deprotect **2.81** and **3.14** to afford pallidol (**1.153**) and ampelopsin F (**3.15**) using the retro-Freidel Crafts conditions employed by Hou and co-workers in 85% and 76% isolated yield, respectively, further demonstrating the versatility of the C3-blocking group strategy for resveratrol oligomer synthesis.

Li and co-workers next evaluated the outcome of oxidative dimerization upon acyl protection of the resorcinol in addition to blocking C3, finding that dimerization of **3.16** with iron (III) chloride hexahydrate delivered the tricuspidadol (**3.17**) and restrytisol B (**3.18**) cores in modest yields (Figure 3.6).¹⁶⁹ While this was certainly an interesting result, again contributing to the knowledge required to impart selectivity for biomimetic dimerization, deprotection efforts did not reveal the corresponding natural products.

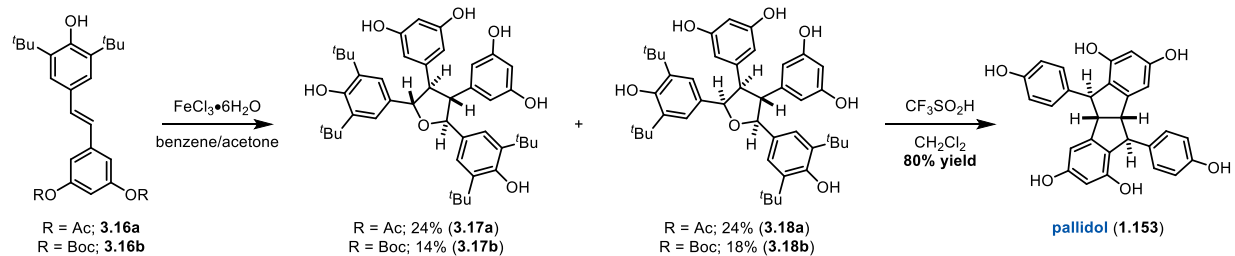
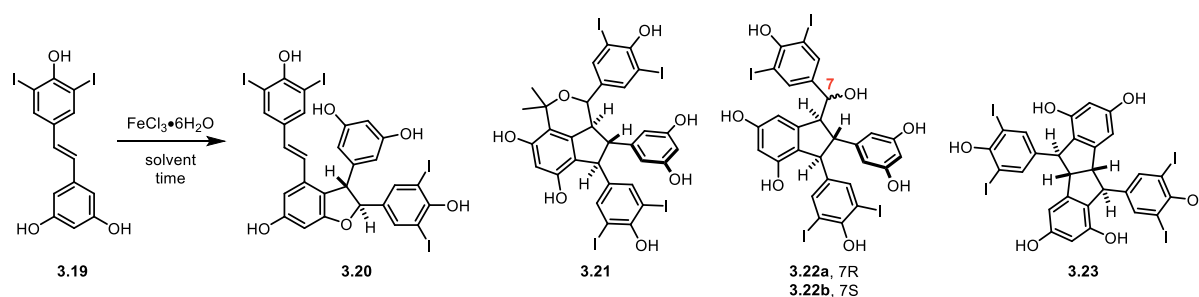


Figure 3.6. Li's approach to protected tetraaryl furan dimers and pallidol (1.153).

Instead, each scaffold further reacted via dehydration under the Brønsted-acid mediated retro-Friedel Crafts conditions to afford pallidol (**1.153**), demonstrating that the removal of *tert*-butyl blocking substituents is challenging the presence of acid-labile benzylic ether moieties, as cleavage to the benzyl cation is highly favored under such conditions. This problem became apparent as well during our group's efforts in the synthesis of nepalensinol B and vateriaphenol C, necessitating the switch from C3-*tert*-butyl to C3-silyl substituents for the successful completion of those natural products (see Section 1.5.2).⁴⁸

Motivated by this drawback in *tert*-butyl cleavage, Li and co-workers subsequently reported the use of halides as C3-blocking substituents for biomimetic resveratrol dimerization (Table 3.4).¹⁷⁰ They prepared the corresponding C3-iodo-resveratrol analog (**3.19**) from the corresponding iodinated benzaldehyde and again evaluated iron (III) chloride hexahydrate for dimerization. They found that the ϵ -viniferin analog **3.20** and a compound resulting from acetone incorporation into the cyclized quinone methide scaffold (**3.21**) were isolated in nearly a 1:1 ratio upon oxidation in acetone for 18 hours (Table 3.4, Entry 1). While the incorporation of benzene as a co-solvent did little to change this result (Table 3.4, Entry 2), aqueous conditions changed the observed product distribution to favor the mixture of benzylic alcohols **3.22a** and **3.22b** arising from water addition to the quinone methide (Table 3.4, Entries 3–4). Finally, extended reaction times and higher oxidant loading also afforded the pallidol scaffold (**3.23**) as a minor product (Table 3.4, Entry 5).

Table 3.4. Li's use of halides as C3-blocking groups for resveratrol dimerization.



Entry	Solvent (ratio)	Time (h)	Isolated yield of dimerization products			
			3.20	3.21	3.22a/3.22b (ratio ^a)	3.23
1 ^b	acetone	18	38	34	-	-
2 ^b	acetone-benzene (2:1)	18	35	30	-	-
3 ^b	acetone-H ₂ O (2:1)	18	-	-	45 (1:0)	-
4 ^b	acetone-buffer (pH = 5.4) (2:1)	24	-	-	35 (1:0)	-
5 ^c	acetone-H ₂ O	36	-	-	32 (1:2)	10

^aDetermined by ¹H NMR. ^b3.0 equiv. of FeCl₃•6H₂O ^c5.0 equiv. of FeCl₃•6H₂O

Importantly, the authors demonstrated that the C3-halides could be cleaved under reducing conditions with either LiAlH₄ or H₂ and Pd/C, providing an orthogonal C3-blocking group strategy for biomimetic resveratrol oligomerization.

3.3 Prior *de novo* efforts in resveratrol oligomer synthesis

The wide-ranging reported biological activities coupled with beautiful and complex molecular architectures have motivated synthetic chemists to target the resveratrol natural product class for some time. As discussed in the preceding section, biomimetic synthesis can be a direct approach to access these molecules, however issues of selectivity have limited the scope of biomimetic efforts to enable systematic study of the corresponding compounds; in fact, few such examples exist.⁴⁵ These challenges could be overcome through *de novo* synthesis of targeted compounds, and indeed multiple research groups have pursued this goal.⁴⁴ The following sections describe selected examples from the *de novo* synthesis literature of resveratrol dimers and higher-order oligomers. The approaches to resveratrol dimers have been broken into two categories: 1) cyclization(s) and/or rearrangement(s) utilizing cationic/quinone methide intermediates, as pioneered by the

Snyder group, and 2) transition-metal mediated approaches to key five-membered rings. The subsequent syntheses of higher order oligomers (trimers and tetramers) by Snyder and co-workers utilize components of each of these strategies and will comprise the final section.

3.3.1 Quinone methide cyclizations to access resveratrol dimers

Snyder and co-workers realized the first targeted total synthesis of resveratrol dimers in 2007 when they reported the preparation of six indane-derived natural products in a modular approach, four of which are highlighted here (Figure 3.7 & Figure 3.8).¹⁷¹ Their approach to accessing the diverse carbocyclic frameworks of these compounds harnessed the reactivity of cationic quinone methide intermediates under acidic conditions for key cyclization events. Starting from protected bromo-resveratrol **3.24**, lithiation and aldol reaction with **3.25** delivered benzylic alcohol **3.26** in 71% yield (Figure 3.7). Exposure of this material to acidic conditions induced cyclization to an intermediate cation (**3.27**) stabilized by conjugation to the adjacent resorcinol moiety. Subsequent trapping of this intermediate with benzyl thiol **3.28** afforded thioether **3.29** in 57% yield. The authors were now set up to perform a Ramberg-Bäcklund reaction to access the desired stilbene,¹⁷² and they chose to employ the Meyers' modification after oxidation of the thioether, forming the necessary halogenated intermediate *in situ* with carbon tetrachloride.¹⁷³ This reaction proceeded with 5:1 selectivity for the desired stilbene isomer, which was chromatographically separable from the undesired alkene. As such, they arrived at the ampelopsin D core (**3.30**) in 40% yield over those two steps, and the corresponding natural product (**3.31**) was revealed upon demethylation with BBr₃ (76% yield). Alternatively, bromination of **3.30** while slowly warming from cryogenic temperatures revealed quinone

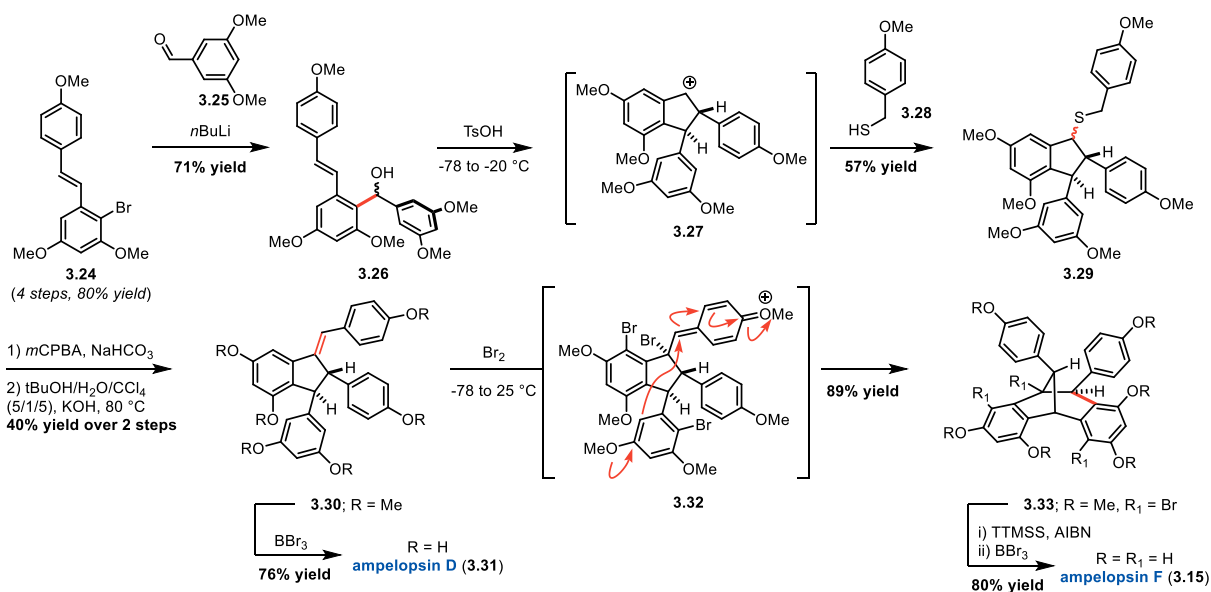


Figure 3.7. Snyder's synthesis of ampelopsin D (3.31) and ampelopsin F (3.15).

methide intermediate **3.32** which is disposed to undergo a 6-*exo-trig* cyclization with the resorcinol on the same face of the indane to deliver the [3.2.1] bicyclooctane core of ampelopsin F (**3.33**). Importantly, this reaction proceeds with concomitant bromination of each resorcinol ring, providing an excellent handle for manipulation to higher-order oligomers. In this case, the synthesis of ampelopsin F (**3.15**) was completed after dehalogenation with tris(trimethylsilyl)silane (TTMSS) and AIBN followed by demethylation with BBr_3 in 80% yield over the two steps. The same strategy, starting from stilbene **3.34**, afforded both quadrangularin A (**1.152**) and pallidol (**1.153**), where in this case the [3.3.0] bicyclooctane forms as a result of the *syn*-configuration of the quinone methide and adjacent resorcinol ring (Figure 3.8). Interestingly, the facial selectivity for the stilbene bromination is opposite for the formation of **3.32** and **3.40**. The authors found through control experiments that both resorcinol rings are brominated prior to the stilbene, with the indane-fused resorcinol brominating first; thus, they invoke a steric argument, rationalizing that the bromonium formation occurs from the opposite face of the stilbene

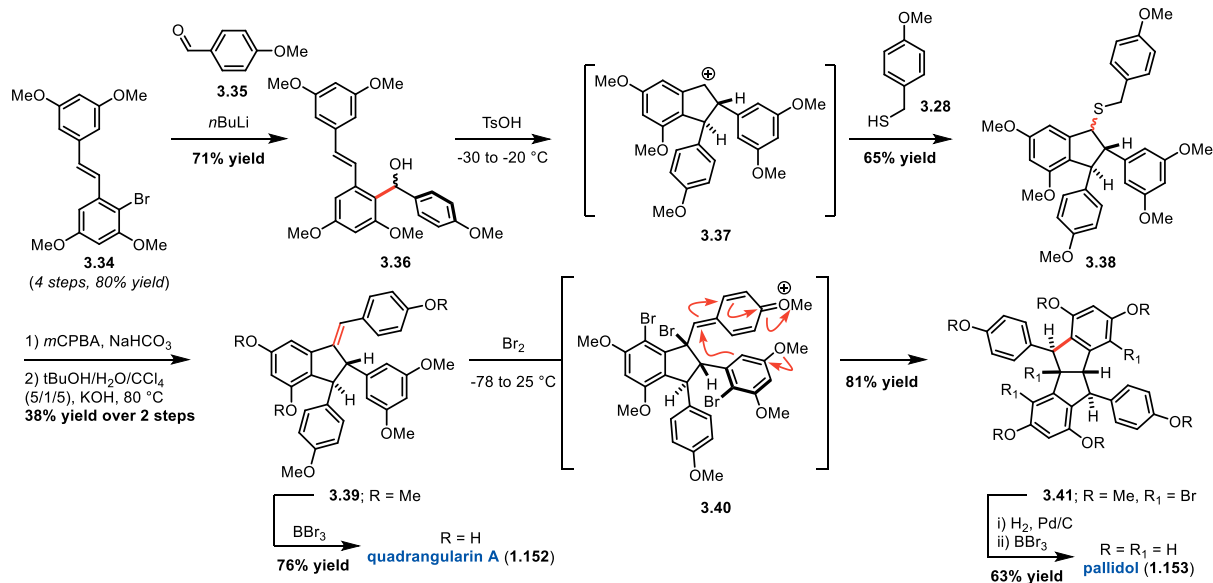


Figure 3.8. Snyder's synthesis of quadrangularin A (1.152) and pallidol (1.153).

relative to the ortho-brominated resorcinol. While this certainly seems reasonable to explain the formation of **3.40**, and subsequently pallidol (**1.153**), the analogous interaction leading to **3.32** would have to occur across the indane ring. It may also be that bromonium formation occurs reversibly by exchanging with free stilbene in solution.^{174,175} In the instance where the quinone methide is formed *anti* to the resorcinol nucleophile, i.e on the opposite face of the indane, it seems likely that a reversible mechanism is operative, as only the products of *syn*-Friedel Crafts cyclization between resorcinol and quinone methide are observed in high yields. This initial report from Snyder and co-workers demonstrated how one might capitalize on the inherent reactivity of these natural product scaffolds for targeted synthesis.

Nicolaou and co-workers followed Snyder's seminal contributions two years later when they reported the synthesis of hopeahainol A (**3.50**) and hopeanol (**3.52**) (Figure 3.9).¹⁷⁶ Benzylic alcohol **3.42** was coupled with α -keto carboxylic acid **3.43** using dicyclohexylcarbodiimide,¹⁷⁷ and the resulting α -keto ester was treated with Grignard

reagent **3.44** to access tertiary alcohol **3.45** after silyl deprotection. Subsequent treatment with acidic conditions resulted in dehydration of **3.45** to reveal an intermediate quinone methide, which was trapped in a 6-*exo-trig* Friedel Crafts cyclization to deliver lactone **3.46**. Base-mediated elimination formed the critical *trans*-stilbene moiety, and subsequent acidic treatment of the newly revealed carboxylic acid afforded condensation with the adjacent phenol to deliver **3.47**. The remaining phenol was acyl protected, and the stilbene was oxidized to the epoxide, which, upon treatment with Lewis acid, was opened to reveal an intermediate quinone methide (**3.48**). A 7-*exo-trig* cyclization ensued to deliver the carbocyclic core (**3.49**) of the desired natural product. This material was brought to the correct oxidation state by treatment with IBX¹⁷⁸ and deprotected with BBr₃ to afford hopeahainol A (**3.50**). Finally, exposure of **3.50** to basic conditions induced Friedel-Crafts cyclization (**3.51**) and conversion to hopeanol (**3.52**) in a manner that mimics the proposed biogenic relationship between these two natural products. Importantly, Nicolaou and co-

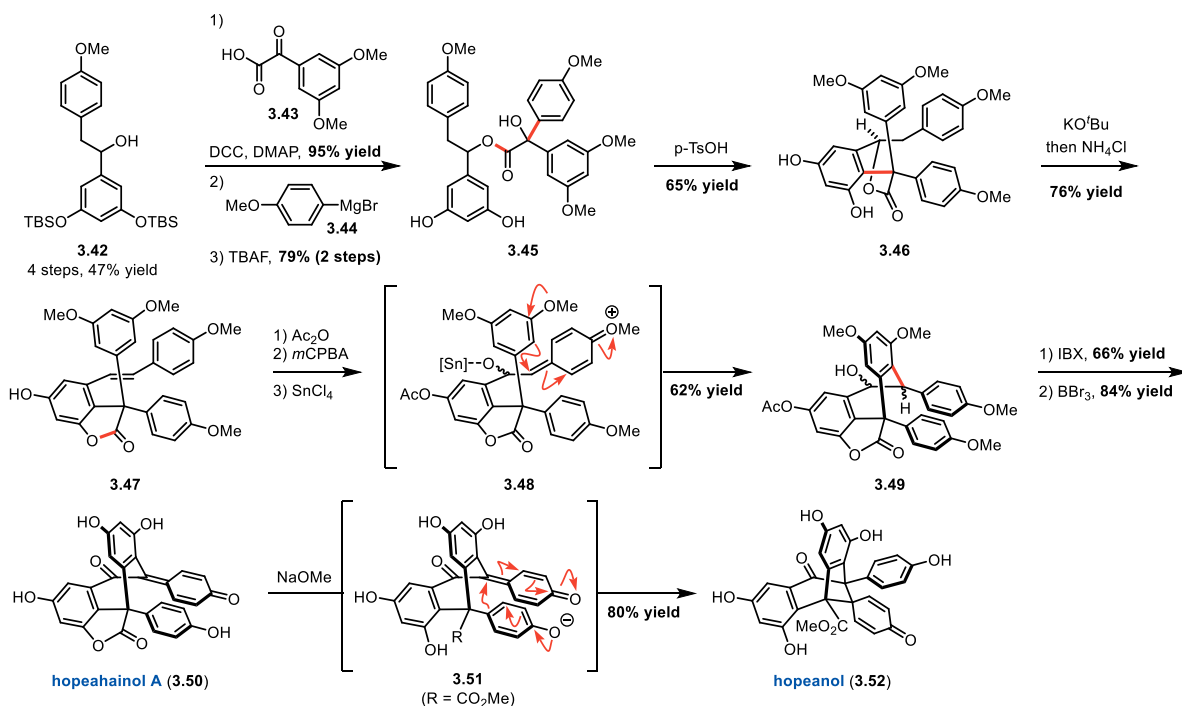


Figure 3.9. Nicolaou's synthesis of hopeahainol A (**3.50**) and hopeanol (**3.52**).

workers were able to develop an asymmetric approach to these compounds that relied upon a Corey-Bakshi-Shibata reduction^{179,180} of the ketone precursor to **3.42**, and each enantiomer of **3.42** was converted to the corresponding enantiomer of the natural product.¹⁸¹ This enabled the biological evaluation of these compounds, and the authors were able to support the reported modest inhibitory activity of (+)-**3.50** against acetylcholinesterase (~4-5 μM); however, they were unable to support the reported cytotoxicity of **3.52** after analysis against multiple cell lines.^{182,183}

Snyder and co-workers also reported an approach to these natural products in 2012 based upon their earlier investigations of quinone methide cyclization to access dibenzocycloheptanes (Figure 3.10).^{171,184} Indeed, treatment of **3.53** (the oxidized product of their prior cyclization starting material) with acid afforded cyclization to **3.54**. This key 7-membered-ring formation occurs via protonation of the stilbene moiety in **3.53** and Friedel-Crafts cyclization onto the resulting quinone methide. At this point Snyder employed a homologation sequence that has become a trademark of sorts for their strategy in this natural product class. First, a Johnson–Corey–Chaykovsky epoxidation^{185,186} converted the ketone to the corresponding epoxide. Next, treatment with acetic acid opened the epoxide to a tertiary benzylic cation which was subsequently trapped with acetate (and later hydrolyzed to the alcohol), and oxidation of the primary alcohol with Dess-Martin Periodinane (DMP) afforded the α -hydroxy aldehyde (**3.55**) in 45% yield over the entire sequence. The authors suggest that the para-methoxy-benzene ring across the 7-membered ring influences the excellent stereocontrol observed for the formation of the tertiary alcohol. Subsequent treatment with aryl Grignard reagent **3.44** afforded vicinal diol **3.56** as a mixture of diastereomers. A Pinacol rearrangement¹⁸⁷ was next conducted, mediated by the

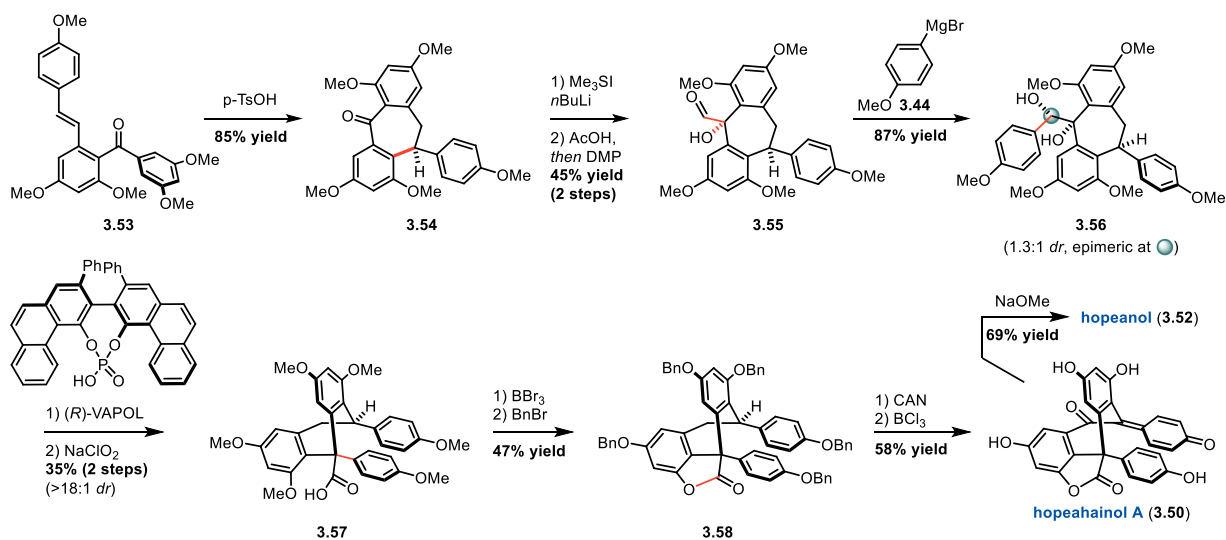


Figure 3.10. Snyder's synthesis of hopeahainol A (3.50) and hopeanol (3.52).

chiral phosphoric acid $(R)\text{-VAPOL}$, followed by a Pinnick-Lindgren oxidation^{188,189} to access the quaternary center in **3.57** in 35% yield and $>18:1$ diastereomeric ratio favoring the desired isomer. At this point, the methyl ethers were exchanged for benzyl ethers, a process which also included condensation of the carboxylic acid moiety onto the adjacent resorcinol, accessing benzolactone **3.58**. Finally, this material underwent both benzylic oxidation and dearomative oxidation upon exposure to ceric ammonium nitrate (CAN), and the benzyl ethers were cleaved with BCl_3 to afford hopeahainol A (**3.50**). Additionally, Snyder and co-workers were able to repeat Nicolaou's conversion of **3.50** to hopeanol (**3.52**).

The Snyder group was able to leverage the same starting material (**3.53**) for the synthesis of hopeahainol D (**3.65**) and heimiol (**3.66**), again utilizing the Friedel-Crafts reactivity of quinone methide intermediates (Figure 3.11).¹⁹⁰ In this example, the authors immediately employed their trademark homologation sequence, subjecting **3.53** to Johnson–Corey–Chaykovsky epoxidation, Meinwald rearrangement,¹⁹¹ and finally Pinnick-Lindgren oxidation of the resulting primary aldehyde to reveal carboxylic acid **3.59**. Subsequent

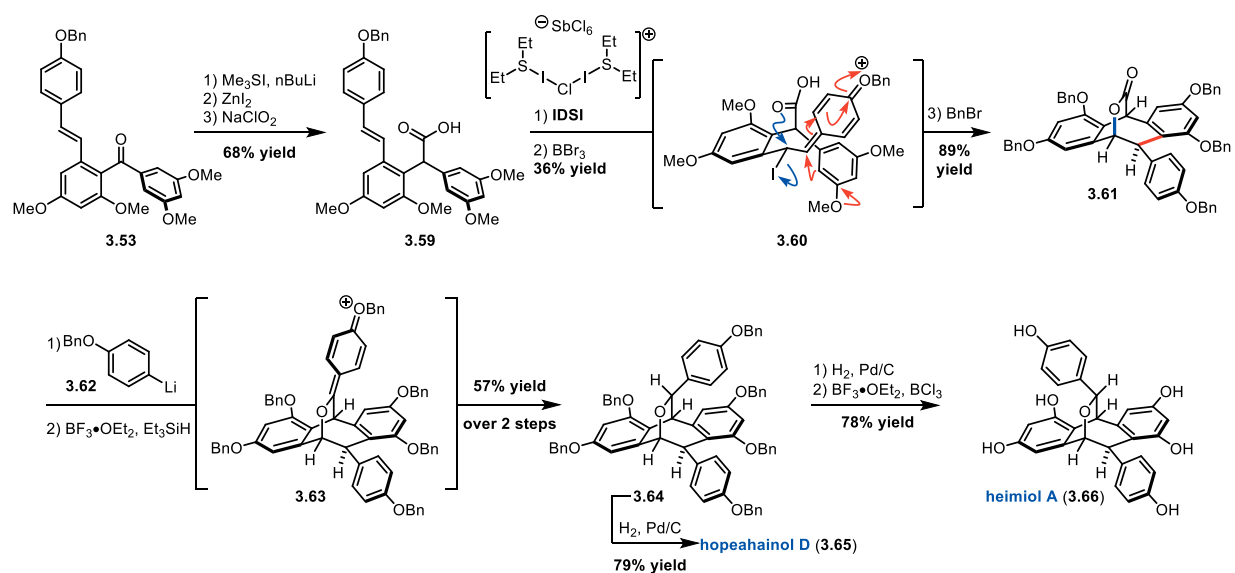


Figure 3.11. Snyder's synthesis of hopeahainol D (3.65) and heimiol A (3.66).

treatment with iodination reagent IDS1 initiated a halolactonization/Friedel-Crafts cascade with quinone methide intermediate **3.60**. While it is unclear which cyclization occurs first in this reaction, the carboxylic acid moiety serves to displace the benzylic halide to form the bridging lactone (blue arrows, Figure 3.11) while the resorcinol moiety and quinone methide engage in a Friedel-Crafts cyclization (red arrows, Figure 3.11). The methyl ethers were also exchanged for benzyl ethers at this stage to allow for more facile deprotection at the end of the synthesis. Addition of the appropriately substituted aryl lithium reagent **3.62** was followed by treatment with Lewis acid and triethylsilane to reduce the intermediate quinone methide **3.63** with a Kishi reduction.¹⁹² Hopeahainol D (**3.65**) was revealed upon hydrogenolysis of the six benzyl ethers in **3.64**, whereas heimiol A (**3.66**) was accessed after hydrogenolysis and Lewis-acid mediated epimerization. Yet again, the Snyder group demonstrated the power quinone methide activation, via selective halogenation or acidic treatment, for the targeted synthesis of resveratrol oligomers.

Building upon Snyder's strategy to access key seven-membered rings exhibited across this natural product class, Chen and co-workers in 2010 reported the synthesis of malibatol

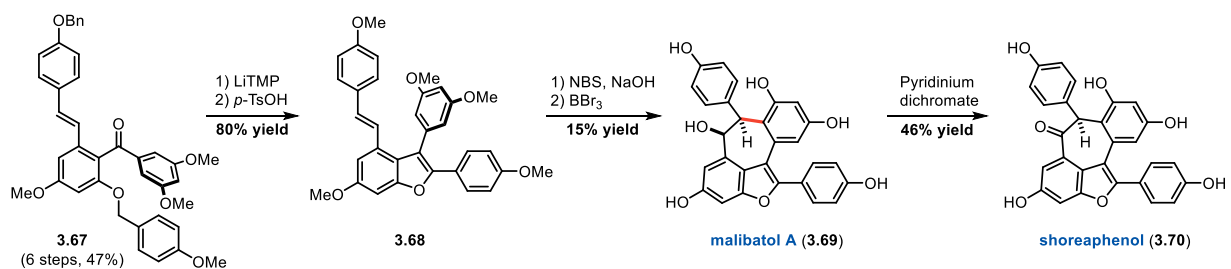


Figure 3.12. Chen's synthesis of malibatol A (3.69) and shoreaphenol (3.70).

A (3.69) and shoreaphenol (3.70) – two benzofuran-containing dimers derived from resveratrol (Figure 3.12).¹⁹³ Starting from the PMB-protected variant of Snyder's key starting benzophenone (3.67), which is available in 6 steps and 47% yield, the authors achieved deprotonation at the benzylic position and subsequent ketone addition by treatment with lithium tetramethylpiperidide (LiTMP).¹⁹⁴ In a second step, acid-mediated dehydration afforded the permethylated viniferifuran analog 3.68. Treatment with NBS and NaOH induced Friedel-Crafts cyclization that proceeds via a quinone methide intermediate, and demethylation afforded malibatol A (3.69). Finally, oxidation of the benzyl alcohol to the corresponding acetophenone moiety proceeded to deliver shoreaphenol (3.70). Chen and co-workers provide yet another example of propensity of this natural product class to engage in Friedel-Crafts reactivity between resorcinol moieties and *in situ* generated quinone methide intermediates to access key C–C bonds. In the next section, key C–C bonds are targeted utilizing transition-metal reactivity to access the indane and dihydrobenzofuran 5-membered rings exhibited across this natural product class.

3.3.2 Construction of 5-membered rings for resveratrol oligomer synthesis

Pauciflorol F (3.73) is a resveratrol-derived natural product that presumably arises from oxidative cleavage of the stilbene moiety of ampelopsin D (3.31). Numerous research groups have targeted the construction and functionalization of this relatively simple indane-derived compound using transition metal catalysis.⁴⁴ Pan, She, and co-workers reported the

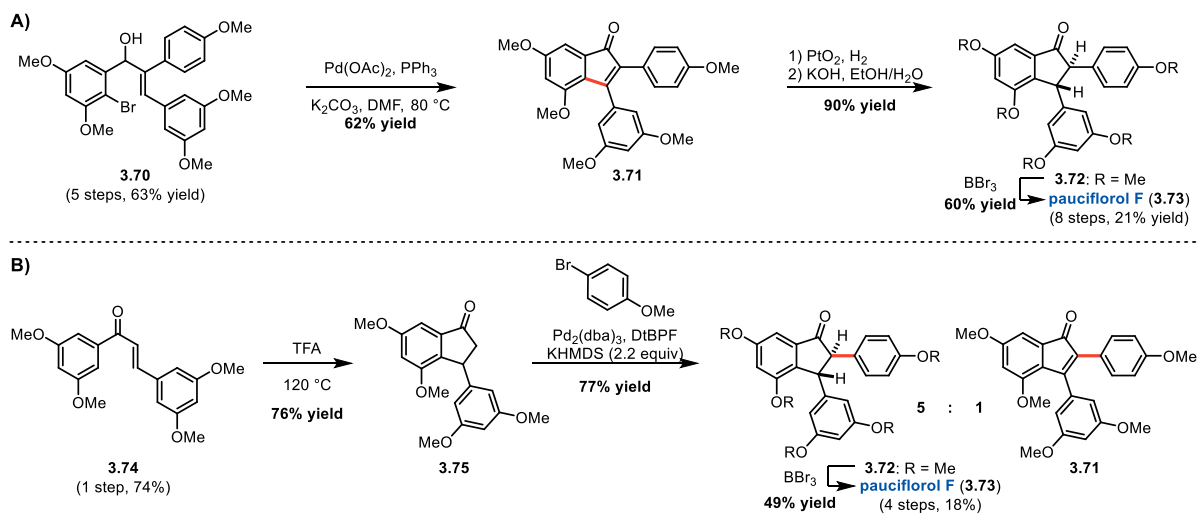


Figure 3.13. Various approaches to diarylindanones utilizing palladium catalysis.

first example of this approach in 2006 (Figure 3.13A).¹⁹⁵ The authors prepared allylic alcohol **3.70** in 5 steps to arrive at their key step. They utilized a 5-*endo* Mizoruki-Heck cyclization reaction to couple the aryl bromide and the alkene and arrive at indenone **3.71**.^{196,197} It is important to notice that **3.71** is at a higher oxidation state than the starting material (**3.70**), suggesting that a Saegusa-Ito oxidation also occurs under these reaction conditions.¹⁹⁸ While it is likely that this result was undesired, the authors had no trouble reducing indenone **3.71** to the *cis*-2,3-dihydroindanone (not shown) prior to base-mediated epimerization to afford the desired *trans*-2,3-dihydroindanone **3.72**. Finally, as demonstrated by Snyder and others (*vide supra*), the methyl ether protecting groups were cleaved with BBr_3 to afford pauciflorol F (**3.73**) in 8 steps and 21% overall yield. Yang and co-workers improved upon this approach, at least in terms of synthetic step count, reporting a 4-step synthesis of **3.73** in 2011 (Figure 3.13B). They chose to start with α,β -unsaturated ketone **3.74**, which is available via aldol condensation in one step from the corresponding acetophenone and benzaldehyde precursors. Exposure to trifluoroacetic acid at elevated temperatures (120 °C) gave indanone **3.75**, arising from a Nazarov cyclization.^{199,200} The

authors next utilized an α -arylation reaction with 4-bromoanisole to arrive at the same *trans*-2,3-dihydroindanone intermediate (**3.72**).^{201,202} As observed previously, the Saegusa-Ito oxidation was also operative under these conditions, giving **3.71** as a minor product. Cleavage of the methyl ethers with BBr₃ proceeded in slightly diminished yield in their hands; nonetheless, pauciflorol F (**3.73**) was prepared in only four steps and 18% overall yield. Multiple groups have since followed this strategy for the preparation of this key indanone fragment.^{203–205} Heo and co-workers were able to improve upon the α -arylation strategy and eliminate **3.71** as a byproduct by utilizing a lower loading (1.1 equiv) of a weaker base (NaO^tBu). Furthermore, they employed baker's yeast to afford a conjugate reduction of **3.71** to access the first asymmetric synthesis of (+)-pauciflorol F (**3.73**).²⁰³ Flynn and co-workers also achieved asymmetric synthesis of each enantiomer of **3.73** by employing a chiral auxiliary during the Nazarov cyclization, and along the way they determined that Heo and co-workers had incorrectly assigned the configuration of their conjugate reduction product.²⁰⁵

While the indane moiety is a critical fragment for the synthesis of resveratrol oligomers, the most important 5-membered ring is undoubtedly the 2,3-diaryldihydrobenzofuran (DHB), as this is present in the vast majority of higher order oligomers isolated to date.⁴⁴ Additionally, a set of oxidized resveratrol oligomers have been observed in which the DHB has been oxidized to the 2,3-diarylbenzofuran. Kim and Choi reported a modular approach to these oxidized scaffolds in 2009 based on a palladium-mediated C–H arylation strategy (Figure 3.14).²⁰⁶ These researchers prepared α -phenoxy acetophenone **3.76** in three steps and subjected this material to cyclodehydration mediated by Bi(OTf)₃ to afford benzofuran **3.77**.²⁰⁷ Next, palladium catalysis was employed to prepare the key 2,3-diarylbenzofuran

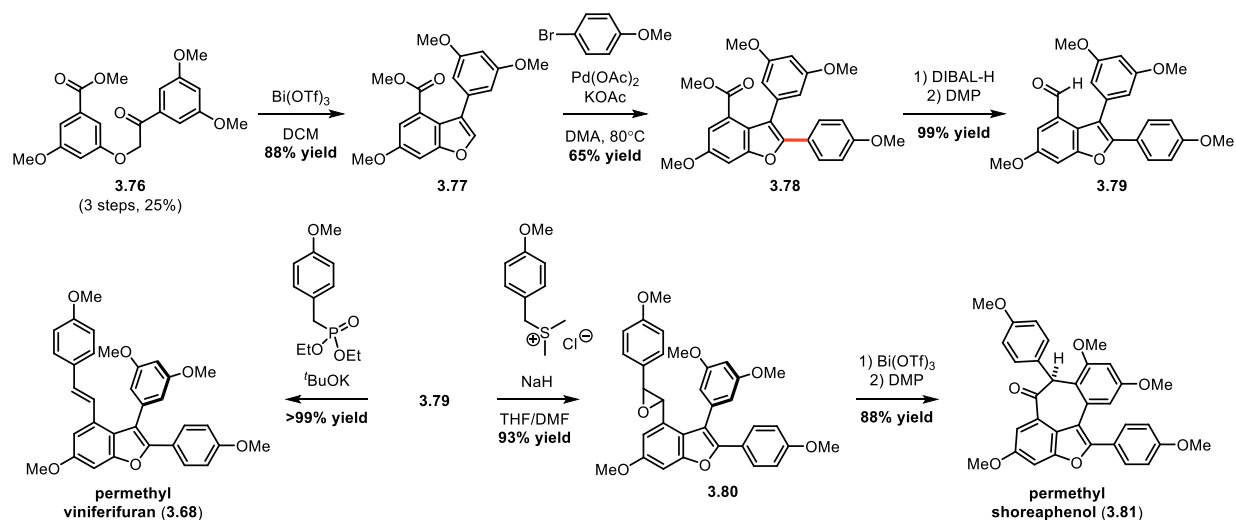


Figure 3.14. Kim and Choi's approach to 2,3-diarylbenzofurans using C–H activation.

moiety (**3.78**) through direct C–H activation.²⁰⁸ In this instance, after oxidative addition of the aryl halide, the reaction presumably proceeds through a concerted metalation-deprotonation (CMD) pathway with the potassium acetate base to afford C2-palladation of the benzofuran.²⁰⁹ Reductive elimination then gives the desired product (**3.79**) in modest yield. Importantly, the remaining mass balance results from two C–H activation events, giving the corresponding benzofuran dimer (not shown) while also generating the active Pd^0 -species. Incorporation of a sacrificial reductant, typically in the form of a phosphine ligand, serves to ameliorate this problem and improve the yield of the desired C–H arylation.²¹⁰ The authors next converted the ester in **3.78** to the aldehyde present in **3.79** by reduction with DIBAL-H to the intermediate benzyl alcohol (not shown) followed by oxidation with DMP. Intermediate **3.79** served as the diverging point for these synthetic efforts. In one direction (left, Figure 3.14), **3.79** was subjected to a Horner-Wadsworth-Emmons (HWE) reaction to deliver permethyl viniferifuran (**3.68**) in excellent yield.^{211–214} In the other direction (right, Figure 3.14), **3.79** was reacted under Johnson–Corey–Chaykovsky conditions with the requisite sulfonium ylide (generated *in situ*) to afford

racemic epoxide **3.80**. Lewis acid activation and cyclization followed by DMP oxidation gave permethyl shoreaphenol (**3.81**) in a manner consistent with the cationic quinone methide cyclization reactions described in the previous section (*vide supra*). In this instance, assisted ionization from the *para*-methoxy phenol presumably opens the activated epoxide to reveal an intermediate cationic quinone methide which is subsequently trapped by a Friedel-Crafts reaction with the adjacent resorcinol moiety. While these efforts from Kim and Choi did not yield natural products, they provided a critical platform for 2,3-diarylbenzofuran synthesis that has been subsequently utilized by multiple research groups.

In 2016, Elofsson and co-workers reported the racemic syntheses of ampelopsin B (**3.85**) and ϵ -viniferin (**3.1**).²¹⁵ Importantly, the cyclopropylmethyl (cPrMe) group was employed as a more labile alternative to the methyl ethers that have previously been used throughout the synthetic efforts in this class, and prior reports have indicated they can be cleaved simply with aqueous hydrochloric acid in methanol.²¹⁶ Starting from benzofuran **3.82**, which was prepared in an analogous manner to the approach utilized by Kim and Choi, the authors utilized C–H activation to arrive at 2,3-diarylbenzofuran **3.83**. The benzofuran was reduced to the *cis*-2,3-diaryldihydrobenzofuran, and the ester was converted to the aldehyde as reported by Kim and Choi to afford **3.84** in 75% yield over the three steps. An HWE reaction afforded the corresponding stilbene intermediate, and exposure of this material to aqueous hydrochloric acid at 80 °C afforded stilbene protonation and cationic quinone methide cyclization in addition to cPrMe cleavage to deliver ampelopsin B (**3.85**). Importantly, this reaction also proceeded with epimerization of the *cis*-2,3-diaryldihydrobenzofuran to the corresponding *trans* isomer, which is known to occur through assisted ionization from *para*- or *ortho*-substituted phenols to relieve the torsional

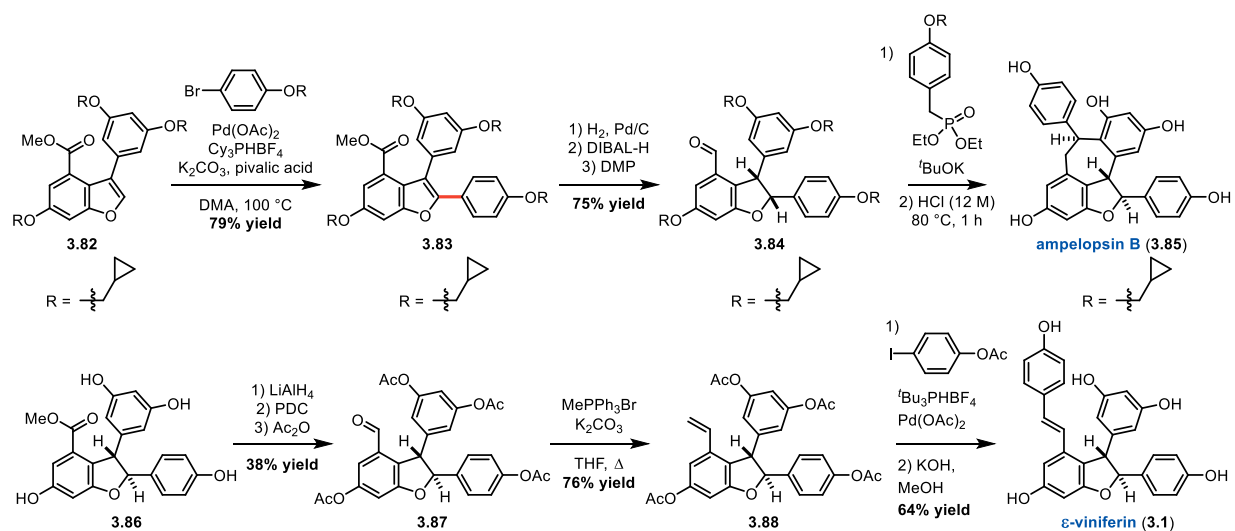


Figure 3.15. Elofsson's approach to ampelopsin B (**3.85**) and ϵ -viniferin (**3.1**).

strain of the syn-disposed aryl groups.²¹⁷ As a result, the authors recognized that they could also access ϵ -viniferin (**3.1**) through this strategy if they simply formed the *trans*-2,3-diaryldihydrobenzofuran sooner and utilized a protecting group that did not require acidic cleavage. Following reduction of **3.83**, the authors instead treated the product with aqueous hydrochloric acid at 100 °C to effect the desired DHB epimerization in addition to cPrMe cleavage to afford **3.86**. The ester moiety was converted to the corresponding aldehyde, again by complete reduction and re-oxidation, and the phenols were acetate-protected to access **3.87**. The authors next employed a Wittig reaction to access styrene **3.88**, and a Heck reaction afforded acetylated ϵ -viniferin, from which the desired natural product (**3.1**) was accessed via base-mediated ester hydrolysis. These efforts from Elofsson and co-workers demonstrate the utility of rapid benzofuran construction and subsequent functionalization to prepare the key DHB fragments in resveratrol oligomeric natural products.

In the same year, Yao and co-workers reported a similar racemic approach to ampelopsin F (**3.15**) relying upon **3.78** as a key intermediate (Figure 3.16).²¹⁸ These researchers employed a Kishi reduction to directly convert **3.78** to the *trans*-DHB followed by a two-

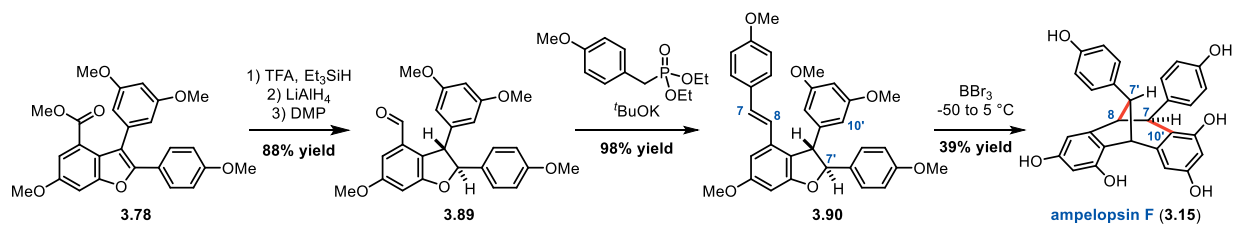
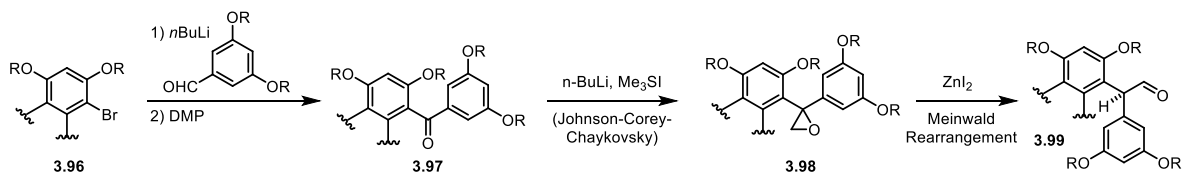


Figure 3.16. Yao's synthesis of ampelopsin F (**3.15**).

step protocol to convert the ester to an aldehyde to afford **3.89**. As demonstrated previously, an HWE reaction proceeds in excellent yield to deliver permethyl ϵ -viniferin (**3.90**). Finally, methyl ether cleavage with BBr_3 under careful temperature control afforded rearrangement to ampelopsin F (**3.15**) in 39% yield. The authors suggest that under the Lewis acidic conditions, assisted ionization from the *para*-substituted phenol helps to cleave the $\text{C}7'\text{-O}$ bond to reveal an intermediate quinone methide. This electrophile is trapped through a vinylogous Friedel-Crafts reaction to form the $\text{C}8\text{-C}7'$ bond while also revealing a second quinone methide. Friedel Crafts attack by the resorcinol moiety affords the $\text{C}7\text{-C}10'$ bond to complete the cationic rearrangement to deliver **3.15**.

Shaw and co-workers reported the first asymmetric approach to the key DHB fragment in 2014 using a different strategy.²¹⁹ These researchers prepared benzophenone **3.91** in 5 steps prior to conversion to the hydrazone (**3.92**) under standard conditions. Oxidation of **3.92** with MnO_2 afforded the corresponding diazo compound, which was directly treated with $\text{Rh}_2(\text{S-PTAD})_4$ to deliver the *cis*-DHB product **3.93** in 90% yield in good diastereo- and enantioselectivity (>95:5 *dr*, 93:7 *er*). This reaction proceeds through intramolecular C–H insertion of the *in situ*-generated rhodium-carbenoid to the methylene of the *para*-methoxybenzyl ether moiety. While this reaction preferentially generates the *cis*-DHB, it is well established that these rings can be epimerized under both acidic and alkaline conditions when substituted with a phenol derivative at the 2-position.^{217,220} As a result,

A. Homologation Sequence



B. Dihydrobenzofuran (DHB) Synthesis

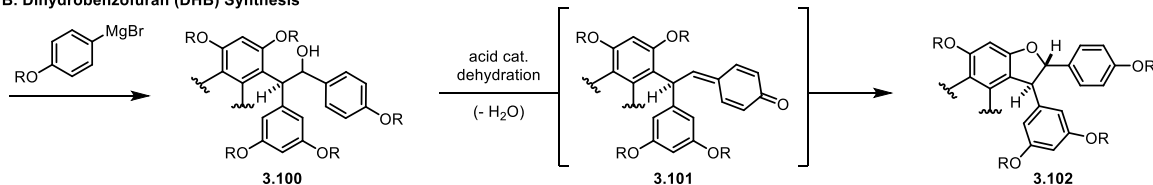


Figure 3.18. Snyder's approach to DHB rings relying upon homologation and cyclization from aryl bromides.

Chaykovsky reaction converts **3.97** to the benzylic epoxide (**3.98**),^{185,186} and a Meinwald rearrangement mediated by ZnI_2 enables a 1,2-hydride shift to give the corresponding benzaldehyde **3.99**.¹⁹¹ The DHB synthesis sequence commences with Grignard addition of a *para*-substituted phenolic aryl magnesium bromide to **3.99** to afford benzyl alcohol **3.100**. The Snyder group finally employs dehydration conditions to eliminate water through assisted ionization from the adjacent phenol to reveal quinone methide intermediate **3.101**, and a 5-*exo-trig* cyclization of the adjacent resorcinol oxygen delivers exclusively the *trans*-isomer of the 2,3-diaryldihydrobenzofuran ring (**3.102**). While it is not depicted in Figure 3.18, this sequence typically also involves a swap in protecting groups from methyl ethers to the more labile benzyl ethers prior to the preparation of epoxide **3.98** as well as global deprotection of **3.100** prior to the dehydration reaction. Most importantly, the overall sequence is racemic. If the stereocenter that is set during the Meinwald rearrangement could be done so in an asymmetric fashion, that would provide the platform for enantioselective preparation of **3.102** using this strategy. Unfortunately, this remains an outstanding challenge that has not been solved. Regardless, as the next section describes, Snyder and

co-workers have leveraged this general approach, in addition to some variations on this theme, for the synthesis of the DHB fragments found in higher order resveratrol oligomers.

3.3.3 Synthesis of higher-order resveratrol oligomers

As described in Section 3.3.1, Snyder's synthesis of ampelopsin F (**3.15**) and pallidol (**1.153**) relied upon stilbene bromination to reveal an intermediate quinone methide for the final cyclization.¹⁷¹ This reaction proceeded with concomitant bromination of both resorcinol rings in each natural product scaffold, requiring hydrodehalogenation for successful dimer syntheses (Figure 3.7 and Figure 3.8). While the arene bromination and hydrodehalogenation may be viewed as a wasteful set of operations for those efforts, the information gleaned about the reactivity of these core dimeric scaffolds proved critical for the synthesis of higher order oligomers, a feat that only the Snyder group had accomplished prior to our own efforts in the Stephenson group.^{44,48} Importantly, the [3.3.0] and [3.2.1] bicyclooctane cores are conserved across higher order oligomers (Figure 3.19); thus, Snyder and co-workers recognized that selective arene halogenation provides a critical functional handle for DHB synthesis to construct resveratrol trimers and tetramers in a modular fashion (*vide supra*, Figure 3.18).²²¹ For example, Snyder and co-workers found that [3.2.1] bicyclooctane **3.103**, the penultimate intermediate in the synthesis of ampelopsin F (**3.15**), undergoes regioselective bromination at C10a in the presence of 1 equivalent of NBS, delivering aryl halide **3.104** in 95% yield. The authors next leveraged their homologation sequence (Figure 3.18A) to arrive at aldehyde **3.105**, where the methyl ethers have been exchanged for benzyl ethers as the phenol protecting groups. Finally, the DHB synthesis sequence (Figure 3.18B) was conducted to arrive at carasiphenol B (**3.106**) in 3% overall yield across 20 steps (Figure 3.19). The authors found that bromination of

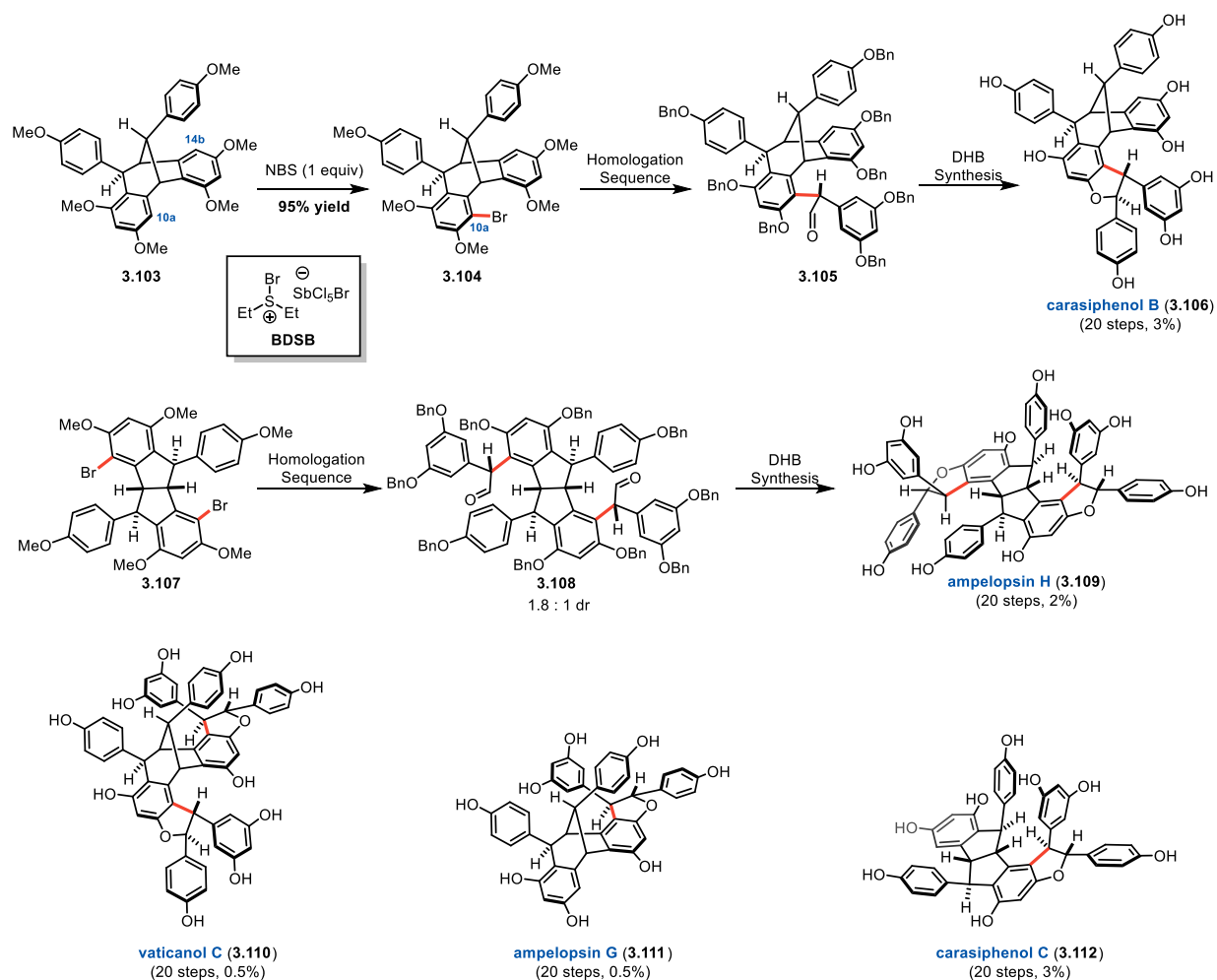


Figure 3.19. Snyder's modular approach to resveratrol trimers and tetramers.

3.103 with an excess of NBS afforded functionalization at both C10a and C14b, and the same homologation and DHB sequences delivered vaticanol C (**3.110**) in 0.5% yield over 20 steps. Finally, the authors were able to reverse the regioselectivity of bromination by employing one of their designer halogenation reagents (**BDSB**) in order to selectively functionalize C14b of **3.103**, leading to the synthesis of ampelopsin G (**3.111**). In a similar fashion, the dibrominated [3.3.0] bicyclic pallidol core **3.107** was converted to bis-aldehyde **3.108** through the Snyder homologation sequence, and DHB synthesis delivered ampelopsin H (**3.109**) in 2% yield over 20 steps. In addition, mono-bromination of **3.107** provided access carasiphenol C (**3.112**). This seminal publication from Snyder and co-

workers represents the first total synthesis of trimeric and tetrameric resveratrol oligomers and truly demonstrates the power of selective arene halogenation for the modular construction of these complex molecules.

The Snyder group followed up this impressive work with the synthesis of vaticanol A (**3.119**) in 2014 (Figure 3.20).²²² This trimeric resveratrol oligomer features a 7,5-fused indane ring system, and it is clear that the stereoselective construction of this core is the key to successful synthesis. Snyder and co-workers recognized that the indane fragment of this natural product has the same relative configuration as pauciflorol F (**3.73**), thus they chose to construct that fragment first using the cationic cyclization they had previously reported, arriving at **3.113** in 44% yield over 8 steps.¹⁷¹ They next utilized a six step sequence to prepare differentially protected, dibrominated ampelopsin D derivative **3.114**. First, a Tebbe olefination converted the ketone in **3.113** to the corresponding exocyclic olefin.²²³ Next, hydroboration-oxidation followed by DMP oxidation gave a primary aldehyde, which was subsequently reacted with the 4-benzyloxy aryl Grignard reagent, and subsequent dehydration with Burgess reagent afforded the protected ampelopsin D core (not shown).²²⁴ Finally, bis-bromination with NBS afforded **3.114** in 38% yield over the six steps. This material was next treated with an excess of *n*-butyl lithium to generate the dianion *in situ*, and reaction with resorcinol-derived benzaldehyde occurred at the more sterically accessible C10b. The intermediate benzyl alcohol was oxidized with DMP, and the benzyl ether at C4b was cleaved under standard hydrogenolysis conditions. The newly revealed C4b-phenol was oxidized with DDQ to reveal an intermediate quinone methide, which was subsequently attacked in a 7-*exo-trig* Friedel Crafts cyclization to afford the C10c–C7b bond of the 7,5-fused ring system. Unfortunately, this reaction afforded both

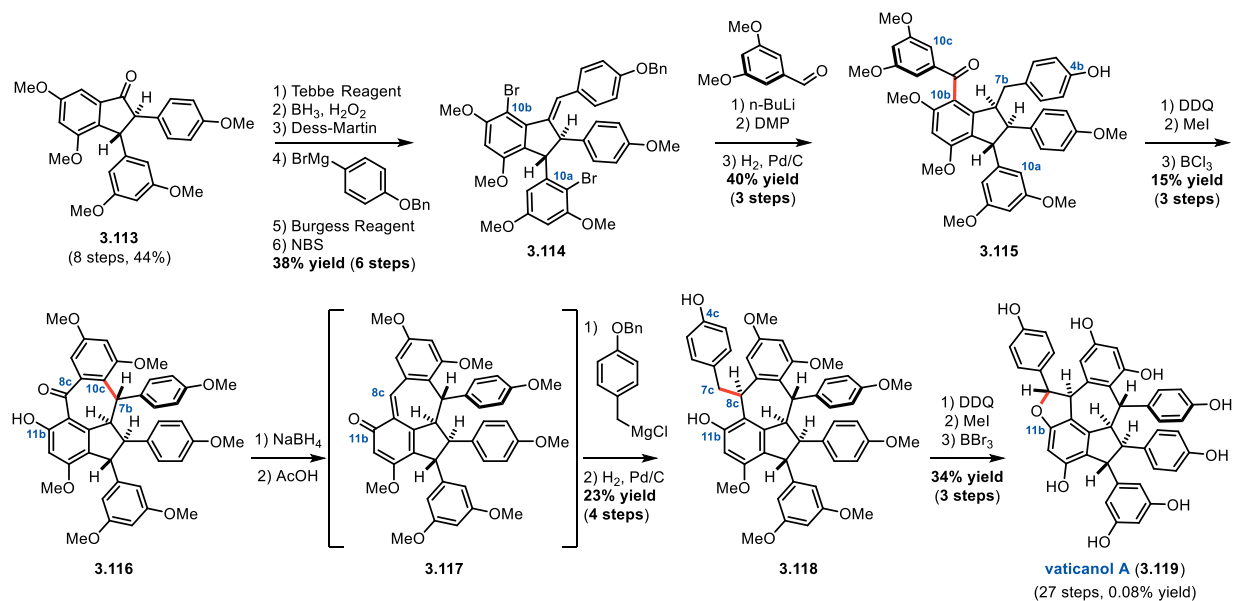


Figure 3.20. Snyder's synthesis of vaticanol A (3.119) harnessing three quinone methide cyclizations.

epimers at C7b in nearly equivalent yield, resulting in only 15% yield of the desired isomer **3.116** following C4b-OH methylation with iodomethane and C11b de-methylation with boron trichloride. Despite this this low yield, the C8c ketone of **3.116** was reduced, and the benzyl alcohol was eliminated through assisted ionization under acidic conditions to reveal an *ortho*-quinone methide (**3.117**). Snyder and co-workers commented that while **3.117** was reasonably stable and could be purified by column chromatography, it was advantageous from a practical standpoint to carry the material forward directly after workup to be reacted with 4-benzyloxy benzyl Grignard to form the C7c–C8c bond, and after hydrogenolysis of the C4c benzyl ether, intermediate **3.118** was accessed in 23% yield over the four steps. A second DDQ oxidation of the C4c phenol resulted in a quinone methide intermediate that was trapped by 5-*exo-trig* cyclization of C11b phenol to deliver the *trans*-DHB. At this point, the authors' attempts to deprotect the cyclization product were unsuccessful, presumably due to deleterious Lewis acid-mediated opening of the DHB ring leading to decomposition. However, Snyder and co-workers found that de-methylation with BBr_3

proceeded smoothly after simply re-protecting the C4c phenol, resulting in the first total synthesis of vaticanol A (**3.119**) in 0.08% yield over 27 steps. While the overall yield and step count does leave something to be desired, Snyder and co-workers again demonstrate the utility of *in situ* generated quinone methides for resveratrol oligomer synthesis.

The final contribution from the Snyder group in terms of *de novo* synthesis of higher order oligomers was their 2014 synthesis of caraphenol A (**3.131**).²²⁵ This resveratrol trimer contains a challenging strained 9-membered ring at the core, and, as a result, the prior strategy of building complexity from one of the prior dimeric precursors was not going to be possible in this case. Instead, Snyder and Wright turned to the tried and true homologation–DHB synthesis sequences to piece this molecule together in an impressive fashion. Starting from benzophenone **3.120**, which is available in 75% yield over three steps, the authors employed their classic homologation sequence followed by DHB synthesis to afford **3.121**. The benzyl alcohol moiety was oxidized twice, first with DMP, and second using a Pinnick-Lindgren oxidation, and the resulting carboxylic acid was alkylated with benzyl bromide **3.122** to afford ester **3.123** in 81% yield over the three steps. Lithium halogen exchange initiated an anionic Fries rearrangement, and silyl protection was conducted in the same pot to afford benzophenone **3.124**.^{226,227} The Snyder homologation sequence preceded Grignard addition and DMP oxidation to deliver ketone **3.125** as an inconsequential 1:1 mixture of diastereomers at C8b. The stereochemical information at C8b was subsequently destroyed upon MOM deprotection and condensation to deliver the C8b benzofuran, and TBAF was employed to cleave the silyl ether to deliver a separable mixture of atropisomers. Importantly, this mixture could be thermally equilibrated to give a 2.8:1 ratio in favor of the desired isomer (**3.127**). The benzyl alcohol

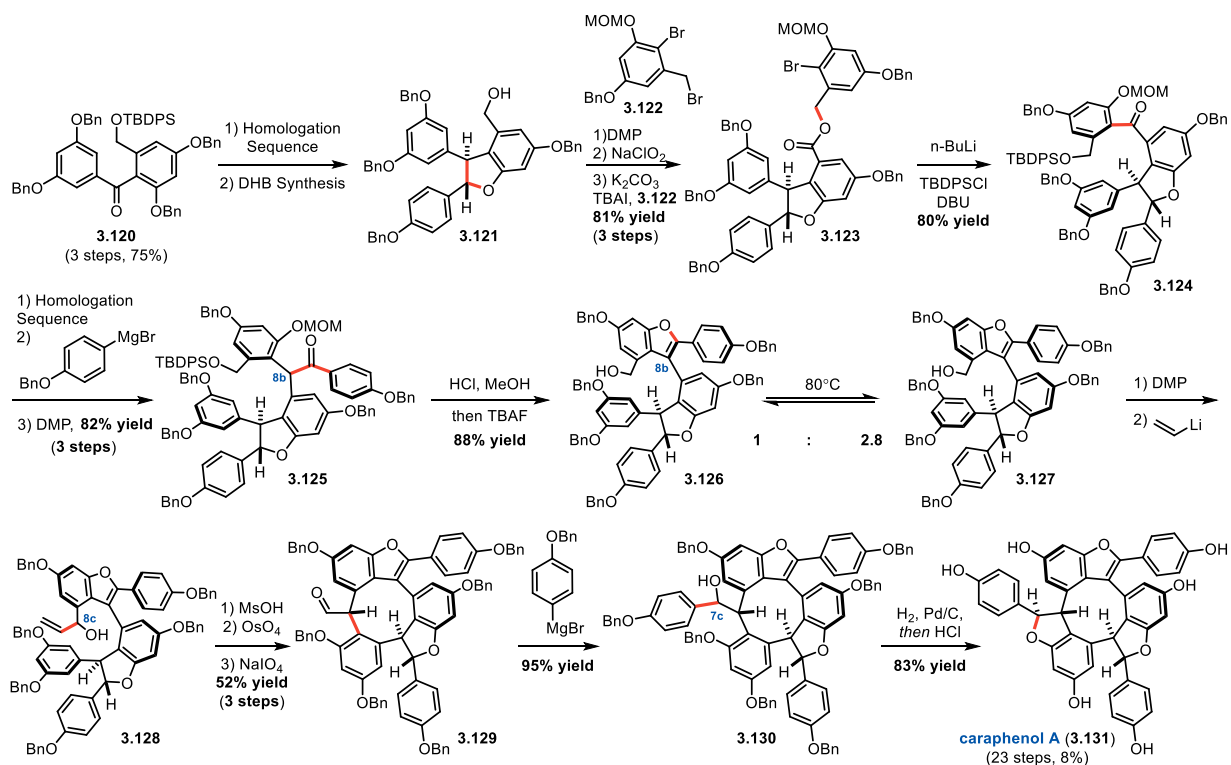


Figure 3.21. Snyder and Wright's synthesis of caraphenol A (3.131).

was next oxidized with DMP and treated with vinyl lithium to afford the C8c allylic alcohol (**3.128**). Friedel-Crafts cyclization proceeded under acidic conditions to close the 9-membered ring, and the alkene was subjected to Johnson–Lemieux oxidation conditions to access **3.129**.²²⁸ Grignard addition to the aldehyde proceeded smoothly to deliver the C7c benzyl alcohol (**3.130**). Finally, after hydrogenolysis of the benzyl ethers under standard conditions, dehydration of the benzyl alcohol via assisted ionization revealed an intermediate quinone methide, and 5-*exo-trig* phenol cyclization delivered the remaining DHB to complete the synthesis of caraphenol A (**3.131**) in 8% yield over 23 steps. Remarkably, Snyder and Wright demonstrated that this route is quite robust, as they were able to prepare greater than 600 mg of **3.131** at the time of publication of this report. Overall, the Snyder group has contributed multiple beautiful approaches to the synthesis of resveratrol oligomers, significantly enhancing the strategic approaches in this field.

3.4 Discovery of a C8–C8' to C3–C8' homolytic bond migration

While the Snyder group has provided a clear blueprint for the *de novo* synthesis of higher order resveratrol oligomers, one of the significant drawbacks to their approach is the overall step count required for trimer and tetramer synthesis. Their key homologation–DHB synthesis sequences are unquestionably powerful, yet they require, at minimum, six synthetic manipulations (eight if phenol protecting group exchange is also necessary) to construct what amounts to a single resveratrol unit. Recognizing this limitation, we postulated that our discovery of the persistent radical equilibrium between **1.151** and **1.156** (see Figure 1.19 in Section 1.5.2) might hold the key for iterative oligomerization in a biomimetic fashion. Previously, the bond dissociation enthalpy for the C8–C8' bond in **1.151** was determined to be 17.0 (± 0.7) kcal/mol following the method reported by Scaiano and co-workers.²²⁹ In this protocol, a combination of the Beer-Lambert law²³⁰ and the van't Hoff equation²³¹ afford an inverse relationship between the absorbance of the persistent

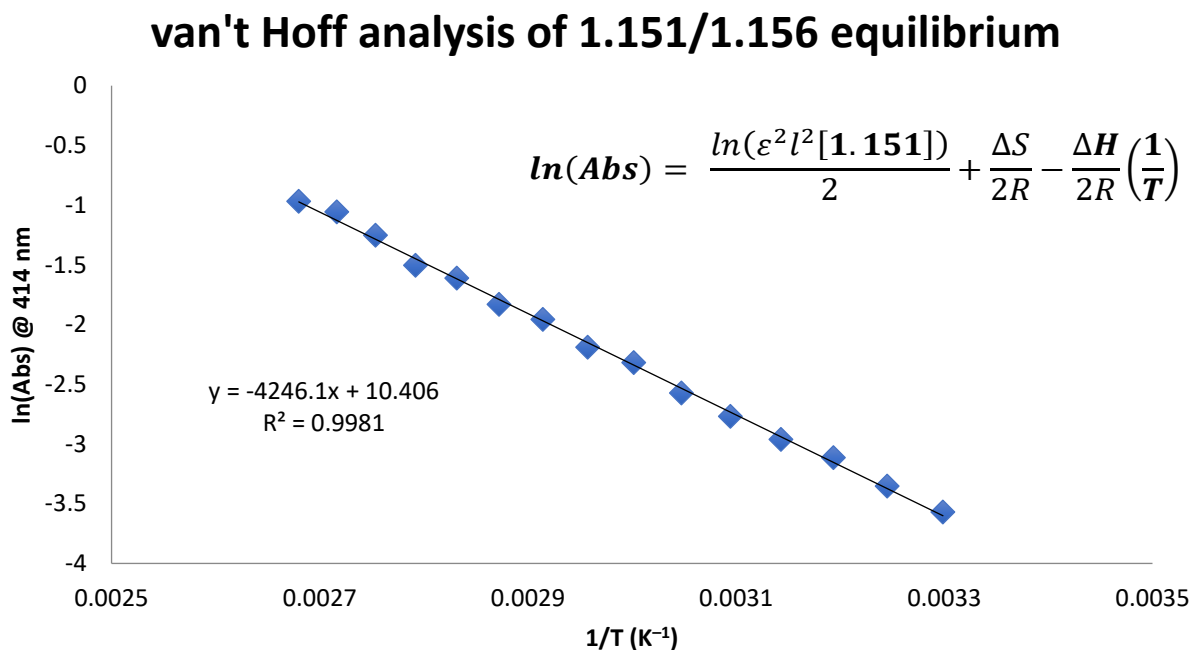
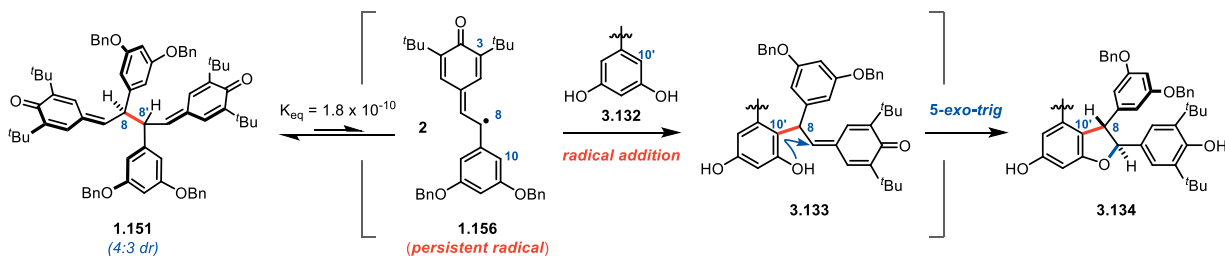


Figure 3.22. van't Hoff analysis of the 1.151/1.156 equilibrium reveals the C8–C8' bond dissociation enthalpy & suggests 1.156 is persistent at elevated temperatures.

radical, measured by UV-vis spectroscopy, and the temperature of the UV-vis acquisition. As is standard for endothermic processes, this affords a van't Hoff plot with a negative slope from which the bond dissociation enthalpy can be derived (Figure 3.22). Importantly, linearity was maintained at all temperatures evaluated, corresponding to a fully reversible equilibrium and suggesting that **1.156** is still persistent at elevated temperatures.

Based on the physical organic studies of this equilibrium, the mechanistic hypothesis for leveraging **1.156** for DHB synthesis was simple (Figure 3.23A). Thermal homolysis of **1.151** would favor formation of the persistent radical **1.156**, and, in the presence of a substituted resorcinol (**3.132**), subsequent radical addition would form the C8–C10' bond exhibited in intermediate **3.133**. Finally, a 5-*exo-trig* cyclization of the phenol onto the quinone methide would forge the C8–C10' DHB in a single transformation. To evaluate this hypothesis, *t*Bu-dihydro-resveratrol **3.135** was prepared from **1.150** under standard conditions for hydrogenation/hydrogenolysis (H₂, Pd/C). A reaction mixture containing quinone methide dimer **1.151** and 2 equivalents of **3.135** was heated in acetone in a pressure

A) Mechanistic Hypothesis for Radical DHB Synthesis:



B) Proof of concept for Radical DHB Synthesis:

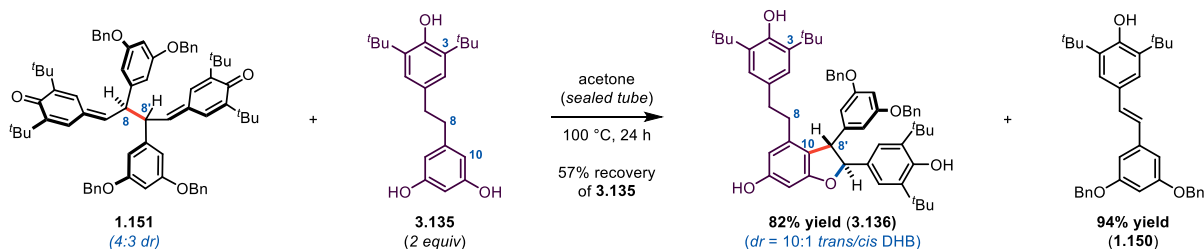


Figure 3.23. Development of a radical DHB synthesis protocol.

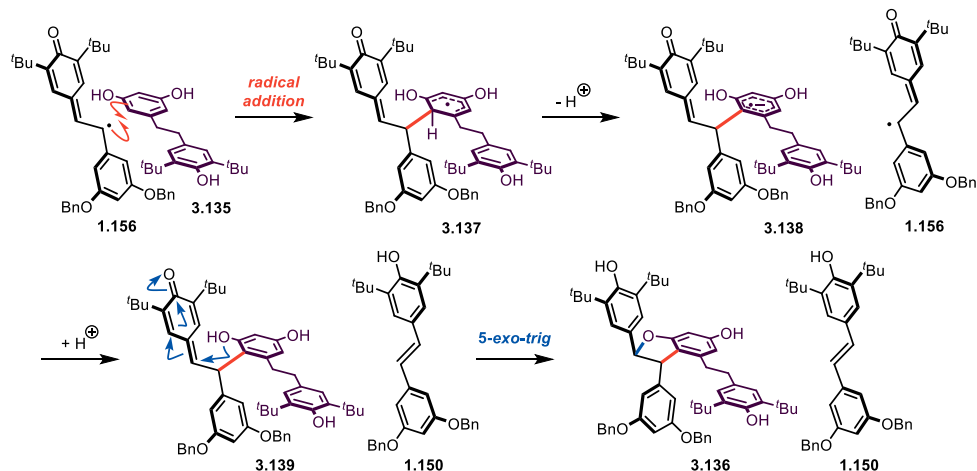


Figure 3.24. Proposed mechanism for radical DHB synthesis.

tube at 100 °C (Figure 3.23B). After 24 hours, full consumption of **1.151** was observed, and after chromatographic purification, ^tBu-dihydro- ϵ -viniferin (**3.136**) was isolated in 82% yield as a 10:1 mixture of DHB isomers, favoring the *trans*-configuration. In addition, the reaction yielded nearly a full equivalent of **1.150** as well as 57% recovery of unreacted **3.135**. These observations inspired the mechanistic proposal given in Figure 3.24. After C8–C8' homolysis of **1.151** gives two equivalents of **1.156**, the persistent radical **1.156** undergoes addition to the resorcinol (**3.135**) to give the C8–C10' bond in **3.137** (highlighted in red). Studer and Curran have reported that cyclohexadienyl radicals such as **3.137** are quite acidic and are rapidly deprotonated to the corresponding radical anion, such as **3.138**.²³² The isolation of **1.150** the end of the reaction is formally a reduction of **1.151**, and it is proposed that the second equivalent of **1.156** arising from C8–C8' homolysis serves as a mild oxidant and proton sponge to rearomatize **3.138** and form **3.139**. Finally, a 5-*exo-trig* cyclization (blue arrows) of the resorcinol onto the quinone methide (and corresponding proton transfer) delivers DHB **3.136** in addition to **1.150**. The discovery that persistent radical **1.156** can deliver the dimeric species **3.136** is a unique contribution to the field given the rapid increase in complexity; the application of this reactivity in the

synthesis of higher-order oligomers represents a challenging proving ground for demonstrating the utility and chemoselectivity achievable with persistent radicals. In principle, biomimetic synthesis of ϵ -viniferin (**3.1**) could be achieved with this strategy by simply oxidizing **3.136** to the corresponding stilbene and removing the *tert*-butyl groups. That second, and most critical, operation has thus far proven to be an insurmountable challenge,⁴⁸ and our group recently evaluated alternative C3-substituents, finding that C3-silyl substituents enabled the synthesis of nepalensinol B (**1.161**) and vateriaphenol C (**1.162**) (see Figure 1.20 in Section 1.5.2).

Therefore, we questioned whether a similar transition from *tert*-butyl to silyl groups at C3 would enable radical DHB synthesis and more facile entry to higher order oligomers. The evaluation of this hypothesis began by conducting the same van't Hoff analysis (Figure 3.25) on the equilibrium between quinone methide dimer **2.69c** and the corresponding persistent radical **3.140** (Figure 3.26). It was determined from the lower temperature

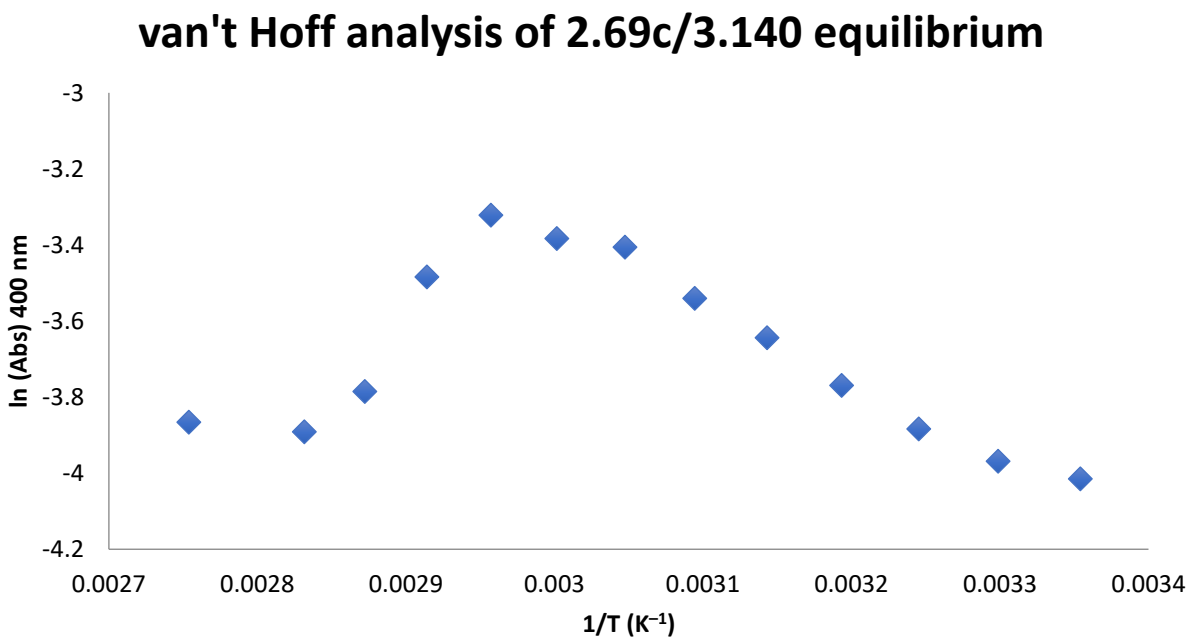


Figure 3.25. van't Hoff analysis of the **2.69c/3.140** equilibrium shows irreversibility at elevated temperatures.

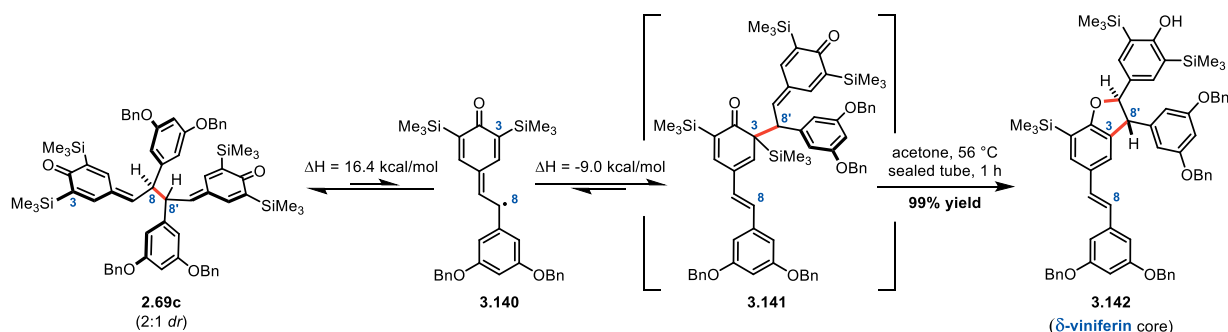


Figure 3.26. Homolysis of the C8–C8' bond of 2.69c at elevated temperature results in homolytic bond migration to the C3–C8' bond.

acquisitions that the C8–C8' bond dissociation enthalpy is 16.4 (\pm 0.5) kcal/mol; however, inspection of the van't Hoff plot beyond 50 °C shows that the **2.69c/3.140** equilibrium does not maintain reversibility at elevated temperature. Laser flash photolysis demonstrated that the recombination rate for **3.140** was an order of magnitude faster than for **1.156**, further supporting that **3.140** is not as persistent as **1.156**.⁴⁸ The predominant decay pathway for **3.140** occurs through the formation of the C3–C8' adduct (**3.141**), which subsequently loses the C3-silyl group to rearomatize the phenol, and cyclization onto the quinone methide affords the C3–C8' DHB found in δ -viniferin (**3.5**). Remarkably, the C8–C8' to C3–C8' homolytic bond migration and subsequent cyclization to **3.142** occurs in nearly quantitative yield after simply heating **2.69c** in degassed acetone at 56 °C for 1 hour (Figure 3.26).

Computations conducted by collaborators in the Pratt group suggest that the C3–C8' dimer **3.141** is 4.2 kcal/mol higher in free energy than the C8–C8' dimer **2.69c** (Figure 3.27). However, the simple fact that **3.140** is in equilibrium with **2.69c** implies that it is also in equilibrium with the C3–C8' dimer **3.141** ($\Delta\Delta H = 7.4$ kcal/mol). Presumably, **3.141** is not observed due to its rapid decomposition to the δ -viniferin core (**3.142**). Computations incorporating a SMD solvent model parameterized for acetone suggests a barrier of 21.7 kcal/mol for the unimolecular expulsion of the TMS cation, implying that this reaction cannot compete with C3–C8' bond homolysis and return to the C8–C8' dimer. As a result,

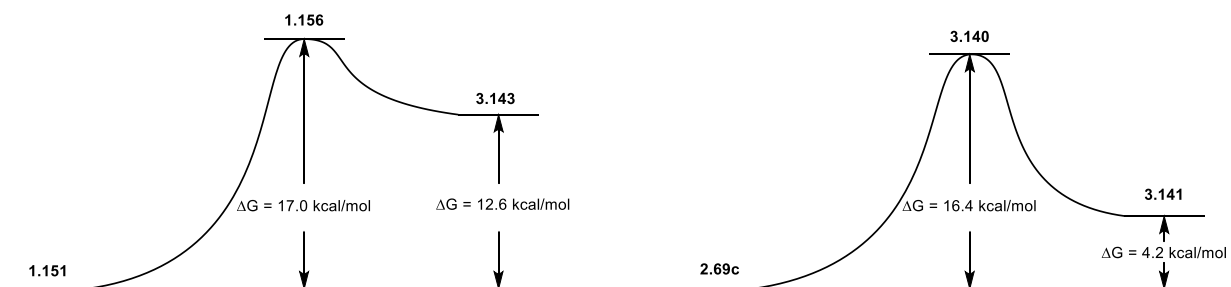
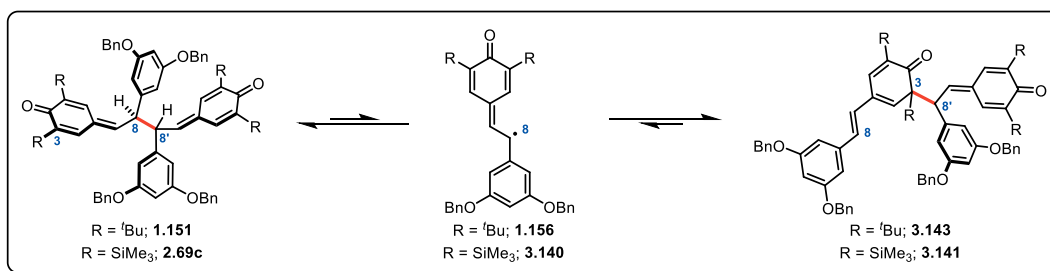


Figure 3.27. Computational investigations of the C8–C8' to C3–C8' homolytic bond migration reveal a clear C3-substituent effect on the free energy of the reaction.

it is likely that adventitious water in the acetone promotes desilylation and concomitant aromatization. Unfortunately, efforts to effect the intermolecular radical C8–C10' DHB synthesis reaction with **2.69c** (the analogous reaction to that depicted in Figure 3.23) were unsuccessful, as even in the presence of a significant excess of exogenous resorcinol, only the C3–C8' DHB product was observed.

While the difference in free energy between **2.69c** and **3.141** is computed to be only 4.2 kcal/mol, the free energy difference of the corresponding *tert*-butylated dimers is 12.6 kcal/mol, the free energy difference of the corresponding *tert*-butylated dimers is 12.6 kcal/mol – consistent with the observed fully reversible equilibrium between the C8–C8' dimer (**1.151**) and the persistent phenoxyl radical(s) derived therefrom (**1.156**) (Figure 3.27). In contrast, the C3–C8' and C8–C8' dimers which lack ortho substitution are computed to be 3.6 kcal/mol apart and therefore are funneled toward the δ -viniferin core. These computations are consistent with the hypothesis that resveratrol oligomerization relies upon equilibration of the C8–C8' and C3–C8' constitutional isomers,⁴⁴ and, in the absence of enzymatic influence, the inherent preference for the C3–C8' product is clear. As

discussed in Section 3.2, numerous research groups have realized the direct conversion of resveratrol (**2.78**) to δ -viniferin (**3.5**) using single electron oxidation strategies (Table 3.1), with Sako's semisynthesis of vitisin B (**3.10**) being the only example of targeted synthesis of a C3–C8' higher order resveratrol oligomer.¹⁵⁸ While Sako's efforts are certainly admirable, they are limited by the requirement that enantiomerically pure ϵ -viniferin (**3.1**) be isolated from natural sources as the synthetic starting material, severely limiting the feasibility of a scalable and sustainable approach to the C3–C8' resveratrol tetramers. Thus, it was hypothesized that the newly discovered C8–C8' to C3–C8' homolytic bond migration could be leveraged as a key step for the synthesis of the vitisin tetramers A–D, which all share the key C3–C8' bond.

3.5 Synthesis of vitisin A & D

The vitisin tetramers arise from the oxidative dimerization of (+)- ϵ -viniferin (**3.1**), which undergoes coupling between C3c and C8b to access **3.144** – the key biosynthetic intermediate for this subset of the natural product class (Figure 3.28).⁴⁴ The quinone methide present in **3.144** can undergo multiple distinct cyclization reactions to arise at the different tetramers. A 5-*exo-trig* cyclization of the adjacent C4c phenol onto the quinone methide can give one of two compounds exhibiting the C3c–C8b dihydrobenzofuran ring. If cyclization gives the *trans*-DHB, vitisin B (**3.10**) is formed. Instead, formation of the *cis*-DHB delivers vitisin C (**3.145**). In addition, a 7-*exo-trig* cyclization from C10a of the pendant resorcinol on to the quinone methide forms the C10a–C7b bond (highlighted in orange, Figure 3.28) embedded in the dibenzocycloheptane of vitisin A (**3.146**). The final tetramer in this subset of the natural product class, vitisin D (**3.148**), comes from a second cyclization of vitisin A. Protonation of the C7c–C8c stilbene generates an intermediate

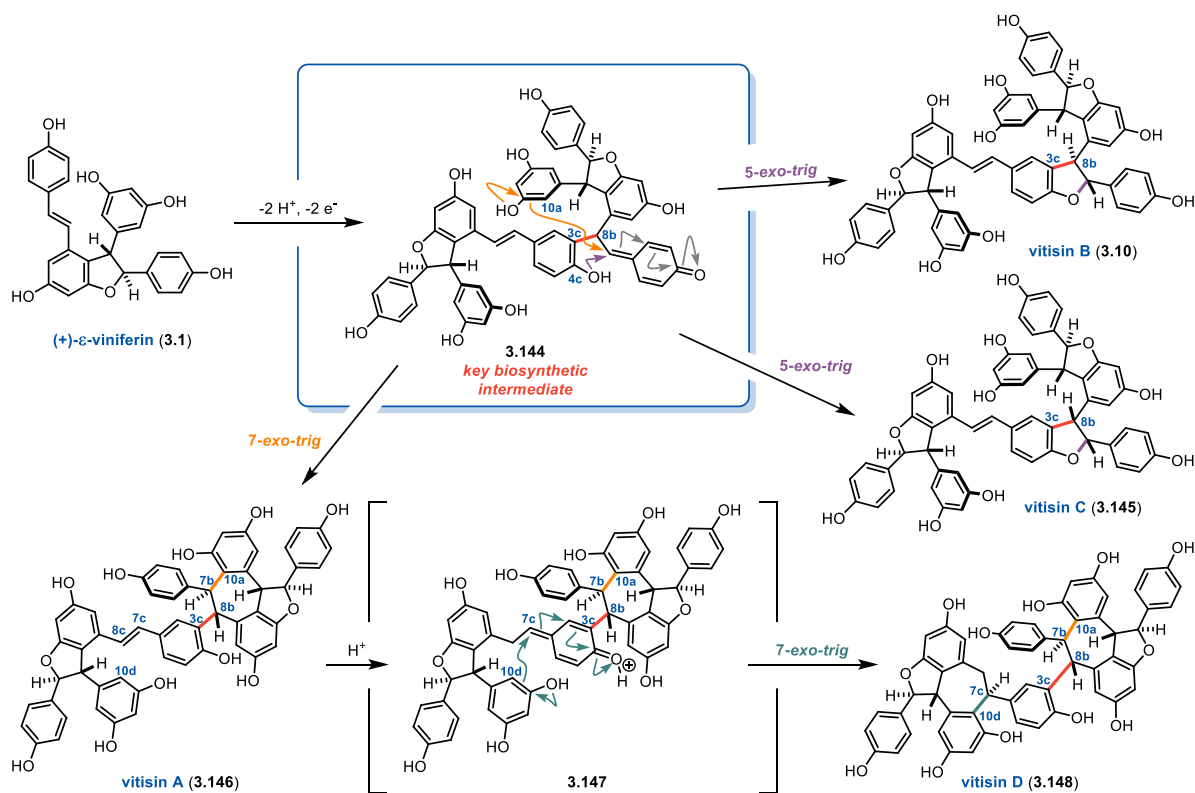


Figure 3.28. Proposed biosynthesis of the C3–C8' resveratrol tetramers.

cationic quinone methide (**3.147**), and *7-exo-trig* cyclization gives the C10d–C7c bond (highlighted in green, Figure 3.28) to form a second dibenzocycloheptane. Studies on the biogenesis of these compounds using isolated material have supported the proposed biosynthesis depicted in Figure 3.28 by establishing that vitisin B (**3.10**) can be converted, presumably through the intermediacy of **3.144**, to vitisin A (**3.146**) under moderately acidic conditions; furthermore **3.146** can subsequently be converted to vitisin D (**3.148**) under acidic conditions at elevated temperature.²³³ Given the shared biosynthesis and supporting literature precedent, we envisioned harnessing the C8–C8' to C3–C8' homolytic bond migration to access an intermediate analogous to **3.144**. Importantly, **3.144** must arise from the coupling of matching ϵ -viniferin enantiomers, as the resulting natural products, vitisin A–D, all exhibit two equivalents of the same (+)- ϵ -viniferin (**3.1**) enantiomer. Thankfully,

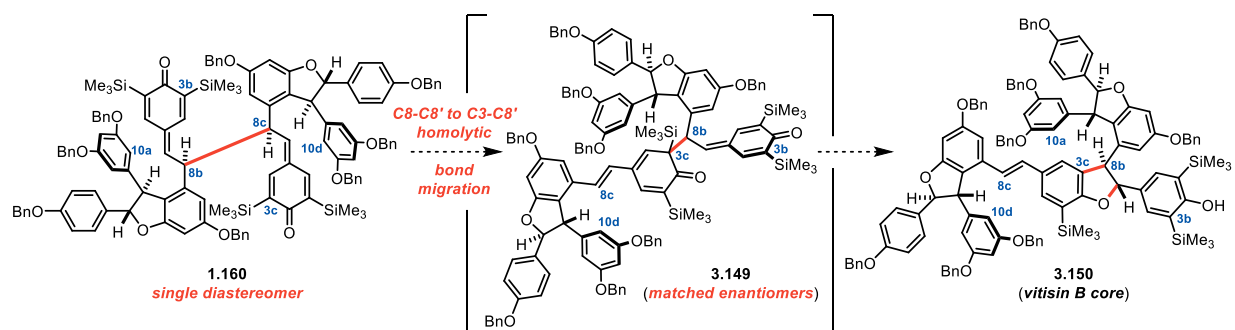


Figure 3.29. Synthetic hypothesis to access vitisin tetramers via a homolytic bond migration strategy.

this problem of dimerization selectivity had already been solved. In the synthesis of nepalensinol B (**1.161**) and vateriaphenol C (**1.162**), as described in Section 1.5.2, the dimerization of a racemic ϵ -viniferin analogue (**1.159**) gave rise to the corresponding bis-quinone methide tetrameric species (**1.160**) as a single diastereomer (Figure 3.29). While the configuration of **1.160** was assigned by analogy to the cyclization products upon treatment with Lewis acid, it is clear that **1.160** results from the coupling of the same ϵ -viniferin enantiomer, as both **1.161** and **1.162** contain two matched enantiomers.⁴⁸ Therefore, the synthetic hypothesis to access the vitisin tetramers was simple – homolytic bond migration of **1.160** would break the C8–C8' bond and deliver the C3–C8' bond between two matched enantiomers of ϵ -viniferin analogs, proceeding through intermediate **3.149**, which is analogous to the key biosynthetic intermediate **3.144**, to deliver vitisin B core **3.150** (Figure 3.29). From there, the corresponding deprotections and/or acid mediated cyclization(s) (Figure 3.28) would deliver the natural products.

This synthetic hypothesis was put forth by my rotation mentor, Dr. Mitch Keylor, in the final weeks of his PhD studies, and, after completing the syntheses of nepalensinol B (**1.161**) and vateriaphenol C (**1.162**), he demonstrated that **1.160** was indeed capable of undergoing homolytic bond migration upon heating in acetone at 56 °C for one hour in ~60% yield to afford **3.150** as an intractable mixture of isomers. Upon Mitch's departure,

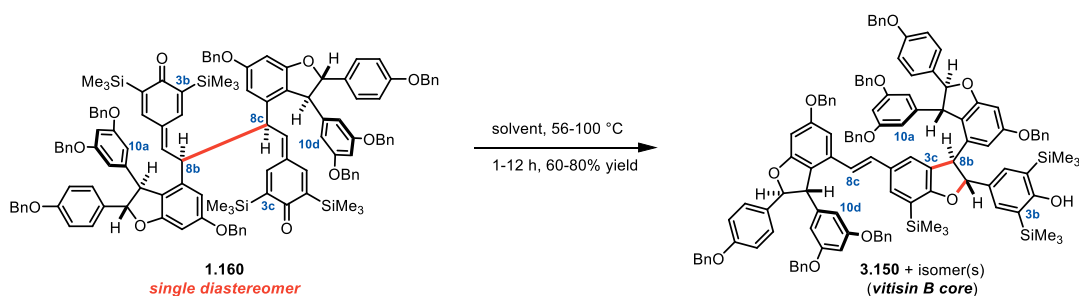
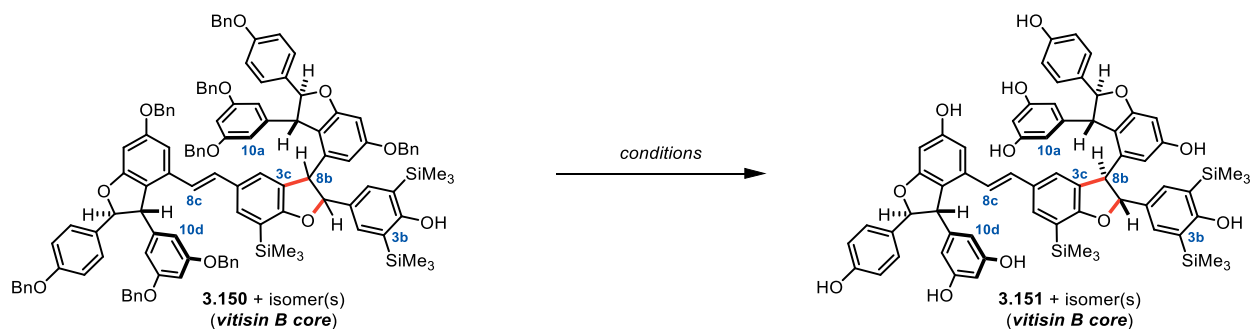


Figure 3.30. Initial studies of the homolytic bond migration targeting the vitisins.

these efforts were spearheaded by Dr. Xu Zhu, a postdoctoral researcher who spent ~4 months in the Stephenson group. Xu examined a range of solvents and temperatures to find that the desired reaction proceeded in 60-80% yield (Figure 3.30). Importantly, we determined that sparging with Ar for ~5 min prior to the reaction was critical to eliminate the formation of **1.159** as a minor side product arising from disproportionation of **1.160**. The issue of isomer separation and characterization of **3.150** remained; however, it was theorized that separation of the diastereomers might occur after benzyl deprotection. Incomplete deprotection would result in challenging mixtures of products, so the deprotection efforts commenced with rather forcing conditions, a summary of which is given in Table 3.5. While it was recognized that debenzylation would be challenging in the presence of the C7c–C8c stilbene, standard hydrogenolysis conditions were first investigated (Entry 1). Unsurprisingly, undesired stilbene reduction was observed. Promoting hydrogenolysis over hydrogenation via transfer hydrogenation catalysis was also investigated, however the desired hydrogenolysis was not observed under reported conditions (Entry 2). Nucleophilic displacement of the benzyl ethers was another strategy that proved not to be viable (Entry 3) despite Porco's recent success with this approach for polyphenol natural product synthesis.²³⁴ Lewis-acid mediated debenzylation was utilized for the deprotection of quadrangularin A,⁴⁵ and these conditions were evaluated for the

Table 3.5. Unsuccessful attempts at debenzoylation of 3.150

Entry	Conditions	Results
1	H ₂ , Pd/C, EtOAc/MeOH (1:1)	Full debenzoylation, stilbene reduction
2	1,4-cyclohexadiene, Pd/C, EtOH, temp.	No conversion
3	Sodium ethanethiolate, DMF, heat	Decomposition of DHB rings
4	BCl ₃ , Me ₅ -benzene, CH ₂ Cl ₂	Decomposition of DHB rings

deprotection of the vitisin B scaffold. These efforts resulted in decomposition, presumably through Lewis-acid activation of the dihydrobenzofuran moieties. At this point, it was determined that a new phenol protecting group strategy was required. Chronologically, this realization coincided with the development of the electrochemical dimerization conditions described in Chapter 2, as well as Xu's departure from the group. We were excited by the possibility that these milder dimerization conditions might allow for a more labile phenol protecting group to be carried through the synthesis to facilitate final deprotections, and it had fallen to me to devise and execute such an approach.

Having exhausted the supply of **1.160**, more of the precursor ϵ -viniferin scaffold **1.159** required preparation in manner that would readily allow for late-stage phenol protecting group evaluation. Previously, Snyder's homologation-DHB synthesis sequence from their preparation of caraphenol A²²⁵ (**3.131**) had been leveraged to construct the southern fragment of **1.159**, as depicted in Figure 3.31. As discussed in Sections 3.3.2 and 3.3.3, this approach to the key 2,3-diaryldihydrobenzofuran is unquestionably powerful, but it requires a long sequence of synthetic manipulations. Snyder and co-workers sourced 3,5-

dibenzoyloxybenzylalcohol **3.155** as the starting material for this key fragment, but at ~\$20/g, our group recognized that a cheaper alternative would allow for a more economical synthesis. As such, benzyl protection of **3.152** (~17x cheaper than **3.155**) gives methyl ester **3.153** in excellent yield on scale. This material was hydrolyzed to the corresponding carboxylic acid with LiOH to give **3.154**, and it was also reduced to **3.155** under standard conditions. Alternatively, Snyder and co-workers prepared **3.154** from **3.155** via oxidation of the alcohol to the carboxylic acid.²²⁵ Regioselective bromination of **3.155** proceeded smoothly with NBS to afford **3.156**, and a Mitsunobu reaction²³⁵ between **3.156** and **3.154** delivered ester **3.157** in 87% yield. From this material, benzophenone **3.120** was prepared in a two-step, one-pot sequence involving an anionic Fries rearrangement^{226,227} followed by silyl protection of the liberated alkoxide. Snyder and co-workers reported that **3.157** was purified by recrystallization following the Mitsunobu reaction, and we also found that the purity of the starting material, in addition to careful temperature control, were critical for the successful conversion to **3.120**. Given the sensitivity of this reaction, each reagent required purification immediately prior to conducting the reaction to ensure reproducibility,

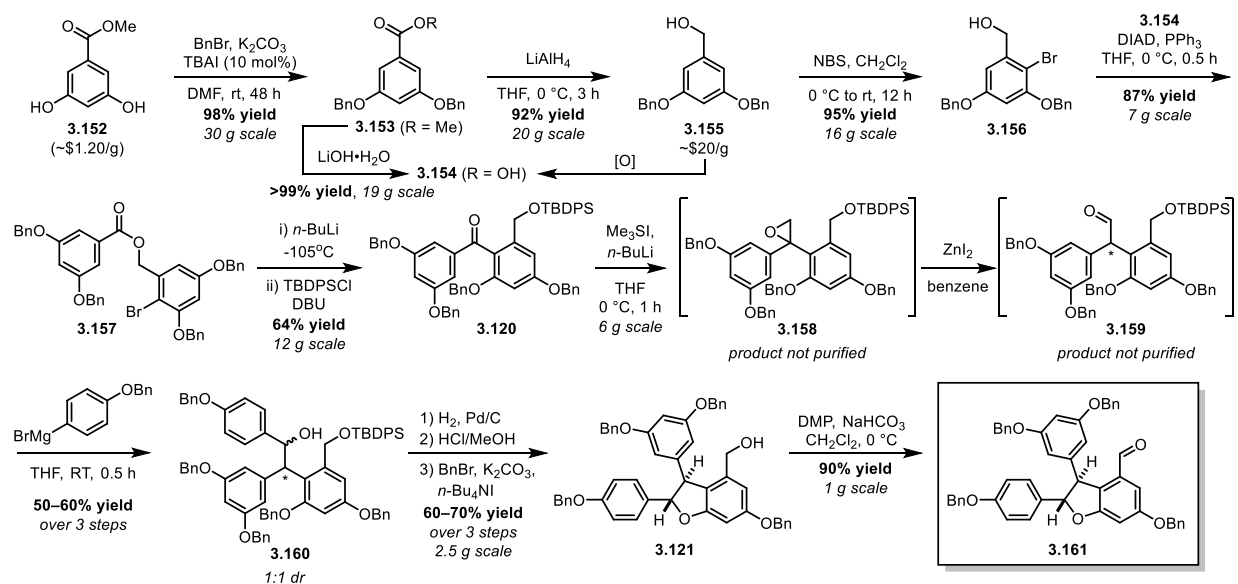


Figure 3.31. Snyder's homologation-DHB synthesis approach to access **3.161**.

significantly increasing the labor required to conduct this single step in the synthetic route. The following three steps, converting **3.120** to **3.160**, required telescoping without intermediate purification due to the instability of both epoxide **3.158** and aldehyde **3.159**, resulting in variable yields in our hands. The DHB was finally constructed after hydrogenolysis of the benzyl ethers in **3.160** and subsequent acid-catalyzed dehydration, and the phenols were re-protected to deliver benzyl alcohol **3.121**. Oxidation of **3.121** ultimately delivered the key aldehyde fragment **3.161** in a sequence the Snyder group counts as 8 steps, but, in reality, is 11 steps from **3.155** or 13 steps from **3.152**. The late-stage benzyl deprotection/reprotection was attractive in that it provided a point at which a diverse protection strategy could be quickly evaluated, but it seemed reasonable that a shorter route could more easily provide access to the **3.161** scaffold for protecting group evaluation.

The route to 2,3-diarylbenzofurans disclosed by Kim and Choi (discussed in Section 3.3.2) was the proposed solution to accessing **3.161** in fewer synthetic manipulations. It was envisioned that ester **3.162** would be the targeted precursor of the **3.161** scaffold, as it would simply require phenol protection and simple redox conversion of the ester to the aldehyde (Figure 3.32). From a retrosynthetic standpoint, **3.162** would arise from the corresponding benzofuran (**3.163**) after reduction, deprotection, and epimerization – all processes that could in principle occur in a single pot. As developed by Kim and Choi, **3.163** would be prepared by C–H arylation of benzofuran **3.164**, which in turn arises from

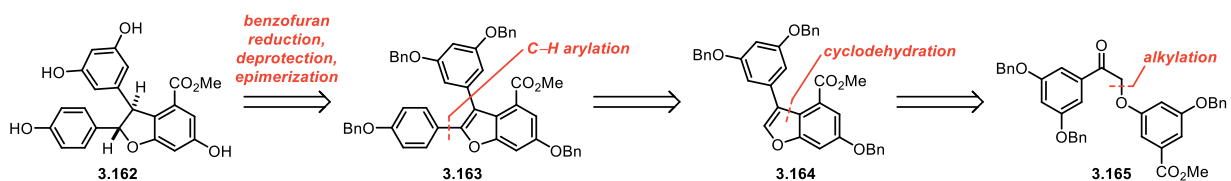


Figure 3.32. Retrosynthetic analysis for the synthesis of key DHB fragment 3.162.

cyclodehydration of **3.165**. Acetophenone **3.165** would be readily prepared from alkylation between two readily available fragments; thus, this approach to dihydrobenzofuran construction was viewed as superior to Snyder's longer sequence.

With the help of Racquel Edjoc, a very studious undergraduate from the University of Ottawa who completed a 4-month internship in the Stephenson group, the execution of this strategy commenced with the preparation of **3.165** (Figure 3.33). Benzyl protection of 3',5'-dihydroxyacetophenone (**3.166**) proceeded smoothly to deliver **3.167**, and subsequent α -bromination with copper (II) bromide afforded α -bromo-acetophenone **3.168** in 74% yield. This material was then combined with readily available **3.169** for alkylation to prepare **3.165** on multi-gram scale. Unfortunately, all acidic conditions that afforded conversion while investigating the cyclodehydration of **3.165** to access **3.164** coincided with acid-mediated benzyl deprotection. This was unsurprising in hindsight given the relative ease with which benzyl ethers have been cleaved under acidic conditions in prior syntheses,⁴⁵ so **3.165** was deprotected under standard hydrogenolysis conditions^b and re-protected to evaluate the desired cyclodehydration. Gratifyingly, TBPDS phenol protection was found

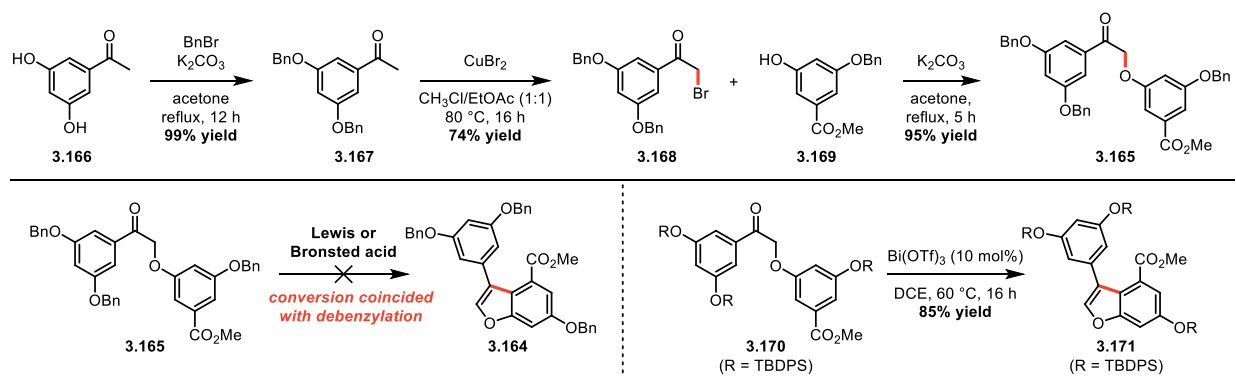


Figure 3.33. Synthesis of the key benzofuran following Kim and Choi's approach.

^bThis resulted in reduction of the acetophenone to the benzyl alcohol, presumably through the enol tautomer, thus requiring oxidation after phenol protection to evaluate the desired cyclodehydration.

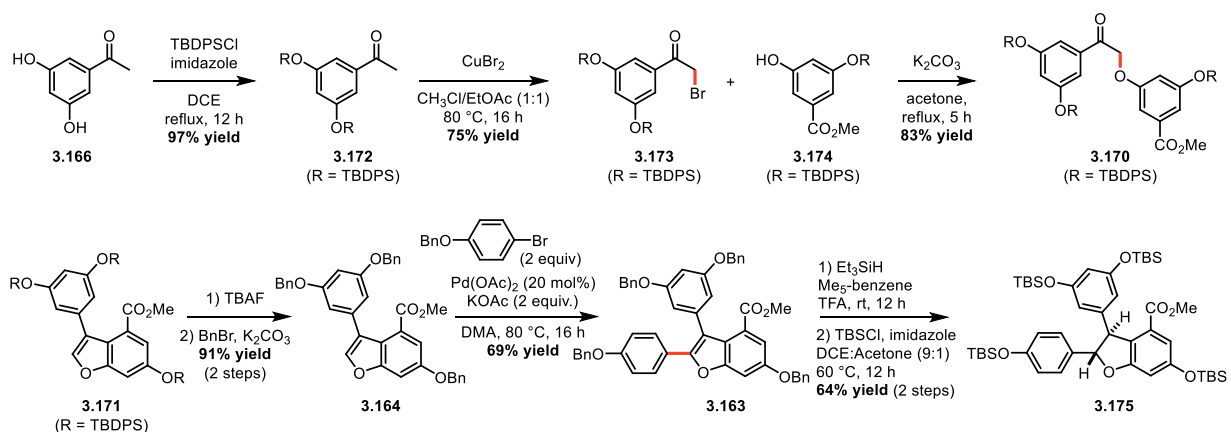


Figure 3.34. First generation synthesis of TBS-protected *trans*-DHB 3.175.

to be competent for the desired reaction, and benzofuran **3.171** was delivered in 85% yield after exposure to 10 mol % of bismuth (III) triflate in dichloroethane at 60 °C for 16 hours. Importantly, the corresponding cyclodehydration precursor (**3.170**) could be prepared on multi-gram scale following the same approach – phenol protection, α -bromination, and alkylation (Figure 3.34). Unfortunately, benzofuran **3.171** was not a competent substrate for the desired C–H arylation under Kim and Choi’s conditions – instead only desilylation was observed. As a result, the silyl groups were replaced with benzyl to deliver **3.164**, which afforded the desired 2,3-diarylbenzofuran **3.163** in 69% yield under Kim and Choi’s optimized conditions.²⁰⁶ Importantly, this material smoothly underwent a Kishi reduction¹⁹² with concomitant acid-mediated debenzoylation to give **3.162** exclusively as the *trans*-isomer, and this material was TBS-protected to access **3.175**. While this route proved robust enough to provide material to complete the synthesis of vitisin A, the additional protecting group manipulations seemed unnecessary. Thus, additional effort was spent to develop a phenol protection approach that would tolerate both the cyclodehydration and C–H arylation while also affording facile cleavage prior to DHB formation.

Isopropyl ethers have been demonstrated to be similarly robust to methyl, yet more readily cleaved,²³⁶ so this protection strategy was employed to access **3.175** in a shorter

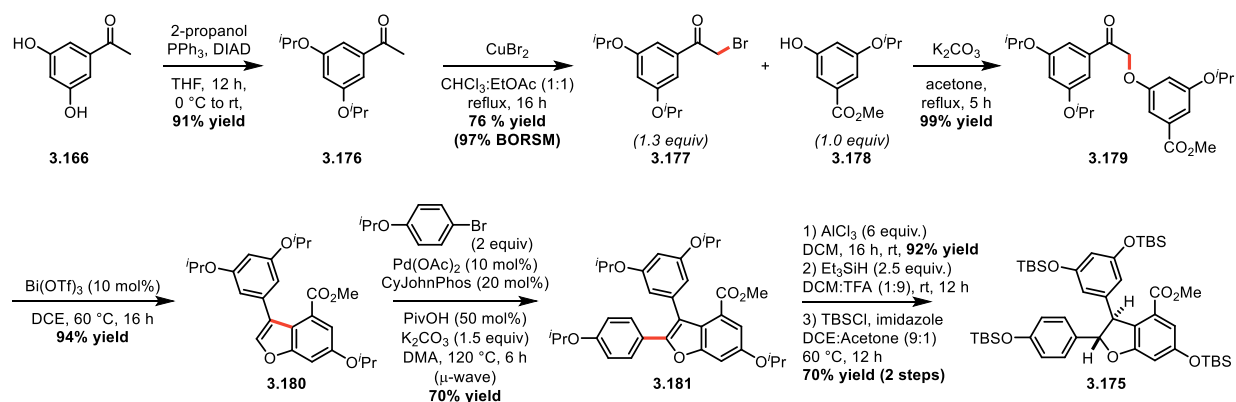
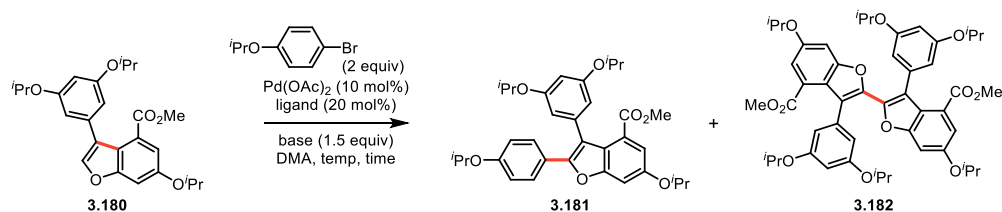


Figure 3.35. Second generation synthesis of key DHB fragment 3.175.

sequence with fewer protecting group manipulations (Figure 3.35). Therefore, the phenols of acetophenone **3.166** were converted to isopropyl ethers (**3.176**) using a Mitsunobu reaction.²³⁵ The same α -bromination conditions delivered the corresponding α -bromo acetophenone **3.177** in 76% yield, with the remainder of the mass balance being the starting material. Increasing the equivalence of copper (II) bromide resulted in formation of the undesired double α -bromination product, thus this reaction was routinely run to ~80% conversion and the recovered starting material was resubjected with each successive batch of material. Alkylation with known phenol **3.178**²³⁷ delivered the corresponding α -phenoxy acetophenone **3.179** in excellent yield. Subsequent cyclodehydration proceeded in 94% yield to deliver benzofuran **3.180**, setting the stage for the key C–H arylation reaction. As described in Table 3.6, Kim and Choi’s conditions afforded poor conversion to the desired product and resulted in significant formation of the undesired dimer **3.182** (Entry 1). This byproduct presumably forms from the C–H activation of two equivalents of starting material with the palladium (II) precatalyst, and reductive elimination forms the active palladium (0) for the desired arylation. As such, phosphine ligands were evaluated to preferentially generate the active catalyst and avoid this deleterious pathway (Entries 2-8). Furthermore, Fagnou and co-workers demonstrated that pivalate bases significantly

Table 3.6. Optimization of the C–H arylation of 3.180 to access 3.181.

Entry	Base	Ligand	Temp. (° C)	Time (h)	Conversion (%)	% Yield (¹ H NMR)	
						3.181	3.182
1	KOAc	-	80	16	50	19	25
2	KOPiv	PPh ₃	80	16	54	40	5
3	KOPiv	XantPhos	100	21	5	5	0
4	KOPiv	CyJohnPhos	100	21	64	62	1
5	KOPiv	Dppbenz	100	21	21	19	2
6	KOPiv	XPhos	100	21	11	11	0
7	KOPiv	SPhos	100	21	24	16	8
8	KOPiv	P(o-tol) ₃	100	21	60	58	2
9 ^a	KOPiv	CyJohnPhos	120	6	90	70 ^b	8

^aReaction conducted under microwave irradiation. ^bIsolated yield.

enhance the rate of concerted metalation-deprotonation (CMD),²³⁸ so potassium pivalate replaced potassium acetate. In all cases, dimer formation was suppressed, and CyJohnPhos was observed to deliver the best conversion to the desired product (Entry 4). To boost conversion, the reaction was conducted using microwave irradiation, resulting in 70% isolated yield of the desired C–H arylation product **3.181**. After C–H arylation, **3.181** was finally converted to **3.175** by Lewis acid-mediated deprotection,²³⁶ Kishi reduction,²¹⁸ and silyl protection (Figure 3.35).

Upon construction of the key DHB fragment and incorporation of a suitably labile phenol protecting group, the remaining task involved conversion of the ester to the corresponding aldehyde (Figure 3.36). This functional group conversion proceeded smoothly in two steps, as reduction of the ester and a Parikh-Doering oxidation²³⁹ delivered aldehyde **3.188** in 72% yield. A Wittig olefination¹⁰⁰ between **3.188** and the corresponding phosphonium salt (**3.187**) was the final step required to access the all-silyl protected ϵ -viniferin analog **3.189**. Phosphonium salt **3.187** was prepared from phenol **3.183** via successive O-silyl

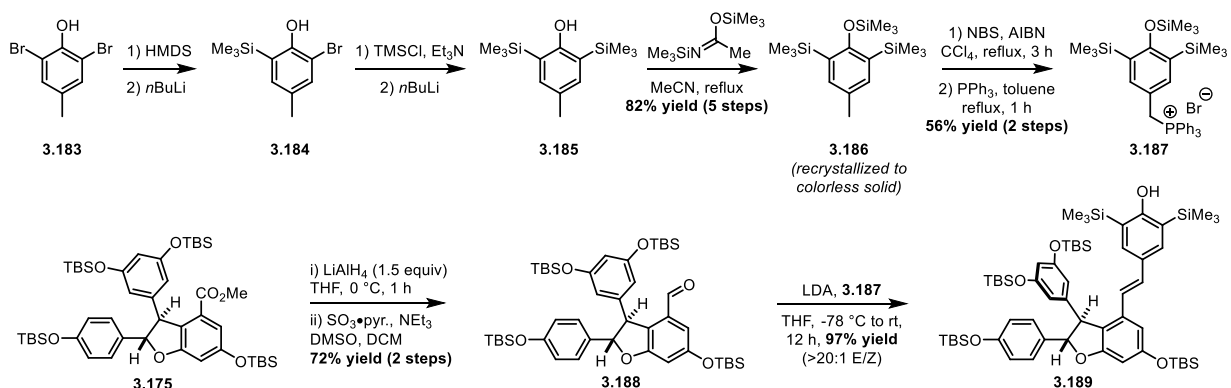


Figure 3.36. Preparation of silyl protected ϵ -viniferin analog 3.189.

protection/retro-Brook rearrangement sequences to prepare the TMS-derivative of BHT (3.185).^{240,241} Silyl protection afforded 3.186, and this entire sequence proceeded without intermediate purification in 82% yield after recrystallization of 3.186. Finally, a Wohl-Ziegler reaction^{242,243} was leveraged to prepare an intermediate benzyl bromide, which, due to significant instability, was immediately carried forward for nucleophilic displacement with triphenylphosphine to arrive at 3.187 (Figure 3.36). Gratifyingly, the olefination reaction between 3.187 and 3.188 delivered 3.189 exclusively as the *E*-isomer in excellent yield following previously optimized conditions.⁴⁸

At this point, our dimerization method utilizing anodic oxidation was employed to access bis-quinone methide tetramer 3.191 (Figure 3.37).⁹⁸ Oxidation of 3.189 under the published conditions to achieve C8b–C8c dimerization of persistent radical 3.190 resulted in low current density and sluggish conversion to the desired product (3.191). This was attributed to poor solubility, as a white solid was observed to deposit on the electrodes over the course of the reaction. This problem was reminiscent of the similar issue encountered upon scaling up the dimerization protocol, thus, the solution was rather simple. Previously, dichloromethane was incorporated as a co-solvent to promote solubility. This strategy was employed again for the preparation of 3.191, and solubility of the reaction was further

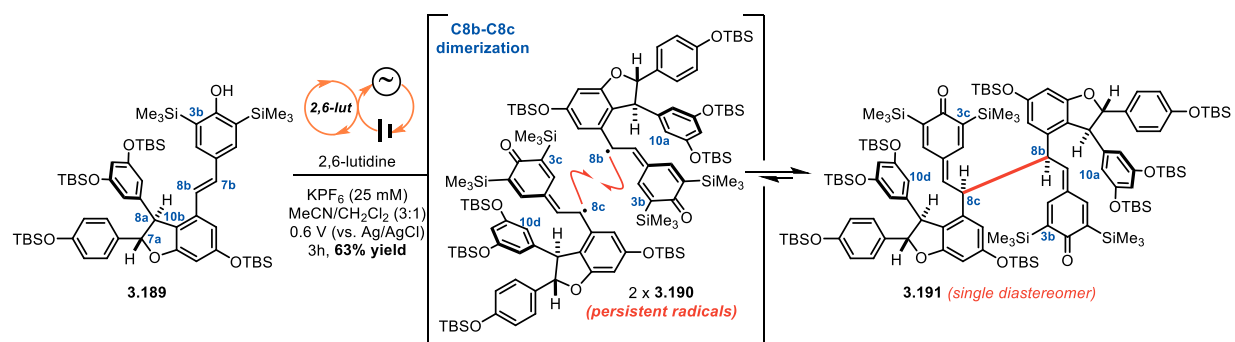


Figure 3.37. Electrochemical dimerization of 3.189 affords key *bis*-quinone methide tetramer 3.190.

promoted by decreasing the electrolyte concentration by half (50 vs. 25 mM).²⁴⁴ This resulted in effectively a trade-off of current density for solubility, leading to a slightly longer reaction time; however, the reaction remained soluble for the duration, and the desired tetrameric product **3.191** was prepared in comparable efficiency (63% yield) to previous efforts on this scaffold (Figure 3.37). Importantly, **3.191** was prepared as a C₂-symmetric single diastereomer, arising from the C8b–C8c coupling of “matched” enantiomers of **3.190** – meeting the critical requirement for potential vitisin tetramer synthesis.

With the silyl-protected tetrameric material in hand, the key C8b–C8c to C3c–C8b homolytic bond migration step was revisited. First, in order to determine if the persistent radicals would escape the solvent cage prior to the formal [1,5]-shift, possibly leading to mismatched C3c–C8b oligomers, a crossover experiment was performed between the benzyl and *para*-methoxy benzyl protected quinone methide dimers **2.69c** and **3.192** (Figure 3.38). Indeed, a nearly statistical mixture of the crossover products (**3.142**, **3.194**, **3.195**, & **3.196**) was observed, suggesting C8–C8' fragmentation and diffusion is competitive with homolytic migration to the C3–C8' bond. However, the dimer model system is not adequate to determine if the stereochemical integrity of **3.191** would be

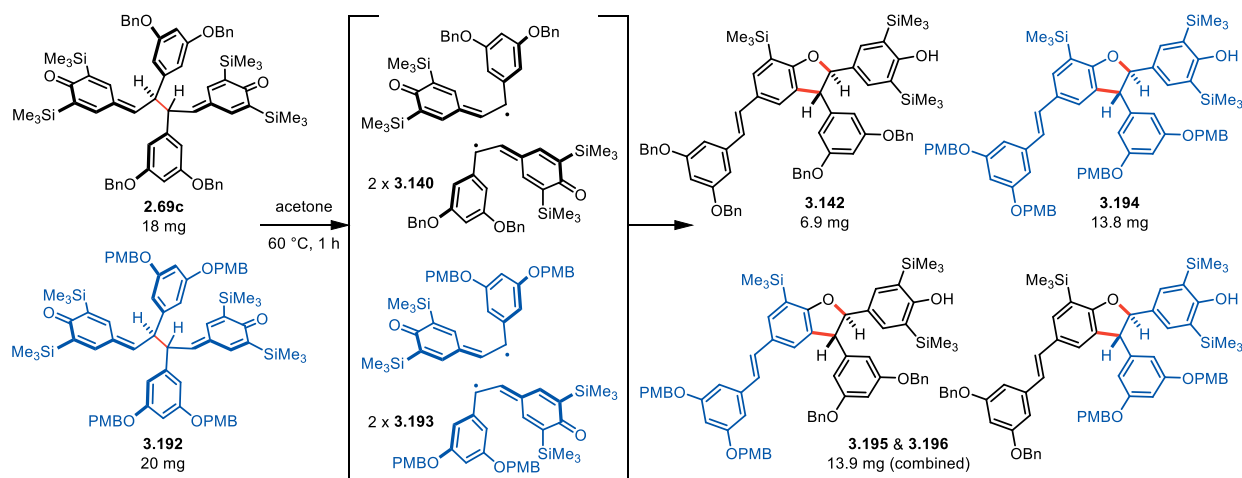


Figure 3.38. Crossover experiment between **2.69c** and **3.192** demonstrates that the persistent radicals escape the solvent cage during the homolytic bond migration.

completely eroded during isomerization, as the corresponding persistent radicals **3.140** and **3.193** are prochiral. Subjecting **3.191** to the thermal isomerization conditions readily accessed the vitisin B core (**3.198**), but as a mixture of four C3c–C8b dihydrobenzofuran (DHB) isomers (Figure 3.39). Increasing the temperature improved the trans/cis ratio of the DHB rings, presumably due to thermal epimerization; however, the facial selectivity of C3c–C8b recombination remained unchanged. Gratifyingly, the TBS ethers were readily cleaved with HF-triethylamine upon completion of the bond migration in a one-pot fashion to afford two compounds – **3.199** and **3.200** (Figure 3.39). These trans-DHB isomers arise

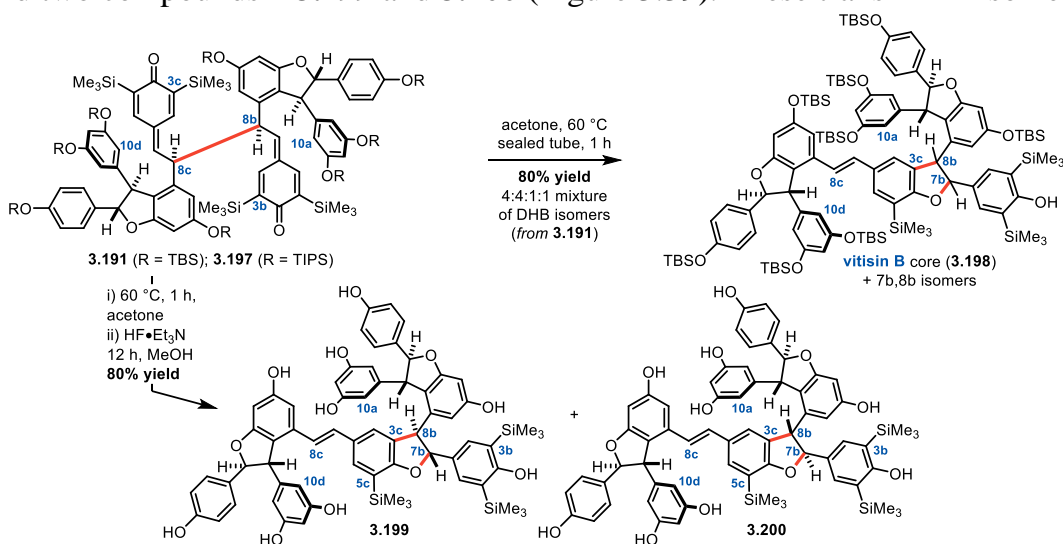


Figure 3.39. Homolytic bond migration proceeds via relative configuration of **3.191**.

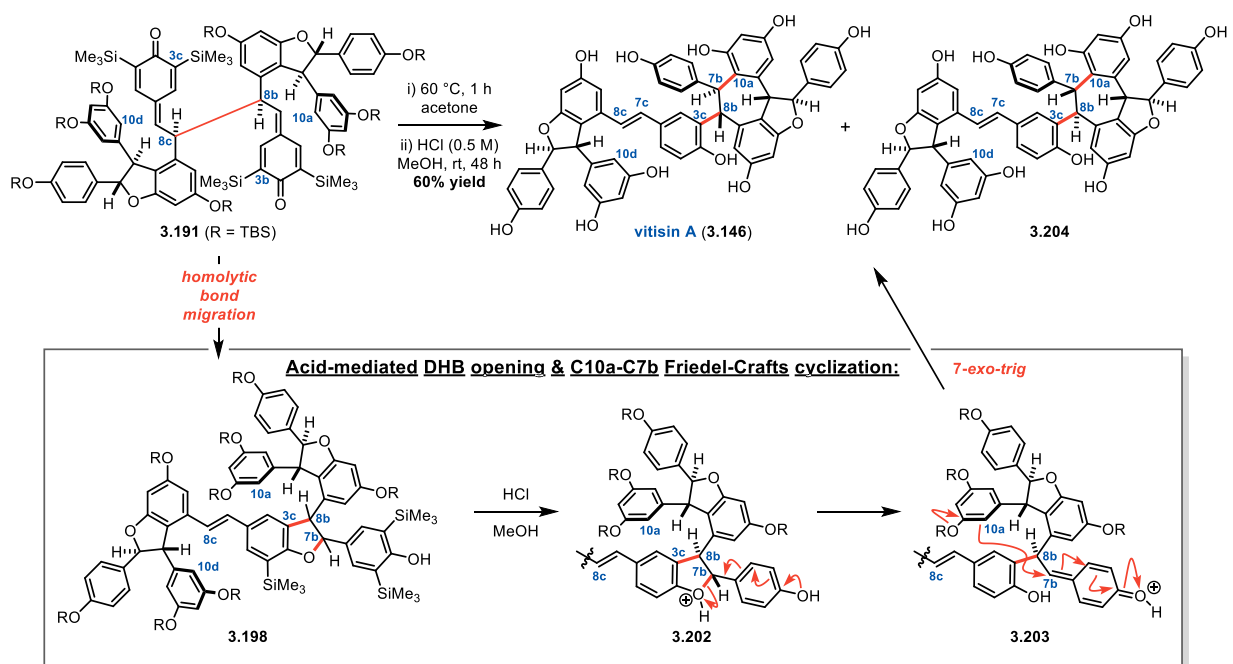


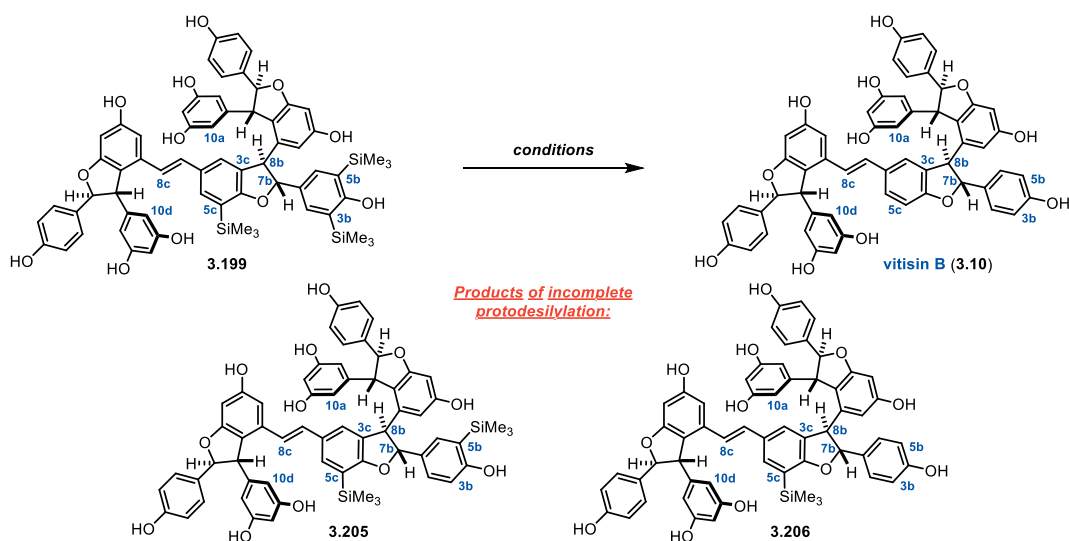
Figure 3.41. Synthesis of vitisin A (3.146) from 3.191 via homolytic bond migration and acid-mediated cyclization.

fashion. Analysis by high-resolution mass spectrometry (HRMS) indicated that the desired mass ($M+H = 907$) was present, and traditional silica gel chromatography afforded isolation of a the most polar TLC “spot” which corresponded to two compounds. Semi-preparative HPLC was utilized to separate this mixture; however, analysis by ^1H NMR indicated that the compounds isolated only contained two dihydrobenzofuran rings. Upon further inspection of ^1H and ^{13}C NMR data and comparison to the isolation literature, it was determined that these two compounds were vitisin A (3.146) and the C7b, C8b-isomer 3.204. As described in Figure 3.28, vitisin A (3.146) and vitisin B (3.10) are proposed to arise from a common intermediate quinone methide (3.144) during biosynthesis, and Niwa and co-workers demonstrated that vitisin A (3.146) can be accessed from vitisin B (3.10) under acidic conditions.²³³ The proposed mechanism for this transformation is given in Figure 3.41. Acid-mediated cleavage of the C7b–O bond upon protonation of the DHB (3.202) affords a quinone methide (3.203) which is reminiscent of the proposed common

biosynthetic intermediate **3.144**. A 7-exo-trig Friedel-Crafts cyclization of C10a on to C7b of the quinone methide ensues to forge the 7-membered ring in a manner consistent with the cyclization approaches discussed in Section 3.3.1. Interestingly, the isolation of only two compounds after cyclization suggests that the C10a–C7b bond formation exclusively delivers the relative *trans*-configuration between C7b and C8b, as depicted in Figure 3.41. As a result, the C8b configuration, which is set during the homolytic bond migration step, dictates the facial selectivity of the cyclization. To date, this route has produced over 30 milligrams of vitisin A (**3.146**), and, starting with 100 mg of **3.191**, 12 milligrams of **3.146** is readily prepared in a single pass after HPLC purification.

As conversion of vitisin A (**3.146**) to vitisin D (**3.148**) under acidic conditions has also been established in the isolation and biosynthesis literature,²³³ attention was focused on the deprotection of the **3.199/3.200** mixture to reveal vitisin B (**3.10**). Previously, protodesilylation of C3/5-TMS resveratrol tetramers was achieved by exposure to trifluoroacetic acid in a 1:1 mixture of nitromethane and dichloromethane.⁴⁸ These conditions were employed for the desilylation of **3.199/3.200**, however, conversion to vitisin A (**3.146**) and **3.204** was observed. It became clear that alkaline conditions might hold the key to desilylation without opening the C7b-C8b dihydrobenzofuran, though it was recognized that ring opening could be feasible upon deprotonation of the C4b phenol. Given the wealth of literature regarding fluoride-mediated protodesilylation,^{245–256} an evaluation of fluoride sources was initiated. A summary of these efforts can be found in Table 3.7. While these investigations were conducted on the **3.199/3.200** mixture, for clarity, Table 3.7 shows only **3.199** and the isomers derived therefrom. These reactions were analyzed by UPLC-MS using a method in which each vitisin B scaffold and the

Table 3.7. Investigation of C3/5 desilylation conditions to access vitisin B (3.10).



Entry	Conditions	Temp.	Yield ^a			
			3.199	3.205	3.206	3.10
1	HF-Et ₃ N (0.3 M), acetone/MeOH (1:1), 12h	60 °C	47	20	-	-
2	HF-Et ₃ N (0.3 M), acetone/MeOH (1:1), 12h	90 °C	-	66	5	-
3	HF-Et ₃ N + AcOH (0.3 M), acetone/MeOH (1:1), 12h	23 °C	63	7	-	-
4	CsF (5 equiv), MeOH/H ₂ O (1:1), 16 h	60 °C	-	45	55	-
5	CsF (10 equiv), MeOH/H ₂ O (1:1), 16 h	60 °C	-	7	93	-
6	CsF (20 equiv), MeOH/H ₂ O (1:1), 16 h	60 °C	-	4	96	-
7	CsF (30 equiv), MeOH/H ₂ O (1:1), 16 h	60 °C	-	-	100	-
8	CsF (10 equiv), MeOH/H ₂ O (1:1), 16 h	90 °C	-	-	100	-
9	CsF (20 equiv), MeOH/H ₂ O (1:1), 16 h	90 °C	-	-	100	-
10	CsF (30 equiv), MeOH/H ₂ O (1:1), 16 h	90 °C	-	-	100	-
11	CsF (30 equiv), MeOH/H ₂ O (1:1), 16 h	120 °C	-	-	-	-

^aYield determined by relative peak area @ 280 nm

corresponding C7b/C8b-epimer (i.e. **3.199** and **3.200**) co-elute, thus the yield of each desilylation reaction was determined by the area of a single peak. First, simply increasing the temperature of the O-desilylation conditions was evaluated, and while protodesilylation began to occur, complete desilylation did not occur (Entries 1-2). Hydrofluoric acid (generated *in situ* from neutralization of triethylamine with acetic acid) offered poor conversion (Entry 3). The evaluation of cesium fluoride gave the first seemingly positive results (Entries 4-10), as the C3b/5b silyl groups were readily cleaved at elevated temperature with an excess of CsF in methanol and water. Extending this reaction to 120 °C resulted in decomposition, but the conditions given in Entry 8 were employed for

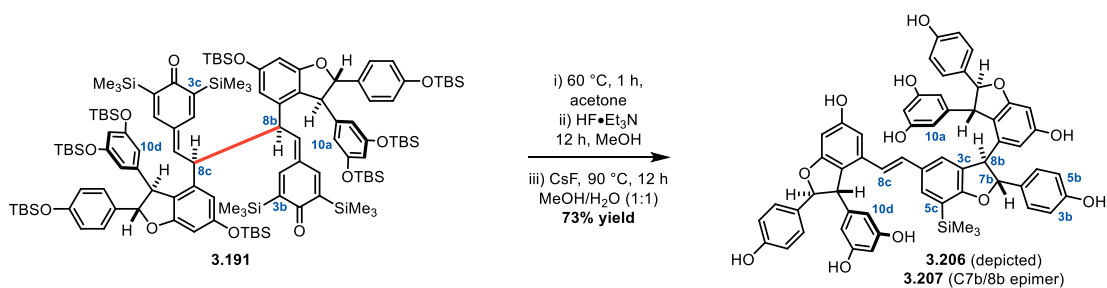
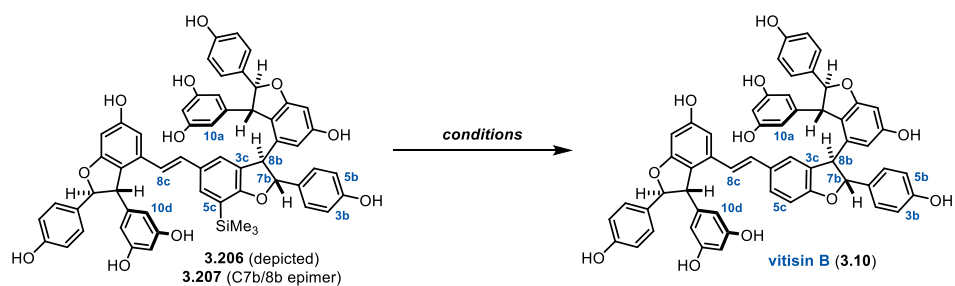


Figure 3.42. Preparation of 3.206/3.207 from 3.191 via homolytic bond migration and desilylation sequence.

C3b/5b desilylation after bond migration and O-desilylation to deliver **3.206** and the corresponding C7b/C8b epimer (**3.207**) in 73% yield. With the end goal seemingly quite near, C5c-desilylation was examined for **3.206/3.207** following the same approach as described for **3.199/3.200** (Table 3.8). First, microwave irradiation was employed to achieve more forcing conditions with CsF in an effort to remove this stubborn group (Entries 1-4). No conversion of the starting material was observed between 90-110 °C and increasing the temperature to 120 °C resulted in decomposition. Next, in an effort to mimic the transmetalation step of a classical Hiyama coupling,²⁵⁷ palladium (II) acetate was employed with an excess of cesium fluoride (Entry 5). It was envisioned that transmetalation to palladium would be followed by protodemetalation; however, the C5c-silyl group remained untouched. Next, the reaction solvent was changed to DMF, theorizing this would result in decreased solvent coordination of the fluoride ions and lead to increased reactivity. Unfortunately, a range of fluoride sources were evaluated (Entries 6-12), and only tetrabutylammonium fluoride (TBAF) arising from a THF solution afforded conversion of the starting material; however, this resulted in decomposition. Aminosulfuranes have been broadly utilized for fluorination reactions,²⁵⁸ so it was hypothesized that this reactivity could be leveraged for the desired C5c-desilylation. Therefore, diethylaminosulfur trifluoride (DAST) was evaluated (Entries 13-17). In

Table 3.8. Unsuccessful attempts at C5c-desilylation.



Entry	Conditions	% Conv.	Outcome
1	CsF (10 equiv), MeOH/H ₂ O (1:1), 6 h, 90 °C (μ-wave)	0	-
2	CsF (10 equiv), MeOH/H ₂ O (1:1), 12 h, 100 °C (μ-wave)	0	-
3	CsF (10 equiv), MeOH/H ₂ O (1:1), 6 h, 110 °C (μ-wave)	0	-
4	CsF (10 equiv), MeOH/H ₂ O (1:1), 6 h, 120 °C (μ-wave)	100	decomp.
5	CsF (50 equiv), Pd(OAc) ₂ (1 equiv), MeOH/H ₂ O (1:1), 16 h, 90 °C	0	-
6	CsF (50 equiv), DMF, 90 °C, 16 h	0	-
7	TBAF-3H ₂ O (3 equiv), DMF, 90 °C, 2 h	0	-
8	TBAF (1M in THF, 10 equiv), DMF, 90 °C, 16 h	100	decomp.
9	KHF ₂ (10 equiv), DMF, 23 °C, 16 h	0	-
10	KHF ₂ (10 equiv), DMF, 23 °C, 16 h	0	-
11	HF-Et ₃ N (10 equiv), DMF, 90 °C, 16 h	0	-
12	Anhydrous CsF (10 equiv), DMF, 90 °C, 16 h	0	-
13	DAST (10 equiv), MeCN, 23 °C, 16 h	0	-
14	DAST (10 equiv), AcOH (10 equiv), DMF, 90 °C, 16 h	0	-
15	DAST (10 equiv), DMF, 90 °C, 16 h	100	decomp.
16	DAST (10 equiv), DMF, 60 °C, 16 h	100	decomp.
17	DAST (10 equiv), DMF, 0 °C to rt, 3 h	100	decomp.
18	TMAF (10 equiv), DMF, 23 °C, 16 h	0	-
19	TMAF (10 equiv), DMF, 60 °C, 16 h	0	-
20	TMAF (10 equiv), DMF, 90 °C, 16 h	100	3.146/3.204

acetonitrile at ambient temperatures the reaction became insoluble immediately, presumably due to phenol deprotonation, thus it was unsurprising that conversion did not occur. However, exposure to DAST in DMF between 0 °C and 90 °C all resulted in total decomposition of the starting material. Finally, tetramethylammonium fluoride (TMAF) has demonstrated excellent reactivity for S_NAr reactions at room temperature,²⁵⁹ so perhaps this reagent could be harnessed to achieve the desired transformation. While the starting material did not convert at ambient temperatures or at 60 °C (Entries 18-19), desilylation did occur at 90 °C (Entry 20). Unfortunately, the only tetrameric products isolated were vitisin A (**3.146**) and the corresponding C7b/C8b epimer (**3.204**) arising from base mediated DHB opening and cyclization. This same mechanism is operative when potassium

carbonate in MeOH is employed for desilylation, which is well-established for the desilylation of TMS-acetylenes.²⁶⁰ It was determined from careful temperature evaluation that base-mediated opening and cyclization occurs prior to desilylation, suggesting that the free phenol adjacent to the silyl group is critical to assist with silyl cleavage.

It is perhaps unsurprising that both acidic and alkaline conditions result in the opening of the C7b/C8b dihydrobenzofuran as it can effectively be viewed as a hemiacetal, where the incorporated aromatic ring only serves to further delocalized positive or negative charge under the respective conditions. With than analogy in mind, an auspicious report from Radner and Wistrand was encountered in which they achieve protodesilylation of aryltrimethylsilanes in the presence of acid-labile ketals.²⁶¹ They found that exposure of their substrates to equimolar amounts of potassium iodide, chlorotrimethylsilane, and water in acetonitrile afforded clean desilylation while preserving the ketals. These conditions were employed for the protodesilylation of **3.199/3.200**, and after just one hour a new peak with the desired molecular weight ($M+H = 907$) was observed by UPLC-MS. After purification by preparative HPLC afforded two compounds, analysis by ¹H NMR revealed that these compounds had the same connectivity and only exhibited the diagnostic peaks for two dihydrobenzofuran rings. However, these products were not vitisin A (**3.146**) and the diastereomer **3.204** – instead, vitisin D (**3.148**) had been isolated along with a diastereomer (**3.209**). Vitisin D (**3.148**) has been proposed to arise from vitisin A (**3.146**) during the biosynthesis of these compounds, as depicted in Figure 3.28, through the intermediacy of a quinone methide (**3.147**), and indeed isolation studies have validated this hypothesis.²³³ Therefore, it is unsurprising that sufficiently acidic conditions would result in the rearrangement of the vitisin B scaffold (**3.199/3.200**) directly to the vitisin D scaffold

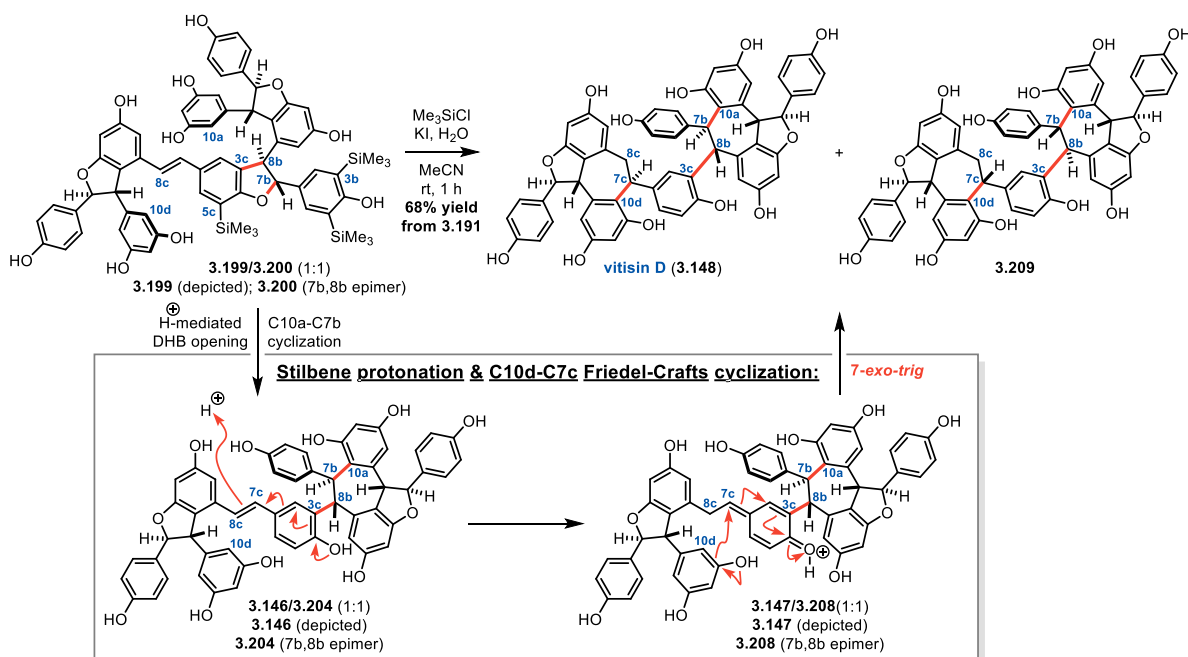


Figure 3.43. Synthesis of vitisin D (3.148) via Friedel-Crafts cyclizations from the vitisin B scaffold.

(3.148/3.209). This is exactly the case for this reaction (Figure 3.43). Under the acidic conditions generated by the mixture of Me_3SiCl , KI , and H_2O in MeCN , protodesilylation occurs in addition to acid-mediated C7b–O cleavage and C10a–C7b Friedel-Crafts cyclization to generate vitisin A (3.146) and diastereomer 3.204, as depicted in Figure 3.41. Next, stilbene protonation at C8c, assisted by the C4c-phenol, reveals quinone methide 3.147/3.208, and subsequent C10d–C7c Friedel-Crafts cyclization forges the second 7-membered ring exhibited in the vitisin D scaffold (3.148/3.209). These two compounds were isolated in a 1:1 ratio which can be traced back to the facial selectivity of the homolytic bond migration. Remarkably, the subsequent cyclization reaction of each vitisin B scaffold is completely selective for one diastereomer of both the vitisin A and vitisin D scaffolds. As with vitisin A, this route to vitisin D is sufficiently robust for biological analysis, as nearly 20 milligrams of the natural product have been prepared to date. It is certainly disappointing that efforts to realize a unified synthesis of each of the vitisin tetramers were

unsuccessful; however, this synthesis demonstrated the utility of persistent radical intermediates while providing material for further biological study of resveratrol tetramers.

3.6 Biological activity of resveratrol tetramers

The structural complexity exhibited by resveratrol tetramers requires innovative solutions for synthesis, providing significant motivation for targeting these natural products from an organic chemistry perspective. However, these complex molecules are broadly interesting beyond the methods developed to synthesize them, as this natural product class has been attributed with wide-spread biological activity.^{44,102,132–135} Numerous studies have relied upon highly labor-intensive extraction and purification processes to acquire material from plant matter; however, despite excellent efforts to improve such processes,²⁶² this approach is not sustainable.²⁶³ Therefore, chemical synthesis is required to supply critical material for detailed investigation of the pharmacological potential of these interesting molecules.²⁶⁴ Given the completed synthesis of vitisin A (**3.146**) and vitisin D (**3.148**) described in the preceding section, this section will summarize the biological activities reported for these compounds to date. Between these two natural products, significantly more data exist regarding the biological activity of vitisin A (**3.146**), which can almost certainly be attributed to a higher propensity for isolation relative to vitisin D (**3.148**). As a result, one might suggest that **3.148** is actually an artifact arising during the isolation of **3.146**, though this seems unlikely due to the significantly acidic conditions required for the cyclization of **3.146** to **3.148** (*vide supra*).²³³

Alzheimer's disease has become one of the leading neurodegenerative conditions that result in a decline in quality of life, as it is associated with impairment of memory and cognition, and it is projected that >100 million people will be afflicted by 2050.²⁶⁵ One of

the pathological hallmarks of this disease is the formation of senile plaques from amyloid- β ($A\beta$) peptides. These peptides are generated through the cleavage of $A\beta$ precursor protein (APP) by β - and γ -secretase enzymes. The enzyme BACE-1 – or β -site APP cleaving enzyme 1 – has been determined to be the critical β -secretase involved in $A\beta$ -plaque formation,^{266–269} therefore it has become a target for inhibition in the development of Alzheimer's therapies.²⁷⁰ Toward this goal, Hu and co-workers evaluated various polyphenolic compounds isolated from *Vitis thunbergii* var. *taiwaniana*, finding that, of the twelve isolated, five – including vitisin A (**3.146**) – showed ability to reduce $A\beta$ levels in cell culture studies at low micromolar concentrations. Control experiments demonstrated that γ -secretase activity was not diminished in the presence of these compounds, and both vitisin A (**3.146**) and ampelopsin C were found to reduce β -secretase activity in cellular assays. Importantly, the cellular BACE-1 levels were not affected, suggesting that these compounds inhibit BACE-1 activity as opposed to diminishing its concentration in the cell through some other mechanism. These results are consistent with a prior report from Choi and co-workers in which they determined that vitisin A (**3.146**) inhibits baculovirus-expressed BACE-1 *in vitro* ($IC_{50} = 0.8 \pm 0.1 \mu M$) using a fluorescence resonance energy transfer (FRET) assay.²⁷¹ Interestingly, vitisin B (**3.10**) was the most potent of the polyphenolic molecules evaluated in this study ($IC_{50} = 0.4 \pm 0.1 \mu M$), and both vitisins exhibited an order of magnitude greater activity than the other (dimeric) compounds, supporting the notion that an increase in chemical complexity in this natural product class also results in increased biological function.⁴⁴ Alternatively, it has been proposed that acetylcholinesterase may be involved in $A\beta$ peptide formation, and vitisin A (**3.146**) has exhibited micromolar potency ($IC_{50} = 1.04 \pm 0.05 \mu M$) for the inhibition of this enzyme.²⁷²

As a result, vitisin A (**3.146**) could possibly be active against the aggregation of A β peptides through two different mechanisms.

Obesity is another disease that, despite recognition of the problems associated with and prevalence of the condition, has continued to affect an increasing portion of the global population.²⁷³ This disease significantly increases the risk of developing additional medical problems, including, but not limited to, cardiovascular disease, type II diabetes, and hypertension.^{274,275} Obesity results from hypertrophy, or the increased size of adipocytes (cells that comprise fat tissue), as well as hyperplasia, or the increased number of adipocytes. Both of these processes lead to increased lipid accumulation and ultimately an increase in body mass; therefore, targeted therapy to reverse this process is of high interest in medicine.²⁷⁶ It has been previously demonstrated that adipocyte maturation, or adipogenesis, occurs through complex cellular process involving gene expression specific to these cells resulting in the synthesis and accumulation of lipids.^{277,278} Recently, Tie and co-workers utilized an *in vitro* study to examine the effects of isolated oligostilbenes on the adipocyte differentiation process in 3T3-L1 cells as a model for influencing adipogenesis. The authors isolated vitisin A-D in addition to cis-vitisin A^c from *Iris lactea* Pall.var. *chinensis* (Fisch.) Koidz and evaluated the influence of these 5 compounds on adipocyte differentiation. They found that three compounds – vitisin A (**3.146**), vitisin B (**3.10**), and cis-vitisin A – significantly inhibited adipogenesis. Interestingly, vitisin C (**3.145**) and vitisin D (**3.148**) had the opposite effect, which is remarkable given the structural similarity between vitisin B (**3.10**) and vitisin C (**3.145**, see Figure 3.28). Nonetheless, the authors showed that treatment of the 3T3-L1 cells with vitisin A (**3.146**), vitisin B (**3.10**), and cis-

^c cis-vitisin A is the Z-stilbene isomer of vitisin A (**3.146**)

vitisin A diminished the expression of adipogenesis genes, including adipocyte fatty acid binding protein 4 (FABP4), peroxisome proliferator activated receptor- γ (PPAR γ), and CCAAT/enhancer binding protein- α (C/EBP α). It has been previously demonstrated that PPAR γ and C/EBP α are involved in the regulation of downstream genes related to fatty acid oxidation and lipid accumulation,²⁷⁹ and, more specifically, the expression of FABP4 is mediated by PPAR γ .²⁸⁰ Unquestionably, further investigation into the specific molecular interactions between the vitisin tetramers and PPAR γ is critical to understanding the observed difference in adipocyte differentiation, and perhaps an increased understanding of this component of the adipogenesis process could lead to the development of targeted therapy to combat obesity.

Inflammation is another broadly applicable indication that is relevant in the progression of numerous diseases.²⁸¹ In 2001, Huang and co-workers disclosed that vitisin A (**3.146**) has anti-inflammatory effects,²⁸² however the mechanism by which this occurs was not studied. Among the cellular processes involved in inflammatory responses, the production of nitric oxide (NO) has been connected to the pathogenesis of diseases such as autoimmune diabetes, cerebral malaria, septic shock, and rheumatoid arthritis.²⁸³ In 2008, Sung and co-workers published a study of the mechanism by which vitisin A (**3.146**) influences lipopolysaccharide(LPS)-induced NO production.²⁸⁴ They found that treatment of RAW 264.7 cells with vitisin A (**3.146**) affords decreased NO production through inhibition of the LPS-induced extracellular signal-regulated kinase 1/2 (ERK1/2) and p38 phosphorylation, thereby resulting in the deactivation of NF- κ B – a major transcription factor. This work was followed by Nassra and co-workers in 2013, who determined the inhibitory activity of both vitisin A (**3.146**) ($IC_{50} = 3.9 \pm 0.7 \mu\text{M}$) and vitisin B (**3.10**) (IC_{50}

= $4.7 \pm 0.5 \mu\text{M}$) on NO production induced by LPS (in this case in BV-2 microglial cells).²⁸⁵ In addition, these authors found that treatment of the cells with vitisin A (**3.146**) or vitisin B (**3.10**) resulted in attenuated expression of the inducible NO synthase protein, further supporting the hypothesis that these resveratrol tetramers influence the genetic regulation of this particular inflammatory response. Finally, Jang and co-workers have invoked an alternative mechanism of action for the activity of vitisin A (**3.146**) against cellular nitric oxide, suggesting that this polyphenol has sufficient radical scavenging activity to protect against NO-induced toxicity.²⁸⁶ The authors reported that vitisin A (**3.146**) and an additional polyphenol, heyneanol A, reduce DNA fragmentation and cell death in human neuroblastoma SH-SY5Y cells induced by sodium nitroprusside. While they show data suggesting that each of these oligomers are better radical scavengers than the precursor compound – resveratrol (**2.78**) – they did not compare the activity of α -tocopherol (**2.82**) in these studies, which, as our collaborative efforts have demonstrated,^{45,98} is critical for completely understanding cellular radical trapping activity. Given that vitisin A (**3.146**) has otherwise been reported to be a modest antioxidant ($\text{EC}_{50} = 13.8 \pm 2.7 \mu\text{M}$),²⁸⁷ additional study is required to definitively determine the mechanism by which vitisin A (**3.146**) affords protection against neuronal NO toxicity.

As with most natural products, vitisin A (**3.146**) has also been evaluated for possible anti-cancer properties. Prostate cancer, in particular, has become the most common cancer in men around the globe.²⁸⁸ While numerous approaches are currently in use to combat this disease, it has been recently established that activation of the tumor necrosis factor(TNF)-related apoptosis-inducing ligand (TRAIL) receptor pathway shows promise as a therapeutic strategy for the selective eradication of cancer cells.^{289–292} Recently, Shin and

co-workers demonstrated that vitisin A (**3.146**) can be used in combination with TRAIL to induce apoptosis in PC-3 prostate cancer cells.²⁹³ While they do not indicate a value for the activity of vitisin A (**3.146**), the compound is employed at micromolar concentrations for the entirety of the study. The authors found that combined treatment with vitisin A (**3.146**) and TRAIL resulted in upregulation of death receptor 5 (DR5) in addition to its expression at the cellular surface. A control experiment in which DR5 was silenced by siRNA transfection eliminated the observed activity of vitisin A (**3.146**), further supporting this role in apoptosis promotion. Furthermore, an increase in the production of reactive oxygen species (ROS) was observed after combination treatment with vitisin A (**3.146**) and TRAIL, which supports the notion that these polyphenolic natural products are not radical trapping antioxidants but instead are involved in different components of the cellular response to oxidative cell death. Clearly, additional work is required to determine the specific role that vitisin A (**3.146**) plays in this process in order to develop cancer treatment selective for the elimination of cancer cells while preserving healthy cells. While this is certainly a worthwhile goal, vitisin A (**3.146**) has also been found to promote apoptosis in rat cardiomyocytes.²⁹⁴ In particular, between 30-300 nM concentrations, vitisin A (**3.146**) was found to increase swelling and depolarization of mitochondria as well as promote cytochrome *c* release from mitochondria – both indications of apoptosis – in a dose-dependent manner. Evaluation of additional polyphenols, including vitisin B (**3.10**), resulted in the observation that the ϵ -viniferin subunit was conserved across compounds that induced cardiomyocyte apoptosis. Therefore, additional study of the specific molecular interactions that occur with this scaffold is required to determine if these polyphenols can afford any therapeutic benefit.

While the preceding observed biological activities of the vitisin tetramers alone is enough to inspire further study now that these molecules have been accessed synthetically, our original inspiration for synthesis resulted from the observed antiviral activity of these compounds. For example, infection from the influenza virus results in the expression of chemokines as part of the inflammatory response in airway epithelial cells.²⁹⁵ One example is the regulated on activation, normal T cell expressed and secreted (RANTES) chemokine. In 2008, Huang and co-workers evaluated the effect of five isolated stilbenes on RANTES production in A549 alveolar epithelial cells infected with the influenza A virus (H1N1).²⁹⁶ They found vitisin A (**3.146**) ($EC_{50} = 0.27 \pm 0.04 \mu\text{M}$) to be the most active compound for RANTES inhibition while also exhibiting cytotoxicity ($CC_{50} = 22.4 \pm 3.3 \mu\text{M}$) at 100-fold higher concentrations. This also resulted in the attenuation of Akt phosphorylation and STAT₁ activation, suggesting that vitisin A (**3.146**) may play a role in the PI3K-Akt and STAT₁ kinase signaling pathways that lead to the genotypic response to H1N1 infection. While these results are certainly inspiring for the development of new influenza therapies, Lee and co-workers reported even more compelling antiviral activity for vitisin B (**3.10**) and vitisin A (**3.146**) when studying the effect of polyphenolic natural products against the hepatitis C virus (HCV).²⁹⁷ It has been approximated that nearly 200 million people worldwide are afflicted with HCV, and this disease leads to numerous chronic inflammatory liver indications, including hepatocellular carcinoma and liver cirrhosis.²⁹⁸ Importantly, Lee and co-workers observed that vitisin B (**3.10**) ($EC_{50} = 0.006 \mu\text{M}$), vitisin A (**3.146**) ($EC_{50} = 0.035 \mu\text{M}$), and wilsonol C ($EC_{50} = 0.016 \mu\text{M}$) demonstrated potent activity against HCV replication while maintaining good cell viability ($CC_{50} > 10 \mu\text{M}$) in all cases in Rluc-J6/JFH1 RNA-transfected Huh7.5 cells using a luciferase assay. They

found that after dosing with 0.5 μM vitisin B (**3.10**), cell viability was maintained over 72 hours, whereas HCV replication was eliminated ($t_{1/2} = 6.28$ h). Furthermore, when vitisin B (**3.10**) was dosed in combination with sofosbuvir, a known NS5B polymerase inhibitor, a synergistic (or at the very least additive) effect was observed in the decrease of viral activity. Analysis of a selection of vitisin B-resistant HCV mutant variants suggested that the NS3 helicase was a possible target for the observed activity, and direct binding between vitisin B (**3.10**) and purified NS3 helicase was confirmed *in vitro*, finding that **3.10** ($\text{IC}_{50} = 0.003$ μM) is a potent inhibitor of the HCV NS3 helicase. Given the poor bioavailability that is traditionally associated with polyphenols, the authors recognized that it was important to conduct a tissue distribution study, and they found that after intraperitoneal (IP) injection in rats (10 mg/kg) the bioavailability was 80.9%. Furthermore, vitisin B (**3.10**) was localized to the liver in higher concentrations than any other organ – exactly where it is required to combat HCV activity. Finally, Lee and co-workers examined the up-regulation of pro-inflammatory cytokines (TNF- α and IL-6), finding that there was not an acute adverse response to vitisin B (**3.10**) treatment, and the authors are currently following up in additional animal models to investigate the feasibility of vitisin B (**3.10**) for HCV therapy.²⁹⁷

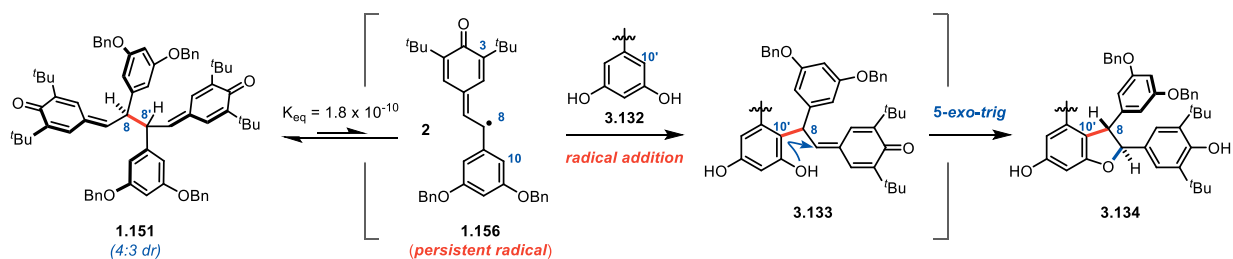
In summary, the vitisin tetramers derived from resveratrol have exhibited some of the most potent biological activity from this natural product class to date, lending further support to the notion that the increased molecular complexity afforded by resveratrol oligomerization also results in enhanced biological activity. Given the synthetic access to vitisin tetramers provided herein, the platform for further study of these interesting molecules has been established. Hopefully this will lead to an increased understanding of

the mechanism(s) by which these molecules influence biological systems and subsequently result in the development of new therapies for multiple indications.

3.7 Future directions – efforts toward resveratrol trimers

While the development of syntheses of two resveratrol tetramers (described in Section 3.5) is a gratifying achievement, this project is by no means complete. Until this point, the story has been told in chronological order; however, a key portion was omitted. Prior to the discovery of the C8–C8' to C3–C8' homolytic bond migration that became the key step for vitisin synthesis, it was discovered that the persistent radical **1.156** is capable of engaging in intermolecular C8–C10' and C7–O bond formation for the construction of DHB rings (Figure 3.44A). While this transformation was initially evaluated for the synthesis of the ϵ -viniferin scaffold (Figure 3.23), it was hypothesized that this intermolecular reactivity of persistent radicals could be applied as the key step for the synthesis of resveratrol trimers (Figure 3.44B). Isolable quinone methide intermediate **3.210** contains two sites at which

A) Mechanistic Hypothesis for Radical DHB Synthesis:



B) Proposed Synthesis of Resveratrol Trimers using Radical DHB Synthesis:

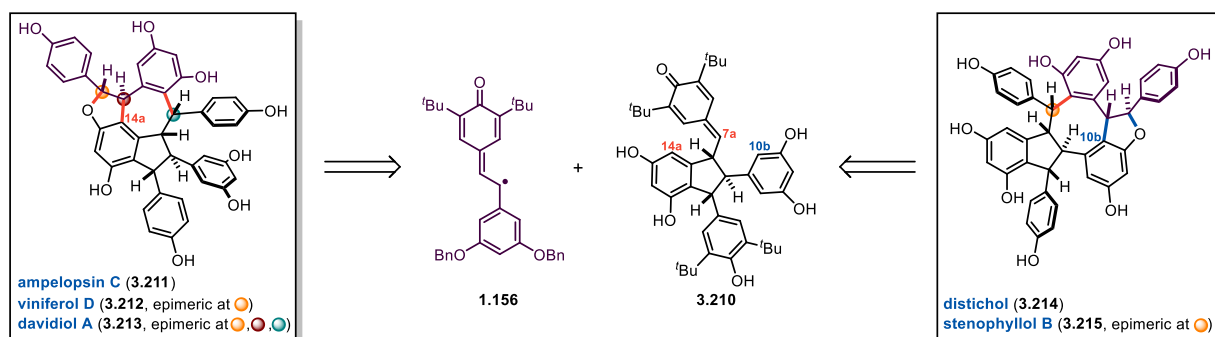


Figure 3.44. Synthetic hypothesis for resveratrol trimers from radical DHB formation.

this oxidative annulation reaction can occur – C14a and C10b. The resulting DHB products would lead to rapid synthesis of resveratrol trimers such as ampelopsin C (**3.211**) and distichol (**3.214**). As described in Section 3.3.3, only one synthesis of a trimeric structure possessing this challenging medium-ring fused core has been achieved, requiring 27 steps for an overall yield of just 0.08%.²²² Therefore, synthesis of resveratrol trimers from this strategy would serve to advance the state-of-the-art approach in the field and provide necessary material for further biological evaluation of this natural product class. The key quinone methide intermediate **3.210** is readily synthesized from **1.151** utilizing the diastereoconvergent cyclization previously described in Section 1.5.2 (Figure 3.45).⁴⁸ Direct debenzoylation of **1.154** in the presence of the quinone methide moiety proved challenging; however, reduction of the quinone methide and hydrogenolysis of the four benzyl ethers followed oxidation back to the quinone methide readily afforded **3.210** in 78% yield over two steps. Preliminary evaluation of solvent, temperature, and heating method for the desired radical DHB synthesis reaction between **1.151** and **1.154** determined that subjecting an acetone solution of the two starting materials to microwave irradiation at 100 °C for 3 hours gave the best conversion to the desired products. Implementation of these conditions on preparative scale resulted in the isolation of nearly 50% yield of trimeric material in a ~3:2 ratio between the C14a (**3.216**) and C10b (**3.217**) adducts (Figure 3.46).

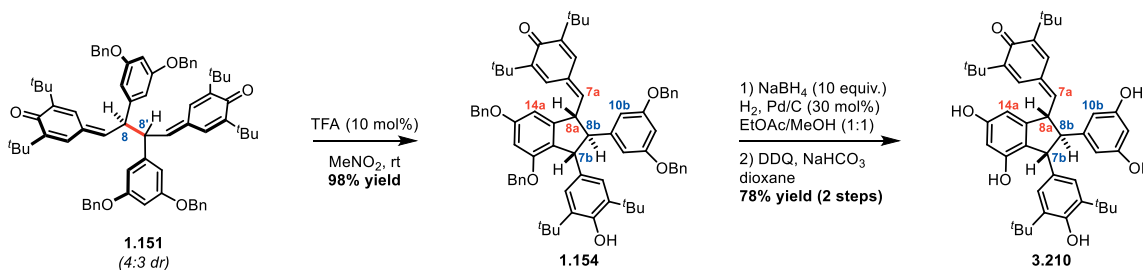


Figure 3.45. Diastereoconvergent cyclization affords synthesis of quinone methide intermediate 3.210.

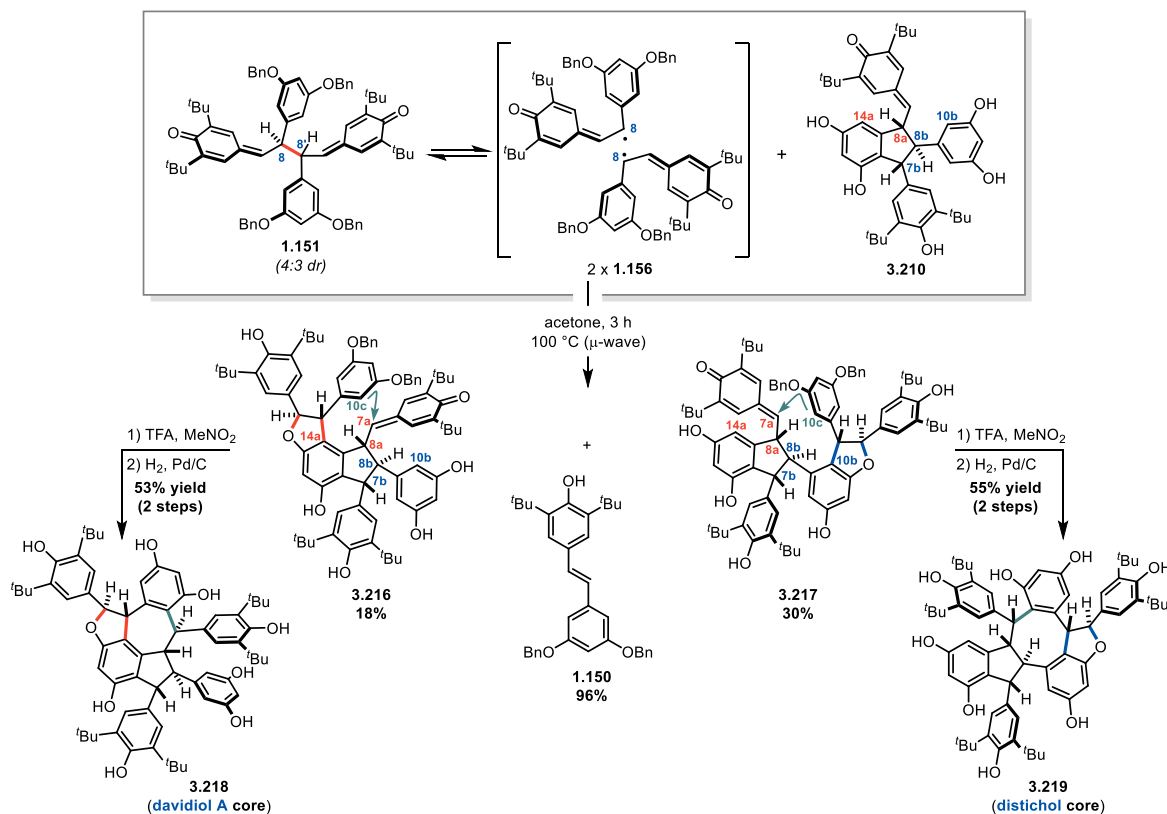


Figure 3.46. Radical DHB synthesis with 3.210 leads to two resveratrol trimer cores. Importantly, **1.150**, the stilbene precursor to **1.151**, was isolated in 96% yield, resulting from one equivalent of **1.156** serving as an oxidant and proton sponge during this transformation. The final C10c–C7a bond of the carbocyclic framework for each resveratrol trimer core was formed via a Brønsted-acid promoted intramolecular Friedel Crafts reaction. The core of davidiol A (**3.218**) was prepared after cyclization of **3.216** and subsequent hydrogenolysis of the remaining two benzyl ethers, and this same two-step protocol from **3.217** afforded the core of distichol (**3.219**). Each of these compounds requires C3-*de-tert*-butylation to achieve to first total synthesis of these natural products, and work to complete this goal is now being spearheaded by two excellent colleagues – Matthew Galliher and Rebeca Roldan. Furthermore, while they continue to optimize the approach to these two compounds, synthesis of resveratrol oligomers from the radical DHB synthesis strategy will

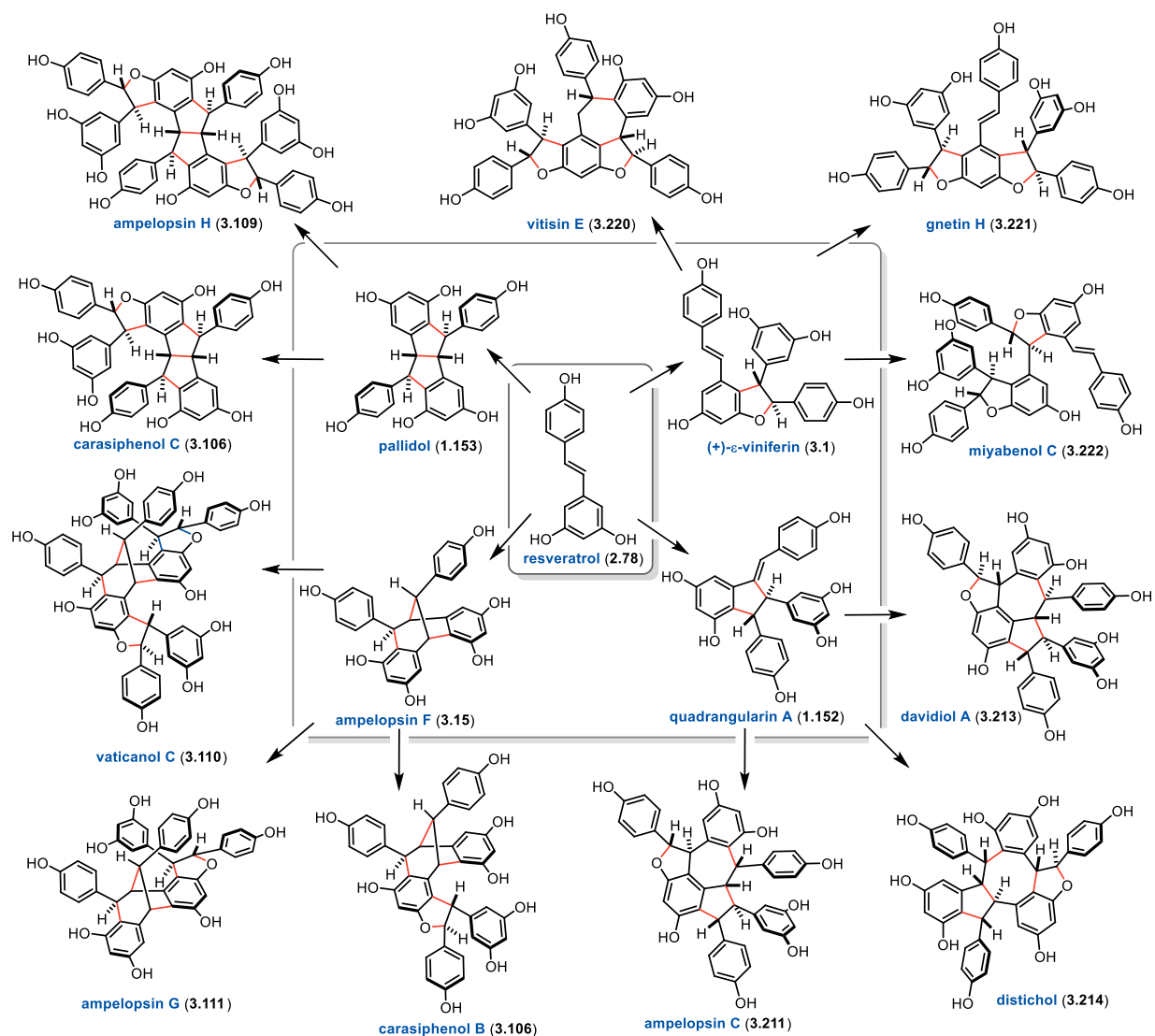


Figure 3.47. Radical DHB synthesis offers an approach for the unified synthesis of higher-order resveratrol oligomers.

by no means be limited to these two natural products. In principle, this reactivity directly mimics the manner in which these molecules are constructed biosynthetically (Figure 3.2), thus many suitably substituted phenols have the potential to act as a scaffold for radical DHB synthesis and lead to the preparation of higher-order resveratrol oligomers. It is reasonable to envision that, with the suitable choice of arene blocking groups and phenol protection, this approach leveraging persistent phenoxyl radicals will afford the unified synthesis of resveratrol oligomers from dimer scaffolds, as depicted in Figure 3.47.

3.8 Conclusions

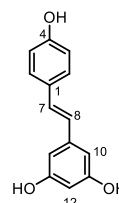
The first total synthesis of C3c–C8b resveratrol tetramers – vitisin A (**3.146**) and vitisin D (**3.148**) – has been accomplished in just 13 and 14 total steps, respectively. This represents just the third total synthesis of resveratrol tetramers, and, in terms of step count and overall yield, it is on par with the state of the art efforts in the field.^{48,221} This synthesis relies upon the intermediacy of persistent radicals – a concept that had minimal precedent in the literature beyond our own research group when these endeavors commenced.⁷ The key C8–C8' to C3–C8' homolytic bond migration step was discovered and developed through careful physical organic analysis of the equilibrium between persistent phenoxyl radicals and their corresponding C8–C8' dimers. Importantly, anodic oxidation offers a mild approach for the generation of these persistent radicals in order to harness their reactivity, and the excellent dimerization diastereoselectivity for the preparation of bis-quinone methide **3.191** from racemic ϵ -viniferin analog **3.189** suggests that an enantioselective approach to **3.189** would allow for asymmetric synthesis of these resveratrol tetramers. The route to **3.189** disclosed herein utilizing a racemic reduction of a benzofuran (**3.163** or **3.181**) provides the necessary platform to achieve this goal, as the asymmetric reduction of either intermediate would allow for enantioselective preparation of **3.189**. Finally, after homolytic bond migration, the intramolecular cyclization reactions that prepared vitisin A (**3.146**) and vitisin D (**3.148**) are consistent with the proposed biogenesis for these natural products. Providing synthetic access to these two compounds will enable further evaluation of their pharmacological potential, and we look forward to the results of those subsequent studies.

3.9 Experimental Procedures and Spectral Data

General Procedures: Unless specifically noted otherwise, all glassware was flame-dried under vacuum (~0.5 Torr) and cooled under inert atmosphere (N₂ or Ar) prior to use. Each reaction container was charged with a Teflon/PTFE-coated magnetic stir bar and sealed with a rubber septum to maintain a positive pressure of inert atmosphere (N₂ or Ar). Reagents sensitive to the atmosphere were transferred via syringe or cannula as necessary. Reactions that required microwave irradiation were conducted in a Biotage Initiator+ Microwave Synthesizer. Reaction conversion was evaluated using analytical thin-layer chromatography (TLC) using Merck silica gel 60 F254 TLC plates. TLC plates were visualized under a dual short wave/long wave UV lamp and/or stained using solutions of *p*-anisaldehyde or potassium permanganate or ceric ammonium molybdate. Stained plates were developed over a heat gun as needed. Either sodium sulfate or magnesium sulfate were utilized to exclude water from worked up reactions, and the solvent was removed on Büchi rotary evaporators and/or a Welch vacuum pump. Reactions were purified via flash column chromatography either with Biotage SNAP Ultra chromatography cartridges using a Biotage Isolera automated purification system or manually using 230-400 mesh silica gel. Final purification of natural products was achieved using reverse phase preparative HPLC on an Agilent 1290 Infinity II Preparative LC/MSD System. All electrochemical experiments were acquired using either a CH1620E electrochemical analyzer (from CH Instruments) or a uSTAT4000 4-Channel Potentiostat/Galvanostat (from Metrohm USA). Bulk electrolysis experiments were performed on discovery scale in open 10-mL vials and in a beaker of the appropriate size (15–40 mL) for the subsequent scale-up experiments. These reactions used RVC panels (reticulated vitreous carbon, 100 ppi, 0.25-inch thickness, 3% relative density, from McMaster Carr) as the working or counter/auxiliary electrodes and a Ag/AgCl (3 M KCl) reference electrode.

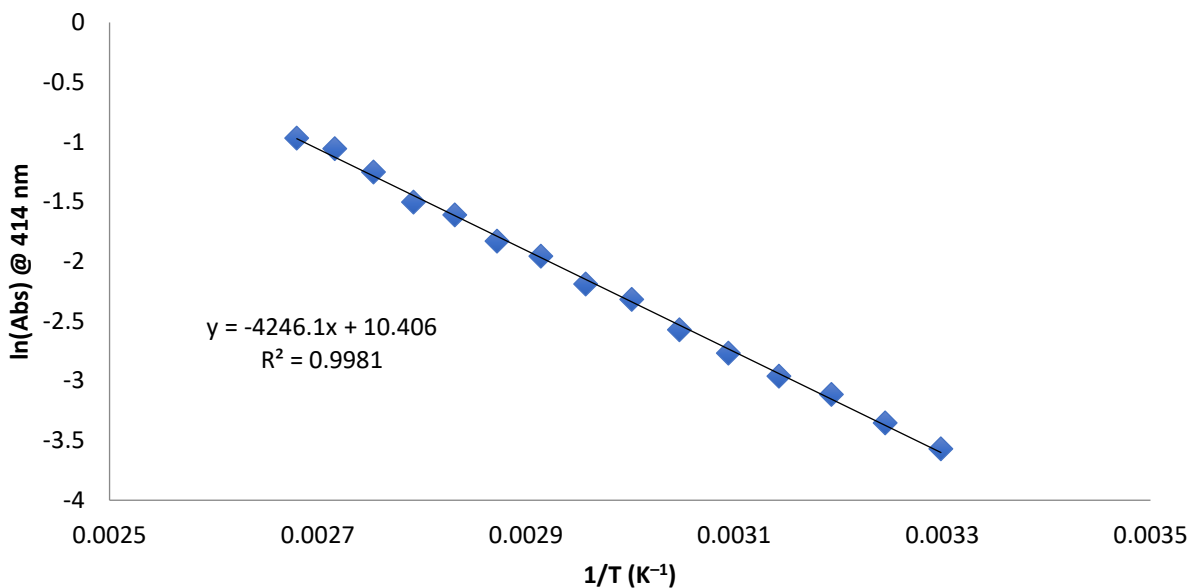
Reaction Materials: Commercially available reagents were used without further purification unless specified. Organic solvents (acetonitrile, dichloromethane, diethyl ether, dimethylformamide, dimethyl sulfoxide, methanol, tetrahydrofuran, and toluene) and amine bases (triethylamine, pyridine, N,N-diisopropylethylamine, and diisopropylamine) were purified prior to use with a Phoenix Solvent Drying System from JC-Meyer Solvent Systems and PureSolv Micro amine drying columns from Innovative Technology, respectively, and kept under a pressure of argon. Solutions of organolithium reagents and Grignard reagents were purchased from Acros Organics and titrated prior to use.

Product Analysis: Product names were obtained using ChemDraw Professional 16.0 from Perkin Elmer. For racemic compounds, the name corresponds to the depicted structure. Nuclear magnetic resonance (NMR) spectra were obtained using an internal deuterium lock on Varian Inova 500 or Varian VNMR 500 and 700 spectrometers. For ¹H spectra, chemical shifts were referenced to the center line of the residual solvent signal (CDCl₃: δ 7.26; acetone-*d*₆: δ 2.05; methanol-*d*₄: δ 3.31) and are reported in parts per million (ppm). Signal multiplicity is reported as follows: (br = broad, s = singlet, d = doublet, t = triplet, dd = doublet of doublets, ddd = doublet of doublet of doublets, m = multiplet), and the associated coupling constants are given in Hertz. For ¹³C spectra, experiments were completely heterodecoupled (broadband) and chemical shifts are reported as ppm using the center line of the solvent signal as reference (CDCl₃: δ 77.16; acetone-*d*₆: δ 29.96; methanol-*d*₄: δ 49.00). The following resveratrol numbering scheme was used for the assignment of ¹H and ¹³C NMR signals. High-resolution mass spectra (HRMS) were acquired using a Micromass AutoSpec Ultima Magnetic Sector mass spectrometer using electrospray ionization (ESI), positive ion mode. We thank James Windak and Paul Lennon at the University of Michigan, Department of Chemistry Instrumentation Facility for conducting the HRMS experiments. Infrared spectra were acquired using a Perkin-Elmer Spectrum BX FT-IR spectrophotometer using an ATR mount with a ZnSe crystal. UV-Vis spectra were recorded on an Agilent Cary 100 UV-Vis spectrophotometer equipped with a 6x6 thermostated multi-cell holder and a Cary temperature controller unit. Electron paramagnetic resonance (EPR) spectra were recorded on a Bruker EMXplus (X-band) equipped with an ER 4119HS cavity in a temperature range from 10 to 50 °C. Samples were typically 50 μM in benzene and the radical concentration was determined using the quantitative EPR package of the Bruker Xenon software.

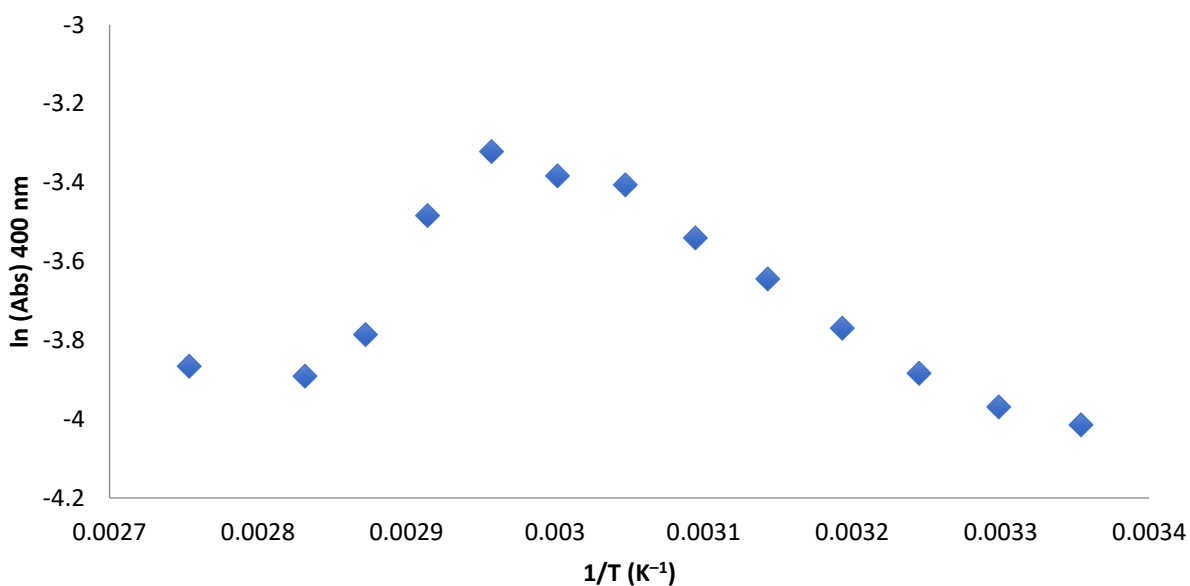


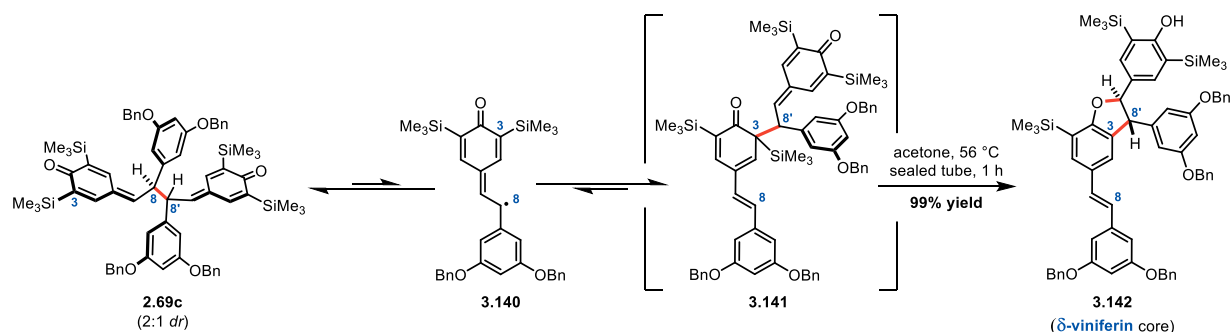
UV-Vis/EPR: The temperature dependent UV-Vis measurements were performed as follows: To a 3.5 mL quartz cuvette was added 2.475 mL of 1,2-dichlorobenzene (dried over sieves) and 25 μL of a 5 mM stock of substrate in 1,2-dichlorobenzene. The cuvette was capped with a rubber septum and purged with nitrogen for 10 minutes. The cuvette was connected to a nitrogen balloon to maintain a pressure of nitrogen throughout the experiment. A cuvette containing only solvent was used as a baseline throughout the experiment to record baseline-corrected data at each temperature. The cuvette was loaded into the multi-cell holder and allowed to equilibrate to each recorded temperature for at least 5 minutes before the absorbance reading. To determine the radical's extinction coefficient, a UV-Vis spectrum of a 50 μM sample in benzene was measured and the solution then transferred into an EPR tube where the radical concentration was determined by EPR at the same temperature. Substitution of Beer's law into the Van't Hoff equation affords an inverse relationship between the natural log of UV-Vis absorbance and temperature.

van't Hoff analysis of 1.151/1.156 equilibrium



van't Hoff analysis of 2.69c/3.140 equilibrium





3.142 - 4-((2R)-3-(3,5-bis(benzyloxy)phenyl)-5-((E)-3,5-bis(benzyloxy)styryl)-7-(trimethylsilyl)-2,3-dihydrobenzofuran-2-yl)-2,6-bis(trimethylsilyl)phenol

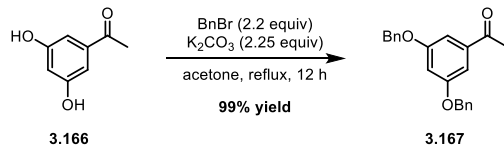
Quinone methide dimer **2.69c** (80 mg, 0.0725 mmol; obtained from our prior report⁹⁸) was dissolved in acetone (1.5 mL, HPLC-grade) in a 2-dram vial charged with a stir bar. The yellow solution was vigorously sparged with a balloon of argon for >5 min to exclude oxygen, and the reaction vial was capped and sealed with parafilm. The vial was heated at 56 °C for 1 hour, during which the solution transitioned from yellow to colorless. After 1 hour had passed, the reaction was cooled to room temperature, the stir bar was removed, and the solvent was evaporated under reduced pressure to afford δ -viniferin core **3.142** (74 mg, 99% yield) as an off-white foam. **Note:** The key to excellent yield for this reaction is the exclusion of oxygen. If not rigorously degassed, disproportionation of **2.69c** occurs as a minor reaction pathway to return half of the dimeric material to the stilbene precursor and resulting in decomposition of the other half. Compound **3.142** was characterized in a prior report from our group.⁴⁸ This same protocol was followed for the crossover experiment between **2.69c** and **3.192** (see Figure 3.38).

¹H NMR (500 MHz, Chloroform-*d*) δ 7.47 – 7.28 (m, 20H), 7.39 (s, overlap, 1H, C6–H), 7.27 (s, 2H, C2'–H), 7.19 (br s, 1H, C2–H), 7.03 (d, *J* = 16.3 Hz, 1H, C7–H), 6.82 (d, *J* = 16.3 Hz, C8–H), 6.74 (d, *J* = 2.2 Hz, 2H, C10–H), 6.60 (t, *J* = 2.2 Hz, 1H, C12'–H), 6.52 (t, *J* = 2.2 Hz, 1H, C12–H), 6.50 (d, *J* = 2.2 Hz, 2H, C10'–H), 5.51 (d, *J* = 9.2 Hz, 1H, C7'–H), 5.07 (s, 4H, C11a–OCH₂C₆H₅), 5.03 (s, 1H, C4'–OH), 5.00 (s, 4H, C11'–H), 4.35 (d, *J* = 9.2 Hz, 1H, C8'–H), 0.39 (s, 9H, C5–Si(CH₃)₃), 0.31 (s, 18H, C3/5'–Si(CH₃)₃)

¹³C NMR (126 MHz, Chloroform-*d*) δ 165.24 (C4), 165.19 (C4'), 160.5 (C11'), 160.4 (C11), 144.3 (C9'), 140.2 (C9), 137.2 (–OCH₂C₆H₅), 136.9 (–OCH₂C₆H₅), 133.8 (C2'), 133.6 (C6), 132.8 (C1'), 130.4 (C1), 129.7 (C7), 129.6 (C3), 128.8 (–OCH₂C₆H₅), 128.3 (–OCH₂C₆H₅), 128.2 (–OCH₂C₆H₅), 127.9 (–OCH₂C₆H₅), 127.8 (–OCH₂C₆H₅), 126.0 (C8), 124.4 (C3'), 124.0 (C2), 120.3 (C5), 108.1 (C10'), 105.6 (C10), 101.4 (C12), 100.8 (C12'), 92.6 (C7'), 70.4 (C11'–OCH₂C₆H₅), 70.3 (C11–OCH₂C₆H₅), 58.3 (C8'), –0.3 (C3/5'–Si(CH₃)₃), –0.9 (C5–Si(CH₃)₃)

IR (Neat): 3606, 2951, 1586, 1497, 1454, 1398, 1294, 1244, 1149, 1057, 1029, 960, 905, 834, 733, 694 cm⁻¹.

HRMS (ESI) *m/z* calculated for C₆₅H₇₁O₆Si₃⁺ ([M+H]⁺) 1031.4533, found 1031.4528.



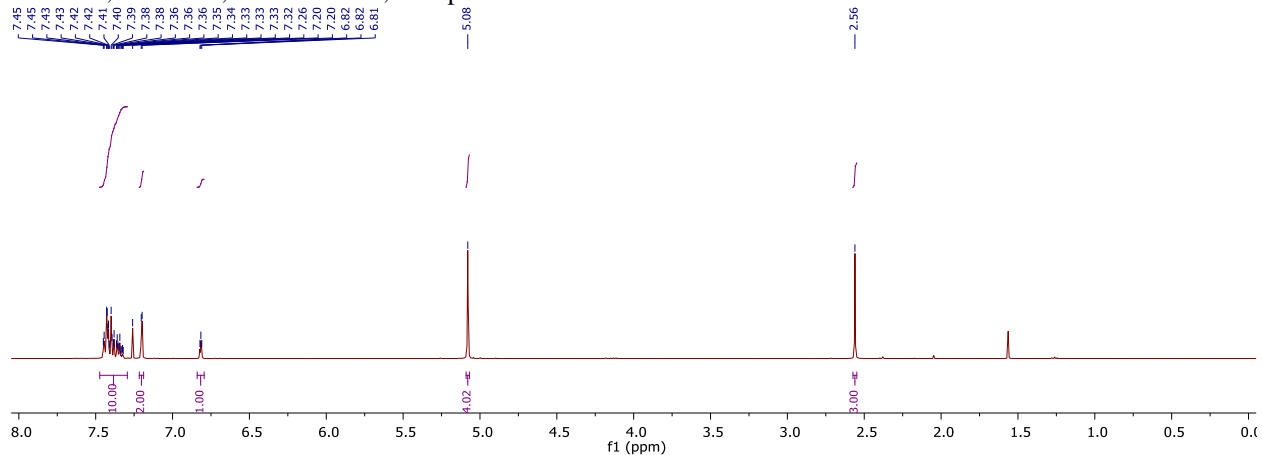
3.167 – 1-(3,5-bis(benzyloxy)phenyl)ethan-1-one

The starting acetophenone **3.166** (5.0 g, 32.9 mmol) and K_2CO_3 (10.2 g, 73.9 mmol, 2.25 equiv) were added to a flame-dried 2-neck 250 mL round bottom flask fitted with a reflux condenser and charged with a stir bar under inert atmosphere. The solids were suspended/dissolved in acetone (90 mL), and to the stirring reaction mixture was added BnBr (8.6 mL, 72.3 mmol, 2.2 equiv) via syringe. The reaction mixture was heated at reflux for 12 hours; after cooling to room temperature, the heterogeneous reaction mixture was filtered over Celite, concentrated, and purified by column chromatography (5-30% EtOAc in Hexanes) to afford the desired product **3.167** as a white solid (10.8 g, 99% yield). The ^1H and ^{13}C NMR data was consistent with the literature data for this compound.²⁹⁹

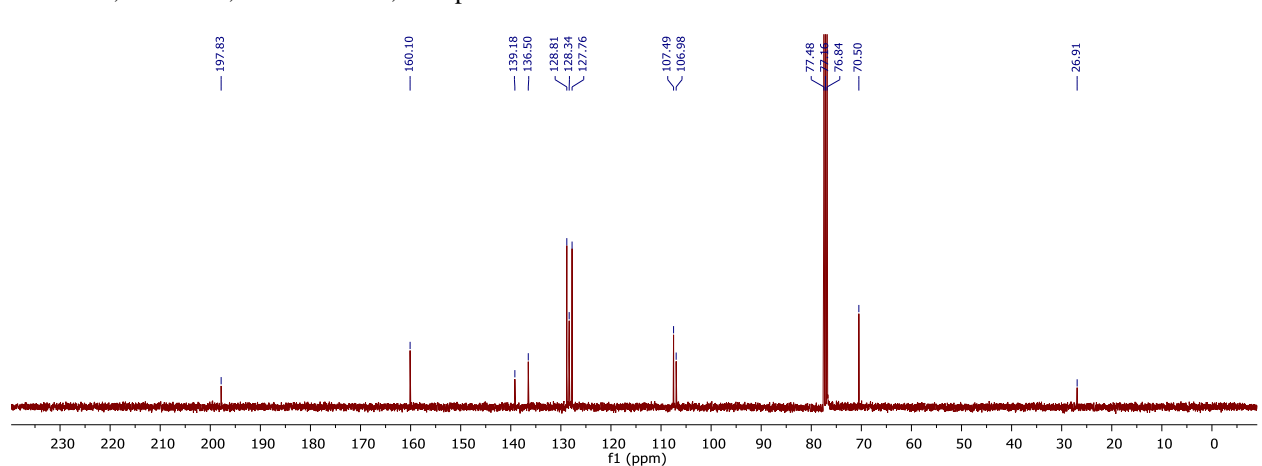
^1H NMR (400 MHz, Chloroform-*d*) δ 7.47 – 7.29 (m, 10H), 7.20 (d, $J = 2.3$ Hz, 2H), 6.82 (t, $J = 2.3$ Hz, 1H), 5.08 (s, 4H), 2.56 (s, 3H).

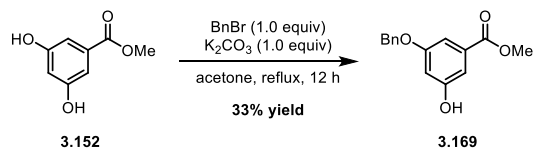
^{13}C NMR (100 MHz, Chloroform-*d*) δ 197.83, 160.10, 139.18, 136.50, 128.81, 128.34, 127.76, 107.49, 106.98, 70.50, 26.91.

^1H NMR, 400 MHz, Chloroform-*d*, Compound **3.167**



^{13}C NMR, 100 MHz, Chloroform-*d*, Compound **3.167**





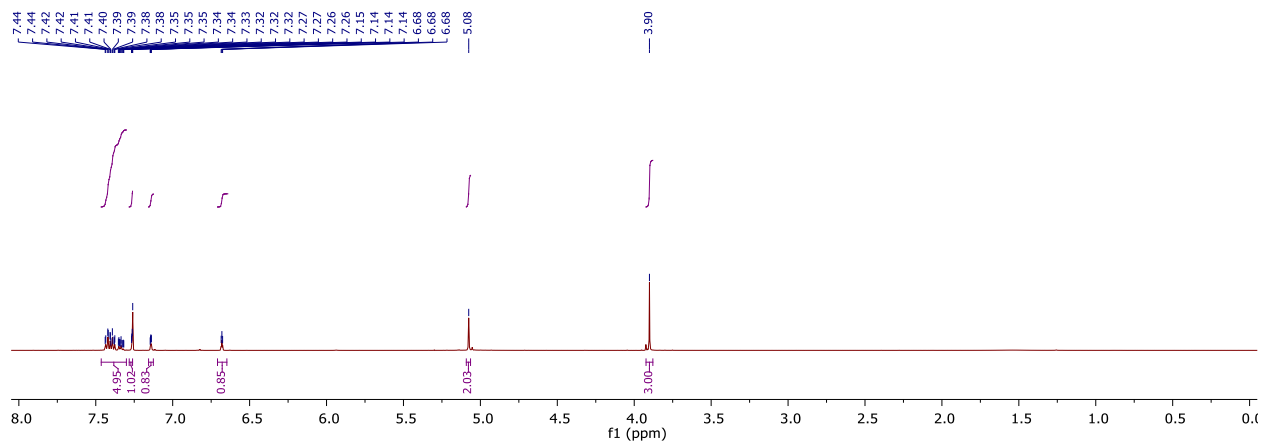
3.169 – methyl 3-(benzyloxy)-5-hydroxybenzoate

The starting ester **3.152** (5.0 g, 29.7 mmol) and K_2CO_3 (4.11 g, 29.7 mmol, 1.0 equiv) were added to a flame-dried 2-neck 250 mL round bottom flask fitted with a reflux condenser and charged with a stir bar under inert atmosphere. The solids were suspended/dissolved in acetone (90 mL), and to the stirring reaction mixture was added BnBr (3.6 mL, 29.7 mmol, 1.0 equiv) via syringe. The reaction mixture was heated at reflux for 12 hours; after cooling to room temperature, the heterogeneous reaction mixture was filtered over Celite, concentrated, and purified by column chromatography (5–30% EtOAc in Hexanes) to afford the desired product **3.169** as a white solid (2.5 g, 33% yield). The ^1H and ^{13}C NMR data was consistent with the literature data for this compound.³⁰⁰

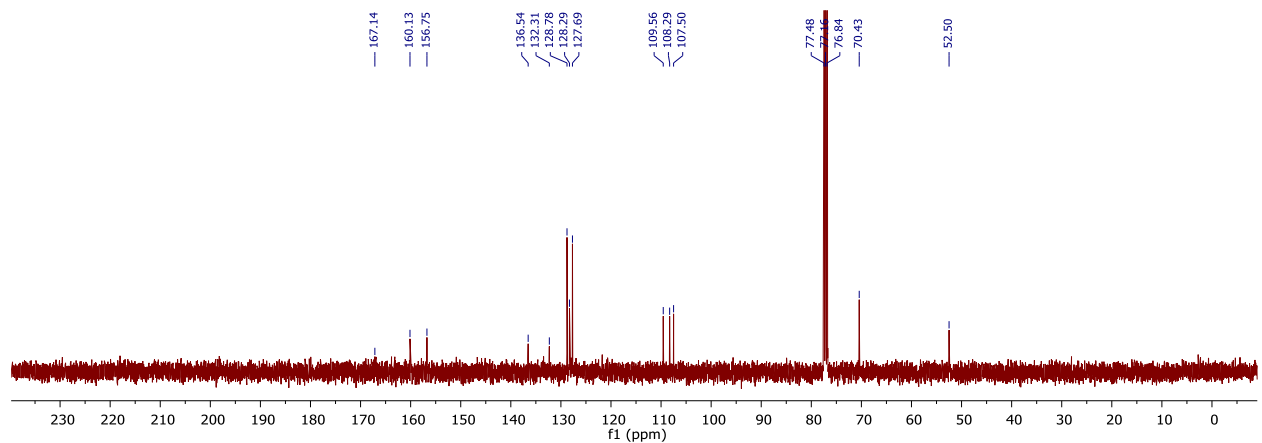
^1H NMR (500 MHz, Chloroform-*d*) δ 7.46 – 7.30 (m, 5H), 7.28 – 7.26 (m, 1H), 7.14 (dd, $J = 2.5, 1.4$ Hz, 1H), 6.68 (t, $J = 2.3$ Hz, 1H), 5.08 (s, 2H), 3.90 (s, 3H).

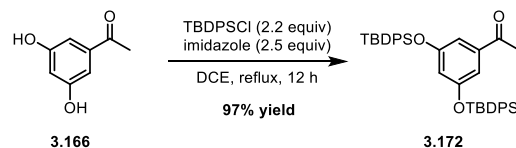
^{13}C NMR (100 MHz, Chloroform-*d*) δ 167.14, 160.13, 156.75, 136.54, 132.31, 128.78, 128.29, 127.69, 109.56, 108.29, 107.50, 70.43, 52.50.

^1H NMR, 500 MHz, Chloroform-*d*, Compound **3.169**



^{13}C NMR, 100 MHz, Chloroform-*d*, Compound **3.169**





3.172 – 1-(3,5-bis((tert-butyl)diphenylsilyloxy)phenyl)ethan-1-one

The starting acetophenone **S9** (5.0 g, 32.9 mmol) and imidazole (5.0 g, 73.9 mmol, 2.25 equiv) were added to a flame-dried round bottom flask fitted with a reflux condenser and charged with a stir bar under inert atmosphere. The solids were suspended in 1,2-dichloroethane (115 mL), and to the stirring suspension was added TBDPSCl (18.8 mL, 72.3 mmol, 2.2 equiv) via syringe. The reaction mixture was heated at reflux for 12 hours; after cooling to room temperature, the heterogeneous reaction mixture was filtered over Celite, concentrated, and purified by column chromatography (0-20% EtOAc in Hexanes) to afford the desired product **S10** as a colorless solid (20 g, 97% yield).

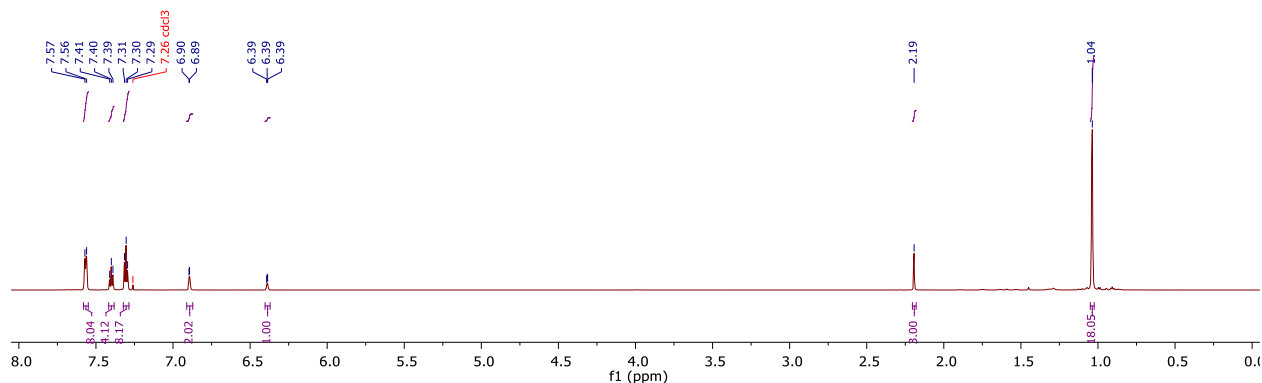
^1H NMR (700 MHz, Chloroform-*d*) δ 7.57 (d, J = 7.6 Hz, 8H), 7.40 (t, J = 7.4 Hz, 4H), 7.30 (t, J = 7.0 Hz, 8H), 6.89 (d, J = 2.5 Hz, 2H), 6.39 (d, J = 2.3 Hz, 1H), 2.19 (s, 3H), 1.04 (s, 18H).

^{13}C NMR (176 MHz, Chloroform-*d*) δ 197.7, 156.5, 138.6, 135.6, 132.5, 130.0, 127.9, 116.4, 113.2, 26.6 (2C), 19.6.

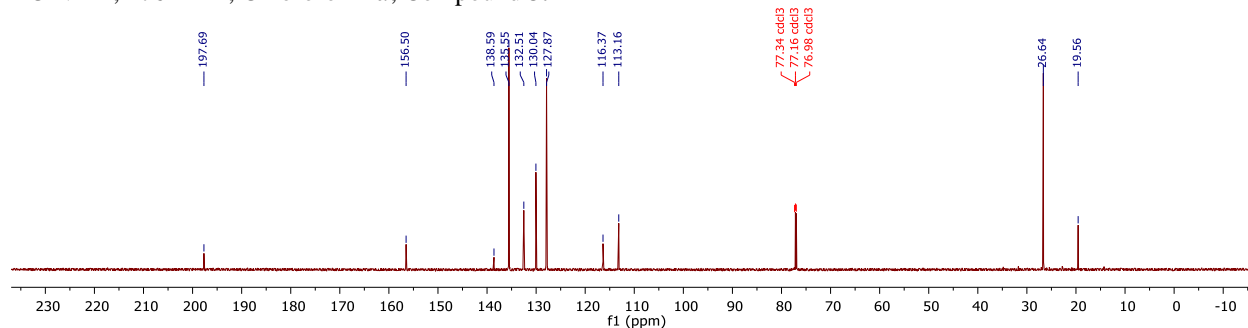
IR (Neat): 2977, 1684, 1589, 1556, 1364, 1298, 1187, 1151, 1110 cm^{-1} .

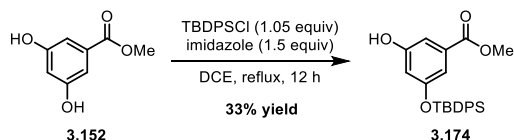
HRMS (ESI) m/z calculated for $\text{C}_{40}\text{H}_{45}\text{O}_3\text{Si}_2^+$ ($[\text{M}+\text{H}]^+$) 629.2902, found 629.2901.

^1H NMR, 700 MHz, Chloroform-*d*, Compound **3.172**



^{13}C NMR, 176 MHz, Chloroform-*d*, Compound **3.172**





3.174 – methyl 3-((*tert*-butyldiphenylsilyloxy)-5-hydroxybenzoate

The starting acetophenone **3.152** (2.0 g, 11.9 mmol) and imidazole (1.2 g, 1.8 mmol, 1.5 equiv) were added to a flame-dried round bottom flask fitted with a reflux condenser and charged with a stir bar under inert atmosphere. The solids were suspended in 1,2-dichloroethane (100 mL), and to the stirring suspension was added TBDPSCI (3.25 mL, 1.25 mmol, 1.05 equiv) via syringe. The reaction mixture was heated at reflux for 12 hours; after cooling to room temperature, the heterogeneous reaction mixture was filtered over Celite, concentrated, and purified by column chromatography (0-40% EtOAc in Hexanes) to afford the desired product **3.174** as a white solid (1.63 g, 33% yield).

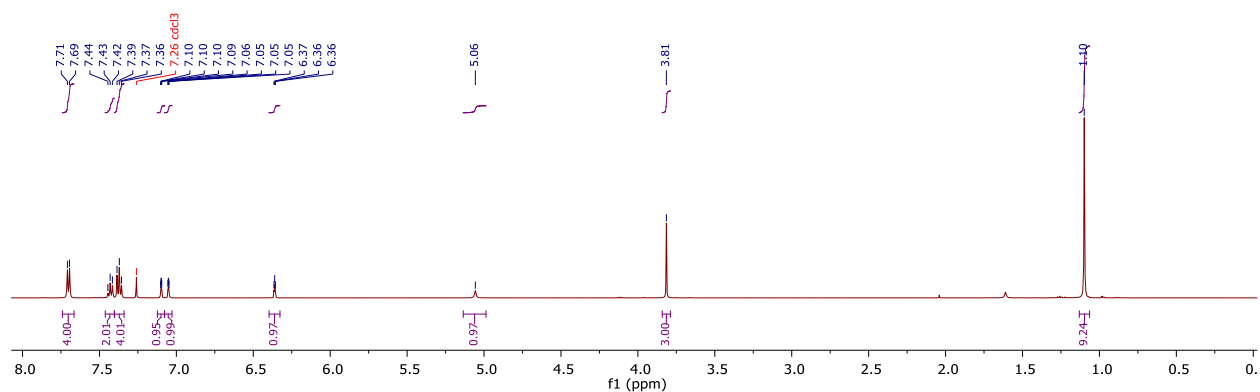
$^1\text{H NMR}$ (500 MHz, Chloroform-*d*) δ 7.70 (d, $J = 6.6$ Hz, 4H), 7.43 (t, $J = 7.3$ Hz, 2H), 7.37 (t, $J = 7.2$ Hz, 4H), 7.10 (dd, $J = 2.2, 1.4$ Hz, 1H), 7.05 (dd, $J = 2.3, 1.4$ Hz, 1H), 6.36 (t, $J = 2.3$ Hz, 1H), 5.06 (s, 1H), 3.81 (s, 3H), 1.10 (s, 9H).

$^{13}\text{C NMR}$ (126 MHz, Chloroform-*d*) δ 166.9, 156.9, 156.3, 135.6, 132.5, 132.0, 130.2, 128.0, 114.0, 111.8, 109.6, 52.3, 26.6, 19.6.

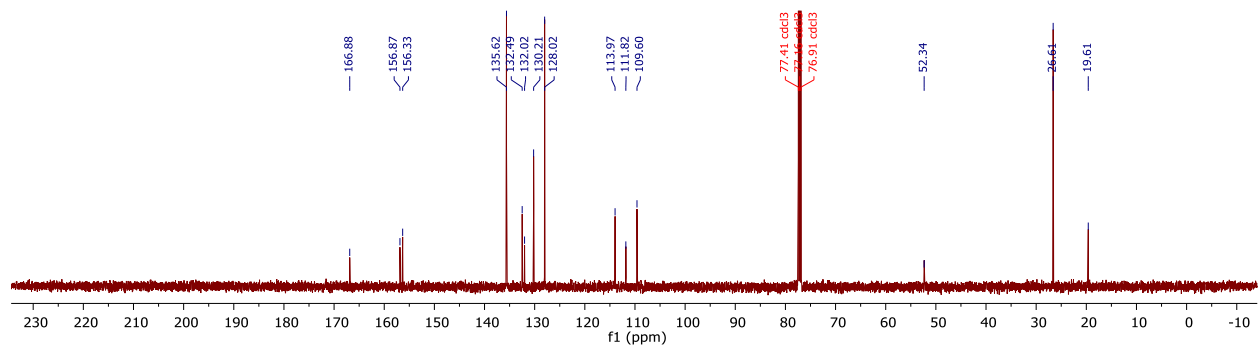
IR (Neat): 3423 (br), 2974, 1724, 1586, 1364, 1298, 1182, 1156, 1124 cm^{-1} .

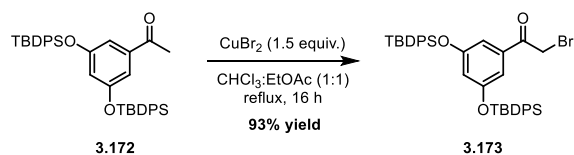
HRMS (ESI) m/z calculated for $\text{C}_{24}\text{H}_{27}\text{O}_4\text{Si}^+$ ($[\text{M}+\text{H}]^+$) 407.1673, found 407.1675.

$^1\text{H NMR}$, 500 MHz, Chloroform-*d*, Compound **3.174**



$^{13}\text{C NMR}$, 126 MHz, Chloroform-*d*, Compound **3.174**





3.173 – 1-(3,5-bis((tert-butyl)phenylsilyloxy)phenyl)-2-bromoethan-1-one

The starting acetophenone **3.172** (7.50 g, 11.9 mmol) was added to a flame-dried round bottom flask fitted with a reflux condenser and charged with a stir bar under inert atmosphere. The starting material was dissolved in a 1:1 solution of CHCl_3 and EtOAc (100 mL), and CuBr_2 (4.00 g, 17.9 mmol, 1.5 equiv) was added to the reaction solution. The reaction was heated at reflux overnight (~16 h), at which point it was cooled to rt and filtered through a plug of Celite in the fume hood, eluting with DCM (~100 mL). The filtrate was transferred to a separatory funnel containing sat'd aq. NaHCO_3 (100 mL). The layers were separated, and the organic layer was washed with aqueous solution of 10% sodium thiosulphate (100 mL). The fully quenched organic layer was subsequently washed with brine, dried over Na_2SO_4 , and concentrated under reduced pressure. The crude product was purified by flash column chromatography (5% to 40% DCM/Hexanes) to afford the desired brominated product **3.173** as a white solid (6.3 g, 75% yield) in addition to unreacted **3.172** as a clear, colorless oil (1.50 g, 2.38 mmol). The yield based on recovered **3.172** is 93%.

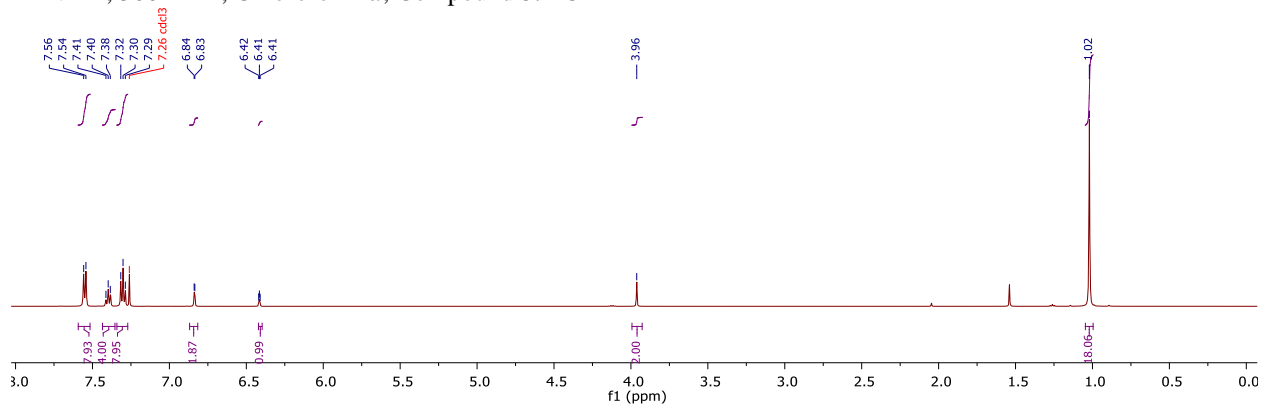
^1H NMR (500 MHz, Chloroform-*d*) δ 7.55 (d, $J = 7.3$ Hz, 8H), 7.40 (t, $J = 7.1$ Hz, 4H), 7.30 (t, $J = 7.4$ Hz, 8H), 6.84 (d, $J = 2.2$ Hz, 2H), 6.42 (d, $J = 2.3$ Hz, 1H), 3.96 (s, 2H), 1.02 (s, 18H).

^{13}C NMR (126 MHz, Chloroform-*d*) δ 190.6, 156.8, 135.6, 135.3, 132.4, 130.2, 128.0, 117.4, 113.6, 31.5, 26.6, 19.6.

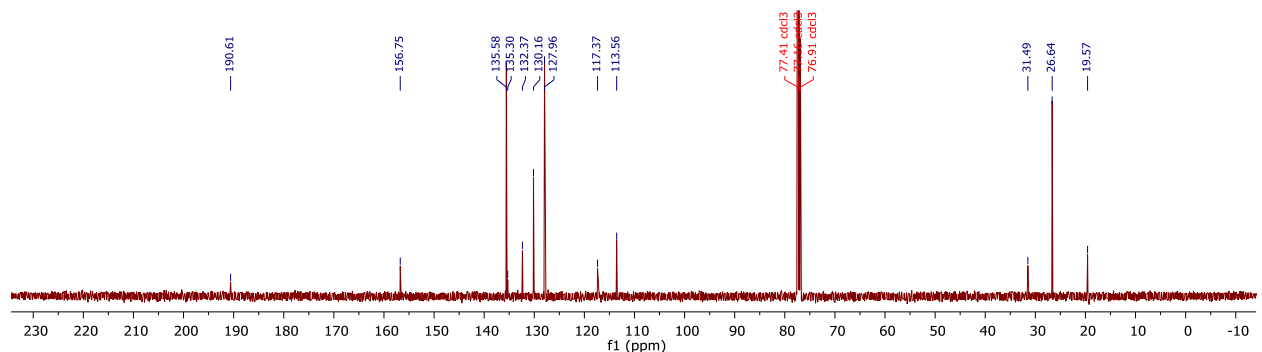
IR (Neat): 2977, 1684, 1589, 1556, 1364, 1298, 1187, 1151, 1110, 742 cm^{-1} .

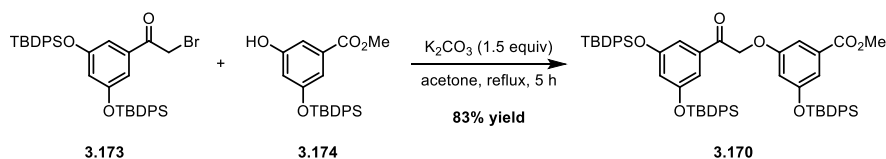
HRMS (ESI) m/z calculated for $\text{C}_{40}\text{H}_{44}\text{BrO}_3\text{Si}_2^+$ ($[\text{M}+\text{H}]^+$) 707.2007, found 707.2001.

^1H NMR, 500 MHz, Chloroform-*d*, Compound **3.173**



^{13}C NMR, 126 MHz, Chloroform-*d*, Compound **3.173**





3.170 - methyl 3-(2-(3,5-bis((tert-butyldiphenylsilyl)oxy)phenyl)-2-oxoethoxy)-5-((tert-butyldiphenylsilyl)oxy)benzoate

A solution of the starting phenol **3.174** (0.65 g, 1.60 mmol, 1.0 equiv) and bromide **3.173** (1.30 g, 1.84 mmol, 1.15 equiv) in acetone (30 mL) was prepared in a flame-dried, 100 mL rb flask fitted with reflux condenser under inert atmosphere. To the stirring solution was added K_2CO_3 (0.331 g, 2.40 mmol, 1.5 equiv) in a single portion, and the reaction was heated to reflux for 5 h. Upon cooling to rt, the crude reaction was concentrated under reduced pressure. The residue was dissolved in EtOAc and added to a sep. funnel containing DI H_2O . The layers were separated, and the organic layer was washed with brine, dried over MgSO_4 , and concentrated. The crude product was purified by flash column chromatography (1%, 2%, 3%, 5%, 8%, 12%, 18% EtOAc in Hexanes, 1.5 CV per step, CV = 200 mL) to afford the product **3.170** as a white foam (1.37 g, 1.33 mmol, 83% yield).

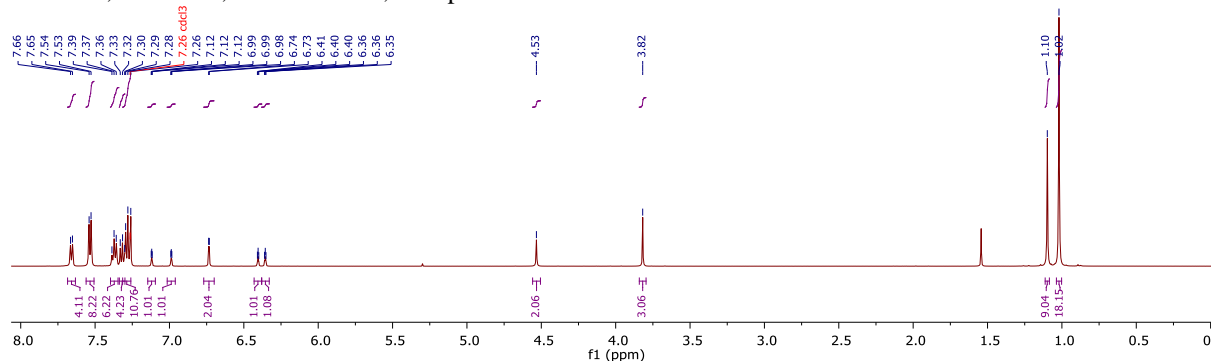
$^1\text{H NMR}$ (500 MHz, Chloroform-*d*) δ 7.66 (d, $J = 6.4$ Hz, 4H), 7.53 (d, $J = 6.5$ Hz, 8H), 7.37 (t, $J = 7.3$ Hz, 6H), 7.32 (d, $J = 7.7$ Hz, 4H), 7.28 (t, $J = 7.5$ Hz, 8H), 7.12 (t, $J = 1.7$ Hz, 1H), 7.02 – 6.96 (m, 1H), 6.73 (d, $J = 2.2$ Hz, 2H), 6.40 (t, $J = 2.2$ Hz, 1H), 6.36 (t, $J = 2.4$ Hz, 1H), 4.53 (s, 2H), 3.82 (s, 3H), 1.10 (s, 9H), 1.02 (s, 18H).

$^{13}\text{C NMR}$ (126 MHz, Chloroform-*d*) δ 192.7, 166.7, 158.7, 156.7, 156.7, 135.6, 135.6, 132.5, 132.3, 131.9, 130.20, 130.18, 128.0, 127.9, 117.2, 114.8, 113.8, 112.6, 111.7, 108.7, 70.3, 52.2, 26.70, 26.66, 19.64, 19.57.

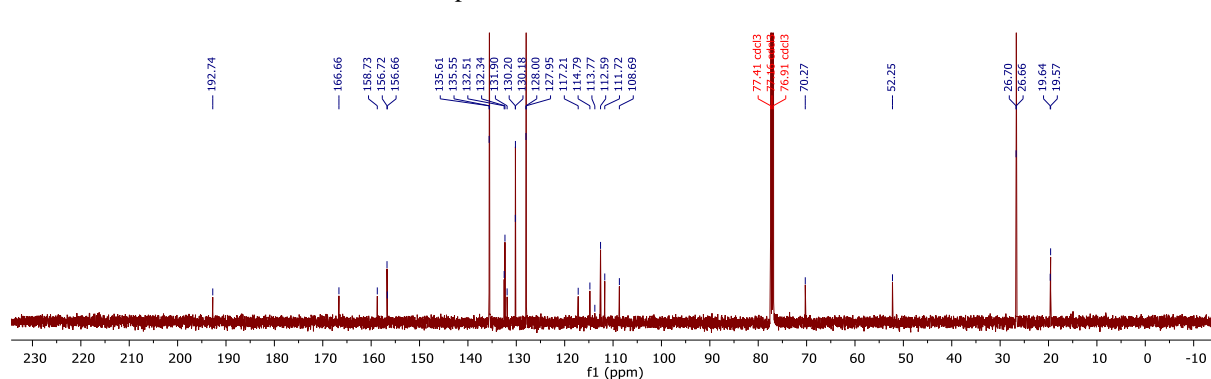
IR (Neat): 2977, 1724, 1684, 1589, 1556, 1364, 1298, 1187, 1151, 1110 cm^{-1} .

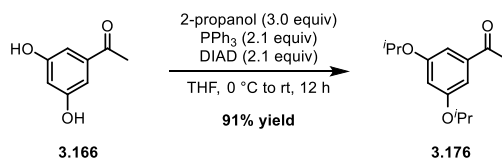
HRMS (ESI) m/z calculated for $\text{C}_{64}\text{H}_{69}\text{O}_7\text{Si}_3^+$ ($[\text{M}+\text{H}]^+$) 1033.4346, found 1033.4336.

$^1\text{H NMR}$, 500 MHz, Chloroform-*d*, Compound **3.170**



$^{13}\text{C NMR}$, 126 MHz, Chloroform-*d*, Compound **3.170**





3.176 – 1-(3,5-diisopropoxyphenyl)ethan-1-one

The starting acetophenone **3.166** (3.00 g, 19.7 mmol), 2-propanol (4.52 mL, 59.2 mmol, 3.0 equiv) and PPh₃ (10.9 g, 41.4 mmol, 2.10 equiv) were added to a flame-dried 250-mL round bottom flask charged with a stir bar under inert atmosphere. The starting materials were dissolved in THF (60 mL), and to the stirring solution was cooled to 0 °C in an ice bath. To the cold solution was added DIAD (8.15 mL, 41.4 mmol, 2.10 equiv) via syringe pump over 20 minutes. The reaction mixture was allowed to warm to room temperature over 12 hours, at which point the reaction was concentrated onto Celite and purified by column chromatography (0-15% EtOAc in Hexanes) to afford the desired product **3.176** as a colorless oil (4.26 g, 91% yield).

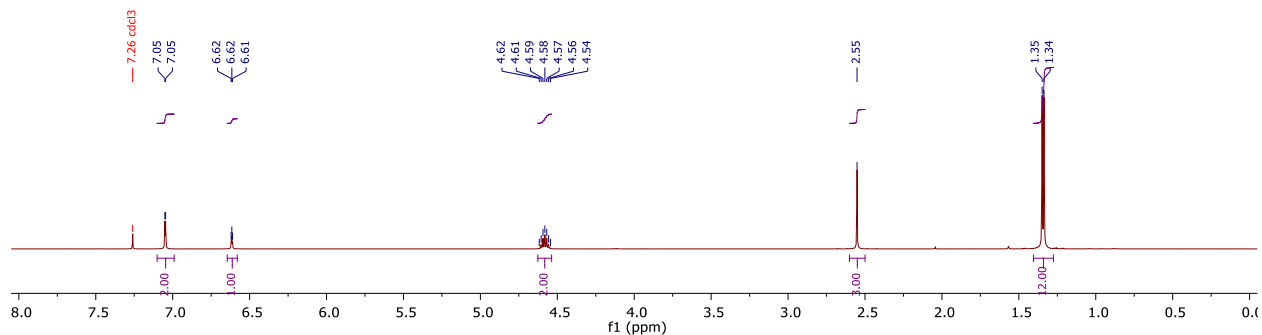
¹H NMR (500 MHz, Chloroform-*d*) δ 7.05 (d, *J* = 2.3 Hz, 2H), 6.62 (t, *J* = 2.3 Hz, 1H), 4.58 (hept, *J* = 6.1 Hz, 2H), 2.55 (s, 3H), 1.34 (d, *J* = 6.0 Hz, 12H).

¹³C NMR (126 MHz, Chloroform-*d*) δ 198.1, 159.2, 139.2, 108.6, 107.9, 70.3, 26.9, 22.1.

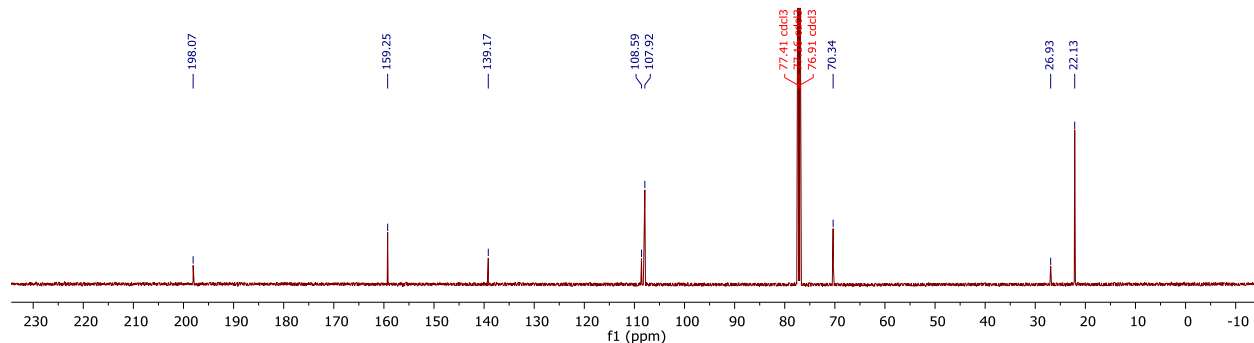
IR (Neat): 2977, 1684, 1589, 1362, 1295, 1184, 1156, 1114 cm⁻¹.

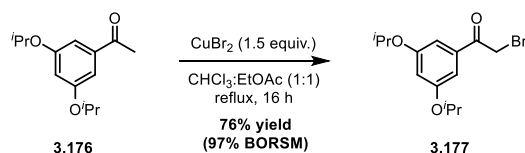
HRMS (ESI) *m/z* calculated for C₁₄H₂₁O₃⁺ ([M+H]⁺) 237.1485, found 237.1496.

¹H NMR, 500 MHz, Chloroform-*d*, Compound **3.176**



¹³C NMR, 126 MHz, Chloroform-*d*, Compound **3.176**





3.177 – 2-bromo-1-(3,5-diisopropoxyphenyl)ethan-1-one

The starting acetophenone **3.176** (5.70 g, 24.1 mmol) was added to a flame-dried 500-mL round bottom flask fitted with a reflux condenser and charged with a stir bar under inert atmosphere. The starting material was dissolved in a 1:1 solution of CHCl_3 and EtOAc (185 mL), and CuBr_2 (8.08 g, 36.2 mmol, 1.5 equiv) was added to the reaction solution. The reaction was heated at reflux overnight (~16 h), at which point it was cooled to rt and filtered through a plug of Celite in the fume hood, eluting with CH_2Cl_2 (~100 mL). The filtrate was transferred to a separatory funnel containing sat'd aq. NaHCO_3 (100 mL). The layers were separated, and the organic layer was washed with aqueous solution of 10% sodium thiosulphate (100 mL). The fully quenched organic layer was subsequently washed with brine, dried over Na_2SO_4 , and concentrated under reduced pressure. The crude product was purified by flash column chromatography (1.5% to 9% EtOAc/Hexanes over 6 steps) to afford the desired brominated product **3.177** as a colorless oil (5.75 g, 76% yield) in addition to unreacted **3.176** as a clear, colorless oil (1.25 g, 22% RSM). The yield based on recovered **3.176** is 97%. At higher conversions, **3.177** reacts further to give the undesired dibrominated material, thus holding the reaction at ~80% conversion was found to be optimal.

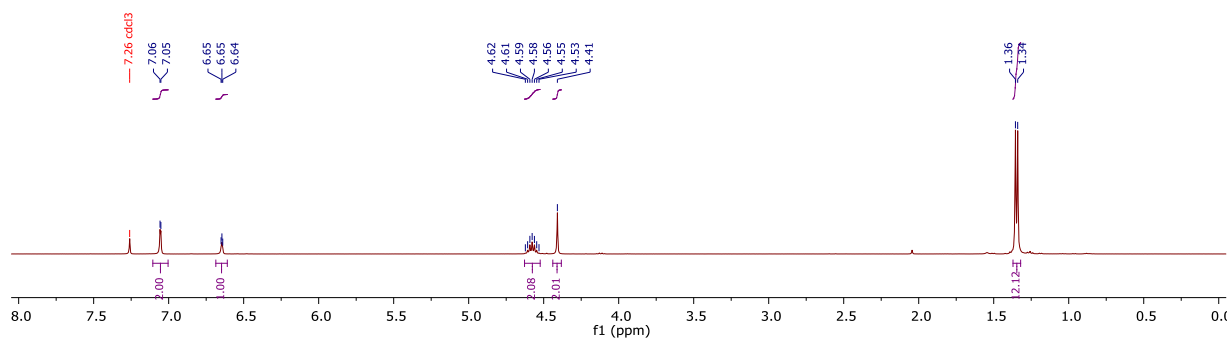
^1H NMR (401 MHz, Chloroform-*d*) δ 7.05 (d, $J = 2.2$ Hz, 2H), 6.65 (t, $J = 2.2$ Hz, 1H), 4.58 (hept, $J = 6.1$ Hz, 2H), 4.41 (s, 2H), 1.35 (d, $J = 6.0$ Hz, 12H).

^{13}C NMR (126 MHz, Chloroform-*d*) δ 191.2, 159.5, 135.9, 109.5, 108.4, 70.5, 31.2, 22.1.

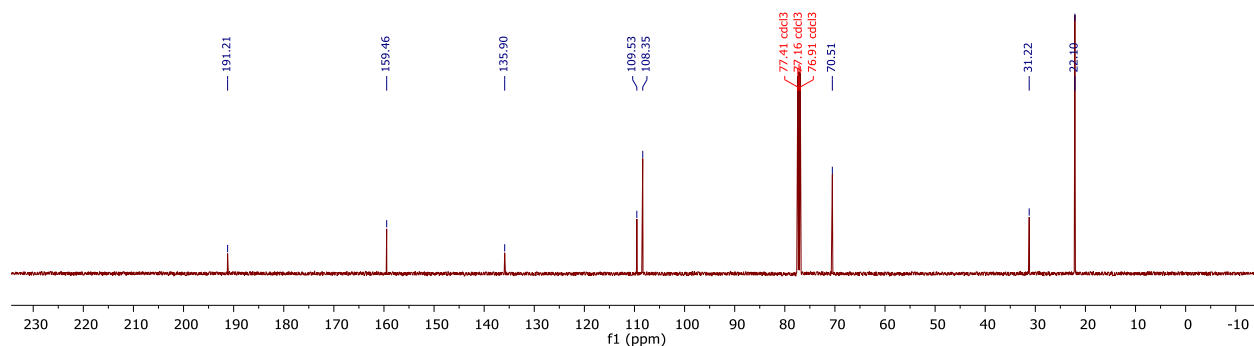
IR (Neat): 2976, 1700, 1599, 1587, 1315, 1298, 1184, 1157, 1112 cm^{-1} .

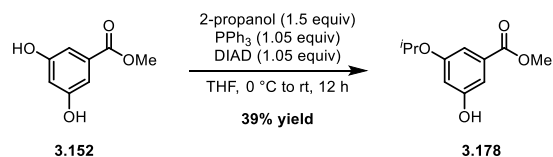
HRMS (ESI) m/z calculated for $\text{C}_{14}\text{H}_{20}\text{BrO}_3^+$ ($[\text{M}+\text{H}]^+$) 315.0590, found 315.0604.

^1H NMR, 401 MHz, Chloroform-*d*, Compound **3.177**



^{13}C NMR, 126 MHz, Chloroform-*d*, Compound **3.177**





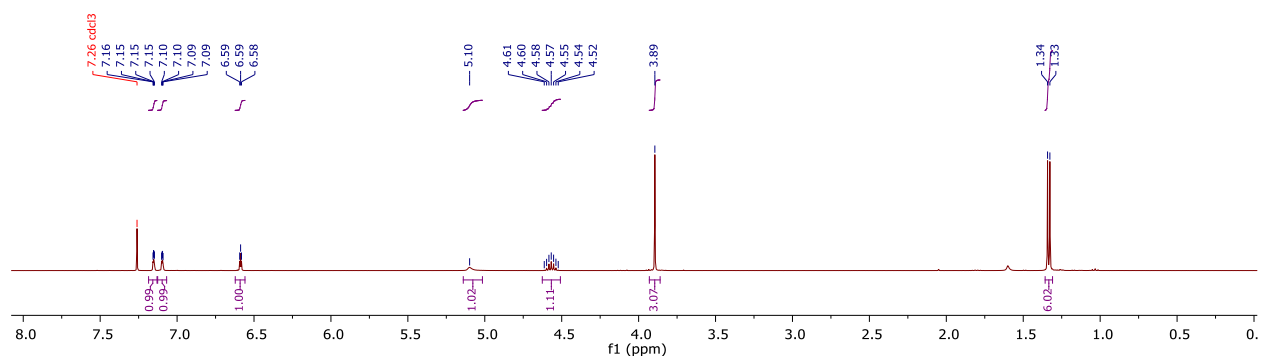
3.178 – methyl 3-hydroxy-5-isopropoxybenzoate

The starting ester **3.152** (6.00 g, 35.7 mmol), 2-propanol (4.10 mL, 53.5 mmol, 1.5 equiv) and PPh₃ (9.83 g, 37.5 mmol, 1.05 equiv) were added to a flame-dried 250-mL round bottom flask charged with a stir bar under inert atmosphere. The starting materials were dissolved in THF (120 mL), and to the stirring solution was cooled to 0 °C in an ice bath. To the cold solution was added DIAD (7.38 mL, 37.5 mmol, 1.05 equiv) via syringe pump over 10 minutes. The reaction mixture was allowed to warm to room temperature over 12 hours, at which point the reaction was concentrated onto Celite and purified by column chromatography (5-30% EtOAc in Hexanes) to afford the desired product **3.178** as a white solid (2.95 g, 39% yield). The ¹H and ¹³C NMR data for this compound were consistent with prior literature reports.²³⁷

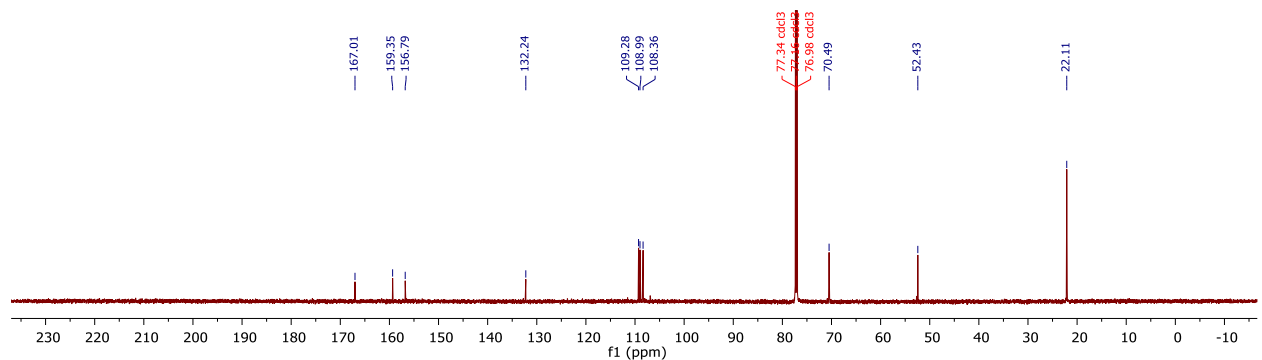
¹H NMR (400 MHz, Chloroform-*d*) δ 7.15 (dd, *J* = 2.3, 1.3 Hz, 1H), 7.10 (dd, *J* = 2.4, 1.3 Hz, 1H), 6.59 (t, *J* = 2.3 Hz, 1H), 5.10 (s, 1H), 4.57 (hept, *J* = 6.1 Hz, 1H), 3.89 (s, 3H), 1.33 (d, *J* = 6.0 Hz, 6H).

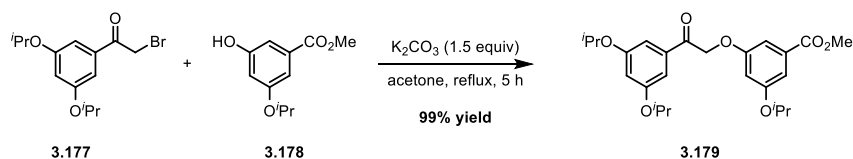
¹³C NMR (176 MHz, Chloroform-*d*) δ 167.0, 159.4, 156.8, 132.2, 109.3, 109.0, 108.4, 70.5, 52.4, 22.1.

¹H NMR, 400 MHz, Chloroform-*d*, Compound **3.178**



¹³C NMR, 176 MHz, Chloroform-*d*, Compound **3.178**





3.179 - methyl 3-(2-(3,5-diisopropoxyphenyl)-2-oxoethoxy)-5-isopropoxybenzoate

A solution of the starting phenol **3.178** (2.95 g, 14.0 mmol, 1.0 equiv) and bromide **3.177** (5.75 g, 18.2 mmol, 1.30 equiv) in acetone (140 mL) was prepared in a flame-dried, 500 mL rb flask fitted with reflux condenser under inert atmosphere. To the stirring solution was added K_2CO_3 (2.91 g, 21.0 mmol, 1.50 equiv) in a single portion, and the reaction was heated to reflux for 5 h. Upon cooling to rt, the crude reaction was concentrated under reduced pressure. The residue was dissolved in EtOAc and added to a sep. funnel containing DI H_2O . The layers were separated, and the organic layer was washed with brine, dried over MgSO_4 , and concentrated. The crude product was purified by flash column chromatography (5% to 40% EtOAc in Hexanes over 10 column volumes) to afford the product **3.179** as a colorless oil (6.20 g, 13.9 mmol, 99% yield).

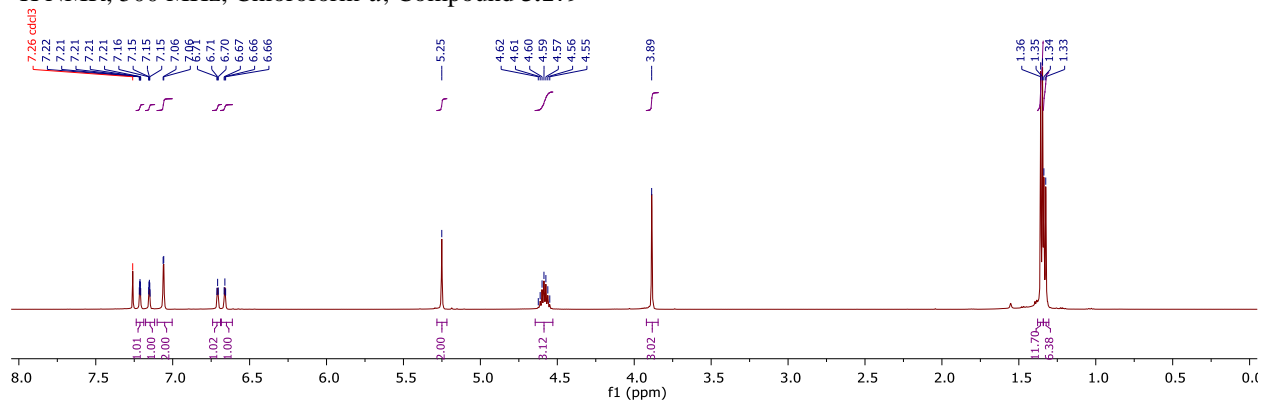
$^1\text{H NMR}$ (500 MHz, Chloroform-*d*) δ 7.21 (dt, $J = 2.3, 1.1$ Hz, 1H), 7.15 (dt, $J = 2.3, 1.1$ Hz, 1H), 7.06 (d, $J = 1.9$ Hz, 2H), 6.71 (d, $J = 2.5$ Hz, 1H), 6.66 (d, $J = 2.4$ Hz, 1H), 5.25 (s, 2H), 4.59 (hept, $J = 6.2$ Hz, 3H), 3.89 (s, 3H), 1.35 (d, $J = 6.0$ Hz, 12H), 1.33 (d, $J = 6.1$ Hz, 6H).

$^{13}\text{C NMR}$ (126 MHz, Chloroform-*d*) δ 193.5, 166.8, 159.5, 159.23, 159.17, 136.3, 132.2, 110.3, 109.3, 108.4, 107.48, 107.43, 70.8, 70.5, 52.4, 22.11, 22.10.

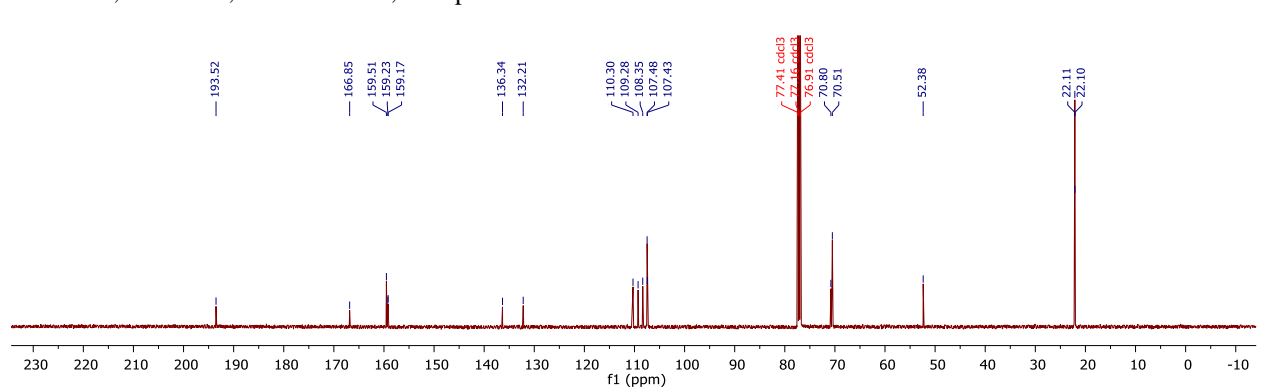
IR (Neat): 2976, 1717, 1700, 1590, 1457, 1437, 1296, 1156, 1112 cm^{-1} .

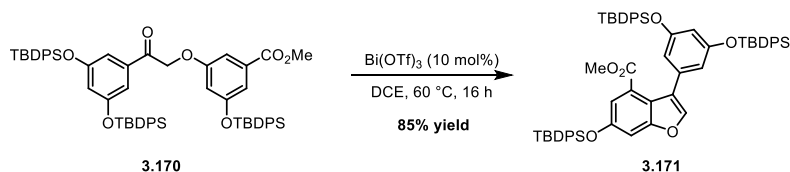
HRMS (ESI) m/z calculated for $\text{C}_{25}\text{H}_{33}\text{O}_7^+$ ($[\text{M}+\text{H}]^+$) 445.2221, found 445.2224.

$^1\text{H NMR}$, 500 MHz, Chloroform-*d*, Compound **3.179**



$^{13}\text{C NMR}$, 126 MHz, Chloroform-*d*, Compound **3.179**





3.171 - methyl 3-(3,5-bis((tert-butyldiphenylsilyl)oxy)phenyl)-6-((tert-butyldiphenylsilyl)oxy)benzofuran-4-carboxylate

The starting acetophenone **3.170** (2.70 g, 2.61 mmol) was added to a flame-dried round bottom flask charged with a stir bar and fitted with a reflux condenser under inert atmosphere. The starting material was dissolved in 1,2-dichloroethane (DCE, 55 mL) and Bi(OTf)₃ (171 mg, 0.261 mmol, 10 mol%) was added to the reaction under a stream of nitrogen. The reaction was heated at 60 °C for 16 hours; after cooling to room temperature, the reaction was filtered through a plug of Celite, eluting with DCM (~150 mL). The filtrate was concentrated and purified by flash column chromatography (0-10% EtOAc in Hexanes) to afford the desired product (2.25 g, 85% yield).

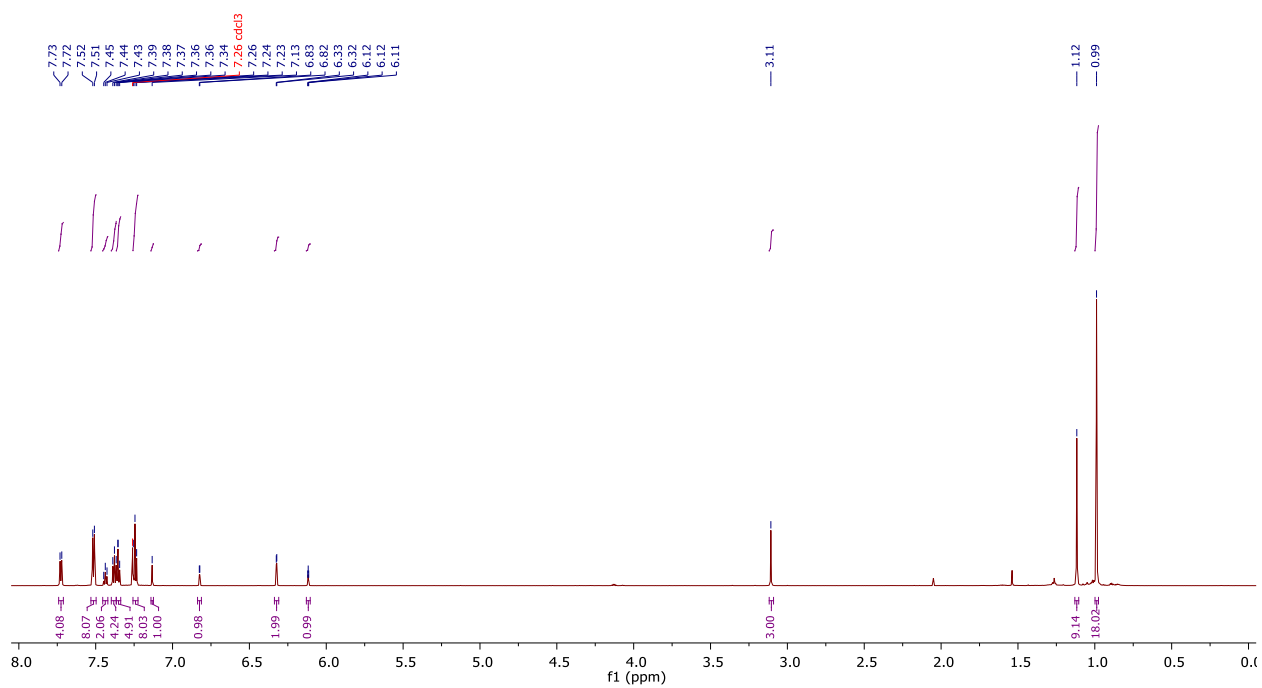
¹H NMR (700 MHz, Chloroform-*d*) δ 7.73 (d, *J* = 8.0 Hz, 4H), 7.51 (d, *J* = 7.3 Hz, 8H), 7.44 (t, *J* = 7.4 Hz, 2H), 7.38 (t, *J* = 7.7 Hz, 4H), 7.37 – 7.34 (m, 5H), 7.24 (t, *J* = 7.5 Hz, 8H), 7.13 (s, 1H), 6.82 (d, *J* = 2.3 Hz, 1H), 6.32 (d, *J* = 2.2 Hz, 2H), 6.12 (t, *J* = 2.2 Hz, 1H), 3.11 (s, 3H), 1.12 (s, 9H), 0.99 (s, 18H).

¹³C NMR (126 MHz, Chloroform-*d*) δ 167.4, 156.4, 155.9, 153.0, 135.64, 135.60, 134.8, 132.8, 132.4, 130.2, 129.9, 128.1, 127.8, 125.2, 122.6, 118.9, 118.3, 113.6, 106.1, 51.2, 26.7, 26.6, 19.6, 19.5.

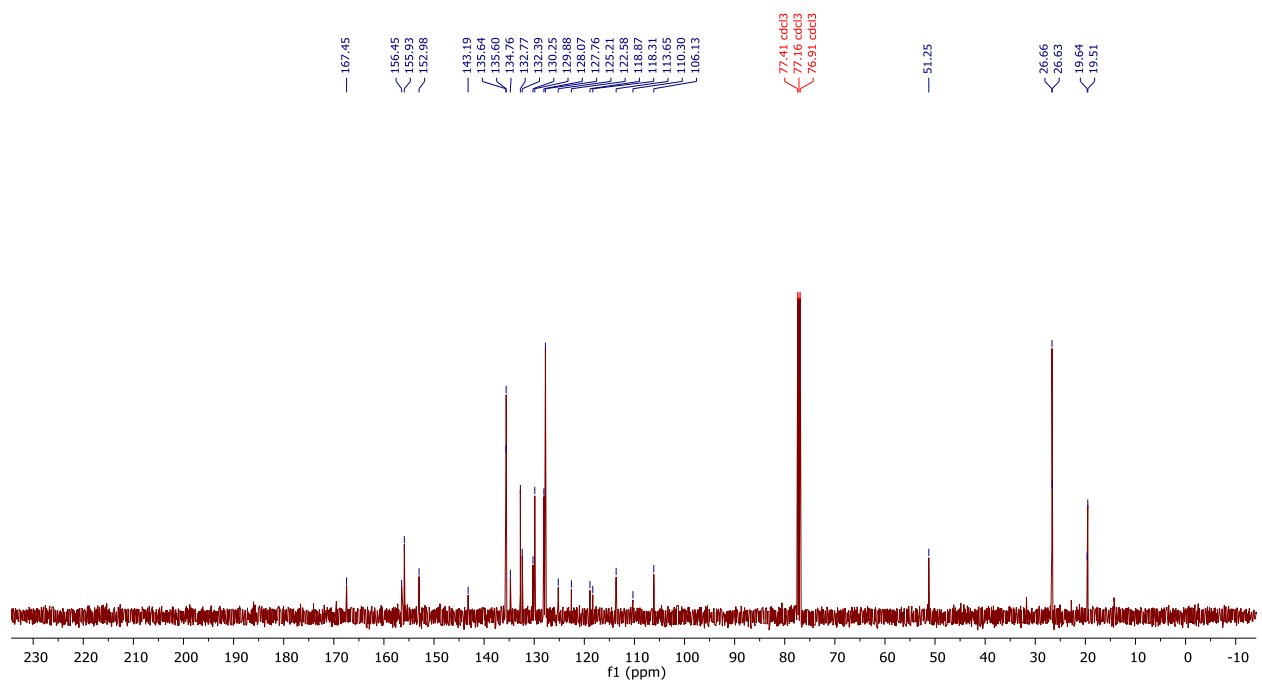
IR (Neat): 2978, 1734, 1589, 1556, 1364, 1298, 1193, 1154, 1110 cm⁻¹.

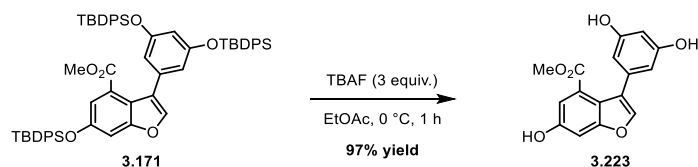
HRMS (ESI) *m/z* calculated for C₆₄H₆₇O₆Si₃⁺ ([M+H]⁺) 1015.4240, found 1015.4238.

¹H NMR, 700 MHz, Chloroform-*d*, Compound **3.171**



¹³C NMR, 126 MHz, Chloroform-*d*, Compound **3.171**





3.223 - methyl 3-(3,5-dihydroxyphenyl)-6-hydroxybenzofuran-4-carboxylate

A solution of the starting benzofuran **3.171** (1.25 g, 1.23 mmol, 1.0 equiv.) in EtOAc (30 mL) was prepared in a flame-dried round bottom flask under inert atmosphere. The solution was cooled to 0 °C in an ice-bath, at which point a solution of TBAF (3.69 mL, 3.69 mmol, 1.0 M in THF, 3 equiv.) was added dropwise to the reaction mixture. After stirring for 1 hour at temperature, the reaction was quenched with 4 N HCl (30 mL), and this mixture was rapidly stirred for 5 minutes, at which point it was added to a separatory funnel containing a solution of saturated aqueous sodium bicarbonate (~100 mL). The layers were separated, and the aqueous layer was extracted with additional EtOAc. The combined organic layers were dried over MgSO₄ and concentrated under reduced pressure. The crude product was purified by flash column chromatography (25% to 100% EtOAc in CH₂Cl₂) to afford the desired product **3.223** as an off-white solid (360 mg, 97% yield).

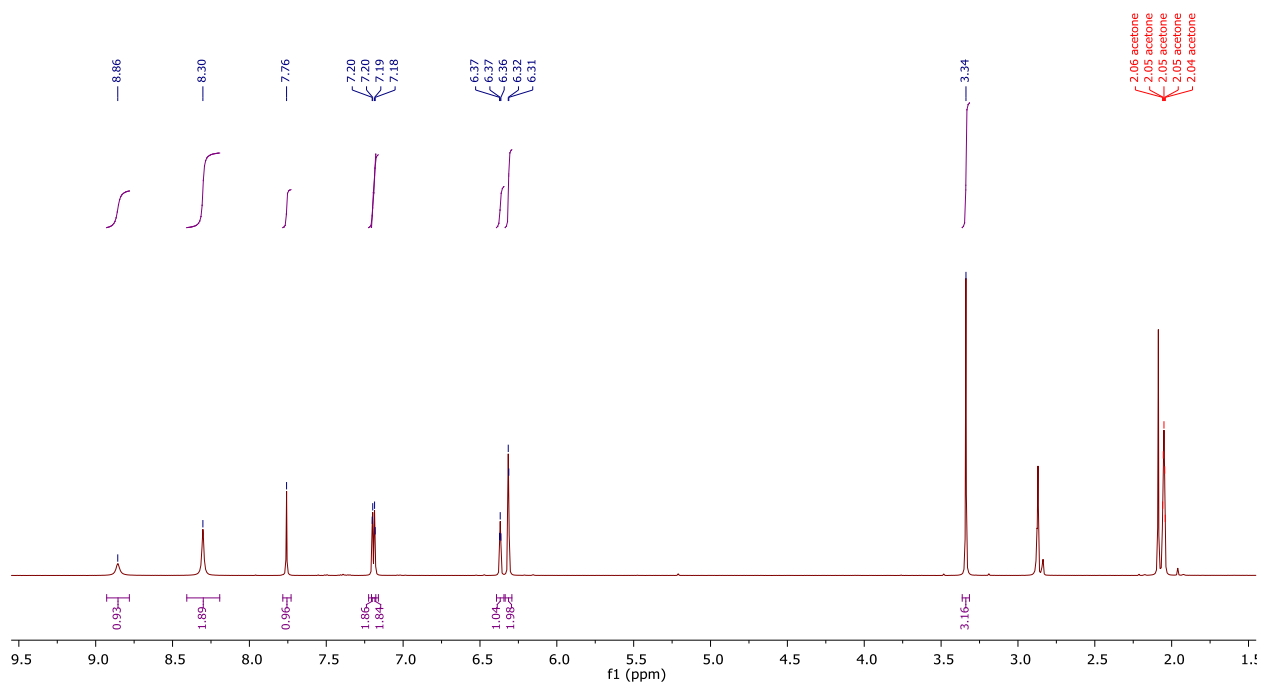
¹H NMR (500 MHz, Acetone-*d*₆) δ 8.86 (s, 1H), 8.30 (s, 2H), 7.76 (s, 1H), 7.20 (d, *J* = 1.8 Hz, 1H), 7.18 (d, *J* = 1.9 Hz, 1H), 6.37 (t, *J* = 2.1 Hz, 1H), 6.31 (d, *J* = 1.8 Hz, 2H), 3.34 (s, 3H).

¹³C NMR (126 MHz, Acetone-*d*₆) δ 168.1, 159.3, 158.0, 156.0, 143.5, 136.0, 127.1, 124.0, 118.4, 114.1, 107.9, 102.3, 102.0, 51.5.

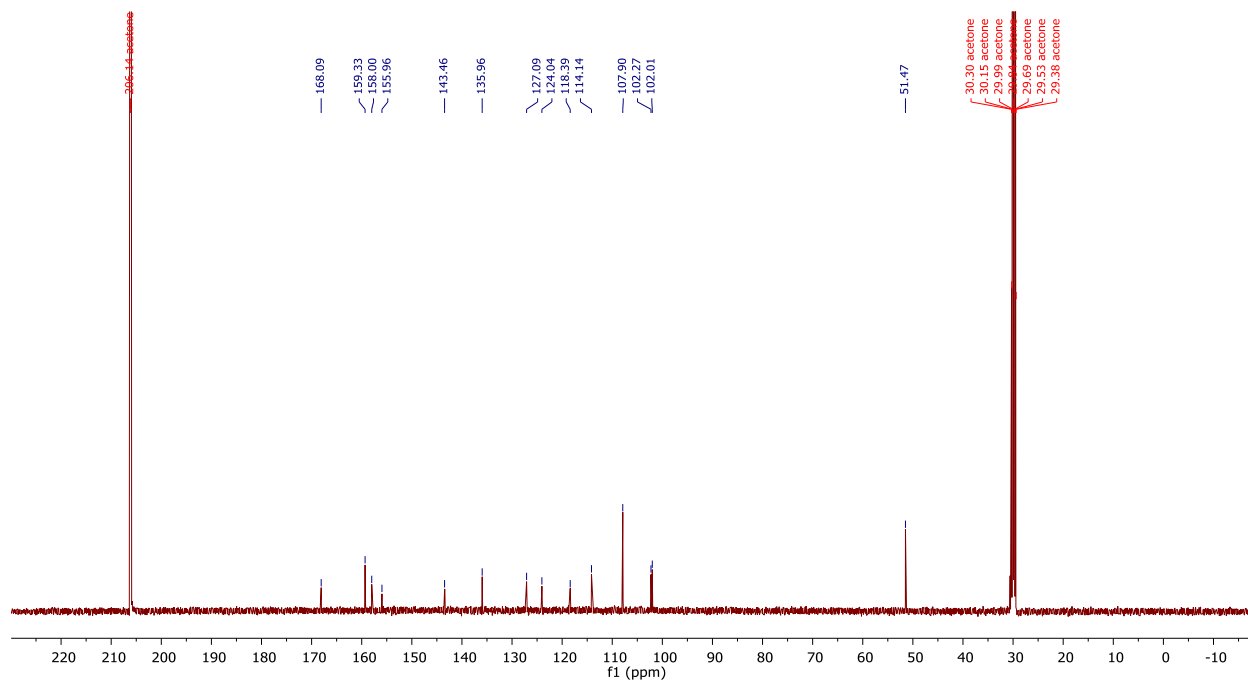
IR (Neat): 3328 (br), 2927, 1684, 1613, 1440, 1341, 1266, 1157, 1135, 1002 cm⁻¹.

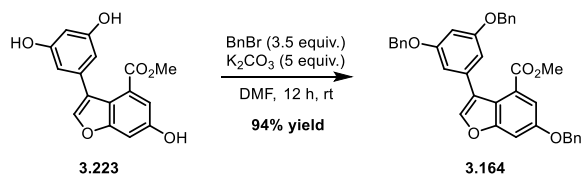
HRMS (ESI) *m/z* calculated for C₁₆H₁₃O₆⁺ ([M+H]⁺) 301.0707, found 301.0697.

¹H NMR, 500 MHz, Acetone-*d*₆, Compound **3.223**



¹³C NMR, 126 MHz, Acetone-*d*₆, Compound **3.223**





3.164 – methyl 6-(benzyloxy)-3-(3,5-bis(benzyloxy)phenyl)benzofuran-4-carboxylate

A flame-dried reaction vial was charged with the starting phenol **3.223** (100 mg, 0.333 mmol) and a stir bar under inert atmosphere. The starting material was dissolved in DMF (3.0 mL), and to the resulting solution was added potassium carbonate (5.0 equiv., 230 mg, 1.67 mmol). The resulting reaction mixture was allowed to stir for 30 min, at which point benzyl bromide (3.5 equiv., 1.4 mL, 1.17 mmol) was added dropwise via syringe. The resulting reaction mixture was allowed to stir for 12 hours, at which point the reaction was diluted with EtOAc (~15 mL) and added to a separatory funnel containing water (~50 mL). The layers were separated, and the aqueous layer was extracted with EtOAc (2 x 15 mL), and the combined organic layers were washed with water (3 x 50 mL), washed with brine (~50 mL), dried over magnesium sulfate, and concentrated under reduced pressure. The crude material was purified via flash column chromatography (0% to 40% EtOAc/Hexanes) to afford the desired product **3.164** as a clear, colorless oil (178 mg, 94% yield).

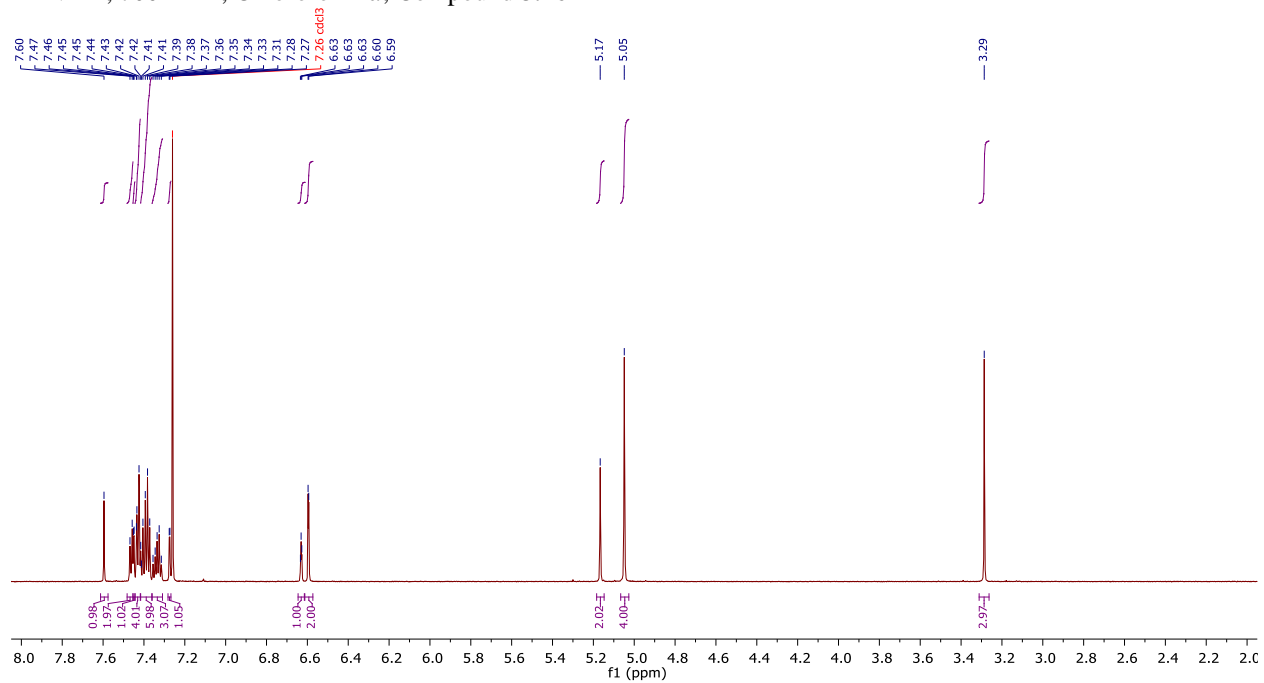
$^1\text{H NMR}$ (700 MHz, Chloroform-*d*) δ 7.60 (s, 1H), 7.46 (d, $J = 7.6$ Hz, 2H), 7.45 (d, $J = 2.3$ Hz, 1H), 7.43 (d, $J = 7.2$ Hz, 4H), 7.39 (m, 6H), 7.34 (m, 3H), 7.27 (d, $J = 2.3$ Hz, 1H), 6.63 (d, $J = 2.3$ Hz, 1H), 6.59 (d, $J = 2.2$ Hz, 2H), 5.17 (s, 2H), 5.05 (s, 4H), 3.29 (s, 3H).

$^{13}\text{C NMR}$ (176 MHz, Chloroform-*d*) δ 167.8, 159.9, 157.0, 156.6, 143.2, 136.9, 136.6, 135.4, 128.8, 128.7, 128.3, 128.2, 127.7, 127.6, 125.7, 122.9, 118.9, 114.0, 107.8, 101.44, 101.42, 71.0, 70.2, 51.6.

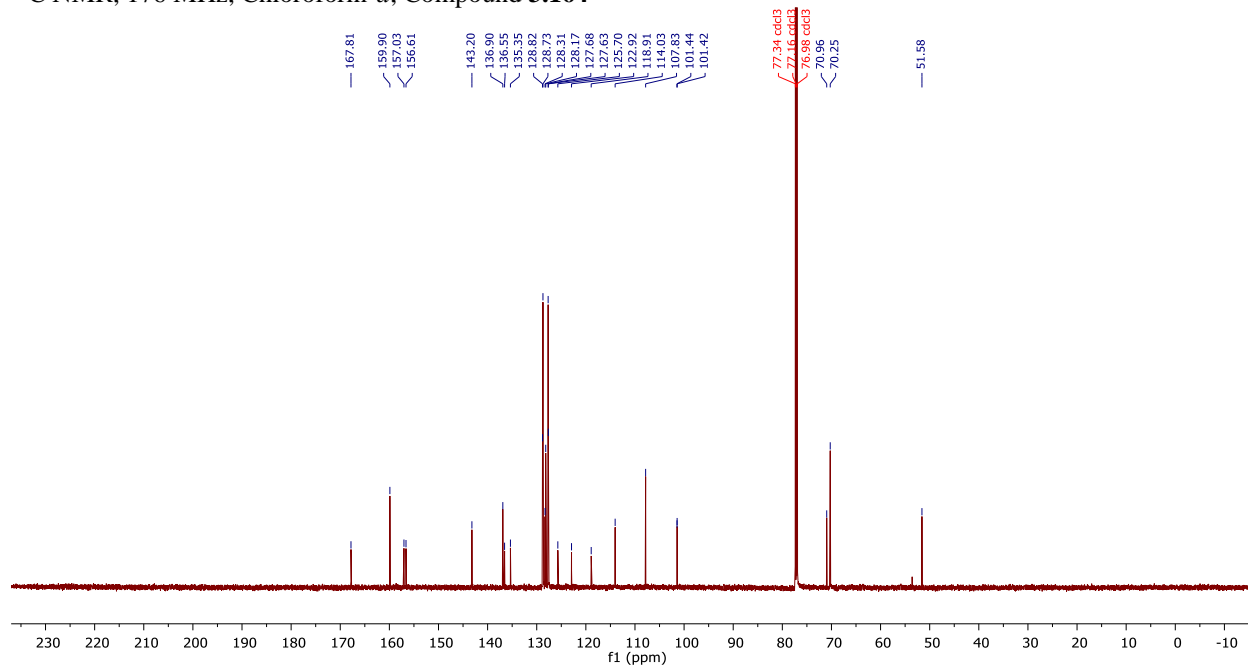
IR (Neat): 3024, 2927, 1684, 1610, 1424, 1339, 1268, 1159, 1135, 1002 cm^{-1} .

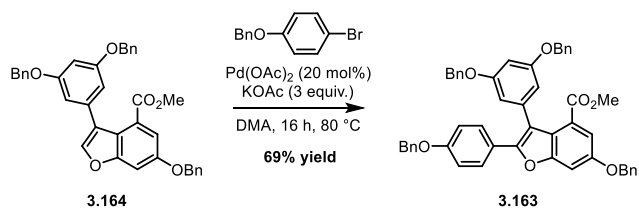
HRMS (ESI) m/z calculated for $\text{C}_{37}\text{H}_{31}\text{O}_6^+$ ($[\text{M}+\text{H}]^+$) 571.2115, found 571.2111.

¹H NMR, 700 MHz, Chloroform-*d*, Compound **3.164**



¹³C NMR, 176 MHz, Chloroform-*d*, Compound **3.164**





3.163 – methyl 6-(benzyloxy)-2-(4-(benzyloxy)phenyl)-3-(3,5-bis(benzyloxy)phenyl)benzofuran-4-carboxylate

A flame-dried round bottom flask was charged with the starting benzofuran **3.164** (590 mg, 1.03 mmol), 4-benzyloxybromobenzene (816 mg, 3.10 mmol), Pd(OAc)₂ (46 mg, 0.21 mmol), and KOAc (304 mg, 3.10 mmol) with a stir bar under inert atmosphere. The solids were dissolved/suspended in DMA (18 mL), and the reaction mixture was sparged with N₂ for >30 min. The resulting reaction mixture was heated at 80 °C for 16 hours, at which point the reaction was diluted with EtOAc (~30 mL) and filtered over Celite, eluting with EtOAc (~100 mL). The filtrate was added to a separatory funnel containing water (~100 mL). The layers were separated, and the organic layer was washed with water (3 x 100 mL), washed with brine (~50 mL), dried over magnesium sulfate, and concentrated under reduced pressure. The crude material was purified via flash column chromatography (4% to 32%, 8 steps in 4% increments, 1.5 CVs per step, polar phase – 2:1 CH₂Cl₂/EtOAc, nonpolar phase – Hexanes) to afford the desired product as a clear, colorless oil (539 mg, 69% yield).

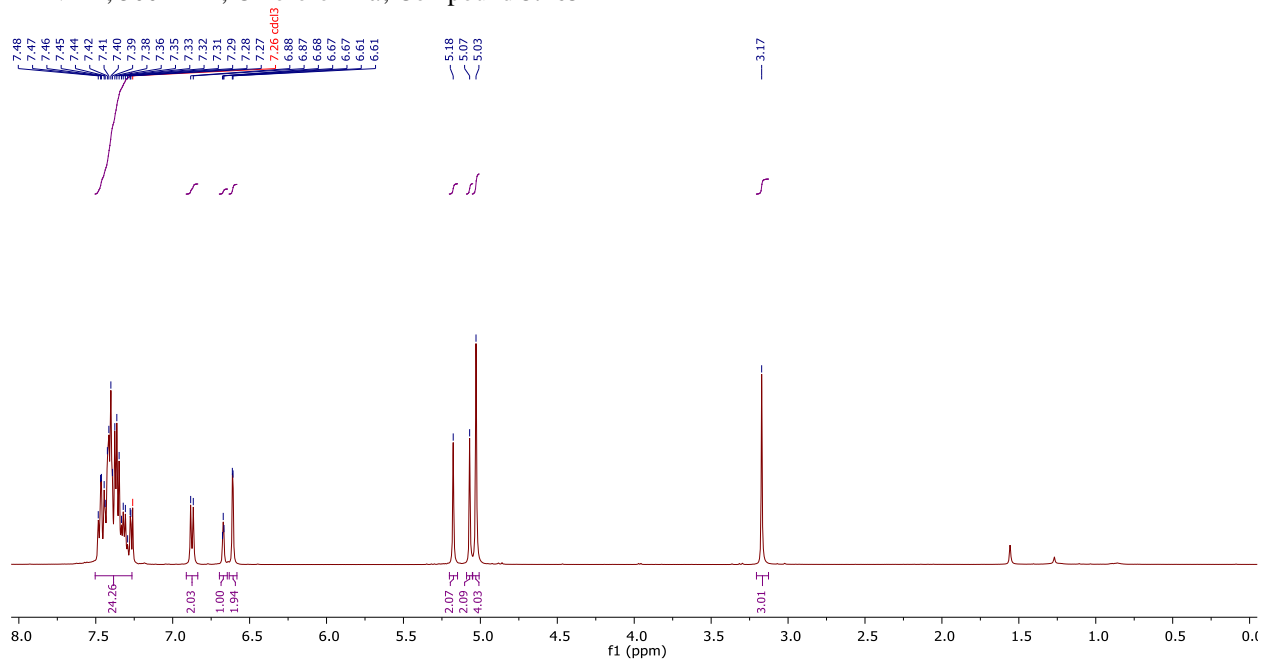
¹H NMR (500 MHz, Chloroform-*d*) δ 7.49 – 7.27 (m, 24H), 6.87 (d, *J* = 8.5 Hz, 2H), 6.67 (t, *J* = 2.4 Hz, 1H), 6.61 (d, *J* = 2.2 Hz, 2H), 5.18 (s, 2H), 5.07 (s, 2H), 5.03 (s, 4H), 3.17 (s, 3H).

¹³C NMR (126 MHz, Chloroform-*d*) δ 167.9, 160.3, 159.0, 156.2, 155.3, 152.0, 136.89, 136.85, 136.82, 136.7, 128.80, 128.76, 128.7, 128.4, 128.3, 128.2, 128.1, 127.63, 127.62, 127.58, 125.3, 123.3, 122.0, 115.9, 114.9, 113.6, 109.0, 102.1, 100.9, 70.9, 70.2, 70.1, 51.6.

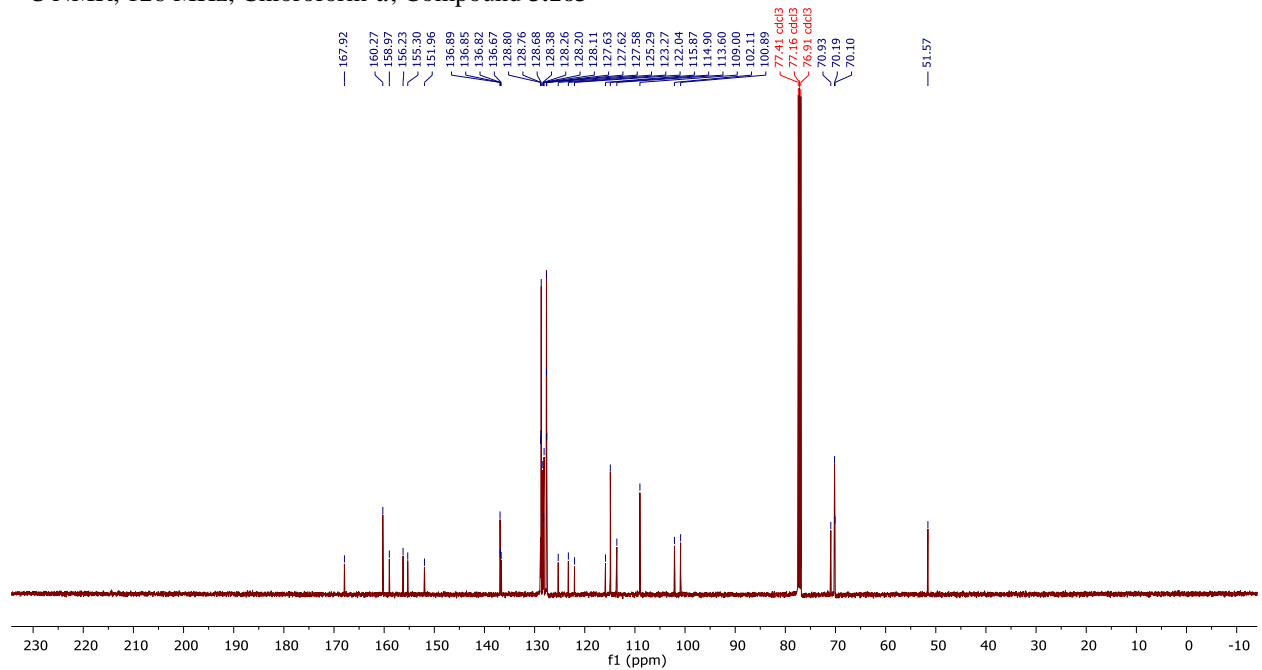
IR (Neat): 3024, 2927, 1684, 1610, 1424, 1339, 1268, 1159, 1135, 1002 cm⁻¹.

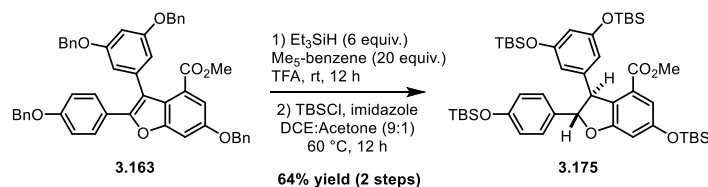
HRMS (ESI) *m/z* calculated for C₅₀H₄₁O₇⁺ ([M+H]⁺) 753.2847, found 753.2830.

¹H NMR, 500 MHz, Chloroform-*d*, Compound **3.163**



¹³C NMR, 126 MHz, Chloroform-*d*, Compound **3.163**





3.175 - methyl (2R,3R)-3-(3,5-bis((tert-butyldimethylsilyl)oxy)phenyl)-6-((tert-butyldimethylsilyl)oxy)-2-(4-((tert-butyldimethylsilyl)oxy)phenyl)-2,3-dihydrobenzofuran-4-carboxylate

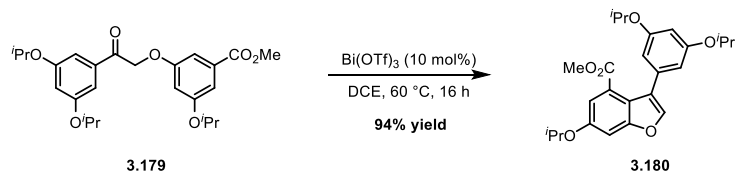
Triethylsilane (197 μL , 1.24 mmol) was added to a stirred solution of **3.163** (155 mg, 0.206 mmol) in trifluoroacetic acid (2 mL). The reaction mixture was allowed to react at room temperature overnight. Upon reaction completion, the solution was cooled to 0 °C and quenched with sat'd aq. NaHCO_3 . The quenched reaction was then extracted with ethyl acetate ($3 \times 10\text{mL}$), and the combined organic layer was dried over MgSO_4 and concentrated under reduced pressure. The crude residue was dissolved in minimal acetone ($\sim 200 \mu\text{L}$), and the resulting solution was diluted with DCE (1.8 mL). Imidazole (77 mg, 1.13 mmol) and TBSCl (155 mg, 1.03 mmol) were added to the reaction solution, and the reaction mixture was heated at 60 °C for 12 hours. Upon completion of the reaction, the reaction was concentrated and purified by flash column chromatography (0 to 10% EtOAc/Hexanes) to afford the desired product as a colorless oil (111 mg, 64% yield). See page 286 for ^1H and ^{13}C NMR spectra for compound **3.175**.

^1H NMR (700 MHz, Chloroform-*d*) δ 7.16 (d, $J = 8.5$ Hz, 2H), 7.05 (d, $J = 2.2$ Hz, 1H), 6.81 (d, $J = 8.5$ Hz, 2H), 6.66 (d, $J = 2.2$ Hz, 1H), 6.21 (t, $J = 2.2$ Hz, 1H), 6.13 (d, $J = 2.2$ Hz, 2H), 5.39 (d, $J = 5.1$ Hz, 1H), 4.71 (d, $J = 5.1$ Hz, 1H), 3.54 (s, 3H), 1.01 (s, 9H), 0.99 (s, 9H), 0.93 (s, 18H), 0.25 (s, 6H), 0.20 (s, 6H), 0.12 (s, 12H).

^{13}C NMR (176 MHz, Chloroform-*d*) δ 166.1, 162.1, 156.8, 155.8, 146.4, 134.3, 128.2, 126.9, 123.6, 120.4, 114.6, 112.5, 110.7, 106.3, 93.3, 57.4, 51.6, 25.85, 25.83, 18.41, 18.39, 18.35, -4.21, -4.25, -4.26, -4.28.

IR (Neat): 2955, 2930, 2895, 2858, 1727, 1161, 1588, 1473, 1343, 1253, 1161, 1030, 833 cm^{-1} .

HRMS (ESI) m/z calculated for $\text{C}_{46}\text{H}_{75}\text{O}_7\text{Si}_4^+$ ($[\text{M}+\text{H}]^+$) 851.4584, found 851.4580.



3.180 - methyl 3-(3,5-bis((tert-butyl)diphenylsilyl)oxy)phenyl)-6-((tert-butyl)diphenylsilyl)oxy)benzofuran-4-carboxylate

The starting acetophenone **3.179** (6.20 g, 13.9 mmol) was added to a flame-dried 500-mL round bottom flask charged with a stir bar and fitted with a reflux condenser under inert atmosphere. The starting material was dissolved in 1,2-dichloroethane (DCE, 200 mL) and Bi(OTf)₃ (915 mg, 1.39 mmol, 10 mol%) was added to the reaction under a stream of nitrogen. The reaction was heated at 60 °C for 16 hours; after cooling to room temperature, the reaction was filtered through a plug of Celite, eluting with CH₂Cl₂ (~200 mL). The filtrate was concentrated and purified by flash column chromatography (0-15% EtOAc in Hexanes) to afford the desired product **3.180** as a colorless oil (5.58 g, 94% yield).

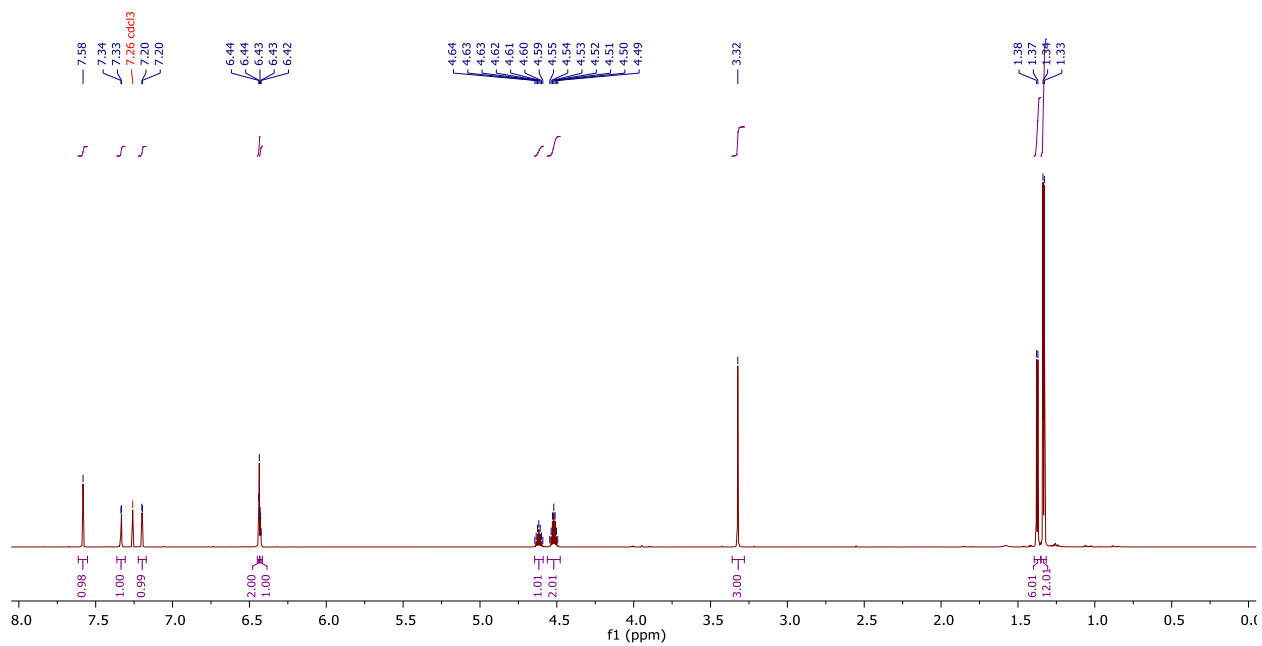
¹H NMR (700 MHz, Chloroform-d) δ 7.58 (s, 1H), 7.33 (d, *J* = 2.3 Hz, 1H), 7.20 (d, *J* = 2.3 Hz, 1H), 6.44 (d, *J* = 2.1 Hz, 2H), 6.43 (d, *J* = 2.2 Hz, 1H), 4.62 (hept, *J* = 6.0 Hz, 1H), 4.52 (hept, *J* = 6.1 Hz, 2H), 3.32 (s, 3H), 1.37 (d, *J* = 6.0 Hz, 6H), 1.33 (d, *J* = 6.1 Hz, 12H).

¹³C NMR (176 MHz, Chloroform-d) δ 167.9, 159.1, 157.1, 155.7, 143.0, 135.3, 125.6, 123.2, 118.8, 115.0, 108.3, 103.0, 102.6, 71.3, 70.0, 51.5, 22.3, 22.1.

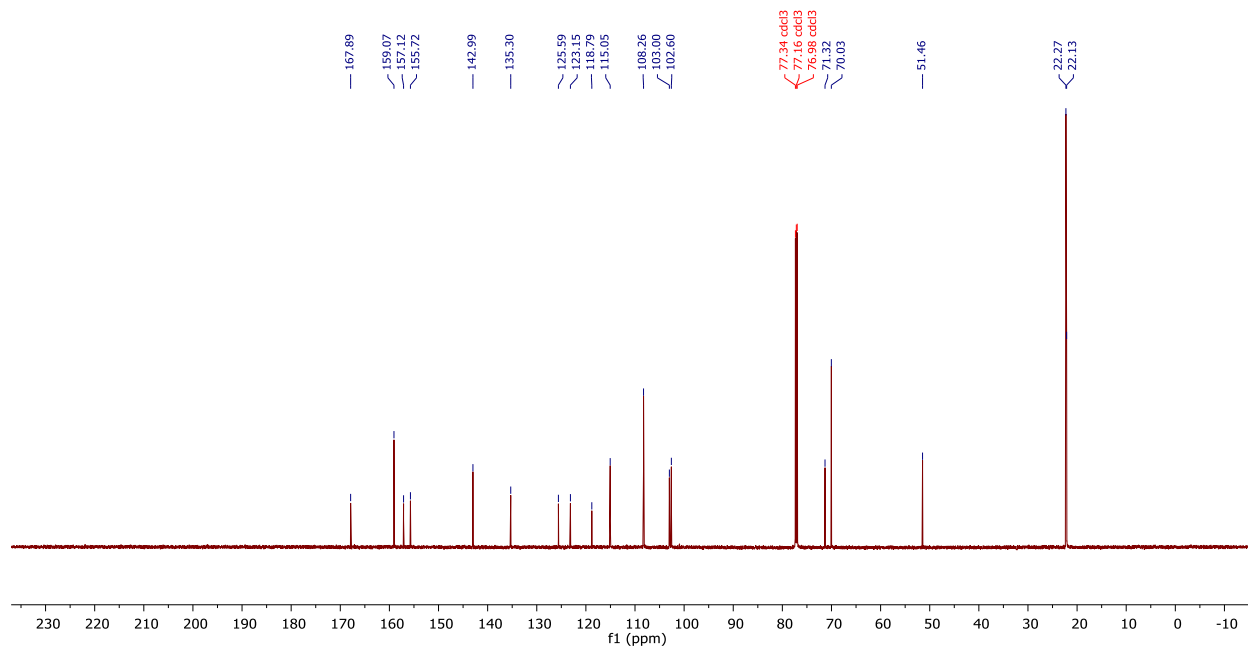
IR (Neat): 2976, 1734, 1718, 1592, 1436, 1317, 1248, 1154, 1136, 1104 cm⁻¹.

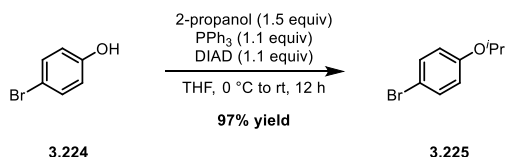
HRMS (ESI) *m/z* calculated for C₂₅H₃₁O₆⁺ ([M+H]⁺) 427.2115, found 427.2126.

¹H NMR, 700 MHz, Chloroform-*d*, Compound **3.180**



¹³C NMR, 126 MHz, Chloroform-*d*, Compound **3.180**





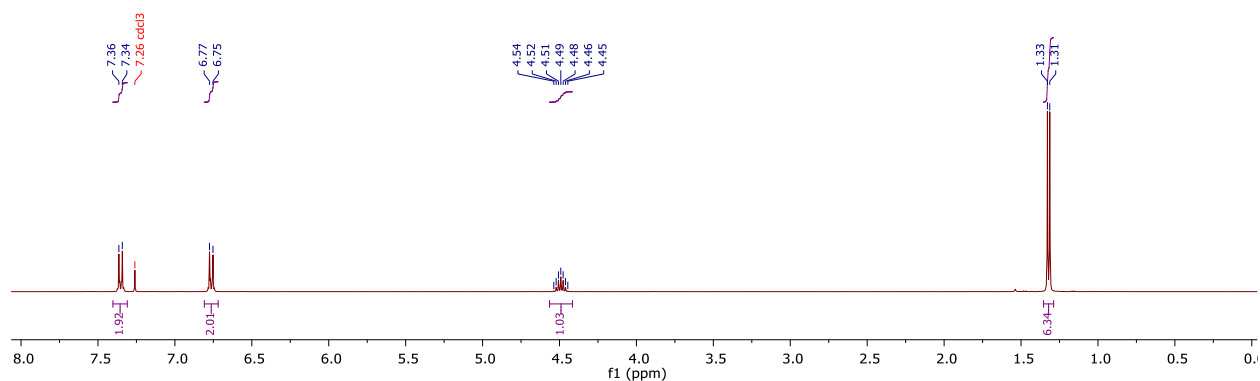
3.225 – 1-bromo-4-isopropoxybenzene

The starting phenol **3.224** (5.00 g, 28.9 mmol), 2-propanol (3.31 mL, 43.4 mmol, 1.5 equiv) and PPh_3 (8.34 g, 31.8 mmol, 1.1 equiv) were added to a flame-dried 250-mL round bottom flask charged with a stir bar under inert atmosphere. The starting materials were dissolved in THF (90 mL), and to the stirring solution was cooled to 0 °C in an ice bath. To the cold solution was added diisopropyl azodicarboxylate (DIAD, 6.26 mL, 31.8 mmol, 1.1 equiv) via syringe pump over 10 minutes. The reaction mixture was allowed to warm to room temperature over 12 hours, at which point the reaction was concentrated onto Celite and purified by column chromatography (0-15% CH_2Cl_2 in Hexanes) to afford the desired product **3.225** as a colorless oil (6.01 g, 97% yield). The ^1H and ^{13}C NMR data for this compound were consistent with prior literature reports.³⁰¹

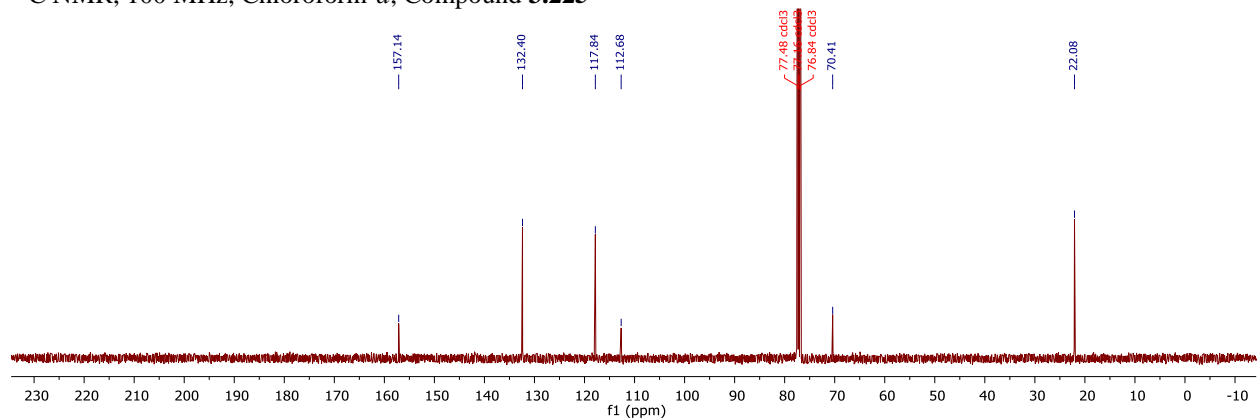
^1H NMR (400 MHz, Chloroform-*d*) δ 7.35 (d, J = 9.0 Hz, 2H), 6.76 (d, J = 8.9 Hz, 2H), 4.49 (hept, J = 6.1 Hz, 1H), 1.32 (d, J = 6.1 Hz, 6H).

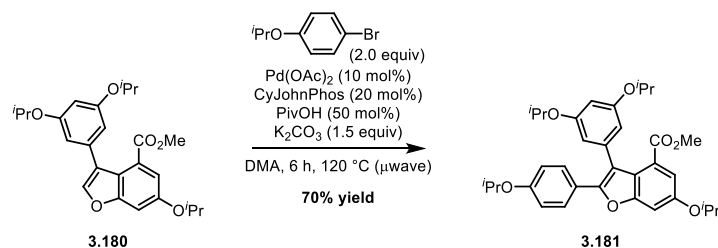
^{13}C NMR (100 MHz, Chloroform-*d*) δ 157.1, 132.4, 117.8, 112.7, 70.4, 22.1.

^1H NMR, 400 MHz, Chloroform-*d*, Compound **3.225**



^{13}C NMR, 100 MHz, Chloroform-*d*, Compound **3.225**





3.181 – methyl 3-(3,5-diisopropoxyphenyl)-6-isopropoxy-2-(4-isopropoxyphenyl)benzofuran-4-carboxylate

A flame-dried round heart-shaped flask was charged with the starting benzofuran **3.180** (1.00 g, 2.34 mmol), 4-isopropoxybromobenzene (**3.225**, 1.01 g, 4.69 mmol), CyJohnPhos (164 mg, 0.469 mmol), pivalic acid (120 mg, 1.17 mmol), potassium carbonate (486 mg, 3.52 mmol), and Pd(OAc)_2 (53 mg, 0.234 mmol) with a stir bar under inert atmosphere. The solids were dissolved/suspended in degassed DMA (15 mL, degassed by Freeze-Pump-Thaw, 3 cycles), and the reaction mixture was degassed by Freeze-Pump-Thaw (3 cycles). The resulting reaction mixture was transferred to a 20-mL microwave vial via cannula under a stream of N_2 . The microwave vial was capped under a stream of N_2 , and the reaction was irradiated at 120 °C for 6 hours. Upon completion of microwave irradiation, the reaction was diluted with EtOAc (~30 mL) and filtered over Celite, eluting with EtOAc (~100 mL). The filtrate was added to a separatory funnel containing water (~100 mL). The layers were separated, and the organic layer was washed with water (3 x 100 mL), washed with brine (~150 mL), dried over magnesium sulfate, and concentrated under reduced pressure. The crude material was purified via flash column chromatography (4% to 24%, 6 steps in 4% increments, 2 CVs per step, polar phase – 3:1 $\text{CH}_2\text{Cl}_2/\text{EtOAc}$, nonpolar phase – Hexanes) to afford the desired product **3.181** as a clear, colorless oil (920 mg, 70% yield).

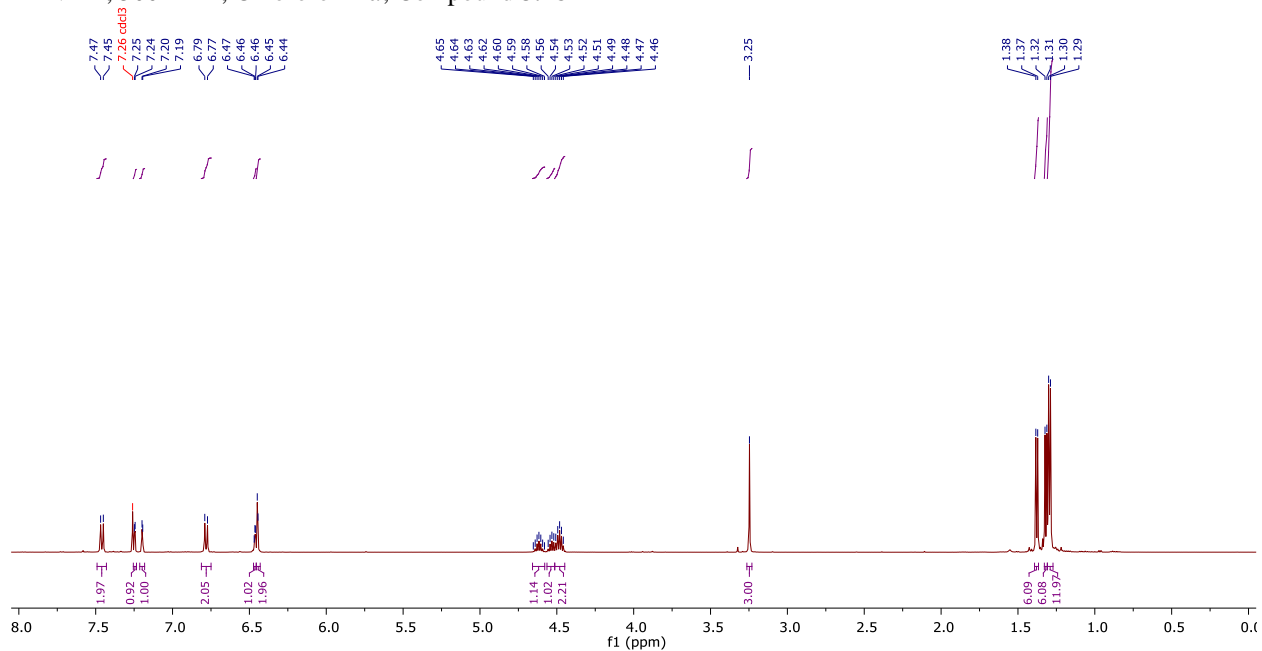
^1H NMR (500 MHz, Chloroform-*d*) δ 7.46 (d, J = 8.9 Hz, 2H), 7.25 (d, J = 2.3 Hz, 1H), 7.20 (d, J = 2.3 Hz, 1H), 6.78 (d, J = 8.9 Hz, 2H), 6.46 (t, J = 2.3 Hz, 1H), 6.45 (d, J = 2.3 Hz, 2H), 4.62 (hept, J = 6.1 Hz, 1H), 4.53 (hept, J = 6.1 Hz, 1H), 4.48 (hept, J = 6.2 Hz, 2H), 3.25 (s, 3H), 1.38 (d, J = 6.1 Hz, 6H), 1.32 (d, J = 6.1 Hz, 6H), 1.29 (d, J = 6.0 Hz, 12H).

^{13}C NMR (126 MHz, Chloroform-*d*) δ 168.0, 159.5, 158.1, 155.4, 155.3, 151.8, 136.7, 128.4, 128.2, 125.2, 122.9, 121.9, 116.0, 115.7, 114.8, 114.6, 109.4, 109.3, 104.1, 104.0, 102.2, 102.0, 71.4, 71.3, 70.02, 70.01, 69.97, 69.93, 51.5, 22.2, 22.13, 22.07.

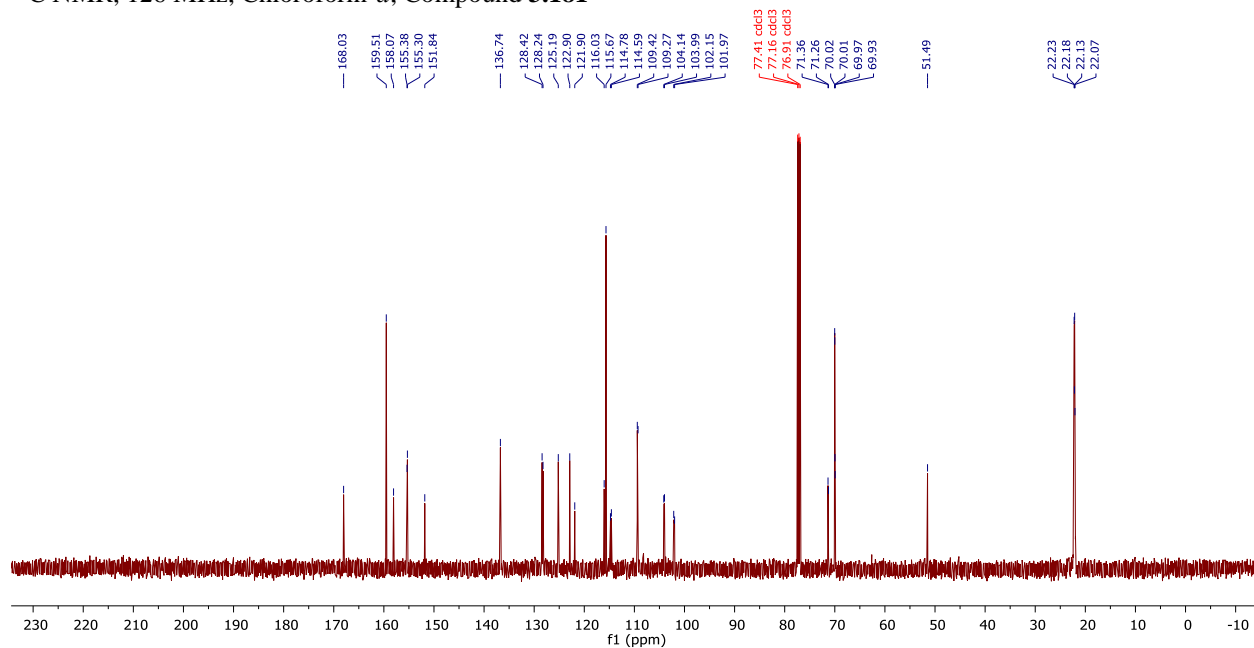
IR (Neat): 2977, 1734, 1700, 1559, 1521, 1343, 1287, 1194, 1176, 1122 cm^{-1} .

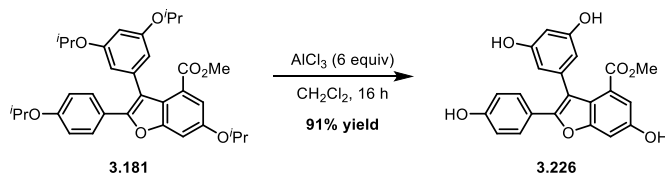
HRMS (ESI) m/z calculated for $\text{C}_{34}\text{H}_{41}\text{O}_7^+$ ($[\text{M}+\text{H}]^+$) 561.2847, found 561.2849.

¹H NMR, 500 MHz, Chloroform-*d*, Compound **3.181**



¹³C NMR, 126 MHz, Chloroform-*d*, Compound **3.181**





3.226 – methyl 3-(3,5-dihydroxyphenyl)-6-hydroxy-2-(4-hydroxyphenyl)benzofuran-4-carboxylate

A flame-dried round bottom flask was charged with the starting benzofuran **3.181** (920 mg, 1.64 mmol) with a stir bar under inert atmosphere. The starting material was dissolved in CH_2Cl_2 (17 mL) and AlCl_3 (1.31 g, 9.85 mmol) was added to the reaction solution in a single portion under a stream of nitrogen. The reaction became yellow and then deep red as the deprotection occurred. After the reaction was complete, it was quenched with sat. aqueous NH_4Cl (~20 mL) and transferred to a separatory funnel containing water (~100 mL) and EtOAc (~100 mL). The layers were separated, and the aqueous layer was washed with EtOAc (3 x 50 mL). The combined organic layers were washed with brine (~200 mL), dried over magnesium sulfate, and concentrated under reduced pressure. The crude material was purified via flash column chromatography (2% to 10%, 5 steps in 2% increments, 2 CVs per step, polar phase – MeOH, nonpolar phase – CH_2Cl_2) to afford the desired product as a white solid (587 mg, 91% yield).

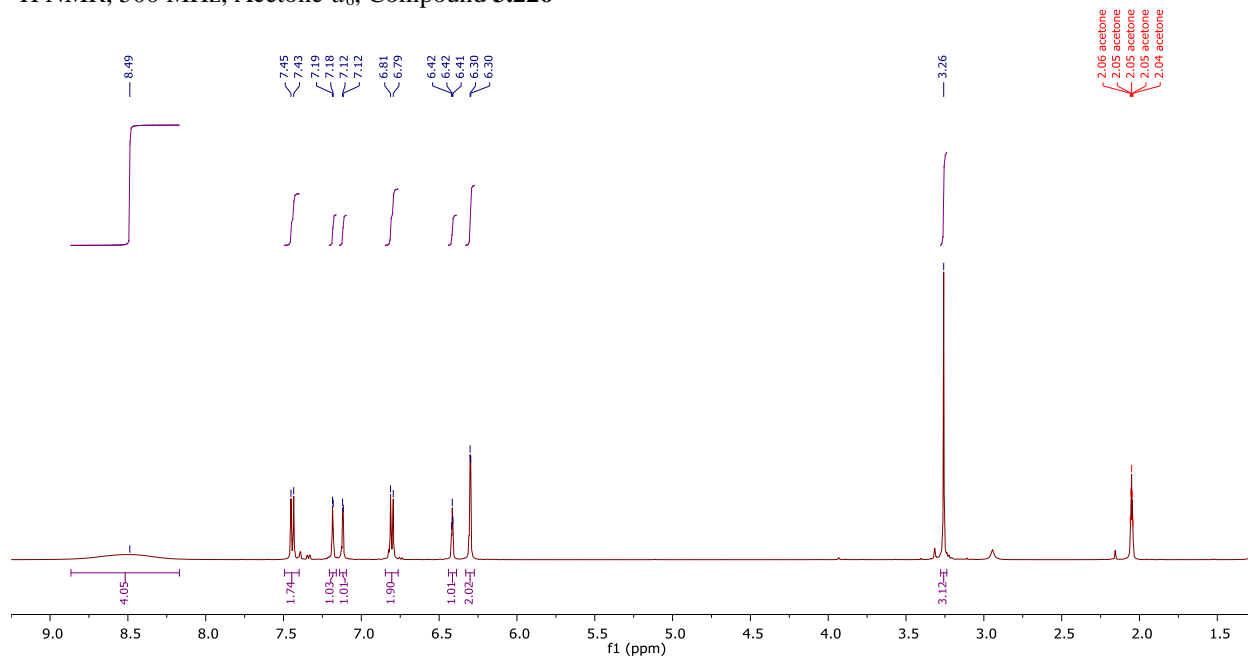
^1H NMR (500 MHz, Acetone- d_6) δ 8.49 (s, 4H), 7.44 (d, $J = 8.8$ Hz, 2H), 7.18 (d, $J = 2.2$ Hz, 1H), 7.12 (d, $J = 2.2$ Hz, 1H), 6.80 (d, $J = 8.8$ Hz, 2H), 6.42 (t, $J = 2.2$ Hz, 1H), 6.30 (d, $J = 2.2$ Hz, 2H), 3.26 (s, 3H).

^{13}C NMR (126 MHz, Acetone- d_6) δ 168.1, 159.8, 158.6, 156.1, 155.6, 152.0, 137.4, 129.1, 126.7, 122.9, 121.6, 116.6, 116.1, 113.8, 109.1, 102.6, 101.4, 51.4.

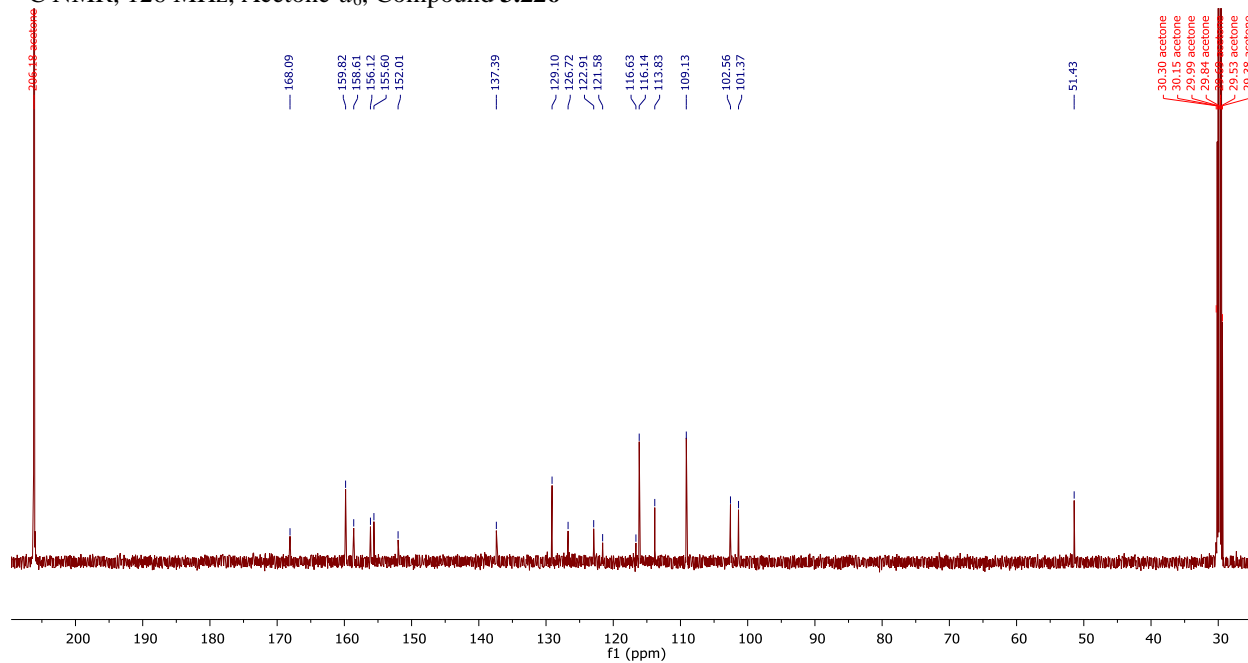
IR (Neat): 3326 (br), 2925, 1684, 1613, 1440, 1341, 1266, 1157, 1135, 1002 cm^{-1} .

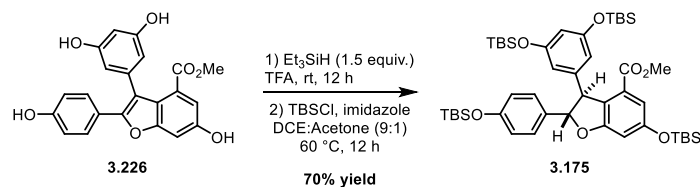
HRMS (ESI) m/z calculated for $\text{C}_{22}\text{H}_{15}\text{O}_7^-$ ($[\text{M}-\text{H}]^-$) 391.0823, found 391.0830.

¹H NMR, 500 MHz, Acetone-*d*₆, Compound **3.226**



¹³C NMR, 126 MHz, Acetone-*d*₆, Compound **3.226**





3.175 - methyl (2R,3R)-3-(3,5-bis((tert-butyldimethylsilyl)oxy)phenyl)-6-((tert-butyldimethylsilyl)oxy)-2-(4-((tert-butyldimethylsilyl)oxy)phenyl)-2,3-dihydrobenzofuran-4-carboxylate

Triethylsilane (305 μL , 1.91 mmol) was added to a stirred solution of **3.226** (500 mg, 1.27 mmol) in trifluoroacetic acid (10 mL). The reaction mixture was stirred at room temperature overnight. Upon reaction completion, the solution was cooled to 0 $^\circ\text{C}$ and carefully quenched with sat'd aq. NaHCO_3 . The quenched reaction was then extracted with ethyl acetate ($3 \times 10\text{mL}$), and the combined organic layer was dried over MgSO_4 and concentrated under reduced pressure. The crude residue was dissolved in minimal acetone ($\sim 500 \mu\text{L}$), and the resulting solution was diluted with DCE (13 mL). Imidazole (476 mg, 6.99 mmol) and TBSCl (957 mg, 6.35 mmol) were added to the reaction solution, and the reaction mixture was heated at 60 $^\circ\text{C}$ for 12 hours. Upon completion of the reaction, the reaction was concentrated and purified by flash column chromatography (0 to 10% EtOAc/Hexanes) to afford the desired product **3.175** as a colorless oil (758 mg, 70% yield).

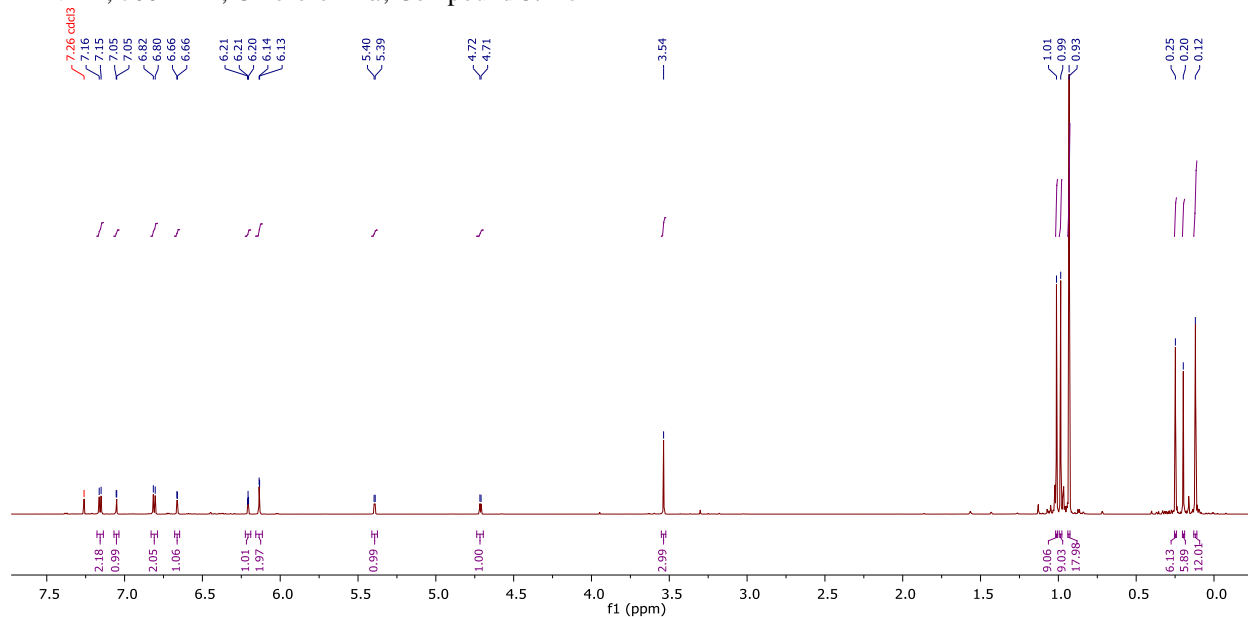
$^1\text{H NMR}$ (700 MHz, Chloroform-*d*) δ 7.16 (d, $J = 8.5$ Hz, 2H), 7.05 (d, $J = 2.2$ Hz, 1H), 6.81 (d, $J = 8.5$ Hz, 2H), 6.66 (d, $J = 2.2$ Hz, 1H), 6.21 (t, $J = 2.2$ Hz, 1H), 6.13 (d, $J = 2.2$ Hz, 2H), 5.39 (d, $J = 5.1$ Hz, 1H), 4.71 (d, $J = 5.1$ Hz, 1H), 3.54 (s, 3H), 1.01 (s, 9H), 0.99 (s, 9H), 0.93 (s, 18H), 0.25 (s, 6H), 0.20 (s, 6H), 0.12 (s, 12H).

$^{13}\text{C NMR}$ (176 MHz, Chloroform-*d*) δ 166.1, 162.1, 156.8, 155.8, 146.4, 134.3, 128.2, 126.9, 123.6, 120.4, 114.6, 112.5, 110.7, 106.3, 93.3, 57.4, 51.6, 25.85, 25.83, 18.41, 18.39, 18.35, -4.21, -4.25, -4.26, -4.28.

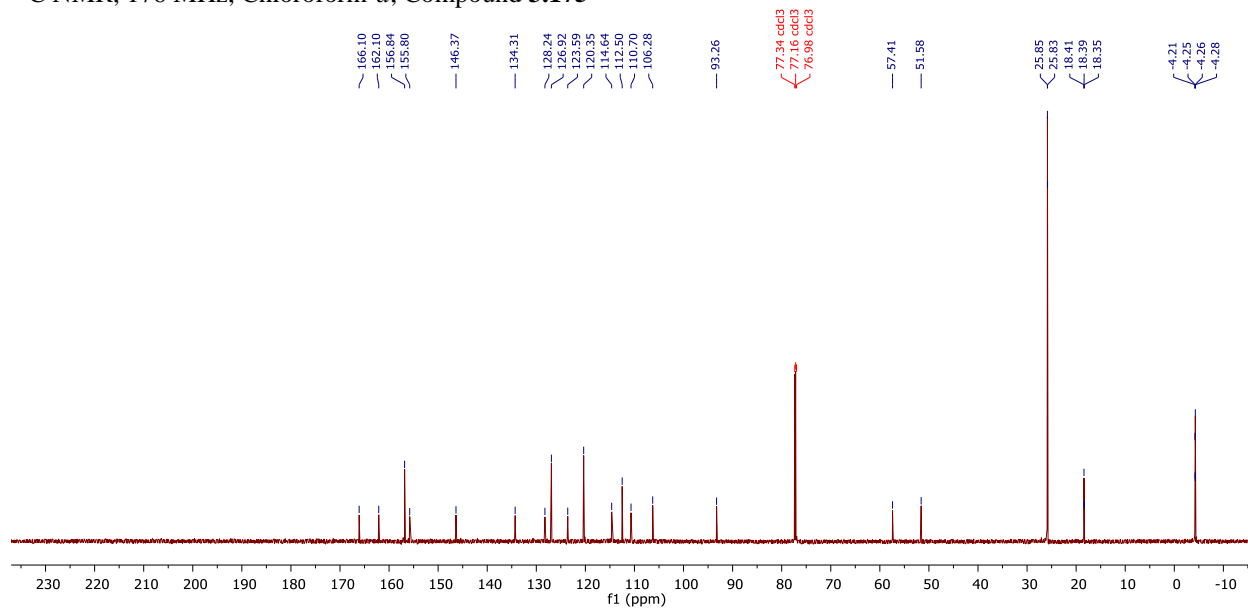
IR (Neat): 2955, 2930, 2895, 2858, 1727, 1161, 1588, 1473, 1343, 1253, 1161, 1030, 833 cm^{-1} .

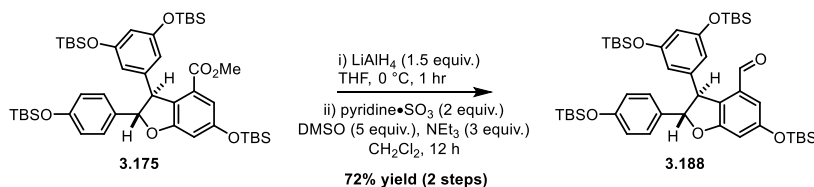
HRMS (ESI) m/z calculated for $\text{C}_{46}\text{H}_{75}\text{O}_7\text{Si}_4^+$ ($[\text{M}+\text{H}]^+$) 851.4584, found 851.4580.

¹H NMR, 700 MHz, Chloroform-*d*, Compound **3.175**



¹³C NMR, 176 MHz, Chloroform-*d*, Compound **3.175**





3.188 - (2R,3R)-3-(3,5-bis((tert-butyldimethylsilyloxy)phenyl)-6-((tert-butyldimethylsilyloxy)oxy)-2-(4-((tert-butyldimethylsilyloxy)phenyl)-2,3-dihydrobenzofuran-4-carbaldehyde

LiAlH_4 (45 mg, 1.18 mmol) was added to a stirred solution of **3.175** (670 mg, 0.787 mmol) in THF (15 mL) in an ice bath. The reaction mixture was allowed to react at 0 °C for 1 hour, at which point it was quenched with Glauber's salt. The precipitate was removed by filtration, and the filtrate was concentrated to afford the crude product, which was resuspended in CH_2Cl_2 (12 mL). To the reaction solution was added DMSO (280 μL , 3.93 mmol) and NEt_3 (330 μL , 2.36 mmol), and the solution was cooled to 0 °C. Pyridine- SO_3 (250 mg, 1.57 mmol) was added to the reaction in a single portion, and the reaction was allowed to warm to room temperature over 12 hours. The solvent was removed by rotatory evaporation, and the crude residue was dissolved in 20 mL of EtOAc/ H_2O (1:1) and transferred to a separatory funnel. The layers were separated, and the aqueous layer was extracted with additional EtOAc. The combined organic layers were washed with 1N HCl, sodium bicarbonate, and brine, then dried over magnesium sulfate and concentrated under reduced pressure. The crude product was purified by flash column chromatography (0 to 10% EtOAc in Hexanes) to afford the desired product **3.188** as a colorless oil (467 mg, 72% yield).

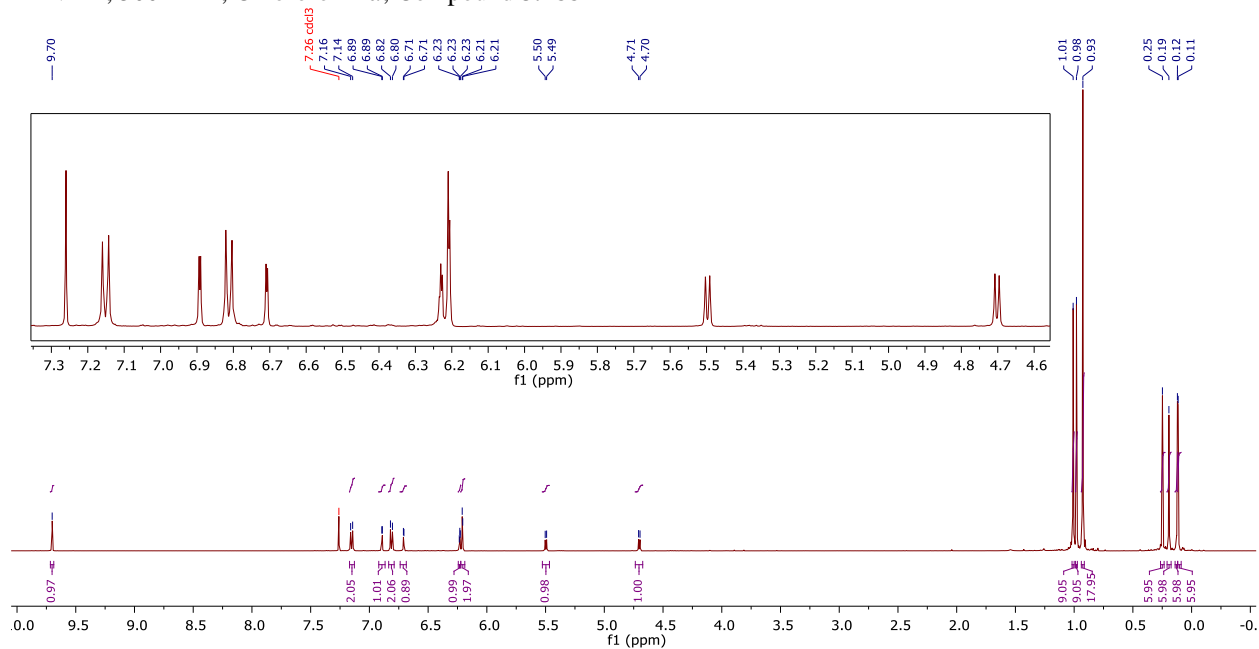
^1H NMR (500 MHz, Chloroform-*d*) δ 9.70 (s, 1H), 7.15 (d, $J = 8.5$ Hz, 2H), 6.89 (d, $J = 2.2$ Hz, 1H), 6.81 (d, $J = 8.5$ Hz, 2H), 6.71 (d, $J = 2.1$ Hz, 1H), 6.23 (t, $J = 2.2$ Hz, 1H), 6.21 (d, $J = 2.2$ Hz, 2H), 5.50 (d, $J = 6.0$ Hz, 1H), 4.70 (d, $J = 6.0$ Hz, 1H), 1.01 (s, 9H), 0.98 (s, 9H), 0.93 (s, 18H), 0.25 (s, 6H), 0.19 (s, 6H), 0.12 (s, 6H), 0.12 (s, 6H).

^{13}C NMR (126 MHz, Chloroform-*d*) δ 190.2, 162.2, 157.5, 157.1, 155.9, 145.5, 133.6, 133.2, 126.9, 124.6, 120.4, 113.1, 112.9, 111.3, 107.7, 94.1, 55.9, 25.83, 25.80, 18.39, 18.36, -4.25, -4.28.

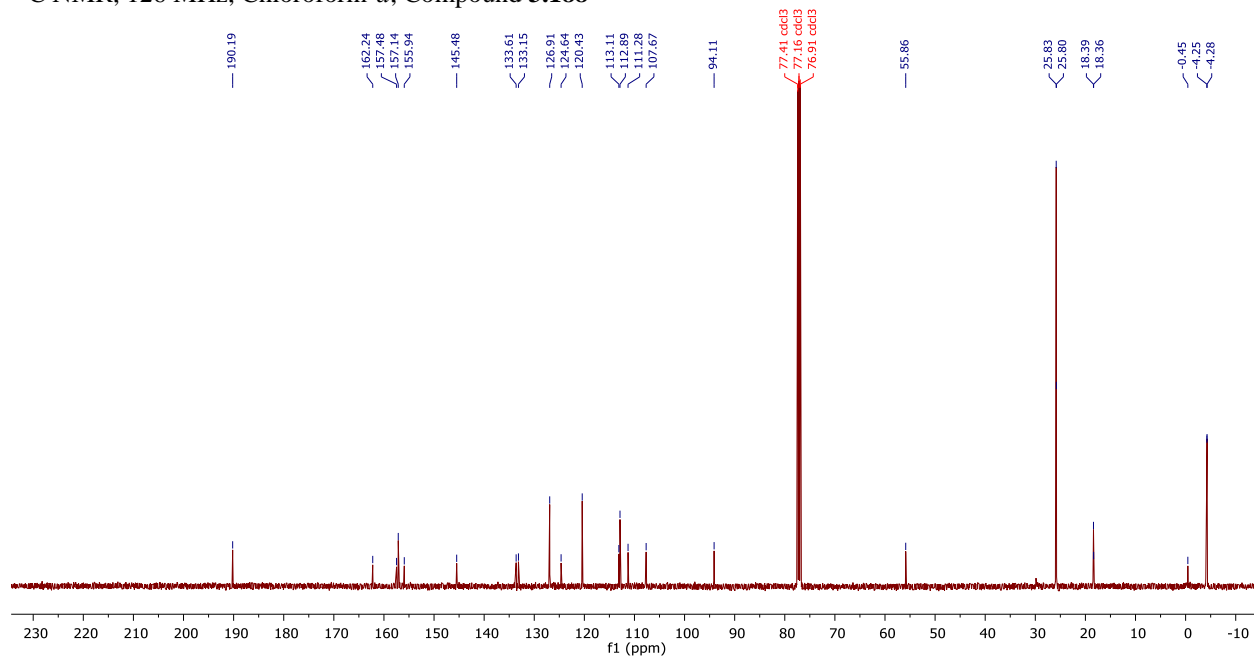
IR (Neat): 2955, 2929, 2858, 1700, 1608, 1589, 1338, 1254, 1163, 1030, 915 cm^{-1} .

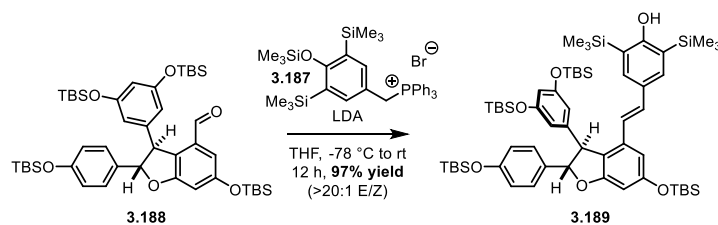
HRMS (ESI) m/z calculated for $\text{C}_{45}\text{H}_{73}\text{O}_6\text{Si}_4^+$ ($[\text{M}+\text{H}]^+$) 821.4479, found 821.4474.

¹H NMR, 500 MHz, Chloroform-*d*, Compound **3.188**



¹³C NMR, 126 MHz, Chloroform-*d*, Compound **3.188**





3.189 - 4-((E)-2-((2S,3S)-3-(3,5-bis((tert-butyl dimethylsilyl)oxy)phenyl)-6-((tert-butyl dimethylsilyl)oxy)-2-(4-((tert-butyl dimethylsilyl)oxy)phenyl)-2,3-dihydrobenzofuran-4-yl)vinyl)-2,6-bis(trimethylsilyl)phenol

Preparation of LDA solution:

Freshly distilled diisopropyl amine (126 μ L, 0.901 mmol) was dissolved in freshly distilled THF (6 mL) in a flame-dried heart-shaped flask. The resulting solution was cooled to -78 $^{\circ}$ C, at which point *n*BuLi (351 μ L, 0.877 mmol, 2.5 M in hexanes) was added. The reaction solution was allowed to stir for 30 min at -78 $^{\circ}$ C prior to using the LDA solution.

Preparation of the ylide:

Phosphonium salt **3.187** was prepared as previously reported by our group.⁴⁸ A flame-dried three-neck round bottom flask was charged with **3.187** (584 mg, 0.877 mmol) under inert atmosphere, and **3.187** was suspended in freshly distilled THF (6 mL). The resulting suspension was cooled to -78 $^{\circ}$ C, at which point the LDA solution (*vide supra*) was added to the suspension via cannula (**Note:** Both solutions were held at -78 $^{\circ}$ C for the duration of the cannulation). As deprotonation to form the ylide occurred, the reaction solution turned a brilliant red color. This solution was allowed to stir at -78 $^{\circ}$ C for 1 hour prior to addition of the aldehyde.

Wittig olefination between the ylide and aldehyde **3.188**:

Aldehyde **3.188** (400 mg, 0.487 mmol) was added to a flame-dried heart-shaped flask and dissolved in freshly distilled THF (5 mL). Upon completion of the ylide formation, the aldehyde solution was added to the ylide solution via cannula (**Note:** The aldehyde solution was at room temperature while the ylide solution was held at -78 $^{\circ}$ C for the duration of the cannulation). Upon complete addition of the aldehyde solution, the reaction was allowed to slowly warm to room temperature overnight (\sim 12 h). The reaction was subsequently diluted with EtOAc (\sim 25 mL) and added to a separatory funnel containing DI water (\sim 50 mL). An aqueous solution of saturated NH_4Cl (\sim 50 mL) was added to the separatory funnel, and the layers were separated. The aqueous layer was extracted with additional EtOAc, and the combined organic layers were washed with aqueous saturated sodium bicarbonate, washed with brine, dried over MgSO_4 , and concentrated. The crude product was purified by flash column chromatography (5% to 35% CH_2Cl_2 in Hexanes, 7 steps, 2 column volumes per step, 300 mL column volumes) to afford the desired product **3.189** as a white foam (498 mg, 97% yield).

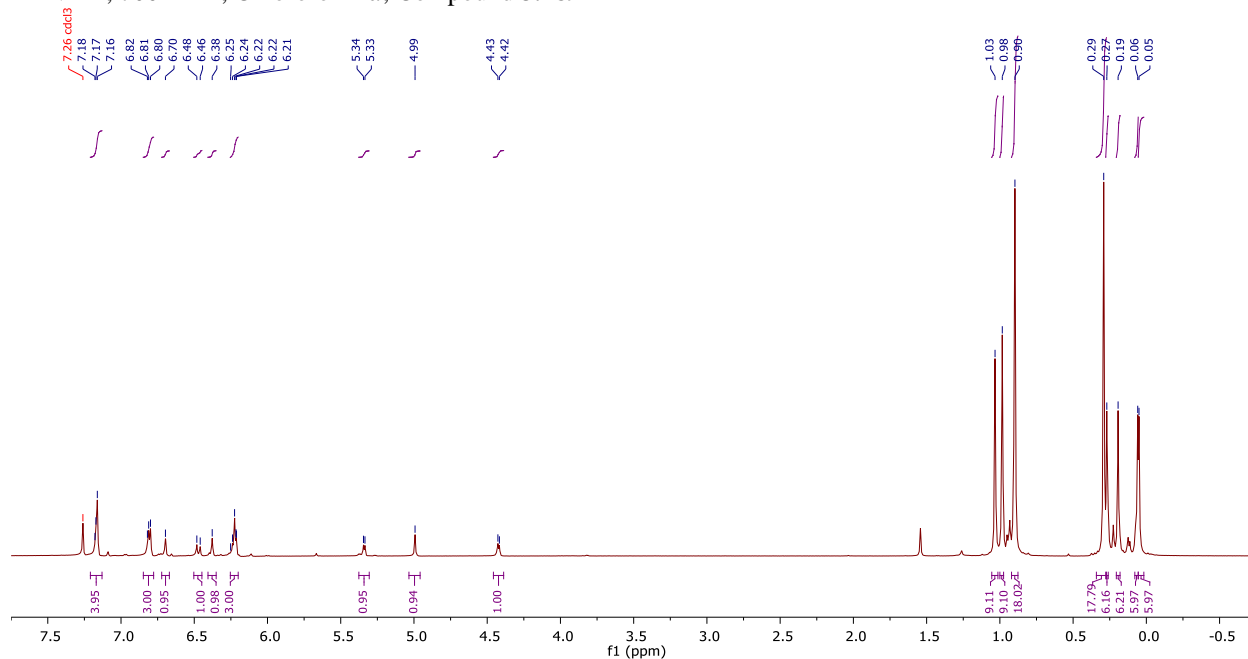
^1H NMR (700 MHz, Chloroform-*d*) δ 7.17 (d, J = 6.6 Hz, 4H), 6.85 – 6.78 (m, 3H), 6.70 (s, 1H), 6.47 (d, J = 16.1 Hz, 1H), 6.38 (s, 1H), 6.25 – 6.20 (m, 3H), 5.34 (d, J = 7.1 Hz, 1H), 4.99 (s, 1H), 4.42 (d, J = 7.1 Hz, 1H), 1.03 (s, 9H), 0.98 (s, 9H), 0.90 (s, 18H), 0.29 (s, 18H), 0.27 (s, 6H), 0.19 (s, 6H), 0.06 (s, 6H), 0.05 (s, 6H).

^{13}C NMR (176 MHz, Chloroform-*d*) δ 165.2, 161.5, 157.1, 157.0, 155.8, 145.0, 135.7, 135.1, 134.1, 129.9, 129.5, 127.2, 124.3, 123.2, 120.3, 120.0, 113.0, 111.4, 108.9, 100.9, 93.6, 57.0, 25.9, 25.8, 18.4, 18.37, 18.35, -4.13, -4.15, -4.21, -4.24, -4.25, -4.4.

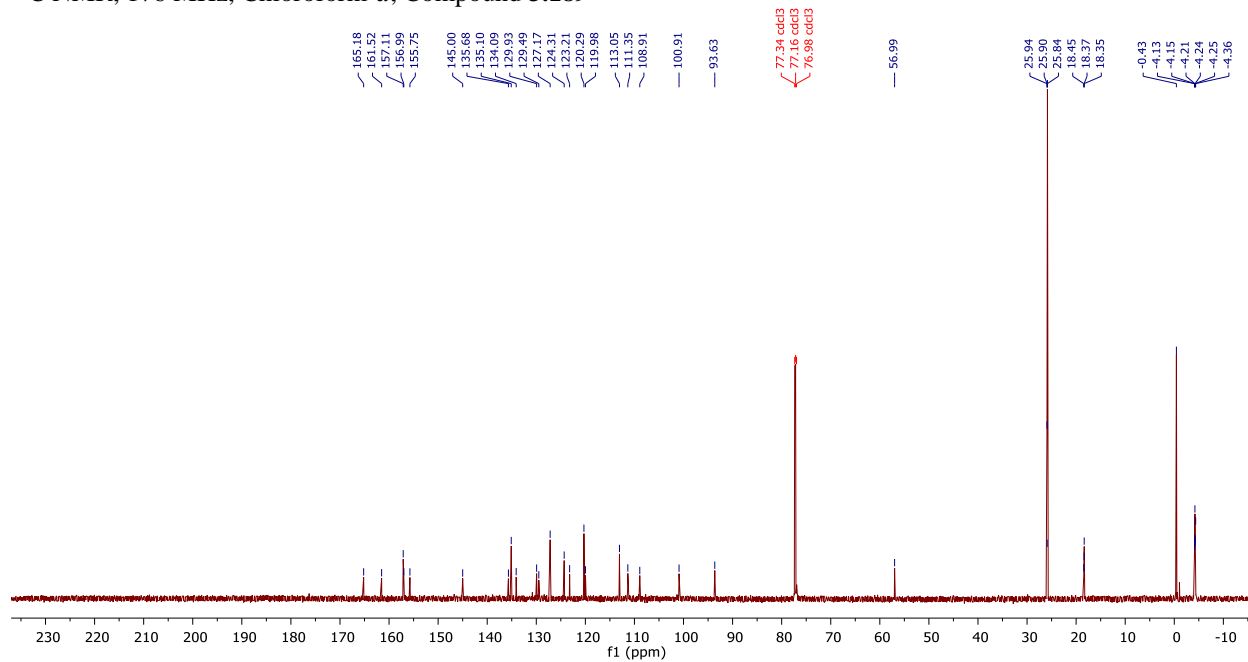
IR (Neat): 3609, 2944, 2892, 2866, 1607, 1584, 1462, 1340, 1264, 1166, 1012, 960, 852 cm^{-1} .

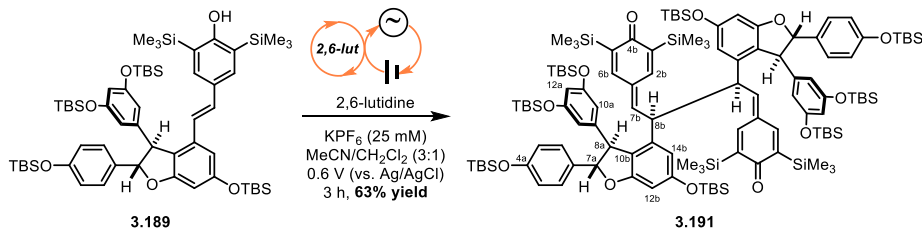
HRMS (ESI) m/z calculated for $\text{C}_{58}\text{H}_{95}\text{O}_6\text{Si}_6^+$ ($[\text{M}+\text{H}]^+$) 1055.5739, found 1055.5725.

¹H NMR, 700 MHz, Chloroform-*d*, Compound **3.189**



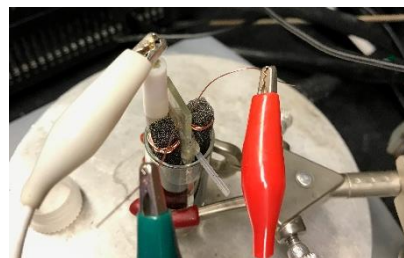
¹³C NMR, 176 MHz, Chloroform-*d*, Compound **3.189**





3.191 - 4,4'-((2S,3S)-2,3-bis((2S,3S)-3-(3,5-bis((tert-butyldimethylsilyloxy)phenyl)-6-((tert-butyldimethylsilyloxy)-2-(4-((tert-butyldimethylsilyloxy)phenyl)-2,3-dihydrobenzofuran-4-yl)butane-1,4-diylidene)bis(2,6-bis(trimethylsilyl)cyclohexa-2,5-dien-1-one)

Protected ϵ -viniferin analogue **3.189** (83 mg, 0.079 mmol) was added to a 10-mL reaction vial charged with a stir bar and KPF₆ (36 mg, 0.2 mmol, 2.5 equiv). The solids were dissolved in a 3:1 MeCN/CH₂Cl₂ (8 mL), and 2,6-lutidine (2.3 μ L, 0.0197 mmol, 0.25 equiv) was added to the reaction solution. Two pieces of 0.25 x 2-inch RVC panel (0.25 inch thickness) were cut. To each, a hole was made near one end, and copper wire was placed through the hole and wrapped around the top of each electrode. One end of the wire was left free in to connect to the alligator clips. These electrodes were carefully placed into the reaction vial along with the reference electrode (Ag/AgCl in 3 M KCl) and a divider (see image). The alligator clips were connected such that the reference (white) and working (green) electrodes were adjacent to each other, while the counter (red) electrode was opposite the divider. Care was taken to ensure the copper wire was not submerged in solvent, nor the active components of the alligator clips touching each other. The reaction was stirred at 750 rpm for 3 h at a constant voltage of 0.6 V. Upon completion of the reaction, the electrodes were removed and rinsed into a collection flask with DCM (~40 mL). The contents of the reaction vial were also rinsed into the collection flask. The solvent was removed on the rotovap, the crude material was resuspended in DCM, and the electrolyte was filtered away with a plug of Celite. The filtrate was then concentrated and purified by column chromatography (10% to 75% DCM in Hexanes) to afford the product as a yellow foam (52 mg, 63% yield). On 500 mg scale, the reaction was conducted with 1 x 2 inch RVC panels (0.25 inch thickness) in a 50 mL beaker in 40 mL of MeCN/CH₂Cl₂. The same ratio of KPF₆ and 2,6-lutidine was used relative to the starting material to yield 312 mg of product. The spectroscopic data for this compound was consistent with our prior report for the benzyl-protected compound.⁴⁸



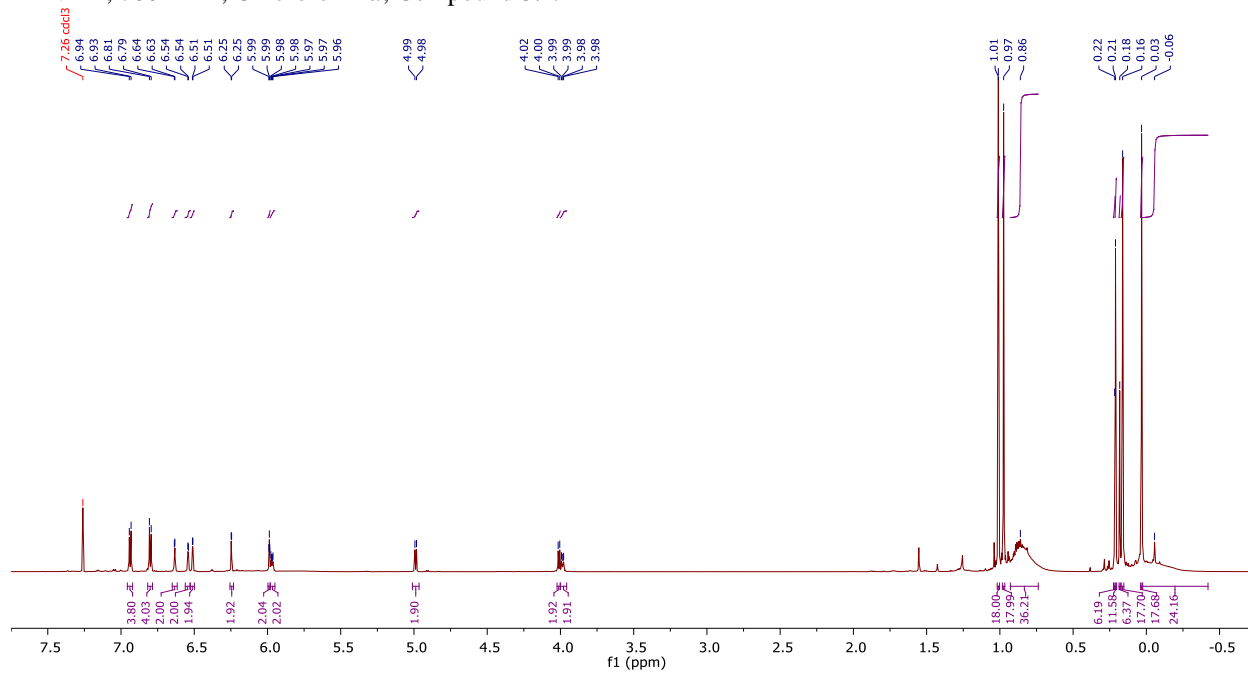
¹H NMR (700 MHz, Chloroform-*d*) δ 6.94 (d, J = 8.5 Hz, 4H, C_{2a}-H), 6.80 (d, J = 8.5 Hz, 4H, C_{3a}-H), 6.63 (d, J = 2.6 Hz, 2H, C_{2/6b}-H), 6.54 (d, J = 2.7 Hz, 2H, C_{2/6b}-H), 6.51 (d, J = 2.0 Hz, 2H, C_{14b}-H), 6.25 (d, J = 1.9 Hz, 2H, C_{12b}-H), 5.99 (t, J = 2.2 Hz, 2H, C_{12a}-H), 5.98 – 5.95 (m, 2H, C_{7b}-H), 4.99 (d, J = 7.6 Hz, 2H, C_{7a}-H), 4.01 (d, J = 7.6 Hz, 2H, C_{8a}-H), 3.99 (dd, J = 7.4, 2.9 Hz, 2H, C_{8b}-H), 1.01 (s, 18H), 0.97 (s, 18H), 0.86 (s, 36H), 0.22 (s, 6H), 0.21 (s, 12H), 0.18 (s, 6H), 0.16 (s, 18H), 0.03 (s, 18H), -0.06 (s, 24H).

¹³C NMR (176 MHz, Chloroform-*d*) δ 192.7, 161.3, 157.3, 156.0, 148.3, 144.5, 142.0, 141.3, 139.8, 138.2, 133.1, 132.5, 127.6, 121.7, 120.3, 111.1, 101.1, 94.2, 55.9, 49.4, 25.9, 25.8, 25.8, 18.4, 18.31, 18.28, -1.2, -1.3, -4.1, -4.17, -4.24.

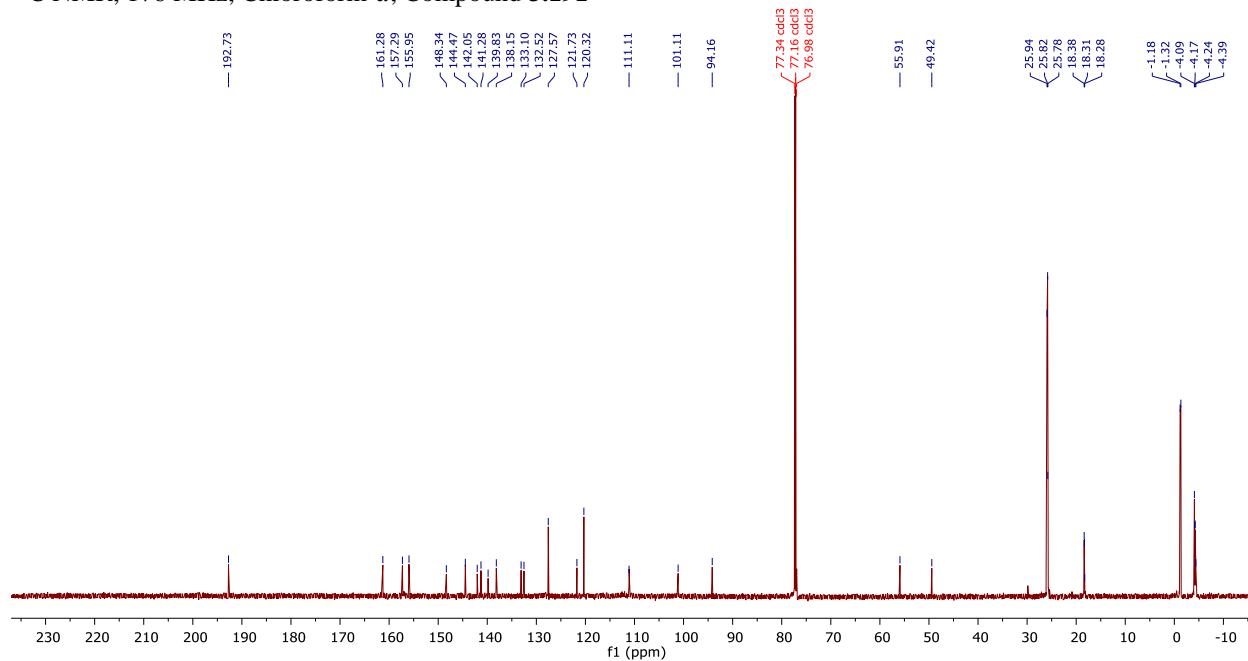
HRMS (ESI) m/z calculated for C₁₁₆H₁₈₇O₁₂Si₁₂⁺ ([M+H]⁺) 2108.1248, found 2108.1228.

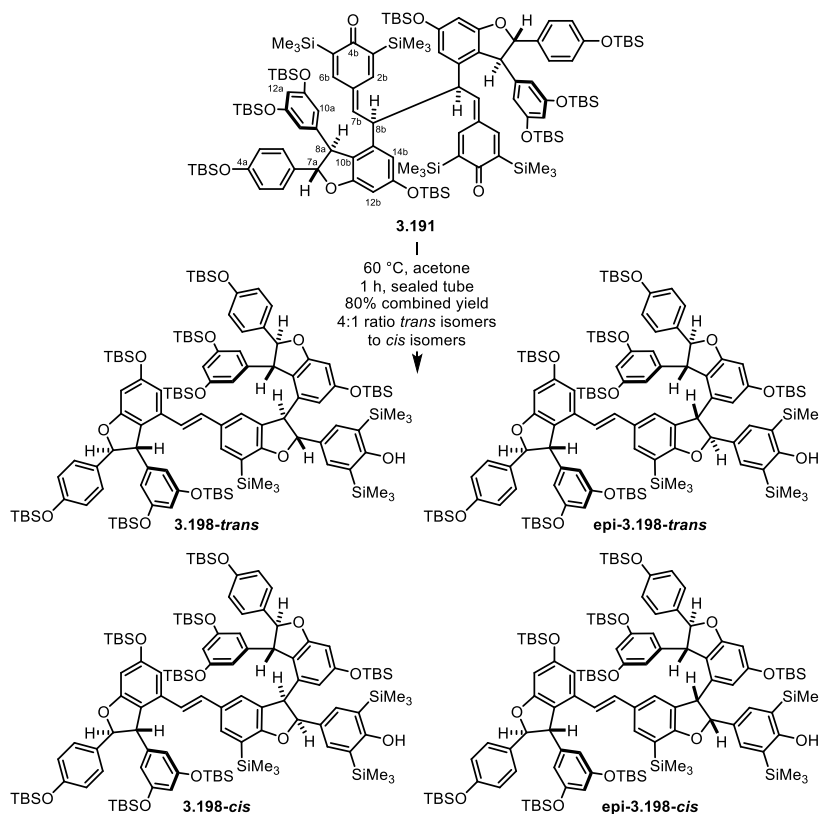
Note: The C_{10a}-H protons are not visible due to extreme broadening in the ¹H NMR spectrum. This is presumably due to hindered/slow rotation in a sterically encumbered environment. In the ¹³C NMR spectrum, the resonances for C_{9a} – C_{12a} were very broadened, further corroborating that rotation of the bulky phenol is likely hindered in this sterically congested system.

¹H NMR, 700 MHz, Chloroform-*d*, Compound **3.191**



¹³C NMR, 176 MHz, Chloroform-*d*, Compound **3.191**





3.198 - 4-((2R,2'S,3R,3'S)-3'-((3,5-bis((tert-butyltrimethylsilyloxy)phenyl)-5-((E)-2-((2S,3S)-3-(3,5-bis((tert-butyltrimethylsilyloxy)phenyl)-6-((tert-butyltrimethylsilyloxy)-2-(4-((tert-butyltrimethylsilyloxy)phenyl)-2,3-dihydrobenzofuran-4-yl)vinyl)-6'-((tert-butyltrimethylsilyloxy)-2'-((4-((tert-butyltrimethylsilyloxy)phenyl)-7-(trimethylsilyloxy)-2,2',3,3'-tetrahydro-[3,4'-bibenzofuran]-2-yl)-2,6-bis(trimethylsilyloxy)phenol

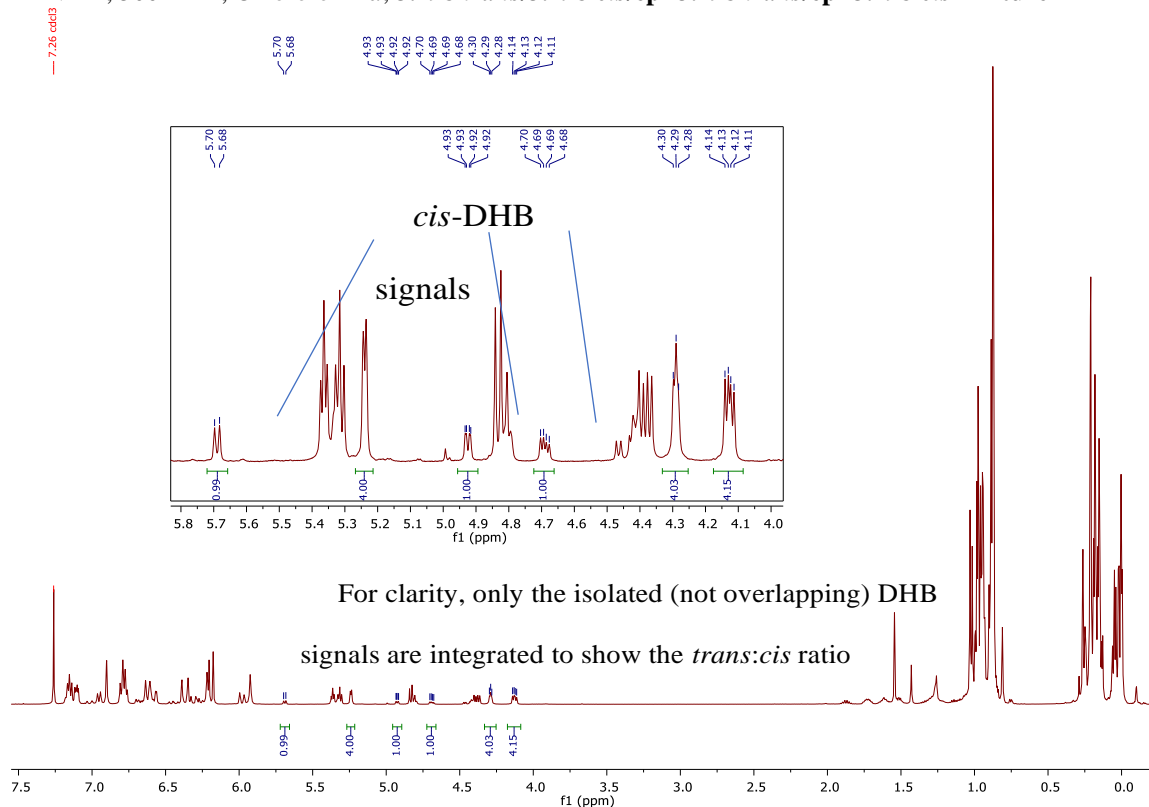
Quinone-methide dimer **3.191** (50 mg, 0.024 mmol) was added to a flame-dried reaction vial charged with a stir bar and dissolved in acetone (1.0 mL, HPLC grade). The reaction solution was sparged with a balloon of Ar for 5 minutes and then sealed under argon with parafilm. The reaction was heated to 60 °C for 1 hour, at which point it was cooled to room temperature, the stir bar was removed, and the solvent was evaporated under reduced pressure. The crude reaction was purified by flash column chromatography (4% to 28% over 7 steps, then 33%, 50%, 66% CH₂Cl₂ in Hexanes, 1 column volume per step, 30 mL column volume) to afford the inseparable mixture of four diastereomers (38.6 mg, 80% yield). Additional rounds of chromatography afforded modest resolution between the *trans*-DHB and *cis*-DHB isomers; however, **3.198-*trans*** and **epi-3.198-*trans*** were not separable from each other, so for targeting the natural products the crude mixture was carried forward for desilylation without purification.

3.198-*trans*/epi-3.198-*trans* mixture:

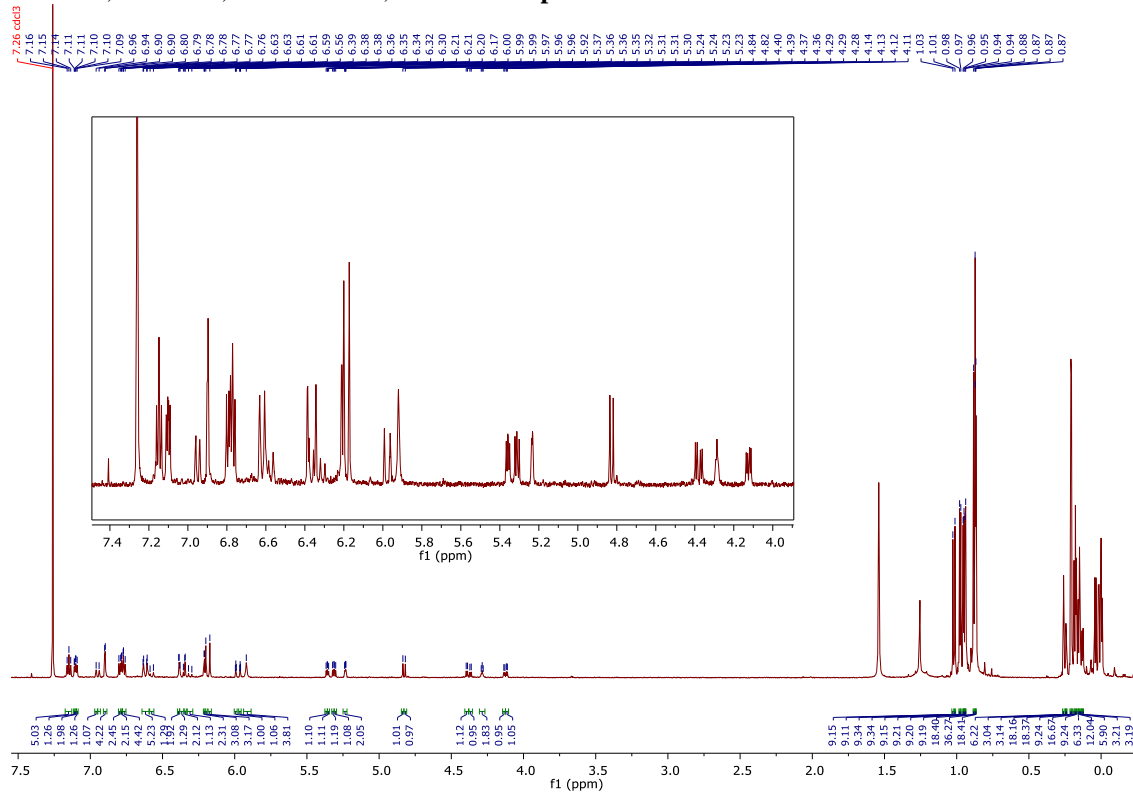
¹H NMR (700 MHz, Chloroform-*d*) δ 7.15 (t, *J* = 8.7 Hz, 5H), 7.11 (d, *J* = 2.0 Hz, 1H), 7.10 (d, *J* = 2.9 Hz, 2H), 7.09 (s, 1H), 6.96 (s, 1H), 6.94 (s, 1H), 6.90 (d, *J* = 3.0 Hz, 4H), 6.80 (d, *J* = 8.5 Hz, 2H), 6.78 (d, *J* = 2.3 Hz, 2H), 6.76 (d, *J* = 8.4 Hz, 4H), 6.62 (dd, *J* = 17.3, 2.4 Hz, 5H), 6.57 (d, *J* = 16.2 Hz, 1H), 6.39 (d, *J* = 2.1 Hz, 2H), 6.37 (d, *J* = 16.1 Hz, 1H), 6.34 (d, *J* = 2.1 Hz, 2H), 6.31 (d, *J* = 16.2 Hz, 1H), 6.21 (d, *J* = 2.2 Hz, 2H), 6.20 (s, 3H), 6.17 (s, 3H), 5.99 (t, *J* = 2.2 Hz, 1H), 5.96 (t, *J* = 2.0 Hz, 1H), 5.92 (s, 4H), 5.36 (d, *J* = 5.2 Hz, 1H), 5.35 (d, *J* = 5.3 Hz, 1H), 5.32 (d, *J* = 6.7 Hz, 1H), 5.31 (d, *J* = 6.8 Hz, 1H), 5.23 (dd, *J* = 4.3, 1.7 Hz, 2H), 4.84 (s, 1H), 4.82 (s, 1H), 4.39 (d, *J* = 6.6 Hz, 1H), 4.37 (d, *J* = 6.5 Hz, 1H), 4.29 (t, *J* = 4.7 Hz, 2H), 4.13 (d, *J* = 5.1 Hz, 1H), 4.12 (d, *J* = 5.0 Hz, 1H), 1.03 (s, 9H), 1.01 (s, 9H), 0.98 (s, 9H), 0.97 (s, 9H), 0.96 (s, 9H), 0.95 (s, 9H), 0.94 (s, 9H), 0.94 (s, 9H), 0.88 (s, 18H), 0.87 (d, *J* = 1.1 Hz, 36H), 0.87 (s, 18H), 0.26 (s, 6H), 0.24 (s, 3H), 0.24 (s, 3H), 0.21 (s, 18H), 0.20 (s, 18H), 0.19 (s, 9H), 0.18 (d, *J* = 1.2 Hz, 17H), 0.17 (s, 9H), 0.16 (s, 6H), 0.15 (d, *J* = 1.5 Hz, 12H), 0.14 (s, 6H), 0.13 (s, 3H), 0.12 (d, *J* = 1.6 Hz, 3H).

HRMS (ESI) *m/z* calculated for C₁₁₃H₁₇₉O₁₂Si₁₁⁺ ([M+H]⁺) 2036.0853, found 2036.0849.

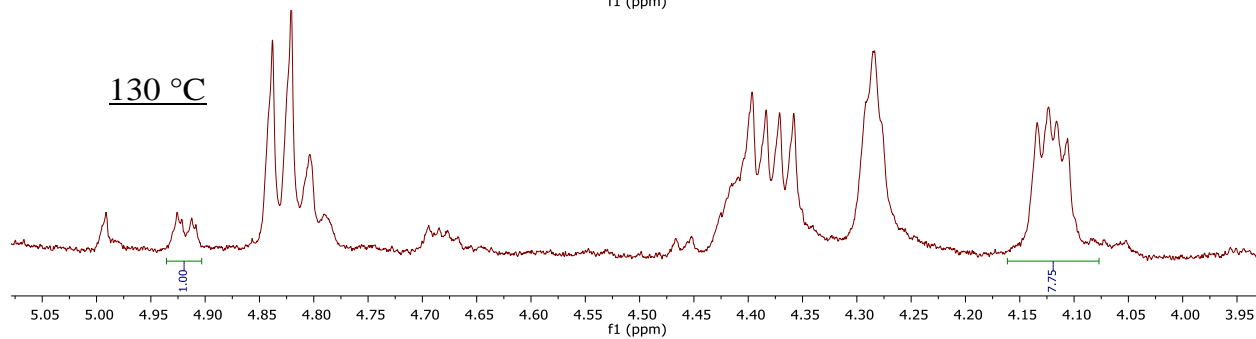
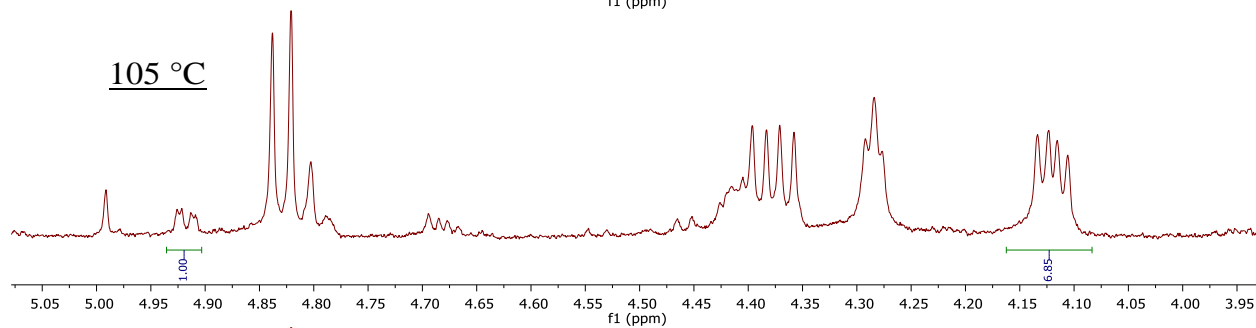
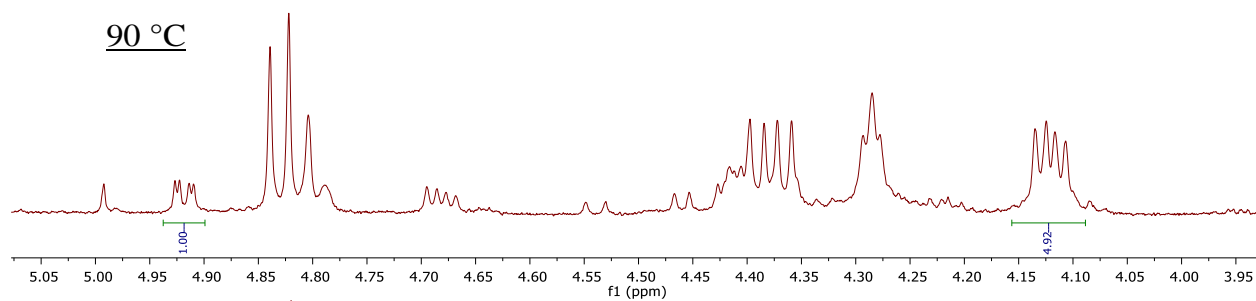
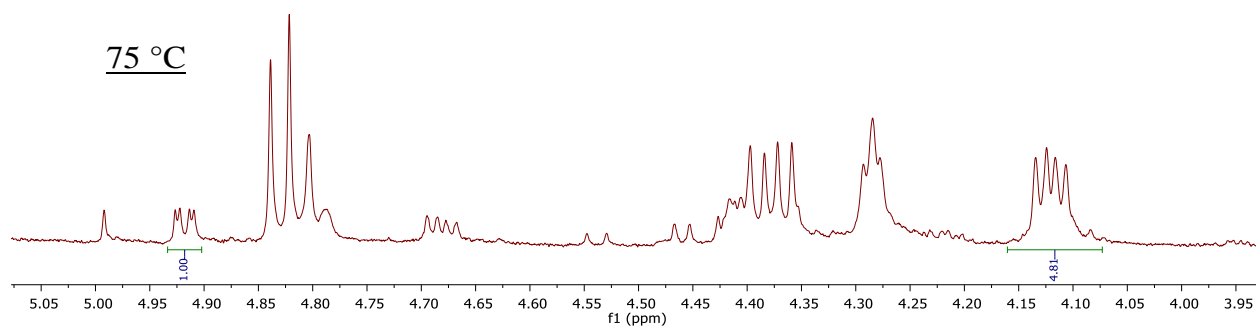
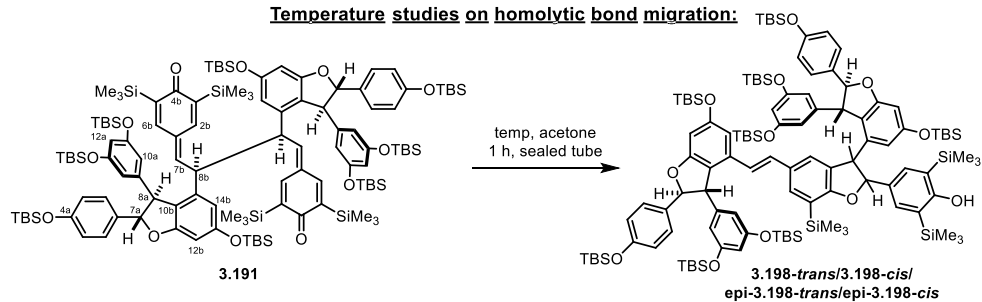
¹H NMR, 500 MHz, Chloroform-*d*, 3.198-*trans*/3.198-*cis*/epi-3.198-*trans*/epi-3.198-*cis* mixture

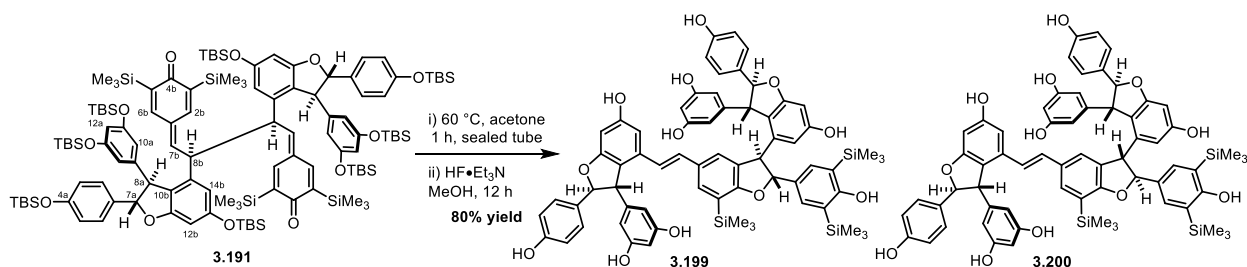


¹H NMR, 700 MHz, Chloroform-*d*, 3.198-*trans*/epi-3.198-*trans* mixture



Temperature studies on homolytic bond migration:





3.199 - 5-((2*S*,3*S*)-4-((*E*)-2-((2*R*,2'*S*,3*R*,3'*S*)-3'-(3,5-dihydroxyphenyl)-6'-hydroxy-2-(4-hydroxy-3,5-bis(trimethylsilyl)phenyl)-2'-(4-hydroxyphenyl)-7-(trimethylsilyl)-2,2',3,3'-tetrahydro-[3,4'-bibenzofuran]-5-yl)vinyl)-6-hydroxy-2-(4-hydroxyphenyl)-2,3-dihydrobenzofuran-3-yl)benzene-1,3-diol

Quinone-methide dimer **3.191** (100 mg, 0.047 mmol) was added to a flame-dried reaction vial charged with a stir bar and dissolved in acetone (1.5 mL, HPLC grade). The reaction solution was sparged with a balloon of Ar for 5 minutes and then sealed under argon with parafilm. The reaction was heated to 60 °C for 1 hour, at which point it was cooled to room temperature, and HF·Et₃N (0.48 mL, 2.94 mmol) was added followed by methanol (1.5 mL). The desilylation stirred for 12 hours, at which point it was transferred to a separatory funnel containing aqueous sat. sodium bicarbonate (~50 mL), and the aqueous layer was extracted with portions EtOAc (3 x 20 mL). The combined organic layers were washed with brine, dried over MgSO₄, and concentrated. For characterization purposes this material was purified by flash column chromatography (10% to 40% in 4 step increments, 2 column volumes per step, Nonpolar solvent – CH₂Cl₂, Polar solvent – 3:1 Acetone/MeOH) to afford the **3.199/3.200** mixture (44 mg, 80% yield). Otherwise when targeting vitisin D (**3.148**) and **3.206**, **3.207**, and **3.209**, this material was carried forward without purification.

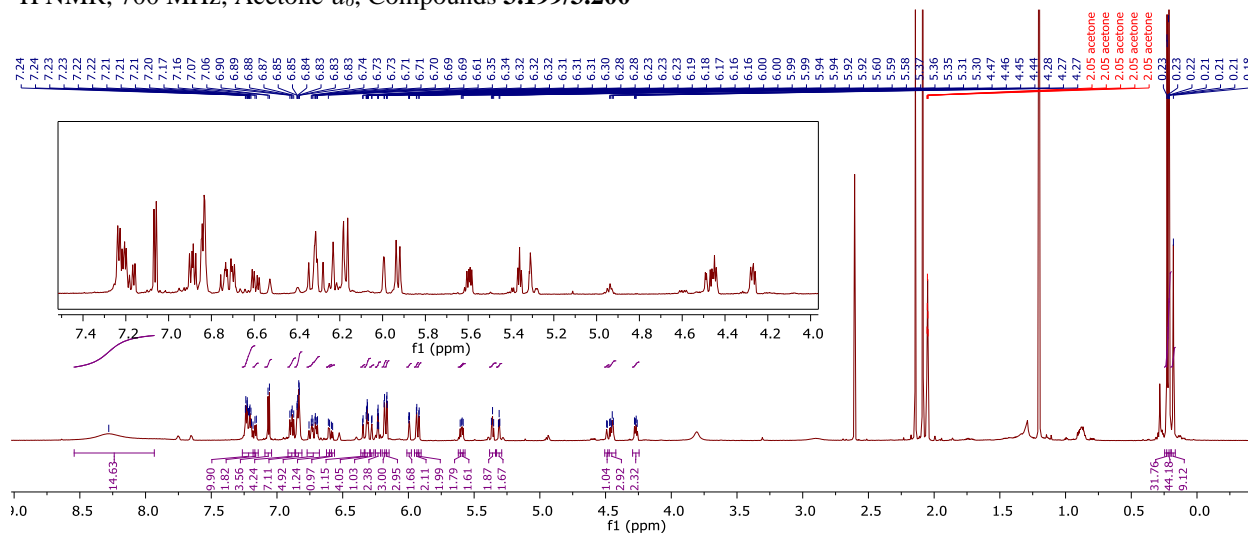
¹H NMR (700 MHz, Acetone-*d*₆) δ 8.28 (s, 15H), 7.26 – 7.18 (m, 10H), 7.16 (d, *J* = 7.4 Hz, 2H), 7.06 (d, *J* = 7.5 Hz, 4H), 6.89 (dd, *J* = 12.3, 8.1 Hz, 4H), 6.86 – 6.81 (m, 7H), 6.77 – 6.68 (m, 5H), 6.60 (d, *J* = 6.4 Hz, 1H), 6.58 (d, *J* = 6.4 Hz, 1H), 6.35 (d, *J* = 2.1 Hz, 1H), 6.31 (ddd, *J* = 6.7, 4.3, 2.0 Hz, 4H), 6.28 (d, *J* = 2.0 Hz, 1H), 6.23 (p, *J* = 1.8 Hz, 2H), 6.18 (d, *J* = 2.5 Hz, 3H), 6.17 – 6.15 (m, 2H), 6.01 – 5.98 (m, 2H), 5.94 (d, *J* = 2.0 Hz, 2H), 5.92 (d, *J* = 2.1 Hz, 1H), 5.60 (d, *J* = 6.1 Hz, 1H), 5.59 (d, *J* = 5.4 Hz, 1H), 5.36 (t, *J* = 5.8 Hz, 2H), 5.31 (t, *J* = 3.7 Hz, 2H), 4.49 (d, *J* = 4.0 Hz, 1H), 4.48 – 4.42 (m, 3H), 4.27 (dd, *J* = 8.9, 5.7 Hz, 2H), 0.23 (d, *J* = 1.1 Hz, 18H), 0.21 (dd, *J* = 2.9, 1.0 Hz, 27H), 0.18 (s, 9H).

¹³C NMR (176 MHz, Acetone-*d*₆) δ 166.4, 164.8, 162.8, 162.7, 160.2, 159.91, 159.87, 159.61, 159.57, 158.3, 158.12, 158.07, 147.4, 147.3, 146.9, 146.8, 136.72, 136.67, 134.65, 134.60, 134.40, 134.36, 134.1, 133.9, 133.8, 132.2, 132.1, 131.6, 131.0, 130.9, 130.8, 128.32, 128.25, 128.15, 127.9, 127.8, 126.8, 126.7, 126.2, 123.5, 123.4, 120.6, 119.65, 119.62, 119.5, 119.3, 116.5, 116.3, 116.2, 107.01, 106.98, 106.45, 106.42, 104.5, 102.4, 102.3, 96.8, 96.7, 94.25, 94.21, 94.18, 94.16, 91.4, 91.3, 69.8, 57.3, 57.1, 57.0, 56.7, 53.0, -0.3, -0.85, -0.86.

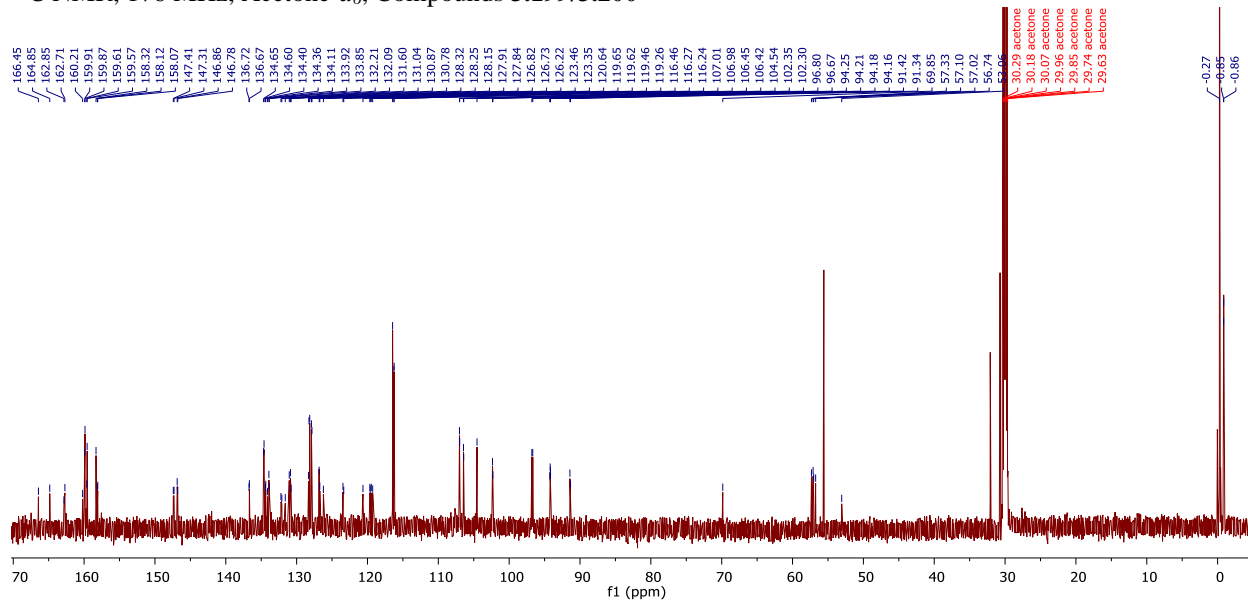
IR (Neat): 3438 (br), 2925, 1613, 1589, 1524, 1442, 1336, 1269, 1154, 1135, 1012 cm⁻¹.

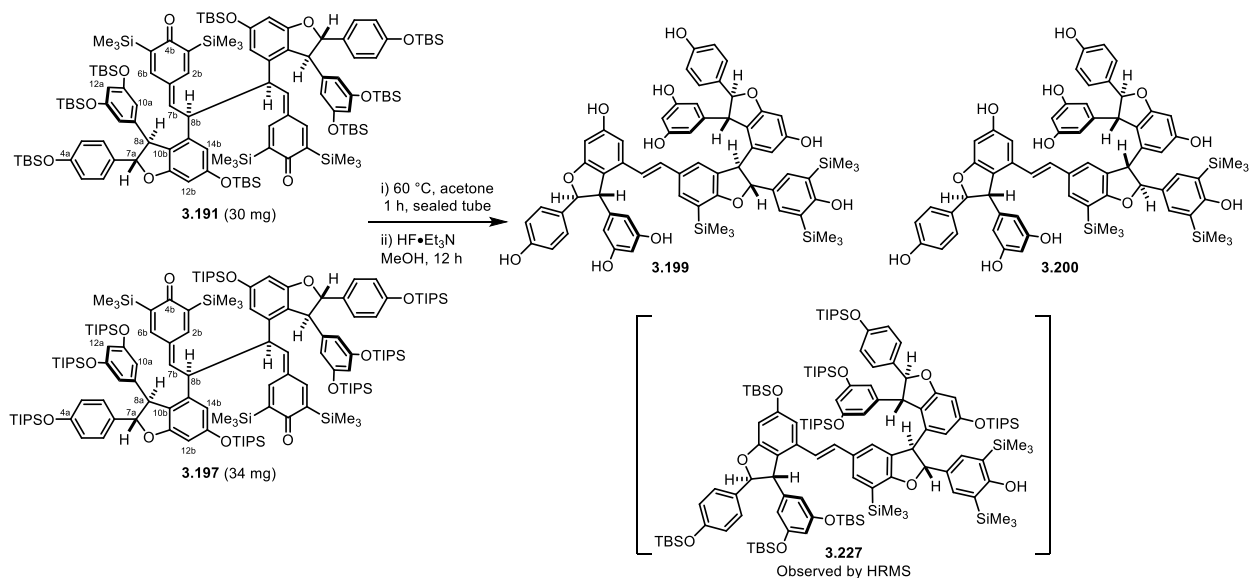
HRMS (ESI) *m/z* calculated for C₆₅H₆₇O₁₂Si₃⁺ ([M+H]⁺) 1123.3935, found 1123.3924.

¹H NMR, 700 MHz, Acetone-*d*₆, Compounds **3.199/3.200**



¹³C NMR, 176 MHz, Acetone-*d*₆, Compounds **3.199/3.200**



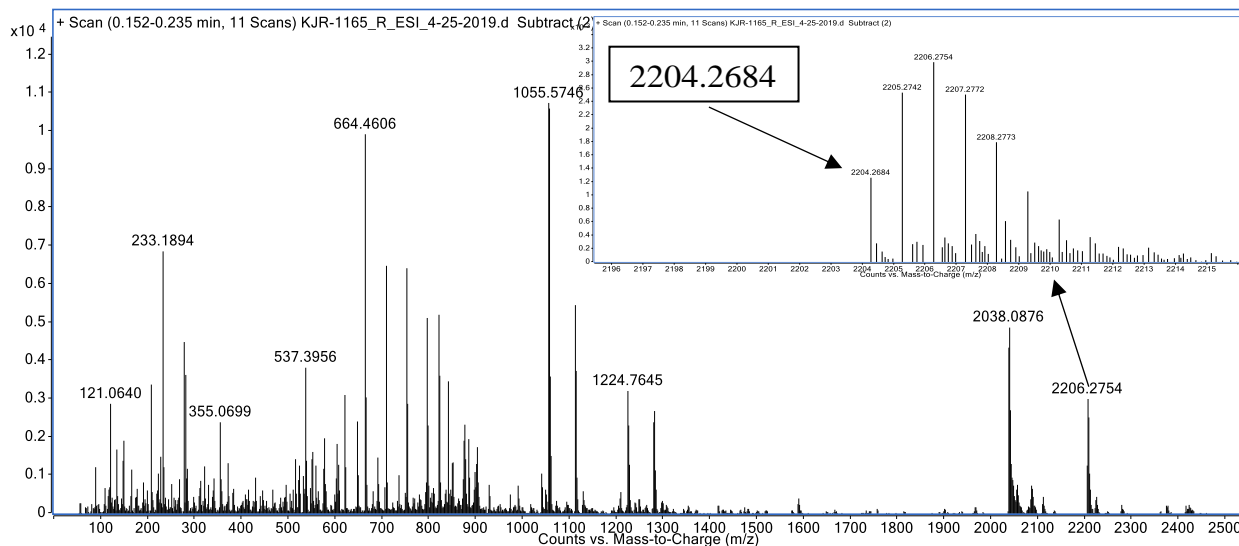


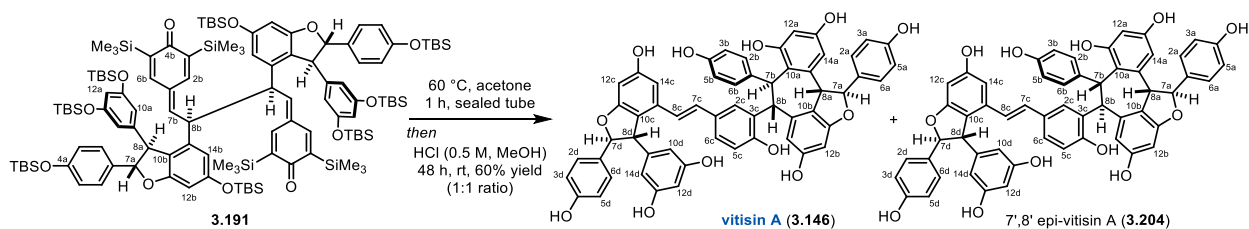
Crossover Experiment with **3.191** and **3.197**

Quinone-methide dimer **3.191** (30 mg, 0.014 mmol) and QMD **3.197** (34 mg, 0.014 mmol) were added to a flame-dried reaction vial charged with a stir bar and dissolved in acetone (1.0 mL, HPLC grade). The reaction solution was sparged with a balloon of Ar for 5 minutes and then sealed under argon with parafilm. The reaction was heated to 60 °C for 1 hour, at which point it was cooled to room temperature, and a 50 μL sample for HRMS analysis was taken. To the remaining HF·Et₃N (0.28 mL, 1.71 mmol) was added followed by methanol (1.0 mL). The desilylation stirred for 12 hours, at which point it was transferred to a separatory funnel containing aqueous sat. sodium bicarbonate (~50 mL), and the aqueous layer was extracted with portions EtOAc (3 x 20 mL). The combined organic layers were washed with brine, dried over MgSO₄, and concentrated. The crude product was purified by flash column chromatography (10% to 40% in 4 step increments, 2 column volumes per step, Nonpolar solvent – CH₂Cl₂, Polar solvent – 3:1 Acetone/MeOH) to afford the **3.199/3.200** mixture (12 mg, 75% yield). See above for characterization of **3.199/3.200**.

Intermediate **S24**:

HRMS (ESI) *m/z* calculated for C₁₂₅H₂₀₃O₁₂Si₁₁⁺ ([M+H]⁺) 2204.2731, found 2204.2684.





Vitisin A (3.146) - (4bS,5S,10S,11R)-10-(5-((E)-2-((2S,3S)-3-(3,5-dihydroxyphenyl)-6-hydroxy-2-(4-hydroxyphenyl)-2,3-dihydrobenzofuran-4-yl)vinyl)-2-hydroxyphenyl)-5,11-bis(4-hydroxyphenyl)-4b,5,10,11-tetrahydrobenzo[6,7]cyclohepta[1,2,3-cd]benzofuran-1,3,8-triol

Quinone-methide dimer **3.191** (140 mg, 0.066 mmol) was added to a flame-dried reaction vial charged with a stir bar and dissolved in acetone (2.0 mL, HPLC grade). The reaction solution was sparged with a balloon of Ar for 5 minutes and then sealed under argon with parafilm. The reaction was heated to 60 °C for 1 hour, and upon cooling to ambient temperature, a solution of hydrochloric acid was added (10 mL, 0.5 M in MeOH). The reaction was sealed under an argon atmosphere and allowed to stir at ambient temperature. After 48 hours, the stir bar was removed and the reaction mixture was directly concentrated on the rotovap and the crude residue was purified by flash column chromatography (8% to 40% in 5 step increments, 2 column volumes per step, Nonpolar solvent – CH₂Cl₂, Polar solvent – 3:1 Acetone/MeOH) to afford a mixture of vitisin A (**3.146**) and its diastereomer (**3.204**) in a ca. 1:1 ratio (35.9 mg, 60% combined yield). This mixture was further purified by prep-HPLC (10% to 65% MeCN/H₂O gradient over 1 hour) to afford pure samples of each compound. The ¹H and ¹³C NMR data for vitisin A (**3.146**) are consistent with literature reports.³⁰²

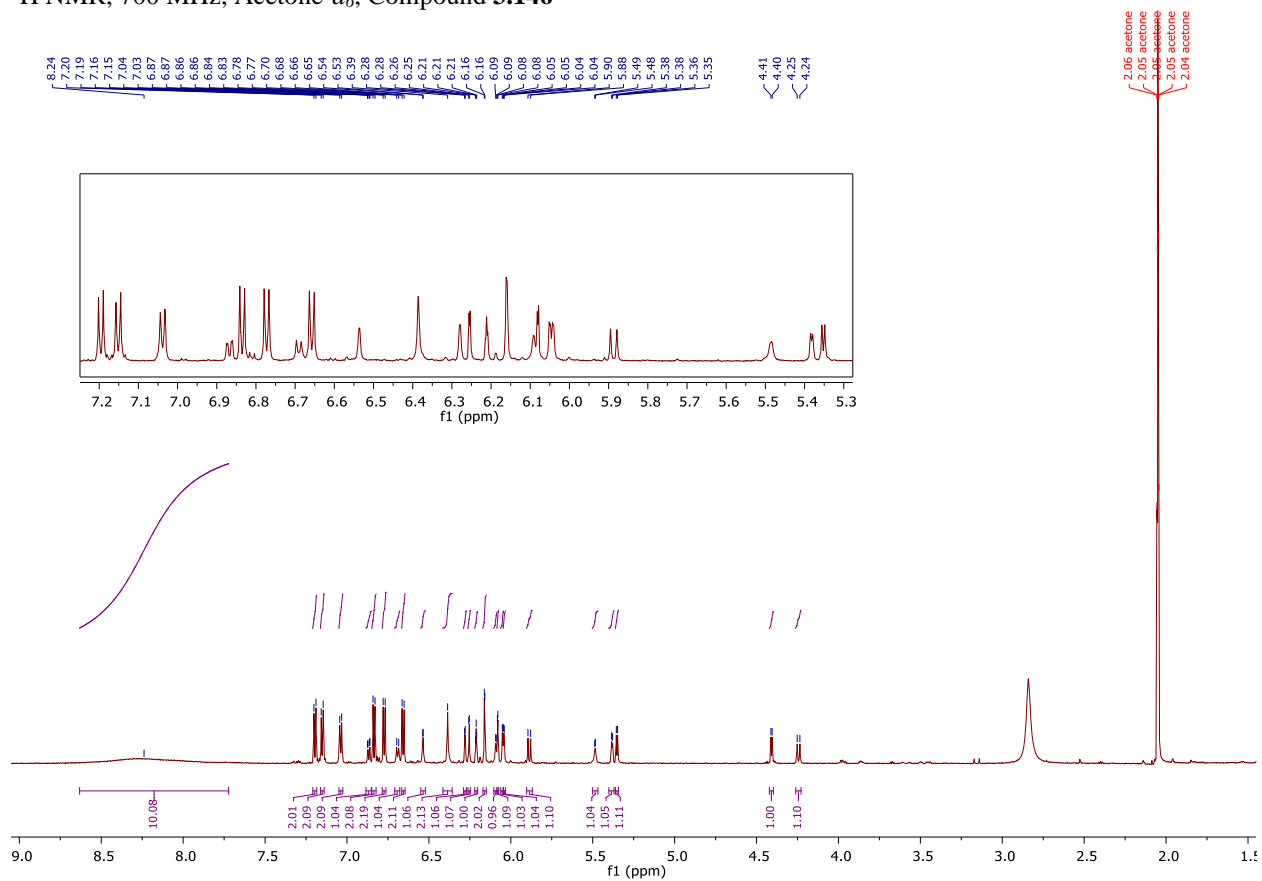
Vitisin A (3.146):

¹H NMR (700 MHz, Acetone-*d*₆) δ 8.24 (s, 10H, ArOH), 7.20 (d, *J* = 8.6 Hz, 2H, C_{2/6a}-H), 7.15 (d, *J* = 8.5 Hz, 2H, C_{2/6d}-H), 7.04 (d, *J* = 8.1 Hz, 2H, C_{2/6b}-H), 6.87 (dd, *J* = 8.4, 2.2 Hz, 1H, C_{6c}-H), 6.84 (d, *J* = 8.6 Hz, 2H, C_{3/5a}-H), 6.77 (d, *J* = 8.6 Hz, 2H, C_{3/5d}-H), 6.69 (d, *J* = 8.4 Hz, 1H, C_{5c}-H), 6.66 (d, *J* = 8.7 Hz, 2H, C_{3/5b}-H), 6.54 (d, *J* = 2.1 Hz, 1H, C_{14a}-H), 6.39 (br s, 2H, C_{7/8c}-H), 6.28 (d, *J* = 2.3 Hz, 1H, C_{12a}-H), 6.25 (d, *J* = 2.1 Hz, 1H, C_{14c}-H), 6.21 (t, *J* = 2.2 Hz, 1H, C_{12d}-H), 6.16 (d, *J* = 2.2 Hz, 2H, C_{10/14d}-H), 6.09 (d, *J* = 2.0 Hz, 1H, C_{2c}-H), 6.08 (d, *J* = 2.1 Hz, 1H, C_{12b}-H), 6.05 (d, *J* = 2.1 Hz, 1H, C_{14b}-H), 6.04 (d, *J* = 2.3 Hz, 1H, C_{12c}-H), 5.89 (d, *J* = 11.5 Hz, 1H, C_{7a}-H), 5.49 (d, *J* = 2.4 Hz, 1H, C_{8b}-H), 5.38 (d, *J* = 3.9 Hz, 1H, C_{7b}-H), 5.35 (d, *J* = 5.3 Hz, 1H, C_{7d}-H), 4.41 (d, *J* = 5.3 Hz, 1H, C_{8d}-H), 4.24 (d, *J* = 11.5 Hz, 1H, C_{8a}-H).

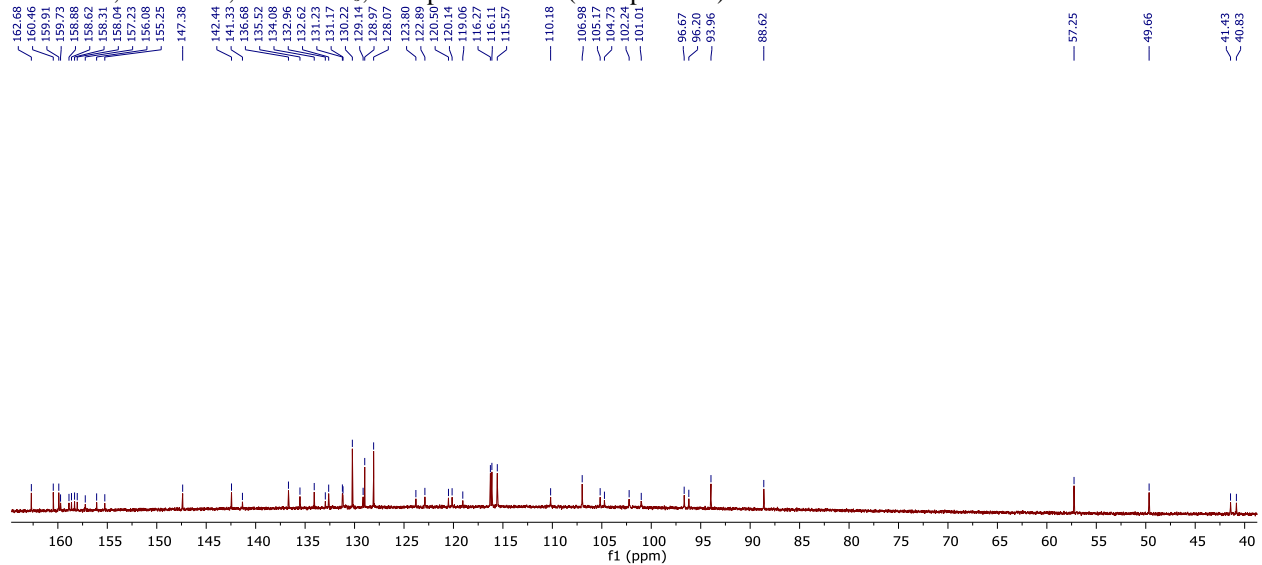
¹³C NMR (176 MHz, Acetone-*d*₆) δ 162.7, 160.5, 159.9, 159.7, 158.9, 158.6, 158.3, 158.0, 157.2, 156.1, 155.2, 147.4, 142.4, 141.3, 136.7, 135.5, 134.1, 133.0, 132.6, 131.23, 131.17, 130.2, 129.1, 129.0, 128.1, 123.8, 122.9, 120.5, 120.1, 119.0, 116.3, 116.1, 115.6, 110.2, 107.0, 105.2, 104.7, 102.2, 101.0, 96.7, 96.2, 94.0, 88.6, 57.2, 49.7, 41.4, 40.8.

HRMS (ESI) *m/z* calculated for C₅₆H₄₃O₁₂⁺ ([M+H]⁺) 907.2749, found 907.2743.

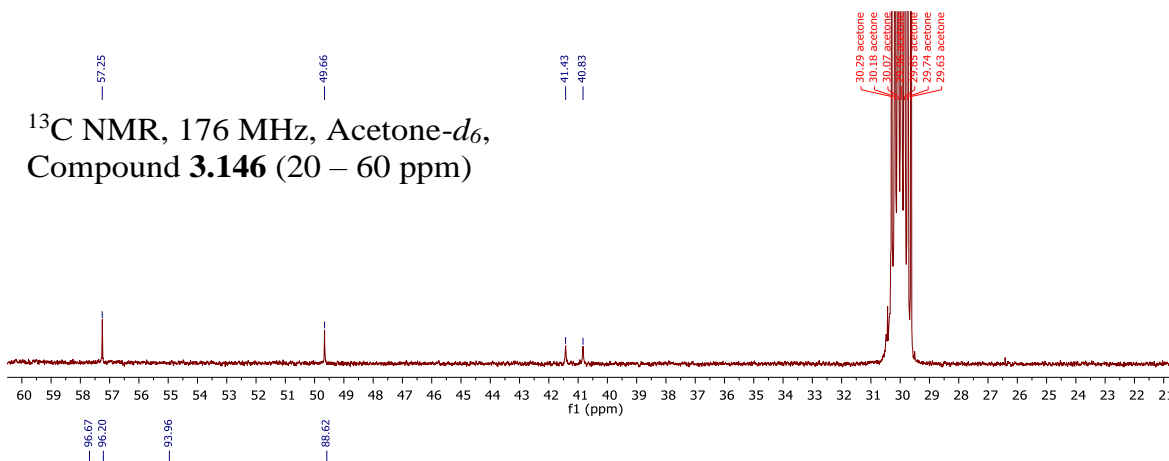
¹H NMR, 700 MHz, Acetone-*d*₆, Compound **3.146**



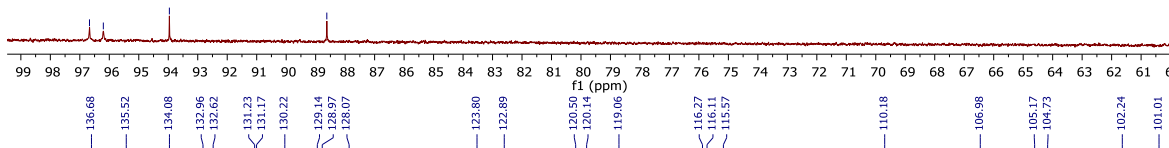
¹³C NMR, 176 MHz, Acetone-*d*₆, Compound **3.146** (full spectrum)



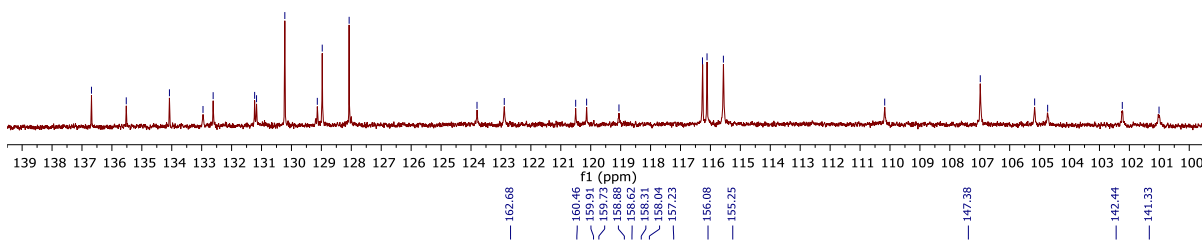
^{13}C NMR, 176 MHz, Acetone- d_6 ,
Compound **3.146** (20 – 60 ppm)



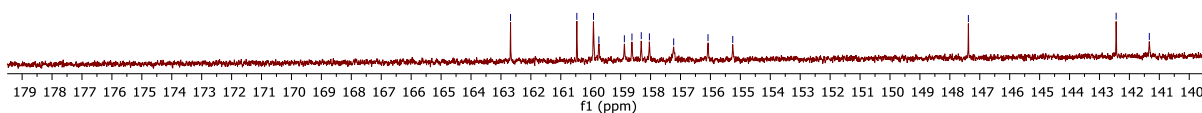
^{13}C NMR, 176 MHz, Acetone- d_6 ,
Compound **3.146** (60 – 100 ppm)



^{13}C NMR, 176 MHz, Acetone- d_6 ,
Compound **3.146** (100 – 140 ppm)



^{13}C NMR, 176 MHz, Acetone- d_6 ,
Compound **3.146** (140 – 180 ppm)



COSY, 500 MHz, Acetone-*d*₆, Compound 3.204

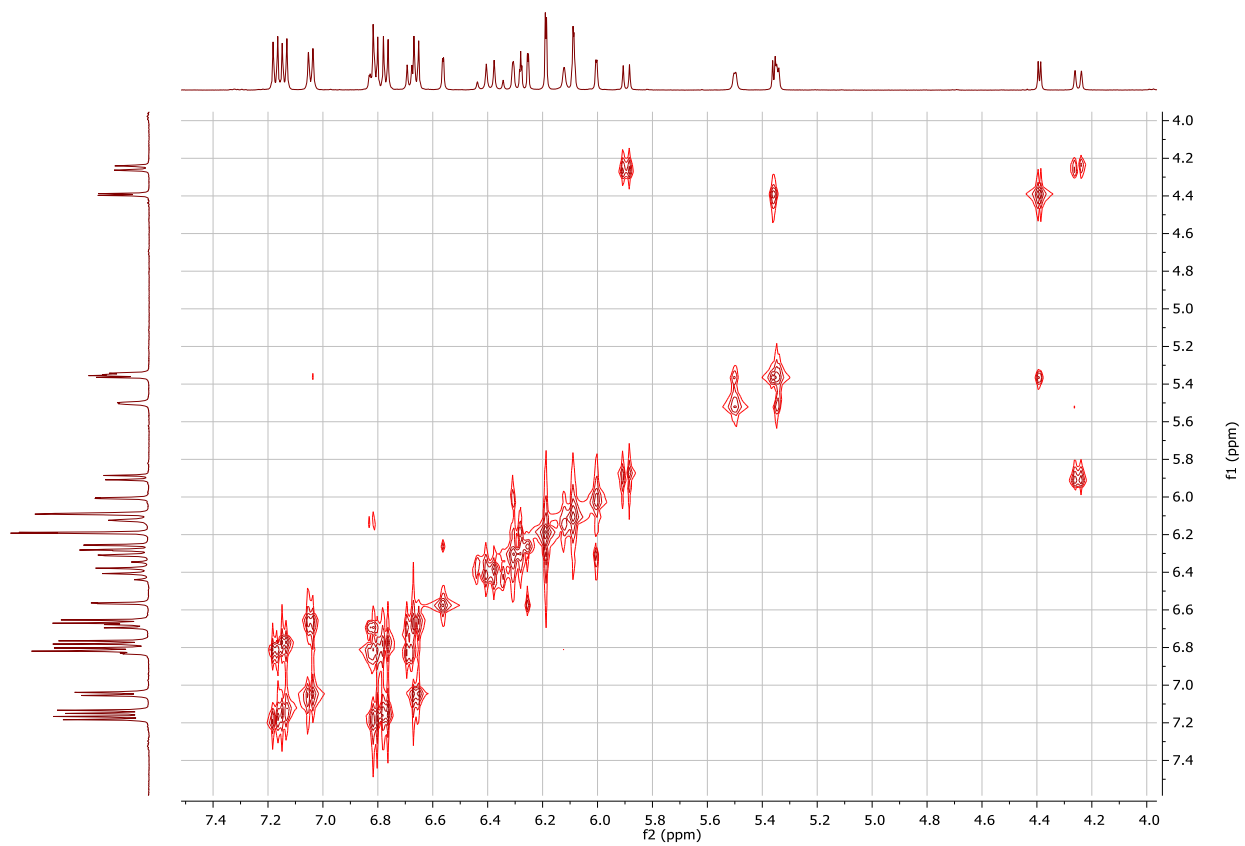


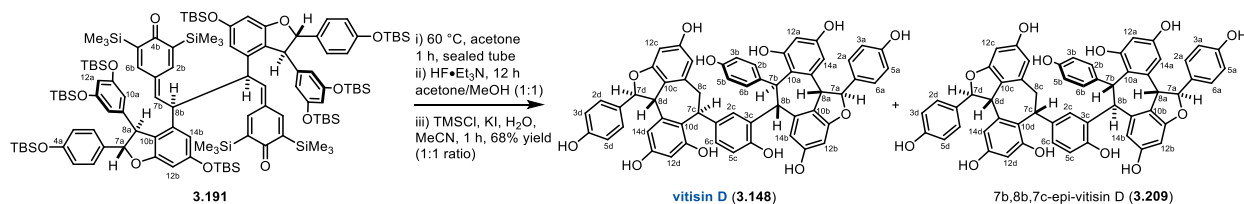
Table 3.9. Comparison of literature and observed ¹H NMR data for vitisin A (3.146).

Assignment	Literature ³⁰²	Observed
	500 MHz, Acetone- <i>d</i> ₆	700 MHz, Acetone- <i>d</i> ₆
2/6a	7.22 (d, <i>J</i> = 8.5 Hz)	7.20 (d, <i>J</i> = 8.6 Hz, 2H)
3/5a	6.86 (d, <i>J</i> = 8.5 Hz)	6.84 (d, <i>J</i> = 8.6 Hz, 2H)
7a	5.91 (d, <i>J</i> = 10.5 Hz)	5.89 (d, <i>J</i> = 11.5 Hz, 1H)
8a	4.26 (d, <i>J</i> = 10.5 Hz)	4.24 (d, <i>J</i> = 11.5 Hz, 1H)
12a	6.28 (d, <i>J</i> = 2.0 Hz)	6.28 (d, <i>J</i> = 2.3 Hz, 1H),
14a	6.55 (d, <i>J</i> = 2.0 Hz)	6.54 (d, <i>J</i> = 2.1 Hz, 1H)
2/6b	7.06 (d, <i>J</i> = 8.5 Hz)	7.04 (d, <i>J</i> = 8.1 Hz, 2H)
3/5b	6.68 (d, <i>J</i> = 8.5 Hz)	6.66 (d, <i>J</i> = 8.7 Hz, 2H)
7b	5.41 (d, <i>J</i> = 3.0 Hz)	5.38 (d, <i>J</i> = 3.9 Hz, 1H)
8b	5.50 (d, <i>J</i> = 3.0 Hz)	5.49 (d, <i>J</i> = 2.4 Hz, 1H)
12b	6.11 (d, <i>J</i> = 2.0 Hz)	6.08 (d, <i>J</i> = 2.1 Hz, 1H)
14b	6.08 (d, <i>J</i> = 2.0 Hz)	6.05 (d, <i>J</i> = 2.1 Hz, 1H)
2c	6.12 (d, <i>J</i> = 2.0 Hz)	6.09 (d, <i>J</i> = 2.0 Hz, 1H)
5c	6.71 (d, <i>J</i> = 8.5 Hz)	6.69 (d, <i>J</i> = 8.4 Hz, 1H)
6c	6.89 (dd, <i>J</i> = 8.5, 2.0 Hz)	6.87 (dd, <i>J</i> = 8.4, 2.2 Hz)
7c	6.41 (br s)	6.39 (br s, 2H)
8c	6.41 (br s)	6.39 (br s, 2H)
12c	6.06 (d, <i>J</i> = 2.0 Hz)	6.04 (d, <i>J</i> = 2.3 Hz, 1H)
14c	6.27 (d, <i>J</i> = 2.0 Hz)	6.25 (d, <i>J</i> = 2.1, 1H)
2/6d	7.17 (d, <i>J</i> = 8.5 Hz)	7.15 (d, <i>J</i> = 8.5 Hz, 2H)
3/5d	6.80 (d, <i>J</i> = 8.5 Hz)	6.77 (d, <i>J</i> = 8.6 Hz, 2H)
7d	5.38 (d, <i>J</i> = 5.0 Hz)	5.35 (d, <i>J</i> = 5.3 Hz, 1H)
8d	4.43 (d, <i>J</i> = 5.0 Hz)	4.41 (d, <i>J</i> = 5.3 Hz, 1H)
10/14d	6.19 (d, <i>J</i> = 2.0 Hz)	6.16 (d, <i>J</i> = 2.2 Hz, 2H)
12d	6.24 (t, <i>J</i> = 2.0 Hz)	6.21 (t, <i>J</i> = 2.2 Hz, 1H)

Note: The 7c/8c signals were anticipated to appear as an AB multiplet characteristic of a stilbene; instead, a broad singlet is observed, which presumably results from the doublets overlapping with each other such that the peripheral peak of each signal is indistinguishable from the baseline.

Table 3.10. Comparison of literature and observed ^{13}C NMR data for vitisin A (3.146).

Assignment	Literature ³⁰²	Observed
	125 MHz, Acetone- <i>d</i> ₆	176 MHz, Acetone- <i>d</i> ₆
1a	131.3	131.2
2/6a	128.3	128.1
3/5a	116.5	116.3
4a	158.5	158.3
7a	88.8	88.6
8a	57.4	57.2
9a	142.6	142.4
10a	120.6	120.5
11a	158.3	158.0
12a	96.9	96.7
13a	156.2	156.1
14a	104.9	104.7
1b	135.7	135.5
2/6b	129.2	129.0
3/5b	115.8	115.6
4b	155.5	155.2
7b	41.0	40.8
8b	41.6	41.4
9b	141.5	141.3
10b	120.5	120.1
11b	157.2	157.2
12b	96.4	96.2
13b	159.1	158.9
14b	110.4	110.2
1c	129.2	129.1
2c	132.7	132.6
3c	136.9	136.7
4c	160.0	159.9
5c	115.8	115.6
6c	124.1	123.8
7c	131.4	131.2
8c	123.0	122.9
9c	134.2	134.1
10c	119.4	119.1
11c	162.8	162.7
12c	101.3	101.0
13c	159.8	159.7
14c	105.3	105.2
1d	133.1	133.0
2/6d	130.4	130.2
3/5d	116.4	116.1
4d	158.8	158.6
7d	94.1	94.0
8d	49.8	49.7
9d	147.6	147.4
10/14d	107.2	107.0
11/13d	160.6	160.5
12d	102.5	102.2



Vitisin D (3.148) - (1S,7S,11bS)-7-(4-hydroxy-3-((4bS,5S,10S,11R)-1,3,8-trihydroxy-5,11-bis(4-hydroxyphenyl)-4b,5,10,11-tetrahydrobenzo[6,7]cyclohepta[1,2,3-cd]benzofuran-10-yl)phenyl)-1-(4-hydroxyphenyl)-1,6,7,11b-tetrahydrobenzo[6,7]cyclohepta[1,2,3-cd]benzofuran-4,8,10-triol

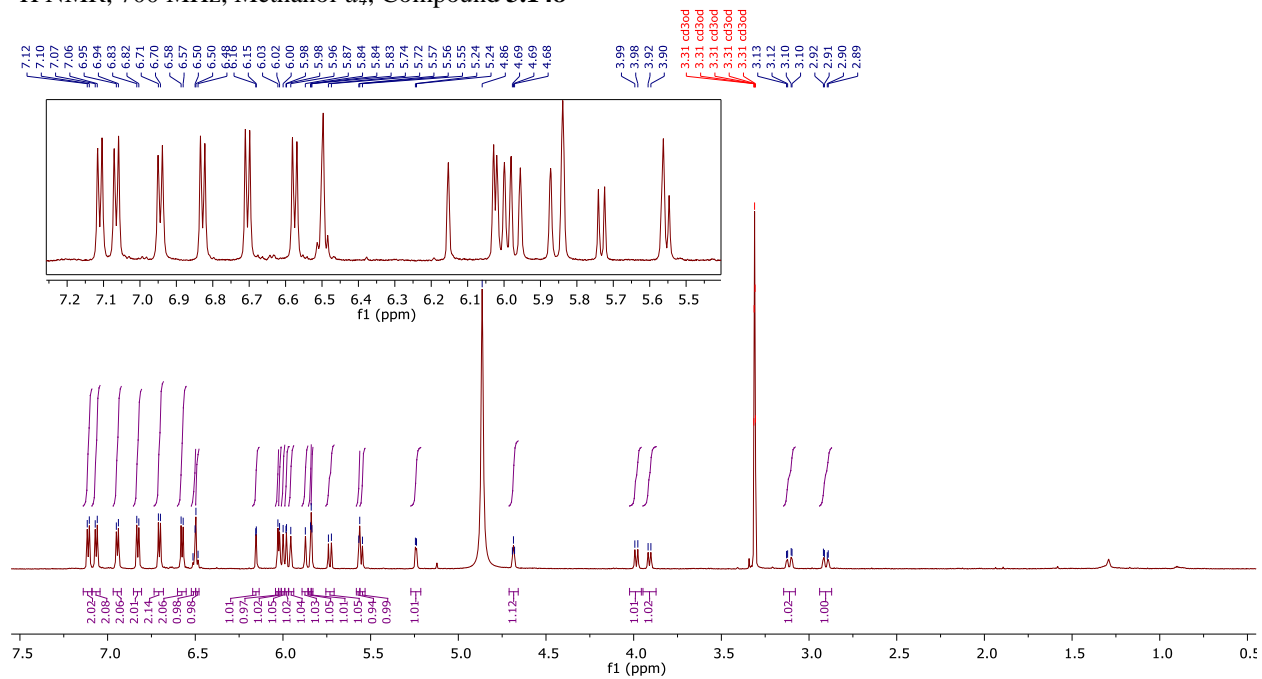
Quinone-methide dimer **3.191** (100 mg, 0.047 mmol) was added to a flame-dried reaction vial charged with a stir bar and dissolved in acetone (1.5 mL, HPLC grade). The reaction solution was sparged with a balloon of Ar for 5 minutes and then sealed under argon with parafilm. The reaction was heated to 60 °C for 1 hour, and upon cooling to ambient temperature, a solution of HF-triethylamine was added (0.48 mL, 2.94 mmol) followed by MeOH (1.5 mL, HPLC grade). The reaction was sealed under an argon atmosphere and allowed to stir at ambient temperature. After 16 hours, the stir bar was removed, and the reaction mixture was added to a separatory funnel containing sat. aq. sodium bicarbonate (~20 mL). The aqueous layer was extracted with portion of EtOAc (3 x 15 mL), and the combined organic layers were washed with brine, dried over MgSO₄, and concentrated under reduced pressure. The crude material was consistent with cleavage of the 8 TBS ethers, so it was directly carried forward for protodesilylation. The material was dissolved in MeCN (1.0 mL) in a reaction vial, and potassium iodide (25 mg, 0.15 mmol), TMSCl (19.4 μL, 0.15 mmol), and water (3 μL, 0.16 mmol) were added. The reaction was allowed to stir at room temperature for 1 hour, at which point it was quenched with triethylamine (0.5 mL) and directly concentrated on the rotovap. The crude residue was purified by flash column chromatography (8% to 40% in 5 step increments, 2 column volumes per step, Nonpolar solvent – CH₂Cl₂, Polar solvent – 3:1 Acetone/MeOH) to afford a mixture of vitisin D (**3.148**) and its diastereomer (**3.209**) in a ca. 1:1 ratio (28.8 mg, 68% combined yield). This mixture was further purified by prep-HPLC (10% to 65% MeCN/H₂O gradient over 1 hour) to afford pure samples of each compound. The ¹H and ¹³C NMR data for vitisin D (**7**) are consistent with literature reports.^{262,303}

Vitisin D (3.148):

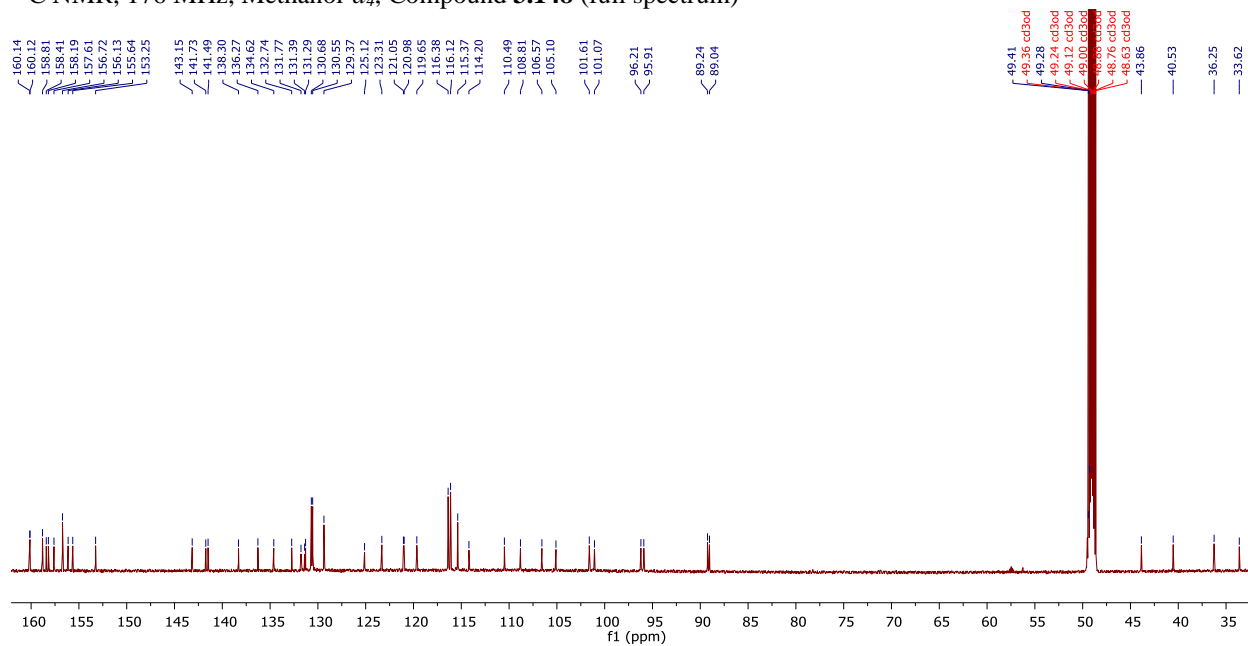
¹H NMR (700 MHz, Methanol-*d*₄) δ 7.11 (d, *J* = 8.2 Hz, 2H, C_{2/6a}-H), 7.06 (d, *J* = 8.2 Hz, 2H, C_{2/6d}-H), 6.94 (d, *J* = 8.2 Hz, 2H, C_{2/6b}-H), 6.83 (d, *J* = 8.1 Hz, 2H, C_{3/5d}-H), 6.70 (d, *J* = 8.2 Hz, 2H, C_{3/5a}-H), 6.57 (d, *J* = 8.3 Hz, 2H, C_{3/5b}-H), 6.51 (d, *J* = 8.4 Hz, 1H, C_{6c}-H), 6.49 (d, *J* = 8.5 Hz, 1H, C_{5c}-H), 6.15 (d, *J* = 2.2 Hz, 1H, C_{12d}-H), 6.03 (s, 1H, C_{14c}-H), 6.02 (s, 1H, C_{12c}-H), 6.00 (s, 1H, C_{12b}-H), 5.98 (d, *J* = 2.1 Hz, 1H, C_{14d}-H), 5.96 (s, 1H, C_{2c}-H), 5.87 (s, 1H, C_{14a}-H), 5.84 (d, *J* = 2.9 Hz, 1H, C_{12a}-H), 5.83 (s, 1H, C_{14b}-H), 5.73 (d, *J* = 11.9 Hz, 1H, C_{7a}-H), 5.56 (d, *J* = 4.2 Hz, 1H, C_{7b}-H), 5.55 (d, *J* = 11.1 Hz, 1H, C_{7d}-H), 5.24 (d, *J* = 4.3 Hz, 1H, C_{8b}-H), 4.68 (t, *J* = 4.0 Hz, 1H, C_{7c}-H), 3.98 (d, *J* = 11.9 Hz, 1H, C_{8a}-H), 3.91 (d, *J* = 11.2 Hz, 1H, C_{8d}-H), 3.11 (dd, *J* = 18.0, 3.8 Hz, 1H, C_{8c}-H), 2.90 (dd, *J* = 17.8, 3.7 Hz, 1H, C_{8c}-H).

¹³C NMR (176 MHz, Methanol-*d*₄) δ 160.14, 160.12, 158.8, 158.4, 158.2, 157.6, 156.7, 156.1, 155.6, 153.2, 143.2, 141.7, 141.5, 138.3, 136.3, 134.6, 132.7, 131.8, 131.4, 131.3, 130.7, 130.6, 129.4, 125.1, 123.3, 121.05, 120.98, 119.6, 116.4, 116.1, 115.4, 114.2, 110.5, 108.8, 106.6, 105.1, 101.6, 101.1, 96.2, 95.9, 89.2, 89.0, 49.4, 49.3, 43.9, 40.5, 36.2, 33.6.

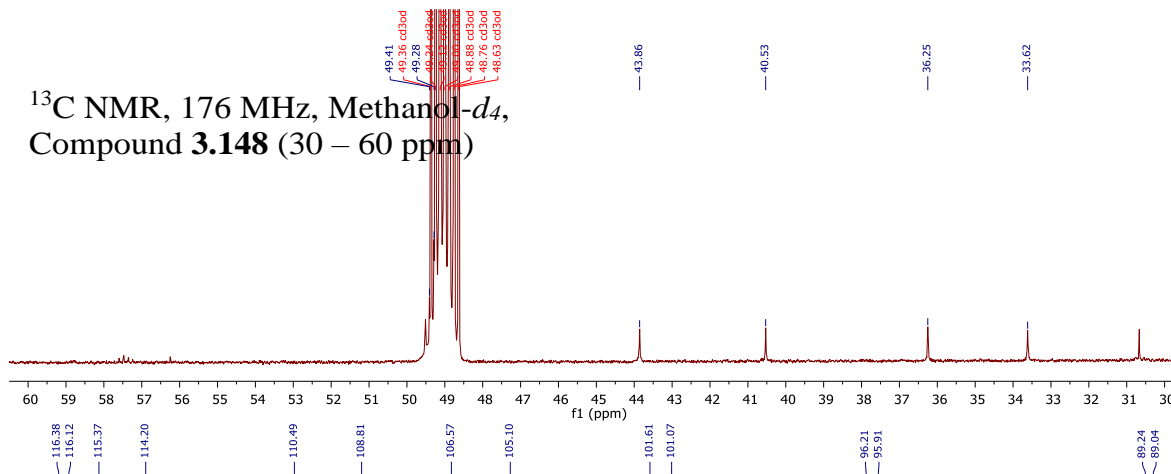
¹H NMR, 700 MHz, Methanol-*d*₄, Compound **3.148**



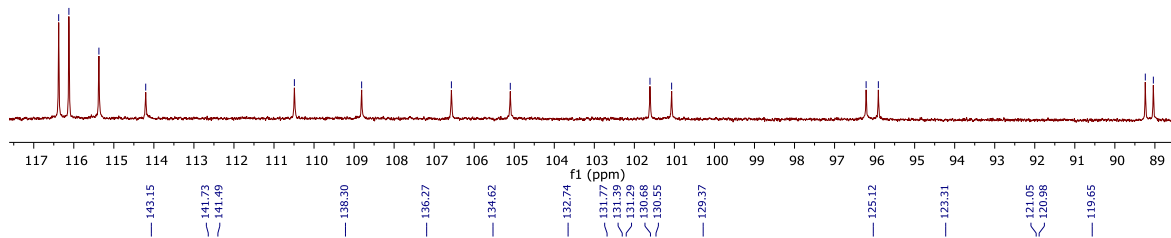
¹³C NMR, 176 MHz, Methanol-*d*₄, Compound **3.148** (full spectrum)



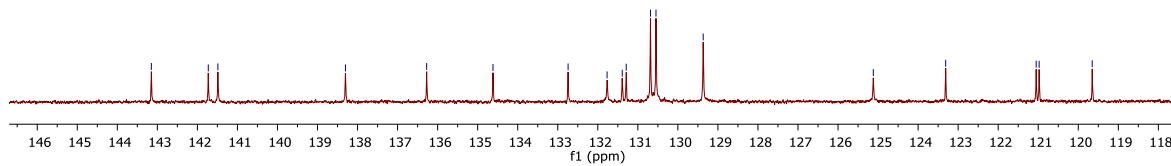
^{13}C NMR, 176 MHz, Methanol- d_4 ,
Compound **3.148** (30 – 60 ppm)



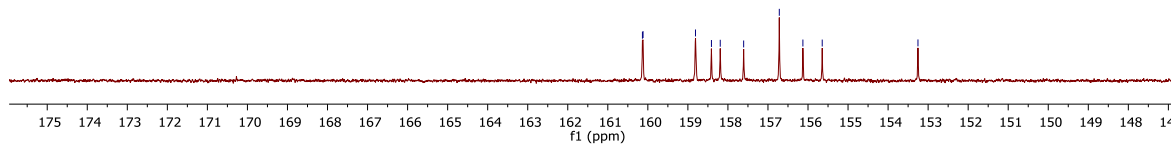
^{13}C NMR, 176 MHz, Methanol- d_4 ,
Compound **3.148** (90 – 118 ppm)



^{13}C NMR, 176 MHz, Methanol- d_4 ,
Compound **3.148** (118 – 146 ppm)



^{13}C NMR, 176 MHz, Methanol- d_4 ,
Compound **3.148** (147 – 175 ppm)



COSY, 700 MHz, Methanol-*d*₄, Compound 3.209

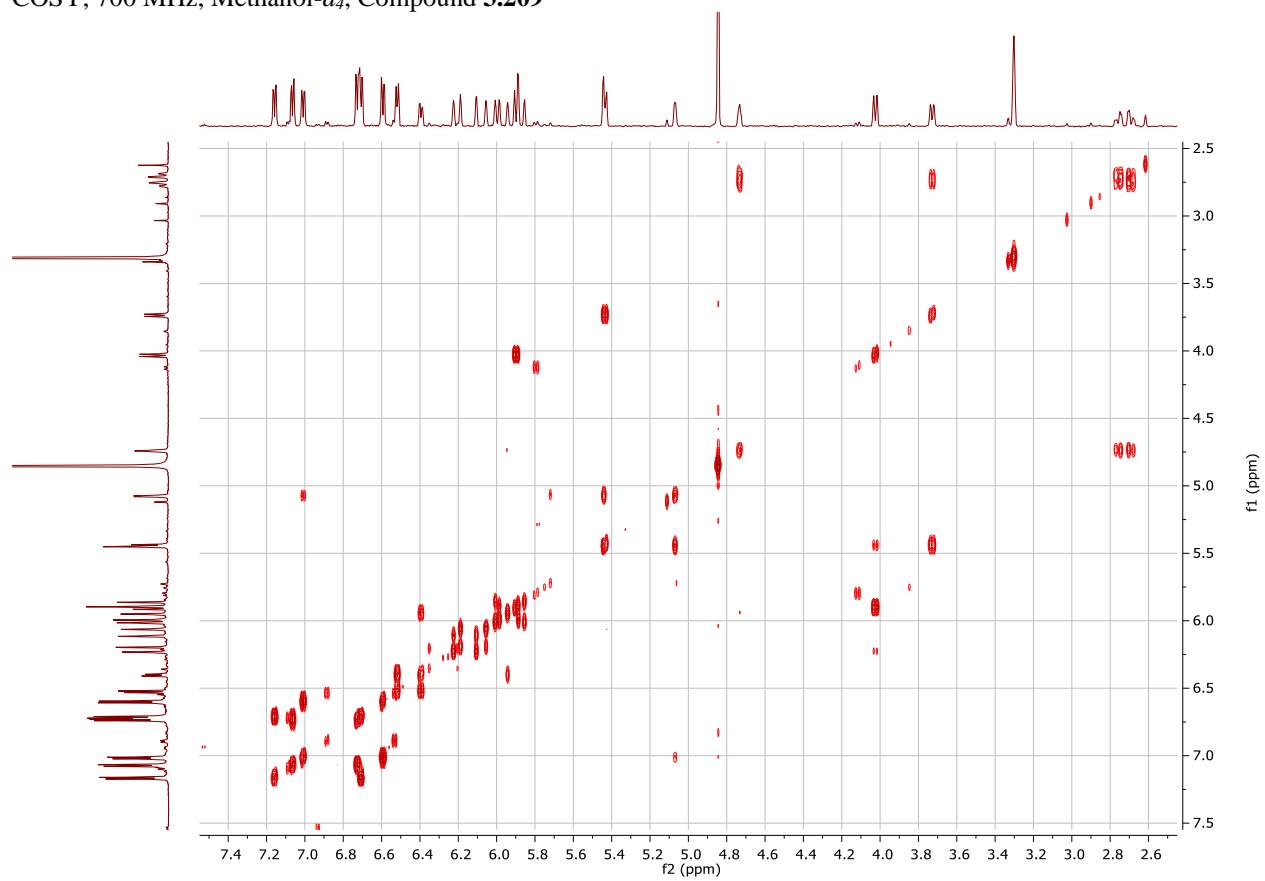


Table 3.11. Comparison of literature and observed ¹H NMR data for vitisin D (3.148).

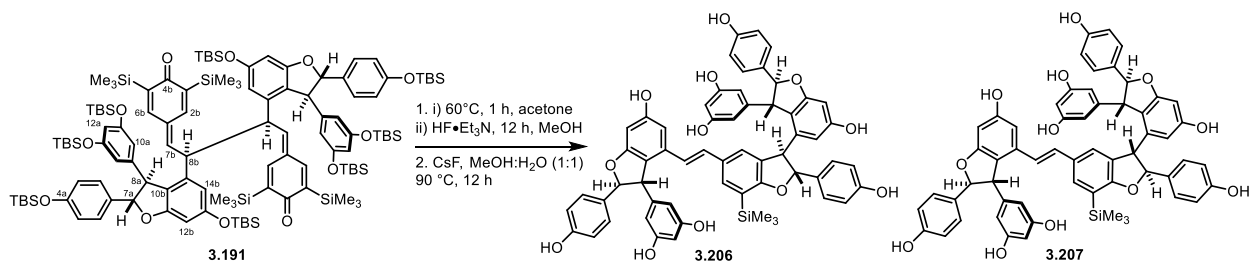
Assignment	Literature		Observed
	300 MHz, CDCl ₂ :CD ₃ OD (7:3) ³⁰³	600 MHz, CD ₃ OD ²⁶²	700 MHz, CD ₃ OD
8c	2.98 (1H br d, <i>J</i> = 16.8 Hz)	2.93 (br d, <i>J</i> = 16.6 Hz)	2.90 (dd, <i>J</i> = 17.8, 3.7 Hz, 1H)
8c	3.15 (1H, br d, <i>J</i> = 16.8 Hz)	3.14 (br d, <i>J</i> = 16.6 Hz)	3.11 (dd, <i>J</i> = 18.0, 3.8 Hz, 1H)
8d	3.90 (1H, d, <i>J</i> = 11.0 Hz)	3.39 (d, <i>J</i> = 11.1 Hz)*	3.91 (d, <i>J</i> = 11.2 Hz, 1H)
8a	4.05 (1H, d, <i>J</i> = 11.6 Hz)	4.01 (d, <i>J</i> = 11.9 Hz)	3.98 (d, <i>J</i> = 11.9 Hz, 1H)
7c	4.70 (1H, br t, <i>J</i> = 4.5 Hz)	4.66 (br t, <i>J</i> = 4.5 Hz)	4.68 (t, <i>J</i> = 4.0 Hz, 1H)
8b	5.26 (1H, d, <i>J</i> = 3.7 Hz)	5.27 (d, <i>J</i> = 3.7 Hz)	5.24 (d, <i>J</i> = 4.3 Hz, 1H)
7b	5.49 (1H, d, <i>J</i> = 3.7 Hz)	5.59 (d, <i>J</i> = 3.7 Hz)	5.56 (d, <i>J</i> = 4.2 Hz, 1H)
7d	5.63 (1H, d, <i>J</i> = 11.0 Hz)	5.58 (d, <i>J</i> = 11.0 Hz)	5.55 (d, <i>J</i> = 11.1 Hz, 1H)
7a	5.70 (1H, d, <i>J</i> = 11.6 Hz)	5.75 (d, <i>J</i> = 11.6 Hz)	5.73 (d, <i>J</i> = 11.9 Hz, 1H)
14b	5.79 (1H, br s)	5.77 (br s)	5.83 (s, 1H)
12a	5.82 (1H, br s)	5.86 (br s)	5.84 (d, <i>J</i> = 2.9 Hz, 1H)
14a	5.89 (1H, br s)	5.87 (br s)	5.87 (s, 1H)
2c	5.92 (1H, br s)	5.90 (br s)	5.96 (s, 1H)
14d	5.98 (1H, br s)	5.99 (br s)	5.98 (d, <i>J</i> = 2.1 Hz, 1H)
12b	6.02 (1H, br s)	6.02 (br s)	6.00 (s, 1H)
12c	6.07 (1H, br s)	6.06 (br s)	6.02 (s, 1H)
14c	6.07 (1H, br s)	6.06 (br s)	6.03 (s, 1H)
12d	6.15 (1H, br s)	6.19 (br s)	6.15 (d, <i>J</i> = 2.2 Hz, 1H)
5c	6.52 (1H, d, <i>J</i> = 7.4 Hz)	6.52 (d, <i>J</i> = 7.4 Hz)	6.49 (d, <i>J</i> = 8.5 Hz, 1H)
6c	6.57 (1H, br d, <i>J</i> = 7.4 Hz)	6.53 (br d, <i>J</i> = 7.4 Hz)	6.51 (d, <i>J</i> = 8.4 Hz, 1H)
3/5b	6.60 (2H, d, <i>J</i> = 8.4 Hz)	6.62 (d, <i>J</i> = 8.4 Hz)	6.57 (d, <i>J</i> = 8.3 Hz, 2H)
3/5a	6.73 (2H, d, <i>J</i> = 8.4 Hz)	6.74 (d, <i>J</i> = 8.4 Hz)	6.70 (d, <i>J</i> = 8.2 Hz, 2H)
3/5d	6.85 (2H, d, <i>J</i> = 8.4 Hz)	6.86 (d, <i>J</i> = 8.4 Hz)	6.83 (d, <i>J</i> = 8.1 Hz, 2H)
2/6b	6.98 (2H, d, <i>J</i> = 8.4 Hz)	6.97 (d, <i>J</i> = 8.4 Hz)	6.94 (d, <i>J</i> = 8.2 Hz, 2H)
2/6d	7.09 (2H, d, <i>J</i> = 8.4 Hz)	7.09 (d, <i>J</i> = 8.4 Hz)	7.06 (d, <i>J</i> = 8.2 Hz, 2H)
2/6a	7.15 (2H, d, <i>J</i> = 8.4 Hz)	7.14 (d, <i>J</i> = 8.4 Hz)	7.11 (d, <i>J</i> = 8.2 Hz, 2H)

*We believe that this signal was incorrectly tabulated in ref. 9 and should instead be 3.93 ppm.

Table 3.12. Comparison of literature and observed ¹³C NMR data for vitisin D (3.148).

Assignment	Literature			Observed
	75 MHz, CD ₃ OD ³⁰³	Recalibrated Shift*	150 MHz, CD ₃ OD ²⁶²	176 MHz, CD ₃ OD
8c	32.1	33.5	33.5	33.6
7c	34.8	36.2	36.2	36.2
7b	39.0	40.4	40.5	40.5
8b	42.2	43.6	43.8	43.9
8d	47.2	48.6	48.6	49.3
8a	47.6	49	48.7	49.4
7d	87.6	89	89.0	89.0
7a	87.8	89.2	89.2	89.2
12c	94.4	95.8	95.9	95.9
12b	94.8	96.2	96.2	96.2
12d	99.6	101	101.1	101.1
12a	100.2	101.6	101.6	101.6
14d	103.6	105	105.1	105.1
14a	105.1	106.5	106.5	106.6
14c	107.4	108.8	108.8	108.8
14b	109.1	110.5	110.5	110.5
5c	112.8	114.2	114.2	114.2
3/5b	114.0	115.4	115.3	115.4
3/5a	114.7	116.1	116.1	116.1
3/5d	115.0	116.4	116.3	116.4
10c	118.2	119.6	119.6	119.6
10a	119.5	120.9	120.96	120.98
10b	119.6	121	121.00	121.05
10d	121.9	123.3	123.3	123.3
6c	123.7	125.1	125.1	125.1
2/6b	128.0	129.4	129.3	129.4
2/6a	129.2	130.6	130.5	130.6
2/6d	129.3	130.7	130.6	130.7
2c	129.9	131.3	131.3	131.3
1d	130.0	131.4	131.4	131.4
1a	130.3	131.7	131.7	131.8
3c	131.3	132.7	132.7	132.7
1c	133.2	134.6	134.6	134.6
1b	134.9	136.3	136.2	136.3
9c	136.9	138.3	138.3	138.3
9b	140.1	141.5	141.4	141.5
9a	140.3	141.7	141.7	141.7
9d	141.8	143.2	143.1	143.2
4c	151.9	153.3	153.2	153.2
4b	154.2	155.6	155.6	155.6
13a	154.7	156.1	156.1	156.1
13d	155.3	156.7	156.6	156.7
11b	155.4	156.8	156.7	156.7
11a	156.2	157.6	157.6	157.6
11c	156.7	158.1	158.1	158.2
4a	157.0	158.4	158.3	158.4
4d	157.3	158.7	158.6	158.8
11d	157.4	158.8	158.7	158.8
13b	158.8	160.2	160.1	160.12
13c	158.8	160.2	160.1	160.14

*We noticed that the ¹³C NMR data from ref. 8 was consistently ~1.4 ppm lower than observed, perhaps due to incorrect referencing of the solvent signal. After recalibrating the data from ref. 8 by adding 1.4 ppm to each signal, it is consistent with the observed data as well as ref. 9.



3.206 - 5-((2*S*,3*S*)-4-((*E*)-2-((2*R*,2'*S*,3*R*,3'*S*)-3'-(3,5-dihydroxyphenyl)-6'-hydroxy-2,2'-bis(4-hydroxyphenyl)-7-(trimethylsilyl)-2,2',3,3'-tetrahydro-[3,4'-bibenzofuran]-5-yl)vinyl)-6-hydroxy-2-(4-hydroxyphenyl)-2,3-dihydrobenzofuran-3-yl)benzene-1,3-diol

Quinone-methide dimer **3.191** (200 mg, 0.095 mmol) was added to a flame-dried reaction vial charged with a stir bar and dissolved in acetone (3.0 mL, HPLC grade). The reaction solution was sparged with a balloon of Ar for 5 minutes and then sealed under argon with parafilm. The reaction was heated to 60 °C for 1 hour, and upon cooling to ambient temperature, a solution of HF-triethylamine was added (0.93 mL, 5.68 mmol) followed by MeOH (3.0 mL, HPLC grade). The reaction was sealed under an argon atmosphere and allowed to stir at ambient temperature. After 16 hours, the stir bar was removed, and the reaction mixture was added to a separatory funnel containing sat. aq. sodium bicarbonate (~50 mL). The aqueous layer was extracted with portion of EtOAc (3 x 25 mL), and the combined organic layers were washed with brine, dried over MgSO₄, and concentrated under reduced pressure. The crude material was dissolved in MeOH/H₂O (1:1, 3.0 mL), and to the reaction mixture was added CsF (143 mg, 0.944 mmol). The reaction was sealed under nitrogen and heated at 90 °C for 12 hours. Upon cooling to room temperature, the reaction mixture was added to separatory funnel containing saturated aqueous NH₄Cl, and the aqueous layer was extracted with portions of EtOAc (3 x 25 mL). The combined organic layers were washed with brine, dried over MgSO₄, and concentrated under reduced pressure. The crude material was purified by flash column chromatography (8% to 40% in 5 step increments, 2 column volumes per step, Nonpolar solvent – CH₂Cl₂, Polar solvent – 3:1 Acetone/MeOH) to afford the **3.206/3.207** mixture (67.5 mg, 73% yield).

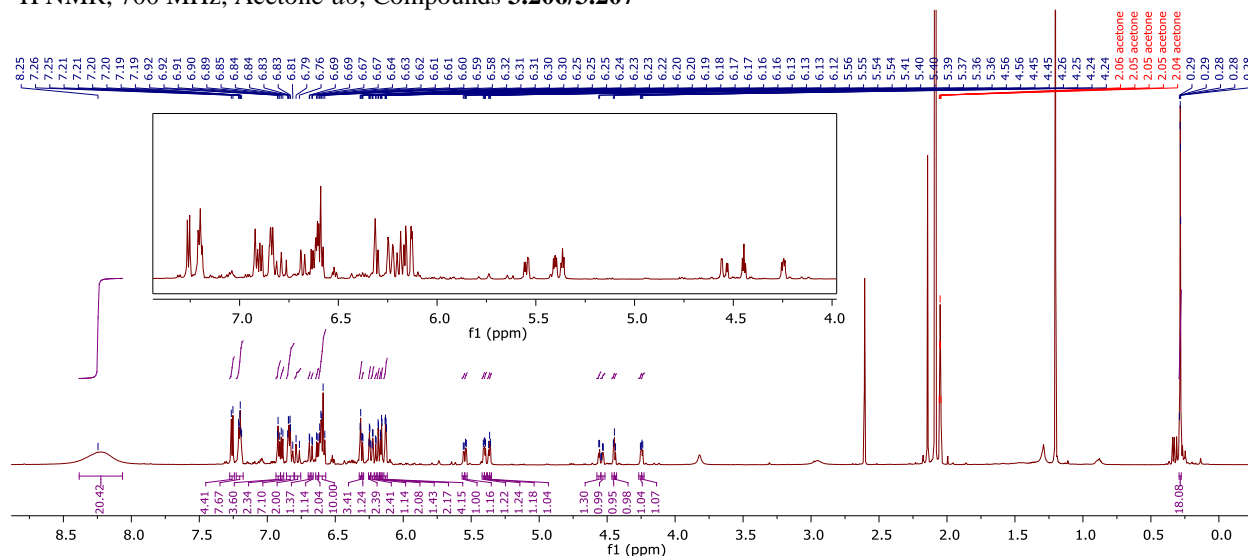
¹H NMR (700 MHz, Acetone-*d*₆) δ 8.25 (s, 20H), 7.26 (d, *J* = 8.3 Hz, 4H), 7.20 (td, *J* = 6.7, 3.1 Hz, 8H), 6.94 – 6.90 (m, 4H), 6.89 (d, *J* = 8.4 Hz, 2H), 6.86 – 6.80 (m, 7H), 6.78 (d, *J* = 17.4 Hz, 2H), 6.69 (d, *J* = 2.0 Hz, 1H), 6.67 (d, *J* = 2.0 Hz, 1H), 6.63 (d, *J* = 6.4 Hz, 2H), 6.62 – 6.57 (m, 10H), 6.31 (d, *J* = 2.7 Hz, 3H), 6.30 (d, *J* = 2.0 Hz, 1H), 6.25 (q, *J* = 2.3 Hz, 2H), 6.24 – 6.21 (m, 2H), 6.20 (d, *J* = 2.1 Hz, 1H), 6.18 (d, *J* = 2.2 Hz, 2H), 6.17 (d, *J* = 2.1 Hz, 1H), 6.16 (d, *J* = 2.2 Hz, 2H), 6.13 (dd, *J* = 5.0, 2.2 Hz, 4H), 5.55 (d, *J* = 4.7 Hz, 1H), 5.54 (d, *J* = 4.2 Hz, 1H), 5.41 (d, *J* = 4.4 Hz, 1H), 5.40 (d, *J* = 4.2 Hz, 1H), 5.37 (d, *J* = 4.8 Hz, 1H), 5.36 (s, 1H), 4.56 (d, *J* = 4.4 Hz, 1H), 4.53 (d, *J* = 4.4 Hz, 1H), 4.45 (s, 1H), 4.44 (d, *J* = 5.6 Hz, 1H), 4.25 (d, *J* = 4.6 Hz, 1H), 4.24 (d, *J* = 4.2 Hz, 1H), 0.29 – 0.28 (m, 18H).

¹³C NMR (176 MHz, Acetone-*d*₆) δ 164.92, 164.86, 162.71, 162.69, 162.47, 162.45, 160.3, 160.2, 159.9, 159.8, 159.5, 158.3, 158.1, 158.0, 157.7, 147.63, 147.55, 147.4, 147.3, 142.8, 142.6, 136.63, 136.59, 134.4, 134.3, 133.89, 133.87, 133.1, 132.9, 132.3, 131.7, 131.31, 131.29, 131.2, 131.1, 130.8, 130.7, 130.2, 129.2, 128.9, 128.2, 128.1, 128.01, 127.95, 127.3, 127.2, 126.9, 126.4, 123.7, 123.6, 120.9, 120.8, 119.71, 119.68, 119.65, 119.64, 116.43, 116.41, 116.2, 115.9, 107.0, 104.7, 104.6, 102.5, 102.3, 96.8, 96.6, 94.2, 94.1, 90.84, 90.76, 57.3, 57.2, 56.9, 56.7, 52.5, 52.3, -0.82, -0.84.

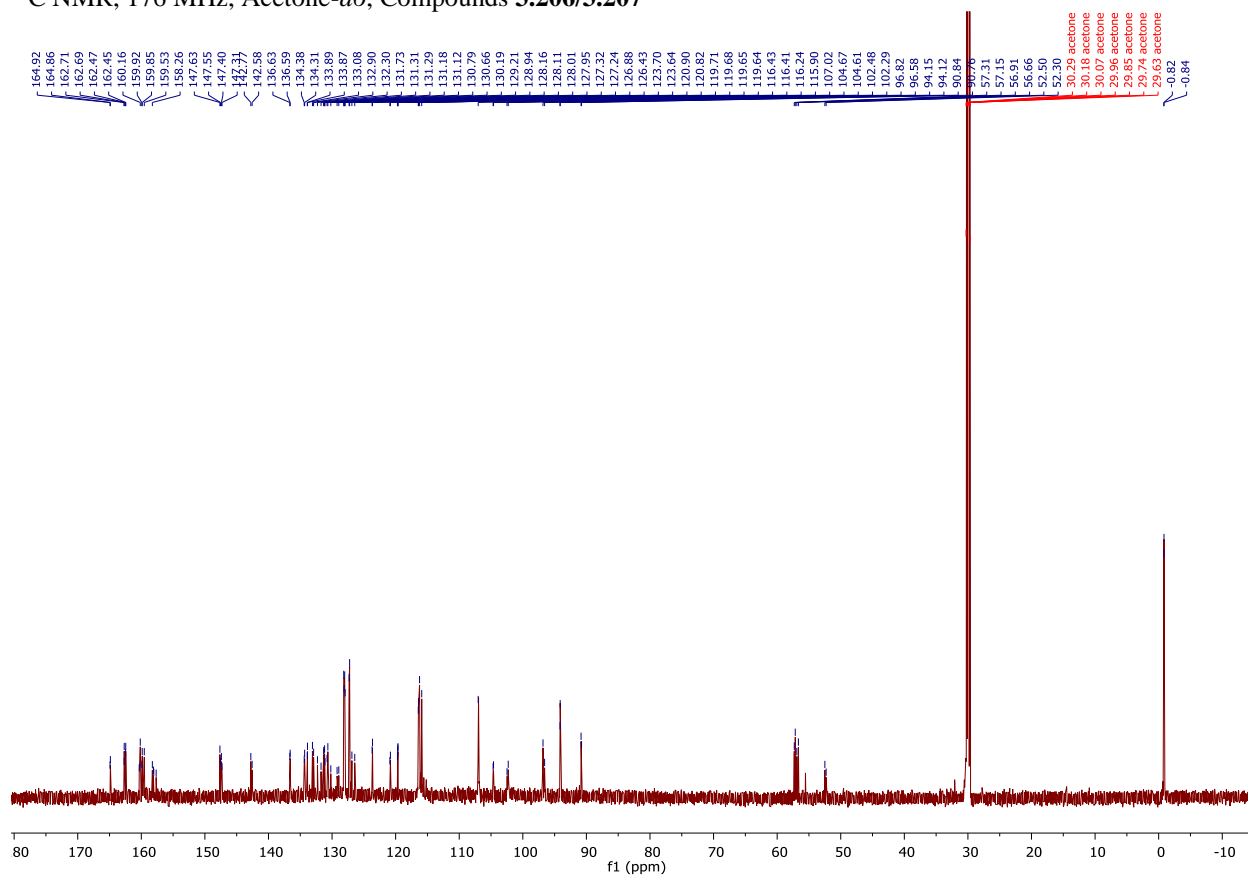
IR (Neat): 3439 (br), 2923, 1617, 1586, 1525, 1444, 1328, 1269, 1158, 1135, 1015 cm⁻¹.

HRMS (ESI) *m/z* calculated for C₅₉H₅₁O₁₂Si⁺ ([M+H]⁺) 979.3144, found 979.3130.

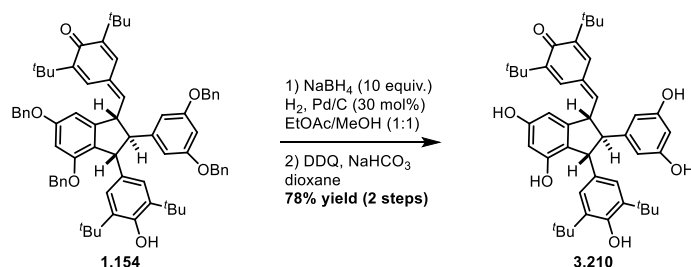
¹H NMR, 700 MHz, Acetone-*d*₆, Compounds **3.206/3.207**



¹³C NMR, 176 MHz, Acetone-*d*₆, Compounds **3.206/3.207**



Preliminary results toward the synthesis of resveratrol trimers:

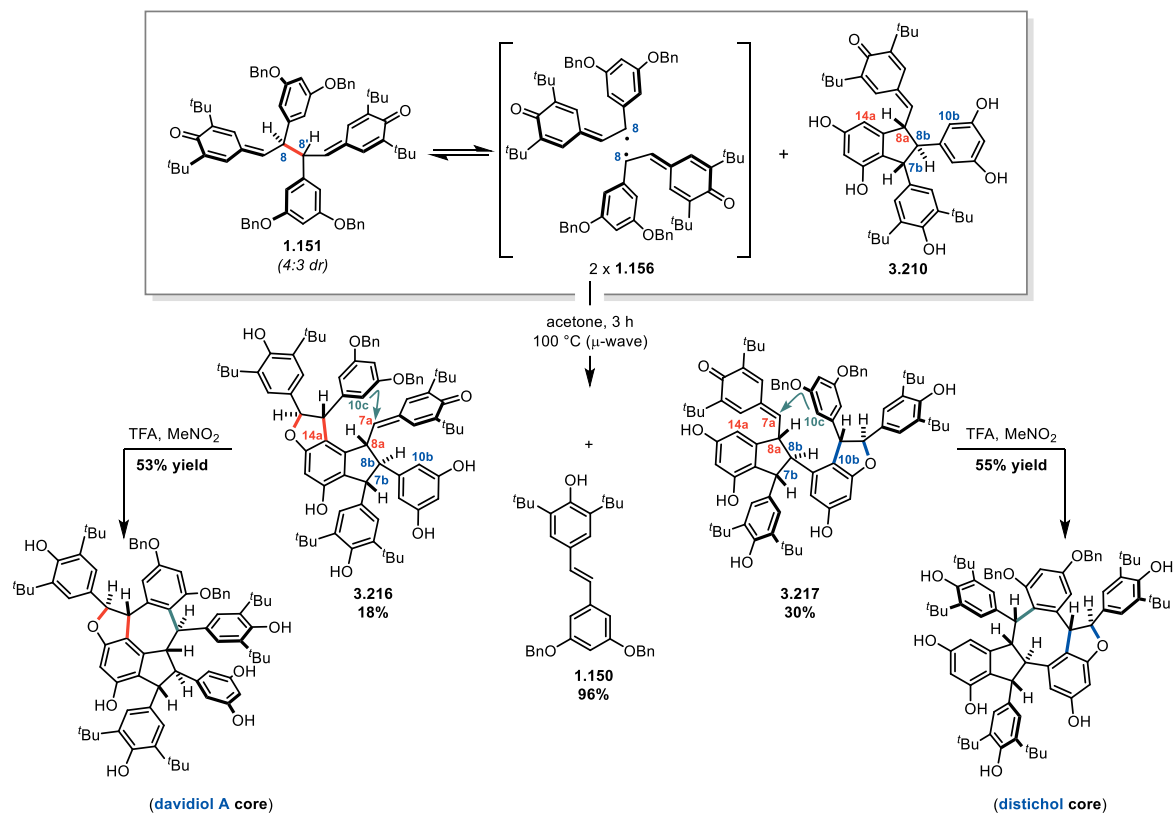


3.210 - 2,6-di-tert-butyl-4-(((1R,2R,3R)-3-(3,5-di-tert-butyl-4-hydroxyphenyl)-2-(3,5-dihydroxyphenyl)-4,6-dihydroxy-2,3-dihydro-1H-inden-1-yl)methylene)cyclohexa-2,5-dien-1-one

The conversion of **1.151** to **1.154** was conducted following the literature report.⁴⁸ Compound **1.154** (2.45 g, 2.36 mmol) and Pd/C (30 wt. %, 251 mg, 0.30 equiv) was subsequently dissolved in EtOAc (41 mL) and methanol (41 mL) under a stream of nitrogen. Sodium borohydride (892 mg, 10 equiv) was added in a single portion, and the reaction mixture was sparged with hydrogen for 30 min. The reaction was stirred under a hydrogen atmosphere overnight (~16 h). Upon completion, the reaction was diluted with EtOAc and filtered over Celite to remove the palladium, eluting with MeOH. The filtrate was washed with water to quench/remove any remaining NaBH₄, then washed with brine, dried over Na₂SO₄, and concentrated to afford the debenzylated/reduced dimer product (1.6 g, 98% yield). The subsequent intermediate compound was carried forward in 400 mg batches. A 0.25 M solution of DDQ (140 mg, 0.617 mmol, 1.05 equiv) was prepared in dioxane (2.5 mL) in a flame-dried heart-shaped flask. The dimer intermediate (400 mg, 0.587 mmol) was added to a flame-dried flask with NaHCO₃ (493 mg, 10 equiv). The mixture was dissolved/suspended in dioxane (60.0 mL, 0.01 M) and stirred at rt under N₂. To the stirring mixture was added DDQ solution dropwise via cannula. Reaction turned initially yellow-green and then to a bright orange-red. As the DDQ is consumed, the hydroquinone precipitates from the solution, which is an indicator of the reaction working. After ~1 h, TLC indicated consumption of starting material, so the reaction was quenched by the addition of Na₂S₂O₃ and stirred for 3-5 minutes. At this point, the mixture was diluted with EtOAc and transferred to a separatory funnel containing sat. aq. Na₂CO₃. The phases were separated, and the organic layer was washed once more with Na₂CO₃, then brine, then dried over Na₂SO₄ and concentrated *in vacuo*. The crude material was purified by flash chromatography, 0-15% Acetone/DCM gradient to afford **3.210** (311 mg, 78% yield). The ¹H NMR and ¹³C data was consistent with the literature report for this compound.⁹²

¹H NMR (500 MHz, Acetone-*d*₆) δ 8.12 (br s, 3H), 7.28 (d, *J* = 2.2 Hz, 1H), 7.20 (br s, 1H), 7.03 (d, *J* = 2.2 Hz, 1H), 6.89 (s, 2H), 6.53 (d, *J* = 9.5 Hz, 1H), 6.33 (d, *J* = 2.0 Hz, 1H), 6.24 (d, *J* = 2.0 Hz, 1H), 6.23 (d, *J* = 2.0 Hz, 1H), 6.17 (d, *J* = 2.0 Hz, 1H), 5.83 (s, 1H), 4.63 (t, *J* = 9.5 Hz, 1H), 4.42 (d, *J* = 8.2 Hz, 1H), 3.02 (dd [apparent triplet], *J* = 8.2 Hz, 1H), 1.34 (s, 18 H), 1.26 (s, 9H), 1.22 (s, 9H)

¹³C NMR (125 MHz, Acetone-*d*₆) δ 187.1, 159.7, 159.5, 155.6, 153.3, 150.3, 148.9, 148.1, 147.2, 145.5, 137.8, 135.9, 134.7, 133.3, 128.2, 124.9, 121.4, 107.5, 104.1, 103.2, 102.0, 66.4, 57.4, 52.9, 35.9, 35.5, 35.2, 30.8, 29.9, 29.8



davidiol A core - (3R,4aS,5R,9bR,10R)-3,5,10-tris(3,5-di-tert-butyl-4-hydroxyphenyl)-4-(3,5-dihydroxyphenyl)-3,4,4a,5,9b,10-hexahydrobenzo[5,6]azuleno[7,8,1-cde]benzofuran-2,6,8-triol
distichol core - (2S,2aS,7aS,12R,12aR)-2,7,12-tris(3,5-di-tert-butyl-4-hydroxyphenyl)-2,2a,7,7a,12,12a-hexahydrobenzo[7,8]indeno[2',1':4,5]cycloocta[1,2,3-cd]benzofuran-4,6,9,11,14-pentaol

A 20 mL microwave vial was charged with **1.151** (100 mg, 0.0962 mmol, 1 equiv) and **3.210** (131 mg, 0.192 mmol, 2 equiv) and the solids were dissolved/suspended in acetone (10 mL, reagent grade purity). The vial was capped, and the reaction was conducted in the Biotage microwave reactor for 3 h at 100 °C. Upon completion of microwave irradiation, the reaction was transferred to a round bottom flask and concentrated on the rotovap. The crude residue was dissolved in minimal CH₂Cl₂ to be wet-loaded onto a flash column for purification at the following gradient – 0.2, 0.4, 0.6, 1.2, 2, 3, 5, 10% Acetone/CH₂Cl₂, 2 column volumes (1 column volume = 200 mL) of each step. The fractions containing trimeric material were further purified by preparative TLC (3% Acetone/CH₂Cl₂) to afford **3.216** (15.9 mg, 18% yield brsm) and **3.217** (26 mg, 30% yield brsm). In addition, unreacted **3.210** (72.6 mg) and a 2:1 mixture of **1.150/1.151** (71.4 mg) was recovered. Each trimeric adduct was cyclized by stirring in a 1 mL solution of TFA:MeNO₂ (1 μL/mL) for 2 h. The cyclization reaction was quenched via the addition of triethylamine, diluted with EtOAc, and added to a sep. funnel. The organic layer was washed with aq. saturated sodium bicarbonate followed by brine, then dried over sodium sulfate and concentrated. The product was purified by prep. TLC in 2.5% acetone/CH₂Cl₂. The two remaining benzyl ethers are readily cleaved via standard hydrogenolysis; however, characterization of each core was conducted prior to debenzoylation.

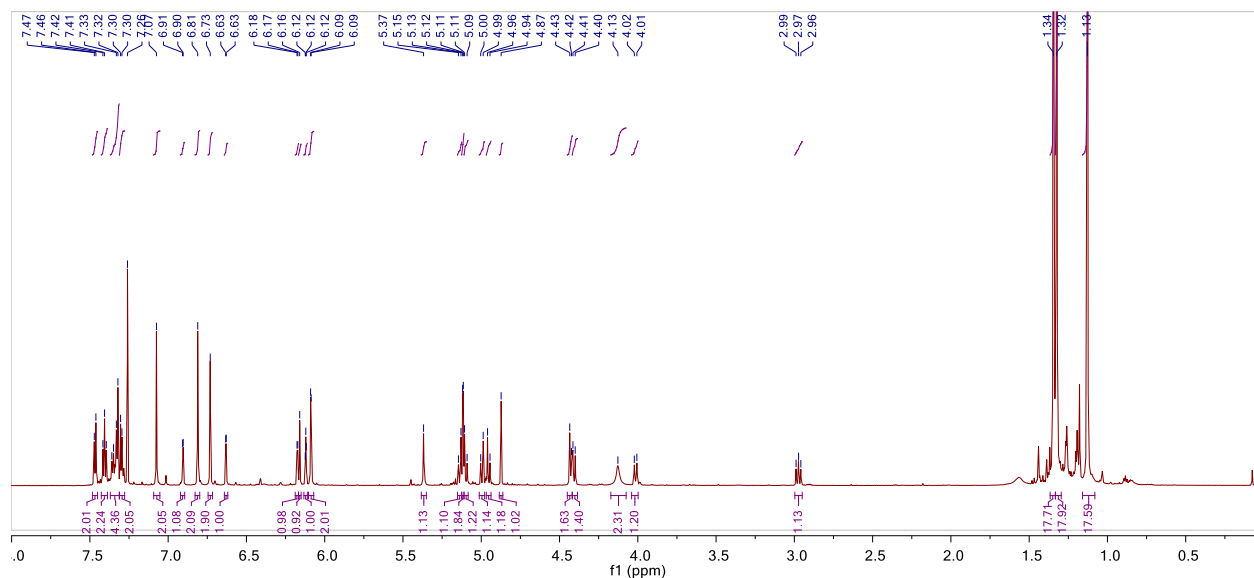
davidiol A core:

¹H NMR (700 MHz, Chloroform-*d*) δ 7.47 (d, *J* = 7.2 Hz, 2H), 7.41 (t, *J* = 7.6 Hz, 2H), 7.37 – 7.31 (m, 4H), 7.30 (d, *J* = 6.1 Hz, 2H), 7.07 (s, 2H), 6.91 (d, *J* = 2.4 Hz, 1H), 6.81 (s, 2H), 6.73 (s, 2H), 6.63 (d, *J* = 2.3 Hz, 1H), 6.17 (d, *J* = 3.7 Hz, 1H), 6.16 (s, 1H), 6.12 (t, *J* = 2.2 Hz, 1H), 6.09 (d, *J* = 2.2 Hz, 2H), 5.37 (s, 1H), 5.14 (d, *J* = 11.3 Hz, 1H), 5.12 (d, *J* = 3.1 Hz, 2H), 5.10 (d, *J* = 11.4 Hz, 1H), 5.00 (d, *J* = 11.1 Hz, 1H), 4.95 (d, *J* = 11.1 Hz, 1H), 4.87 (s, 1H), 4.43 (d, *J* = 7.8 Hz, 2H), 4.41 (d, *J* = 10.1 Hz, 1H), 4.13 (s, 2H), 4.01 (d, *J* = 11.3 Hz, 1H), 3.00 – 2.95 (m, 1H), 1.34 (s, 18H), 1.32 (s, 18H), 1.13 (s, 18H).

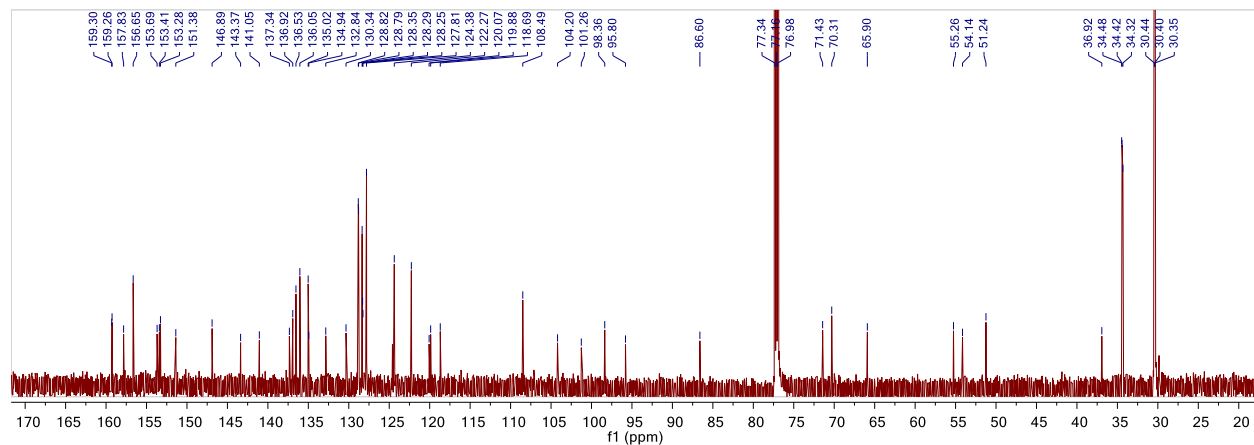
^{13}C NMR (176 MHz, Chloroform-*d*) δ 159.30, 159.26, 157.83, 156.65, 153.69, 153.41, 153.28, 151.38, 146.89, 143.37, 141.05, 137.34, 136.92, 136.53, 136.05, 135.02, 134.94, 132.84, 130.34, 128.82, 128.79, 128.35, 128.29, 128.25, 127.81, 124.38, 122.27, 120.07, 119.88, 118.69, 108.49, 104.20, 101.26, 98.36, 95.80, 86.60, 71.43, 70.31, 65.90, 55.26, 54.14, 51.24, 36.92, 34.48, 34.42, 34.32, 30.44, 30.40, 30.35.

daidiol A core:

^1H NMR (700 MHz, Chloroform-*d*)

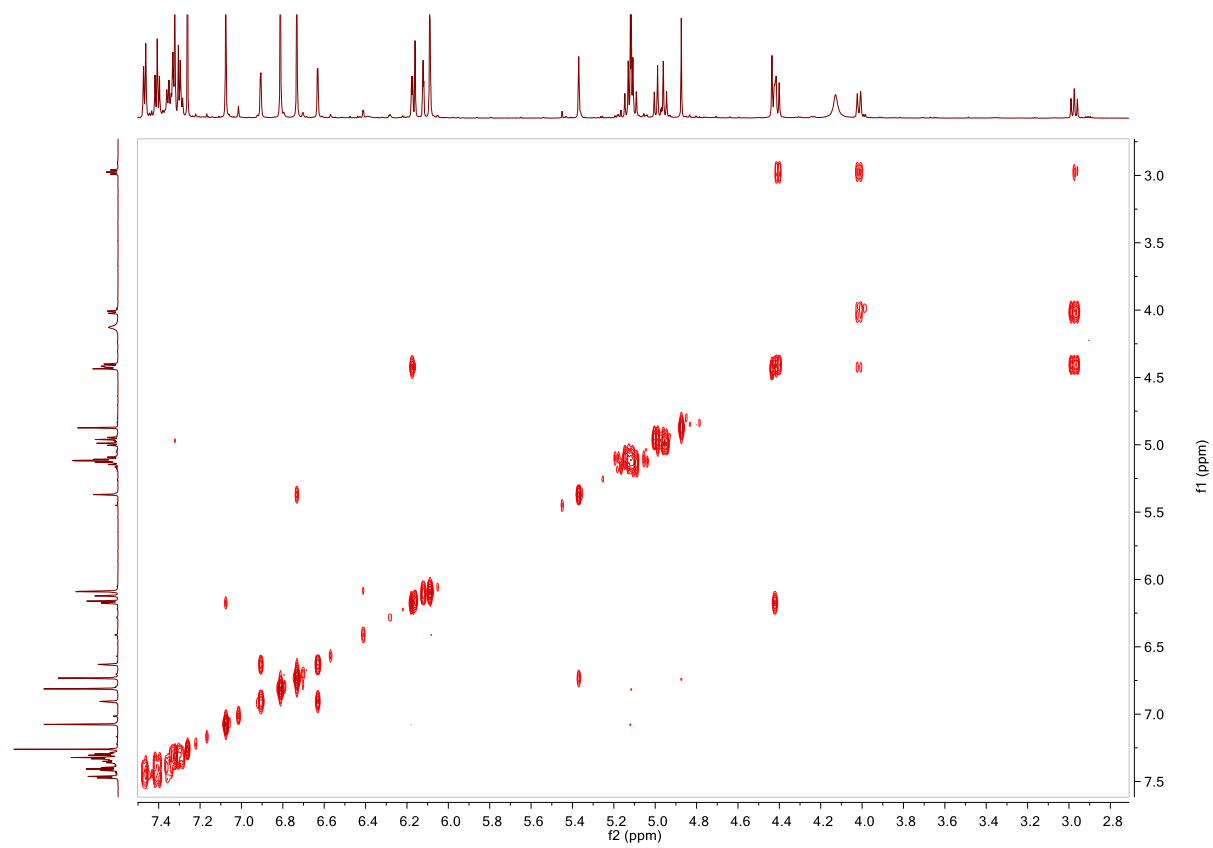


^{13}C NMR (176 MHz, Chloroform-*d*)



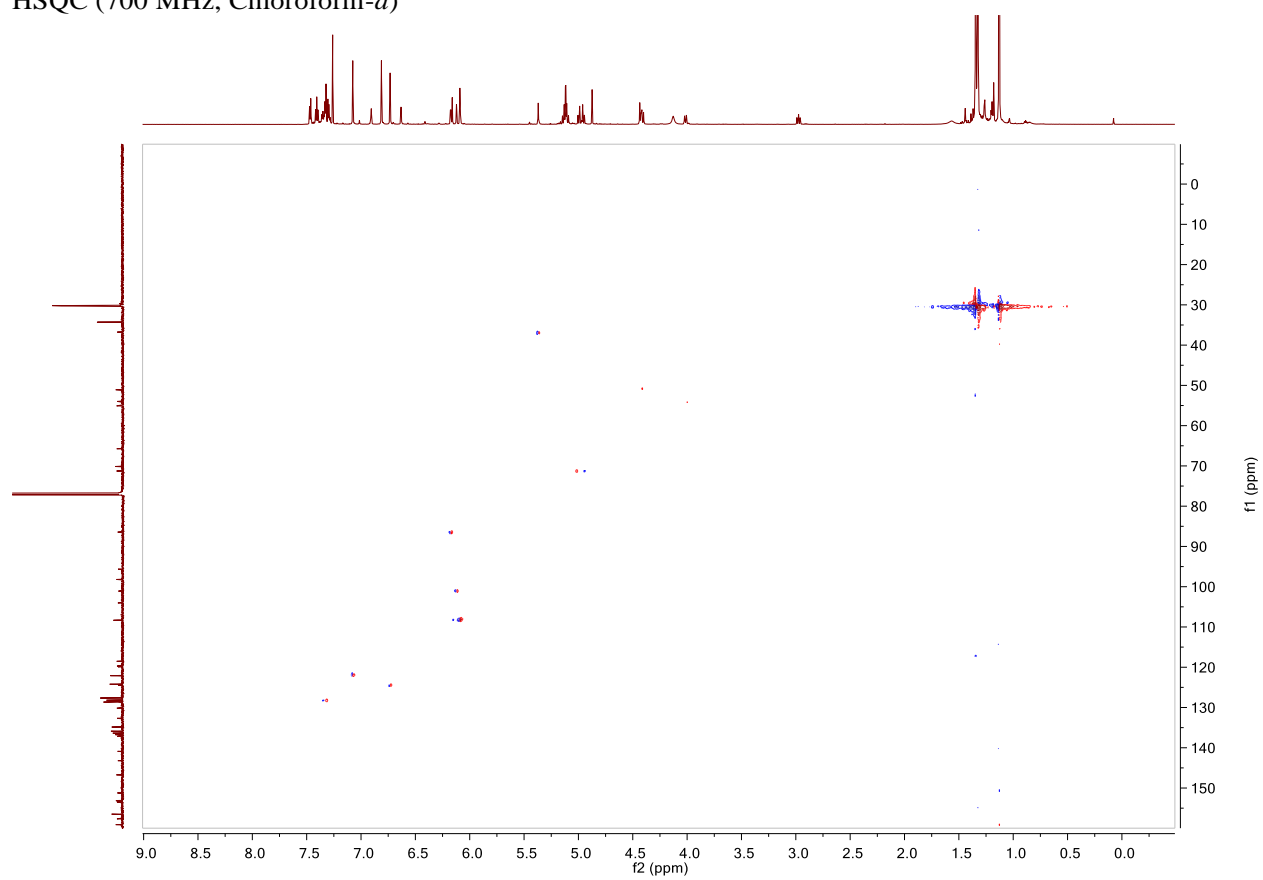
dauidiol A core:

COSY (700 MHz, Chloroform-*d*)



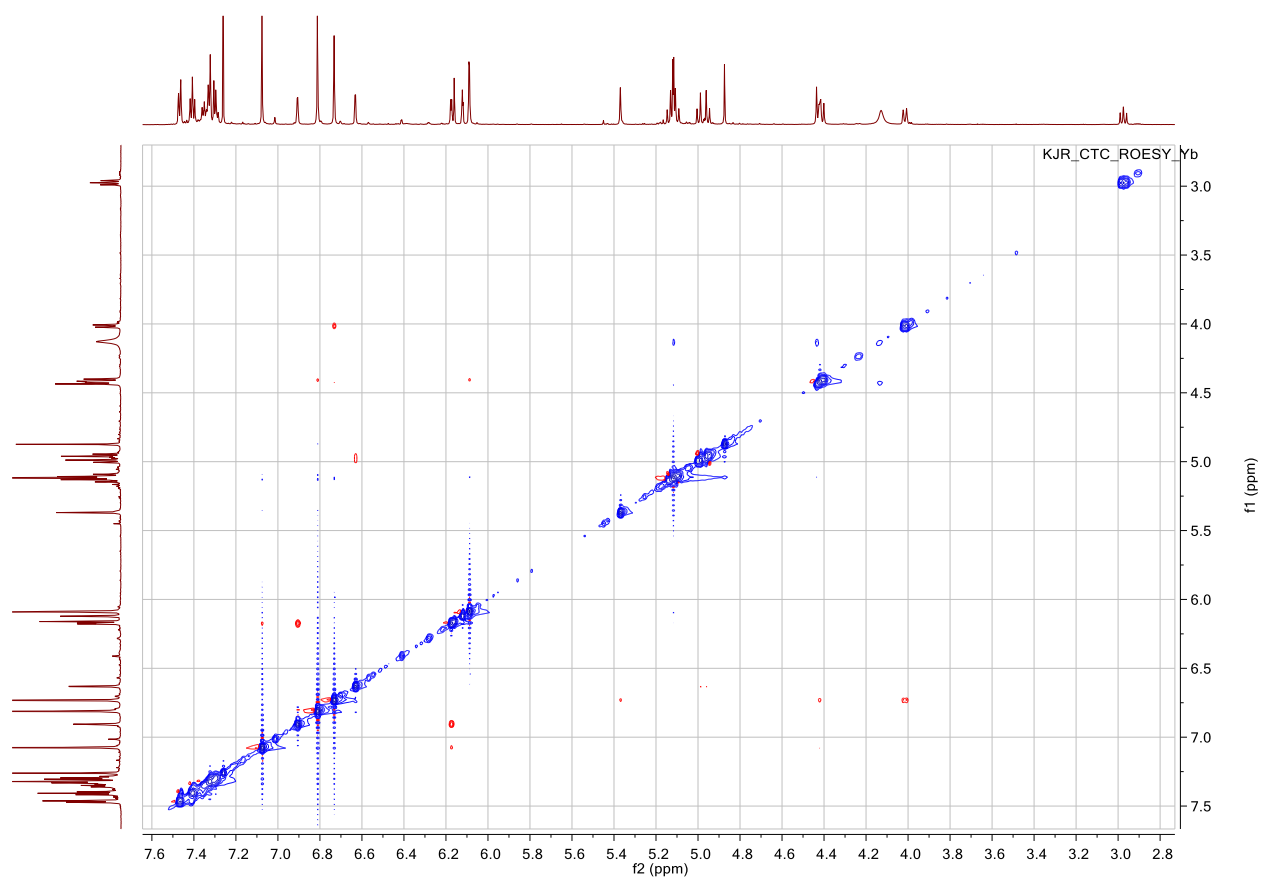
dauidiol A core:

HSQC (700 MHz, Chloroform-*d*)



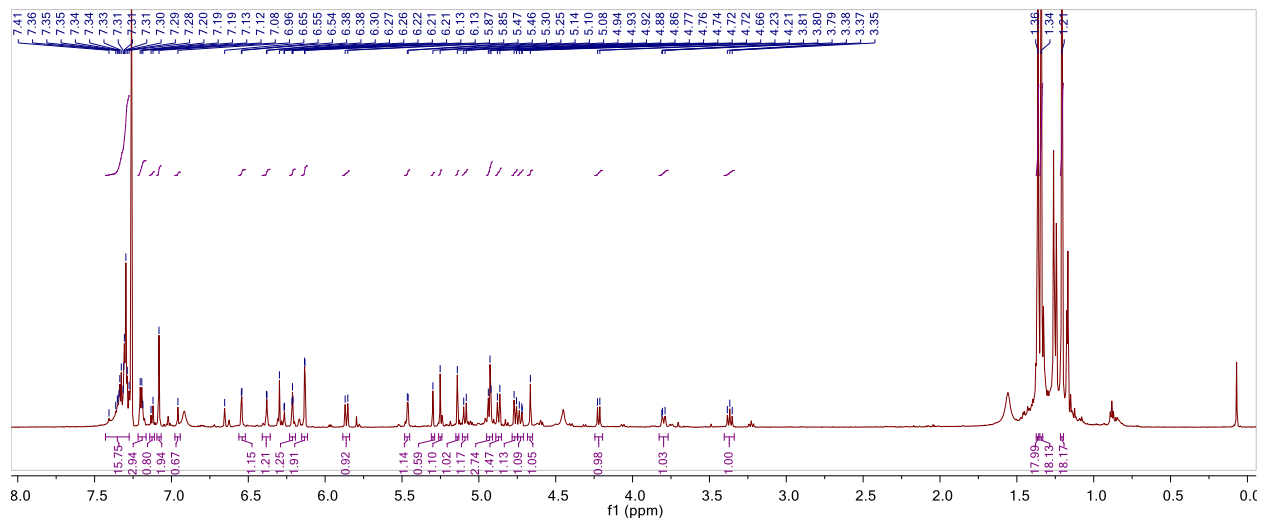
dauidiol A core:

ROESY (700 MHz, Chloroform-*d*)

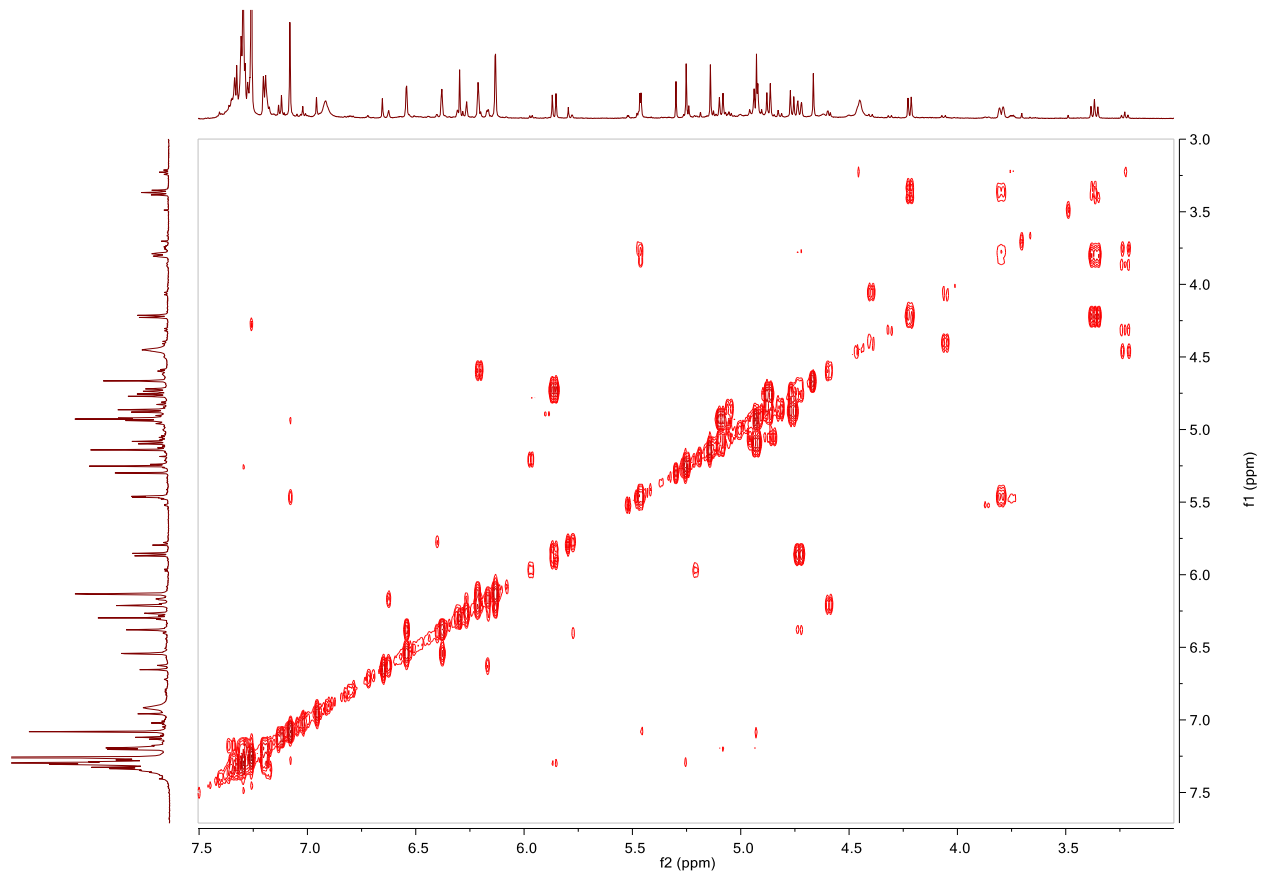


distichol core:

^1H NMR (700 MHz, Chloroform-*d*) δ 7.43 – 7.27 (m, 16H), 7.20 (d, $J = 7.3$ Hz, 3H), 7.13 (d, $J = 9.1$ Hz, 1H), 7.08 (s, 2H), 6.96 (s, 1H), 6.54 (d, $J = 2.4$ Hz, 1H), 6.38 (d, $J = 2.4$ Hz, 1H), 6.21 (d, $J = 2.4$ Hz, 1H), 6.13 (d, $J = 2.2$ Hz, 2H), 5.86 (d, $J = 12.1$ Hz, 1H), 5.46 (d, $J = 3.9$ Hz, 1H), 5.30 (s, 1H), 5.25 (s, 1H), 5.14 (s, 1H), 5.09 (d, $J = 11.8$ Hz, 1H), 4.93 (t, $J = 6.1$ Hz, 3H), 4.87 (d, $J = 11.2$ Hz, 1H), 4.76 (d, $J = 11.0$ Hz, 1H), 4.75 – 4.71 (m, 1H), 4.66 (s, 1H), 4.22 (d, $J = 10.3$ Hz, 1H), 3.83 – 3.77 (m, 1H), 3.37 (t, $J = 11.1$ Hz, 1H), 1.36 (s, 18H), 1.34 (s, 18H), 1.21 (s, 18H).

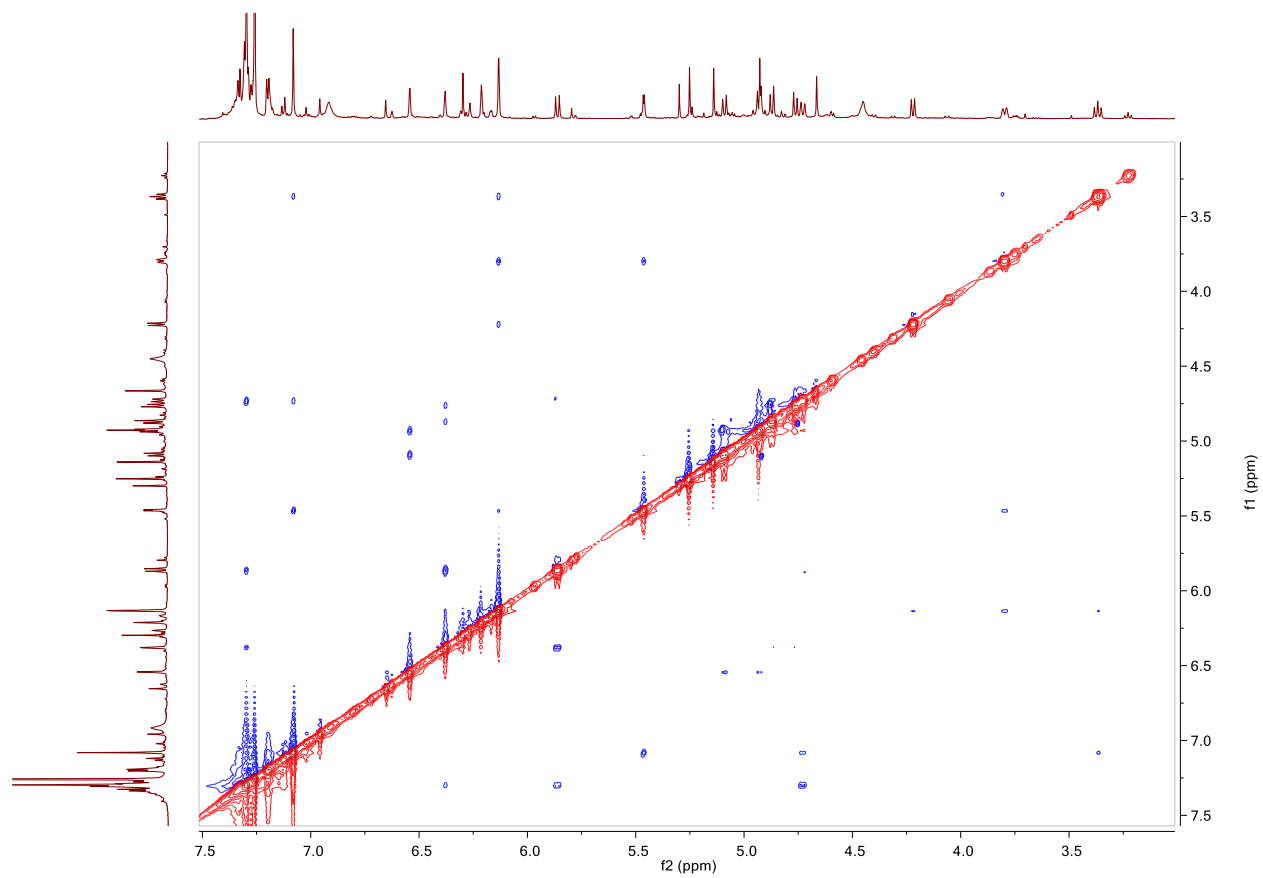


COSY (700 MHz, Chloroform-*d*)



distichol core:

ROESY (700 MHz, Chloroform-*d*)



Computational Data.

Calculations were carried out at the B3LYP-D3 level of theory with the 6-311G(d,p) basis set as implemented in the Gaussian 16 suite of programs.

Table 3.13. Enthalpies and free energies (in kcal/mol) for the dimerization of resveratrol radicals to dimers.

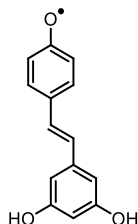
R = H	ΔH_r	ΔG_r	R = <i>t</i> Bu	ΔH_r	ΔG_r	R = SiMe ₃	ΔH_r	ΔG_r
3.210	0.0	0.0	1.156	0.0	0.0	3.140	0.0	0.0
3.211	-16.2	-1.7	1.151	-23.4	-5.1	2.69c	-25.3	-6.1
3.212	-12.6	1.1	3.143	-9.6	7.5	3.141	-17.9	-1.9

Table 3.14. Relative enthalpies and free energies (in kcal/mol) for R = *t*Bu and TMS.

R = <i>t</i> Bu	$\Delta\Delta H_r$	$\Delta\Delta G_r$	R = SiMe ₃	$\Delta\Delta H_r$	$\Delta\Delta G_r$
1.151	0.0	0.0	2.69c	-1.9	-1.1
3.143	13.9	12.6	3.141	5.5	3.1

Optimized Structures and B3LYP-D3/6-311G(d,p) Energies

resveratrol radical (**3.210**)

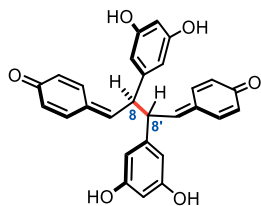


Enthalpy= -765.728708 Free Energy= -765.788163

0.2			
C	4.11301400	-1.28211300	0.00000700
C	2.76489500	-1.09696700	0.00000700
C	2.19113900	0.21564700	-0.00000100
C	3.08432200	1.33160200	-0.00000600
C	4.43837800	1.17148200	-0.00000700
C	5.04462100	-0.15566200	-0.00000700
O	6.27368500	-0.31983900	0.00000300
C	0.78165400	0.46213200	-0.00000100
C	-0.21287900	-0.47040700	0.00000300
C	-1.64492200	-0.21869100	0.00000200
C	-2.50670500	-1.32505300	0.00000200
C	-3.88976200	-1.14198600	0.00000000
C	-4.43262400	0.13997900	-0.00000100
C	-3.57506100	1.24592300	-0.00000100
C	-2.19644600	1.07911000	0.00000000
O	-4.17269700	2.47182900	-0.00000300
O	-4.66234800	-2.26464600	0.00000000
H	4.55384800	-2.27215400	0.00001400

H	2.11164200	-1.96156700	0.00001400
H	2.65749300	2.33008200	-0.00000900
H	5.11686100	2.01638400	-0.00001000
H	0.50273100	1.51207600	-0.00000600
H	0.05991000	-1.52090200	0.00000700
H	-2.11773600	-2.33548600	0.00000300
H	-5.50380100	0.30730200	-0.00000300
H	-1.55710700	1.95421000	0.00000100
H	-3.49801500	3.15848500	-0.00000300
H	-5.59268300	-2.01717000	-0.00000100

resveratrol dimer (C8–C8', meso) (**3.211**)



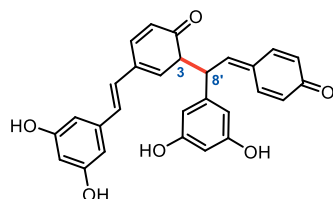
Enthalpy= -1531.483309 Free Energy= -1531.579064

0 1

C	-2.49402300	1.58114400	0.34129800
C	-1.19547500	1.35151600	0.65930800
C	-0.12294700	0.76074100	-0.20442800
C	0.12294900	-0.76074700	0.20443200
C	1.19547300	-1.35152200	-0.65930900
C	2.49402400	-1.58114500	-0.34130700
H	-0.44450400	0.75371100	-1.24646600
C	-3.07629300	1.31140400	-0.96796100
C	-4.38875800	1.48675100	-1.20769200
C	-5.31794700	1.96890000	-0.16795900
C	-4.71037400	2.27650200	1.14043900
C	-3.39650600	2.09723600	1.36654600
C	3.39650000	-2.09724400	-1.36655700
C	4.71037000	-2.27650800	-1.14045700
C	5.31795200	-1.96889200	0.16793300
C	4.38876800	-1.48674300	1.20767100
C	3.07630200	-1.31139800	0.96794800
O	-6.51662700	2.10697000	-0.38075800
O	6.51663100	-2.10697500	0.38072900
C	1.17745500	1.54405500	-0.11465300
C	1.80419300	1.73964200	1.11319200
C	3.05620500	2.35472400	1.16531000
C	3.67622500	2.80442000	0.00283000
C	3.03319600	2.62695600	-1.22147800
C	1.78909900	1.99550600	-1.28515900
O	3.63233900	2.46944600	2.39524600
C	-1.17745400	-1.54406000	0.11466200
C	-1.78909300	-1.99551400	1.28517000
C	-3.03319200	-2.62695900	1.22149300
C	-3.67622900	-2.80441500	-0.00281200
C	-3.05621400	-2.35471600	-1.16529400

C	-1.80419900	-1.73963900	-1.11318000
O	-3.63235700	-2.46942900	-2.39522700
O	-3.68169600	-3.08762700	2.32756900
H	0.44451000	-0.75371700	1.24646800
H	0.88973500	-1.58247800	-1.67636300
O	3.68170500	3.08762000	-2.32755200
H	-0.88974400	1.58246500	1.67636600
H	-2.43390700	0.94668100	-1.75817200
H	-2.96992000	2.32326800	2.33943800
H	2.96990800	-2.32328400	-2.33944400
H	2.43392100	-0.94667100	1.75816100
H	1.36801000	1.39656000	2.04253000
H	4.64909900	3.28206900	0.02250900
H	1.30857200	1.84347600	-2.24655700
H	4.50498900	2.86689800	2.30798100
H	-1.30855900	-1.84349000	2.24656500
H	-4.64910600	-3.28205900	-0.02248700
H	-1.36802100	-1.39655500	-2.04251900
H	-4.50500900	-2.86687500	-2.30795800
H	-3.15123200	-2.90727800	3.11027600
H	3.15124900	2.90726500	-3.11026100
H	-5.38289500	2.64733100	1.90514300
H	-4.82611500	1.27479100	-2.17642300
H	5.38288600	-2.64734400	-1.90516300
H	4.82613100	-1.27477900	2.17639800

resveratrol dimer (C3–C8') (3.212)



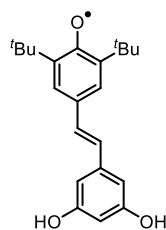
Enthalpy= -1531.477449 Free Energy= -1531.574575

0 1

H	3.51207300	0.62267400	1.74214200
C	3.36634000	-0.15119400	0.99417700
C	2.11483700	-0.52442400	0.67355100
H	1.97704400	-1.31639600	-0.05701400
C	4.60958200	-0.69835700	0.44254400
C	7.05543300	-1.69289400	-0.52247800
C	4.63319400	-1.59528900	-0.63208200
C	5.82439100	-0.29702800	1.02408800
C	7.03381400	-0.79519300	0.54364900
C	5.84879300	-2.08508700	-1.10333400
H	3.72891500	-1.91943200	-1.12846000
H	5.82117400	0.39993300	1.85677200
H	8.00898900	-2.06447300	-0.88050700
C	0.86966200	0.01876700	1.20924500
C	-1.57451600	1.12557900	2.35741100
C	0.87025700	1.12517900	2.17133300

C	-0.32045400	-0.48963900	0.81523000
C	-1.63561600	0.02026600	1.29765800
C	-0.25188000	1.63602600	2.71363100
H	1.82417000	1.55327100	2.45688900
H	-0.34676100	-1.30954100	0.10351300
H	-0.22648000	2.45309900	3.42496400
O	-2.60512000	1.56358500	2.84433600
O	8.24075900	-0.44158000	1.07460000
H	8.10124000	0.17377200	1.80144900
O	5.79922900	-2.95490300	-2.15380500
H	6.69273000	-3.22066600	-2.39347400
H	-2.18179500	-0.81070900	1.76161800
C	-2.57781500	0.53361900	0.12532500
H	-3.46483900	0.88782300	0.65261000
C	-2.96998100	-0.58937000	-0.78910100
H	-2.42448300	-0.67550800	-1.72369000
C	-1.96148500	1.72518400	-0.59072000
C	-0.79444300	3.97444200	-1.78597300
C	-0.94758500	1.56779000	-1.53262700
C	-2.39384000	3.00890500	-0.24327600
C	-1.80726600	4.12540900	-0.83909700
C	-0.36976600	2.69253900	-2.12584400
H	-0.56923100	0.59466400	-1.81456500
H	-3.16402800	3.13528700	0.51019100
H	-0.35833500	4.85860400	-2.23747900
C	-3.93643900	-1.51047200	-0.54280200
C	-5.93720500	-3.54813100	-0.08078700
C	-4.19576400	-2.56543900	-1.51701700
C	-4.74454100	-1.51850100	0.67285700
C	-5.67348200	-2.46783700	0.89223600
C	-5.12376800	-3.51756200	-1.31039900
H	-3.60551700	-2.55989900	-2.42871000
H	-4.58479900	-0.74180200	1.41266500
H	-6.27682000	-2.48302200	1.79259100
H	-5.31666900	-4.30310700	-2.03164600
O	-2.18228300	5.40143400	-0.53579900
H	-2.87863100	5.37812300	0.12876000
O	0.61910800	2.46723300	-3.03859500
H	0.94780500	3.30869700	-3.37091100
O	-6.78150400	-4.41140900	0.12400200

di-ortho-*tert*-butyl resveratrol radical

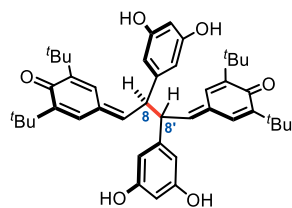


Enthalpy= -1080.122264 Free Energy= -1080.204399

0 2			
C	-2.23772700	1.28927800	0.00013900

C	-0.89426400	1.04300400	0.00004500
C	-0.35194100	-0.27458700	0.00003200
C	-1.24973700	-1.37741100	0.00012100
C	-2.61096500	-1.23388100	0.00021800
C	-3.17194500	0.13655300	0.00022900
O	-4.40125400	0.31815400	0.00032000
C	1.05580100	-0.54141900	-0.00006600
C	2.06461300	0.37481400	-0.00016000
C	3.49288200	0.10002600	-0.00025900
C	4.37296900	1.19187000	-0.00035900
C	5.75274000	0.98612800	-0.00045900
C	6.27516200	-0.30433000	-0.00045900
C	5.39934600	-1.39568200	-0.00035900
C	4.02364900	-1.20631900	-0.00025900
O	5.97620500	-2.63202700	-0.00036400
O	6.54409600	2.09625300	-0.00055400
C	-2.80721700	2.71410300	0.00015200
C	-1.69342100	3.77861200	0.00004400
C	-3.66900100	2.93431200	1.26779700
C	-3.66919400	2.93425800	-1.26737100
C	-3.56340200	-2.43605100	0.00031400
C	-2.80002900	-3.77427100	0.00028500
C	-4.45276000	-2.40040400	-1.26696800
C	-4.45257300	-2.40035100	1.26772500
H	-0.20287000	1.87268800	-0.00002100
H	-0.80829800	-2.36587900	0.00010900
H	1.31869000	-1.59564500	-0.00006300
H	1.80917300	1.42968200	-0.00016500
H	4.00049000	2.20853100	-0.00036200
H	7.34349900	-0.48895900	-0.00053500
H	3.37001400	-2.07084900	-0.00018100
H	5.28922100	-3.30633400	-0.00029000
H	7.46993300	1.83260800	-0.00061400
H	-1.05908500	3.70845700	-0.88844000
H	-2.14791700	4.77230600	0.00005900
H	-1.05894800	3.70849400	0.88843300
H	-4.51571200	2.25176500	1.29098500
H	-4.04659500	3.96133800	1.28126000
H	-3.07010000	2.78312000	2.17091800
H	-4.04678800	3.96128400	-1.28082200
H	-3.07042900	2.78302500	-2.17057700
H	-4.51590900	2.25171200	-1.29040100
H	-2.17173800	-3.88775900	0.88854400
H	-3.51933800	-4.59689900	0.00035600
H	-2.17187000	-3.88779700	-0.88806300
H	-5.06819200	-1.50369300	-1.28953200
H	-5.10882500	-3.27619400	-1.27996900
H	-3.83618700	-2.42693900	-2.17045100
H	-5.10863500	-3.27614200	1.28086000
H	-3.83586700	-2.42684700	2.17111800
H	-5.06800300	-1.50364100	1.29034100

simplified *tert*-butyl resveratrol dimer 5A (C8–C8', meso)



Enthalpy= -2160.281829 Free Energy= -2160.416858

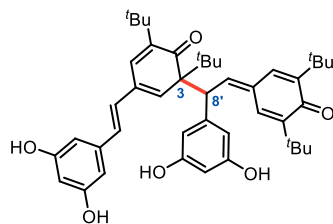
0 1

C	-2.70905000	-0.71620600	0.84926300
C	-1.39572500	-1.05406500	0.77481800
C	-0.21123500	-0.14493200	0.76998500
C	0.21123600	0.14493400	-0.76998800
C	1.39572800	1.05406200	-0.77483300
C	2.70905200	0.71619600	-0.84927000
H	-0.47544100	0.82701300	1.18955100
C	-3.18566200	0.62924000	1.09494900
C	-4.49346100	0.96573800	1.04731600
C	-5.49760400	-0.08951800	0.70904700
C	-5.01646400	-1.47547200	0.42685900
C	-3.69905800	-1.73670000	0.56045000
C	3.69906500	1.73669500	-0.56048900
C	5.01647100	1.47546700	-0.42689900
C	5.49760300	0.08949900	-0.70903200
C	4.49345700	-0.96575800	-1.04728700
C	3.18565900	-0.62925600	-1.09492600
O	-6.69779500	0.17709600	0.66775100
O	6.69779100	-0.17712400	-0.66770200
C	0.98372800	-0.69426300	1.53160300
C	1.36878000	-2.02753200	1.41392000
C	2.54445500	-2.46909400	2.02270100
C	3.35658800	-1.59136800	2.73247600
C	2.96844900	-0.25680500	2.84578600
C	1.78110600	0.18813400	2.26556200
O	2.86191600	-3.78662600	1.84994700
C	-0.98372900	0.69427500	-1.53159700
C	-1.78110300	-0.18810800	-2.26557700
C	-2.96844800	0.25684000	-2.84578900
C	-3.35659200	1.59139800	-2.73244700
C	-2.54446400	2.46911100	-2.02265100
C	-1.36878800	2.02753900	-1.41387900
O	-2.86193100	3.78663700	-1.84986800
O	-3.80719700	-0.57063500	-3.53435000
H	0.47543300	-0.82701200	-1.18955700
H	1.17828500	2.09925500	-0.57581200
O	3.80720200	0.57068200	3.53432800
C	4.98883300	-2.39110500	-1.33363200
C	5.90751400	-2.37772500	-2.57906400
C	3.82081600	-3.35660400	-1.61307300
C	5.76885300	-2.94183400	-0.11488900
C	6.02960400	2.53441400	0.02793800
C	6.70753900	2.05465100	1.33540100
C	7.09433000	2.77142900	-1.06869700
C	5.34751100	3.88367900	0.32199800

C	-6.02959000	-2.53440800	-0.02802300
C	-5.34748500	-3.88365100	-0.32215300
C	-7.09430800	-2.77148900	1.06860400
C	-6.70753500	-2.05459000	-1.33546100
C	-4.98884300	2.39107800	1.33368700
C	-5.76888100	2.94181700	0.11495900
C	-3.82082900	3.35658200	1.61312400
C	-5.90750900	2.37767600	2.57912900
H	-1.17827900	-2.09925200	0.57576900
H	-2.44581600	1.38215100	1.31914800
H	-3.31462200	-2.73415100	0.38658200
H	3.31463400	2.73415300	-0.38664900
H	2.44581100	-1.38217100	-1.31910600
H	0.79672000	-2.74795000	0.84532200
H	4.28671500	-1.91175200	3.18680000
H	1.50174700	1.23357600	2.34765400
H	3.70841600	-3.97695700	2.26736500
H	-1.50173900	-1.23354700	-2.34769300
H	-4.28672000	1.91178900	-3.18676600
H	-0.79673200	2.74794500	-0.84526200
H	-3.70844400	3.97696800	-2.26726000
H	-3.47233400	-1.47239900	-3.49822200
H	3.47235000	1.47244800	3.49816500
H	6.78309000	-1.75222700	-2.41674100
H	6.24277600	-3.39567300	-2.80069900
H	5.36459900	-2.00354900	-3.45213000
H	4.22285800	-4.35053300	-1.82549400
H	3.15562200	-3.45074800	-0.75137500
H	3.23636500	-3.04933500	-2.48537600
H	5.13149800	-2.93450000	0.77172800
H	6.65776000	-2.34992100	0.08885700
H	6.07016100	-3.97566600	-0.30956300
H	5.95677900	1.82823000	2.09881400
H	7.36515900	2.83963100	1.72097900
H	7.30101000	1.15894300	1.16409200
H	7.64649900	1.85924500	-1.28348900
H	7.80135400	3.53836700	-0.73740500
H	6.62306200	3.12259000	-1.99162500
H	4.60349400	3.79965900	1.12042300
H	6.10095700	4.60383300	0.64999500
H	4.85953600	4.30005500	-0.56399100
H	-4.85950300	-4.30006800	0.56381400
H	-6.10092400	-4.60379700	-0.65018400
H	-4.60347100	-3.79958300	-1.12057600
H	-7.64648700	-1.85932200	1.28344200
H	-7.80132400	-3.53842000	0.73727800
H	-6.62303200	-3.12268800	1.99151300
H	-5.95678000	-1.82812800	-2.09886700
H	-7.30101500	-1.15889600	-1.16410800
H	-7.36514900	-2.83955800	-1.72107200
H	-6.07018900	3.97564600	0.30964800
H	-5.13153900	2.93449300	-0.77166700
H	-6.65779000	2.34990400	-0.08878000
H	-3.15564800	3.45074100	0.75141700
H	-4.22287500	4.35050500	1.82556400
H	-3.23636300	3.04930700	2.48541500

H	-6.24277800	3.39561800	2.80077900
H	-6.78308000	1.75217100	2.41680900
H	-5.36458000	2.00349500	3.45218400

simplified *tert*-butyl resveratrol dimer 5B (C3–C8')



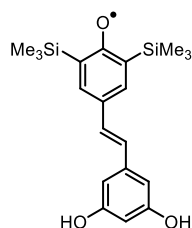
Enthalpy= -2160.259756 Free Energy= -2160.396832

0 1			
C	2.71055100	-2.41548300	-1.79167000
C	1.76856500	-1.45514700	-1.68007200
C	1.97730000	-0.21205700	-0.95988400
C	3.28257000	0.01315700	-0.37539200
C	4.28204300	-0.89250000	-0.43818000
C	4.05046800	-2.17379500	-1.17243600
O	4.94263700	-3.01614100	-1.26180800
C	0.92913600	0.63687700	-0.80745800
C	0.88688400	1.92226400	-0.02298600
C	0.49764100	3.07188000	-0.94513600
C	1.34323000	4.17472800	-1.03188300
C	1.02761200	5.24121600	-1.87864400
C	-0.12737700	5.21417500	-2.65483400
C	-0.95631200	4.09404700	-2.59162800
C	-0.65026500	3.02650800	-1.74915400
O	-2.06340100	4.10427000	-3.39007400
O	1.90005000	6.28812600	-1.90051700
C	-0.00690300	1.68687200	1.29004000
C	-1.41546700	1.38805500	0.89134900
C	-2.03165000	0.20451800	1.09397300
C	-1.31049400	-0.86712500	1.77298500
C	-0.03473600	-0.78187200	2.21197700
C	0.70547000	0.48322900	1.97241700
O	1.88390400	0.60158000	2.27540900
C	-3.40773400	0.01532700	0.63483600
C	-4.11451700	-1.12872000	0.63556500
C	-5.49056900	-1.30209100	0.15986100
C	-5.95747800	-2.60227800	-0.05713000
C	-7.25459300	-2.81543600	-0.52815100
C	-8.10310800	-1.74117700	-0.77894700
C	-7.64131200	-0.44240400	-0.54794600
C	-6.35044300	-0.21566000	-0.08331000
O	-8.52461400	0.56894800	-0.79580900
O	-7.63599800	-4.11028300	-0.72378600
H	0.78473000	-1.59389400	-2.11089400
H	3.42455200	0.93178400	0.17021200
H	-0.01187300	0.34266700	-1.26295000
H	1.87793600	2.13762300	0.36568300

H	2.25746400	4.23158000	-0.45659200
H	-0.38978000	6.02891500	-3.32026500
H	-1.30296600	2.16200700	-1.73719100
H	-2.53367000	3.26989400	-3.29361100
H	1.59346200	6.95059800	-2.52817000
H	-1.95908700	2.18319000	0.39966500
H	-1.85434900	-1.78661800	1.93521700
H	-3.64537400	-2.04144200	0.99043700
H	-5.32458600	-3.46191100	0.12482800
H	-9.11651700	-1.88351600	-1.13698600
H	-6.02771700	0.80001700	0.11732300
H	-8.10966700	1.41238700	-0.58879400
H	-8.54362000	-4.13312600	-1.04368900
C	2.45378300	-3.74761100	-2.51033500
C	2.63478000	-4.91875800	-1.51433000
C	1.02060900	-3.82582200	-3.06934800
C	3.43331300	-3.90746600	-3.69750600
H	3.65221700	-4.95671600	-1.13102200
H	1.94626200	-4.81494700	-0.67004600
H	2.41486200	-5.86663800	-2.01515200
H	0.82516400	-3.04129200	-3.80623700
H	0.88179400	-4.78772600	-3.56911000
H	0.26809400	-3.75483900	-2.27830400
H	3.22618500	-4.84481400	-4.22321500
H	3.30959800	-3.08625500	-4.40992900
H	4.46615700	-3.92132800	-3.35634300
C	5.63713600	-0.65950900	0.24489100
C	5.67584400	0.69667000	0.97544900
C	5.88704100	-1.76575200	1.29899700
C	6.76987000	-0.66831700	-0.80863900
H	5.54901500	1.53583500	0.28480100
H	4.90720000	0.76429500	1.75031700
H	6.64870100	0.81524700	1.45913300
H	5.92628100	-2.75034700	0.83779300
H	6.83895100	-1.58042500	1.80603800
H	5.09633600	-1.76177900	2.05451400
H	7.72897600	-0.46958200	-0.32027700
H	6.83030800	-1.62971500	-1.31459200
H	6.60403000	0.11289700	-1.55668500
C	0.68308100	-1.94509700	2.91155900
C	1.16889900	-1.49713800	4.31076000
H	1.65011700	-2.33786400	4.81894100
H	1.88782400	-0.68342300	4.23882600
H	0.32575600	-1.16893100	4.92624000
C	1.88810900	-2.40496400	2.05616000
H	1.56279900	-2.71752600	1.06050400
H	2.62057100	-1.61097600	1.93905000
H	2.37626400	-3.25842500	2.53583400
C	-0.24833500	-3.15668900	3.10123800
H	-1.12201100	-2.91240400	3.71294100
H	-0.59299900	-3.56115200	2.14494300
H	0.29910100	-3.95223600	3.61204600
C	-0.01164900	2.92020700	2.32859900
C	1.38560200	3.53194400	2.54059900
H	1.33050000	4.25148700	3.36298800
H	2.12725000	2.77796400	2.79489100

H	1.72188400	4.07834700	1.65950900
C	-0.95956300	4.05069800	1.87065900
H	-0.83300200	4.90496900	2.54119400
H	-0.74286800	4.39050800	0.85811500
H	-2.00911100	3.75319500	1.92228500
C	-0.52875800	2.39084800	3.68499400
H	-0.69514400	3.22913700	4.36707600
H	-1.47705000	1.85887100	3.57012800
H	0.19014500	1.71880000	4.15778500
H	-3.86935000	0.91353400	0.23204000

di-ortho-TMS resveratrol radical



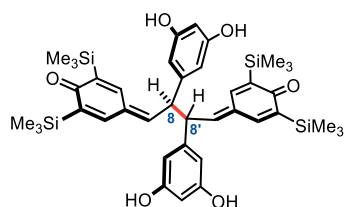
Enthalpy= -1583.020820 Free Energy= -1583.115667

0 2

C	-1.87055300	1.26821400	0.00011300
C	-0.52478200	1.02250300	0.00001800
C	0.01628000	-0.30281100	0.00000600
C	-0.89891700	-1.39955700	0.00009600
C	-2.25979700	-1.23638700	0.00019300
C	-2.79969300	0.12861300	0.00020500
O	-4.03317300	0.32098200	0.00029800
C	1.41992700	-0.58105200	-0.00009200
C	2.43579500	0.32885200	-0.00018400
C	3.86135300	0.04407100	-0.00028400
C	4.74878400	1.13015100	-0.00036500
C	6.12709500	0.91481500	-0.00046300
C	6.63999400	-0.37951600	-0.00048100
C	5.75685300	-1.46518300	-0.00040000
C	4.38259100	-1.26628800	-0.00030300
O	6.32568100	-2.70483600	-0.00042400
O	6.92597000	2.01907600	-0.00053700
C	-1.20529600	4.25855800	-0.00001600
C	-3.67161100	3.22919800	1.54956600
C	-3.67186300	3.22912100	-1.54914500
C	-2.52494000	-4.28818300	0.00026900
C	-4.56724000	-2.56407700	-1.54875100
C	-4.56701400	-2.56402200	1.54952500
H	0.16579200	1.85887700	-0.00005000
H	-0.47394400	-2.40027600	0.00008500
H	1.67512400	-1.63730800	-0.00008900
H	2.18693900	1.38523700	-0.00018500
H	4.38318800	2.14928600	-0.00035300
H	7.70699600	-0.57172000	-0.00055600
H	3.72283100	-2.12608500	-0.00024300
H	5.63490400	-3.37529900	-0.00036300

H	7.85015100	1.74959100	-0.00060100
H	-0.57174800	4.15362400	-0.88613100
H	-1.60226000	5.27827600	-0.00000900
H	-0.57160200	4.15366700	0.88600000
H	-4.46479200	2.47889500	1.56059200
H	-4.12921100	4.22296500	1.57841400
H	-3.07072300	3.10747900	2.45551600
H	-4.12946700	4.22288700	-1.57797000
H	-3.07112300	3.10735500	-2.45518700
H	-4.46504600	2.47881700	-1.56000300
H	-1.88878500	-4.37799300	0.88615100
H	-3.21012300	-5.14139800	0.00033500
H	-1.88891300	-4.37802500	-0.88570100
H	-5.09679400	-1.60926200	-1.56011700
H	-5.30359700	-3.37328800	-1.57652300
H	-3.95818200	-2.62998700	-2.45501500
H	-5.30336500	-3.37323400	1.57743400
H	-3.95782400	-2.62989700	2.45570300
H	-5.09656900	-1.60920800	1.56093400
Si	-2.62478700	3.01037800	0.00013100
Si	-3.50246100	-2.67022600	0.00031100

simplified TMS resveratrol dimer 5A (C8–C8', meso)



Enthalpy= -3166.081932 Free Energy= -3166.241069

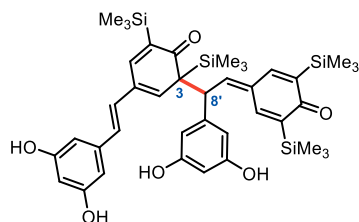
0 1

C	-2.68040100	0.60606900	-0.97111900
C	-1.36862800	0.95349500	-0.93370300
C	-0.18821600	0.05122100	-0.79018100
C	0.18821800	-0.05121200	0.79017500
C	1.36862600	-0.95349100	0.93369900
C	2.68040100	-0.60607000	0.97111000
H	-0.44628100	-0.96428700	-1.09427300
C	-3.15960700	-0.76639100	-1.03673400
C	-4.46709300	-1.09050500	-0.90738700
C	-5.45842700	-0.01305100	-0.68256700
C	-4.99372200	1.39082600	-0.60527800
C	-3.68122500	1.65132800	-0.79909200
C	3.68122100	-1.65133400	0.79908700
C	4.99371800	-1.39083700	0.60527400
C	5.45843000	0.01303800	0.68256200
C	4.46709900	1.09049800	0.90737300
C	3.15961200	0.76638900	1.03671800
O	-6.65823500	-0.28197600	-0.56265000
O	6.65824000	0.28195500	0.56265300
C	1.02787800	0.50318200	-1.58134600

C	1.41078000	1.84157700	-1.62609200
C	2.60159700	2.20469200	-2.25769900
C	3.43266000	1.24494700	-2.82542100
C	3.04738700	-0.09438200	-2.77401900
C	1.84389900	-0.46402200	-2.17471000
O	2.90927800	3.53547300	-2.25480600
C	-1.02787600	-0.50316600	1.58134100
C	-1.84388600	0.46404100	2.17471500
C	-3.04737600	0.09440800	2.77402500
C	-3.43266200	-1.24491700	2.82541600
C	-2.60161300	-2.20466700	2.25768000
C	-1.41079200	-1.84155700	1.62607600
O	-2.90930900	-3.53544300	2.25477300
O	-3.90430900	1.00305300	3.32375400
H	0.44628800	0.96429600	1.09426600
H	1.15250200	-2.01613500	0.87157000
O	3.90433100	-1.00302300	-3.32373700
C	6.26947600	3.03403000	2.47260400
C	3.65829100	4.03816800	1.14388400
C	6.07691500	3.23843600	-0.60362500
C	7.00040300	-2.20207300	-1.54200600
C	7.62002600	-2.81692900	1.43809200
C	5.37938500	-4.35544700	-0.03187600
C	-5.37939900	4.35543600	0.03187200
C	-7.62004300	2.81690100	-1.43807600
C	-7.00039200	2.20205300	1.54201800
C	-6.07689900	-3.23842000	0.60364200
C	-3.65828200	-4.03817700	-1.14387800
C	-6.26947700	-3.03406400	-2.47258800
H	-1.15251000	2.01614000	-0.87156600
H	-2.42484500	-1.54875700	-1.18556500
H	-3.31017700	2.67297200	-0.75783800
H	3.31016900	-2.67297700	0.75783700
H	2.42485200	1.54875700	1.18554400
H	0.82487800	2.62805400	-1.17030900
H	4.37440200	1.50637200	-3.29305600
H	1.56616700	-1.51211900	-2.12939000
H	3.76699800	3.67717000	-2.66882600
H	-1.56614400	1.51213600	2.12940200
H	-4.37440300	-1.50633600	3.29305800
H	-0.82490100	-2.62803500	1.17028100
H	-3.76706000	-3.67712900	2.66873200
H	-3.56626400	1.89325800	3.18248200
H	3.56629900	-1.89323100	-3.18245000
H	7.08790700	2.31571500	2.38850200
H	6.69518600	4.04054700	2.53193700
H	5.73453600	2.83797600	3.40639000
H	4.01220700	5.06758400	1.25774700
H	3.02797000	4.00283900	0.25159400
H	3.04505300	3.80616000	2.02014100
H	5.46049600	3.01625800	-1.47755600
H	6.96664400	2.60916700	-0.65576300
H	6.37778100	4.28937100	-0.65113000
H	6.20914700	-1.98135100	-2.26470700
H	7.63724000	-2.99083000	-1.95408200
H	7.59839000	-1.29640000	-1.42122800

H	8.09383200	-1.84063600	1.55987100
H	8.38699200	-3.54419700	1.15418100
H	7.20600300	-3.12118200	2.40377900
H	4.59492600	-4.32282500	-0.79465700
H	6.08446000	-5.14062400	-0.32106900
H	4.91876900	-4.66069000	0.91267200
H	-4.91879400	4.66068000	-0.91268100
H	-6.08447700	5.14060800	0.32107000
H	-4.59493300	4.32281900	0.79464600
H	-8.09385000	1.84060700	-1.55984400
H	-8.38700800	3.54417200	-1.15416500
H	-7.20602800	3.12114800	-2.40376800
H	-6.20912900	1.98134300	2.26471500
H	-7.59837000	1.29637200	1.42124600
H	-7.63723700	2.99080400	1.95409600
H	-6.37759300	-4.28939900	0.65126300
H	-5.46055200	-3.01602700	1.47757000
H	-6.96673100	-2.60928900	0.65567800
H	-3.02795700	-4.00284600	-0.25159000
H	-4.01219800	-5.06759300	-1.25773800
H	-3.04504600	-3.80617100	-2.02013700
H	-6.69520000	-4.04057700	-2.53189100
H	-7.08790000	-2.31573800	-2.38849700
H	-5.73454200	-2.83804000	-3.40638200
Si	6.27827400	-2.69849200	0.12482500
Si	5.12929100	2.86614000	0.98387200
Si	-5.12928200	-2.86614900	-0.98386700
Si	-6.27828000	2.69847500	-0.12481900

simplified TMS resveratrol dimer 5B (C3–C8^{*})



Enthalpy= -3166.070238 Free Energy= -3166.234398

0 1

C	5.52692700	0.19612000	-0.15477300
C	4.33618100	0.78981400	0.09594200
C	3.10027200	0.04625800	0.30293700
C	3.19699800	-1.40517300	0.29581400
C	4.35441900	-2.06358300	0.05236900
C	5.58857200	-1.28237200	-0.20421800
O	6.65167900	-1.86182100	-0.45134100
C	1.93480800	0.73200100	0.43166700
C	0.56370200	0.14478000	0.58232900
C	0.00742200	0.42316600	1.98141700
C	-0.41208000	-0.64676100	2.76586200
C	-0.98280700	-0.40808000	4.01984600
C	-1.14264300	0.89154400	4.49246200

C	-0.71154200	1.95753800	3.70185300
C	-0.12309700	1.73201100	2.45958000
O	-0.90266100	3.21466100	4.19875900
O	-1.37885500	-1.50083600	4.73537100
C	-0.48815100	0.59081500	-0.51307300
C	-1.69154700	-0.26366800	-0.38391200
C	-2.96892400	0.18988200	-0.46671400
C	-3.17015300	1.62646600	-0.56100300
C	-2.16231100	2.53611900	-0.59125300
C	-0.76643000	2.07918100	-0.53837800
O	0.15588000	2.90232500	-0.52152000
C	-4.08807100	-0.74672600	-0.40590700
C	-5.38920000	-0.46279000	-0.59380000
C	-6.50760100	-1.40792100	-0.53052000
C	-7.75526600	-0.98967300	-1.00480800
C	-8.84702900	-1.85946600	-0.97833900
C	-8.71350500	-3.14970300	-0.47436400
C	-7.46962800	-3.56371600	0.01064400
C	-6.37355900	-2.70869500	-0.01207500
O	-7.40354700	-4.83459300	0.50563600
O	-10.02965100	-1.38268700	-1.46432200
H	4.25553300	1.87353600	0.12786100
H	2.29567000	-1.97210400	0.50069000
H	1.97219700	1.81397800	0.40335900
H	0.62969900	-0.93915100	0.48613200
H	-0.31823200	-1.67065000	2.42587500
H	-1.59555000	1.09702800	5.45600500
H	0.20912600	2.57261200	1.86661900
H	-0.59928500	3.86238500	3.55285700
H	-1.74964500	-1.21511100	5.57657600
H	-1.51959200	-1.32624800	-0.23556500
H	-4.19441600	1.98441300	-0.55721500
H	-5.67740000	0.55476700	-0.84094800
H	-7.89605500	0.00607700	-1.40647900
H	-9.54888300	-3.83987700	-0.43843000
H	-5.42750700	-3.04671300	0.39590600
H	-6.50856900	-5.01011400	0.81340000
H	-10.70393600	-2.06596200	-1.39329200
C	7.76511800	0.74182300	-2.19691000
C	6.76084300	2.99272800	-0.33538400
C	8.41002900	0.65402300	0.83097200
H	7.93965200	-0.33292200	-2.27955400
H	7.03626600	1.03142200	-2.95967000
H	8.70247100	1.26529100	-2.40947900
H	6.38454100	3.25970000	0.65683800
H	7.67000500	3.57613100	-0.51019700
H	6.01969000	3.30951900	-1.07548000
H	9.35766600	1.17850800	0.67367800
H	8.05747900	0.88855400	1.83964500
H	8.59298200	-0.42094900	0.77322200
C	2.77175000	-4.66182300	0.35506800
C	5.04819900	-4.48053000	-1.72032700
C	5.71165800	-4.53471400	1.30741600
H	2.40479600	-4.36272300	1.34176500
H	2.03957000	-4.34186900	-0.39315800
H	2.80359700	-5.75538800	0.33474100

H	6.01804000	-4.03042800	-1.94156200
H	5.14343600	-5.56861100	-1.78940400
H	4.33612300	-4.15461700	-2.48436500
H	5.81860900	-5.62378600	1.29315600
H	6.68861900	-4.08603100	1.11593100
H	5.38905900	-4.23947000	2.31008500
C	-1.63425200	5.25283400	-1.98124200
H	-1.76758200	6.33811400	-1.93794900
H	-0.56495000	5.03312000	-1.99083500
H	-2.06690700	4.89932300	-2.92192000
C	-1.70211400	5.03673900	1.11585100
H	-2.12380200	4.48823400	1.96366900
H	-0.61944700	4.89139000	1.09717200
H	-1.90837500	6.10085000	1.26309200
C	-4.30213100	4.72754800	-0.51274800
H	-4.77568500	4.34342300	-1.42143200
H	-4.79678100	4.26871800	0.34857200
H	-4.49969700	5.80287500	-0.47016500
C	1.68057100	1.21494800	-2.78442300
H	1.77432600	1.27117300	-3.87394800
H	1.59069600	2.22982100	-2.39324200
H	2.59354400	0.77175200	-2.38530500
C	0.54816200	-1.64518000	-2.44145300
H	0.87823600	-1.89894600	-3.45375900
H	1.35903100	-1.91515200	-1.76098500
H	-0.32281300	-2.26400600	-2.21257800
C	-1.23778600	0.63957600	-3.54321900
H	-0.95537400	0.36393100	-4.56398400
H	-2.16638600	0.12127600	-3.29601600
H	-1.43521300	1.71434400	-3.53067300
H	-3.79961300	-1.77555700	-0.20637900
Si	7.13845700	1.14587400	-0.46756800
Si	4.48985800	-3.95445800	-0.00083500
Si	-2.44144200	4.40958200	-0.50583300
Si	0.15908800	0.19583500	-2.36452400

References

- (1) Gomberg, M. AN INSTANCE OF TRIVALENT CARBON: TRIPHENYLMETHYL. *J. Am. Chem. Soc.* **1900**, 22 (11), 757–771. <https://doi.org/10.1021/ja02049a006>.
- (2) Schoepfle, C.; Bachmann, W. Moses Gomberg 1866-1947. *J. Am. Chem. Soc.* **1947**, 69 (12), 2921–2925. <https://doi.org/10.1021/ja01204a641>.
- (3) Lankamp, H.; Nauta, W. T.; MacLean, C. A New Interpretation of the Monomer-Dimer Equilibrium of Triphenylmethyl- and Alkylsubstituted-Diphenyl Methyl-Radicals in Solution. *Tetrahedron Lett.* **1968**, 9 (2), 249–254. [https://doi.org/10.1016/S0040-4039\(00\)75598-5](https://doi.org/10.1016/S0040-4039(00)75598-5).
- (4) Griller, D.; Ingold, K. U. Persistent Carbon-Centered Radicals. *Acc. Chem. Res.* **1976**, 9 (1), 13–19. <https://doi.org/10.1021/ar50097a003>.
- (5) Bordwell, F. G.; Cheng, J.; Ji, G. Z.; Satish, A. V.; Zhang, X. Bond Dissociation Energies in DMSO Related to the Gas Phase Values. *J. Am. Chem. Soc.* **1991**, 113 (26), 9790–9795. <https://doi.org/10.1021/ja00026a012>.
- (6) Blanksby, S. J.; Ellison, G. B. Bond Dissociation Energies of Organic Molecules. *Acc. Chem. Res.* **2003**, 36 (4), 255–263. <https://doi.org/10.1021/ar020230d>.
- (7) Romero, K. J.; Galliher, M. S.; Pratt, D. A.; Stephenson, C. R. J. Radicals in Natural Product Synthesis. *Chem. Soc. Rev.* **2018**, 47 (21), 7851–7866. <https://doi.org/10.1039/C8CS00379C>.
- (8) Bergh, H. E. van den; Callear, A. B. Experimental Determination of the Oscillator Strength of the B(2B1)—X(2A2) Transition of the Free Allyl Radical. *Trans. Faraday Soc.* **1970**, 66 (0), 2681–2684. <https://doi.org/10.1039/TF9706602681>.
- (9) Claridge, R. F. C.; Fischer, H. Self-Termination and Electronic Spectra of Substituted Benzyl Radicals in Solution. *J. Phys. Chem.* **1983**, 87 (11), 1960–1967. <https://doi.org/10.1021/j100234a026>.
- (10) Schreiner, K.; Berndt, A. ESR Spectrum of a Perpendicular Benzyl Radical. *Angew. Chem. Int. Ed. Engl.* **13** (2), 144–145. <https://doi.org/10.1002/anie.197401441>.
- (11) Curran, D. P.; Rakiewicz, D. M. Tandem Radical Approach to Linear Condensed Cyclopentanoids. Total Synthesis of (+-)-Hirsutene. *J. Am. Chem. Soc.* **1985**, 107 (5), 1448–1449. <https://doi.org/10.1021/ja00291a077>.
- (12) Fischer, H. The Persistent Radical Effect: A Principle for Selective Radical Reactions and Living Radical Polymerizations. *Chem. Rev.* **2001**, 101 (12), 3581–3610. <https://doi.org/10.1021/cr990124y>.
- (13) Studer Armido. The Persistent Radical Effect in Organic Synthesis. *Chem. – Eur. J.* **2001**, 7 (6), 1159–1164. [https://doi.org/10.1002/1521-3765\(20010316\)7:6<1159::AID-CHEM1159>3.0.CO;2-I](https://doi.org/10.1002/1521-3765(20010316)7:6<1159::AID-CHEM1159>3.0.CO;2-I).

- (14) Jasperse, C. P.; Curran, D. P.; Fevig, T. L. Radical Reactions in Natural Product Synthesis. *Chem. Rev.* **1991**, *91* (6), 1237–1286. <https://doi.org/10.1021/cr00006a006>.
- (15) Studer, A.; Curran, D. P. Catalysis of Radical Reactions: A Radical Chemistry Perspective. *Angew. Chem. Int. Ed.* **2016**, *55* (1), 58–102. <https://doi.org/10.1002/anie.201505090>.
- (16) Helm, M. D.; Da Silva, M.; Sucunza, D.; Findley, T. J. K.; Procter, D. J. A Dialdehyde Cyclization Cascade: An Approach to Pleuromutilin. *Angew. Chem. Int. Ed.* **2009**, *48* (49), 9315–9317. <https://doi.org/10.1002/anie.200905490>.
- (17) Fazakerley, N. J.; Helm, M. D.; Procter, D. J. Total Synthesis of (+)-Pleuromutilin. *Chem. – Eur. J.* **2013**, *19* (21), 6718–6723. <https://doi.org/10.1002/chem.201300968>.
- (18) Wang, X.; Ma, Z.; Lu, J.; Tan, X.; Chen, C. Asymmetric Synthesis of Ageliferin. *J. Am. Chem. Soc.* **2011**, *133* (39), 15350–15353. <https://doi.org/10.1021/ja207386q>.
- (19) Snider, B. B. Manganese(III)-Based Oxidative Free-Radical Cyclizations. *Chem. Rev.* **1996**, *96* (1), 339–364. <https://doi.org/10.1021/cr950026m>.
- (20) Tan, X.; Chen, C. Regiocontrol in MnIII-Mediated Oxidative Heterobicyclizations: Access to the Core Skeletons of Oroidin Dimers. *Angew. Chem. Int. Ed.* **2006**, *45* (26), 4345–4348. <https://doi.org/10.1002/anie.200601208>.
- (21) Hashimoto, S.; Katoh, S.; Kato, T.; Urabe, D.; Inoue, M. Total Synthesis of Resiniferatoxin Enabled by Radical-Mediated Three-Component Coupling and 7-Endo Cyclization. *J. Am. Chem. Soc.* **2017**, *139* (45), 16420–16429. <https://doi.org/10.1021/jacs.7b10177>.
- (22) Hrovat, D. A.; Borden, W. T. Ab Initio Calculations of the Relative Resonance Stabilization Energies of Allyl and Benzyl Radicals. *J. Phys. Chem.* **1994**, *98* (41), 10460–10464. <https://doi.org/10.1021/j100092a014>.
- (23) Sears, J. E.; Boger, D. L. Total Synthesis of Vinblastine, Related Natural Products, and Key Analogues and Development of Inspired Methodology Suitable for the Systematic Study of Their Structure–Function Properties. *Acc. Chem. Res.* **2015**, *48* (3), 653–662. <https://doi.org/10.1021/ar500400w>.
- (24) Vukovic, J.; Goodbody, A. E.; Kutney, J. P.; Misawa, M. Production of 3', 4'-anhydrovinblastine: A Unique Chemical Synthesis. *Tetrahedron* **1988**, *44* (2), 325–331. [https://doi.org/10.1016/S0040-4020\(01\)85824-5](https://doi.org/10.1016/S0040-4020(01)85824-5).
- (25) Beatty, J. W.; Stephenson, C. R. J. Synthesis of (–)-Pseudotabersonine, (–)-Pseudovincadifformine, and (+)-Coronaridine Enabled by Photoredox Catalysis in Flow. *J. Am. Chem. Soc.* **2014**, *136* (29), 10270–10273. <https://doi.org/10.1021/ja506170g>.
- (26) Bruncko, M.; Crich, D.; Samy, R. Chemistry of Cyclic Tautomers of Tryptophan: Formation of a Quaternary Center at C3a and Total Synthesis of the Marine Alkaloid (+)-Ent-Debromoflustramine B. *J. Org. Chem.* **1994**, *59* (19), 5543–5549. <https://doi.org/10.1021/jo00098a011>.
- (27) Movassaghi, M.; Schmidt, M. A. Concise Total Synthesis of (–)-Calycanthine, (+)-Chimonanthine, and (+)-Folicanthine. *Angew. Chem. Int. Ed.* **2007**, *46* (20), 3725–3728. <https://doi.org/10.1002/anie.200700705>.
- (28) Furst Laura; Narayanam Jagan M. R.; Stephenson Corey R. J. Total Synthesis of (+)-Gliocladin C Enabled by Visible-Light Photoredox Catalysis. *Angew. Chem. Int. Ed.* **2011**, *50* (41), 9655–9659. <https://doi.org/10.1002/anie.201103145>.

- (29) Wu, K.; Du, Y.; Wang, T. Visible-Light-Mediated Construction of Pyrroloindolines via an Amidyl Radical Cyclization/Carbon Radical Addition Cascade: Rapid Synthesis of (±)-Flustramide B. *Org. Lett.* **2017**, *19* (20), 5669–5672. <https://doi.org/10.1021/acs.orglett.7b02837>.
- (30) Gentry, E. C.; Rono, L. J.; Hale, M. E.; Matsuura, R.; Knowles, R. R. Enantioselective Synthesis of Pyrroloindolines via Noncovalent Stabilization of Indole Radical Cations and Applications to the Synthesis of Alkaloid Natural Products. *J. Am. Chem. Soc.* **2018**, *140* (9), 3394–3402. <https://doi.org/10.1021/jacs.7b13616>.
- (31) Schnermann Martin J.; Overman Larry E. A Concise Synthesis of (–)-Aplyviolene Facilitated by a Strategic Tertiary Radical Conjugate Addition. *Angew. Chem. Int. Ed.* **2012**, *51* (38), 9576–9580. <https://doi.org/10.1002/anie.201204977>.
- (32) Garnsey, M. R.; Slutskyy, Y.; Jamison, C. R.; Zhao, P.; Lee, J.; Rhee, Y. H.; Overman, L. E. Short Enantioselective Total Syntheses of Cheloviolenes A and B and Dendrillolide C via Convergent Fragment Coupling Using a Tertiary Carbon Radical. *J. Org. Chem.* **2017**. <https://doi.org/10.1021/acs.joc.7b02458>.
- (33) Cha, J. Y.; Yeoman, J. T. S.; Reisman, S. E. A Concise Total Synthesis of (–)-Maoecrystal Z. *J. Am. Chem. Soc.* **2011**, *133* (38), 14964–14967. <https://doi.org/10.1021/ja2073356>.
- (34) Riehl, P. S.; DePorre, Y. C.; Armaly, A. M.; Groso, E. J.; Schindler, C. S. New Avenues for the Synthesis of Ent-Kaurene Diterpenoids. *Tetrahedron* **2015**, *71* (38), 6629–6650. <https://doi.org/10.1016/j.tet.2015.04.116>.
- (35) Olguín-Urbe, S.; Mijangos, M. V.; Amador-Sánchez, Y. A.; Sánchez-Carmona, M. A.; Miranda, L. D. Expedited Synthesis of Matrine Analogues through an Oxidative Cascade Addition/Double-Cyclization Radical Process. *Eur. J. Org. Chem.* **2017**, *2017* (17), 2481–2485. <https://doi.org/10.1002/ejoc.201700208>.
- (36) Lebedev, O. L.; Kazarnovskii, S. N. Catalytic oxidation of aliphatic amines with hydrogen peroxide. *Russ. J. Gen. Chem.* **1960**, *30* (5), 1631–1635.
- (37) Mahoney, L. R.; Mendenhall, G. D.; Ingold, K. U. Calorimetric and equilibrium studies on some stable nitroxide and iminoxy radicals. Approximate oxygen-hydrogen bond dissociation energies in hydroxylamines and oximes <https://pubs.acs.org/doi/abs/10.1021/ja00807a018> (accessed May 5, 2018).
- (38) Fischer, H. Unusual Selectivities of Radical Reactions by Internal Suppression of Fast Modes. *J. Am. Chem. Soc.* **1986**, *108* (14), 3925–3927. <https://doi.org/10.1021/ja00274a012>.
- (39) Leifert, D.; Studer, A. The Persistent Radical Effect in Organic Synthesis. *Angew. Chem. Int. Ed.* **2020**, *59* (1), 74–108. <https://doi.org/10.1002/anie.201903726>.
- (40) Amatov, T.; Gebauer, M.; Pohl, R.; Cisařová, I.; Jahn, U. Oxidative Radical Cyclizations of Diketopiperazines Bearing an Amidomalonate Unit. Heterointermediate Reaction Sequences toward the Asperparalines and Stephacidins. *Free Radic. Res.* **2016**, *50* (sup1), S6–S17. <https://doi.org/10.1080/10715762.2016.1223295>.
- (41) Amatov Tynchtyk; Pohl Radek; Cisařová Ivana; Jahn Ullrich. Synthesis of Bridged Diketopiperazines by Using the Persistent Radical Effect and a Formal Synthesis of Bicyclomycin. *Angew. Chem. Int. Ed.* **2015**, *54* (41), 12153–12157. <https://doi.org/10.1002/anie.201504883>.

- (42) Kapras, V.; Vyklicky, V.; Budesinsky, M.; Cisarova, I.; Vyklicky, L.; Chodounska, H.; Jahn, U. Total Synthesis of Ent-Pregnanolone Sulfate and Its Biological Investigation at the NMDA Receptor. *Org. Lett.* **2018**, *20* (4), 946–949. <https://doi.org/10.1021/acs.orglett.7b03838>.
- (43) Xu, J.; Caro-Diaz, E. J. E.; Trzoss, L.; Theodorakis, E. A. Nature-Inspired Total Synthesis of (–)-Fusarisetin A. *J. Am. Chem. Soc.* **2012**, *134* (11), 5072–5075. <https://doi.org/10.1021/ja300807e>.
- (44) Keylor, M. H.; Matsuura, B. S.; Stephenson, C. R. J. Chemistry and Biology of Resveratrol-Derived Natural Products. *Chem. Rev.* **2015**, *115* (17), 8976–9027. <https://doi.org/10.1021/cr500689b>.
- (45) Matsuura, B. S.; Keylor, M. H.; Li, B.; Lin, Y.; Allison, S.; Pratt, D. A.; Stephenson, C. R. J. A Scalable Biomimetic Synthesis of Resveratrol Dimers and Systematic Evaluation of Their Antioxidant Activities. *Angew. Chem. Int. Ed.* **2015**, *54* (12), 3754–3757. <https://doi.org/10.1002/anie.201409773>.
- (46) Becker, H. D. New Stable Phenoxy Radicals. Oxidation of Hydroxystilbenes. *J. Org. Chem.* **1969**, *34* (5), 1211–1215. <https://doi.org/10.1021/jo01257a006>.
- (47) Neumann, W. P.; Uzick, W.; Zarkadis, A. K. Sterically Hindered Free Radicals. 14. Substituent-Dependent Stabilization of Para-Substituted Triphenylmethyl Radicals. *J. Am. Chem. Soc.* **1986**, *108* (13), 3762–3770. <https://doi.org/10.1021/ja00273a034>.
- (48) Keylor, M. H.; Matsuura, B. S.; Griesser, M.; Chauvin, J.-P. R.; Harding, R. A.; Kirillova, M. S.; Zhu, X.; Fischer, O. J.; Pratt, D. A.; Stephenson, C. R. J. Synthesis of Resveratrol Tetramers via a Stereoconvergent Radical Equilibrium. *Science* **2016**, *354* (6317), 1260–1265. <https://doi.org/10.1126/science.aaj1597>.
- (49) Nicholson, W. Account of the New Electrical or Galvanic Apparatus of Sig. Alex. Volta, and Experiments Performed with the Same. *J. Nat. Philos. Chem. Arts* **1800**, *4*, 179.
- (50) Russell, C. Enterprise and electrolysis... <https://www.chemistryworld.com/news/enterprise-and-electrolysis--/3001445.article> (accessed Jan 14, 2020).
- (51) Faraday, M. Siebente Reihe von Experimental-Untersuchungen über Elektrizität. *Ann. Phys.* **1834**, *109* (23–30), 433–451. <https://doi.org/10.1002/andp.18341092307>.
- (52) Lund, H. A Century of Organic Electrochemistry. *J. Electrochem. Soc.* **2002**, *149* (4), S21. <https://doi.org/10.1149/1.1462037>.
- (53) Kolbe, H. Beobachtungen über die oxydirende Wirkung des Sauerstoffs, wenn derselbe mit Hülfe einer elektrischen Säule entwickelt wird. *J. Für Prakt. Chem.* **1847**, *41* (1), 137–139. <https://doi.org/10.1002/prac.18470410118>.
- (54) Hou, M.; Chen, L.; Guo, Z.; Dong, X.; Wang, Y.; Xia, Y. A Clean and Membrane-Free Chlor-Alkali Process with Decoupled Cl₂ and H₂/NaOH Production. *Nat. Commun.* **2018**, *9* (1), 1–8. <https://doi.org/10.1038/s41467-018-02877-x>.
- (55) Botte, G. G. Electrochemical Manufacturing in the Chemical Industry. *Electrochem. Soc. Interface* **2014**, *23* (3), 49–55. <https://doi.org/10.1149/2.F04143if>.
- (56) Möhle, S.; Zirbes, M.; Rodrigo, E.; Gieshoff, T.; Wiebe, A.; Waldvogel, S. R. Modern Electrochemical Aspects for the Synthesis of Value-Added Organic Products. *Angew. Chem. Int. Ed.* **2018**, *57* (21), 6018–6041. <https://doi.org/10.1002/anie.201712732>.

- (57) Yan, M.; Kawamata, Y.; Baran, P. S. Synthetic Organic Electrochemical Methods Since 2000: On the Verge of a Renaissance. *Chem. Rev.* **2017**. <https://doi.org/10.1021/acs.chemrev.7b00397>.
- (58) Shatskiy, A.; Lundberg, H.; Kärkäs, M. D. Organic Electrosynthesis: Applications in Complex Molecule Synthesis. *ChemElectroChem* **2019**, *6* (16), 4067–4092. <https://doi.org/10.1002/celec.201900435>.
- (59) Moeller, K. D. Synthetic Applications of Anodic Electrochemistry. *Tetrahedron* **2000**, *56* (49), 9527–9554. [https://doi.org/10.1016/S0040-4020\(00\)00840-1](https://doi.org/10.1016/S0040-4020(00)00840-1).
- (60) Sperry, J. B.; Wright, D. L. The Application of Cathodic Reductions and Anodic Oxidations in the Synthesis of Complex Molecules. *Chem. Soc. Rev.* **2006**, *35* (7), 605–621. <https://doi.org/10.1039/B512308A>.
- (61) Frontana-Urbe, B. A.; Little, R. D.; Ibanez, J. G.; Palma, A.; Vasquez-Medrano, R. Organic Electrosynthesis: A Promising Green Methodology in Organic Chemistry. *Green Chem.* **2010**, *12* (12), 2099–2119. <https://doi.org/10.1039/C0GC00382D>.
- (62) Wiebe, A.; Gieshoff, T.; Möhle, S.; Rodrigo, E.; Zirbes, M.; Waldvogel, S. R. Electrifying Organic Synthesis. *Angew. Chem. Int. Ed.* **2018**, *57* (20), 5594–5619. <https://doi.org/10.1002/anie.201711060>.
- (63) Moeller, K. D. Using Physical Organic Chemistry To Shape the Course of Electrochemical Reactions. *Chem. Rev.* **2018**, *118* (9), 4817–4833. <https://doi.org/10.1021/acs.chemrev.7b00656>.
- (64) Kingston, C.; Palkowitz, M. D.; Takahira, Y.; Vantourout, J. C.; Peters, B. K.; Kawamata, Y.; Baran, P. S. A Survival Guide for the “Electro-Curious.” *Acc. Chem. Res.* **2019**. <https://doi.org/10.1021/acs.accounts.9b00539>.
- (65) Corey, E. J.; Sauers, R. R. The Synthesis of Pentacyclosqualene (8,8'-Cycloönocerene) and the α - and β -Onoceradienes I. *J. Am. Chem. Soc.* **1959**, *81* (7), 1739–1743. <https://doi.org/10.1021/ja01516a054>.
- (66) Ruzicka, L.; Janot, M. M. Höhere Terpenverbindungen L. Zur Kenntnis Des Sclareols. *Helv. Chim. Acta* **1931**, *14* (1), 645–650. <https://doi.org/10.1002/hlca.19310140162>.
- (67) Shizuri, Y.; Okuno, Y.; Shigemori, H.; Yamamura, S. Efficient Synthesis of (\pm)-8,14-Cedranoxide Using Electrochemical Method as a Key Step. *Tetrahedron Lett.* **1987**, *28* (52), 6661–6664. [https://doi.org/10.1016/S0040-4039\(00\)96939-9](https://doi.org/10.1016/S0040-4039(00)96939-9).
- (68) Pfitzner, K. E.; Moffatt, J. G. A New and Selective Oxidation of Alcohols. *J. Am. Chem. Soc.* **1963**, *85* (19), 3027–3028. <https://doi.org/10.1021/ja00902a036>.
- (69) Vedejs, E.; Peterson, M. J. Stereochemistry and Mechanism in the Wittig Reaction. In *Topics in Stereochemistry*; John Wiley & Sons, Ltd, 2007; pp 1–157.
- (70) Moeller, K. D. Intramolecular Carbon-Carbon Bond Forming Reactions at the Anode. In *Electrochemistry VI Electroorganic Synthesis: Bond Formation at Anode and Cathode*; Steckhan, E., Ed.; Topics in Current Chemistry; Springer Berlin Heidelberg: Berlin, Heidelberg, 1997; pp 49–86.
- (71) Kam, T.-S.; Lim, T.-M.; Tan, G.-H. Electrochemical Oxidation of Aspidofractinine-Type Alkaloids: Formation of Kopsine, Kopsidine, Kopsinitarine and Bisindole Derivatives. *J. Chem. Soc. [Perkin 1]* **2001**, No. 14, 1594–1604. <https://doi.org/10.1039/B103962H>.

- (72) Elgrishi, N.; Rountree, K. J.; McCarthy, B. D.; Rountree, E. S.; Eisenhart, T. T.; Dempsey, J. L. A Practical Beginner's Guide to Cyclic Voltammetry. *J. Chem. Educ.* **2018**, *95* (2), 197–206. <https://doi.org/10.1021/acs.jchemed.7b00361>.
- (73) Kam, T.-S.; Yoganathan, K.; Chuah, C.-H.; Wei, C. Aspidofractinine Alkaloids from a New *Kopsia* Species. *Phytochemistry* **1993**, *32* (5), 1343–1346. [https://doi.org/10.1016/S0031-9422\(00\)95118-5](https://doi.org/10.1016/S0031-9422(00)95118-5).
- (74) Roth, H. G.; Romero, N. A.; Nicewicz, D. A. Experimental and Calculated Electrochemical Potentials of Common Organic Molecules for Applications to Single-Electron Redox Chemistry. *Synlett* **2016**, *27* (5), 714–723. <https://doi.org/10.1055/s-0035-1561297>.
- (75) Shono, T. Synthesis of Alkaloidal Compounds Using an Electrochemical Reaction as a Key Step. In *Electrochemistry III*; Stekchan, E., Ed.; Topics in Current Chemistry; Springer Berlin Heidelberg, 1988; pp 131–151.
- (76) Shankaraiah, N.; da Silva, W. A.; Andrade, C. K. Z.; Santos, L. S. Enantioselective Total Synthesis of (S)-(-)-Quinolactacin B. *Tetrahedron Lett.* **2008**, *49* (27), 4289–4291. <https://doi.org/10.1016/j.tetlet.2008.04.130>.
- (77) Louafi, F.; Moreau, J.; Shahane, S.; Golhen, S.; Roisnel, T.; Sinbandhit, S.; Hurvois, J.-P. Electrochemical Synthesis and Chemistry of Chiral 1-Cyanotetrahydroisoquinolines. An Approach to the Asymmetric Syntheses of the Alkaloid (-)-Crispine A and Its Natural (+)-Antipode. *J. Org. Chem.* **2011**, *76* (23), 9720–9732. <https://doi.org/10.1021/jo2017982>.
- (78) Mirabal-Gallardo, Y.; Piérola, J.; Shankaraiah, N.; Santos, L. S. Enantioselective Total Synthesis of (S)-(+)-Lennoxamine through Asymmetric Hydrogenation Mediated by L-Proline-Tetrazole Ruthenium Catalyst. *Tetrahedron Lett.* **2012**, *53* (28), 3672–3675. <https://doi.org/10.1016/j.tetlet.2012.05.033>.
- (79) Duan, S.; Moeller, K. D. Anodic Coupling Reactions: Probing the Stereochemistry of Tetrahydrofuran Formation. A Short, Convenient Synthesis of Linalool Oxide. *Org. Lett.* **2001**, *3* (17), 2685–2688. <https://doi.org/10.1021/ol0162670>.
- (80) Sutterer, A.; Moeller, K. D. Reversing the Polarity of Enol Ethers: An Anodic Route to Tetrahydrofuran and Tetrahydropyran Rings. *J. Am. Chem. Soc.* **2000**, *122* (23), 5636–5637. <https://doi.org/10.1021/ja001063k>.
- (81) Mihelcic, J.; Moeller, K. D. Oxidative Cyclizations: The Asymmetric Synthesis of (-)-Alliacol A. *J. Am. Chem. Soc.* **2004**, *126* (29), 9106–9111. <https://doi.org/10.1021/ja048085h>.
- (82) Garegg, P. J.; Johansson, R.; Ortega, C.; Samuelsson, B. Novel Reagent System for Converting a Hydroxy-Group into an Iodogroup in Carbohydrates with Inversion of Configuration. Part 3. *J. Chem. Soc. [Perkin 1]* **1982**, No. 0, 681–683. <https://doi.org/10.1039/P19820000681>.
- (83) Miller, A. K.; Hughes, C. C.; Kennedy-Smith, J. J.; Gradl, S. N.; Trauner, D. Total Synthesis of (-)-Heptemerone B and (-)-Guanacastepene E. *J. Am. Chem. Soc.* **2006**, *128* (51), 17057–17062. <https://doi.org/10.1021/ja0660507>.
- (84) Brown, H. C.; Chandrasekharan, J.; Ramachandran, P. V. Chiral Synthesis via Organoboranes. 14. Selective Reductions. 41. Diisopinocampheylchloroborane, an Exceptionally Efficient Chiral Reducing Agent. *J. Am. Chem. Soc.* **1988**, *110* (5), 1539–1546. <https://doi.org/10.1021/ja00213a030>.

- (85) Whitesell, J. K. Cyclohexyl-Based Chiral Auxiliaries. *Chem. Rev.* **1992**, *92* (5), 953–964. <https://doi.org/10.1021/cr00013a010>.
- (86) Dess, D. B.; Martin, J. C. Readily Accessible 12-I-5 Oxidant for the Conversion of Primary and Secondary Alcohols to Aldehydes and Ketones. *J. Org. Chem.* **1983**, *48* (22), 4155–4156. <https://doi.org/10.1021/jo00170a070>.
- (87) Vougioukalakis, G. C.; Grubbs, R. H. Ruthenium-Based Heterocyclic Carbene-Coordinated Olefin Metathesis Catalysts. *Chem. Rev.* **2010**, *110* (3), 1746–1787. <https://doi.org/10.1021/cr9002424>.
- (88) Rosen, B. R.; Werner, E. W.; O'Brien, A. G.; Baran, P. S. Total Synthesis of Dixiamycin B by Electrochemical Oxidation. *J. Am. Chem. Soc.* **2014**, *136* (15), 5571–5574. <https://doi.org/10.1021/ja5013323>.
- (89) Horn, E. J.; Rosen, B. R.; Chen, Y.; Tang, J.; Chen, K.; Eastgate, M. D.; Baran, P. S. Scalable and Sustainable Electrochemical Allylic C–H Oxidation. *Nature* **2016**, *533* (7601), 77–81. <https://doi.org/10.1038/nature17431>.
- (90) Vogt, T. Phenylpropanoid Biosynthesis. *Mol. Plant* **2010**, *3* (1), 2–20. <https://doi.org/10.1093/mp/ssp106>.
- (91) Quideau, S.; Deffieux, D.; Douat-Casassus, C.; Pouységu, L. Plant Polyphenols: Chemical Properties, Biological Activities, and Synthesis. *Angew. Chem. Int. Ed.* **2011**, *50* (3), 586–621. <https://doi.org/10.1002/anie.201000044>.
- (92) Li, W.; Li, H.; Li, Y.; Hou, Z. Total Synthesis of (±)-Quadrangularin A. *Angew. Chem. Int. Ed.* **2006**, *45* (45), 7609–7611. <https://doi.org/10.1002/anie.200603097>.
- (93) Li, W.; Li, H.; Luo, Y.; Yang, Y.; Wang, N. Biosynthesis of Resveratrol Dimers by Regioselective Oxidative Coupling Reaction. *Synlett* **2010**, *8*, 1247–1250. <https://doi.org/10.1055/s-0029-1219787>.
- (94) Li, W.; Dong, T.; Chen, P.; Liu, X.; Liu, M.; Han, X. Concise Synthesis of Several Oligostilbenes from the Enzyme-Promoted Oxidation of Brominated Resveratrol. *Tetrahedron* **2017**, *73* (21), 3056–3065. <https://doi.org/10.1016/j.tet.2017.04.021>.
- (95) Hong, F.-J.; Low, Y.-Y.; Chong, K.-W.; Thomas, N. F.; Kam, T.-S. Biomimetic Oxidative Dimerization of Anodically Generated Stilbene Radical Cations: Effect of Aromatic Substitution on Product Distribution and Reaction Pathways. *J. Org. Chem.* **2014**, *79* (10), 4528–4543. <https://doi.org/10.1021/jo500559r>.
- (96) Chong, K.-W.; Hong, F.-J.; Thomas, N. F.; Low, Y.-Y.; Kam, T.-S. Electrochemically Mediated Oxidative Transformations of Substituted 4-Methoxystilbenes: Effect of Ortho-Substituted Nucleophilic Groups. *J. Org. Chem.* **2017**, *82* (12), 6172–6191. <https://doi.org/10.1021/acs.joc.7b00753>.
- (97) Corduneanu, O.; Janeiro, P.; Brett, A. M. O. On the Electrochemical Oxidation of Resveratrol. *Electroanalysis* **2006**, *18* (8), 757–762. <https://doi.org/10.1002/elan.200503469>.
- (98) Romero, K. J.; Galliher, M. S.; Raycroft, M. A. R.; Chauvin, J.-P. R.; Bosque, I.; Pratt, D. A.; Stephenson, C. R. J. Electrochemical Dimerization of Phenylpropenoids and the Surprising Antioxidant Activity of the Resultant Quinone Methide Dimers. *Angew. Chem. Int. Ed.* **2018**, *57* (52), 17125–17129. <https://doi.org/10.1002/anie.201810870>.
- (99) Connelly, N. G.; Geiger, W. E. Chemical Redox Agents for Organometallic Chemistry. *Chem. Rev.* **1996**, *96* (2), 877–910. <https://doi.org/10.1021/cr940053x>.

- (100) Wittig, G.; Schöllkopf, U. Über Triphenyl-phosphin-methylene als olefinbildende Reagenzien (I. Mitteil. *Chem. Ber.* **1954**, *87* (9), 1318–1330. <https://doi.org/10.1002/cber.19540870919>.
- (101) Tucker, J. W.; Narayanam, J. M. R.; Shah, P. S.; Stephenson, C. R. J. Oxidative Photoredox Catalysis: Mild and Selective Deprotection of PMB Ethers Mediated by Visible Light. *Chem. Commun.* **2011**, *47* (17), 5040–5042. <https://doi.org/10.1039/C1CC10827A>.
- (102) Baur, J. A.; Sinclair, D. A. Therapeutic Potential of Resveratrol: The in Vivo Evidence. *Nat. Rev. Drug Discov.* **2006**, *5* (6), 493–506. <https://doi.org/10.1038/nrd2060>.
- (103) Luque-Contreras, D.; Carvajal, K.; Toral-Rios, D.; Franco-Bocanegra, D.; Campos-Peña, V. Oxidative Stress and Metabolic Syndrome: Cause or Consequence of Alzheimer's Disease? <https://new.hindawi.com/journals/omcl/2014/497802/> (accessed Jan 18, 2020).
- (104) Ingold, K. U.; Pratt, D. A. Advances in Radical-Trapping Antioxidant Chemistry in the 21st Century: A Kinetics and Mechanisms Perspective. *Chem. Rev.* **2014**, *114* (18), 9022–9046. <https://doi.org/10.1021/cr500226n>.
- (105) Porter, N. A. Mechanisms for the Autoxidation of Polyunsaturated Lipids. *Acc. Chem. Res.* **1986**, *19* (9), 262–268. <https://doi.org/10.1021/ar00129a001>.
- (106) Yin, H.; Xu, L.; Porter, N. A. Free Radical Lipid Peroxidation: Mechanisms and Analysis. *Chem. Rev.* **2011**, *111* (10), 5944–5972. <https://doi.org/10.1021/cr200084z>.
- (107) Roschek, B.; Tallman, K. A.; Rector, C. L.; Gillmore, J. G.; Pratt, D. A.; Punta, C.; Porter, N. A. Peroxyl Radical Clocks. *J. Org. Chem.* **2006**, *71* (9), 3527–3532. <https://doi.org/10.1021/jo0601462>.
- (108) Pratt, D. A.; Tallman, K. A.; Porter, N. A. Free Radical Oxidation of Polyunsaturated Lipids: New Mechanistic Insights and the Development of Peroxyl Radical Clocks. *Acc. Chem. Res.* **2011**, *44* (6), 458–467. <https://doi.org/10.1021/ar200024c>.
- (109) Burton, G. W.; Ingold, K. U. Vitamin E: Application of the Principles of Physical Organic Chemistry to the Exploration of Its Structure and Function. *Acc. Chem. Res.* **1986**, *19* (7), 194–201. <https://doi.org/10.1021/ar00127a001>.
- (110) Krumova, K.; Friedland, S.; Cosa, G. How Lipid Unsaturation, Peroxyl Radical Partitioning, and Chromanol Lipophilic Tail Affect the Antioxidant Activity of α -Tocopherol: Direct Visualization via High-Throughput Fluorescence Studies Conducted with Fluorogenic α -Tocopherol Analogues. *J. Am. Chem. Soc.* **2012**, *134* (24), 10102–10113. <https://doi.org/10.1021/ja301680m>.
- (111) Li, B.; Harjani, J. R.; Cormier, N. S.; Madarati, H.; Atkinson, J.; Cosa, G.; Pratt, D. A. Besting Vitamin E: Sidechain Substitution Is Key to the Reactivity of Naphthyridinol Antioxidants in Lipid Bilayers. *J. Am. Chem. Soc.* **2013**, *135* (4), 1394–1405. <https://doi.org/10.1021/ja309153x>.
- (112) Haidasz, E. A.; Van Kessel, A. T. M.; Pratt, D. A. A Continuous Visible Light Spectrophotometric Approach To Accurately Determine the Reactivity of Radical-Trapping Antioxidants. *J. Org. Chem.* **2016**, *81* (3), 737–744. <https://doi.org/10.1021/acs.joc.5b02183>.
- (113) Zolotova, N. V.; Denisov, Y. T.; Volod'kin, A. A.; Yershov, V. V.; Galiyeva, F. A. Kinetic Characteristics of Methylene Quinones as Inhibitors of Polypropylene

- Oxidation. *Polym. Sci. USSR* **1981**, 23 (1), 163–168. [https://doi.org/10.1016/0032-3950\(81\)90310-5](https://doi.org/10.1016/0032-3950(81)90310-5).
- (114) Zavitsas, A. A.; Chatgialoglu, C. Energies of Activation. The Paradigm of Hydrogen Abstractions by Radicals. *J. Am. Chem. Soc.* **1995**, 117 (43), 10645–10654. <https://doi.org/10.1021/ja00148a006>.
- (115) Montgomery, J. A.; Frisch, M. J.; Ochterski, J. W.; Petersson, G. A. A Complete Basis Set Model Chemistry. VI. Use of Density Functional Geometries and Frequencies. *J. Chem. Phys.* **1999**, 110 (6), 2822–2827. <https://doi.org/10.1063/1.477924>.
- (116) Jonsson, M.; Lind, J.; Reitberger, T.; Eriksen, T. E.; Merenyi, G. Free Radical Combination Reactions Involving Phenoxy Radicals. *J. Phys. Chem.* **1993**, 97 (31), 8229–8233. <https://doi.org/10.1021/j100133a018>.
- (117) Bosque, I.; Magallanes, G.; Rigoulet, M.; Kärkäs, M. D.; Stephenson, C. R. J. Redox Catalysis Facilitates Lignin Depolymerization. *ACS Cent. Sci.* **2017**, 3 (6), 621–628. <https://doi.org/10.1021/acscentsci.7b00140>.
- (118) Bazin, M.-A.; Kihel, L. E.; Jouanne, M.; Lancelot, J.-C.; Rault, S. Synthesis of New Avenalamic Carboxamide Derivatives in the Ferulic Series. *Synth. Commun.* **2008**, 38 (22), 3947–3959. <https://doi.org/10.1080/00397910802238817>.
- (119) Yang, L. X.; Huang, K. X.; Li, H. B.; Gong, J. X.; Wang, F.; Feng, Y. B.; Tao, Q. F.; Wu, Y. H.; Li, X. K.; Wu, X. M.; Zeng, S.; Spencer, S.; Zhao, Y.; Qu, J. Design, Synthesis, and Examination of Neuron Protective Properties of Alkenylated and Amidated Dehydro-Silybin Derivatives. *J. Med. Chem.* **2009**, 52 (23), 7732–7752. <https://doi.org/10.1021/jm900735p>.
- (120) Previtiera, L.; Della Greca, M.; Molinaro, A.; Monaco, P. Dihydrobenzofuran Neolignans from *Arum Italicum*. *HETEROCYCLES* **1994**, 38 (5), 1099. <https://doi.org/10.3987/COM-94-6681>.
- (121) Chauvin, J.-P. R.; Griesser, M.; Pratt, D. A. Hydropersulfides: H-Atom Transfer Agents Par Excellence. *J. Am. Chem. Soc.* **2017**, 139 (18), 6484–6493. <https://doi.org/10.1021/jacs.7b02571>.
- (122) Burton, G. W.; Doba, T.; Gabe, E.; Hughes, L.; Lee, F. L.; Prasad, L.; Ingold, K. U. Autoxidation of Biological Molecules. 4. Maximizing the Antioxidant Activity of Phenols. *J. Am. Chem. Soc.* **1985**, 107 (24), 7053–7065. <https://doi.org/10.1021/ja00310a049>.
- (123) Siemann, E. H.; Creasy, L. L. Concentration of the Phytoalexin Resveratrol in Wine. *Am. J. Enol. Vitic.* **1992**, 43 (1), 49–52.
- (124) 進野々村; 宏加奈川; 有浩牧本. タデ科植物成分の研究 (第1報). *YAKUGAKU ZASSHI* **1963**, 83 (10), 988–990. https://doi.org/10.1248/yakushi1947.83.10_988.
- (125) Renaud, S.; de Lorgeril, M. Wine, Alcohol, Platelets, and the French Paradox for Coronary Heart Disease. *The Lancet* **1992**, 339 (8808), 1523–1526. [https://doi.org/10.1016/0140-6736\(92\)91277-F](https://doi.org/10.1016/0140-6736(92)91277-F).
- (126) Law, M.; Stampfer, M.; Barker, D. J. P.; Mackenbach, J. P.; Wald, N.; Rimm, E.; Kunst, A. E. Why Heart Disease Mortality Is Low in France: The Time Lag explanationCommentary: Alcohol and Other Dietary Factors May Be importantCommentary: Intrauterine Nutrition May Be importantCommentary: Heterogeneity of Populations Should Be Taken into accountAuthors' Response. *BMJ* **1999**, 318 (7196), 1471–1480. <https://doi.org/10.1136/bmj.318.7196.1471>.

- (127) Fuchs, F. D.; Chambless, L. E. Is the Cardioprotective Effect of Alcohol Real? *Alcohol* **2007**, *41* (6), 399–402. <https://doi.org/10.1016/j.alcohol.2007.05.004>.
- (128) He, S.; Yan, X. From Resveratrol to Its Derivatives: New Sources of Natural Antioxidant. *Curr. Med. Chem.* **2013**, *20* (8), 1005–1017.
- (129) Milne, J. C.; Lambert, P. D.; Schenk, S.; Carney, D. P.; Smith, J. J.; Gagne, D. J.; Jin, L.; Boss, O.; Perni, R. B.; Vu, C. B.; Bemis, J. E.; Xie, R.; Disch, J. S.; Ng, P. Y.; Nunes, J. J.; Lynch, A. V.; Yang, H.; Galonek, H.; Israelian, K.; Choy, W.; Iffland, A.; Lavu, S.; Medvedik, O.; Sinclair, D. A.; Olefsky, J. M.; Jirousek, M. R.; Elliott, P. J.; Westphal, C. H. Small Molecule Activators of SIRT1 as Therapeutics for the Treatment of Type 2 Diabetes. *Nature* **2007**, *450* (7170), 712–716. <https://doi.org/10.1038/nature06261>.
- (130) Banks, A. S.; Kon, N.; Knight, C.; Matsumoto, M.; Gutiérrez-Juárez, R.; Rossetti, L.; Gu, W.; Accili, D. SirT1 Gain of Function Increases Energy Efficiency and Prevents Diabetes in Mice. *Cell Metab.* **2008**, *8* (4), 333–341. <https://doi.org/10.1016/j.cmet.2008.08.014>.
- (131) Jang, M.; Cai, L.; Udeani, G. O.; Slowing, K. V.; Thomas, C. F.; Beecher, C. W. W.; Fong, H. H. S.; Farnsworth, N. R.; Kinghorn, A. D.; Mehta, R. G.; Moon, R. C.; Pezzuto, J. M. Cancer Chemopreventive Activity of Resveratrol, a Natural Product Derived from Grapes. *Science* **1997**, *275* (5297), 218–220. <https://doi.org/10.1126/science.275.5297.218>.
- (132) Aggarwal, B. B.; Bhardwaj, A.; Aggarwal, R. S.; Seeram, N. P.; Shishodia, S.; Takada, Y. Role of Resveratrol in Prevention and Therapy of Cancer: Preclinical and Clinical Studies. *Anticancer Res.* **2004**, *24* (5A), 2783–2840.
- (133) Frémont, L. Biological Effects of Resveratrol. *Life Sci.* **2000**, *66* (8), 663–673. [https://doi.org/10.1016/S0024-3205\(99\)00410-5](https://doi.org/10.1016/S0024-3205(99)00410-5).
- (134) Harikumar, K. B.; Aggarwal, B. B. Resveratrol: A Multitargeted Agent for Age-Associated Chronic Diseases. *Cell Cycle* **2008**, *7* (8), 1020–1035. <https://doi.org/10.4161/cc.7.8.5740>.
- (135) Vang, O.; Ahmad, N.; Baile, C. A.; Baur, J. A.; Brown, K.; Csiszar, A.; Das, D. K.; Delmas, D.; Gottfried, C.; Lin, H.-Y.; Ma, Q.-Y.; Mukhopadhyay, P.; Nalini, N.; Pezzuto, J. M.; Richard, T.; Shukla, Y.; Surh, Y.-J.; Szekeres, T.; Szkudelski, T.; Walle, T.; Wu, J. M. What Is New for an Old Molecule? Systematic Review and Recommendations on the Use of Resveratrol. *PLOS ONE* **2011**, *6* (6), e19881. <https://doi.org/10.1371/journal.pone.0019881>.
- (136) Singh, A. P.; Singh, R.; Verma, S. S.; Rai, V.; Kaschula, C. H.; Maiti, P.; Gupta, S. C. Health Benefits of Resveratrol: Evidence from Clinical Studies. *Med. Res. Rev.* **2019**, *39* (5), 1851–1891. <https://doi.org/10.1002/med.21565>.
- (137) Berman, A. Y.; Motechin, R. A.; Wiesenfeld, M. Y.; Holz, M. K. The Therapeutic Potential of Resveratrol: A Review of Clinical Trials. *NPJ Precis. Oncol.* **2017**, *1*. <https://doi.org/10.1038/s41698-017-0038-6>.
- (138) Langcake, P.; Pryce, R. J. The Production of Resveratrol by *Vitis Vinifera* and Other Members of the Vitaceae as a Response to Infection or Injury. *Physiol. Plant Pathol.* **1976**, *9* (1), 77–86. [https://doi.org/10.1016/0048-4059\(76\)90077-1](https://doi.org/10.1016/0048-4059(76)90077-1).
- (139) Langcake, P.; McCarthy, W. V. The Relationship of Resveratrol Production to Infection of Grapevine Leaves by *Botrytis Cinerea*. *VITIS - J. Grapevine Res.* **1979**, *18* (3), 244–244.

- (140) Langcake, P. Disease Resistance of *Vitis* Spp. and the Production of the Stress Metabolites Resveratrol, ϵ -Viniferin, α -Viniferin and Pterostilbene. *Physiol. Plant Pathol.* **1981**, *18* (2), 213–226. [https://doi.org/10.1016/S0048-4059\(81\)80043-4](https://doi.org/10.1016/S0048-4059(81)80043-4).
- (141) Coggon, P.; King, T. J.; Wallwork, S. C. The Structure of Hopeaphenol. *Chem. Commun. Lond.* **1966**, No. 13, 439–440. <https://doi.org/10.1039/C19660000439>.
- (142) Aiba, C. J.; Corrêa, R. G. C.; Gottlieb, O. R. Natural Occurrence of Erdtman's Dehydrodiisoeugenol. *Phytochemistry* **1973**, *12* (5), 1163–1164. [https://doi.org/10.1016/0031-9422\(73\)85034-4](https://doi.org/10.1016/0031-9422(73)85034-4).
- (143) Langcake, P.; Pryce, R. J. Oxidative Dimerisation of 4-Hydroxystilbenes in Vitro: Production of a Grapevine Phytoalexin Mimic. *J. Chem. Soc. Chem. Commun.* **1977**, No. 7, 208–210. <https://doi.org/10.1039/C39770000208>.
- (144) Langcake, P.; Pryce, R. J. A New Class of Phytoalexins from Grapevines. *Experientia* **1977**, *33* (2), 151–152. <https://doi.org/10.1007/BF02124034>.
- (145) Davin, L. B.; Bedgar, D. L.; Katayama, T.; Lewis, N. G. On the Stereoselective Synthesis of (+)-Pinoresinol in *Forsythia Suspensa* from Its Achiral Precursor, Coniferyl Alcohol. *Phytochemistry* **1992**, *31* (11), 3869–3874. [https://doi.org/10.1016/S0031-9422\(00\)97544-7](https://doi.org/10.1016/S0031-9422(00)97544-7).
- (146) Davin, L. B.; Wang, H.-B.; Crowell, A. L.; Bedgar, D. L.; Martin, D. M.; Sarkanen, S.; Lewis, N. G. Stereoselective Bimolecular Phenoxy Radical Coupling by an Auxiliary (Dirigent) Protein Without an Active Center. *Science* **1997**, *275* (5298), 362–367. <https://doi.org/10.1126/science.275.5298.362>.
- (147) Kim, K.-W.; Smith, C. A.; Daily, M. D.; Cort, J. R.; Davin, L. B.; Lewis, N. G. Trimeric Structure of (+)-Pinoresinol-Forming Dirigent Protein at 1.95 Å Resolution with Three Isolated Active Sites. *J. Biol. Chem.* **2015**, *290* (3), 1308–1318. <https://doi.org/10.1074/jbc.M114.611780>.
- (148) Pickel, B.; Constantin, M.-A.; Pfannstiel, J.; Conrad, J.; Beifuss, U.; Schaller, A. An Enantiocomplementary Dirigent Protein for the Enantioselective Laccase-Catalyzed Oxidative Coupling of Phenols. *Angew. Chem. Int. Ed.* **2010**, *49* (1), 202–204. <https://doi.org/10.1002/anie.200904622>.
- (149) Robinson, R. LXIII.—A Synthesis of Tropinone. *J. Chem. Soc. Trans.* **1917**, *111* (0), 762–768. <https://doi.org/10.1039/CT9171100762>.
- (150) Nicolaou, K. C.; Vourloumis, D.; Winssinger, N.; Baran, P. S. The Art and Science of Total Synthesis at the Dawn of the Twenty-First Century. *Angew. Chem. Int. Ed.* **2000**, *39* (1), 44–122. [https://doi.org/10.1002/\(SICI\)1521-3773\(20000103\)39:1<44::AID-ANIE44>3.0.CO;2-L](https://doi.org/10.1002/(SICI)1521-3773(20000103)39:1<44::AID-ANIE44>3.0.CO;2-L).
- (151) Robinson, R. LXXV.—A Theory of the Mechanism of the Phytochemical Synthesis of Certain Alkaloids. *J. Chem. Soc. Trans.* **1917**, *111* (0), 876–899. <https://doi.org/10.1039/CT9171100876>.
- (152) Fan, G.-J.; Liu, X.-D.; Qian, Y.-P.; Shang, Y.-J.; Li, X.-Z.; Dai, F.; Fang, J.-G.; Jin, X.-L.; Zhou, B. 4,4'-Dihydroxy-Trans-Stilbene, a Resveratrol Analogue, Exhibited Enhanced Antioxidant Activity and Cytotoxicity. *Bioorg. Med. Chem.* **2009**, *17* (6), 2360–2365. <https://doi.org/10.1016/j.bmc.2009.02.014>.
- (153) Wang, M.; Jin, Y.; Ho, C.-T. Evaluation of Resveratrol Derivatives as Potential Antioxidants and Identification of a Reaction Product of Resveratrol and 2,2-Diphenyl-1-Picrylhydrazyl Radical. *J. Agric. Food Chem.* **1999**, *47* (10), 3974–3977. <https://doi.org/10.1021/jf990382w>.

- (154) Takaya, Y.; Terashima, K.; Ito, J.; He, Y.-H.; Tateoka, M.; Yamaguchi, N.; Niwa, M. Biomimic Transformation of Resveratrol. *Tetrahedron* **2005**, *61* (43), 10285–10290. <https://doi.org/10.1016/j.tet.2005.08.023>.
- (155) Nicotra, S.; Cramarossa, M. R.; Mucci, A.; Pagnoni, U. M.; Riva, S.; Forti, L. Biotransformation of Resveratrol: Synthesis of Trans-Dehydrodimers Catalyzed by Laccases from Myceliophthora Thermophyla and from Trametes Pubescens. *Tetrahedron* **2004**, *60* (3), 595–600. <https://doi.org/10.1016/j.tet.2003.10.117>.
- (156) Shang, Y.-J.; Qian, Y.-P.; Liu, X.-D.; Dai, F.; Shang, X.-L.; Jia, W.-Q.; Liu, Q.; Fang, J.-G.; Zhou, B. Radical-Scavenging Activity and Mechanism of Resveratrol-Oriented Analogues: Influence of the Solvent, Radical, and Substitution. *J. Org. Chem.* **2009**, *74* (14), 5025–5031. <https://doi.org/10.1021/jo9007095>.
- (157) Song, T.; Zhou, B.; Peng, G.-W.; Zhang, Q.-B.; Wu, L.-Z.; Liu, Q.; Wang, Y. Aerobic Oxidative Coupling of Resveratrol and Its Analogues by Visible Light Using Mesoporous Graphitic Carbon Nitride (Mpg-C₃N₄) as a Bioinspired Catalyst. *Chem. – Eur. J.* **2014**, *20* (3), 678–682. <https://doi.org/10.1002/chem.201303587>.
- (158) Sako, M.; Hosokawa, H.; Ito, T.; Inuma, M. Regioselective Oxidative Coupling of 4-Hydroxystilbenes: Synthesis of Resveratrol and ϵ -Viniferin (E)-Dehydrodimers. *J. Org. Chem.* **2004**, *69* (7), 2598–2600. <https://doi.org/10.1021/jo035791c>.
- (159) Li, C.; Lu, J.; Xu, X.; Hu, R.; Pan, Y. pH-Switched HRP-Catalyzed Dimerization of Resveratrol: A Selective Biomimetic Synthesis. *Green Chem.* **2012**, *14* (12), 3281–3284. <https://doi.org/10.1039/C2GC36288K>.
- (160) Sarkanen, K. V.; Wallis, A. F. A. Oxidative Dimerizations of (E)- and (Z)-Isoeugenol (2-Methoxy-4-pro-Penylphenol) and (E)- and (Z)-2,6-Dimethoxy-4-Propenylphenol. *J. Chem. Soc. [Perkin 1]* **1973**, No. 0, 1869–1878. <https://doi.org/10.1039/P19730001869>.
- (161) Ponzoni, C.; Beneventi, E.; Cramarossa, M. R.; Raimondi, S.; Trevisi, G.; Pagnoni, U. M.; Riva, S.; Forti, L. Laccase-Catalyzed Dimerization of Hydroxystilbenes. *Adv. Synth. Catal.* **2007**, *349* (8–9), 1497–1506. <https://doi.org/10.1002/adsc.200700043>.
- (162) Jeandet, P.; Sobarzo-Sánchez, E.; Silva, A. S.; Clément, C.; Nabavi, S. F.; Battino, M.; Rasekhian, M.; Belwal, T.; Habtemariam, S.; Koffas, M.; Nabavi, S. M. Whole-Cell Biocatalytic, Enzymatic and Green Chemistry Methods for the Production of Resveratrol and Its Derivatives. *Biotechnol. Adv.* **2019**, 107461. <https://doi.org/10.1016/j.biotechadv.2019.107461>.
- (163) Yao, C.-S.; Lin, M.; Wang, Y.-H. Synthesis of the Active Stilbenoids by Photooxidation Reaction of Trans- ϵ -Viniferin. *Chin. J. Chem.* **2004**, *22* (11), 1350–1355. <https://doi.org/10.1002/cjoc.20040221127>.
- (164) Pezet, R. Purification and Characterization of a 32-kDa Laccase-like Stilbene Oxidase Produced by Botrytis Cinerea Pers.:Fr. *FEMS Microbiol. Lett.* **1998**, *167* (2), 203–208. <https://doi.org/10.1111/j.1574-6968.1998.tb13229.x>.
- (165) Huffman, M. A.; Fryszkowska, A.; Alvizo, O.; Borra-Garske, M.; Campos, K. R.; Canada, K. A.; Devine, P. N.; Duan, D.; Forstater, J. H.; Grosser, S. T.; Halsey, H. M.; Hughes, G. J.; Jo, J.; Joyce, L. A.; Kolev, J. N.; Liang, J.; Maloney, K. M.; Mann, B. F.; Marshall, N. M.; McLaughlin, M.; Moore, J. C.; Murphy, G. S.; Nawrat, C. C.; Nazor, J.; Novick, S.; Patel, N. R.; Rodriguez-Granillo, A.; Robaire, S. A.; Sherer, E. C.; Truppo, M. D.; Whittaker, A. M.; Verma, D.; Xiao, L.; Xu, Y.; Yang, H. Design

- of an in Vitro Biocatalytic Cascade for the Manufacture of Islatravir. *Science* **2019**, *366* (6470), 1255–1259. <https://doi.org/10.1126/science.aay8484>.
- (166) Müller, E.; Mayer, R.; Spanagel, H.-D.; Scheffler, K. über Sauerstoffradikale, XIX. Dehydrierung hydroxyphenyl-substituierter äthylene. *Justus Liebigs Ann. Chem.* **1961**, *645* (1), 53–65. <https://doi.org/10.1002/jlac.19616450106>.
- (167) Sarkanen, K. V.; Wallis, A. F. A. Oxidative Dimerization of Methyl (E)-4-Hydroxy-3,5-Di-T-Butylcinnamate with Potassium Ferricyanide. *J. Chem. Soc. [Perkin 1]* **1973**, No. 0, 1878–1881. <https://doi.org/10.1039/P19730001878>.
- (168) Velu, S. S.; Buniyamin, I.; Ching, L. K.; Feroz, F.; Noorbacha, I.; Gee, L. C.; Awang, K.; Wahab, I. A.; Weber, J.-F. F. Regio- and Stereoselective Biomimetic Synthesis of Oligostilbenoid Dimers from Resveratrol Analogues: Influence of the Solvent, Oxidant, and Substitution. *Chem. – Eur. J.* **2008**, *14* (36), 11376–11384. <https://doi.org/10.1002/chem.200801575>.
- (169) Yang, Y.; Liu, Q.; Chen, P.; Li, W. FeCl₃·6H₂O Oxidation of Protected Resveratrol for the Synthesis of Tetraarylfuran-Type Oligostilbenes. *Tetrahedron Lett.* **2014**, *55* (32), 4455–4457. <https://doi.org/10.1016/j.tetlet.2014.06.046>.
- (170) Liu, M.; Dong, T.; Guan, X.; Shao, Z.; Li, W. Regioselective Biomimetic Oxidation of Halogenated Resveratrol for the Synthesis of (±)-ε-Viniferin and Its Analogues. *Tetrahedron* **2018**, *74* (29), 4013–4019. <https://doi.org/10.1016/j.tet.2018.06.005>.
- (171) Snyder, S. A.; Zografos, A. L.; Lin, Y. Total Synthesis of Resveratrol-Based Natural Products: A Chemoselective Solution. *Angew. Chem. Int. Ed.* **2007**, *46* (43), 8186–8191. <https://doi.org/10.1002/anie.200703333>.
- (172) Taylor, R. J. K. Recent Developments in Ramberg–Bäcklund and Episulfone Chemistry. *Chem. Commun.* **1999**, No. 3, 217–227. <https://doi.org/10.1039/A806615I>.
- (173) Meyers, C. Y.; Malte, A. M.; Matthews, W. S. Ionic Reactions of Carbon Tetrachloride. Survey of Reactions with Ketones, Alcohols, and Sulfones. *J. Am. Chem. Soc.* **1969**, *91* (26), 7510–7512. <https://doi.org/10.1021/ja01054a049>.
- (174) Brown, R. S. Investigation of the Early Steps in Electrophilic Bromination through the Study of the Reaction with Sterically Encumbered Olefins. *Acc. Chem. Res.* **1997**, *30* (3), 131–137. <https://doi.org/10.1021/ar960088e>.
- (175) Rodebaugh, R.; Fraser-Reid, B. Evidence for Cyclic Bromonium Ion Transfer in Electrophilic Bromination of Alkenes: Reaction of ω-Alkenyl Glycosides with Aqueous N-Bromosuccinimide. *Tetrahedron* **1996**, *52* (22), 7663–7678. [https://doi.org/10.1016/S0040-4020\(96\)00349-3](https://doi.org/10.1016/S0040-4020(96)00349-3).
- (176) Nicolaou, K. C.; Wu, T. R.; Kang, Q.; Chen, D. Y.-K. Total Synthesis of Hopeahainol A and Hopeanol. *Angew. Chem. Int. Ed.* **2009**, *48* (19), 3440–3443. <https://doi.org/10.1002/anie.200900438>.
- (177) Sheehan, J. C.; Hess, G. P. A New Method of Forming Peptide Bonds. *J. Am. Chem. Soc.* **1955**, *77* (4), 1067–1068. <https://doi.org/10.1021/ja01609a099>.
- (178) Frigerio, M.; Santagostino, M.; Sputore, S. A User-Friendly Entry to 2-Iodoxybenzoic Acid (IBX). *J. Org. Chem.* **1999**, *64* (12), 4537–4538. <https://doi.org/10.1021/jo9824596>.
- (179) Hirao, A.; Itsuno, S.; Nakahama, S.; Yamazaki, N. Asymmetric Reduction of Aromatic Ketones with Chiral Alkoxy-Amineborane Complexes. *J. Chem. Soc. Chem. Commun.* **1981**, No. 7, 315–317. <https://doi.org/10.1039/C39810000315>.

- (180) Corey, E. J.; Bakshi, R. K.; Shibata, S. Highly Enantioselective Borane Reduction of Ketones Catalyzed by Chiral Oxazaborolidines. Mechanism and Synthetic Implications. *J. Am. Chem. Soc.* **1987**, *109* (18), 5551–5553. <https://doi.org/10.1021/ja00252a056>.
- (181) Nicolaou, K. C.; Kang, Q.; Wu, T. R.; Lim, C. S.; Chen, D. Y.-K. Total Synthesis and Biological Evaluation of the Resveratrol-Derived Polyphenol Natural Products Hopeanol and Hopeahainol A. *J. Am. Chem. Soc.* **2010**, *132* (21), 7540–7548. <https://doi.org/10.1021/ja102623j>.
- (182) Ge, H. M.; Xu, C.; Wang, X. T.; Huang, B.; Tan, R. X. Hopeanol: A Potent Cytotoxin with A Novel Skeleton from *Hopea exalata*. *Eur. J. Org. Chem.* **2006**, *2006* (24), 5551–5554. <https://doi.org/10.1002/ejoc.200600661>.
- (183) Ge, H. M.; Zhu, C. H.; Shi, D. H.; Zhang, L. D.; Xie, D. Q.; Yang, J.; Ng, S. W.; Tan, R. X. Hopeahainol A: An Acetylcholinesterase Inhibitor from *Hopea hainanensis*. *Chem. – Eur. J.* **2008**, *14* (1), 376–381. <https://doi.org/10.1002/chem.200700960>.
- (184) Snyder, S. A.; Thomas, S. B.; Mayer, A. C.; Breazzano, S. P. Total Syntheses of Hopeanol and Hopeahainol A Empowered by a Chiral Brønsted Acid Induced Pinacol Rearrangement. *Angew. Chem. Int. Ed.* **2012**, *51* (17), 4080–4084. <https://doi.org/10.1002/anie.201107730>.
- (185) Johnson, A. W.; LaCount, R. B. The Chemistry of Ylids. VI. Dimethylsulfonium Fluorenylide—A Synthesis of Epoxides1. *J. Am. Chem. Soc.* **1961**, *83* (2), 417–423. <https://doi.org/10.1021/ja01463a040>.
- (186) Corey, E. J.; Chaykovsky, M. Dimethyloxosulfonium Methylide ((CH₃)₂SOCH₂) and Dimethylsulfonium Methylide ((CH₃)₂SCH₂). Formation and Application to Organic Synthesis. *J. Am. Chem. Soc.* **1965**, *87* (6), 1353–1364. <https://doi.org/10.1021/ja01084a034>.
- (187) Rickborn, B. 3.2 - The Pinacol Rearrangement. In *Comprehensive Organic Synthesis*; Trost, B. M., Fleming, I., Eds.; Pergamon: Oxford, 1991; pp 721–732.
- (188) Bal, B. S.; Childers, W. E.; Pinnick, H. W. Oxidation of α,β -Unsaturated Aldehydes. *Tetrahedron* **1981**, *37* (11), 2091–2096. [https://doi.org/10.1016/S0040-4020\(01\)97963-3](https://doi.org/10.1016/S0040-4020(01)97963-3).
- (189) Lindgren, B. O.; Nilsson, T.; Husebye, S.; Mikalsen, Ø.; Leander, K.; Swahn, C.-G. Preparation of Carboxylic Acids from Aldehydes (Including Hydroxylated Benzaldehydes) by Oxidation with Chlorite. *Acta Chem. Scand.* **1973**, *27*, 888–890. <https://doi.org/10.3891/acta.chem.scand.27-0888>.
- (190) Snyder, S. A.; Wright, N. E.; Pflueger, J. J.; Breazzano, S. P. Total Syntheses of Heimiol A, Hopeahainol D, and Constrained Analogues. *Angew. Chem. Int. Ed.* **2011**, *50* (37), 8629–8633. <https://doi.org/10.1002/anie.201103575>.
- (191) Meinwald, J.; Labana, S. S.; Chadha, M. S. Peracid Reactions. III.1 The Oxidation of Bicyclo [2.2.1]heptadiene2. *J. Am. Chem. Soc.* **1963**, *85* (5), 582–585. <https://doi.org/10.1021/ja00888a022>.
- (192) Lewis, M. D.; Cha, J. K.; Kishi, Y. Highly Stereoselective Approaches to α - and β -C-Glycopyranosides. *J. Am. Chem. Soc.* **1982**, *104* (18), 4976–4978. <https://doi.org/10.1021/ja00382a053>.
- (193) Chen, D. Y.-K.; Kang, Q.; Wu, T. R. Modular Synthesis of Polyphenolic Benzofurans, and Application in the Total Synthesis of Malibatol A and

- Shoreaphenol. *Molecules* **2010**, *15* (9), 5909–5927. <https://doi.org/10.3390/molecules15095909>.
- (194) Lappert, M. F.; Slade, M. J.; Singh, A.; Atwood, J. L.; Rogers, R. D.; Shakir, R. Structure and Reactivity of Sterically Hindered Lithium Amides and Their Diethyl Etherates: Crystal and Molecular Structures of [Li{N(SiMe₃)₂}(OEt)₂]₂ and tetrakis(2,2,6,6-Tetramethylpiperidinolithium). *J. Am. Chem. Soc.* **1983**, *105* (2), 302–304. <https://doi.org/10.1021/ja00340a031>.
- (195) 陈博卢江平; CHEN Bo, L. J.-P. (±)-Pauciflorol F的全合成. *有机化学* **26** (9), 1300–1302.
- (196) Mizoroki, T.; Mori, K.; Ozaki, A. Arylation of Olefin with Aryl Iodide Catalyzed by Palladium. *Bull. Chem. Soc. Jpn.* **1971**, *44* (2), 581–581. <https://doi.org/10.1246/bcsj.44.581>.
- (197) Heck, R. F.; Nolley, J. P. Palladium-Catalyzed Vinylic Hydrogen Substitution Reactions with Aryl, Benzyl, and Styryl Halides. *J. Org. Chem.* **1972**, *37* (14), 2320–2322. <https://doi.org/10.1021/jo00979a024>.
- (198) Ito, Y.; Hirao, T.; Saegusa, T. Synthesis of α,β -Unsaturated Carbonyl Compounds by palladium(II)-Catalyzed Dehydrosilylation of Silyl Enol Ethers. *J. Org. Chem.* **1978**, *43* (5), 1011–1013. <https://doi.org/10.1021/jo00399a052>.
- (199) Habermas, K. L.; Denmark, S. E.; Jones, T. K. The Nazarov Cyclization. In *Organic Reactions*; American Cancer Society, 2004; pp 1–158.
- (200) Vinogradov, M. G.; Turova, O. V.; Zlotin, S. G. Nazarov Reaction: Current Trends and Recent Advances in the Synthesis of Natural Compounds and Their Analogs. *Org. Biomol. Chem.* **2017**, *15* (39), 8245–8269. <https://doi.org/10.1039/C7OB01981E>.
- (201) Palucki, M.; Buchwald, S. L. Palladium-Catalyzed α -Arylation of Ketones. *J. Am. Chem. Soc.* **1997**, *119* (45), 11108–11109. <https://doi.org/10.1021/ja972593s>.
- (202) Hamann, B. C.; Hartwig, J. F. Palladium-Catalyzed Direct α -Arylation of Ketones. Rate Acceleration by Sterically Hindered Chelating Ligands and Reductive Elimination from a Transition Metal Enolate Complex. *J. Am. Chem. Soc.* **1997**, *119* (50), 12382–12383. <https://doi.org/10.1021/ja9727880>.
- (203) Lee, B. H.; Choi, Y. L.; Shin, S.; Heo, J.-N. Stereoselective Palladium-Catalyzed α -Arylation of 3-Aryl-1-Indanones: An Asymmetric Synthesis of (+)-Pauciflorol F. *J. Org. Chem.* **2011**, *76* (16), 6611–6618. <https://doi.org/10.1021/jo2009164>.
- (204) Zhong, C.; Zhu, J.; Chang, J.; Sun, X. Concise Total Syntheses of (±)isopaucifloral F, (±)quadrangularin A, and (±)pallidol. *Tetrahedron Lett.* **2011**, *52* (22), 2815–2817. <https://doi.org/10.1016/j.tetlet.2011.03.002>.
- (205) Kerr, D. J.; Miletic, M.; Manchala, N.; White, J. M.; Flynn, B. L. Asymmetric Synthesis of (+)- and (-)-Pauciflorol F: Confirmation of Absolute Stereochemistry. *Org. Lett.* **2013**, *15* (16), 4118–4121. <https://doi.org/10.1021/ol401752u>.
- (206) Kim, I.; Choi, J. A Versatile Approach to Oligostilbenoid Natural Products – Synthesis of Permethylated Analogues of Viniferifuran, Malibatol A, and Shoreaphenol. *Org. Biomol. Chem.* **2009**, *7* (13), 2788–2795. <https://doi.org/10.1039/B901911A>.
- (207) Abu-Hashem, A. A.; Hussein, H. A. R.; Aly, A. S.; Gouda, M. A. Synthesis of Benzofuran Derivatives via Different Methods. *Synth. Commun.* **2014**, *44* (16), 2285–2312. <https://doi.org/10.1080/00397911.2014.894528>.

- (208) Ohta, A.; late) Yasuo Akita, (the; Ohkuwa, T.; Chiba, M.; Fukunaga, R.; Miyafuji, A.; Nakata, T.; Tani, N.; Aoyagi, Y. Palladium-Catalyze Arylation of Furan, Thiophene, Benzo[b]furan and Benzo[b]thiophene. *HETEROCYCLES* **1990**, *31* (11), 1951. <https://doi.org/10.3987/COM-90-5467>.
- (209) Kapdi, A. R. Organometallic Aspects of Transition-Metal Catalysed Regioselective C–H Bond Functionalisation of Arenes and Heteroarenes. *Dalton Trans.* **2014**, *43* (8), 3021–3034. <https://doi.org/10.1039/C3DT52737A>.
- (210) Kim, K.; Kim, I. Total Synthesis of Diptoindonesin G via a Highly Efficient Domino Cyclodehydration/Intramolecular Friedel–Crafts Acylation/Regioselective Demethylation Sequence. *Org. Lett.* **2010**, *12* (22), 5314–5317. <https://doi.org/10.1021/ol102322g>.
- (211) Horner, L.; Hoffmann, H.; Wippel, H. G. Phosphororganische Verbindungen, XII. Phosphinoxyde als Olefinierungsreagenzien. *Chem. Ber.* **1958**, *91* (1), 61–63. <https://doi.org/10.1002/cber.19580910113>.
- (212) Horner, L.; Hoffmann, H.; Wippel, H. G.; Klahre, G. Phosphororganische Verbindungen, XX. Phosphinoxyde als Olefinierungsreagenzien. *Chem. Ber.* **1959**, *92* (10), 2499–2505. <https://doi.org/10.1002/cber.19590921017>.
- (213) Wadsworth, W. S.; Emmons, W. D. The Utility of Phosphonate Carbanions in Olefin Synthesis. *J. Am. Chem. Soc.* **1961**, *83* (7), 1733–1738. <https://doi.org/10.1021/ja01468a042>.
- (214) Boutagy, J.; Thomas, R. Olefin Synthesis with Organic Phosphonate Carbanions. *Chem. Rev.* **1974**, *74* (1), 87–99. <https://doi.org/10.1021/cr60287a005>.
- (215) Lindgren, A. E. G.; Öberg, C. T.; Hillgren, J. M.; Elofsson, M. Total Synthesis of the Resveratrol Oligomers (±)-Ampelopsin B and (±)-ε-Viniferin. *Eur. J. Org. Chem.* **2016**, *2016* (3), 426–429. <https://doi.org/10.1002/ejoc.201501486>.
- (216) Nagata, W.; Okada, K.; Itazaki, H.; Uyeo, S. Synthetic Studies on Isoquinoline Alkaloids. II. Selective Conversion of 3, 9, 10-Substituted Tetrahydroprotoberberines into 3, 9, 10-Substituted 14-Deoxoprotopines. Total Synthesis of 3, 9, 10-Substituted 5, 6, 7, 8, 13, 14-Hexahydrodibenz (C, G) Azecines. *Chem. Pharm. Bull. (Tokyo)* **1975**, *23* (11), 2878–2890. <https://doi.org/10.1248/cpb.23.2878>.
- (217) Kurosawa, W.; Kan, T.; Fukuyama, T. An Efficient Synthesis of Optically Active Trans-2-Aryl-2,3-Dihydrobenzofuran-3-Carboxylic Acid Esters via C–H Insertion Reaction. *Synlett* **2003**, *2003* (7), 1028–1030. <https://doi.org/10.1055/s-2003-39316>.
- (218) Zhang, J.; Zhang, J.; Kang, Y.; Shi, J.; Yao, C. A Facile and Practical Total Synthetic Route for Ampelopsin F and Permethylated ε-Viniferin. *Synlett* **2016**, *27* (10), 1587–1591. <https://doi.org/10.1055/s-0035-1561419>.
- (219) Soldi, C.; Lamb, K. N.; Squitieri, R. A.; González-López, M.; Di Maso, M. J.; Shaw, J. T. Enantioselective Intramolecular C–H Insertion Reactions of Donor–Donor Metal Carbenoids. *J. Am. Chem. Soc.* **2014**, *136* (43), 15142–15145. <https://doi.org/10.1021/ja508586t>.
- (220) Natori, Y.; Tsutsui, H.; Sato, N.; Nakamura, S.; Nambu, H.; Shiro, M.; Hashimoto, S. Asymmetric Synthesis of Neolignans (–)-Epi-Conocarpan and (+)-Conocarpan via Rh(II)-Catalyzed C–H Insertion Process and Revision of the Absolute Configuration of (–)-Epi-Conocarpan. *J. Org. Chem.* **2009**, *74* (11), 4418–4421. <https://doi.org/10.1021/jo900502d>.

- (221) Snyder, S. A.; Gollner, A.; Chiriac, M. I. Regioselective Reactions for Programmable Resveratrol Oligomer Synthesis. *Nature* **2011**, *474* (7352), 461–466. <https://doi.org/10.1038/nature10197>.
- (222) Jepsen, T. H.; Thomas, S. B.; Lin, Y.; Stathakis, C. I.; de Miguel, I.; Snyder, S. A. Harnessing Quinone Methides: Total Synthesis of (±)-Vaticanol A. *Angew. Chem. Int. Ed.* **2014**, *53* (26), 6747–6751. <https://doi.org/10.1002/anie.201402858>.
- (223) Tebbe, F. N.; Parshall, G. W.; Reddy, G. S. Olefin Homologation with Titanium Methylene Compounds. *J. Am. Chem. Soc.* **1978**, *100* (11), 3611–3613. <https://doi.org/10.1021/ja00479a061>.
- (224) Atkins, G. M.; Burgess, E. M. The Reactions of an N-Sulfonylamine Inner Salt. *J. Am. Chem. Soc.* **1968**, *90* (17), 4744–4745. <https://doi.org/10.1021/ja01019a052>.
- (225) Wright, N. E.; Snyder, S. A. 9-Membered Carbocycle Formation: Development of Distinct Friedel–Crafts Cyclizations and Application to a Scalable Total Synthesis of (±)-Caraphenol A. *Angew. Chem. Int. Ed.* **2014**, *53* (13), 3409–3413. <https://doi.org/10.1002/anie.201311299>.
- (226) Fries, K.; Finck, G. Über Homologe Des Cumaranon Und Ihre Abkömmlinge. *Berichte Dtsch. Chem. Ges.* **1908**, *41* (3), 4271–4284. <https://doi.org/10.1002/cber.190804103146>.
- (227) Fries, K.; Pfaffendorf, W. Über Ein Kondensationsprodukt Des Cumaranon Und Seine Umwandlung in Oxindirubin. *Berichte Dtsch. Chem. Ges.* **1910**, *43* (1), 212–219. <https://doi.org/10.1002/cber.19100430131>.
- (228) Pappo, R.; Allen, J., D. S.; Lemieux, R. U.; Johnson, W. S. Notes - Osmium Tetroxide-Catalyzed Periodate Oxidation of Olefinic Bonds. *J. Org. Chem.* **1956**, *21* (4), 478–479. <https://doi.org/10.1021/jo01110a606>.
- (229) Frenette, M.; Aliaga, C.; Font-Sanchis, E.; Scaiano, J. C. Bond Dissociation Energies for Radical Dimers Derived from Highly Stabilized Carbon-Centered Radicals. *Org. Lett.* **2004**, *6* (15), 2579–2582. <https://doi.org/10.1021/ol049111j>.
- (230) Beer. Bestimmung Der Absorption Des Rothen Lichts in Farbigen Flüssigkeiten. *Ann. Phys.* **1852**, *162* (5), 78–88. <https://doi.org/10.1002/andp.18521620505>.
- (231) Hoff, M. J. H. van't. Etudes de Dynamique Chimique. *Recl. Trav. Chim. Pays-Bas* **1884**, *3* (10), 333–336. <https://doi.org/10.1002/recl.18840031003>.
- (232) Studer, A.; Curran, D. P. The Electron Is a Catalyst. *Nat. Chem.* **2014**, *6* (9), 765–773. <https://doi.org/10.1038/nchem.2031>.
- (233) Takaya, Y.; Yan, K.-X.; Terashima, K.; He, Y.-H.; Niwa, M. Biogenetic Reactions on Stilbenetetramers from Vitaceae Plants. *Tetrahedron* **2002**, *58* (45), 9265–9271. [https://doi.org/10.1016/S0040-4020\(02\)01191-2](https://doi.org/10.1016/S0040-4020(02)01191-2).
- (234) Smith, M. J.; Reichl, K. D.; Escobar, R. A.; Heavey, T. J.; Coker, D. F.; Schaus, S. E.; Porco, J. A. Asymmetric Synthesis of Griffipavixanthone Employing a Chiral Phosphoric Acid-Catalyzed Cycloaddition. *J. Am. Chem. Soc.* **2019**, *141* (1), 148–153. <https://doi.org/10.1021/jacs.8b12520>.
- (235) Mitsunobu, O.; Yamada, M. Preparation of Esters of Carboxylic and Phosphoric Acid via Quaternary Phosphonium Salts. *Bull. Chem. Soc. Jpn.* **1967**, *40* (10), 2380–2382. <https://doi.org/10.1246/bcsj.40.2380>.
- (236) Banwell, M. G.; Flynn, B. L.; Stewart, S. G. Selective Cleavage of Isopropyl Aryl Ethers by Aluminum Trichloride†. *J. Org. Chem.* **1998**, *63* (24), 9139–9144. <https://doi.org/10.1021/jo9808526>.

- (237) Bowler, J. M.; Hervert, K. L.; Kearley, M. L.; Miller, B. G. Small-Molecule Allosteric Activation of Human Glucokinase in the Absence of Glucose. *ACS Med. Chem. Lett.* **2013**, *4* (7), 580–584. <https://doi.org/10.1021/ml400061x>.
- (238) Liégault, B.; Lapointe, D.; Caron, L.; Vlassova, A.; Fagnou, K. Establishment of Broadly Applicable Reaction Conditions for the Palladium-Catalyzed Direct Arylation of Heteroatom-Containing Aromatic Compounds. *J. Org. Chem.* **2009**, *74* (5), 1826–1834. <https://doi.org/10.1021/jo8026565>.
- (239) Parikh, J. R.; Doering, W. v. E. Sulfur Trioxide in the Oxidation of Alcohols by Dimethyl Sulfoxide. *J. Am. Chem. Soc.* **1967**, *89* (21), 5505–5507. <https://doi.org/10.1021/ja00997a067>.
- (240) Akai, S.; Ikawa, T.; Takayanagi, S.; Morikawa, Y.; Mohri, S.; Tsubakiyama, M.; Egi, M.; Wada, Y.; Kita, Y. Synthesis of Biaryl Compounds through Three-Component Assembly: Ambidentate Effect of the Tert-Butyldimethylsilyl Group for Regioselective Diels–Alder and Hiyama Coupling Reactions. *Angew. Chem. Int. Ed.* **2008**, *47* (40), 7673–7676. <https://doi.org/10.1002/anie.200803011>.
- (241) Ikawa, T.; Nishiyama, T.; Nosaki, T.; Takagi, A.; Akai, S. A Domino Process for Benzyne Preparation: Dual Activation of O-(Trimethylsilyl)phenols by Nonafluorobutanesulfonyl Fluoride. *Org. Lett.* **2011**, *13* (7), 1730–1733. <https://doi.org/10.1021/ol200252c>.
- (242) Wohl, A. Bromierung Ungesättigter Verbindungen Mit N-Brom-Acetamid, Ein Beitrag Zur Lehre Vom Verlauf Chemischer Vorgänge. *Berichte Dtsch. Chem. Ges. B Ser.* **1919**, *52* (1), 51–63. <https://doi.org/10.1002/cber.19190520109>.
- (243) Ziegler, K.; Schenck, G.; Krockow, E. W.; Siebert, A.; Wenz, A.; Weber, H. Die Synthese Des Cantharidins. *Justus Liebigs Ann. Chem.* **1942**, *551* (1), 1–79. <https://doi.org/10.1002/jlac.19425510102>.
- (244) Romero, K. J.; Keylor, M. H.; Griesser, M.; Zhu, X.; Strobel, E. J.; Pratt, D. A.; Stephenson, C. R. J. Synthesis of Vitisins A and D Enabled by a Persistent Radical Equilibrium. *J. Am. Chem. Soc.* **2020**, *142* (14), 6499–6504. <https://doi.org/10.1021/jacs.0c01714>.
- (245) Corey, E. J.; Fleet, G. W. J.; Kato, M. A Biogenetic Approach to the Synthesis of a Prostanoid Precursor. *Tetrahedron Lett.* **1973**, *14* (40), 3963–3966. [https://doi.org/10.1016/S0040-4039\(01\)87084-2](https://doi.org/10.1016/S0040-4039(01)87084-2).
- (246) Clive, D. L. J.; Tao, Y.; Bo, Y.; Hu, Y.-Z.; Selvakumar, N.; Sun, S.; Daigneault, S.; Wu, Y.-J. Synthetic Studies on calicheamicinylII—synthesis of (–)-Calicheamicinone and Models Representing the Four Sugars Andthe Aromatic System. *Chem. Commun.* **2000**, No. 15, 1341–1350. <https://doi.org/10.1039/B001204L>.
- (247) Kraus, G. A.; Bae, J. Synthesis of N-(2-Methylpropyl)-2E-Undecene-8,10-Diynamide, a Novel Constituent of Echinacea Angustifolia. *Tetrahedron Lett.* **2003**, *44* (29), 5505–5506. [https://doi.org/10.1016/S0040-4039\(03\)01253-X](https://doi.org/10.1016/S0040-4039(03)01253-X).
- (248) Mukai, C.; Nomura, I.; Kitagaki, S. Efficient Construction of the Bicyclo[5.3.0]decenone Skeleton Based on the Rh(I)-Catalyzed Allenic Pauson–Khand Reaction. *J. Org. Chem.* **2003**, *68* (4), 1376–1385. <https://doi.org/10.1021/jo020649h>.

- (249) Kirkham, J. E. D.; Courtney, T. D. L.; Lee, V.; Baldwin, J. E. Asymmetric Synthesis of Cytotoxic Sponge Metabolites R-Strongyloidiols A and B. *Tetrahedron Lett.* **2004**, *45* (29), 5645–5647. <https://doi.org/10.1016/j.tetlet.2004.05.122>.
- (250) Bellina, F.; Carpita, A.; Mannocci, L.; Rossi, R. First Total Synthesis of Naturally Occurring (–)-Nitidon and Its Enantiomer. *Eur. J. Org. Chem.* **2004**, *2004* (12), 2610–2619. <https://doi.org/10.1002/ejoc.200400101>.
- (251) Bergueiro, J.; Montenegro, J.; Saá, C.; López, S. Synthesis of 11-Cis-Retinoids by Hydrosilylation–Protodesilylation of an 11,12-Didehydro Precursor: Easy Access to 11- and 12-Mono- and 11,12-Dideuteroretinoids. *Chem. – Eur. J.* **2012**, *18* (44), 14100–14107. <https://doi.org/10.1002/chem.201202260>.
- (252) Schinzer, D.; Heathcock, C. H. Fluoride-Catalyzed Conversion of Acylsilanes to Aldehydes and Ketones. *Tetrahedron Lett.* **1981**, *22* (20), 1881–1884. [https://doi.org/10.1016/S0040-4039\(01\)90467-8](https://doi.org/10.1016/S0040-4039(01)90467-8).
- (253) Toyota, M.; Terashima, S. A Novel Synthesis of the Basic Carbon Framework of Fredericamycin A. Promising Routes for the Spiro Chiral Center Construction of the CD-Ring System. *Tetrahedron Lett.* **1989**, *30* (7), 829–832. [https://doi.org/10.1016/S0040-4039\(01\)80627-4](https://doi.org/10.1016/S0040-4039(01)80627-4).
- (254) Reiffen, M.; Hoffmann, R. W. Carben-Reaktionen XIII Cycloheptatrienyliden Aus Trimethylsilyl-Tropylium-Tetrafluorborat. *Tetrahedron Lett.* **1978**, *19* (13), 1107–1110. [https://doi.org/10.1016/S0040-4039\(01\)94473-9](https://doi.org/10.1016/S0040-4039(01)94473-9).
- (255) Hagen, S. E.; Domagala, J. M.; Heifetz, C. L.; Johnson, J. Synthesis and Biological Activity of 5-Alkyl-1,7,8-Trisubstituted-6-Fluoroquinoline-3-Carboxylic Acids. *J. Med. Chem.* **1991**, *34* (3), 1155–1161. <https://doi.org/10.1021/jm00107a040>.
- (256) Mills, R. J.; Taylor, N. J.; Snieckus, V. Directed Ortho Metalation of N,N-Diethylbenzamides. Silicon Protection of Ortho Sites and the O-Methyl Group. *J. Org. Chem.* **1989**, *54* (18), 4372–4385. <https://doi.org/10.1021/jo00279a028>.
- (257) Hatanaka, Y.; Hiyama, T. Cross-Coupling of Organosilanes with Organic Halides Mediated by a Palladium Catalyst and Tris(diethylamino)sulfonium Difluorotrimethylsilicate. *J. Org. Chem.* **1988**, *53* (4), 918–920. <https://doi.org/10.1021/jo00239a056>.
- (258) Hudlický, M. Fluorination with Diethylaminosulfur Trifluoride and Related Aminofluorosulfuranes. In *Organic Reactions*; American Cancer Society, 2004; pp 513–637.
- (259) Schimmler, S. D.; Ryan, S. J.; Bland, D. C.; Anderson, J. E.; Sanford, M. S. Anhydrous Tetramethylammonium Fluoride for Room-Temperature S_NAr Fluorination. *J. Org. Chem.* **2015**, *80* (24), 12137–12145. <https://doi.org/10.1021/acs.joc.5b02075>.
- (260) Sowden, M. J.; Ward, J. S.; Sherburn, M. S. Synthesis and Properties of 2,3-Diethynyl-1,3-Butadienes. *Angew. Chem. Int. Ed.* **2020**, *59* (10), 4145–4153. <https://doi.org/10.1002/anie.201914807>.
- (261) Radner, F.; Wistrand, L.-G. A Convenient Method for the Protodesilylation of Aryltrimethylsilanes. *Tetrahedron Lett.* **1995**, *36* (28), 5093–5094. [https://doi.org/10.1016/0040-4039\(95\)00948-C](https://doi.org/10.1016/0040-4039(95)00948-C).
- (262) Lv, H.; Zhou, W.; Wang, X.; Wang, Z.; Suo, Y.; Wang, H. Extraction and Separation of Vitisin D, Ampelopsin B and Cis-Vitisin A from *Iris Lactea* Pall. Var. *Chinensis* (Fisch.) Koidz by Alkaline Extraction–Acid Precipitation and High-Speed Counter-

- Current Chromatography. *J. Chromatogr. Sci.* **2016**, *54* (5), 744–751. <https://doi.org/10.1093/chromsci/bmv249>.
- (263) Davis, R. A.; Beattie, K. D.; Xu, M.; Yang, X.; Yin, S.; Holla, H.; Healy, P. C.; Sykes, M.; Shelper, T.; Avery, V. M.; Elofsson, M.; Sundin, C.; Quinn, R. J. Solving the Supply of Resveratrol Tetramers from Papua New Guinean Rainforest Anisoptera Species That Inhibit Bacterial Type III Secretion Systems. *J. Nat. Prod.* **2014**, *77* (12), 2633–2640. <https://doi.org/10.1021/np500433z>.
- (264) Newman, D. J.; Cragg, G. M. Natural Products as Sources of New Drugs over the Nearly Four Decades from 01/1981 to 09/2019. *J. Nat. Prod.* **2020**. <https://doi.org/10.1021/acs.jnatprod.9b01285>.
- (265) Brookmeyer, R.; Johnson, E.; Ziegler-Graham, K.; Arrighi, H. M. Forecasting the Global Burden of Alzheimer’s Disease. *Alzheimers Dement.* **2007**, *3* (3), 186–191. <https://doi.org/10.1016/j.jalz.2007.04.381>.
- (266) Hussain, I.; Powell, D.; Howlett, D. R.; Tew, D. G.; Meek, T. D.; Chapman, C.; Gloger, I. S.; Murphy, K. E.; Southan, C. D.; Ryan, D. M.; Smith, T. S.; Simmons, D. L.; Walsh, F. S.; Dingwall, C.; Christie, G. Identification of a Novel Aspartic Protease (Asp 2) as β -Secretase. *Mol. Cell. Neurosci.* **1999**, *14* (6), 419–427. <https://doi.org/10.1006/mcne.1999.0811>.
- (267) Lin, X.; Koelsch, G.; Wu, S.; Downs, D.; Dashti, A.; Tang, J. Human Aspartic Protease Memapsin 2 Cleaves the β -Secretase Site of β -Amyloid Precursor Protein. *Proc. Natl. Acad. Sci.* **2000**, *97* (4), 1456–1460. <https://doi.org/10.1073/pnas.97.4.1456>.
- (268) Sinha, S.; Anderson, J. P.; Barbour, R.; Basi, G. S.; Caccavello, R.; Davis, D.; Doan, M.; Dovey, H. F.; Frigon, N.; Hong, J.; Jacobson-Croak, K.; Jewett, N.; Keim, P.; Knops, J.; Lieberburg, I.; Power, M.; Tan, H.; Tatsuno, G.; Tung, J.; Schenk, D.; Seubert, P.; Suomensaaari, S. M.; Wang, S.; Walker, D.; Zhao, J.; McConlogue, L.; John, V. Purification and Cloning of Amyloid Precursor Protein β -Secretase from Human Brain. *Nature* **1999**, *402* (6761), 537–540. <https://doi.org/10.1038/990114>.
- (269) Vassar, R.; Bennett, B. D.; Babu-Khan, S.; Kahn, S.; Mendiaz, E. A.; Denis, P.; Teplow, D. B.; Ross, S.; Amarante, P.; Loeloff, R.; Luo, Y.; Fisher, S.; Fuller, J.; Edenson, S.; Lile, J.; Jarosinski, M. A.; Biere, A. L.; Curran, E.; Burgess, T.; Louis, J.-C.; Collins, F.; Treanor, J.; Rogers, G.; Citron, M. β -Secretase Cleavage of Alzheimer’s Amyloid Precursor Protein by the Transmembrane Aspartic Protease BACE. *Science* **1999**, *286* (5440), 735–741. <https://doi.org/10.1126/science.286.5440.735>.
- (270) Hu, J.; Lin, T.; Xu, J.; Ding, R.; Wang, G.; Shen, R.; Zhang, Y.; Chen, H. Polyphenols Isolated from Leaves of *Vitis Thunbergii* Var. *Taiwaniana* Regulate APP Related Pathway. *Bioorg. Med. Chem. Lett.* **2016**, *26* (2), 505–511. <https://doi.org/10.1016/j.bmcl.2015.11.085>.
- (271) Choi, Y. H.; Yoo, M. Y.; Choi, C. W.; Cha, M.-R.; Yon, G. H.; Kwon, D. Y.; Kim, Y. S.; Park, W.-K.; Ryu, S. Y. A New Specific BACE-1 Inhibitor from the Stembark Extract of *Vitis Vinifera*. *Planta Med.* **2009**, *75* (5), 537–540. <https://doi.org/10.1055/s-0029-1185311>.
- (272) Jang, M. H.; Piao, X. L.; Kim, J. M.; Kwon, S. W.; Park, J. H. Inhibition of Cholinesterase and Amyloid- β Aggregation by Resveratrol Oligomers from *Vitis Amurensis*. *Phytother. Res.* **2008**, *22* (4), 544–549. <https://doi.org/10.1002/ptr.2406>.

- (273) Mitchell, N. S.; Catenacci, V. A.; Wyatt, H. R.; Hill, J. O. Obesity: Overview of an Epidemic. *Psychiatr. Clin. North Am.* **2011**, *34* (4), 717–732. <https://doi.org/10.1016/j.psc.2011.08.005>.
- (274) Kopelman, P. G. Obesity as a Medical Problem. *Nature* **2000**, *404* (6778), 635–643. <https://doi.org/10.1038/35007508>.
- (275) Blüher, M. Adipose Tissue Dysfunction Contributes to Obesity Related Metabolic Diseases. *Best Pract. Res. Clin. Endocrinol. Metab.* **2013**, *27* (2), 163–177. <https://doi.org/10.1016/j.beem.2013.02.005>.
- (276) Tie, F.-F.; Luan, G.-X.; Zhou, W.-N.; Wang, Z.-H.; Shi, X.-B.; Li, G.; Wang, H.-L. Effects of the Oligostilbenes from *Iris Lactea* Pall. Var. *Chinensis* (Fisch.) Koidz on the Adipocytes Differentiation of 3T3-L1 Cells. *Pharmazie* **2018**, *73* (2), 98–103.
- (277) Rosen, E. D.; MacDougald, O. A. Adipocyte Differentiation from the inside out. *Nat. Rev. Mol. Cell Biol.* **2006**, *7* (12), 885–896. <https://doi.org/10.1038/nrm2066>.
- (278) Camp, H. S.; Ren, D.; Leff, T. Adipogenesis and Fat-Cell Function in Obesity and Diabetes. *Trends Mol. Med.* **2002**, *8* (9), 442–447. [https://doi.org/10.1016/S1471-4914\(02\)02396-1](https://doi.org/10.1016/S1471-4914(02)02396-1).
- (279) Park, U.-H.; Jeong, J.-C.; Jang, J.-S.; Sung, M.-R.; Youn, H.; Lee, S.-J.; Kim, E.-J.; Um, S.-J. Negative Regulation of Adipogenesis by Kaempferol, a Component of *Rhizoma Polygonati Falcatum* in 3T3-L1 Cells. *Biol. Pharm. Bull.* **2012**, *35* (9), 1525–1533. <https://doi.org/10.1248/bpb.b12-00254>.
- (280) Kopecky, J.; Clarke, G.; Enerbäck, S.; Spiegelman, B.; Kozak, L. P. Expression of the Mitochondrial Uncoupling Protein Gene from the aP2 Gene Promoter Prevents Genetic Obesity. *J. Clin. Invest.* **1995**, *96* (6), 2914–2923. <https://doi.org/10.1172/JCI118363>.
- (281) Chen, L.; Deng, H.; Cui, H.; Fang, J.; Zuo, Z.; Deng, J.; Li, Y.; Wang, X.; Zhao, L. Inflammatory Responses and Inflammation-Associated Diseases in Organs. *Oncotarget* **2017**, *9* (6), 7204–7218. <https://doi.org/10.18632/oncotarget.23208>.
- (282) Huang, K.-S.; Lin, M.; Cheng, G.-F. Anti-Inflammatory Tetramers of Resveratrol from the Roots of *Vitis Amurensis* and the Conformations of the Seven-Membered Ring in Some Oligostilbenes. *Phytochemistry* **2001**, *58* (2), 357–362. [https://doi.org/10.1016/S0031-9422\(01\)00224-2](https://doi.org/10.1016/S0031-9422(01)00224-2).
- (283) O’Shea, J. J.; Ma, A.; Lipsky, P. Cytokines and Autoimmunity. *Nat. Rev. Immunol.* **2002**, *2* (1), 37–45. <https://doi.org/10.1038/nri702>.
- (284) Mi Jeong Sung; Davaatseren, M.; Kim, W.; Sung Kwang Park; Kim, S.-H.; Haeng Jeon Hur; Myung Sunny Kim; Kim, Y.-S.; Dae Young Kwon. Vitisin A Suppresses LPS-Induced NO Production by Inhibiting ERK, p38, and NF-κB Activation in RAW 264.7 Cells. *Int. Immunopharmacol.* **2009**, *9* (3), 319–323. <https://doi.org/10.1016/j.intimp.2008.12.005>.
- (285) Nassra, M.; Krisa, S.; Papastamoulis, Y.; Kapche, G. D.; Bisson, J.; André, C.; Konsman, J.-P.; Schmitter, J.-M.; Mérillon, J.-M.; Waffo-Tégou, P. Inhibitory Activity of Plant Stilbenoids against Nitric Oxide Production by Lipopolysaccharide-Activated Microglia. *Planta Med.* **2013**, *79* (11), 966–970. <https://doi.org/10.1055/s-0032-1328651>.
- (286) Jang, M.; Cho, E. J.; Piao, X.-L. Protective Effects of Resveratrol Oligomers from *Vitis Amurensis* against Sodium Nitroprusside-Induced Neurotoxicity in Human

- Neuroblastoma SH-SY5Y Cells. *Arch. Pharm. Res.* **2015**, *38* (6), 1263–1269. <https://doi.org/10.1007/s12272-014-0505-3>.
- (287) Huang, Y.-L.; Tsai, W.-J.; Shen, C.-C.; Chen, C.-C. Resveratrol Derivatives from the Roots of *Vitis Thunbergii*. *J. Nat. Prod.* **2005**, *68* (2), 217–220. <https://doi.org/10.1021/np049686p>.
- (288) Niraula, S.; Le, L. W.; Tannock, I. F. Treatment of Prostate Cancer With Intermittent Versus Continuous Androgen Deprivation: A Systematic Review of Randomized Trials. *J. Clin. Oncol.* **2013**, *31* (16), 2029–2036. <https://doi.org/10.1200/JCO.2012.46.5492>.
- (289) Voortman, J.; Resende, T. P.; Hassan, M. A. I. A. E.; Giaccone, G.; Kruyt, F. A. E. TRAIL Therapy in Non-small Cell Lung Cancer Cells: Sensitization to Death Receptor-mediated Apoptosis by Proteasome Inhibitor Bortezomib. *Mol. Cancer Ther.* **2007**, *6* (7), 2103–2112. <https://doi.org/10.1158/1535-7163.MCT-07-0167>.
- (290) Mirandola, P.; Gobbi, G.; Sponzilli, I.; Malinverno, C.; Cavazzoni, A.; Alfieri, R.; Petronini, P. G.; Vitale, M. TRAIL-Induced Apoptosis of FHIT-Negative Lung Cancer Cells Is Inhibited by FHIT Re-Expression. *J. Cell. Physiol.* **2009**, *220* (2), 492–498. <https://doi.org/10.1002/jcp.21801>.
- (291) Li, G.; Fu, D.; Liang, W.; Fan, L.; Chen, K.; Shan, L.; Hu, S.; Ma, X.; Zhou, K.; Cheng, B. CYC1 Silencing Sensitizes Osteosarcoma Cells to TRAIL-Induced Apoptosis. *Cell. Physiol. Biochem.* **2014**, *34* (6), 2070–2080. <https://doi.org/10.1159/000366402>.
- (292) Wu, X.; Yang, N.; Zhou, W.; Xu, J.; Chen, J.; Zheng, F.; Long, Z.; Yue, C.; Ai, K.; Liu, L.; Wan, X.; Liu, Q. Up-Regulation of P21 Inhibits TRAIL-Mediated Extrinsic Apoptosis, Contributing Resistance to SAHA in Acute Myeloid Leukemia Cells. *Cell. Physiol. Biochem.* **2014**, *34* (2), 506–518. <https://doi.org/10.1159/000363018>.
- (293) Shin, D.; Kwon, H.-Y.; Sohn, E. J.; Nam, M. S.; Kim, J. H.; Lee, J. C.; Ryu, S.-Y.; Park, B.; Kim, S.-H. Upregulation of Death Receptor 5 and Production of Reactive Oxygen Species Mediate Sensitization of PC-3 Prostate Cancer Cells to TRAIL Induced Apoptosis by Vitisin A. *Cell. Physiol. Biochem.* **2015**, *36* (3), 1151–1162. <https://doi.org/10.1159/000430286>.
- (294) Seya, K.; Kanemaru, K.; Sugimoto, C.; Suzuki, M.; Takeo, T.; Motomura, S.; Kitahara, H.; Niwa, M.; Oshima, Y.; Furukawa, K.-I. Opposite Effects of Two Resveratrol Tetramers, Vitisin A and Hopeaphenol on Apoptosis of Myocytes Isolated from Adult Rat Heart. *J. Pharmacol. Exp. Ther.* **2008**. <https://doi.org/10.1124/jpet.108.143172>.
- (295) Matsukura, S.; Kokubu, F.; Kubo, H.; Tomita, T.; Tokunaga, H.; Kadokura, M.; Yamamoto, T.; Kuroiwa, Y.; Ohno, T.; Suzaki, H.; Adachi, M. Expression of RANTES by Normal Airway Epithelial Cells after Influenza Virus A Infection. *Am. J. Respir. Cell Mol. Biol.* **1998**, *18* (2), 255–264. <https://doi.org/10.1165/ajrcmb.18.2.2822>.
- (296) Huang, Y.-L.; Loke, S.-H.; Hsu, C.-C.; Chiou, W.-F. (+)-Vitisin A Inhibits Influenza A Virus-Induced RANTES Production in A549 Alveolar Epithelial Cells through Interference with Akt and STAT1 Phosphorylation. *Planta Med.* **2008**, *74* (2), 156–162. <https://doi.org/10.1055/s-2007-993786>.
- (297) Lee, S.; Yoon, K. D.; Lee, M.; Cho, Y.; Choi, G.; Jang, H.; Kim, B.; Jung, D.-H.; Oh, J.-G.; Kim, G.-W.; Oh, J.-W.; Jeong, Y.-J.; Kwon, H. J.; Bae, S. K.; Min, D.-H.;

- Windisch, M. P.; Heo, T.-H.; Lee, C. Identification of a Resveratrol Tetramer as a Potent Inhibitor of Hepatitis C Virus Helicase. *Br. J. Pharmacol.* **2016**, *173* (1), 191–211. <https://doi.org/10.1111/bph.13358>.
- (298) Shepard, C. W.; Finelli, L.; Alter, M. J. Global Epidemiology of Hepatitis C Virus Infection. *Lancet Infect. Dis.* **2005**, *5* (9), 558–567. [https://doi.org/10.1016/S1473-3099\(05\)70216-4](https://doi.org/10.1016/S1473-3099(05)70216-4).
- (299) Shang, C.; Kang, Y.; Yang, Q.; Zhu, Q.; Yao, C. Versatile and Enantioselective Total Synthesis of Naturally Active Gnetulin. *Adv. Synth. Catal.* **2019**, *361* (16), 3768–3776. <https://doi.org/10.1002/adsc.201900336>.
- (300) Vutukuri, D. R.; Bharathi, P.; Yu, Z.; Rajasekaran, K.; Tran, M.-H.; Thayumanavan, S. A Mild Deprotection Strategy for Allyl-Protecting Groups and Its Implications in Sequence Specific Dendrimer Synthesis. *J. Org. Chem.* **2003**, *68* (3), 1146–1149. <https://doi.org/10.1021/jo026469p>.
- (301) Xiong, X.; Tan, F.; Yeung, Y.-Y. Zwitterionic-Salt-Catalyzed Site-Selective Monobromination of Arenes. *Org. Lett.* **2017**, *19* (16), 4243–4246. <https://doi.org/10.1021/acs.orglett.7b01899>.
- (302) Oshima, Y.; Kamijou, A.; Moritani, H.; Namao, K.; Ohizumi, Y. Vitisin A and Cis-Vitisin A, Strongly Hepatotoxic Plant Oligostilbenes from *Vitis Coignetiae* (Vitaceae). *J. Org. Chem.* **1993**, *58* (4), 850–853. <https://doi.org/10.1021/jo00056a016>.
- (303) Ohshima, Y.; Shinoda, K.; Takaya, Y.; Ohta, T.; Niwa, M.; Hisamichi, K.; Takeshita, M. Vitisins D and E, Novel Oligostilbenes from *Vitis Coignetiae* Stem Barks. *HETEROCYCLES* **1997**, *46* (1), 169. <https://doi.org/10.3987/COM-97-S62>.